DEVELOPMENT AND POTENTIAL MECHANISMS OF LOW MOLECULAR WEIGHT DRUGS FOR CANCER IMMUNOTHERAPY

EDITED BY: Yanfeng Gao, Bin Zhang and Xuanming Yang

PUBLISHED IN: Frontiers in Immunology, Frontiers in Oncology and Frontiers in Pharmacology

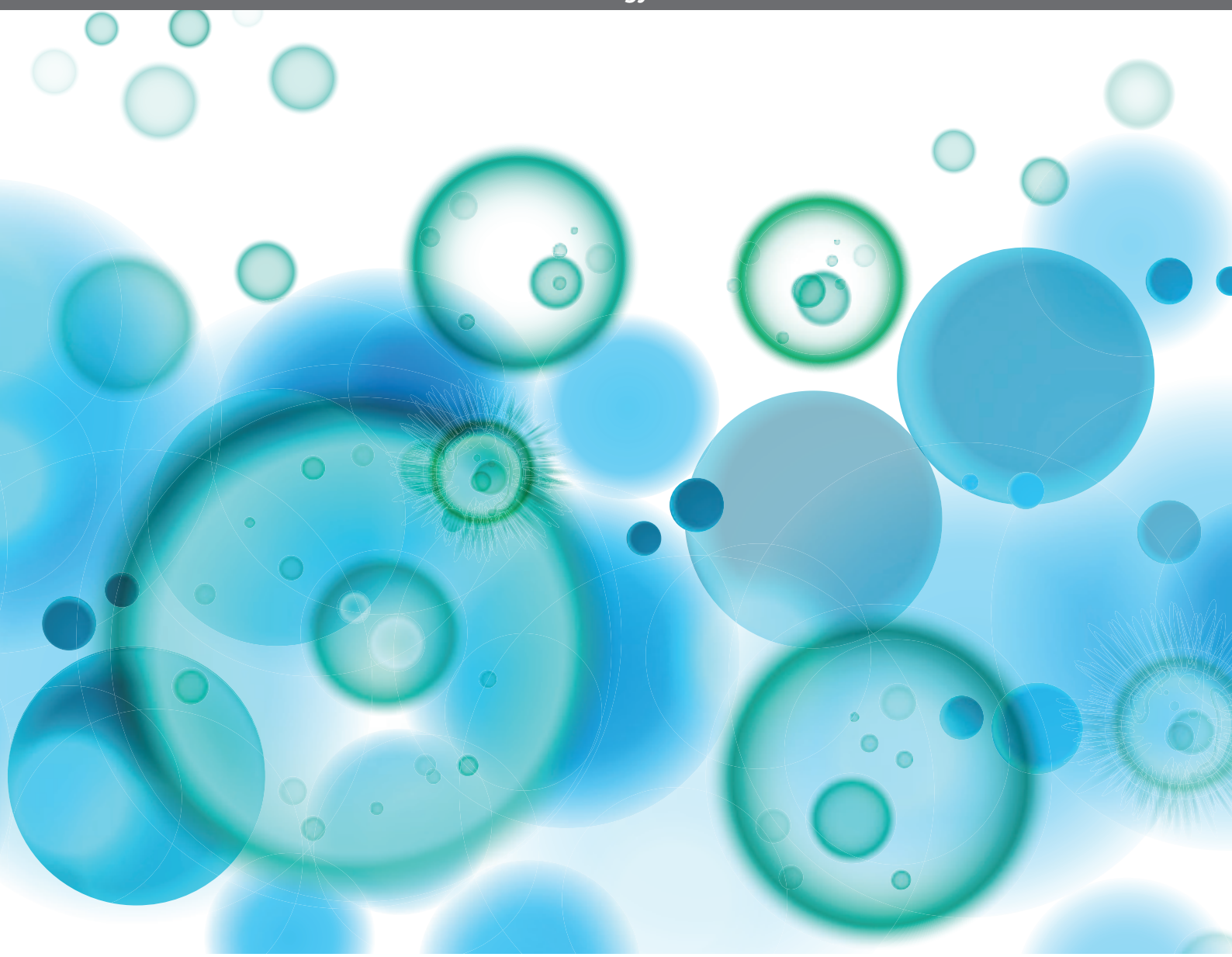

frontiers Research Topics

frontiers

ISSN 1664-8714
ISBN 978-2-88976-316-0
DOI 10.3389/978-2-88976-316-0

About Frontiers

Frontiers is more than just an open-access publisher of scholarly articles: it is a pioneering approach to the world of academia, radically improving the way scholarly research is managed. The grand vision of Frontiers is a world where all people have an equal opportunity to seek, share and generate knowledge. Frontiers provides immediate and permanent online open access to all its publications, but this alone is not enough to realize our grand goals.

Frontiers Journal Series

The Frontiers Journal Series is a multi-tier and interdisciplinary set of open-access, online journals, promising a paradigm shift from the current review, selection and dissemination processes in academic publishing. All Frontiers journals are driven by researchers for researchers; therefore, they constitute a service to the scholarly community. At the same time, the Frontiers Journal Series operates on a revolutionary invention, the tiered publishing system, initially addressing specific communities of scholars, and gradually climbing up to broader public understanding, thus serving the interests of the lay society, too.

Dedication to Quality

Each Frontiers article is a landmark of the highest quality, thanks to genuinely collaborative interactions between authors and review editors, who include some of the world's best academicians. Research must be certified by peers before entering a stream of knowledge that may eventually reach the public - and shape society; therefore, Frontiers only applies the most rigorous and unbiased reviews.
Frontiers revolutionizes research publishing by freely delivering the most outstanding research, evaluated with no bias from both the academic and social point of view. By applying the most advanced information technologies, Frontiers is catapulting scholarly publishing into a new generation.

What are Frontiers Research Topics?

Frontiers Research Topics are very popular trademarks of the Frontiers Journals Series: they are collections of at least ten articles, all centered on a particular subject. With their unique mix of varied contributions from Original Research to Review Articles, Frontiers Research Topics unify the most influential researchers, the latest key findings and historical advances in a hot research area! Find out more on how to host your own Frontiers Research Topic or contribute to one as an author by contacting the Frontiers Editorial Office: frontiersin.org/about/contact

DEVELOPMENT AND POTENTIAL MECHANISMS OF LOW MOLECULAR WEIGHT DRUGS FOR CANCER IMMUNOTHERAPY

Topic Editors:
Yanfeng Gao, Sun Yat-sen University, China
Bin Zhang, Northwestern University, United States
Xuanming Yang, Shanghai Jiao Tong University, China

Citation: Gao, Y., Zhang, B., Yang, X., eds. (2022). Development and Potential Mechanisms of Low Molecular Weight Drugs for Cancer Immunotherapy. Lausanne: Frontiers Media SA. doi: 10.3389/978-2-88976-316-0

Table of Contents

frontiers | Frontiers in Immunology

EDITORIAL
published: 17 May 2022
doi: 10.3389/fimmu.2022.920442

Editorial: Development and Potential Mechanisms of Low Molecular Weight Drugs for Cancer Immunotherapy

Yanfeng Gao[1]*, *Xuanming Yang*[2] *and Bin Zhang*[3]

[1] School of Pharmaceutical Sciences (Shenzhen), Sun Yat-sen University, Shenzhen, China, [2] School of Life Science and Biotechnology, Shanghai Jiao Tong University, Shanghai, China, [3] Department of Medicine-Division of Hematology/Oncology, Northwestern University Feinberg School of Medicine, Chicago, IL, United States

Keywords: cancer immunotherapy, innate immunity, immune checkpoint, drug repositioning, small molecular inhibitor

Editorial on the Research Topic

Development and Potential Mechanisms of Low Molecular Weight Drugs for Cancer Immunotherapy

Cancer immunotherapy has gained great progress during the last decade. More than ten PD-1/PD-L1 antibodies were approved globally. However, the response rate in certain types of cancer is still need to be improved. On the other hand, low molecular weight therapeutics, such as proteins, peptides and small molecules, have gained more attention recently with their advantages including greater penetration, oral bioavailability, easy modification and fine control of bioavailability, meanwhile avoiding some severe immune related adverse events associated with antibodies. Therefore, they are considered as the next-generation of cancer immunotherapy candidates. However, their application and regulation role in cancer immunotherapy are largely needed to be explored.

The present Research Topic "Development and Potential Mechanisms of Low Molecular Weight Drugs for Cancer Immunotherapy" accepted twelve articles including seven research articles, four review articles and one case report. These articles covered a broad area including small molecule agents targeting immune checkpoint PD-1 and IDO, anti-PD-1 development and novel combination strategies, repositioning of vitamin C and curcumin derivates, cGAS inhibitor and bacteria to modulate the innate immunity.

Up to now, seven PD-1/PD-L1 antibody entities has been approved FDA. Toripalimab is the first PD-1 antibody approved by CFDA for the treatment of melanoma (second-line) in December, 2018. Zhang et al. described the development and clinical application of Toripalimab in China. Aside from the long-term survival benefits of Toripalimab monotherapy in Chinese melanoma patients, the combination with axitinib also exhibited an impressive clinical outcome. Meanwhile, Yang et al. reported a 58-year-old female patient with renal cell carcinoma resistant to both anti-PD-1 monotherapy and standard-dose axitinib. Interestingly, after the low dose of axitinib was given, the regulatory T cells decreased gradually with the tumor regressed. These results suggested that synergistic effects can be achieved by the combination of targeted therapy and anti-PD-1, and the treatment timing and dosage is critical for combinational efficacy. On the other hand, a series of chemotherapeutic agents are reported to induce the apoptosis and autophagy of tumor cells, which could lead to immunogenic cell death (ICD). But the high dosage and inappropriate timing would

OPEN ACCESS

Edited and reviewed by:
Catherine Sautes-Fridman, INSERM U1138 Centre de Recherche des Cordeliers (CRC), France

***Correspondence:**
Yanfeng Gao
gaoyf29@mail.sysu.edu.cn

Specialty section:
This article was submitted to Cancer Immunity and Immunotherapy, a section of the journal Frontiers in Immunology

Received: *14 April 2022*
Accepted: *28 April 2022*
Published: *17 May 2022*

Citation:
Gao Y, Yang X and Zhang B (2022) Editorial: Development and Potential Mechanisms of Low Molecular Weight Drugs for Cancer Immunotherapy. Front. Immunol. 13:920442. doi: 10.3389/fimmu.2022.920442

impair the antitumor immune response. Yuan et al. reported that a low-dose chemotherapy/autophagy enhancing regimen (CAER) could induce the death of tumor cells with higher levels of autophagy. These results further emphasized the importance of precise combination of these antitumor strategies.

Although anti-PD (PD-1/PD-L1) antibodies have made great clinical success, the therapeutic resistance and immune-related adverse events are still concerns. Moreover, the poor ability of solid tumor penetration and injection-only administration property promote the development of low molecular weight therapeutics. Wang et al. reported the discovery of a PD-1/PD-L1 inhibitor PDI-1 with antitumor activity. Sasikumar and Ramachandra summarized the small molecules targeting PD-1 for cancer immunotherapy. The structure, function and mechanism were analyzed. More importantly, the ongoing clinical trials of the small molecules and experience learned were also discussed. The development of inhibitors targeting other immune checkpoints is also thought to be helpful to improve the anti-PD therapeutic efficacy. Unfortunately, the IDO1 inhibitor epacadostat failed in phase III clinical trials. Shao et al. discovered that the IDO1 metabolite kynurenine could restrict the antitumor effects of CAR-T therapy in solid tumor. Therefore, IDO1 inhibitor was used as a combination by nanomaterial based delivery system to improve its therapeutic efficacy.

Drug repositioning comes from the idea that we can discover the novel mechanisms or indications of the approved drugs and natural products with identified toxicity. Curcumin is a well-known anticancer natural product. Wang et al. reported a novel curcumin derivative to inhibit colon cancer cells through changing the mitochondrial membrane potential and inducing endoplasmic reticulum (ER)-stress. Sohail et al. summarized the recent progress of a lipophilic analog of curcumin (dimethoxycurcumin) which maintains the anticancer potency but improves the systematic bioavailability. Similar as curcumin to regulate the production of Reactive oxygen species (ROS), vitamin C elicits antitumor activity through oxidant and epigenetic mechanisms. Kouakanou et al. summarized the recent progress of vitamin C to modulate the function of immune cells, and to improve their antitumor effects, such as adoptive cellular therapies.

Modulation of the signaling pathways of innate immune system can amplify the antitumor response or relieve the immune-related side effects, such as Toll-like receptors (TLRs) and cGAS-STING pathways. The components from bacteria have been considered as the powerful immune stimulator historically in clinic. Yang et al. discovered that the engineered anaerobic *Salmonella typhimurium* strain YB1 could initiate the phagocytosis function of macrophages and neutrophils and thus inhibit tumor growth and metastasis. Yu et al. established an intratumoral injection model by using PcrV protein from *Pseudomonas aeruginosa* and found tumor growth suppression effects. PcrV protein could activate the TLR4/MyD88 pathway and thus induce the innate immune response, such as potentiate the M1 polarization of macrophage. Chu et al. discovered a natural monoterpenoid compound perillaldehyde (PAH), derived from *Perilla frutescens*, could elicit cGAS inhibitory effects and have the potential to treat autoimmune syndrome. These studies open a window to develop novel strategies to strengthen the cancer immunotherapy or control the side effects.

Although no low molecular weight immunotherapeutic drugs have been approved up to now, more and more encouraging results have been reported from clinical trials. We believe that this Research Topic will help us to understand the development of next-generation of therapeutic agents for cancer immunotherapy in "post anti-PD era".

AUTHOR CONTRIBUTIONS

YG wrote the manuscript. XY and BZ revised the text. All authors contributed to the article and approved the submitted version.

FUNDING

This work was supported by grants from the National Natural Science Foundation of China (No. U20A20369).

Conflict of Interest: The authors declare that the research was conducted in the absence of any commercial or financial relationships that could be construed as a potential conflict of interest.

Publisher's Note: All claims expressed in this article are solely those of the authors and do not necessarily represent those of their affiliated organizations, or those of the publisher, the editors and the reviewers. Any product that may be evaluated in this article, or claim that may be made by its manufacturer, is not guaranteed or endorsed by the publisher.

frontiers in Immunology

ORIGINAL RESEARCH
published: 22 March 2021
doi: 10.3389/fimmu.2021.661357

Indoleamine 2,3-Dioxygenase 1 Inhibitor-Loaded Nanosheets Enhance CAR-T Cell Function in Esophageal Squamous Cell Carcinoma

Jingwen Shao[1,2†], *Lin Hou*[1,3†], *Jinyan Liu*[1†], *Yulin Liu*[1], *Jie Ning*[3], *Qitai Zhao*[1] *and Yi Zhang*[1,2,4,5*]

[1] Biotherapy Center, The First Affiliated Hospital of Zhengzhou University, Zhengzhou, China, [2] School of Life Sciences, Zhengzhou University, Zhengzhou, China, [3] School of Pharmacy, Zhengzhou University, Zhengzhou, China, [4] Henan Key Laboratory for Tumor Immunology and Biotherapy, Zhengzhou, China, [5] State Key Laboratory of Esophageal Cancer Prevention & Treatment, Zhengzhou University, Zhengzhou, China

OPEN ACCESS

Edited by:
Xuanming Yang,
Shanghai Jiao Tong University, China

Reviewed by:
Weidong Han,
People's Liberation Army General Hospital, China
Xiaoyan Qiu,
Peking University, China

***Correspondence:**
Yi Zhang
yizhang@zzu.edu.cn

†These authors have contributed equally to this work and share first authorship

Specialty section:
This article was submitted to Cancer Immunity and Immunotherapy, a section of the journal Frontiers in Immunology

Received: 30 January 2021
Accepted: 05 March 2021
Published: 22 March 2021

Citation:
Shao J, Hou L, Liu J, Liu Y, Ning J, Zhao Q and Zhang Y (2021) Indoleamine 2,3-Dioxygenase 1 Inhibitor-Loaded Nanosheets Enhance CAR-T Cell Function in Esophageal Squamous Cell Carcinoma. Front. Immunol. 12:661357. doi: 10.3389/fimmu.2021.661357

In chimeric antigen receptor (CAR)-T cell therapy, the role and mechanism of indoleamine 2, 3 dioxygenase 1 (IDO1) in enhancing antitumor immunity require further study. IDO1 is one of the most important immunosuppressive proteins in esophageal squamous cell carcinoma (ESCC). However, the IDO1 inhibitor, epacadostat, has failed in phase III clinical trials; its limited capacity to inhibit IDO1 expression at tumor sites was regarded as a key reason for clinical failure. In this study, we innovatively loaded the IDO1 inhibitor into hyaluronic acid-modified nanomaterial graphene oxide (HA-GO) and explored its potential efficacy in combination with CAR-T cell therapy. We found that inhibition of the antitumor effect of CAR-T cells in ESCC was dependent on the IDO1 metabolite kynurenine. Kynurenine could suppress CAR-T cell cytokine secretion and cytotoxic activity. Inhibiting IDO1 activity significantly enhanced the antitumor effect of CAR-T cells *in vitro* and *in vivo*. Our findings suggested that IDO1 inhibitor-loaded nanosheets could enhance the antitumor effect of CAR-T cells compared with free IDO1 inhibitor. Nanosheet-loading therefore provides a promising approach for improving CAR-T cell therapeutic efficacy in solid tumors.

Keywords: ESCC, combinatorial immunotherapy, IDO1, CAR-T, epacadostat, hyaluronic acid-modified nanomaterial graphene oxide

INTRODUCTION

The application of chimeric antigen receptor (CAR)-T cell therapy in cancer, following the successful application of CD19 CAR-T cells in eradicating hematologic malignancies, has re-energized cancer immunotherapy research (1, 2). Nonetheless, the solid tumor microenvironment poses many challenges for the application of CAR-T cell therapy (3). To kill solid tumor cells, CAR-T cells must traffic from the blood to solid tumor sites, and then infiltrate the stromal elements to

elicit specific cytotoxicity. Their efficacy in solid tumors is constrained by the limited infiltration of immune-cell to the tumor site, heterogeneity of tumor antigen expression, and the immunosuppressive environment (4, 5). Recent efforts have focused on combination therapy to improve CAR-T cell efficacy in solid tumors.

IDO1 mediates the metabolism of tryptophan into kynurenine (KYN), a immunosuppressive metabolite (6). This metabolic pathway creates an immunosuppressive environment in tumors and in tumor-draining lymph nodes (7). The depletion of tryptophan and accumulation of immunosuppressive tryptophan catabolites can induce T cell anergy and apoptosis (8, 9). Importantly, the IDO1 pathway serves as a negative feedback mechanism that is followed by $CD8^+$ T cell infiltration (10). Although IDO1 is induced mainly by T cell-mediated IFN-γ, IDO1 overexpression disables T cells (11, 12). IDO1 is produced principally by tumor cells, and is overexpressed in many types of human cancers. Both IDO1 expression by tumor cells and high levels of serum KYN are associated with poor prognosis in patients (13–15). Therefore, tryptophan catabolism has become an attractive target for reducing tumor progression and improving antitumor immunity in cancer therapy (16).

The lymphocyte-dependent IDO1 inhibitor (17), epacadostat (INCB024360), have entered human clinical trials over the years, but all have failed. A recent phase III ECHO-301 trial, testing the combination of epacadostat and pembrolizumab in melanoma, did not show better outcomes than pembrolizumab alone. This led to the halting of other phase III trials of IDO1 inhibitors (18). Since the phase I and phase II trials of epacadostat have shown a good clinical effect (19–21), further study of this drug should not be abandoned. Analysis of the clinical trial results indicates that the dose of epacadostat might be one of the reasons for its failure. Using higher epacadostat doses, to improve target coverage, is an option worth investigating (18, 19, 22, 23). Considering the complex tumor microenvironment in the solid tumors, the ability of the drug to reach the tumor site may be a major reason for IDO1 inhibitor failure in solid tumors; improving this may enhance clinical outcomes.

Graphene oxide (GO) has attracted attention as a promising multi-functional tool with applications in diverse fields, including biomedical engineering (24). Nano-graphene oxide (NGO), which has a large surface area for loading of aromatic drugs, has shown great potential in drug delivery (25). Hence, epacadostat can be easily loaded onto GO nanosheets. Further, many tumor cells show upregulated expression of hyaluronic acid (HA) receptors, making HA a utilized as a capping agent for tumor-specific targeted and controlled drug release (26, 27). Hyaluronic acid-modified graphene oxide (HA-GO) nanosheets have been used in other fields of cancer therapy (27), their ability to enhance CAR-T-induced cell death has not previously been studied.

Therefore, we present the first study evaluating the effects of combining CAR-T cells and IDO1 inhibitors. We combined an IDO1 inhibitor with mesothelin CAR-T cells, using epacadostat-loaded HA-GO nanosheets. This work provides a novel strategy to enhance the efficacy of CAR-T cells in solid tumors.

MATERIALS AND METHODS

Bioinformatics Analysis

Level 3 mRNA sequencing data and clinical information about esophageal cancer were downloaded from UCSC Xena (http://xena.ucsc.edu/). The Spearman correlation between IDO1 and immune-related gene expression in a wide range of solid tumors was downloaded from the cBioPortal for Cancer Genomics (https://www.cbioportal.org) and visualized using a heatmap in R, using the package "pheatmap." The correlation between IDO1 expression and overall survival in ESCC was calculated using the R packages "survival" and "survminer." The "high" and "low" IDO1-expression groups were allocated based on the IDO1 expression threshold. Immune-cell abundance was estimated using the R packages "ssGSEA" and "CIBERSORT," using the supplied cell markers. Samples with $P < 0.05$ were selected for further analysis. Spearman correlation analysis of IDO1 expression and immune-cell abundance was performed using the R package "corrplot."

Cell Lines

The human ESCC cell lines (EC109, EC1, TE1, KYSE70, KYSE150, and KYSE450), normal human esophageal epithelial cell line (HET-1A), and human embryonic kidney cell line 293T were purchased from the Chinese Academy of Sciences Cell Repertoire in Shanghai, China,. All cell lines were confirmed free of mycoplasma contamination, and were cultured in DMEM or RPMI-1640 (HyClone, Logan, UT) containing 10% FBS (Sigma-Aldrich), 100 U/mL penicillin, and 100 mg/mL streptomycin, at 37°C with 5% CO_2. EC1 cells were transduced with a retroviral vector encoding human IDO1 shRNA (EC1-shIDO1) or an empty vector (EC1-control), and with a puromycin-resistance gene. Transduced cells were single-cell cloned by limiting dilution.

T Cell Isolation and CAR-T Cell Preparation

$CD3^+$ T cells from peripheral blood mononuclear cells (PBMCs) were isolated using an autoMACS cell separation device with human CD3 MicroBeads (Miltenyi Biotec). Cells were suspended at a final concentration of 2×10^6/ml in complete RPMI-1640 medium supplemented with 10% FBS, 100 U/mL penicillin, and 100 g/mL streptomycin (28). $CD3^+$ T cells were activated using anti-CD3/CD28 conjugated magnetic beads (Invitrogen) at a bead/T cell ratio of 1:1, and then cultured with 100 IU/mL IL-2 (Beijing SL Pharmaceutical, Beijing, China). To generate mesothelin (MSLN)-specific CAR-T cells, we engineered a fusion protein encoding a fully human scFv m912 specific for MSLN (provided by D. Dimitrov), linked to the CD28/CD3ζ domain, as previously described (29).

Western Blot

Complete cell lysates were clarified by centrifugation and subjected to SDS-PAGE (using 10% polyacrylamide gels). Polyvinylidene fluoride (PVDF) membranes (Bio-Rad, Hercules, CA) were incubated after protein transfer with anti-IDO1 antibody (Adipogen, San Diego, CA), or with anti-β-actin (Cell Signaling Technology) as a loading control.

Quantitative Real-Time PCR (qPCR)

Total cellular RNA was extracted using TRIzol (Invitrogen, Carlsbad, CA). RNA quality and concentration were detected using a NanoDrop 2000 spectrophotometer (Thermo Fisher Scientific). RNA was reverse transcribed to cDNA using a PrimeScript RT reagent Kit (TaKaRa, Dalian, China). qRT-PCR was performed on a Real-Time PCR System (Agilent Stratagene, Santa Clara, CA), and the data were analyzed by comparative Ct quantification.

Flow Cytometry and Intracellular Cytokine Staining

Antibodies were purchased from BioLegend. In total, 5×10^5 cells were collected by centrifugation and were washed twice with PBS. The cells were then stained with fluorescence-conjugated antibodies for 20 min in the dark. For analysis of intracellular cytokines, some PBMCs were stimulated with brefeldin (1 3 brefeldin; BioLegend), PMA (1 mg/mL; Sigma-Aldrich), and ionomycin (1 mg/mL; Sigma-Aldrich) for 5 h. Tumor-infiltrating lymphocytes (TILs) from mouse tumors were directly harvested. TILs and stimulated cells were then stained with antibodies against CD45 and CD3 for 20 min on ice in the dark, followed by the addition of 4% formalin. After washing using permeabilization washing buffer, cells were stained with antibodies against IFN-γ, IL-2, and TNF-α for 20 min. Data were acquired on a FACSCanto II flow cytometer (BD Biosciences, Franklin Lakes, NJ).

Cytotoxicity Assay

CAR-T cells with or without KYN treatment were then cocultured with transduced cancer cells at different effector-to-target (E:T) ratios for 6 h. The tumor cells were then incubated with Annexin-V (BioLegend) for 15 min at 4°C in the dark, and propidium iodide (Sigma-Aldrich) was added before flow cytometry analysis. For the luciferase assay (30), EC1 cells and EC109 cells expressing luciferase (hereafter "luc-EC1 cells" and "luc-EC109 cells") were treated with PBS, IDO1 inhibitor, IDO1i-loaded nanosheets, and nanosheets for 2 h. Then, 1×10^4 cells per well were placed in a 96-well round-bottom microtiter plate with CAR-T cells, at E:T ratios ranging from 5:1 to 1:1, or alone. After 24 h of coculturing, the supernatant was discarded for ELISA assay. The cells were then transferred into a 96-well black assay plate (Corning 3603) within 50 μL of Dual-Luciferase Reporter Media, followed by incubation at room temperature for 10 min. Fluorescence was then measured using the Xenogen IVIS-200 Spectrum camera imaging system.

Degranulation Assay

For the degranulation assay, MSLN-CAR-T cells, or KYM-treated MSLN-CAR-T cells, were cocultured with EC1 or transduced EC1 cells for 6 h in complete medium. After stimulation, cells were washed and labeled with anti-CD8 and anti-CD107a antibodies for 20 min at 4°C.

Preparation and Characterization of HA-GO-IDO1i Nanosheets

HA-GO was synthesized according to our previous report (27). In brief, HA was first aminated (HA-NH_2) for the reaction with carboxylic acids of GO. Accordingly, HA-NH_2 was conjugated with GO in the presence of EDC and NHS at room temperature.

For INCB024360 loading, 5 mg of INCB024360 and HA-GO were dissolved in 500 μL ethanol and 3 mL water, respectively. INCB024360 was then added dropwise to the HA-GO solution, and the resulting mixture was stirred at room temperature for 12 h. Finally, the solution was dialyzed against distilled water for 24 h using a dialysis membrane (MW = 12,000 Da) to remove free drugs, and was lyophilized for further use. INCB024360 drug loading was calculated as follows:

Drug loading (%) = weight of INCB024360 in nanosheets / weight of the whole formulation × 100 %.

INCB024360 encapsulation efficiency was calculated as follows:

Encapsulation efficiency (%) = weight of INCB024360 in nanosheets / weight of INCB024360 initially provided × 100 %.

The resultant formulation of HA-GO-IDO1i was characterized by UV-Vis spectrophotometry, and observed by atomic force microscopy (AFM).

Cell Proliferation

To determine the effects of the nanosheets on the proliferation of ESCC cells, EC1 cells were seeded in a 96-well plate at a density of 2×10^4 cells/well. After incubating for 1 d, free IDO1i, HA-GO, and HA-GO-IDO1i (at the same IDO1i concentration, 50 μM) were used for treatment for 24 h, 48 h, or 72 h. Then, 10 μL CCK-8 was added to each well, and the cells were incubated for 2 h in a 37°C incubator, and absorbance (OD) was measured at 450 nm using a spectrophotometer. A blank background group, comprising wells with only DMEM medium. Each group had four replicates.

ELISA

Concentrations of IFN-γ, IL-2, and KYN (all from CUSABIO) were analyzed by ELISA, according to the manufacturers' instructions. Absorbance at 450 nm was measured on a Molecular Devices Multifilter F5 plate reader.

In Vivo Assays and Quantitative Biodistribution of Nanosheets in Organs

Female NOD-SCID mice (aged 4–6 weeks) were purchased from Beijing Vital River Laboratory Animal Technology Company. Animal care procedures and experiments were approved by the Institute Animal Care and Use Committee of the First Affiliated Hospital of Zhengzhou University (approval number 2019-41). EC1 cells were inoculated subcutaneously into the right flank of female NOD-SCID mice (4–6 weeks old). Tumor volume was estimated as length (mm) × width (mm)^2/2. When the tumors reached 200–300 mm^3, the mice were injected *via* the tail vein with 100 μL of IR783, GO-IR783, or HA-GO-IR783 (at the same IR783 concentration, 0.8 mg/kg). The mice were sacrificed 24 h after injection, and the organs were collected for imaging of IR783 fluorescence (720 nm excitation and 790 nm filter), using a Xenogen IVIS-200 Spectrum camera imaging system. Images were acquired and analyzed using Living Image version 4.4 (Caliper Life Sciences, Waltham, MA).

For further *in vivo* assays, NOD-SCID mice were injected subcutaneously with luc-EC1 cells, and developed tumor nodules ~7 d later; they were then divided randomly into groups. When the primary tumor reached ~50 mm^3, the mice were subcutaneously injected at their tail-base with 100 μL of PBS, IDO1i, or HA-GO-IDO1i (at the same IDO1i concentration, 100 μg/100 μL). Twelve hours after injection, the mice were infused with 1 × 10^7 MSLN-CAR-T cells. After 7 d, the phenotypes and cytokines of the CD3$^+$ T cells from the tumor tissues were evaluated using flow cytometry. For histopathological analysis, the major organs (liver, spleen, kidney, heart, and lung) were collected and embedded in paraffin. The sections were stained with hematoxylin and eosin (H&E).

Statistical Analysis

The results were analyzed *via* ANOVA or a one-tailed Mann–Whitney U test, using GraphPad Prism 5.0 (GraphPad Software, La Jolla, CA). The statistical significance threshold was set at $P < 0.05$.

RESULTS

IDO1 Accumulation in ESCC May Restrict the Efficiency of CAR-T Cell Therapy

We studied the correlation between IDO1 expression and the immune signature in multiple solid tumors. IDO1 expression was closely correlated with immune-related gene expression (**Figure 1A**). We therefore focused on examining the function

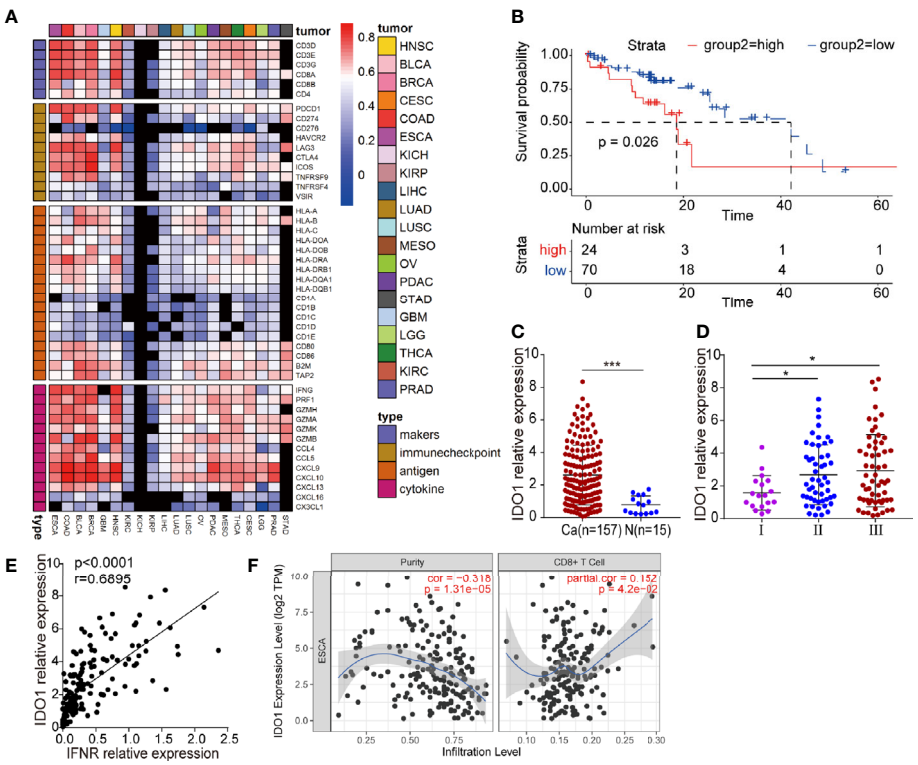

FIGURE 1 | IDO1 expression in ESCC. **(A)** Heatmap showing the correlation between IDO1 and immune-related gene expression in a wide range of solid tumors. Cells present Spearman correlation coefficients ($P < 0.05$); black cells are not significant. **(B)** Correlation between IDO1 expression and overall survival in ESCC. **(C–E)** Correlation between IDO1 expression and clinical prognosis in ESCC. **(E)** Simple linear regression, revealing an inverse relationship between IFNR and IDO1 expression, in ESCC patients from the TCGA database. **(F)** The relationship between IDO1 expression and CD8$^+$ T cell infiltration in ESCC, in the TIMER database. *$P < 0.05$, ***$P < 0.001$ (repeated-measures one-way ANOVA or Student's *t*-test).

of IDO1 in ESCC. Cancer Genome Atlas (TCGA) sequencing data were used to analyze the correlation of IDO1 expression with the pathological staging and survival of patients with ESCC. Average overall survival was lower in patients with high IDO1 expression than in those with low IDO1 expression (**Figure 1B**). IDO1 expression was significantly higher at tumor sites than in adjacent normal tissues (**Figure 1C**), and IDO1 expression was lower in samples from patients diagnosed at an earlier stage than in those diagnosed at a late stage (**Figure 1D**). This reveals that IDO1 expression was associated with an unfavorable clinical outcome in patients with ESCC, suggesting that the IDO1 pathways might serve as negative feedback mechanisms. As IDO1 is mainly induced by T-cell-mediated IFN-γ, we suggested that expression of IDO1 was significantly positively correlated with the expression of IFNR in ESCC (**Figure 1E**), as well as with the infiltration of $CD8^+$ T cell (**Figure 1F**).

We then assessed whether IDO1 expression affects CAR-T-induced cell death. First, we examined IDO1 expression in the esophageal cancer cell lines: IDO1 expression was highest in EC1, and almost absent from KYSE70 (**Supplementary Figure S1A**). As for IFN-γ induces IDO1 expression in tumor cells, IFN-γ induced IDO1 expression in all lines, except KYSE70 (**Supplementary Figure S1B**, **Figure 2A**). We therefor selected EC1 as the model for further study. The shRNA treatment reduced IDO1 mRNA expression (**Supplementary Figure S1C**, **Figure 2B**). The cytotoxicity of MSLN-CAR-T cells was inhibited in the EC1-control cells, compared with the EC1-shIDO1 cells *in vitro* (**Figure 2C**).

To evaluate the effect of tumor-derived IDO1 on MSLN-CAR-T therapy, we injected EC1-control and EC1-shIDO1 cells into NOD/SCID mice (**Figure 2D**). Seven days later, we injected human non-transduced T cells, or MSLN-CAR-T cells, intravenously. Although both the shIDO1-injected and control tumors grew rapidly after the infusion of human non-transduced T cells, only the shIDO1 tumors were inhibited by MSLN-CAR-T cells. In contrast, the control tumors were resistant to MSLN-CAR-T cell inhibition (**Figure 2E**). The expression of PD-1 and TIM3 was lower in the shIDO1-tumor-infiltrated CAR-T cells than in the control-tumor-infiltrated CAR-T cells (**Figure 2F**). There was no significant difference in CD28 production between the shIDO1 and control tumors (**Figure 2G**). The expression of IFN-g and IL-2 was higher in shIDO1-tumor-infiltrated CAR-T cells than in control-tumor-infiltrated CAR-T cells (**Figure 2H**). These results suggest that IDO1 can inhibit CAR-T cell function in ESCC.

IDO1 Inhibits Mesothelin CAR-T Cell Function *via* Its Metabolite KYN

IDO1 is most widely studied for its role in mediating the metabolism of tryptophan into KYN (31), which was documented inhibits T cell function (32, 33). But the effects of the KYN on CAR-T cells is unknown. We assessed that even at low concentrations (50 μM), KYN significantly promoted PD-1 and Tim-3 expression in CAR-T cells *in vitro* (**Figure 3A**). In contrast, KYN significantly inhibited the expression of the CAR-T cell functional cytokines, IFN-γ and IL-2 (**Figure 3B**). After treatment with KYN, the CAR-T cells were cocultured with IDO1 tumor cells for 4h. Flow cytometric analysis revealed that KYN inhibited MSLN-CAR-T cell cytotoxicity in a dose-dependent manner (**Figures 3C, D**).

Nanosheet-Based Delivery of IDO1 Inhibitor

HA-GO-IDO1i nanosheets were synthesized as described (**Figure 4A**). GO showed a broad spectral peak, at 231 nm, and HA was strongly absorbed at 200 nm. After the formation of HA-GO, the absorption red-shifted from 231 to 260 nm, whereas the characteristic peak of HA was maintained, suggesting that the reaction occurred between HA and GO. INCB024360 showed a broad peak at 290 nm. The HA-GO-IDO1i nanosheets also

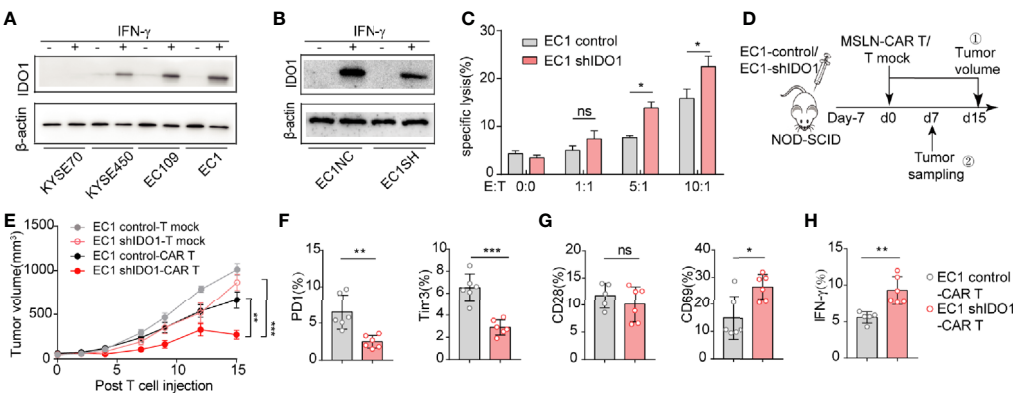

FIGURE 2 | IDO1 accumulation in ESCC may restrict the effectiveness of CAR-T cell therapy. **(A)** Western blot analysis of IDO1 and β-actin levels in ESCC cells treated with or without IFN-γ. **(B)** Western blot analysis of IDO1 and β-actin levels in EC1 cells stably expressing shControl or shIDO1. **(C)** Apoptosis was determined by Annexin-V/PI staining of shControl or shIDO1 cells after 6 h of CAR-T cell culture. **(D)** Schematic of the experiments using SCID/Beige mice, comparing the antitumor effects of MSLN-CAR-T cells in the groups treated with EC1-shControl or EC1-shIDO1 cells. **(E)** Tumor volume was evaluated for 15 d. Expression of **(F)** PD-1,TIM-3, **(G)** CD28, and CD69 in tumor-infiltrated CAR-T cells. **(H)** Proportions of IFN-γ, IL-2, and perforin in tumor-infiltrated CAR-T cells. $^*P < 0.05$, $^{**}P < 0.01$, $^{***}P < 0.001$, ns, Not statistically significant (repeated-measures one-way ANOVA or Student's *t*-test).

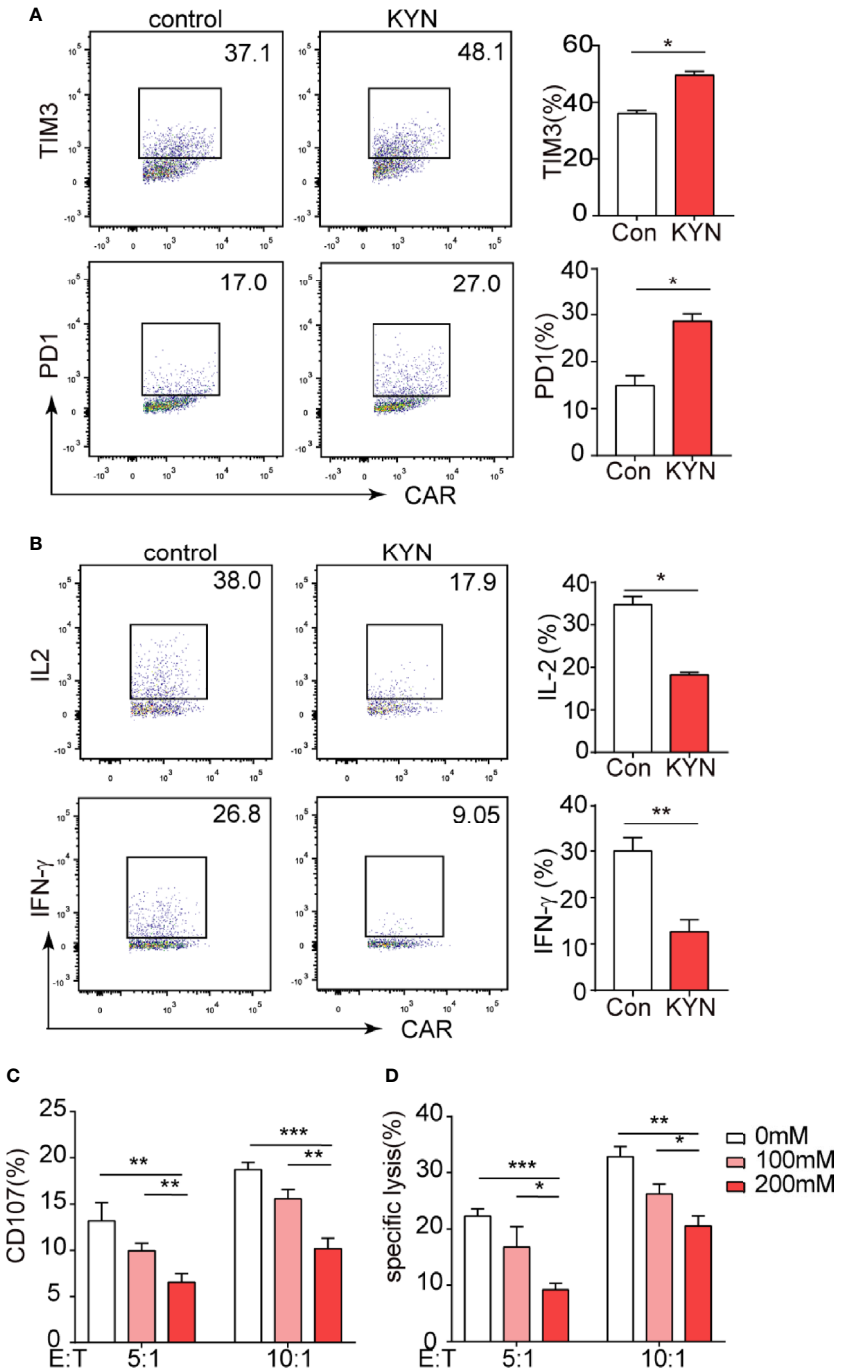

FIGURE 3 | IDO1 can inhibit MSLN-CAR-T cell function *via* its metabolite kynurenine. **(A, B)** MSLN-CAR-T cells were cultured in the absence or presence of KYN (50 μM) with IL-2 (50 U/mL) for 24 h. TIM3, PD-1, IFN-γ, and IL-2 were then detected *via* flow cytometry. **(C)** CAR-T cells treated with different concentrations of KYN were cocultured with tumor cells, to test CAR-T-mediated killing of tumor cells. Tumor cell apoptosis was determined *via* annexin V/PI staining. **(D)** CAR-T cell CD107 expression was detected *via* staining with anti-CD107a antibody or isotype control antibody, and was analyzed using flow cytometry. *$P < 0.05$, **$P < 0.01$, ***$P < 0.001$ (repeated-measures one-way ANOVA or Student's t-test).

showed a broad peak at 290 nm, suggesting that IDO1i was loaded onto HA-GO (**Figure 4B**). It is possible for IDO1i to be encapsulated into these nanosheets with drug loading as high as 40.0%, mainly *via* π-π stacking, with encapsulation efficiency of 63.2%. The morphologies of the GO, HA-GO, and HA-GO-IDO1i nanosheets were evaluated using atomic force microscopy. After HA modification, the GO particles were smaller and better dispersed. HA-GO-IDO1i remained as

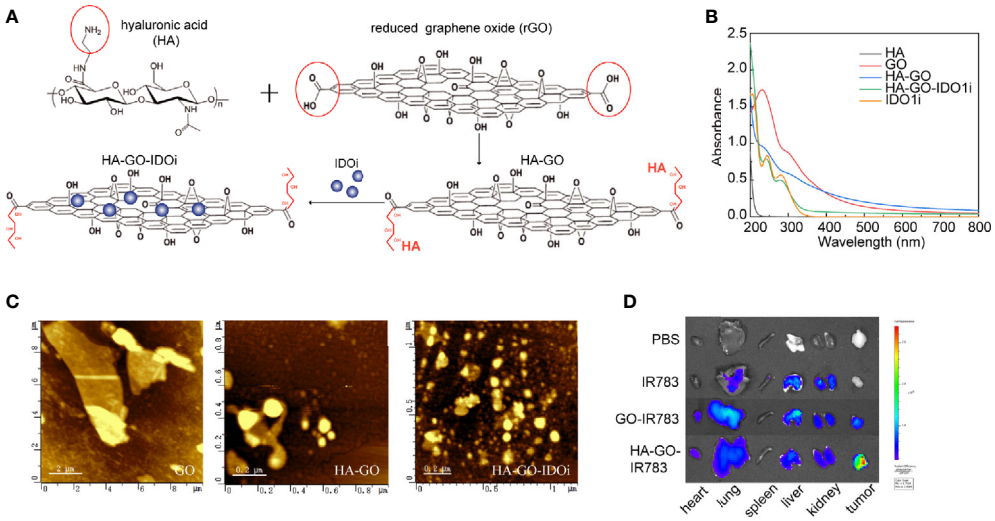

FIGURE 4 | Nanosheet-based delivery system carrying the IDO1 inhibitor. **(A)** Schematic of GO-HA-IDO1i nanosheet synthesis. **(B)** UV-Vis-NIR absorption spectra of the various GO nanosheets. **(C)** Atomic force microscopy images of the various GO nanosheets. **(D)** *Ex vivo* imaging of IR783-labeled HA-GO nanosheets in various organs at 24 h post-injection.

nanometer-sized lamellar structures (**Figure 4C**). The fluorescence images of organs from mice sacrificed 24 h post-injection demonstrated the superior tumor-targeting ability of the HA-GO nanosheets (**Figure 4D**). The nanosheets accumulated mainly in the reticuloendothelial system organs (liver, lung, and kidney), as well as in the tumors; the fluorescence was still detectable after 24 h. The fluorescence signals in the liver, lung, and kidney were lower in the HA-GO-injected mice than in the GO-injected mice. These results indicated that HA-GO nanosheets have greater tumor-targeting potential than GO alone, and can enhance the accumulation of GO nanosheets and IDO1i at the tumor site.

IDO1 Inhibitor-Loaded Nanosheets Mitigate the Inhibitory Effects of Tryptophan Metabolites

Cellular uptake of HA-GO nanosheets was evaluated *in vitro*. Epacadostat is a selective inhibitor which created to bond with the active site of IDO1 enzyme by forming a coordinate covalent bond with ferrous iron of heme (34). KYN production in cells cultured with or without the IDO1 inhibitor was measured *via* ELISA, suppression of KYN production was greatest in the HA-GO-IDO1i group (**Figure 5A**; **Supplementary Figure S2A**). ESCC cell proliferation did not differ significantly between the control group and the groups treated with non-loaded IDO1i or non-loaded nanosheets (**Figure 5B**). We next assessed the effect of the IDO1 inhibitor-loaded nanosheets on CAR-T cell cytotoxicity. After cocultured with luc-EC1 tumor cells that were firstly treated with IDO1i, CAR-T cells showed robust cytotoxicity in HA-GO-IDO1i group (**Figure 5C**, **Supplementary Figure S2B**). CD107 expression was used as another indicator of CAR-T cell cytotoxicity(**Figure 5D**, **Supplementary Figure S3C**). Further, HA-GO-IDO1i treatment significantly inhibited the expression of the CAR-T cell functional cytokines, IFN-γ and IL-2 (**Figure 5E**, **Supplementary Figure S3D**)

IDO1 Inhibitor-Loaded Nanosheets Protect CAR-T Cells Against Damage by IDO1-Positive Tumors *In Vivo*

To evaluate the effect of HA-GO-IDO1i in tumors treated with MSLN-CAR-T cells, we injected luc-EC1 cells subcutaneously, and treated mice with different forms of IDO1i (IDO1i or HA-GO-IDO1i), CAR-T cells, or with both agents. The mice were intravenously injected with the IDO1 inhibitor 24 h before the CAR-T cells were injected (**Figure 6A**). In the MSLN-CAR-T cell group, HA-GO-IDO1i treatment strongly suppressed tumor cell growth (**Figures 6B, C**); importantly, changes in tumor volume revealed that HA-GO-IDO1i was more effective than IDO1i. Further, in the MSLN-CAR-T group, tumor-infiltrated-CAR-T cell expression of PD-1 and TIM3 was lower, whereas that of IFN-γ and IL-2 was higher, in the HA-GO-IDO1i-treated group than in the IDO1i-treated group (**Figures 6D–F**). To assess whether the nanosheets were biocompatible, the major organs (heart, liver, spleen, lung, and kidney) from the four treatment groups were collected 7 d post-injection (**Supplementary Figure S3**). We did not detect any toxicity of the HA-GO-IDO1i nanosheets to mice. Therefore, using nanosheet-loaded IDO1 inhibitors is more effective than direct application of IDO1 inhibitors for promoting CAR-T cell function in treating esophageal cancer. The improvement in CAR-T cell function is mainly manifested by the increased expression of functional molecules and reduced expression of inhibitory molecules.

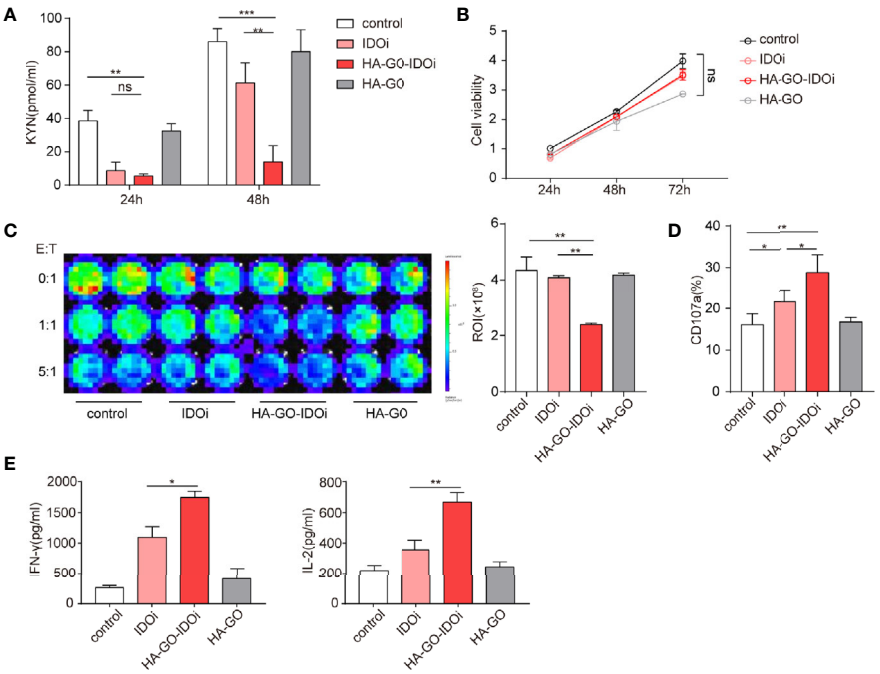

FIGURE 5 | IDO1 inhibitor-loaded nanosheets can mitigate the inhibitory effects of tryptophan metabolites. **(A)** KYN production of EC1 cells cultured with or without IDO1 inhibitor, measured *via* ELISA. **(B)** Effects of nanosheets on ESCC EC1 cell proliferation; **(C)** CAR-T-mediated killing of tumor cells. EC1 cells carrying the firefly luciferase gene were cocultured with CAR-T cells at different ratios, after 24 h of culture with or without IDO1 inhibitor. Luminescence was used to determine percentage tumor cell death. **(D)** CD107a expression of CAR-T cells cocultured with EC1 cells at different E:T ratios for 6 h. The EC1 cells were first cultured with or without IDO1 inhibitor for 24 h. **(E)** Cytokine production of CAR-T cells cocultured with EC1 cells with or without IDO1 inhibitor. IFN-γ and IL-2 secretion of CAR-T cells, detected *via* ELISA. $^{*}P < 0.05$, $^{**}P < 0.01$, $^{***}P < 0.001$, ns, Not statistically significant (repeated-measures one-way ANOVA or Student's *t*-test).

DISCUSSION

The importance of IDO1 in limiting the effectiveness of immunotherapy has recently been demonstrated. Instead of directly influencing cancer cells, IDO1 achieves this by powerfully inhibiting the immune system; in particular, it inhibits T cell activity (10, 35). In this study, high IDO1 expression was associated with immune infiltration and poor survival in patients with ESCC. This suggests that the IDO1 pathway might serve as an important negative feedback mechanism. Considering its immunosuppressive activity, targeting IDO1 might benefit patients with a preexisting T cell-inflamed tumor microenvironment. CAR-T cell treatment of hematologic tumors has recently been shown to be highly effective. This has inspired efforts to apply it to solid tumors in the clinic. However, CAR-T cells have shown limited clinical efficacy for treating solid tumors. The immunosuppressive molecules in the microenvironment, including IDO1, present major hurdles for CAR-T therapy in solid tumors. Thus, blocking IDO1 may enhance CAR-T cell cytotoxicity toward solid tumors.

IDO1 has been found to inhibit CAR-T therapy through the action of tryptophan metabolites in hematologic (36) and solid tumors (37). However, the effect of IDO1 on CAR-T therapy in ESCC patients has not previously been studied. In this study, we investigated whether IDO1 expression by ESCC can inhibit the antitumor effect of CAR-T cells *via* its metabolite KYN. Consistent with a previous report (38), KYN inhibited the cytokine secretion and cytotoxic activity of CAR-T cells, suggesting that production of tryptophan metabolites by IDO1 may at least partially underlie resistance to CAR-T therapy in IDO1-positive tumor cells. Since the immunosuppressive function of IDO1 in tumors is well established; research has therefore focused on inhibitors to block its immunoregulatory function (39). Epacadostat, a hydroxyamidine small-molecule inhibitor, potently suppresses tryptophan metabolism, and has been regarded as a potent adjuvant. However, the first phase 3 trial to evaluate its efficacy in combination with pembrolizumab in advanced melanoma showed no evidence that epacadostat improved outcomes (40).

Multiple hypotheses have been improved to explain the discrepancy between the early phase clinical trial success of epacadostat and the failure of the phase 3 (ECHO-301) trial; these include differences between the treatment populations, inappropriately low epacadostat dosing, and incomplete suppression of intratumoral KYN. The phase 3 trial used 100 mg epacadostat, based on the phase I trial, despite higher doses being tolerated and no maximum-tolerated dose being established (41). This dose was chosen as it was deemed that maximal inhibition of IDO1 activity occurred at doses ≥ 100 mg,

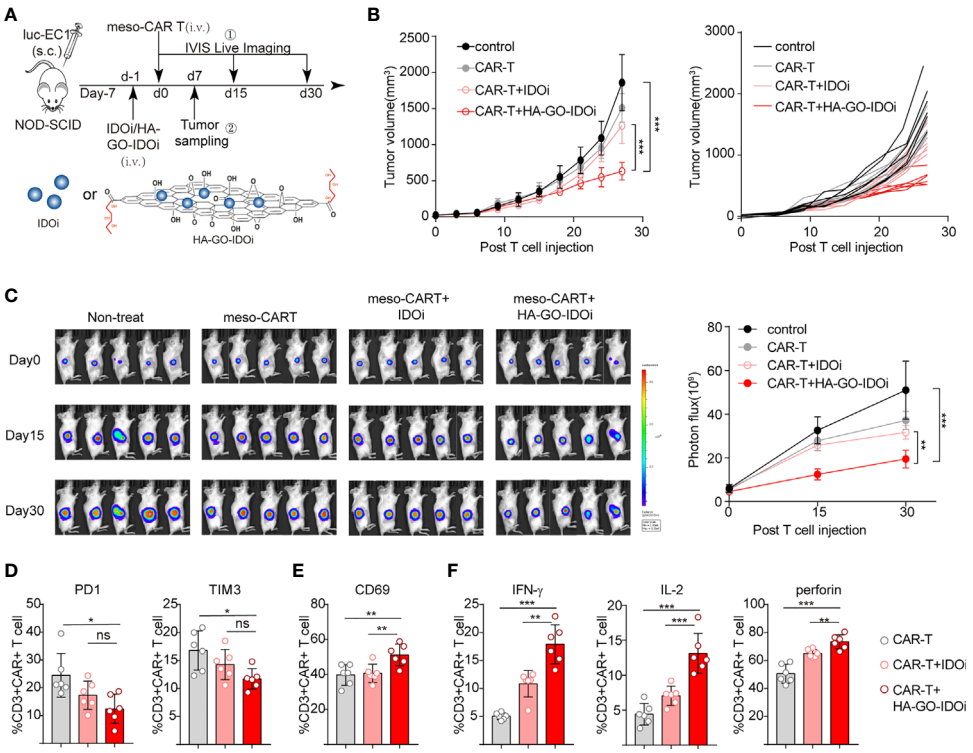

FIGURE 6 | IDO1 inhibitor-loaded nanosheets protect CAR-T cells against the deleterious effects of IDO1-positive tumors *in vivo*. **(A)** Schematic of the experiments using NOD-SCID mice, comparing the antitumor effects of IDO1 inhibitor (IDO1i or HA-GO-IDO1i), MSLN-CAR-T cells, or the combination of both, on IDO1-positive tumors (originating from luc-EC1 cells). **(B)** Tumor volume was evaluated for 30 d. **(C)** Longitudinal measurements of luc-EC1 cell bioluminescence in mice. Expression of **(D)** PD-1, TIM-3, and **(E)** CD69 in tumor-infiltrated CAR-T cells. **(F)** Expression of IFN-γ, IL-2, and perforin in tumor-infiltrated CAR-T cells. $^{*}P < 0.05$, $^{**}P < 0.01$, $^{***}P < 0.001$, ns, Not statistically significant (repeated-measures one-way ANOVA or Student's *t*-test).

with no further reduction in peripheral blood KYN at higher doses. Notably, a simultaneous early phase study used 300 mg of epacadostat; the reported models imply a higher likelihood of IDO1 inhibition at this dose (19, 22). These reports suggest that the current dose of epacadostat was not sufficient to reverse the immunosuppressive environment by blocking IDO1. The optimal dose of epacadostat is being studied in ongoing clinical trials.

In order to deliver IDO1 inhibitors to tumors more efficiently, a novel strategy to enhance the upload of epacadostat into tumor sites is required. Given their capacity for controlled and targeted drug release to specific cells, nanomaterials are critical in tumor therapy (42–45). Lu et al. (46)have revealed that INCB24360 delivery *via* a chlorin-based metal-organic framework achieved positive outcomes using combination photodynamic therapy and IDO1 inhibition. In this study, we loaded an IDO1 inhibitor onto an HA-GO nanomaterial; this material delivers the IDO1 inhibitor into cancer cells *via* receptor-mediated endocytosis pathways (27). Our findings demonstrate that a single treatment with HA-GO-IDO1i downregulates KYN production in esophageal cancer cells—the nanomaterial-based delivery system was able to alter the concentration of KYN and tryptophan in the tumor microenvironment before CAR-T infusion. The HA-GO-loaded IDO1 inhibitor reversed IDO1-induced inhibition of CAR-T therapy more effectively than direct application of free IDO1, both *in vitro* and *in vivo*.

In summary, we have demonstrated that IDO1 expression by esophageal tumors inhibits MSLN-CAR-T activity; blocking IDO1 activity reverses the inhibition of CAR-T-induced cell death. Mechanistically, we investigated whether the immunosuppressive function of IDO1 occurs *via* suppression of CAR-T cell cytokine secretion and cytotoxic activity by the IDO1 metabolite KYN. Importantly, the IDO1 inhibitor-loaded nanosheets exhibited greater ability to restore the function of mesothelin CAR-T cells than direct application of free IDO1 inhibitor, both *in vitro* and *in vivo*. These findings demonstrate the importance of blocking IDO1 in restoring the ability of CAR-T cell to kill cancer cells. Further, this study reveals that applying IDO1 inhibitor-loaded nanosheets to treat solid tumors enhances drug influx at the tumor sites. These findings provide a new strategy to enhance the antitumor effect of CAR-T cell therapy, and a promising approach for the treatment of solid tumors.

DATA AVAILABILITY STATEMENT

Publicly available datasets were analyzed in this study. This data can be found here: http://xena.ucsc.edu/.

ETHICS STATEMENT

The animal study was reviewed and approved by Ethics Committee of the First Affiliated Hospital of Zhengzhou University.

AUTHOR CONTRIBUTIONS

JS, LH, JL, and YZ designed this work and analyzed the data. JS, JL, JN, YL, and QZ helped with, or performed, the experiments and analyses. LH and JN helped to provide the nanosheets. JL, QZ, and LH helped in revising the manuscript. JS and YZ wrote the manuscript. All authors contributed to the article and approved the submitted version.

FUNDING

This study was supported by the National Natural Science Foundation of China [Grant No. 82001659], the Program of the Major Research Plan of the National Natural Science Foundation of China [Grant No. 91942314], and the National Science and Technology Major Project of China [Grant No. 2020ZX09201-009].

SUPPLEMENTARY MATERIAL

The Supplementary Material for this article can be found online at: https://www.frontiersin.org/articles/10.3389/fimmu.2021.661357/full#supplementary-material

REFERENCES

1. Newick K, O'Brien S, Moon E, Albelda SM. CAR T Cell Therapy for Solid Tumors. *Annu Rev Med* (2017) 68:139–52. doi: 10.1146/annurev-med-062315-120245
2. Shen C, Zhang Z, Zhang Y. Chimeric Antigen Receptor T Cell Exhaustion during Treatment for Hematological Malignancies. *BioMed Res Int* (2020) 2020:8765028. doi: 10.1155/2020/8765028
3. Zhao L, Cao YJ. Engineered T Cell Therapy for Cancer in the Clinic. *Front Immunol* (2019) 10:2250. doi: 10.3389/fimmu.2019.02250
4. Lesch S, Benmebarek MR, Cadilha BL, Stoiber S, Subklewe M, Endres S, et al. Determinants of response and resistance to CAR T cell therapy. *Semin Cancer Biol* (2020) 65:80–90. doi: 10.1016/j.semcancer.2019.11.004
5. Tian Y, Li Y, Shao Y, Zhang Y. Gene modification strategies for next-generation CAR T cells against solid cancers. *J Hematol Oncol* (2020) 13 (1):54. doi: 10.1186/s13045-020-00890-6
6. Hirata F, Ohnishi T, Hayaishi O. Indoleamine 2,3-dioxygenase. Characterization and properties of enzyme. O2- complex. *J Biol Chem* (1977) 252(13):4637–42. doi: 10.1016/S0021-9258(17)40208-0
7. Hornyák L, Dobos N, Koncz G, Karányi Z, Páll D, Szabó Z, et al. The Role of Indoleamine-2,3-Dioxygenase in Cancer Development, Diagnostics, and Therapy. *Front Immunol* (2018) 9:151. doi: 10.3389/fimmu.2018.00151
8. Brochez L, Chevolet I, Kruse V. The rationale of indoleamine 2,3-dioxygenase inhibition for cancer therapy. *Eur J Cancer* (2017) 76:167–82. doi: 10.1016/j.ejca.2017.01.011
9. Platten M, Wick W, Van den Eynde BJ. Tryptophan catabolism in cancer: beyond IDO and tryptophan depletion. *Cancer Res* (2012) 72(21):5435–40. doi: 10.1158/0008-5472.Can-12-0569
10. Spranger S, Spaapen RM, Zha Y, Williams J, Meng Y, Ha TT, et al. Up-regulation of PD-L1, IDO, and T(regs) in the melanoma tumor microenvironment is driven by CD8(+) T cells. *Sci Trans Med* (2013) 5 (200):200ra116. doi: 10.1126/scitranslmed.3006504
11. Zhai L, Ladomersky E, Lauing KL, Wu M, Genet M, Gritsina G, et al. Infiltrating T Cells Increase IDO1 Expression in Glioblastoma and Contribute to Decreased Patient Survival. *Clin Cancer Res* (2017) 23 (21):6650–60. doi: 10.1158/1078-0432.Ccr-17-0120
12. Noonepalle SK, Gu F, Lee EJ, Choi JH, Han Q, Kim J, et al. Promoter Methylation Modulates Indoleamine 2,3-Dioxygenase 1 Induction by Activated T Cells in Human Breast Cancers. *Cancer Immunol Res* (2017) 5 (4):330–44. doi: 10.1158/2326-6066.Cir-16-0182
13. Kiyozumi Y, Baba Y, Okadome K, Yagi T, Ishimoto T, Iwatsuki M, et al. IDO1 Expression Is Associated With Immune Tolerance and Poor Prognosis in Patients With Surgically Resected Esophageal Cancer. *Ann Surg* (2019) 269 (6):1101–8. doi: 10.1097/sla.0000000000002754
14. Takada K, Kohashi K, Shimokawa M, Haro A, Osoegawa A, Tagawa T, et al. Co-expression of IDO1 and PD-L1 in lung squamous cell carcinoma: Potential targets of novel combination therapy. *Lung Cancer* (2019) 128:26–32. doi: 10.1016/j.lungcan.2018.12.008
15. Lecerf C, Kamal M, Vacher S, Chemlali W, Schnitzler A, Morel C, et al. Immune gene expression in head and neck squamous cell carcinoma patients. *Eur J Cancer* (2019) 121:210–23. doi: 10.1016/j.ejca.2019.08.028
16. Triplett TA, Garrison KC, Marshall N, Donkor M, Blazeck J, Lamb C, et al. Reversal of indoleamine 2,3-dioxygenase-mediated cancer immune suppression by systemic kynurenine depletion with a therapeutic enzyme. *Nat Biotechnol* (2018) 36(8):758–64. doi: 10.1038/nbt.4180
17. Liu X, Shin N, Koblish HK, Yang G, Wang Q, Wang K, et al. Selective inhibition of IDO1 effectively regulates mediators of antitumor immunity. *Blood* (2010) 115(17):3520–30. doi: 10.1182/blood-2009-09-246124
18. Long GV, Dummer R, Hamid O, Gajewski TF, Caglevic C, Dalle S, et al. Epacadostat plus pembrolizumab versus placebo plus pembrolizumab in patients with unresectable or metastatic melanoma (ECHO-301/KEYNOTE-252): a phase 3, randomised, double-blind study. *Lancet Oncol* (2019) 20(8):1083–97. doi: 10.1016/s1470-2045(19)30274-8
19. Komiya T, Huang CH. Updates in the Clinical Development of Epacadostat and Other Indoleamine 2,3-Dioxygenase 1 Inhibitors (IDO1) for Human Cancers. *Front Oncol* (2018) 8:423. doi: 10.3389/fonc.2018.00423
20. Mitchell TC, Hamid O, Smith DC, Bauer TM, Wasser JS, Olszanski AJ, et al. Epacadostat Plus Pembrolizumab in Patients With Advanced Solid Tumors: Phase I Results From a Multicenter, Open-Label Phase I/II Trial (ECHO-202/KEYNOTE-037). *J Clin Oncol* (2018) 36(32):3223–30. doi: 10.1200/jco.2018.78.9602
21. Epacadostat Shows Value in Two SCCHN Trials. *Cancer Discovery* (2017) 7 (9):Of2. doi: 10.1158/2159-8290.Cd-nb2017-100
22. Muller AJ, Manfredi MG, Zakharia Y, Prendergast GC. Inhibiting IDO pathways to treat cancer: lessons from the ECHO-301 trial and beyond. *Semin Immunopathol* (2019) 41(1):41–8. doi: 10.1007/s00281-018-0702-0
23. Labadie BW, Bao R, Luke JJ. Reimagining IDO Pathway Inhibition in Cancer Immunotherapy *via* Downstream Focus on the Tryptophan-Kynurenine-Aryl Hydrocarbon Axis. *Clin Cancer Res* (2019) 25(5):1462–71. doi: 10.1158/1078-0432.Ccr-18-2882
24. Karki N, Tiwari H, Tewari C, Rana A, Pandey N, Basak S, et al. Functionalized graphene oxide as a vehicle for targeted drug delivery and bioimaging applications. *J Mater Chem B* (2020) 8(36):8116–48. doi: 10.1039/d0tb01149e
25. Gonçalves G, Vila M, Portolés MT, Vallet-Regi M, Gracio J, Marques PA. Nano-graphene oxide: a potential multifunctional platform for cancer therapy. *Adv Healthcare Mater* (2013) 2(8):1072–90. doi: 10.1002/adhm.201300023

26. Brown TJ. The development of hyaluronan as a drug transporter and excipient for chemotherapeutic drugs. *Curr Pharm Biotechnol* (2008) 9(4):253–60. doi: 10.2174/138920108785161514
27. Hou L, Feng Q, Wang Y, Yang X, Ren J, Shi Y, et al. Multifunctional hyaluronic acid modified graphene oxide loaded with mitoxantrone for overcoming drug resistance in cancer. *Nanotechnology* (2016) 27(1):15701. doi: 10.1088/0957-4484/27/1/015701
28. Zhang Z, Li F, Tian Y, Cao L, Gao Q, Zhang C, et al. Metformin Enhances the Antitumor Activity of CD8(+) T Lymphocytes via the AMPK-miR-107-Eomes-PD-1 Pathway. *J Immunol* (2020) 204(9):2575–88. doi: 10.4049/jimmunol.1901213
29. Feng Y, Xiao X, Zhu Z, Streaker E, Ho M, Pastan I, et al. A novel human monoclonal antibody that binds with high affinity to mesothelin-expressing cells and kills them by antibody-dependent cell-mediated cytotoxicity. *Mol Cancer Ther* (2009) 8(5):1113–8. doi: 10.1158/1535-7163.Mct-08-0945
30. He P, Tan Z, Wei Z, Wan CL, Yang SS. Co-expressing LRP6 With Anti-CD19 CAR-T Cells for Improved Therapeutic Effect Against B-ALL. *Front Oncol* (2020) 10:1346. doi: 10.3389/fonc.2020.01346
31. Greene LI, Bruno TC, Christenson JL, D'Alessandro A, Culp-Hill R, Torkko K, et al. A Role for Tryptophan-2,3-dioxygenase in CD8 T-cell Suppression and Evidence of Tryptophan Catabolism in Breast Cancer Patient Plasma. *Mol Cancer Res* (2019) 17(1):131–9. doi: 10.1158/1541-7786.Mcr-18-0362
32. Sledzińska A, Hemmers S, Mair F, Gorka O, Ruland J, Fairbairn L, et al. TGF-β signalling is required for $CD4^+$ T cell homeostasis but dispensable for regulatory T cell function. *PloS Biol* (2013) 11(10):e1001674. doi: 10.1371/journal.pbio.1001674
33. Liu Y, Liang X, Dong W, Fang Y, Lv J, Zhang T, et al. Tumor-Repopulating Cells Induce PD-1 Expression in CD8(+) T Cells by Transferring Kynurenine and AhR Activation. *Cancer Cell* (2018) 33(3):480–94.e7. doi: 10.1016/j.ccell.2018.02.005
34. Yue EW, Sparks R, Polam P, Modi D, Douty B, Wayland B, et al. INCB24360 (Epacadostat), a Highly Potent and Selective Indoleamine-2,3-dioxygenase 1 (IDO1) Inhibitor for Immuno-oncology. *ACS Med Chem Lett* (2017) 8 (5):486–91. doi: 10.1021/acsmedchemlett.6b00391
35. Zhang Z, Liu S, Zhang B, Qiao L, Zhang Y, Zhang Y. T Cell Dysfunction and Exhaustion in Cancer. *Front Cell Dev Biol* (2020) 8:17. doi: 10.3389/fcell.2020.00017
36. Ninomiya S, Narala N, Huye L, Yagyu S, Savoldo B, Dotti G, et al. Tumor indoleamine 2,3-dioxygenase (IDO) inhibits CD19-CAR T cells and is downregulated by lymphodepleting drugs. *Blood* (2015) 125(25):3905–16. doi: 10.1182/blood-2015-01-621474
37. O'Rourke DM, Nasrallah MP, Desai A, Melenhorst JJ, Mansfield K, Morrissette JJD, et al. A single dose of peripherally infused EGFRvIII-directed CAR T cells mediates antigen loss and induces adaptive resistance in patients with recurrent glioblastoma. *Sci Trans Med* (2017) 9(399). doi: 10.1126/scitranslmed.aaa0984
38. Chen Z, Dai Y, Huang X, Chen K, Gao Y, Li N, et al. Combined Metabolomic Analysis of Plasma and Tissue Reveals a Prognostic Risk Score System and Metabolic Dysregulation in Esophageal Squamous Cell Carcinoma. *Front Oncol* (2020) 10:1545. doi: 10.3389/fonc.2020.01545
39. Günther J, Däbritz J, Wirthgen E. Limitations and Off-Target Effects of Tryptophan-Related IDO Inhibitors in Cancer Treatment. *Front Immunol* (2019) 10:1801. doi: 10.3389/fimmu.2019.01801
40. Koblish HK, Hansbury MJ, Bowman KJ, Yang G, Neilan CL, Haley PJ, et al. Hydroxyamidine inhibitors of indoleamine-2,3-dioxygenase potently suppress systemic tryptophan catabolism and the growth of IDO-expressing tumors. *Mol Cancer Ther* (2010) 9(2):489–98. doi: 10.1158/1535-7163.Mct-09-0628
41. Beatty G, O'Dwyer P, Clark J, Shi J, Bowman K, Scherle P, et al. First-in-Human Phase I Study of the Oral Inhibitor of Indoleamine 2,3-Dioxygenase-1 Epacadostat (INCB024360) in Patients with Advanced Solid Malignancies. *Clin Cancer Res* (2017) 23(13):3269–76. doi: 10.1158/1078-0432.Ccr-16-2272
42. Liu Z, Jiang W, Nam J, Moon JJ, Kim BYS. Immunomodulating Nanomedicine for Cancer Therapy. *Nano Lett* (2018) 18(11):6655–9. doi: 10.1021/acs.nanolett.8b02340
43. Chaturvedi VK, Singh A, Singh VK, Singh MP. Cancer Nanotechnology: A New Revolution for Cancer Diagnosis and Therapy. *Curr Drug Metab* (2019) 20(6):416–29. doi: 10.2174/1389200219666180918111528
44. Moy AJ, Tunnell JW. Combinatorial immunotherapy and nanoparticle mediated hyperthermia. *Adv Drug Delivery Rev* (2017) 114:175–83. doi: 10.1016/j.addr.2017.06.008
45. Wu H, Huang W, Zhou X, Min Y. Immunological Effects of Aggregation-Induced Emission Materials. *Front Immunol* (2020) 11:575816. doi: 10.3389/fimmu.2020.575816
46. Lu K, He C, Guo N, Chan C, Ni K, Weichselbaum RR, et al. Chlorin-Based Nanoscale Metal-Organic Framework Systemically Rejects Colorectal Cancers via Synergistic Photodynamic Therapy and Checkpoint Blockade Immunotherapy. *J Am Chem Soc* (2016) 138(38):12502–10. doi: 10.1021/jacs.6b06663

Conflict of Interest: The authors declare that the research was conducted in the absence of any commercial or financial relationships that could be construed as a potential conflict of interest.

frontiers in Oncology

ORIGINAL RESEARCH
published: 30 March 2021
doi: 10.3389/fonc.2021.658254

A Local and Low-Dose Chemotherapy/Autophagy-Enhancing Regimen Treatment Markedly Inhibited the Growth of Established Solid Tumors Through a Systemic Antitumor Immune Response

Jia Yuan[†], *Xianlin Yuan*[†], *Kunlong Wu*[‡], *Junxia Gao*[‡] *and Liangping Li*[*]

Institute of Clinical Oncology, Research Center of Cancer Diagnosis and Therapy, and Department of Clinical Oncology, The First Affiliated Hospital of Jinan University, Guangzhou, China

Chemotherapy is one of the main options for the treatment of a variety of malignant tumors. However, the severe side effects resulting from the killing of normal proliferating cells limit the application of cancer-targeting chemotherapeutic drugs. To improve the efficacy of classic systemic chemotherapy, the local delivery of high-dose chemotherapeutic drugs was developed as a method to enhance local drug concentrations and minimize systemic toxicity. Studies have demonstrated that chemotherapy is often accompanied by cancer-associated immunogenic cell death (ICD) and that autophagy is involved in the induction of ICD. To improve the efficacy of local cancer chemotherapy, we hypothesized that the local delivery of chemotherapeutic plus autophagy-enhancing agents would enhance the promotive effects of ICD on the antitumor immune response. Here, we report that a low-dose chemotherapy/autophagy enhancing regimen (CAER) not only resulted in the increased death of B16F10 and 4T1 tumor cells, but also induced higher levels of autophagy *in vitro*. Importantly, the local delivery of the CARE drugs significantly inhibited tumor growth in B16F10 and 4T1 tumor-bearing mice. Systemic antitumor T-cell immunity was observed *in vivo*, including neoantigen-specific T-cell responses. Furthermore, bioinformatic analysis of human breast cancer and melanoma tissues showed that autophagy-associated gene expression was upregulated in tumor samples. Increased autophagy and immune cell infiltration in tumor tissues were positively correlated with good prognosis of tumor patients. This work highlights a new approach to improve the effects of local chemotherapy and enhance systemic antitumor immunity.

Keywords: local chemotherapy, ICD, autophagy, neoantigens, immunotherapy

OPEN ACCESS

Edited by:
Xuanming Yang,
Shanghai Jiao Tong University, China

Reviewed by:
Liufu Deng,
Shanghai Jiao Tong University, China
Yang-xin Fu,
University of Texas Southwestern Medical Center, United States

***Correspondence:**
Liangping Li
liangping_li@jnu.edu.cn;
liangping_li@yahoo.com

[†]*These authors have contributed equally to this work and share first authorship*

[‡]*These authors have contributed equally to this work and share last authorship*

Specialty section:
This article was submitted to Cancer Immunity and Immunotherapy, a section of the journal Frontiers in Oncology

Received: *25 January 2021*
Accepted: *12 March 2021*
Published: *30 March 2021*

Citation:
Yuan J, Yuan X, Wu K, Gao J and Li L (2021) A Local and Low-Dose Chemotherapy/Autophagy-Enhancing Regimen Treatment Markedly Inhibited the Growth of Established Solid Tumors Through a Systemic Antitumor Immune Response. Front. Oncol. 11:658254. doi: 10.3389/fonc.2021.658254

INTRODUCTION

After more than 100 years of development, chemotherapy has become the mainstay of treatment for a variety of cancers. Chemotherapeutic agents can inhibit cancer cell proliferation and survival through a variety of mechanisms, including by affecting the chemical structure of DNA, interrupting nucleic acid synthesis and transcription, and interfering with mitotic tubulin synthesis (1). To improve treatment efficiency, high-dose systemic chemotherapy was developed as a method to treat hematopoietic and solid tumors. However, high-dose chemotherapy also kills normal proliferating cells, thereby unavoidably leading to severe side effects, such as severe bone marrow failure and immune suppression (2, 3). Multiple infections secondary to immunosuppression resulting from routine systemic chemotherapy can reduce the prognosis and survival of cancer patients. In high-dose chemotherapy regimens, blood progenitor cell transplantation was used to reduce bone marrow- and immune-associated toxicities (4, 5). These observations highlight the need to enhance the effects of chemotherapy and reduce its side effects.

To reduce chemotherapy-related cytotoxicity, local delivery of chemotherapeutic drugs was proposed as a method to maximize local drug concentrations in the immediate tumor environment while also minimizing systemic exposure and nontarget organ toxicity (6, 7). In models of lymph node metastasis, the antitumor efficacy of local chemotherapy for regional lymph node metastasis was reported to be better than that of systemic chemotherapy, and the treatment was deemed to be safe (8). The development of interventional therapy provides a new approach for the local delivery of chemotherapeutic agents. For instance, local intra-arterial chemotherapy with a high-dose cyclophosphamide+epirubicin+5-fluorouracil (CEF) regimen for triple-negative breast cancer reduced treatment duration and increased the lesion remission rate when compared with that of the control group (routine neoadjuvant chemotherapy with CEF), while showing similar toxicity (9). Although this study highlighted the efficacy of local chemotherapy, it also revealed that chemotherapeutic agents exert a significant toxic effect, even with local application.

To reduce the side effects of regional cancer therapy, new methods must be developed that allow the synergistic eradication of cancer cells by different agents. There is increasing evidence that chemotherapy not only directly kills tumor cells, but also indirectly attacks them by activating the immune system (10). Several studies have demonstrated that chemotherapeutic agents such as anthracycline, platinum, and taxane, in addition to inducing cancer cell apoptosis, can also promote the release of tumor antigens, which further activate immune cells, and finally generate a systemic anticancer immune response (11, 12). This process is known as immunogenic cell death (ICD).

Chemotherapy-induced ICD is reported to be closely associated with autophagy (13). Autophagy is characterized by the encapsulation, processing, and degradation of various cytoplasmic components. It not only maintains cellular homeostasis in conditions of internal and external stress, but also shapes the immune response to cancer (14–16). The level of autophagy in cancer cells affects the release of several cytokines and danger signals that instruct immune effectors to induce immune responses (17–19). When autophagy is hyperactivated, tumor-derived cytoplasmic components are made available for lysosomal hydrolysis, thereby promoting antigen processing in dying tumor cells (20, 21). Additionally, highly activated autophagy can increase the secretion of adenosine triphosphate (ATP) by dying tumor cells, and ATP acts as a vital signal for the activation of dendritic cells (DCs) and cytotoxic T cells and their recruitment into the local tumor microenvironment (22, 23).

Rapamycin, one of the most commonly used autophagy-inducing agents, can promote cancer cell autophagy *via* inhibition of the mTOR pathway, thereby inhibiting tumor growth (24, 25). However, systemic rapamycin administration can also suppress the immune system by blocking mTOR on T cells, leading to reduced interleukin (IL-2) production and inhibition of T-cell proliferation, which impair antitumor immune responses (26, 27).

These observations led us to speculate that local delivery of chemotherapeutic and autophagy-enhancing drugs (chemotherapy/autophagy-enhancing regimen, CAER) might enhance the efficacy of local cancer treatment. Here, we report that a low-dose local CAER could activate autophagy and enhance autophagy-associated death *in vitro*. The local delivery of low-dose CAER drugs not only efficiently inhibit the growth of the treated malignant melanoma- and breast cancer-derived tumors, but also of the contralateral nontreated ones. Further analysis showed that the immune system was activated to target the cancer cells. This research provides a new therapeutic approach for the treatment of cancer *via* the local delivery of CAER drugs with systemic antitumor T-cell responses and reduced side effects.

MATERIALS AND METHODS

Reagents

Rapamycin (Rap) (Sigma, USA) was dissolved in DMSO and then diluted with RPMI medium. Chemotherapeutic drugs paclitaxel (PTX) and adriamycin (ADM) were purchased from the First Affiliated Hospital of Jinan University (Guangzhou, China). PMA/Ionomycin (P/I) were purchased from Sigma, USA. The peptides for immunogenic B16F10 and 4T1 mutations were synthesized by Sangon Biotech (Shanghai, China) accordingly previous publication (**Figure S3A**). Propidium iodide (PI) was purchased from BioLegend, USA. LC3B antibody was from Cell Signaling, USA. Anti-CD3, anti-CD4, anti-CD8, and anti-FOXP3 antibodies were purchased from Abcam, Cambridge, UK. Antibodies used for flow cytometry assay were as follows: anti-CD16/32 mAb (BD Biosciences, USA), anti-CD3-PEcy5, anti-CD4-FITC, anti-CD8-FITC, anti-IFN-γ-APC, anti-TNF-α-PE, and anti-FOXP3-PE (BioLegend, USA).

Traditional (2D) and 3D Cell Culture and *In Vitro* Cell Proliferation Assays

Colony Formation Assay

Cells were seeded in 12-well plates (300 cells/well) and cultured under normal *in vitro* culture conditions (2D). After five days of incubation, B16F10 and 4T1 cells were either vehicle-treated or treated with low-dose of single chemotherapy drugs (2.5 μg/mL PTX or 0.05 μg/mL ADM) for two days, or with combination of two drugs as following: the same low-dose of chemotherapeutic drugs for 12 h, followed by treatment with 0.014 μg/mL rapamycin (15 nM) for another 36 h. The medium was changed every three to four days. After two weeks, cells were stained with 0.1% crystal violet in methanol for 15 min, and the number of colonies (containing 50 or more cells) was visualized and quantified by light microscopy (CKX31, OLYMPUS, Japan).

Spheroid Formation and Autophagic Cell Death Staining Assay

A total of 600 B16F10 and 4T1 cells/well were seeded in ultra-low attachment 96-well plates in RPMI 1640/DMEM to establish spheroid cultures (3D). After three days, the cells were treated with vehicle or chemotherapeutic drugs (5 μg/mL PTX or 0.1 μg/mL ADM) for 6–8 h followed by treatment with 0.023 μg/mL rapamycin (25 nM) for another 16–24 h. Finally, the diameter of each spheroid was measured after one week. The spheroids were stained with PI to determine the level of autophagic cell death.

Autophagy Assays

Monodansylcadaverine (MDC) Staining for Autophagy

The entire dynamic autophagic process (autophagic flux) can be measured using the autofluorescent dye MDC, which specifically marks autophagic vacuoles. In brief, 2000 cells of B16F10 or 4T1 were seeded in a 96-well plate in RPMI 1640/DMEM culture medium and incubated for two days at 37°C. Then, the cells were treated with vehicle or a low dose of chemotherapeutic drugs (5 μg/mL PTX or 0.1 μg/mL ADM) for 6–8 h, followed by treatment with rapamycin (25 nM) for another 16–24 h. The cells were then stained with MDC (Solarbio, USA) and observed using fluorescence microscopy.

LC3 Immunofluorescence and WB Assay

To measure the level of autophagy, cells were treated as described in section 2.3.1. The cells were then fixed in cold absolute methanol and blocked with 1% BSA in PBST buffer (PBS with 0.1% Tween 20) for 1 h and incubated with the primary antibody against LC3B overnight at 4°C. The cells were subsequently incubated with a fluorochrome-conjugated secondary antibody diluted in blocking buffer for 1 h at room temperature in the dark. Finally, the stained samples were mounted in Prolong Diamond Antifade with DAPI (Invitrogen, USA). Fluorescence images were acquired and processed using ImageJ software.

Quantified tumor cell lysates protein prepared from B16F10 or 4T1 cells were loaded onto SDS-PAGE and transferred to a PVDF membranes. The primary antibodies used were LC3 (1:1000) and GAPDH (1:1000). Primary antibodies were incubated overnight at 4°C followed by washing and the application of secondary HRP-conjugated antibody. The immunoreactive bands were visualized with a chemiluminescent substrate.

Autophagosome Ultrastructure Assay

The autophagosomes of B16F10 and 4T1 cells were directly identified by transmission electron microscopy. Cells were fixed and embedded. Thin sections (90 nm) were examined at 80 kV with a JEOL 1200EX transmission electron microscope. Autophagosomes were defined as double-membrane vacuoles (0.1–1.0 μm).

Mouse Models and *In Vivo* Local Treatment

Mice were purchased from Guangdong Animal Center (Guangzhou, China) and were kept in specific pathogen-free conditions. The animal experiment was conducted at Jinan University (Guangzhou, China), complying with the national guidelines for the care and use of laboratory animal.

The melanoma model was established with six–eight-week-old female C57BL/6 mice. 3×10^4 B16F10 cells were implanted subcutaneously on both sides of abdomen (left implanted tumor used for local treatment injection, right one for observation of tumor growth). Five days after inoculation, mice were randomly distributed into various groups. Local treatment schedule: PTX (10μg, 10μg and 15μg) were intratumorally injected into tumors at left side on day 5, 9 and 11; rapamycin (2.5μg, 2.5μg and 5μg) were injected intratumorally at left side on day 7, 9 and 11. The last two injections were carried out as the following scheme: PTX (10μg and 15μg) and rapamycin (2.5μg and 5μg) were separately injected into tumors in 6-8h interval on day 9 and 11.

The mouse breast carcinoma model was established with six–eight-week-old female BALB/c mice. BALB/c mice were implanted subcutaneously with 3×10^5 4T1 cells on both sides of abdomen. Seven days after inoculation, BALB/c mice were randomly distributed into various groups. Local treatment schedule: ADM (0.4μg, 0.4μg and 0.8μg) were injected intratumorally into tumor of left side on day 7, 11 and 13. Rapamycin (2.5μg, 2.5μg and 5μg) were injected intratumorally on day 9, 11 and 13. The last two injections were as following: ADM (0.4μg and 0.8μg) and rapamycin (2.5μg and 5μg) were separately injected into tumors in 6–8h interval on day 11 and 13.

C57BL/6 or BALB/c mice were killed on day 21 or day 30 after tumor cells inoculation. Tumor volume was measured with a caliper and calculated using the formula $(A\times B^2)/2$ (A as the largest and B the smallest diameter of the tumor).

In Vitro Generation of Mature Bone Marrow-Derived Dendritic Cells (BMDCs) and Antigen Stimulation of Lymphocytes

BMDCs were prepared from tibias and femurs of six–eight-week-old healthy female C57BL/6 and BALB/c mice. Bone marrow cells were passed through a 40 μm cell strainer (BD Falcon). After centrifugation at 200 × *g* for 3 min, red blood cells

were lysed with 2 mL of ACK lysis buffer (Biolegend, USA) for 10 min. The remaining cells were then plated in six-well plates at a density of 1×10^6 cells/mL in RPMI 1640 medium supplemented with 10% FBS, 20 ng/mL mouse granulocyte macrophage colony-stimulating factor (GM-CSF) (Peprotech, USA), 10 ng/mL mouse IL-4 (Peprotech), and 50 μM β-mercaptoethanol (Sigma, USA). Half of the medium was replaced with an equal volume of fresh medium containing the cytokines every three days. Seven days after the initial plating, non- and semi-adherent cells were harvested and regarded as mature BMDCs, and were loaded with mitomycin C treated tumor cells (1:5) or long peptides (20 μg/mL) for two days.

Spleens were harvested under sterile conditions from C57BL/6 and BALB/c mice with local treatment and T cells were isolated as responder cells using a 40 μm cell strainer. Mixing splenocytes with the antigen loaded BMDCs (10:1). After 72–96 h of incubation, cell clusters were observed and imaged under light microscope (CKX31, OLYMPUS, Japan).

Immunological Assays

Immunohistochemistry (IHC) Assay

Tumors were fixed with 4% paraformaldehyde. Tumor tissue slides were stained with antibodies against CD3, CD4, CD8 and FOXP3. IHC images were acquired using light microscope. CD4, CD8 and FOXP3 stained areas were quantified within manually pre-defined tumor regions *via* computerized image analysis Imagine J software.

IFN-γ ELISpot Assay

5×10^5 splenocytes were added into anti-IFN-γ coated multiscreen 96-well plates. BMDCs loaded with tumor cells (1:5) or 20 μg/mL peptides were added as reactants. After 12–16h of incubation at 37°C, cytokine secretion was detected with an anti-IFN-γ antibody (ELISpot) Kit (DAKEWE, Shenzhen). IFN-γ spots were scanned and quantified using a ELISPOT analyzer and ImmunoSpot Professional Software (CTL-ImmunoSpot® S6 FluoroSpot, USA). P/I (500 ng/mL PMA and 1 μg/mL ionomycin) were used for positive control.

Flow Cytometric Assay

Single cell samples were pre-incubated with anti-CD16/32 mAb for 15 minutes at 4°C, and then stained for 30 minutes at 4°C with various combinations of fluorochrome-conjugated antibodies: anti-CD3-PEcy5, anti-CD4-FITC and anti-CD8-FITC. For intracellular cytokine staining, mouse immune cells were restimulated with antigen-loaded DC in complete RPMI 1640 media and 50 IU/mL recombinant IL-2 (Peprotech, USA) at 37°C. After an hour, 1 × GolgiStop and 1 × GolgiPlug (BD Biosciences, USA) were incubated for another 4–8 hours at 37°C. Then, cells were permeabilized using a Fixation and Permeabilization Kit (BD, USA) and stained with antibodies: anti-IFN-γ-APC, anti-TNF-α-PE and anti-FOXP3-PE. Stained cells were acquired using a flow cytometer (FASC Canto II, BD, USA) and BD FACSDiva software. The data were further analyzed with FlowJo software (version 10.4).

Data Mining From Public Databases

The online website Gene Expression Profiling Interactive Analysis (GEPIA; available at http://gepia.cancer-pku.cn/index.html) was used to investigate the differential expression of autophagy-related 5 (ATG5) in breast invasive carcinoma (BRCA) and skin cutaneous melanoma (SKCM) tissues and explore the prognostic value of the differential expression of ATG5 in BRCA and SKCM patients. The Tumor IMmune Estimation Resource (TIMER) database—a comprehensive resource for the automatic analysis and visualization of the association between immune infiltration levels and a series of variables (https://cistrome.shinyapps.io/timer/)—was used to explore the correlation between ATG5 expression and the abundance of six types of immune cells ($CD4^+$ T cells, $CD8^+$ T cells, B cells, neutrophils, DCs, and macrophages) in BRCA and SKCM.

Statistical Analysis

All values were expressed as means ± SD. Statistically significant differences among individual treatments and the corresponding control groups were determined by the Student's *t*-test or analysis of variance (ANOVA). The Kaplan–Meier method was used to assess animal survival times and the log-rank test was used to test differences between groups of mice. Experiments were independently repeated at least three times. All analyses were carried out using GraphPad Prism 5. A P-value <0.05 was considered to be statistically significant.

RESULTS

Rapamycin Enhanced the Inhibitory Effects of Chemotherapeutic Drugs on B16F10/4T1 Cancer Cell Proliferation and Cell Death in Both 2D and 3D Cultures

To explore the antitumor effects of the classic chemotherapeutic plus autophagy-enhancing agents *in vitro*, we utilized two classic cancer cell lines, namely, B16F10, a malignant melanoma cell line, and 4T1, a triple-negative breast cancer cell line. The IC50 values of PTX for B16F10 cells, of ADM for 4T1 cells, and of rapamycin for both cell lines were determined by MTT assays (**Figures S1A, B**). Low dose chemotherapy (2.5–5.0 μg/mL PTX or 0.05–0.10 μg/mL ADM) was then used to investigate the synergistic effects of the chemotherapeutic drugs with rapamycin. First, a contact-dependent plate clone-formation assay was performed to assess the proliferative ability of the cancer cells. We measured cancer cell proliferation *in vitro* after treatment with the single drugs or with a CAER drugs (**Figures 1A, B**) and found that, at a low concentration (15 nM), rapamycin alone only slightly inhibited the proliferation of the two types of cancer cells (approximately 25% inhibition). A low dosage of each chemotherapeutic agent (5 μg/mL PTX or 0.1 μg/mL ADM) led to an approximately 50% inhibition of cancer cell proliferation. As expected, a combination of low-dose chemotherapy plus rapamycin (PTX+rapamycin for B16F10 cells and ADM+rapamycin for 4T1 cells) elicited a synergistic

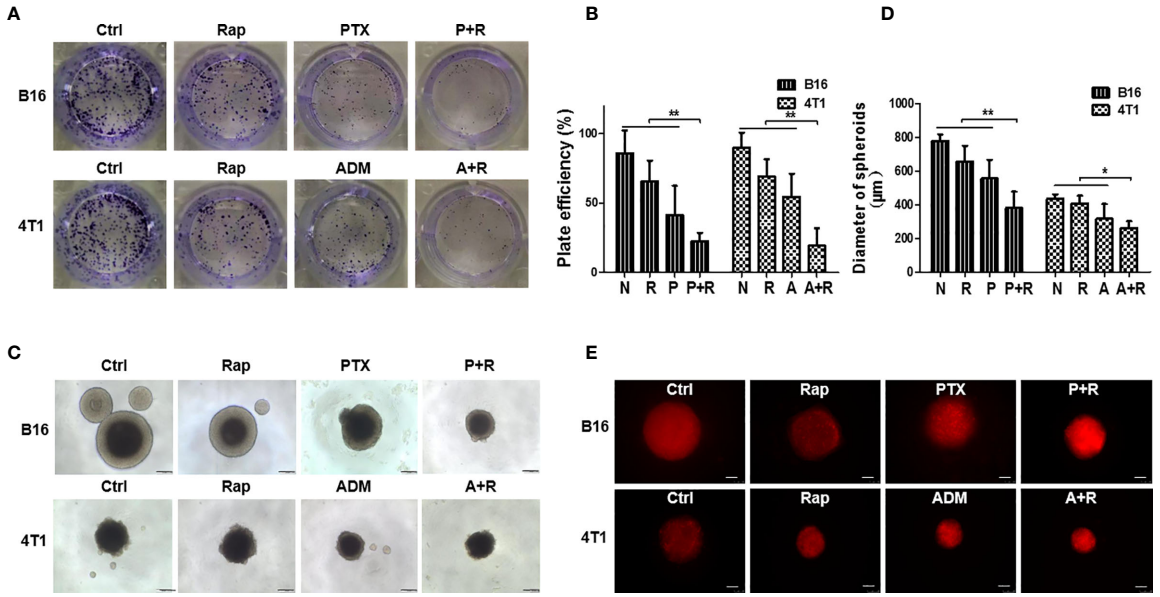

FIGURE 1 | Rapamycin enhanced the inhibitory effects of chemotherapy on B16F10/4T1 cancer cell proliferation and induction of cell death. **(A)** Colony-formation assay for the proliferation of B16F10 and 4T1 cells under different drug treatments. **(B)** Graph of the statistical analysis of the plating efficiency. **(C)** Spheroid formation was used to evaluate tumor cell proliferation in 3D cultures (scale bars: 200 μm). **(D)** Graph of the statistical analysis of spheroid diameter. **(E)** Autophagy-associated death of cancer cell spheroids was measured by propidium iodide (PI) staining and imaged using red fluorescence (scale bars: 250 μm). B16: B16F10. Ctrl: negative control group. Rap: rapamycin. P+R, PTX+Rap; A+R, ADM+Rap. Bars and error bars represent means ± SD, respectively, of three independent experiments. $^{*}P < 0.05$, $^{**}P < 0.01$ by Student's *t*-test.

inhibitory effect on cancer growth (approximately 80%), indicating that a low-dose CAER could inhibit the proliferative ability of B16F10 and 4T1 cells.

To mimic *in vivo* conditions, we treated cancer cell spheroids generated under 3D-culture conditions with the double concentrations of the drugs (10 μg/mL PTX or 0.2 μg/mL ADM). Cancer cells treated with the CAER formed smaller spheroids than cells in the negative control group or those treated with each drug alone (**Figures 1C, D**). Additionally, the PI staining results indicated that cell death was higher in the B16F10- and 4T1-derived spheroids treated with PTX+ rapamycin or ADM+rapamycin, respectively than the negative control group or those treated with each drug alone (**Figure 1E**). Together, these results demonstrated that the CAER synergistically inhibited B16F10/4T1 cell proliferation and enhanced cell death *in vitro*.

CAER Treatment Increased the Activation of Autophagy

To clarify whether treatment using the CAER could hyperactivate autophagy in cancer cells, we treated B16F10 and 4T1 cells with 5 μg/mL PTX or 0.1 μg/mL ADM, respectively, for 6–8 h, and then with rapamycin (25 nM) for another 16–24 h. Firstly, WB showed that the relative protein expression of LC3-II/LC3-I was significantly increased after CAER treatment. The ratio of LC3-II to LC3-I is proportional to the level of autophagy (**Figures 2A, B**). Secondly, we measured the autophagic flux in the cancer cells by MDC assay. Autophagic flux staining was nearly undetectable in the control cells, and was also weak in cells treated with the individual drugs. In comparison, cells treated with the CAER drugs showed substantially stronger autophagic flux staining (**Figure 2C**). Thirdly, we measured the expression level of the autophagy-specific marker LC3B by immunofluorescence staining, and found that LC3B staining was strongest in cells treated with the CAER, followed by those treated with PTX or ADM alone, and then by the control, normal medium-treated cells (**Figures 2D, E**). Finally, observation by electron microscopy showed that CAER-treated B16F10 and 4T1 cells contained more autophagosomes than those treated with either PTX or ADM alone or that seen in control cells (**Figure 2F**). Taken together, these findings showed that the CAER could induce the hyperactivation of autophagy in B16F10 and 4T1 cells.

Local Treatment With the CAER Strongly Inhibited the Growth of B16F10 Cell-/4T1 Cell-Derived Tumors *In Vivo*

To test whether the low-dose CAER could inhibit tumor growth *in vivo*, we established tumor models in C57BL/6 or BALB/c mice by injecting B16F10 or 4T1 cells into both sides of the abdomen of the animals and then delivered the drugs locally into one tumor at left side (**Figures 3A, D**). Analysis of the growth curve of the locally injected tumors (LI-TUs) indicated that local monotherapy with PTX for B16F10 cell-derived tumors (**Figure 3A**) or ADM for 4T1-derived tumors (**Figure 3D**) exerted a significantly greater antitumor than rapamycin treatment alone.

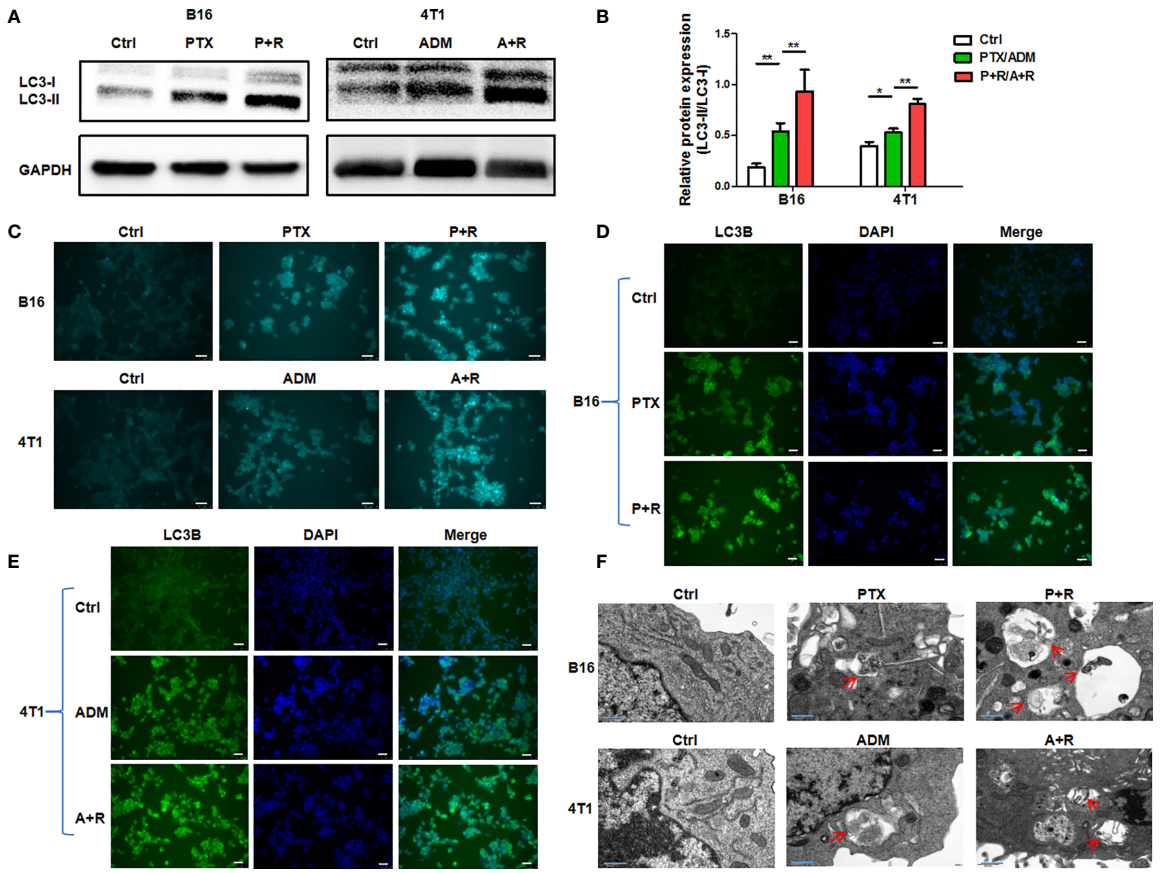

FIGURE 2 | The induction of hyperautophagy by low-dose CAER treatment. **(A)** The autophagy marker LC3-II/LC3-I was detected in B16F10 (left panel) and 4T1 (right panel) cells using WB. Cells were incubated with a low concentration of paclitaxel (PTX; 5 μg/mL) or adriamycin (ADM; 0.1 μg/mL) for 6–8 h and then with rapamycin (25 nM) for 16–24h **(B)** Graph of the statistical analysis of WB. **(C)** The autophagic flux in B16F10 and 4T1 cells was detected by monodansylcadaverine (MDC) assay. (scale bars: 25 μm). **(D, E)** The autophagy marker LC3B was detected in B16F10 cells using immunofluorescence. The treatment was the same as in **Figure 1A** (scale bars: 25 μm). **(F)** Transmission electron micrographs of autophagosomes/autolysosomes induced by the chemotherapeutic agents and rapamycin in B16F10 and 4T1 cells (scale bars: 0.4 μm). *$P < 0.05$, **$P < 0.01$ by Student's t-test.

However, treatment using the CAER conferred greater antitumor activity than PTX, ADM, or rapamycin treatment alone.

Surprisingly, we observed that the growth of the contralateral, noninjected tumors (NI-TUs) was also inhibited in mice of the groups treated with the CAER [PTX+rapamycin for B16F10 cell-derived tumors (**Figures 3A, B**) and ADM+rapamycin for 4T1 cell-derived tumors (**Figures 3D, E**)]. Survival curve analysis indicated that the CAER also improved the survival of mice in both the B16F10 (**Figure 3C**) and 4T1 (**Figure 3F**) tumor model groups. These data indicated that the local application of the CAER to LI-TUs can activate a systemic antitumor immune response and inhibit the growth of distantly contralateral NI-TUs.

Systemic Anti-Tumor Immune Response Induced by Local CAER Treatment

To investigate the immunological changes after local CAER treatment, we analyzed the local (tumor) and systemic (spleen and blood) immune responses in the mouse tumor models using immunohistochemical (IHC) and flow cytometric assays. IHC staining showed that infiltration by $CD3^+$, $CD4^+$, and $CD8^+$ T cells was significantly greater in B16F10-derived tumor tissues administered the CAER than control group or single drug group (**Figure 4A**). T cell infiltration increased two- to three- fold: [PTX+rapamycin *vs*. control: approximately 10% *vs*. 3% of $CD3^+$, 4% *vs*. 1% of $CD4^+$, and 6% *vs*. 3% of $CD8^+$ T cells (**Figure 4B**)]. $FoxP3^+$ T cells (Tregs) significantly reduced: 41% *vs*. 32% of $CD4^+$ T cells from analysis of **Figure 4A**. Similar results were obtained for the 4T1-derived tumor models (**Figures 4C, D**).

To analyze the systemic immune response after local treatments, we measured the levels of IFN-γ secreted by T cells in the spleen and peripheral blood of B16F10 tumor model mice through flow cytometry. Spleen data showed that $CD4^+$ T cells and $CD8^+$ T cells from the CAER treatment groups (PTX +rapamycin) secreted greater amounts of IFN-γ than those in the PBS or PTX monotherapy groups (**Figure 4E**). $CD8^+$ T cells (1.10% increasing) responded more obvious than $CD4^+$ T cells

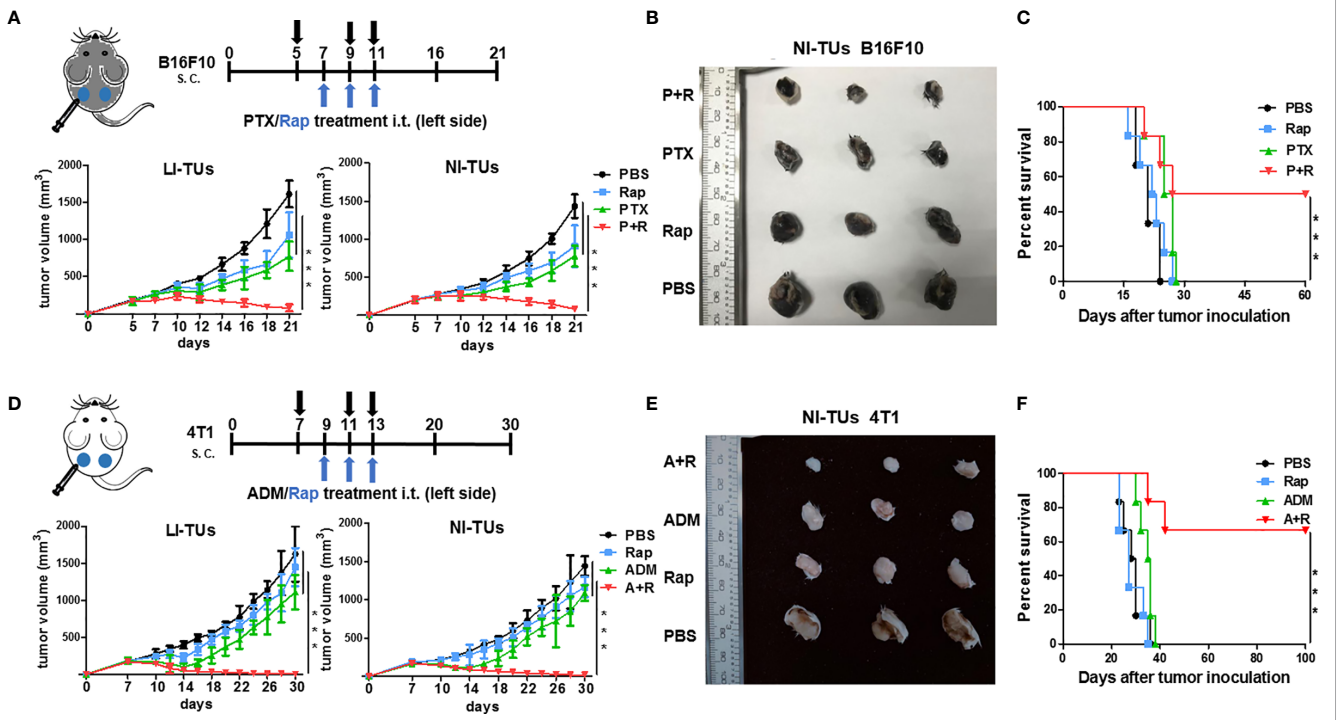

FIGURE 3 | The inhibition of *in vivo* tumor growth using a local CAER treatment. **(A)** The treatment scheme (upper panel) and *in vivo* growth curve (lower panel) of B16F10 cell-derived tumors. **(B)** Representative images of B16F10 cell-derived noninjected tumors on day 16. **(C)** The survival curves for C57BL/6 mice bearing B16F10 cell-derived tumors. **(D)** The treatment scheme (upper panel) and *in vivo* growth curve (lower panel) of 4T1 cell-derived tumors. **(E)** Representative images of 4T1 cell-derived noninjected tumors on day 20. **(F)** The survival curves for BALB/c mice bearing 4T1 cell-derived tumors. LI-TUs, locally injected tumors; NI-TUs, noninjected tumors; n = 5–6 mice/group. ***$P < 0.001$ by Student's t-test.

(0.49% increasing). Meanwhile, Tregs decreased 4.95% in the CAER group of the spleen (**Figure 4F**). In blood analysis for B16F10, $CD8^+$ T cells (2.61% increasing) were triggered more obviously than $CD4^+$ T cells (1.12% increasing), but Tregs decreased 2.97% in the CAER therapy group (**Figures 4G, H**). Similar results could be found in 4T1 tumor models (**Figures 4I–L**): the CAER (A+R) treatment promoted the activation of more T cells or inhibition of Tregs in tumor, spleen and blood of 4T1 tumor-bearing BALB/c mice.

Local CAER Treatment Induced a Tumor Antigen-Specific T-Cell Response *In Vivo*

Our results demonstrated that local CAER treatment could trigger systemic antitumor immunity in two cancer models in mice with different genetic backgrounds. To further elucidate the mechanisms underlying these immunological changes, we performed *ex vivo* stimulation to determine whether CAER treatment could activate tumor-reactive T cells in tumors derived from B16F10 or 4T1 cells. Splenocytes from B16F10-bearing C57BL/6 mice or 4T1-bearing BALB/c mice treated with the local CAER were stimulated with mature DCs loaded with intact B16F10 or 4T1 tumor cells treated with mitomycin C. ELISpot assay data showed that splenocytes from mice treated using the local CAER exhibited a stronger response to tumor cell-derived antigens than those isolated from mice in the control group (**Figures 5A, B**).

To analyze the T-cell responses in the different groups in more detail, we used flow cytometry to analyze intracellular cytokine levels (IFN-γ and TNF-α staining). The data showed that the secretion of both cytokines was significantly upregulated in the PTX+rapamycin and ADM+rapamycin treatment groups when compared with controls. The incubation of tumor cells with splenic T cells derived from B16F10-bearing mice treated with the local CAER led to the activation of a greater number of tumor antigen-specific $CD4^+$ T cells and $CD8^+$ T cells than that with T cells in the other treatment groups (**Figures 5C, D**). $CD8^+$ T cell responded in two-fold more than CD4+ T cell (IFN-γ secreted $CD8^+$ T cells increase to 1.84%, while $CD4^+$ T cells to 0.98%; the secretion of TNF-α was increased to 3.36% of $CD8^+$ T cells, while 1.65% of $CD4^+$ T cells). Similarly, both of $CD4^+$ T cells and $CD8^+$ T cells were activated in the CAER treatment group of 4T1 tumor-bearing BALB/c mice and CD8+ T cells responded dominantly (IFN-γ secreted $CD8^+$ T cells increase to 6.32%, while $CD4^+$ T cells to 1.61%; the secretion of TNF-α was increased to 9.28% in $CD8^+$ T cells, while to 1.94% in $CD4^+$ T cells) (**Figures 5E, F**). These results showed that, compared with the other treatments, local CAER administration activated a greater number of tumor-reactive T cells *in vivo*.

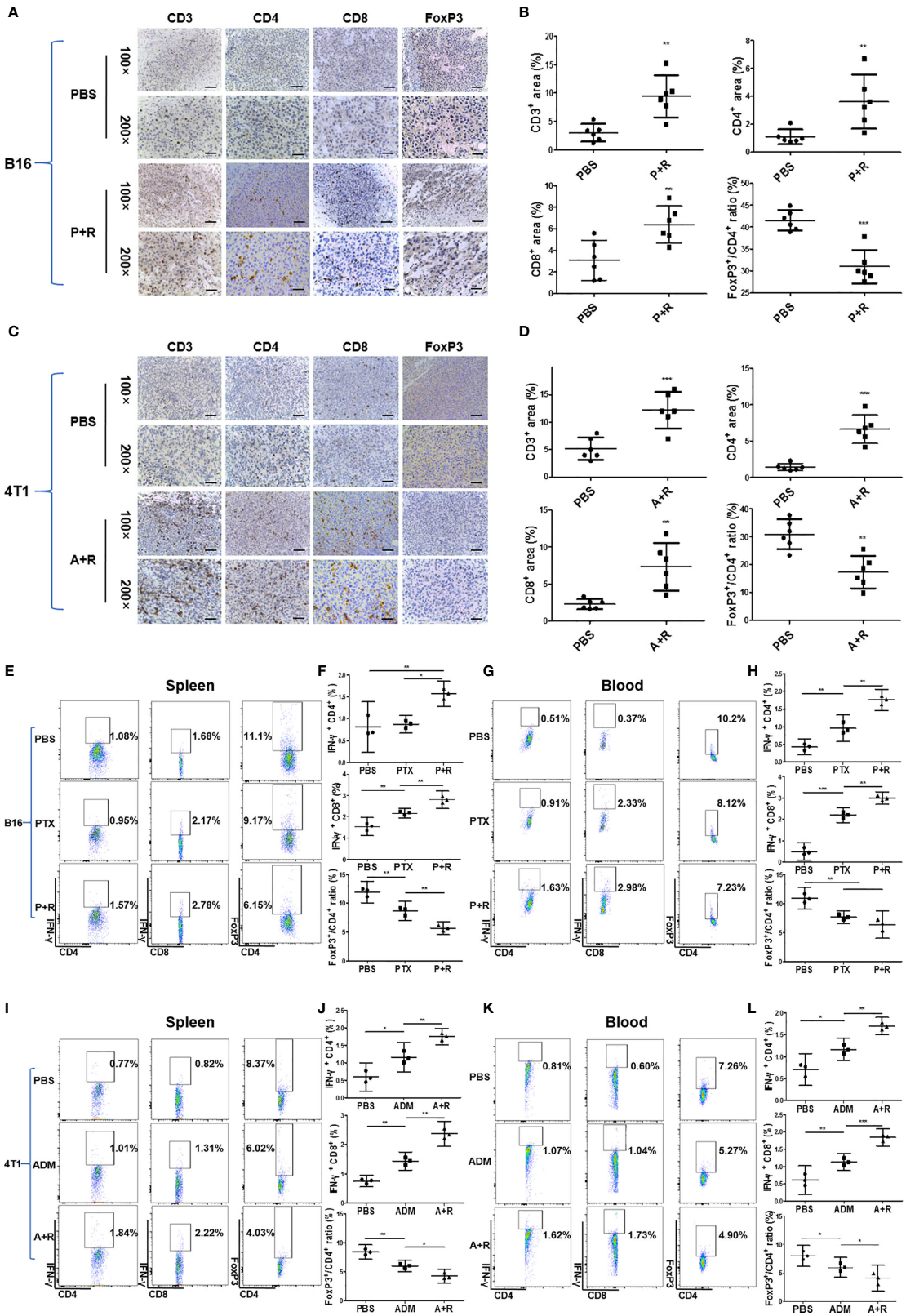

FIGURE 4 | Continued

FIGURE 4 | Immunological analysis of the local and systemic effects after local CAER treatment. **(A, C)** Immunological analysis of treated tumors in B16F10 and 4T1 mouse models. Representative images showing immunohistochemical (IHC) staining of CD3, CD4, CD8, and FOXP3 in tumor samples on day 16 (B16F10 cells) or day 20 (4T1 cells). Phosphate-buffered saline (PBS) was used as control (scale bars: 50 μm). **(B, D)** Graph of the statistical analysis of the IHC staining results in the B16F10 mouse model and the 4T1 mouse model. **(E, G)** Flow cytometric analysis of the spleen and peripheral blood in B16F10 tumor models. Flow cytometric analysis of the percentages of IFN-γ-producing $CD4^+$ T cells, $CD8^+$ T cells, and $FoxP3^+$ T cells in the spleen and peripheral blood of C57BL/6 tumor model mice under the different treatment groups (PBS, PTX, and P+R groups) on day 16. **(F, H)** Graph of the statistical analysis of the flow cytometry results for B16F10 tumor models. **(I, K)** Flow cytometric analysis of the spleen and peripheral blood in 4T1 tumor models. Spleen and peripheral blood were analyzed by flow cytometry to determine the percentages of IFN-γ-producing $CD4^+$ T cells, $CD8^+$ T cells, and $FoxP3^+$ T cells in BALB/c tumor model mice of the different treatment groups (PBS, ADM, and A+R groups) on day 20. **(J, L)** Graph of the statistical analysis of the flow cytometry results for 4T1 tumor models. $^*P < 0.05$, $^{**}P < 0.01$, $^{***}P < 0.001$ by Student's *t*-test.

Local CAER Treatment Induced Neoantigen-Specific T-Cell Responses

Because tumor-specific neoantigens are key targets for antitumor immune responses, we next sought to verify whether the CAER could activate neoantigen-specific T cells. We previously synthesized and prescreened mutant neoantigen peptides from B16F10 and 4T1 cells (28) (**Figure S3A**). Three mutant peptides (B16-M27, B16-M30, and B16-M33) derived from B16F10 cells, and three (4T1-M8, 4T1-M17, and 4T1-M27) from 4T1 cells, were used for the subsequent experiments.

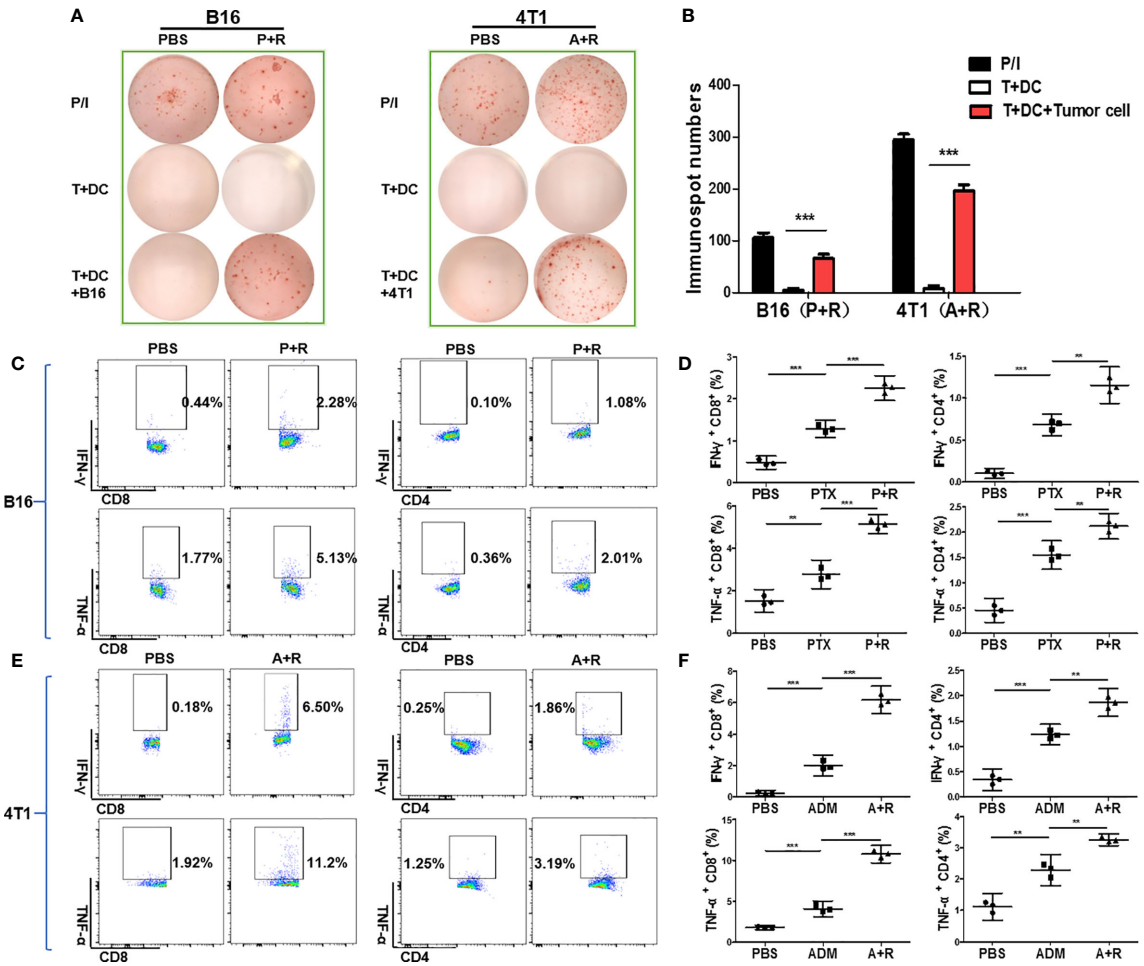

FIGURE 5 | Local CAER treatment increased the number of tumor-reactive T cells *in vivo*. **(A)** ELISpot analysis for immune responses to T cells under the different treatments (PBS, PTX/ADM, and P+R/A+R). The immune responses of splenocytes isolated from B16F10 tumor-bearing C57BL/6 mice or 4T1 tumor-bearing BABL/c mice of the different treatment groups were tested by ELISpot for the recognition of B16F10 and 4T1 tumor cells. **(B)** Graph of the statistical analysis of ImmunoSpot numbers. **(C, E)** Flow cytometric analysis of CD4/CD8 surface and intracellular cytokine (IFN-γ and TNF-α) staining to detect the activation of splenic T cells incubated with B16F10 or 4T1 tumor cells. **(D, F)** Graph of the statistical analysis of the flow cytometry results in the B16F10 and 4T1 models. P/I, PMA +ionomycin (positive control). $^{**}P < 0.01$, $^{***}P < 0.001$ by Student's *t*-test.

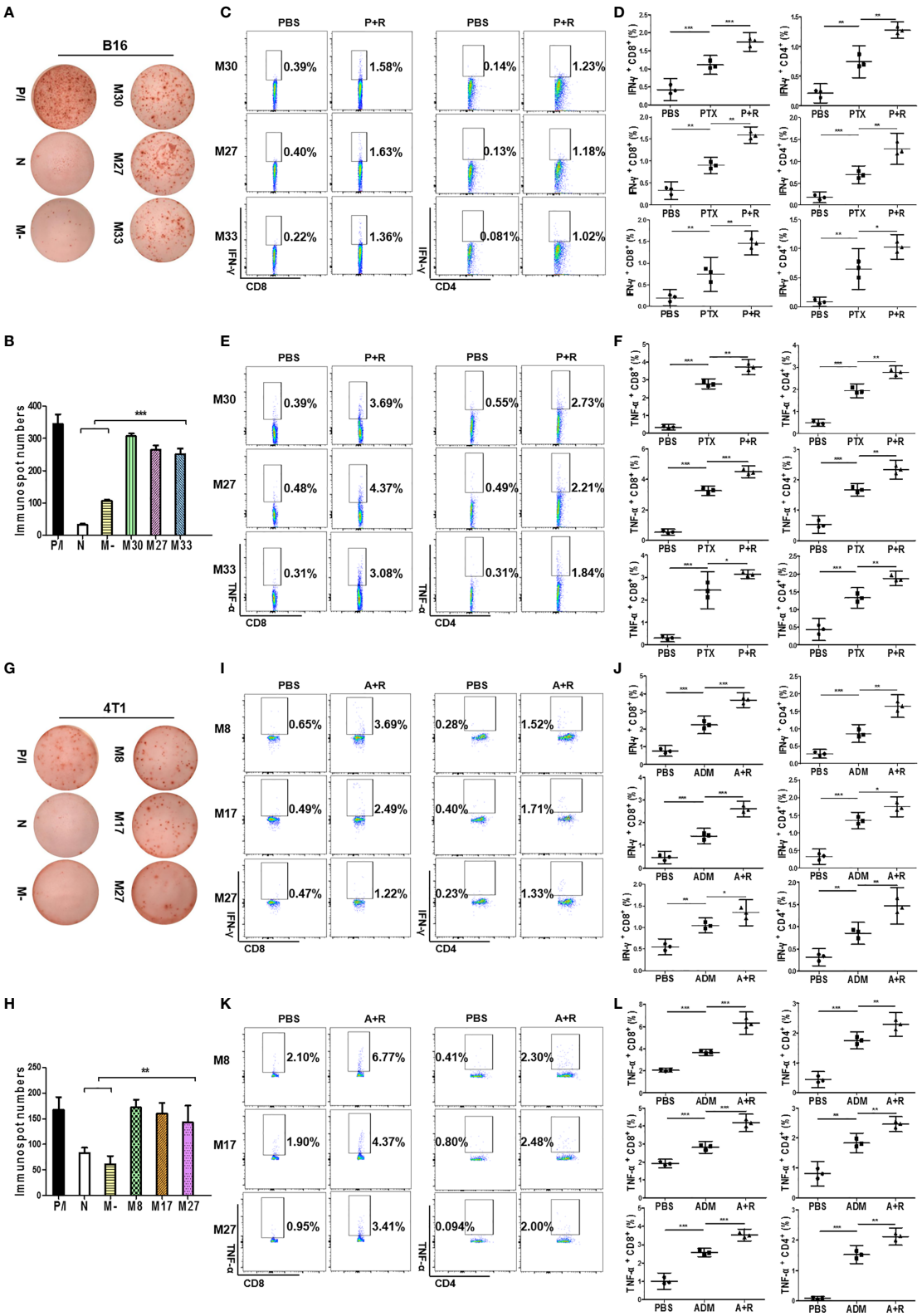

FIGURE 6 | Continued

FIGURE 6 | Local CAER Treatment induce neoantigen-specific T-cell responses. **(A)** IFN-γ ELISpot assay for T cell immune responses targeting neoantigens. Splenocytes from B16F10 cell-derived, tumor-bearing C57BL/6 mice under the different treatments (PBS, PTX, and P+R) were stimulated by BMDCs plus neoantigen peptides (M30, M27 and M33) and detected by IFN-γ ELISpot assay. **(B)** Graph of the statistical analysis of ImmunoSpot numbers in the B16F10 model. **(C, E)** Flow cytometric analysis of intracellular cytokine (IFN-γ and TNF-α) secretion levels during neoantigen-specific T cell immune responses in the B16F10 model. **(D, F)** Graph of the statistical analysis of the flow cytometry results in the B16F10 model. **(G)** IFN-γ ELISpot assay for T cell immune responses targeting neoantigens. Splenocytes from 4T1 cell-derived, tumor-bearing BABL/c mice under the different treatments (PBS, ADM, and A+R) were stimulated by BMDCs plus neoantigen peptides (M8, M17, M27) and detected by IFN-γ ELISpot assay. **(H)** Graph of the statistical analysis of ImmunoSpot numbers in the 4T1 model. **(I, K)** Flow cytometric analysis of intracellular cytokine (IFN-γ and TNF-α) secretion levels during neoantigen-specific T cell immune responses in the 4T1 model. **(J, L)** Graph of the statistical analysis of the flow cytometry results in the 4T1 model. N, no peptide; M-, negative peptide. $^{*}P < 0.05$, $^{**}P < 0.01$, $^{***}P < 0.001$ by Student's *t*-test.

Splenocytes from C57BL/6 mice bearing B16F10 cell-derived tumors and administered the CAER regimen were incubated with peptide-loaded (B16-M27, B16-M30, or B16-M33) DCs to evaluate the neoantigen-reactive T cell immune response. ELISpot assays showed that all the peptide-loaded DCs stimulated T cells to produce IFN-γ (**Figures 6A, B**). To determine the composition of the neoantigen-reactive T-cell population, we next analyzed intracellular cytokine staining by flow cytometry. The analysis demonstrated that, when incubated with neoantigen peptides, splenic T cells isolated from C57BL/6 mice bearing B16F10 cell-derived tumors and treated with CAER generated more activated $CD4^+$ and $CD8^+$ T cells than those isolated from mice in the other treatment groups (**Figures 6C–F**). B16-M30 treatment induced increases in IFN-γ/TNF-α levels of 1.19%/3.30% in $CD8^+$ T cells and 1.09%/2.18% in $CD4^+$ T cells; for B16-M27, the increases were 1.23%/3.89% and 1.05%/1.72%, respectively; and for B16-M33, the respective increases were 1.14%/2.77% and 0.939%/1.53%.

Similar results were obtained for 4T1 cell-derived tumor-bearing BALB/c mice, further indicating that treatment with a local CAER could enhance neoantigen-specific T cell responses (4T1-M8 treatment induced increases in IFN-γ/TNF-α levels of 3.04%/4.67% in $CD8^+$ T cells and 1.24%/1.89% in $CD4^+$ T cells; for 4T1-M17, the increases were 2.00%/2.47% and 1.31%/1.68%, respectively; and for 4T1-M27, the respective increases were 0.75%/2.46% and 1.10%/1.91%) (**Figures 6G–L**). These results indicated that $CD8^+$ T cells elicited the strongest responses to the three neoantigens from each cell line.

Bioinformatic Analysis of the Expression of the Autophagy Biomarker ATG5 and the Relationship Between ATG5 and Immune Cell Infiltration Levels in BRCA and SKCM

To assess the status of autophagy in human breast carcinoma (BRCA) and skin cutaneous melanoma (SKCM), we first analyzed the levels of autophagy in these human cancer types based on data obtained from the GEPIA website. ATG5, a key autophagy-related gene, is reported to be positively correlated with the level of autophagy (29–31). We found that the ATG5 expression level was markedly higher in BRCA and SKCM tissues than in matched normal tissues (**Figure 7A**). Furthermore, the expression level of ATG5 was increased with increasing clinical staging in BRCA and SKCM patients (**Figure 7B**). Next, we generated Kaplan–Meier plots to investigate the prognostic value of the level of autophagy in patients with BRCA and SKCM, with the results showing that high ATG5 expression levels were correlated with better disease-free survival (DFS) (**Figure 7C** upper panel) and forepart of overall survival (OS) (**Figure 7C** lower panel). These data indicated that early-stage BRCA and SKCM might respond better to low-dose CAER treatment. In addition, higher concentrations of CAER drugs might be required to treat late-stage BRCA and SKCM.

Subsequently, we employed the TIMER database to determine whether any correlation existed between ATG5 expression and immune cell infiltration. TIMER-based analysis indicated that infiltration by $CD4^+$/$CD8^+$ T cells and DCs was significantly reduced with arm-level deletion of ATG5 in BRCA and SKCM tissues (**Figure 7D**). We next focused on the correlations between ATG5 expression and the infiltration of six immune cell types in BRCA and SKCM using the TIMER database. As shown in **Figure 7E**, ATG5 expression was markedly correlated with B cell, $CD8^+$ T cell (maximum correlation), $CD4^+$ T cell, macrophage, neutrophil, and DC infiltration. Meanwhile, the correlations between ATG5 expression and the abundance of the six types of immune cells in different types of BRCA and SKCM were also studied (**Figures S4A, B**). Finally, due to the promise associated with immune checkpoint inhibitor therapy for cancer treatment, we further determined the association between ATG5 and PD-1 and CTLA-4 expression (**Figure S4C**), and found that there was a negative correlation between ATG5 and PD-1 ($r = -0.069$, $P < 0.05$) as well as between ATG5 and CTLA-4 ($r = -0.04$, $P = 0.11$) in BRCA and SKCM tumors. Combined, these data indicated that the level of autophagy was correlated with the prognosis of BRCA and SKCM patients and immune cell infiltration in BRCA and SKCM tumors.

DISCUSSION

Cancer chemotherapy-associated immune suppression remains a key drawback for cancer treatment. The suppression of immunity is associated with the dosage and route of chemotherapeutic drug administration. High-dose systemic chemotherapy always destroys bone marrow stem cells and immune cells and results in severe immune suppression (2).

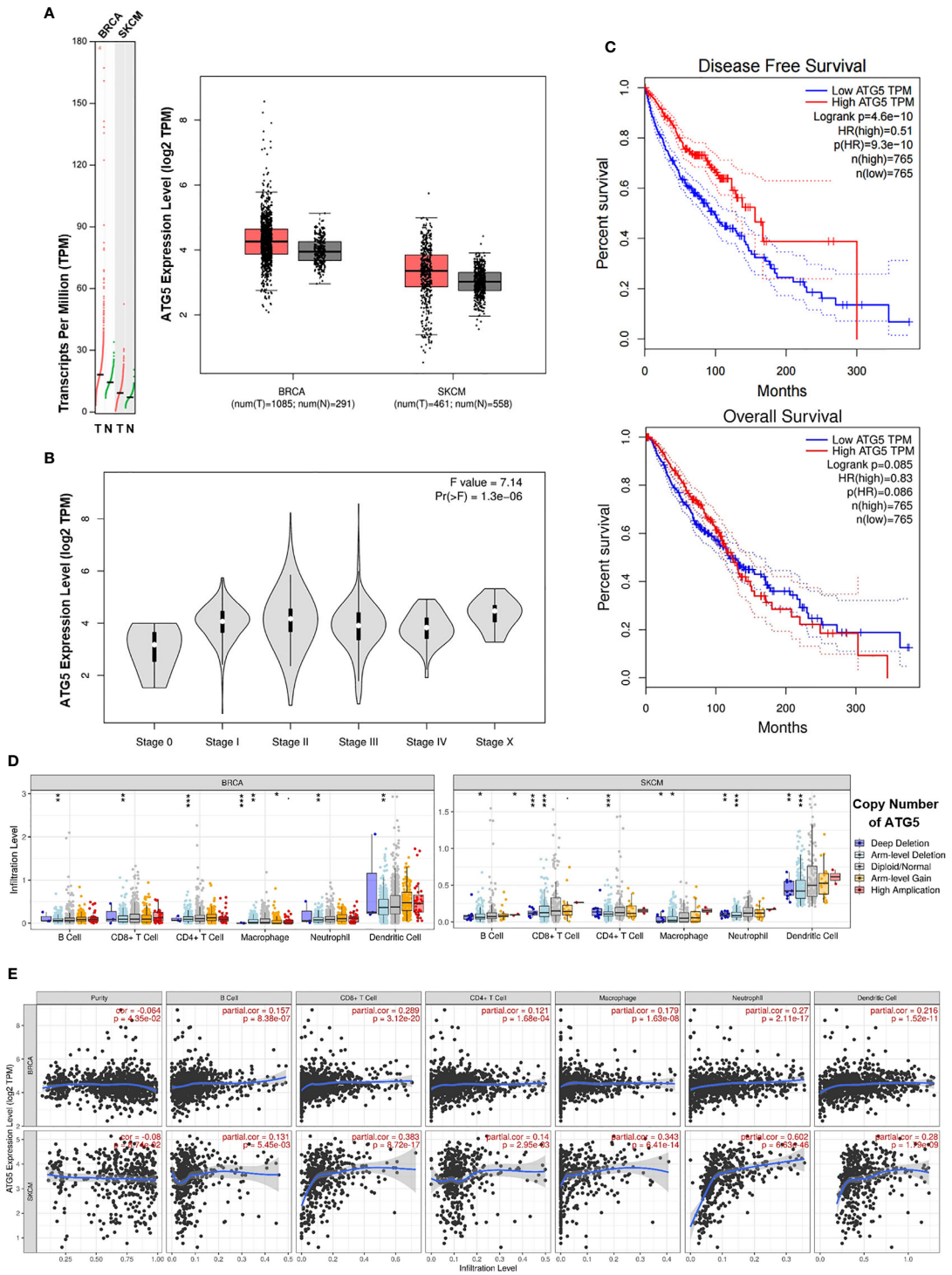

FIGURE 7 | Bioinformatic analysis of the expression of the autophagy biomarker ATG5 and the relationship between ATG5 and immune infiltration levels in BRCA and SKCM. **(A)** The ATG5 mRNA (left panel) and protein expression (right panel) levels were higher in BRCA and SKCM tissue than in normal tissue. **(B)** ATG5 expression levels in different clinical stages in BRCA and SKCM patients. **(C)** Kaplan–Meier survival curves of disease-free survival (upper panel) and overall survival (lower panel) for high and low ATG5 expression groups in BRCA and SKCM patients. **(D)** A comparison of immune infiltration levels among BRCA (left panel) and SKCM (right panel) tumors with different ATG5 gene copy number status. **(E)** The correlation between ATG5 expression and the abundance of six types of immune cells (B cells, $CD8^+$ T cells, $CD4^+$ T cells, macrophages, neutrophils, and dendritic cells) in BRCA (upper panel) and SKCM tissues (lower panel). BRCA, breast invasive carcinoma; SKCM, skin cutaneous melanoma. $^*P < 0.05$, $^{**}P < 0.01$, $^{***}P < 0.001$.

To reduce chemotherapy-related cytotoxicity, the local delivery of chemotherapeutic drugs was proposed and tested in clinical trials. The results of these trials revealed that this approach could reduce systemic toxicity and prolong the survival of cancer patients (7, 32). However, local high-dose chemotherapy still destroys a large number of tumor-reactive T cells that infiltrate the regional tumor tissue and normal tissue cells nearby, which further promotes the progression of the disease (3).

To avoid these potentially harmful effects, we designed a local cancer CAER treatment that combined low-dose chemotherapy with low-dose autophagy therapy. *In vitro*, we demonstrated that low-dose autophagy-inducing rapamycin (25 nM) could greatly enhance cancer-inhibiting effects of low-dose chemotherapeutic drug administration. Additionally, this regimen also resulted in higher rates of cell death, as determined by *in vitro* PI-staining assays.

We successfully applied this strategy in animal models, which led to the complete eradication of well-established tumors derived from both B16F10 and 4T1 cells. Tumor growth was significantly inhibited in mice from the two models treated with low-dose CAER, while mouse survival was significantly improved. Additionally, we observed a large number of infiltrated $CD3^+$ T cells in LI-TUs and NI-TUs. Importantly, local CAER administration also led to the eradication of distant NI-TUs. These observations indicate that local drug injection has a therapeutic effect in remote regions, and even the whole body, through systemic antitumor immune responses. We further analyzed the tumor, spleen, and peripheral blood and found increased numbers of $CD3^+$ T (both $CD4^+$ and $CD8^+$ T cells) in the combination-treatment groups, whereas the numbers of $CD4^+$ $FoxP3^+$ T cells were decreased. These results suggested that treatment using local administration of a combination of CAER can induce a strong systemic antitumor immune response.

Tumor antigens, especially neoantigens, are key targets for anticancer immunotherapy (33–35). The local administration of CAER agents to tumor cells can lead not only to increased tumor cell death but also to the release of a larger amount of tumor antigens, including neoantigens, for antigen presentation (36–38). With our local therapy regimen, the tumors were quickly eradicated, concomitant with the infiltration of a large number of T cells. To determine whether neoantigen-specific T cells were activated by this local treatment, we examined the neoantigen-specific immune response based on previous neoepitope-related studies in these two tumor models by next-generation sequencing (28). We found that a local CAER could activate neoantigen-specific $CD4^+$ and $CD8^+$ T cells, as evidenced by flow cytometric analysis of intracellular IFN-γ and TNF-α staining. These experiments demonstrated that our strategy could lead to the activation of T cells that target these neoantigens, thereby triggering systemic immune responses.

Our animal model data demonstrated that the hyperactivation of autophagy in cancer cells was associated with systemic antitumor immune responses. To assess the relationship between autophagy and immunity in human cancers, we measured the expression levels of autophagy-related genes in BRCA and SKCM through bioinformatics tools. The results indicated that the level of autophagy was higher in early-stage BRCA and SKCM tissue, while Kaplan–Meier plots demonstrated that higher levels of autophagy were correlated with more favorable DFS and better forepart of OS among BRCA and SKCM patients. When exploring the possible reasons behind the clinical prognosis, we further discovered that immune cell infiltration, especially that by $CD8^+$ T cells, was markedly correlated with the level of autophagy in BRCA and SKCM tumors. This suggest that high levels of autophagy in tumor samples, together with T-cell infiltration, can serve as a predictor of better tumor prognosis and has positive clinical significance.

The applicability of this research is mainly reflected in the following two aspects. First, although neoantigen-based vaccines have shown promising efficacy, the application of personalized neoantigen-based vaccines remains limited owing to multiple factors, including an unavoidable original sample error, tumor heterogeneity, predictive accuracy, and high cost (39). Treatment using our CAER could induce ICD and lead to the release of a higher amount of endogenous neoantigens, thereby enhancing tumor immunogenicity and triggering systemic immune responses without the need for sequencing to identify mutant neoantigen sequences. These advantages render our method more convenient than some of those previously reported (40, 41). Furthermore, combining our regimen with other immunomodulators is expected to further improve its efficacy. Indeed, robust antitumor responses were achieved with local chemotherapy combined with a CTLA-4 blockade in murine models of melanoma and prostate cancer (42). These observations suggest that treatment using a local CAER combined with immune checkpoint inhibitors or immunoadjuvants may represent a promising option for cancer immunotherapy in the future (43–46). In this sense, our study broadens the range of neoantigen-related treatments and may provide a new option for the treatment of patients with advanced malignant tumors.

In summary, the key finding of this study was that cancer treatment using local administration of CAER generated an effective local and systemic antitumor response in mice. Our work revealed that hyperactivated autophagy can boost chemotherapy-induced antitumor immunity, especially the activation of neoantigen-specific T cells. Accordingly, local CAER therapy not only reduced systemic toxicity, but also modified the tumor microenvironment, thereby inducing anticancer immunity.

DATA AVAILABILITY STATEMENT

The original contributions presented in the study are included in the article/**Supplementary Material**. Further inquiries can be directed to the corresponding author.

ETHICS STATEMENT

The animal study was reviewed and approved by Jinan University Experimental Animal Center.

AUTHOR CONTRIBUTIONS

JY and XY performed the experiments and wrote the paper. KW and JG performed data processing and statistical analysis. LL designed, proposed, and supervised this project. All authors contributed to the article and approved the submitted version.

FUNDING

This project was supported by National Key Research & Development Projects (2016YFC1303404 and 2016YFA0101103) of the Ministry of Science and Technology, and Guangdong Science and Technology Project (2014A020211006) from the Guangdong Science and Technology Innovation Commission, of the People's Republic of China.

ACKNOWLEDGMENTS

We thank Professor Wende Li of Guangzhou Institute of Zoology for presenting gifting us the B16F10 and 4T1 cell lines. We also thank Charlesworth for polishing our manuscript.

SUPPLEMENTARY MATERIAL

The Supplementary Material for this article can be found online at: https://www.frontiersin.org/articles/10.3389/fonc.2021.658254/full#supplementary-material

REFERENCES

1. DeVita VT, Chu E. A History of Cancer Chemotherapy. *Cancer Res* (2008) 68:8643–53. doi: 10.1158/0008-5472.CAN-07-6611
2. van der Wall E, Beijnen JH, Rodenhuis S. High-dose chemotherapy regimens for solid tumors. *Cancer Treat Rev* (1995) 21:105–32. doi: 10.1016/0305-7372(95)90023-3
3. Hunter WL, Burt HM, Machan L. Local delivery of chemotherapy: a supplement to existing cancer treatments. *Adv Drug Deliv Rev* (1997) 26:199–207. doi: 10.1016/S0169-409X(97)00035-5
4. Sukru O, Ugur S, Nuri K, Fikret A, Taner D. An overview of high dose chemotherapy with autologous stem cell rescue for germ cell tumors in current practice. *J B U ON* (2017) 22:306–11.
5. Jeremy W, Le Deley M-C, Uta D, Le Teuff G, Bernadette B, Nathalie G, et al. High-Dose Chemotherapy and Blood Autologous Stem-Cell Rescue Compared with Standard Chemotherapy in Localized High-Risk Ewing Sarcoma: Results of Euro-E.W.I.N.G.99 and Ewing-2008. *J Clin Oncol* (2018) 36:JCO2018782516. doi: 10.1200/JCO.2018.78.2516
6. Krukiewicz K, Zak JK. Biomaterial-based regional chemotherapy: Local anticancer drug delivery to enhance chemotherapy and minimize its side-effects. *Mat Sci Eng C* (2016) 62:927–42. doi: 10.1016/j.msec.2016.01.063
7. Falke LL, van Vuuren Stefan H, Filis K, Farshad R, Nguyen TQ, Veldhuis JG, et al. Local therapeutic efficacy with reduced systemic side effects by rapamycin-loaded subcapsular microspheres. *Biomaterials* (2015) 42:151–60. doi: 10.1016/j.biomaterials.2014.11.042
8. Heegon K, Hyeonjeong H, Moonkyoung J, Junhee H, Ho PJ. Management of lymph node metastasis via local chemotherapy can prevent distant metastasis and improve survival in mice. *J Controlled Release* (2021) 329:847–57. doi: 10.1016/j.jconrel.2020.10.016
9. He J, Wang X, Guan H, Chen W, Wang M, Wu H, et al. Clinical efficacy of local targeted chemotherapy for triple-negative breast cancer. *Radiol Oncol* (2011) 45:123–8. doi: 10.2478/v10019-011-0014-7
10. Nowak AK, Lake RA, Marzo AL, Scott B, Heath WR, Collins EJ, et al. Induction of tumor cell apoptosis in vivo increases tumor antigen cross-presentation, cross-priming rather than cross-tolerizing host tumor-specific CD8 T cells. *J Immunol (Baltimore Md.: 1950)* (2003) 170:4905–13. doi: 10.4049/jimmunol.170.10.4905
11. Yi-Jun W, Rochelle F, Jian Y, Lin Z. Immunogenic effects of chemotherapy-induced tumor cell death. *Genes Dis* (2018) 5:194–203. doi: 10.1016/j.gendis.2018.05.003
12. Niels H, Sara M, Matthias K, Inka Z, Axel B, Anna S, et al. Localization and density of immune cells in the invasive margin of human colorectal cancer liver metastases are prognostic for response to chemotherapy. *Cancer Res* (2011) 71:5670–7. doi: 10.1158/0008-5472.CAN-11-0268
13. Martins I, Michaud M, Sukkurwala AQ, Adjemian S, Ma Y, Shen S, et al. Premortem autophagy determines the immunogenicity of chemotherapy-induced cancer cell death. *Autophagy* (2012) 8:413–15. doi: 10.4161/auto.19009
14. Zhenyu Z, Elsa S, Michael K. Autophagy, Inflammation, and Immunity: A Troika Governing Cancer and Its Treatment. *Cell* (2016) 166:288–98. doi: 10.1016/j.cell.2016.05.051
15. Ma Y, Galluzzi L, Zitvogel L, Kroemer G. Autophagy and Cellular Immune Responses. *Immunity* (2013) 39:211–27. doi: 10.1016/j.immuni.2013.07.017
16. Kuballa P, Nolte WM, Castoreno AB, Xavier RJ. Autophagy and the immune system. *Annu Rev Immunol* (2012) 30:611–46. doi: 10.1146/annurev-immunol-020711-074948
17. Michaud M, Martins I, Sukkurwala AQ, Adjemian S, Ma Y, Pellegatti P, et al. Autophagy-Dependent Anticancer Immune Responses Induced by Chemotherapeutic Agents in Mice. *Science* (2011) 334:1573–7. doi: 10.1126/science.1208347
18. Michaud M, Xie X, Pedro JMB, Zitvogel L, White E, Kroemer G. An autophagy-dependent anticancer immune response determines the efficacy of melanoma chemotherapy. *OncoImmunology* (2014) 3:e944047. doi: 10.4161/21624011.2014.944047
19. Hernandez C, Huebener P, Schwabe RF. Damage-associated molecular patterns in cancer: a double-edged sword. *Oncogene* (2016) 35:5931–41. doi: 10.1038/onc.2016.104
20. Federico P, Manuel BPJ, Lorenzo G, Guido K. Autophagy in natural and therapy-driven anticancer immunosurveillance. *Autophagy* (2017) 13:2163–70. doi: 10.1080/15548627.2017.1310356
21. van de Ven R, Hilton TL, Hu HM, Dubay CJ, Haley D, Paustian C, et al. Autophagosome-based strategy to monitor apparent tumor-specific CD8 T cells in patients with prostate cancer. *OncoImmunology* (2018) 7:e1466766. doi: 10.1080/2162402X.2018.1466766
22. Shaun M, Dudek-Peric AM, Garg AD, Heleen R, Seyma D, Van Eygen S, et al. An autophagy-driven pathway of ATP secretion supports the aggressive phenotype of $BRAF^{V600E}$ inhibitor-resistant metastatic melanoma cells. *Autophagy* (2017) 13:1512–27. doi: 10.1080/15548627.2017.1332550
23. Fader CM, Aguilera MO, Colombo MI. ATP is released from autophagic vesicles to the extracellular space in a VAMP7-dependent manner. *Autophagy* (2012) 8:1741–56. doi: 10.4161/auto.21858
24. Srivastava RK, Utley A, Shrikant PA. Rapamycin. *OncoImmunology* (2014) 1:1189–90. doi: 10.4161/onci.20663
25. Jung CH, Ro S, Cao J, Otto NM, Kim D. mTOR regulation of autophagy. *FEBS Lett* (2010) 584:1287–95. doi: 10.1016/j.febslet.2010.01.017

26. Chaoul N, Fayolle C, Desrues B, Oberkampf M, Tang A, Ladant D, et al. Rapamycin Impairs Antitumor CD8+ T-cell Responses and Vaccine-Induced Tumor Eradication. *Cancer Res* (2015) 75:3279–91. doi: 10.1158/0008-5472.CAN-15-0454
27. Li Q, Rao R, Vazzana J, Goedegebuure P, Odunsi K, Gillanders W, et al. Regulating Mammalian Target of Rapamycin To Tune Vaccination-Induced CD8. *J Immunol* (2012) 188:3080–7. doi: 10.4049/jimmunol.1103365
28. Sebastian K, Mathias V, van de Roemer N, Mustafa D, Martin L, Jan D, et al. Mutant MHC class II epitopes drive therapeutic immune responses to cancer. *Nature* (2015) 520:692–6. doi: 10.1038/nature14426
29. Cassidy LD, Young AR, Pérez-Mancera PA, Nimmervoll B, Jaulim A, Chen HC, et al. A novel Atg5 -shRNA mouse model enables temporal control of Autophagy in vivo. *Autophagy* (2018) 14:1256–66. doi: 10.1080/15548627.2018.1458172
30. Arbogast F, Arnold J, Hammann P, Kuhn L, Chicher J, Murera D, et al. ATG5 is required for B cell polarization and presentation of particulate antigens. *Autophagy* (2019) 15:280–94. doi: 10.1080/15548627.2018.1516327
31. Pyo J, Yoo S, Ahn H, Nah J, Hong S, Kam T, et al. Overexpression of Atg5 in mice activates autophagy and extends lifespan. *Nat Commun* (2013) 4:604–12. doi: 10.1038/ncomms3300
32. Bohatyrewicz A, Karaczun M, Kotrych D, Ziętek P, Kołodziej Ł, Jurewicz A. Solitary breast cancer metastasis to pelvic bone treated with a unique method of surgery combined with local doxorubicin administration. *Contemp Oncol* (2017) 21:306–10. doi: 10.5114/wo.2017.72402
33. Kishton RJ, Lynn RC, Restifo NP. Strength in Numbers: Identifying Neoantigen Targets for Cancer Immunotherapy. *Cell* (2020) 183:591–3. doi: 10.1016/j.cell.2020.10.011
34. Jiang T, Shi T, Zhang H, Hu J, Song Y, Wei J, et al. Tumor neoantigens: from basic research to clinical applications. *J Hematol Oncol* (2019) 12:263–70. doi: 10.1186/s13045-019-0787-5
35. Sarah C. Neoantigen vaccine proven safe and immunogenic. *Nat Rev Drug Discovery* (2020) 19:838. doi: 10.1038/d41573-020-00194-x
36. Chen H, Yang G, Xiao J, Zheng L, You L, Zhang T. Neoantigen-based immunotherapy in pancreatic ductal adenocarcinoma (PDAC). *Cancer Lett* (2020) 490:12–9. doi: 10.1016/j.canlet.2020.06.011
37. Jiao HX, Lei MX, Li Y, Quan WY, Yong P, Wei WX. Progress in Neoantigen Targeted Cancer Immunotherapies. *Front Cell Dev Biol* (2020) 8:728. doi: 10.3389/fcell.2020.00728
38. Xuhui W, Man L, Kebai R, Chunyu X, Jianping L, Qianwen Y, et al. On-Demand Autophagy Cascade Amplification Nanoparticles Precisely Enhanced Oxaliplatin-Induced Cancer Immunotherapy. *Adv Mat (Deerfield Beach Fla.)* (2020) 32:e2002160. doi: 10.1002/adma.202002160
39. Lancaster EM, David Jablons, Kratz JR. Applications of Next-Generation Sequencing in Neoantigen Prediction and Cancer Vaccine Development. *Genet Test Mol Biomark* (2020) 24:59–66. doi: 10.1089/gtmb.2018.0211
40. Li Q, Ding Z. The Ways of Isolating Neoantigen-Specific T Cells. *Front Oncol* (2020) 10:1347. doi: 10.3389/fonc.2020.01347
41. Sachie H, Emiko N, Hiroko B, Hiroko M, Wataru M, Takako N, et al. Neoantigen prediction in human breast cancer using RNA sequencing data. *Cancer Sci* (2020) 112:465–75. doi: 10.1111/CAS.14720
42. Ariyan CE, Brady MS, Siegelbaum RH, Hu J, Bello DM, Rand J, et al. Robust Antitumor Responses Result from Local Chemotherapy and CTLA-4 Blockade. *Cancer Immunol Res* (2018) 6:189–200. doi: 10.1158/2326-6066.CIR-17-0356
43. ChiPing H, ChunChie W, ChihRong S. Combination of novel intravesical xenogeneic urothelial cell immunotherapy and chemotherapy enhances anti-tumor efficacy in preclinical murine bladder tumor models. *Cancer Immunol Immunother* (2020) 6:1–15. doi: 10.1007/s00262-020-02775-6
44. Davern M, Lysaght J. Cooperation between chemotherapy and immunotherapy in gastroesophageal cancers. *Cancer Lett* (2020) 495:89–99. doi: 10.1016/J.CANLET.2020.09.014
45. Yadong W, Xiaoying Y, Xu T, Ziqi J, Zhongxing B, Lei C, et al. Neoadjuvant immunotherapy plus chemotherapy achieved pathologic complete response in stage IIIB lung adenocarcinoma harbored EGFR G779F: a case report. *Ann Palliat Med* (2020) 9:4339–45. doi: 10.21037/apm-20-1692
46. Wu D, Fan Y, Yan H, Li D, Zhao Z, Chen X, et al. Oxidation-sensitive polymeric nanocarrier-mediated cascade PDT chemotherapy for synergistic cancer therapy and potentiated checkpoint blockade immunotherapy. *Chem Eng J* (2021) 404:126481–. doi: 10.1016/J.CEJ.2020.126481

Conflict of Interest: The authors declare that the research was conducted in the absence of any commercial or financial relationships that could be construed as a potential conflict of interest.

frontiers in Immunology

ORIGINAL RESEARCH
published: 22 April 2021
doi: 10.3389/fimmu.2021.655637

Perillaldehyde Inhibition of cGAS Reduces dsDNA-Induced Interferon Response

Lei Chu[1†], Chenhui Li[1†], Yongxing Li[1], Qiuya Yu[1], Huansha Yu[2], Chunhui Li[1], Wei Meng[1], Juanjuan Zhu[1], Quanyi Wang[1], Chen Wang[1] and Shufang Cui[1*]*

[1] State Key Laboratory of Natural Medicines, School of Life Science and Technology, China Pharmaceutical University, Nanjing, China, [2] Experimental Animal Center, Shanghai Pulmonary Hospital, Tongji University School of Medicine, Shanghai, China

Cyclic GMP-AMP synthase (cGAS), serving as a primary sensor of intracellular DNA, is essential to initiate anti-microbial innate immunity. Inappropriate activation of cGAS by self-DNA promotes severe autoinflammatory diseases such as Aicardi–Goutières syndrome (AGS); thus, inhibition of cGAS may provide therapeutic benefit in anti-autoimmunity. Here we report that perillaldehyde (PAH), a natural monoterpenoid compound derived from *Perilla frutescens*, suppresses cytosolic-DNA-induced innate immune responses by inhibiting cGAS activity. Mice treated with PAH are more susceptible to herpes simplex virus type 1 (HSV-1) infection. Moreover, administration with PAH markedly ameliorates self-DNA-induced autoinflammatory responses in a mouse model of AGS. Collectively, our study reveals that PAH can effectively inhibit cGAS-STING signaling and could be developed toward the treatment of cGAS-mediated autoimmune diseases.

Keywords: cyclic GMP-AMP synthase (cGAS), perillaldehyde, herpes simplex virus type 1 (HSV-1), innate immunity, autoimmune disease

OPEN ACCESS

Edited by:
Yan-feng Gao,
Sun Yat-sen University, China

Reviewed by:
Chunfu Zheng,
Fujian Medical University, China
Xiaohuan Guo,
Tsinghua University, China

***Correspondence:**
Chen Wang
cwang1971@cpu.edu.cn
Shufang Cui
sfcui@cpu.edu.cn

[†]These authors have contributed equally to this work

Specialty section:
This article was submitted to Cancer Immunity and Immunotherapy, a section of the journal Frontiers in Immunology

Received: *19 January 2021*
Accepted: *24 March 2021*
Published: *22 April 2021*

Citation:
Chu L, Li C, Li Y, Yu Q, Yu H, Li C, Meng W, Zhu J, Wang Q, Wang C and Cui S (2021) Perillaldehyde Inhibition of cGAS Reduces dsDNA-Induced Interferon Response. Front. Immunol. 12:655637. doi: 10.3389/fimmu.2021.655637

INTRODUCTION

The innate immune system is initiated as the front-line defense against microbes or damaged self-component *via* germline-encoded pattern-recognition receptors (PRRs) (1). cGAS is a key intracellular DNA sensor that catalyzes the conversion of GTP and ATP to cyclic GMP-AMP (2′3′-cGAMP), which serves as a second messenger to bind and activate the endoplasmic adaptor protein stimulator of interferon genes (STING) (2, 3). cGAMP binding induces a conformation change and trafficking of STING, which activates the downstream effectors TANK-binding kinase 1 (TBK1) and interferon regulatory factor 3 (IRF3). Subsequently, phosphorylated IRF3 dimerizes and translocates into the nucleus to produce type I interferon (IFN) and other proinflammatory cytokines (4–6).

While detection of foreign DNA plays an indispensable role in pathogen defense, aberrant activation of cGAS by self-DNA can promote severe autoimmune diseases. Trex1 is a DNA 3′ repair exonuclease that degrades cytosolic DNA, and deficiency of Trex1 leads to the accumulation of cytosolic DNA (7, 8). Loss-of-function mutations in *Trex1* have been identified in autoimmune disorders such as Aicardi–Goutières syndrome (AGS) and familial chilblain lupus in human patients (9, 10). *Trex1*$^{-/-}$ mice develop the severe early onset systemic autoinflammatory disease with a short lifespan of 2–3 months (8).

Deletion of *Cgas* is sufficient to suppress the autoimmune disease phenotype in the *Trex1*$^{-/-}$ mouse model of AGS (11). In addition, increased cGAS mRNA levels and production of cGAMP have been observed in Systemic Lupus Erythematosus (SLE) patients, indicating that cGAS-STING signaling is also involved in a subset of SLE patients. These observations together demonstrate the importance of cGAS inhibition in treating cGAS-mediated autoimmunity and that cGAS may be a potential drug target for preventing autoinflammation.

Natural products have long been valuable resources for discovering and developing novel molecules to treat various human diseases (12). *Perilla frutescens* has been used as an ingredient in Chinese herbal medicine. By suppressing proinflammatory cytokines and inducing anti-inflammatory cytokines, *Perilla frutescens* leaf extract effectively ameliorates dextran sulfate sodium (DSS)-induced colitis (13). Volatile monoterpenoid Perillaldehyde (PAH), the major component and the most effective ingredient of *Perilla frutescens* leaf (14), is biologically active and exhibits anti-inflammatory (13, 15, 16), antifungal activity (17, 18), antioxidant (19), and anti-tumor effects (20, 21). Despite the multi-functionality of PAH, the effect of PAH in innate immunity has not been characterized well. In this study, we report that PAH specifically impairs the cytosolic DNA-induced innate signaling and inflammatory responses by inhibiting the activity of cGAS. PAH suppresses type I IFN and IFN stimulated gene (ISGs) expression triggered by HT-DNA but not poly(I:C) or cGAMP. Mice treated with PAH are more susceptible to herpes simplex virus type 1 (HSV-1) infection. Furthermore, PAH administration alleviates autoinflammatory responses in *Trex1*$^{-/-}$ bone marrow-derived macrophages (BMDMs) and the autoimmune disorder in *Trex1*$^{-/-}$ mice.

MATERIALS AND METHODS

Mice

Trex1$^{+/-}$ mice were kindly licensed by Dr. Tomas Lindahl and Dr. Deborah Barnes (Cancer Research UK, London) and provided by Dr. Nan Yan (University of Texas Southwestern Medical Center). *Trex1*$^{-/-}$ mice were generated by further mating the male and female *Trex1*$^{+/-}$ mice and were genotyped by standard PCR. All mice used in this study were on C57BL/6 background. 4 weeks old *Trex1*$^{-/-}$ mice were started to drug administration. All mice were maintained under specific pathogen-free (SPF) circumstances at the Center for New Drug Safety Evaluation and Research, China Pharmaceutical University. All animal works were carried out following the National Institutes of Health Guide for the Care and Use of Laboratory Animals.

Cell Culture and Transfection

MEF, HFF, and Vero cells were cultured in DMEM medium (Invitrogen), supplemented with 10% FBS (Gibco) and 1% penicillin–streptomycin (Invitrogen). L929 cells and BMDMs were cultured in RMPI-1640 (Gibco) plus 10% FBS and 1% penicillin–streptomycin. BMDMs were generated as previously reported (22). All cells were cultured at 37°C and 5% CO_2. Lipofectamine 3000 (Invitrogen) was used for transfection according to the manufacture's procedure. cGAMP stimulation was performed with a permeabilization buffer (50 mM HEPES pH 7, 100 mM KCl, 3 mM $MgCl_2$, 0.1 mM DTT, 85 mM sucrose, 0.2% BSA, 1 mM ATP, and 0.1 mM GTP with 10 $\mu g \cdot ml^{-1}$ digitonin (Sigma-Aldrich)) at 37°C for 30 min, followed by replacing with fresh medium.

Virus

HSV-1, GFP-HSV-1, VSV, and GFP-VSV were propagated and titrated by standard plaque assay on Vero cells.

Reagents and Antibodies

PAH, CMC-Na, Poly(I:C), and HT-DNA were purchased from Sigma-Aldrich. cGAMP was obtained from Invivogen. ISD was prepared by annealing equimolar amounts of sense and antisense DNA oligonucleotides at 95°C for 10 min, then cooled to room temperature. Antibodies: anti-IRF3 (CST, #4302), anti-Phospho-IRF3 (CST, #4947), anti-TBK1 (Abcam, ab40676), anti-Phospho-TBK1 (CST, #5483), anti-cGAS (CST, #31659), anti-STING (CST, #13647), anti-RIG-I (CST, #4200), anti-MAVS (CST, #4983), anti-Histone H3 (CST, #4499), anti-GAPDH (Santa Cruz, sc-32233), anti-ISG15 (Santa Cruz, sc-166755), anti-Rabbit IgG (H+L) (Jackson, 111-035-003), anti-Mouse IgG (H+L) (Jackson, 115-035-003).

Western Blot Analysis

Cell pellets were collected and lysed with lysis buffer (50 mM Tris-HCl pH 7.5, 150 mM NaCl, 1% Triton X-100) containing 1× EDTA-Free Protease inhibitor cocktail (Roche) and 1 mM PMSF (Sigma-Aldrich). The resuspended cell pellets were incubated on ice for 30 min, followed by centrifugation at 12,000 rpm for 15 min at 4°C. The supernatants were collected for SDS-PAGE. The bands were probed with indicated primary and secondary antibodies and visualized using a SuperSignal West Pico chemiluminescence ECL kit (Pierce).

The native PAGE assay was performed as described previously (23). Briefly, cell pellets were lysed with native lysis buffer (50 mM Tris-HCl pH 7.5, 150 mM NaCl, 1% NP-40, 1× EDTA-Free Protease inhibitor cocktail, 1 mM PMSF, and 1mM orthovanadate). The resuspended cell pellets were incubated on ice for 30 min followed by centrifugation at 12,000 rpm for 15 min at 4°C. The supernatants were collected for native sample preparation. After pre-run in the electrophoresis buffer (25 mM Tris-HCl, pH 8.4, 192 mM glycine with and without 0.2% deoxycholate in the cathode and anode chamber, respectively), native samples were loaded to gel and electrophorese for 60 min at 25 mA. Then the gel was soaked into 0.1% SDS-containing electrophoresis buffer for 30 min at room temperature, followed by standard immunoblot analysis.

For subcellular fraction assay, cell pellets were lysed with buffer A (10 mM HEPES pH 7.9, 1.5 mM $MgCl_2$, 1 mM KCl, 0.5 mM DTT, and 1 mM PMSF), then 0.2% NP-40 was added after incubation on ice for 15 min. The supernatants were collected as the cytoplasmic fraction after centrifugation for 5 min at 4,000 rpm. The pellets were washed twice with buffer A and then resuspended with buffer C (20 mM HEPES, pH 7.9, 25% glycerol, 0.42 M sodium chloride, 1.5 mM $MgCl_2$, 0.2 mM

EDTA, 0.5 mM DTT, and 2 mM PMSF). After incubation on ice for 0.5–2 h, the supernatants were collected as the nucleic fraction by centrifugation for 15 min at 12,000 rpm. The cytoplasmic and nucleic fractions were analyzed by standard immunoblot analysis.

Immunofluorescence and Confocal Microscopy

Cells were fixed for 15 min with 4% paraformaldehyde in PBS, washed with PBS, and permeabilized with 0.25% Triton X-100 in PBS for 20 min, then washed and blocked with 5% BSA for 1 h. After incubation with indicated primary antibodies overnight at 4°C, fluorescent-conjugated secondary antibodies were incubated for 2 h at room temperature. Slides were mounted with a fluorescent mounting medium (Dako) after DAPI (Sigma-Aldrich) staining and captured using a confocal microscope (LSM800, Carl Zeiss) with a 63× oil objective.

RNA Isolation and Quantitative PCR Analysis

Total RNA from cells was isolated with TRIzol reagent (Invitrogen) according to the manufacturer's instruction. cDNA was synthesized with 0.5 μg RNA and HiScript III Q RT SuperMix for qPCR (Vazyme). Real-time PCR was performed using ChamQ SYBR qPCR Master Mix (Low ROX Premixed) (Vazyme). Data were normalized to the expression of mouse *Gapdh* or human *GAPDH* through the comparative Ct method ($2^{-\triangle\triangle Ct}$).

MTS Assay

According to the manufacturer's instructions, cell viability was measured by CellTiter 96 AQueous One Solution Cell Proliferation Assay (MTS) kit (Promega).

ALT and AST Analysis

The levels of aspartate aminotransferase (AST) and alanine aminotransferase (ALT) in serum were measured by Siemens Dimension® Xpand Plus™ biochemical autoanalyzer.

Detection of Autoantibodies

The hearts from WT mice were lysated in RIPA lysis buffer. The protein extractions were separated by SDS-PAGE and transferred to PVDF membrane, and then incubated with 1:200 dilution of serum overnight at 4°C. Autoantibodies were detected with horseradish peroxidase conjugated anti-mouse IgG.

Enzyme-Linked Immunosorbent Assay

Concentrations of the cytokines in culture supernatants or serum were measured by ELISA kit (4A Biotech, CME0116) according to the manufacturer's instructions.

Hematoxylin and Eosin

Tissues were fixed in 4% paraformaldehyde, paraffin-embedded, cut into 5 mm sections, and stained with hematoxylin and eosin.

Viral Infection

Viral infection assays were executed as described in the figures. Briefly, 8–12 weeks old WT C57BL/6 mice (16–22 g, initially) were orally administered with vehicle (0.03% CMC-Na solution) or PAH at 120 $mg{\bullet}kg^{-1}$ body weight once per day for up to 2 weeks. The body weight of each mouse was measured daily. The mice were injected intravenously with HSV-1 for 12 h after PAH administration. Then the serum and tissues were collected for analysis of RNA and cytokines. For a durable anti-infection study, HSV-1-infected mice were monitored for another 7 days with drug administration. Meanwhile, the body weight of each mouse was measured daily.

Flow Cytometry

L929 cells seeded in 12-well plates were treated with vehicle or PAH (200 μM) for 6 h, and then infected with GFP-HSV-1 (MOI = 0.3) or GFP-VSV (MOI = 0.4) for 16 h. Cell populations were suspended in PBS buffer after trypsin digestion. Then, the ratios of GFP-positive cells were analyzed by flow cytometry (Attune NxT Flow Cytometer; Thermo Fisher Scientific). In flow cytometry gating, cells were first gated for single cells (forward scatter area *versus* side scatter area) and further analyzed for their GFP expression. The results were analyzed by FlowJo.

Plaque Assay

The titers of the virus in the supernatant were determined by standard plaque assay with Vero cells. After infection with virus-contained supernatant for 2 h, cell monolayers were washed twice with pre-warmed DMEM medium, followed by incubation with a mixed media (1× MEM, 2% FBS, 1% Low Melting Point Agarose) until the formation of the plaques. Then the cells were fixed with 4% paraformaldehyde and stained with crystal violet. The titers of the virus were measured by counting the plaques.

cGAS Enzymatic Activity Assay *In Vitro*

cGAS activity was analyzed as described previously (24). The enzymatic activity of cGAS was measured with purified recombinant full-length cGAS in 100 μl reaction buffer (2 mM cGAS, 0.2 mM ATP, 0.2 mM GTP, 100 mM NaCl, 40 mM Tris-HCl pH 7.5, 1 mM $MgCl_2$ and 0.01 $mg{\bullet}ml^{-1}$ dsDNA). Then the reaction buffer was heated at 99°C to denature proteins. After centrifugation at 12,000 g for 10 min, the supernatants were collected and extracted with ACQUITYUPLC® BEH Amide Colum, which was previously equilibrated with running buffer (1% Formic acid solution). All samples were analyzed using a Waters XEVO® TQD system (Waters Corp.) equipped with electrospray ionization (ESI).

Statistical Analyses

Statistical analyses were performed with GraphPad Prism 8. A standard two-tailed unpaired Student's t-test was performed for statistical analyses of two groups or as indicated in the figure legends. All analyzed data are expressed as mean ± standard deviation (SD). Differences with a P-value <0.05 were considered significant.

RESULTS

PAH Inhibits Cytosolic DNA-Triggered Type I IFN Production

To exclude the potential cytotoxicity effect of PAH on the innate immune system, we first determined the *in vitro* cytotoxicity of

PAH on different cells. Two murine cell lines, L929 (murine fibrosarcoma cells) and MEF (mouse embryonic fibroblasts) and one human cell line HFF (human foreskin fibroblasts), were incubated with different doses of PAH for 24 h, and then the cell viability was quantified by MTS assay. There was no significant cytotoxic side effect for L929, MEF, and HFF at the dose of 500, 250, and 200 μM, respectively (**Figure 1A**). Next, we incubated L929 cells with 300 μM PAH and measured the induction of type I IFNs and downstream genes upon various stimuli. PAH markedly inhibited the IRF3-responsive genes (*Ifnb*, *Ifna4*, and *Cxcl10*) expression stimulated by DNA mimics ISD or HT-DNA (herring testis DNA), whereas did not affect these antiviral genes expression triggered by poly(I:C) (a ligand of RNA sensor) or cGAMP (2′3′-cGAMP, a ligand that directly activates STING) (**Figure 1B**).

To substantiate the specific inhibitory effect of PAH on cytosolic DNA-induced type I IFN expression, we incubated L929, MEF, and HFF cells with different doses of PAH. As expected, PAH crippled intracellular DNA-induced IRF3-responsive gene expression in a dose-dependent manner in all three cell lines (**Figures 1C–E**). Consistently, PAH markedly decreased the induction of the same set of genes triggered by HSV-1 in these cell lines (**Figure 1F**). The inhibitory activity of PAH on DNA-induced type I IFN production was not the result of cytotoxicity, as PAH had no effect on the cell viability at the used dosage. Collectively, these data suggest that PAH is a specific inhibitor of the DNA-sensing signaling pathway.

PAH Directly Inhibits cGAS Activity

As cGAS is the primary intracellular DNA sensor, we suspected that PAH inhibited the DNA-sensing pathway by targeting cGAS. We obtained *Cgas*-deficient L929 cells *via* CRISPR-Cas9-mediated targeting to test whether PAH suppressed cGAS-mediated DNA-sensing signaling. Administration of PAH impaired the DNA-induced antiviral gene expression in WT L929, whereas such inhibitory effect vanished in *Cgas*-deficient L929 cells (**Figure 2A**), indicating the inhibition of the DNA-sensing pathway by PAH required the presence of cGAS.

Next, we tested whether PAH regulated the protein levels of cGAS and other essential components for the host's innate defense against viruses. As illustrated in **Figure 2B**, PAH did not affect the endogenous protein levels of cGAS and other molecules involved in cGAS-STING/RIG-MAVS signaling, suggesting the inhibitory effect of PAH on the DNA-sensing pathway to be a consequence of impaired cGAS enzyme activity. We performed *in vitro* dose-titration experiments with recombinant human cGAS and measured cGAMP production using HPLC-MS to test this hypothesis (**Figure 2C**). As expected, PAH effectively inhibited cGAMP production with a biochemical IC_{50} (half maximal inhibitory concentration) value of 31.3 μM (**Figure 2C**). To further determine the physiological inhibition of PAH on cGAS-mediated signaling, we performed concentration–response analysis in different mouse and human cell lines. As determined by RT-qPCR, PAH showed dose-dependent inhibition on the *Ifnb*/*IFNB* expression with cellular IC_{50} of 151.6 ± 8.9 μM for L929, 40.3 ± 2.93 μM for MEF, and 55.79 ± 3.25 μM for HFF cells (**Figure 2D**). Altogether, these data indicate that PAH suppresses DNA-induced type I IFN signaling by directly inhibiting the enzymatic activity of cGAS.

PAH Suppresses cGAS-Mediated Innate Immune Response

Upon sensing intracellular DNA, cGAS initiates a series of downstream signaling transduction events, including TBK1 phosphorylation and IRF3 phosphorylation/dimerization, critical for inducing the antiviral type I IFN responses. To explore whether PAH inhibited the activation of cGAS-mediated innate immune signaling, we checked the impact of PAH on these phenomena. Compared with the control group, PAH markedly attenuated the phosphorylation of TBK1 and IRF3 when stimulated with HT-DNA (**Figure 3A**). Likewise, native western blotting revealed that the dimerization of IRF3 was greatly impaired by PAH treatment (**Figure 3A**). In contrast, PAH had no or marginal effect on these processes when treated with poly(I:C) (**Figure 3B**) or cGAMP (**Figure 3C**), indicating PAH specifically suppressed DNA-induced downstream signaling transduction by targeting cGAS.

Next, we performed subcellular fractionation analysis to test whether PAH inhibited the nuclear translocation of IRF3. Consistent with the phosphorylation and dimerization results, PAH considerably decreased the nuclear translocation of IRF3. (**Figures 3D, E**). Confocal microscopy also revealed that PAH markedly suppressed HT-DNA-induced IRF3 nuclear translocation, whereas it did not affect that when stimulated with poly(I:C) (**Figures 3F, G**). Altogether, these data establish that PAH specifically inhibits the cGAS-mediated innate immune response.

PAH Restricts the Host Innate Antiviral Defense *In Vitro*

As IFN-β protects host cells against virus infection, we detected the secretion of IFN-β in cell supernatant *via* ELISA. Compared with the control group, PAH suppressed the IFN-β secretion in a dose-dependent manner upon stimulated with HT-DNA (**Figure S1**) or HSV-1 (**Figure 4A**). L929 cells were pre-incubated with PAH and then infected with HSV-1 to explore whether PAH impaired the host innate defense against HSV-1. As expected, L929 cells incubated with PAH were more susceptible to HSV-1 infection as determined by the crystal violet staining assay (**Figures 4B, C**). Consistently, PAH administration increased the titer of HSV-1 virus as quantified by the standard plaque assay (**Figure 4D**).

Moreover, we challenged L929 cells with GFP-HSV-1 virus to detect viral replication by fluorescence microscopy. Compared with the control group, treatment of PAH markedly impaired host defense against GFP-HSV-1 virus infection, as shown by the stronger GFP-positive signal and an increased number of the GFP-positive cells (**Figure 4E**). Consistently, FACS results also showed that treatment with PAH led to an increased number of GFP-positive cells (**Figures 4F, G**). Unexpectedly, PAH, to some extent, inhibited the host defense against VSV infection (**Figures S2A–F**), perhaps partially due to the protective role of cGAS in RNA virus infection (25, 26). These data reveal that PAH impairs

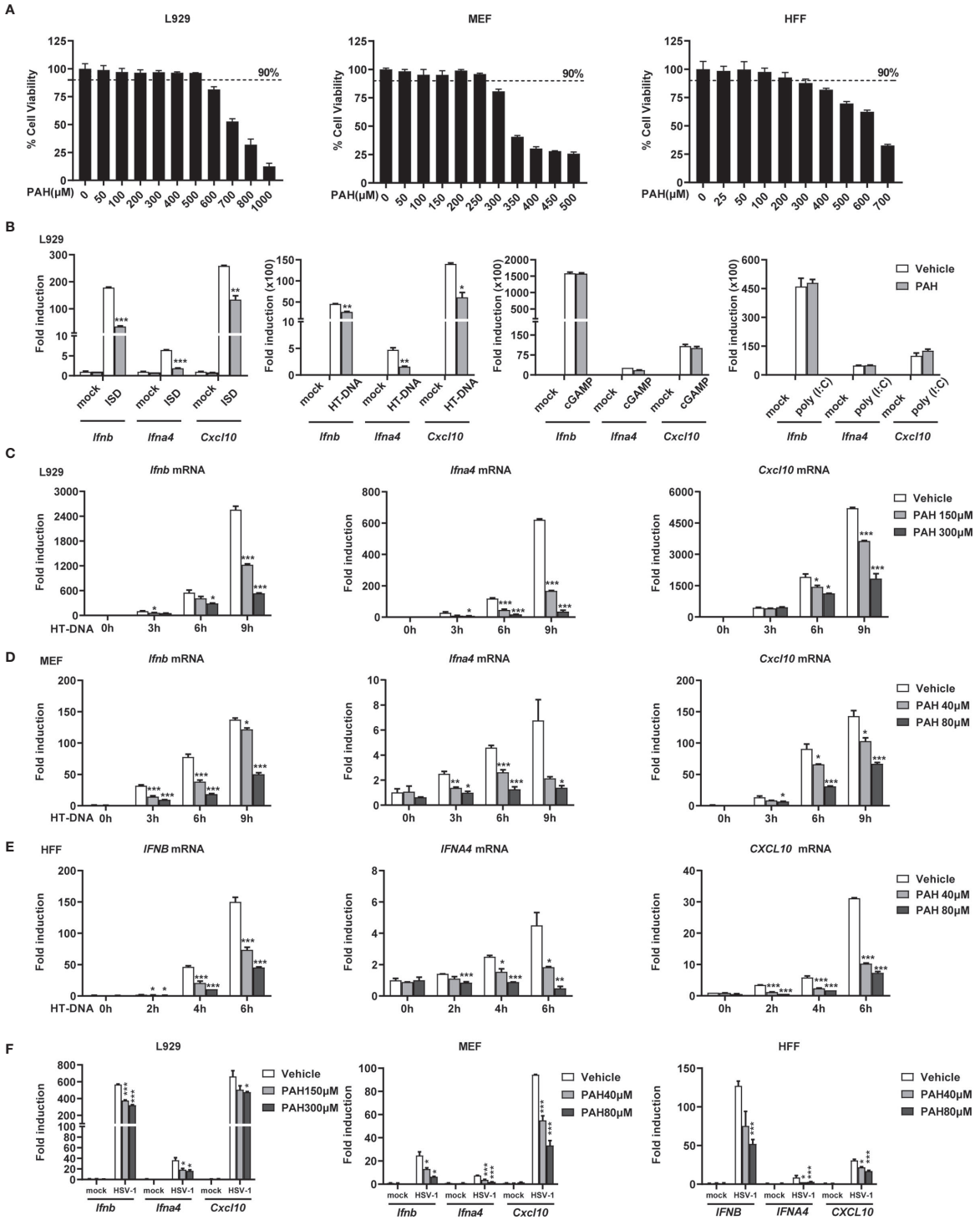

FIGURE 1 | PAH inhibits cytosolic DNA-triggered type I IFNs production. **(A)** L929, MEF, and HFF cells were treated with indicated PAH concentrations for 24 h, and then the cell proliferation was measured by MTS assay. **(B)** L929 cells were treated with Vehicle or PAH (300 μM) for 6 h and then stimulated with ISD (4 μg•ml^{-1}), HT-DNA (4 μg•ml^{-1}), cGAMP (1 μg•ml^{-1}), or poly(I:C) (3 μg•ml^{-1}). The induction of *Ifnb*, *Ifna4*, and *Cxcl10* mRNA expression was then measured by qPCR. **(C–E)** L929 **(C)**, MEF **(D)**, or HFF **(E)** cells were treated with Vehicle or PAH for 6 h and then stimulated with HT-DNA (4 μg•ml^{-1}) for the indicated times. The induction of *Ifnb*, *Ifna4*, and *Cxcl10* mRNA expression was then measured by qPCR. **(F)** L929, MEF, or HFF cells were treated with Vehicle or PAH for 6 h and then infected with HSV-1 (MOI = 1) for 6 h (L929 and MEF) or 3 h (HFF). The induction of *Ifnb*, *Ifna4*, and *Cxcl10* mRNA expression was then measured by qPCR. All of the experiments were repeated at least three times. Data in **(A–F)** are presented as mean ± SD. *$P < 0.05$, **$P < 0.01$, ***$P < 0.001$.

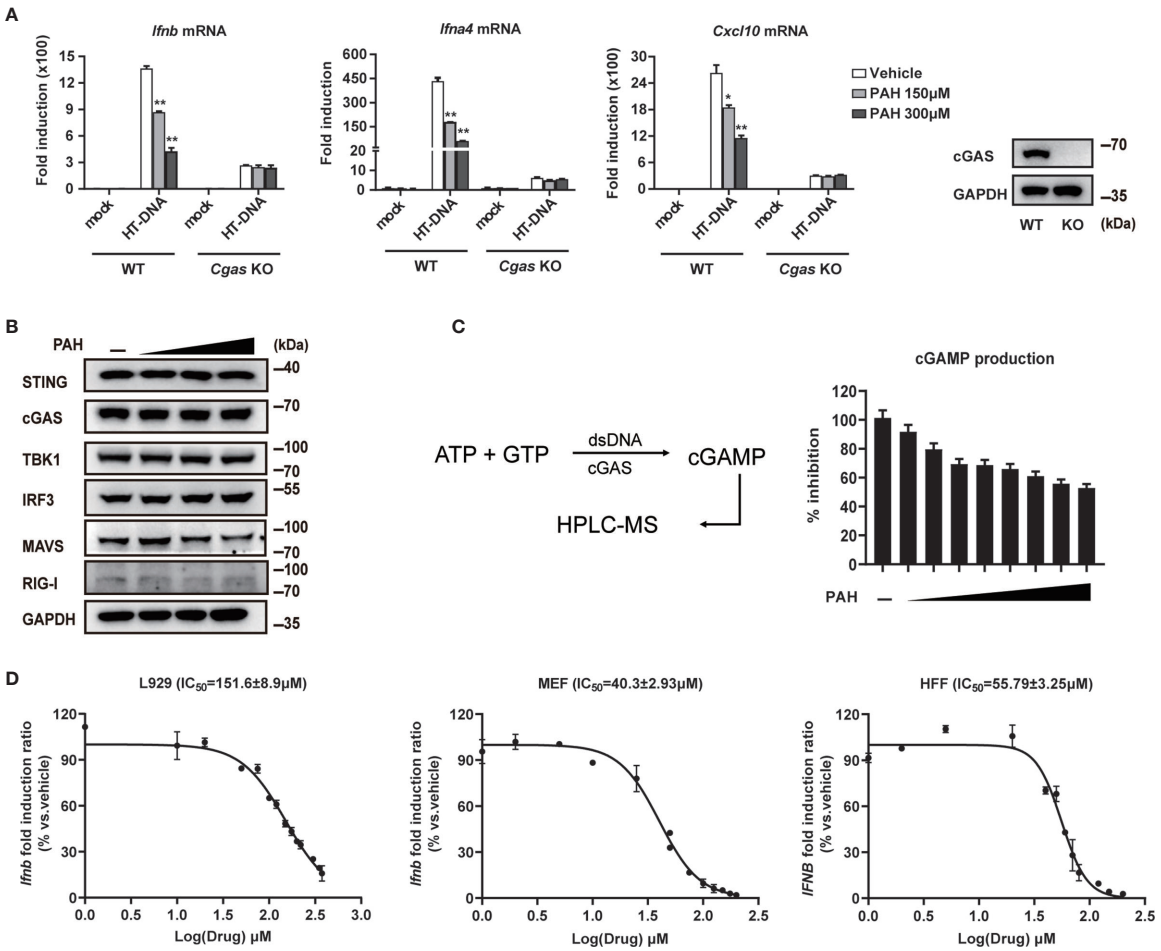

FIGURE 2 | PAH directly inhibits cGAS activity. **(A)** WT or *Cgas*-deficient L929 cells were treated with Vehicle or PAH for 6 h and then stimulated with HT-DNA (4 μg•ml^{-1}) for 6 h. The induction of *Ifnb*, *Ifna4*, and *Cxcl10* mRNA expression was then measured by qPCR (left panel). The cGAS protein levels were examined by immunoblot (right panel). **(B)** L929 cells were treated with a Vehicle or different PAH doses (0 to 300 μM) for 6 h, and then the cell lysates were immunoblotted with the indicated antibodies. **(C)** Schematic of dsDNA-dependent cGAS synthesis of cGAMP and measurement by HPLC-MS (left panel). The cGAMP production was measured in the presence of a Vehicle or different PAH doses (0 to 40 μM) (right panel). **(D)** L929, MEF, and HFF cells were treated with indicated concentrations of PAH for 6 h, followed by stimulation with HT-DNA for 6 h. The induction of *Ifnb* mRNA expression was then measured by qPCR. All of the experiments were repeated at least three times. Data in **(A, C, D)** are presented as mean ± SD. $^{*}P < 0.05$, $^{**}P < 0.01$.

the host innate defense against viruses by dampening IFN-I signaling *in vitro*.

PAH Restricts the Host Innate Defense Against HSV-1 Infection *In Vivo*

The 8–12 weeks old WT mice were pretreated with PAH according to the previous research to explore the potential role of PAH on host defense against viral infection *in vivo* (15). Briefly, mice were orally administered with PAH or Vehicle (0.03% CMC-Na solution) at 120 mg•kg^{-1} body weight once per day for 2 weeks, followed by HSV-1 infection *via* tail vein injection (i.v.) for 12 h. Notably, PAH administration did not affect the mice's body weight (**Figure 5A**). In addition, pretreatment with PAH for two weeks did not change the basal levels of serum aspartate aminotransferase (AST) as well as alanine aminotransferase (ALT) (**Figure 5B**), suggesting the safety and lack of *in vivo* toxicity for PAH under the used dosage. Next, we examined the production of IFN-β *in vivo*. Compared with the infected control mice, mice treated with PAH showed a more severe defect in serum IFN-β production after HSV-1 infection (**Figure 5C**). Consistently, the mRNA levels of *Ifnb* and ISGs (*Cxcl10*, *Isg15*, and *Isg56*) were severely crippled in the hearts and spleens of infected PAH-treated mice, as compared with the infected control mice (**Figures 5D, E**). It's noteworthy that pretreatment with PAH did not affect the basal levels of serum IFN-β and the basal ISG mRNA levels of the hearts and spleens (**Figures S3A–C**), revealing that PAH did not change the *in vivo* immune circumstance.

Furthermore, we studied the durable anti-infection effect of PAH *in vivo*. Mice were pretreated with PAH as described above,

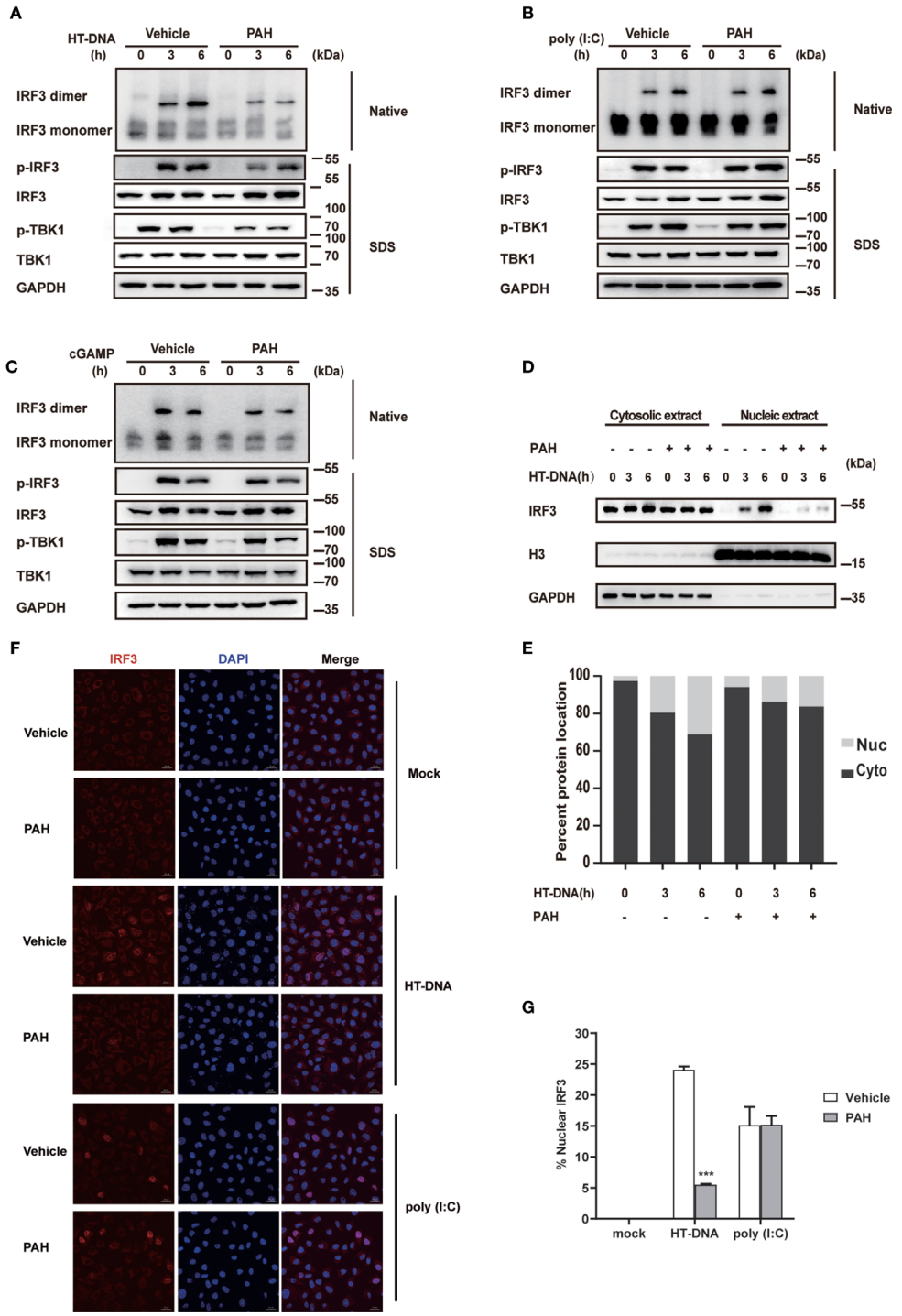

FIGURE 3 | PAH suppresses cGAS-mediated innate immune response. **(A–C)** L929 cells were treated with Vehicle or PAH (200 μM) for 6 h and then stimulated with HT-DNA (4 μg•ml^{-1}) **(A)**, poly(I:C) (3 μg•ml^{-1}) **(B)**, or cGAMP (1 μg•ml^{-1}) **(C)** for the indicated times. The cell extracts were analyzed for TBK1 and IRF3 phosphorylation by SDS-PAGE or IRF3 dimerization by native PAGE. **(D, E)** L929 cells were treated with Vehicle or PAH (200 μM) for 6 h and then stimulated with HT-DNA (4 μg•ml^{-1}) for the indicated times. The IRF3 protein levels in cytoplasmic (Cyto) and nuclear (Nuc) fractions were analyzed by immunoblot **(D)**. The relative ratio of indicated proteins in Cyto and Nuc was analyzed by Image J **(E)**. **(F)** L929 cells were treated with Vehicle or PAH (200 μM) for 6 h, and then stimulated with HT-DNA (4 μg•ml^{-1}) or poly(I:C) (3 μg•ml^{-1}) for 4 h before staining with an antibody against IRF3 (red) and imaged by confocal microscopy. Scale bars represent 10 μm. **(G)** The relative ratio of nuclear IRF3 from **(F)** was analyzed by Image J. All of the experiments were repeated at least three times. Data in **(G)** are presented as mean ± SD. ***$p < 0.001$.

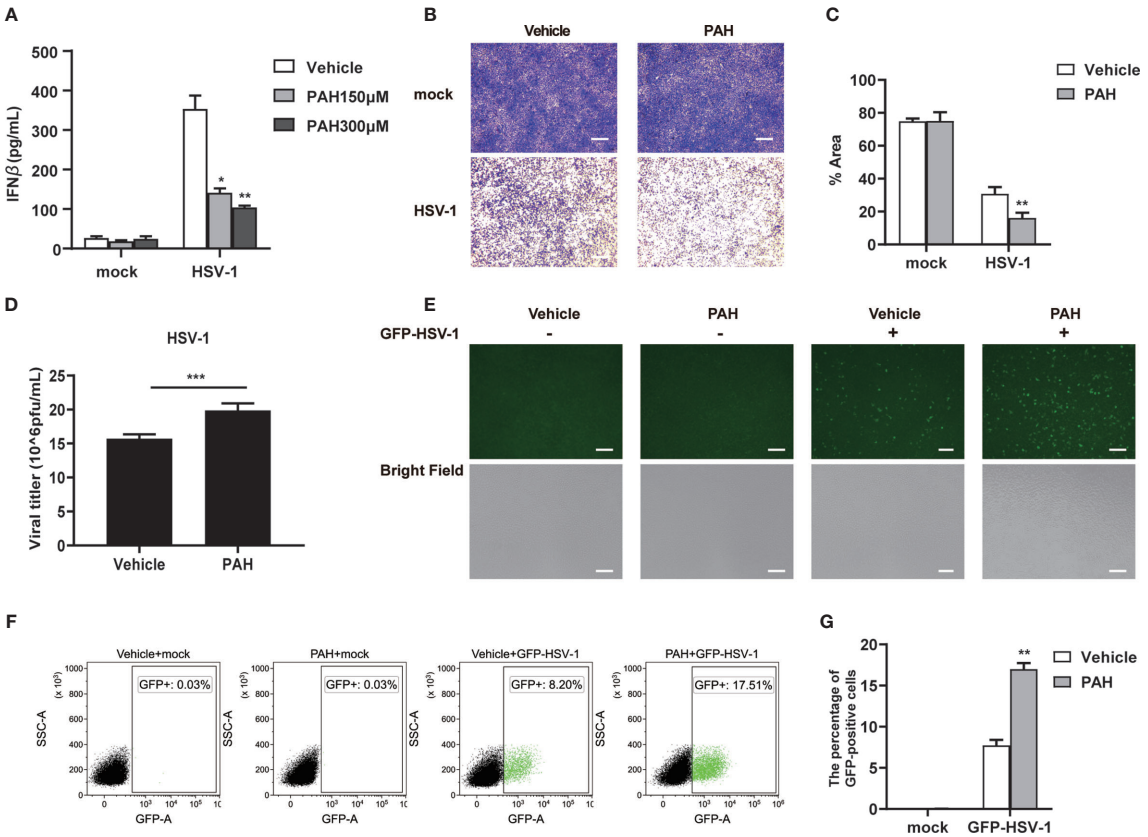

FIGURE 4 | PAH restricts the host innate defense against HSV-1 *in vitro*. **(A)** L929 cells were treated with Vehicle or indicated PAH concentrations for 6 h and then stimulated with HSV-1 (MOI = 1) for 9 h. The supernatants were collected, and ELISA determined the amounts of IFN-*β*. **(B)** L929 cells were treated with Vehicle or PAH (200 μM) for 6 h and then infected with HSV-1 (MOI = 1). The proliferation of cells was examined by crystal violet staining. Scale bars represent 100 μm. **(C)** The statistical analysis of stained cell ratios from **(B)**. **(D)** L929 cells were treated with Vehicle or PAH (200 μM) for 6 h and then infected with HSV-1 (MOI = 1). The titers of HSV-1 were determined by standard plaque assay. **(E)** L929 cells were treated with Vehicle or PAH (200 μM) for 6 h and then infected with GFP-HSV-1 (MOI = 0.3) for 16 h. GFP-HSV-1 replication was visualized by fluorescence microscopy. Scale bars represent 100 μm. **(F)** L929 cells were treated with Vehicle or PAH (200 μM) for 6 h and then infected with GFP-HSV-1 (MOI = 0.3) for 16 h. GFP-HSV-1 replication was visualized by flow cytometry. **(G)** The statistical analysis of GFP-positive cell ratios from **(F)**. All of the experiments were repeated at least three times. Data in **(A, C, D, G)** are presented as mean ± SD. **P*< 0.05, ***P*< 0.01, ****P*< 0.001.

followed by infection with HSV-1. Each mouse's body weight was measured daily for another 7 days with drug administration (**Figure 5F**). There was no significant difference between PAH-treated mice's body weight and that of control mice (**Figures 5G, H**), suggesting PAH itself had no *in vivo* toxicity. In comparison, infection with HSV-1 markedly decreased the body weight of Vehicle group mice. Moreover, treatment with PAH exacerbated the body weight loss after infection with the HSV-1 virus (**Figures 5G, H**). Altogether, these data suggest that PAH suppresses the host defense against HSV-1 infection *in vivo*.

PAH Inhibits cGAS-Mediated Autoimmunity in Mice

Abnormal activation of cGAS by self-DNA is linked to severe autoimmune diseases such as AGS, and inhibition of cGAS provides a powerful therapeutic strategy. As *Trex1*$^{-/-}$ mice are a tractable model to study AGS disease, we investigated whether PAH could be utilized to treat the autoimmune phenotype in *Trex1*$^{-/-}$ mice. First, we incubated BMDMs with different doses of PAH. Compared with BMDMs from WT mice, *Trex1*$^{-/-}$ BMDMs exhibited an aberrant upregulation of the ISG15 protein levels and the phosphorylation levels of IRF3 and TBK1 (**Figure 6A**). Administration of PAH decreased the levels of ISG15 protein and that of IRF3/TBK1 phosphorylation in a dose-dependent manner in *Trex1*$^{-/-}$ BMDMs (**Figure 6A**). Likewise, PAH effectively decreased self-DNA-induced expression of *Ifnb* and a panel of ISGs gene (*Cxcl10*, *Isg15*, *Isg56*, *Ifit2*, *Ifit3*, and *Ifi44*) in *Trex1*$^{-/-}$ BMDMs (**Figure 6B**).

To explore the potential therapeutic effect of PAH in cGAS-mediated autoimmune disease *in vivo*, 4 weeks old *Trex1*$^{-/-}$ mice were started to drug administration for up to 2 weeks as previously described (**Figure 6C**). Two weeks of treatment with PAH had no effect on the bodyweight of *Trex1*$^{-/-}$ mice (**Figures S4A**, **B**), revealing the *in vivo* safety of PAH in *Trex1*$^{-/-}$ mice. Then we examined the effects of PAH on the expression of

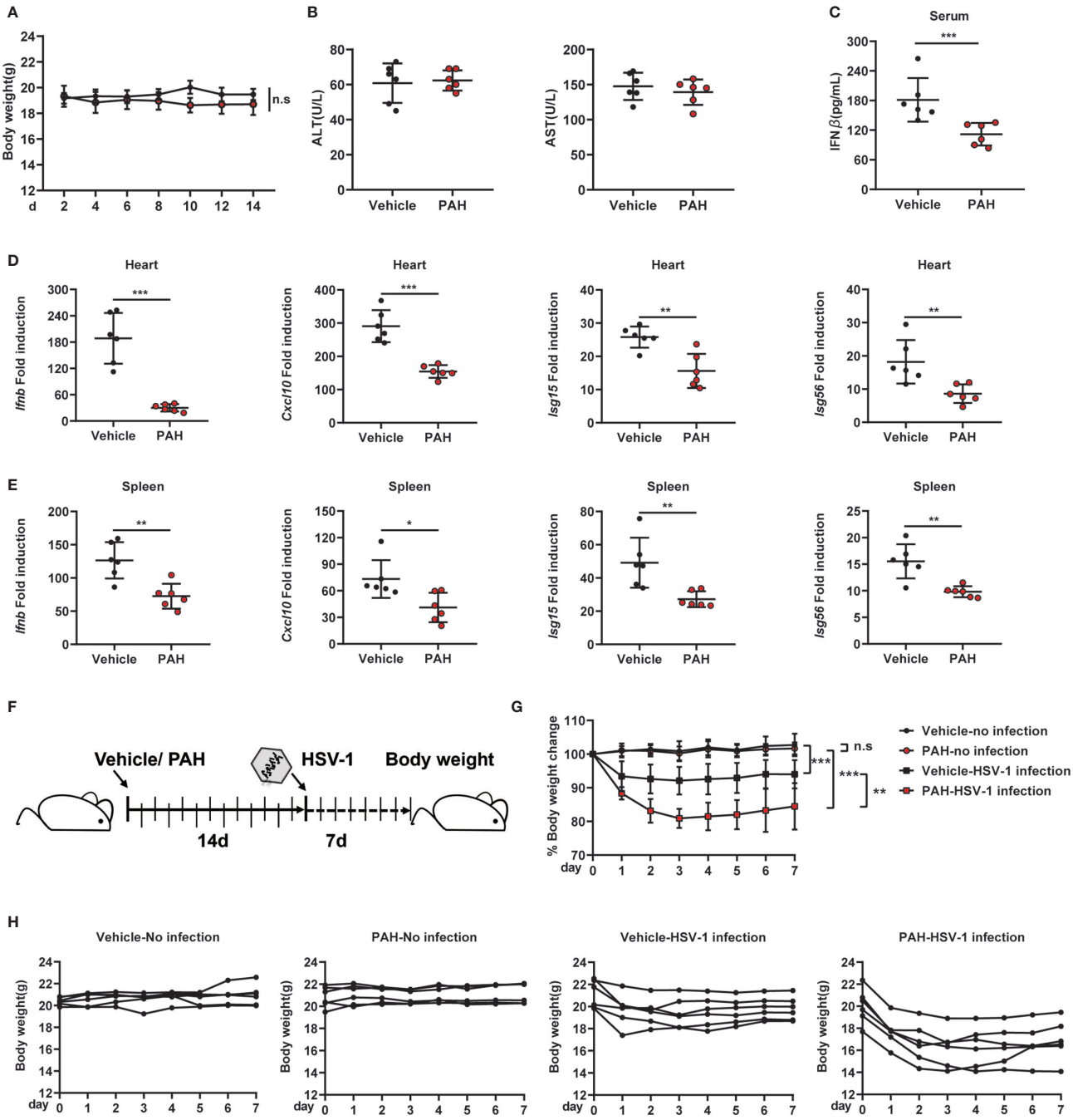

FIGURE 5 | PAH restricts the host innate defense against HSV-1 infection *in vivo*. **(A)** Mice were orally administered Vehicle (0.03% CMC-Na solution) or 120 mg•kg^{-1} PAH once per day for 14 days, then injected with HSV-1 intravenously. The time course of mice body weight. **(B)** Mice were orally administered Vehicle (0.03% CMC-Na solution) or 120 mg•kg^{-1} PAH once per day for 14 days, then the levels of aspartate aminotransferase (AST) and alanine aminotransferase (ALT) in serum were measured at the 14th day. **(C–E)** Mice were treated as in **(A)**. The concentrations of serum IFN-β of mice were measured by ELISA **(C)**, and the levels of *Ifnb*, *Cxcl10*, *Isg15*, and *Isg56* mRNA expression in the hearts **(D)** and spleens **(E)** of mice were measured by qPCR. **(F)** Schematic of drug administration and durable study after HSV-1 infection *in vivo*. **(G)** The time course of merged body weight from mice treated in **(F)**. **(H)** The time course of body weight from each mouse treated in **(F)**. Data in **(A–E, G–H)** are representative of two independent experiments (mean ± SD). n.s, no significance. *P < 0.05, **P < 0.01, ***P < 0.001.

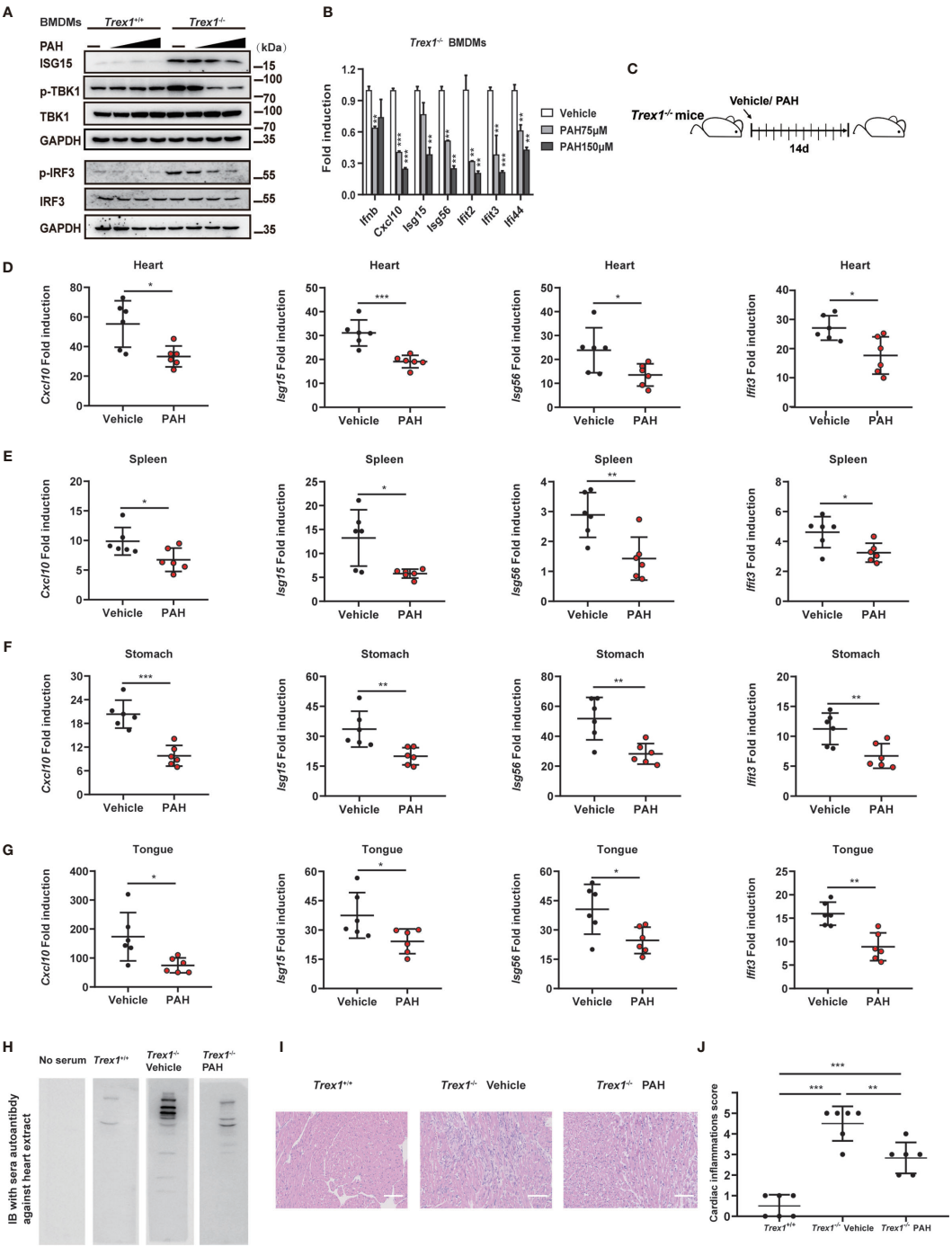

FIGURE 6 | PAH inhibits cGAS-mediated autoimmunity in mice. **(A)** BMDMs from *Trex1*$^{+/+}$ or *Trex1*$^{-/-}$ mice were treated with different PAH doses (0 to 250 μM) for 6 h, then the cell lysates were immunoblotted with the indicated antibodies. **(B)** BMDMs from *Trex1*$^{-/-}$ mice were treated with indicated concentrations of PAH. The baseline of *Ifnb*, *Cxcl10*, *Isg15*, *Isg56*, *Ifit2*, *Ifit3*, and *Ifi44* mRNA expression was then measured by qPCR. **(C)** Schematic of *Trex1*$^{-/-}$ mice drug administration *in vivo*. 4 weeks old *Trex1*$^{-/-}$ mice were orally administered Vehicle (0.03% CMC-Na solution) or 120 mg• kg^{-1} PAH once per day for 14 days. **(D–G)** The levels of *Cxcl10*, *Isg15*, *Isg56*, and *Ifit3* mRNA expression in the heart **(D)**, spleen **(E)**, stomach **(F)**, and tongue **(G)** of mice treated in **(C)** were measured by qPCR. **(H)** Representative autoantibodies blotting band of heart extracts from WT mice. Heart extracts were blotted with serum from *Trex1*$^{+/+}$, *Trex1*$^{-/-}$ (Vehicle), and *Trex1*$^{-/-}$ (PAH) mice and detected using HRP-conjugated anti-mouse IgG. **(I)** Representative H&E-stained heart tissue sections from *Trex1*$^{+/+}$, *Trex1*$^{-/-}$ (Vehicle), and *Trex1*$^{-/-}$ (PAH) mice. Scale bars represent 100 μm. **(J)** Pathological scores of cardiac inflammations in *Trex1*$^{-/-}$ mice administrated with the Vehicle or PAH for 14 days. Data in **(A, B)** were repeated at least three times, data in **(D–J)** are representative of two independent experiments. Data in **(B, D–G)** are presented as mean ± SD. *P< 0.05, **P< 0.01, ***P < 0.001.

ISGs in different tissues. As expected, PAH inhibited the expression of multiple ISGs genes (*Cxcl10*, *Isg15*, *Isg56*, and *Ifit3*) in the heart (**Figure 6D**), spleen (**Figure 6E**), stomach (**Figure 6F**), and tongue (**Figure 6G**) of *Trex1*$^{-/-}$ mice. Treatment with PAH decreased the abundance of sera autoantibodies (**Figure 6H**). Consistent with this observation, hematoxylin and eosin (H&E) and heart pathological scoring results showed that PAH administration could effectively alleviate the inflammation in the heart of *Trex1*$^{-/-}$ mice (**Figures 6I, J**). Collectively, these data reveal that inhibition of cGAS activity by PAH could potentially provide a therapeutic strategy for cGAS-mediated autoimmune diseases.

DISCUSSION

Recent researches have addressed the pivotal roles of cGAS in host innate defense against microbes such as bacteria (27), DNA viruses (28), RNA viruses (26) as well as retroviruses (29). Additionally, cGAS is the predominant sensor of mislocalized self-DNA from the nucleus or damaged mitochondrial (30), which resulted from many kinds of cellular or circumstance insults. The self-DNA sensing ability of cGAS has emerged as an important mechanism for developing inflammatory diseases and cancers. Thus small-molecular antagonists of cGAS may be useful for the treatment of diseases related to dysregulated cGAS signaling. In the present study, we identified that a natural monoterpenoid small molecule PAH could potently and selectively inhibit dsDNA-dependent cGAS enzymatic activity *in vitro* and *in vivo*. Our findings revealed that PAH might be beneficial in the therapy of cGAS-related autoimmune diseases.

Given its critical role in dsDNA-induced innate immunity, efforts to discover inhibitors of cGAS have been taken for the last few years, and several small molecules have been reported. By high-throughput screen with recombinant m-cGAS, RU.521 was identified as a specific inhibitor of cGAS enzyme without interfering with another innate immune signaling in both biochemical and cellular assays (31). Albeit its promise in mouse studies, RU.521 was demonstrated to be a poor inhibitor of human cGAS, underscoring the importance of species difference when screening cGAS inhibitors (32). In the later effort to discover human-cGAS-specific small-molecule inhibitors, G140 and G150 were identified to be potent and specific inhibitors of h-cGAS with cell-based activity (32). However, whether these compounds worked *in vivo* or had utility for the treatment of cGAS-related diseases were unknown. Combining high throughput cGAS fluorescence polarization (FP)-based assay and structure-based chemical optimization, PF-06928215, and related compounds were screened to inhibit cGAS enzymatic activity with high binding affinity as well as low IC_{50} values in the biochemical assay (33). Nevertheless, these compounds failed to inhibit cGAS activity in cellular assays for unknown reasons. Antimalarial drugs (AMDs) such as hydroxychloroquine (HCQ) were shown to interact with the cGAS/dsDNA complex by *in silico* screening and inhibit IFN-β production *in vitro*, although with a poor selectivity (34). Curiously, HCQ did not affect or even increased the ISG expression in the tissues of *Trex1*$^{-/-}$ mice or peripheral blood cells (PBMCs) from SLE patients (35). So far, the most promising cGAS inhibitor came from synthesized AMD derivative X6, which could attenuate the autoimmune disease phenotype in *Trex1*$^{-/-}$ mice (35). Given these observations, it is still urgent to develop new cGAS inhibitors with good efficiency/specificity and a safety profile. Here we characterized that PAH specifically inhibited cGAS activity *via* biochemical and cell-based assays. The suppression effect of PAH on cGAS-mediated innate immune signaling held in both mouse and human cells. *In vivo*, PAH impaired HSV-1-triggered antiviral gene expression and attenuated auto-inflammatory responses in *Trex1*$^{-/-}$ mice.

Consistent with our research, PAH was useful in ameliorating inflammatory diseases such as intestinal inflammation (15) and inflammatory skin diseases (19). As a perspective natural bioactive product, PAH shows several potential superiorities in future drug development. First, PAH exhibits beneficial therapeutic effects in several mouse disease models, including depression-like behavior (36), colitis inflammation (15), cancer (20), and atherosclerosis (37). Administration of PAH showed no side effects and toxicity in these models, revealing the biological safety of PAH *in vivo*. Second, the pharmacological effect of PAH has been improved *via* an optimized drug delivery system. Meanwhile, the pharmacokinetic parameters and tissue distribution of PAH have been reported previously (38).

It's noteworthy that there are some limitations of our study. First, treatment with PAH did not eliminate the pathological autoimmune phenotype in *Trex1*$^{-/-}$ mice, and little is known about whether PAH can prolong the survival of *Trex1*$^{-/-}$ mice. A longer period of treatment or treatment with mothers of pups immediately after birth would help understand the outcomes. Although the IC_{50} values of cGAS inhibitors are cell-type dependent, the cellular IC_{50} values of PAH seem to be high. One possible explanation is the poor water solubility or cell penetration. Chemical optimization or a proper solvent may be helpful for PAH to overcome the membrane barriers. Third, we do not yet understand the inhibitory mechanisms of PAH. As PAH showed an inhibitory effect on both mouse and human cGAS, we suspected that PAH structurally disrupted cGAS binding with dsDNA or functioned on the conserved active sites of cGAS. The exact mechanism(s) responsible remains to be determined. The co-crystal structural and interdisciplinary approach will be necessary to dissect how PAH inhibited the cGAS activity.

PAH can also be considered for the treatment of other cGAS-related diseases such as cancer. The cGAS-STING-mediated inflammatory response can promote tumorigenesis and metastasis in a tumor-type-dependent and stage-specific manner. For example, the carcinogen DMBA could induce nuclear DNA leakage and activate cGAS-STING-dependent cytokine production, supporting inflammation-driven skin carcinogenesis (39). cGAMP produced in brain metastatic breast and lung cancer cells could transfer to the astrocyte and activated the STING pathway, promoting tumor growth and

chemo-resistance (40). In chromosomal instability tumor cells, genomic DNA existed in cytoplasm activated cGAS-STING and downstream NF-κB signaling, promoting tumor cell invasion and metastasis (41). Indeed, PAH showed an inhibitory effect on gastric cancer growth by inducing cell autophagy (20). Considering that the activation of cGAS-STING signaling is implicated in some types of cancer, it is perspective that PAH may have an application in treating cancers.

DATA AVAILABILITY STATEMENT

The raw data supporting the conclusions of this article will be made available by the authors without undue reservation.

ETHICS STATEMENT

The animal study was reviewed and approved by the Institutional Animal Care and Use Committee of China Pharmaceutical University and the Institutional Ethics Committee of China Pharmaceutical University.

AUTHOR CONTRIBUTIONS

SC and CW conceived the experiments. LC, CheL, YL, QY, HY, ChuL, WM, JZ, QW and SC conducted the experiments. SC and LC analyzed the results. SC and CW wrote the manuscript. All authors contributed to the article and approved the submitted version.

FUNDING

This study is supported by the National Natural Science Foundation of China (31801076, 81802000), the Natural Science Foundation of the Jiangsu province (BK20180555), the China Postdoctoral Science Foundation (2018M630641), the National Key R&D Program of China (2016YFA0501800), the Project Program of State Key Laboratory of Natural Medicines (SKLNMZZ202002), the "Double First-Class" Project of China Pharmaceutical University (CPU2018GF10).

ACKNOWLEDGMENTS

We thank Dr. Tomas Lindahl and Dr. Deborah Barnes (Cancer Research UK) for the license of *Trex1*$^{+/-}$ mice, Dr. Nan Yan (University of Texas Southwestern Medical Center) for providing the *Trex1*$^{+/-}$ mice.

SUPPLEMENTARY MATERIAL

The Supplementary Material for this article can be found online at: https://www.frontiersin.org/articles/10.3389/fimmu.2021.655637/full#supplementary-material

Supplementary Figure 1 | PAH Suppresses HT-DNA-triggered IFN-β Secretion. L929 cells were treated with Vehicle or indicated PAH concentrations for 6 h, and then stimulated with HT-DNA (4 μg•ml^{-1}) for 9 h. The supernatants were collected, and ELISA determined the amounts of IFN-β. Data are representative of three independent experiments (mean ± SD). ***$P < 0.001$.

Supplementary Figure 2 | PAH Restricts the Host Innate Defense against VSV *in vitro*. **(A)** L929 cells were treated with Vehicle or PAH for 6 h and then infected with VSV (MOI = 0.5) for 6 h. The induction of *Ifnb*, *Ifna4*, and *Cxcl10* mRNA expression was then measured by qPCR. **(B)** L929 cells were treated with Vehicle or PAH (200 μM) for 6 h and then infected with VSV (MOI = 1). The proliferation of cells was examined by crystal violet staining. Scale bars represent 100 μm. **(C)** The statistical analysis of stained cell ratios from **(B)**. **(D)** L929 cells were treated with Vehicle or PAH (200 μM) for 6 h and then infected with VSV (MOI = 1). The titers of VSV were determined by standard plaque assay. **(E)** L929 cells were treated with Vehicle or PAH (200 μM) for 6 h and then infected with GFP-VSV (MOI = 0.4) for 16 h. GFP-VSV replication was visualized by fluorescence microscopy. Scale bars represent 100 μm. **(F)** L929 cells were treated with Vehicle or PAH (200 μM) for 6 h and then infected with GFP-VSV (MOI = 0.4) for 16 h. GFP-VSV replication was visualized by flow cytometry. **(G)** The statistical analysis of GFP-positive cell ratios from (F). All of the experiments were repeated at least three times. Data in **(A, C, D, F)** are presented as mean ± SD. *$P< 0.05$, ***$P< 0.001$.

Supplementary Figure 3 | The Effect of PAH on Basal Immune Circumstance *in vivo*. **(A)** Mice were orally administered with Vehicle (0.03% CMC-Na solution) or 120 mg• kg^{-1} PAH once per day for 14 days, then the concentrations of serum IFN-β of mice were measured by ELISA. **(B, C)** The levels of *Ifnb*, *Cxcl10*, *Isg15*, and *Isg56* mRNA expression in the hearts **(B)** and spleens **(C)** of mice from **(A)** were measured by qPCR. Data in **(A–C)** are representative of two independent experiments.

Supplementary Figure 4 | The Time Course of Body Weight from *Trex1*$^{-/-}$ mice. **(A)** The time course of body weight from each *Trex1*$^{-/-}$ mouse treated in (**Figure 6C**). **(B)** The time course of merged body weight from mice treated in (**Figure 6C**). Data in **(A, B)** are representative of two independent experiments. Data in **(B)** are presented as mean ± SD.

REFERENCES

1. Takeuchi O, Akira S. Pattern Recognition Receptors and Inflammation. *Cell* (2010) 140(6):805–20. doi: 10.1016/j.cell.2010.01.022
2. Gao P, Ascano M, Wu Y, Barchet W, Gaffney BL, Zillinger T, et al. Cyclic [G(2',5') Pa(3',5')P] is the Metazoan Second Messenger Produced by DNA-Activated Cyclic GMP-AMP Synthase. *Cell* (2013) 153(5):1094–107. doi: 10.1016/j.cell.2013.04.046
3. Ablasser A, Goldeck M, Cavlar T, Deimling T, Witte G, Rohl I, et al. Cgas Produces a 2'-5'-Linked Cyclic Dinucleotide Second Messenger That Activates STING. *Nature* (2013) 498(7454):380–4. doi: 10.1038/nature12306
4. Ishikawa H, Barber GN. STING is an Endoplasmic Reticulum Adaptor That Facilitates Innate Immune Signalling. *Nature* (2008) 455(7213):674–8. doi: 10.1038/nature07317
5. Ishikawa H, Ma Z, Barber GN. STING Regulates Intracellular DNA-Mediated, Type I Interferon-Dependent Innate Immunity. *Nature* (2009) 461(7265):788–92. doi: 10.1038/nature08476
6. Tanaka Y, Chen ZJ. STING Specifies IRF3 Phosphorylation by TBK1 in the Cytosolic DNA Signaling Pathway. *Sci Signal* (2012) 5(214):ra20. doi: 10.1126/scisignal.2002521
7. Yang YG, Lindahl T, Barnes DE. Trex1 Exonuclease Degrades Ssdna to Prevent Chonic Checkpoint Activation and Autoimmune Disease. *Cell* (2007) 131(5):873–86. doi: 10.1016/j.cell.2007.10.017
8. Morita M, Stamp G, Robins P, Dulic A, Rosewell I, Hrivnak G, et al. Gene-Targeted Mice Lacking the Trex1 (Dnase III) 3'–>5' DNA Exonuclease Develop Inflammatory Myocarditis. *Mol Cell Biol* (2004) 24(15):6719–27. doi: 10.1128/MCB.24.15.6719-6727.2004

9. Crow YJ, Hayward BE, Parmar R, Robins P, Leitch A, Ali M, et al. Mutations in the Gene Encoding the 3'-5' DNA Exonuclease TREX1 Cause Aicardi-Goutieres Syndrome At the AGS1 Locus. *Nat Genet* (2006) 38(8):917–20. doi: 10.1038/ng1845
10. Rice G, Newman WG, Dean J, Patrick T, Parmar R, Flintoff K, et al. Heterozygous Mutations in TREX1 Cause Familial Chilblain Lupus and Dominant Aicardi-Goutieres Syndrome. *Am J Hum Genet* (2007) 80 (4):811–5. doi: 10.1086/513443
11. Gao D, Li T, Li XD, Chen X, Li QZ, Wight-Carter M, et al. Activation of Cyclic GMP-AMP Synthase by Self-DNA Causes Autoimmune Diseases. *Proc Natl Acad Sci U S A* (2015) 112(42):E5699–705. doi: 10.1073/pnas.1516465112
12. Newman DJ, Cragg GM. Natural Products as Sources of New Drugs Over the Nearly Four Decades From 01/1981 to 09/2019. *J Nat Prod* (2020) 83(3):770–803. doi: 10.1021/acs.jnatprod.9b01285
13. Urushima H, Nishimura J, Mizushima T, Hayashi N, Maeda K, Ito T. Perilla Frutescens Extract Ameliorates DSS-Induced Colitis by Suppressing Proinflammatory Cytokines and Inducing Anti-Inflammatory Cytokines. *Am J Physiol Gastrointest Liver Physiol* (2015) 308(1):G32–41. doi: 10.1152/ajpgi.00294.2014
14. Bumblauskiene L, Jakstas V, Janulis V, Mazdzieriene R, Ragazinskiene O. Preliminary Analysis on Essential Oil Composition of Perilla L. Cultivated in Lithuania. *Acta Pol Pharm* (2009) 66(4):409–13. doi: 10.1055/s-0029-1234773
15. Uemura T, Yashiro T, Oda R, Shioya N, Nakajima T, Hachisu M, et al. Intestinal Anti-Inflammatory Activity of Perillaldehyde. *J Agric Food Chem* (2018) 66(13):3443–8. doi: 10.1021/acs.jafc.8b00353
16. Ueda H, Yamazaki M. Anti-Inflammatory and Anti-Allergic Actions by Oral Administration of a Perilla Leaf Extract in Mice. *Biosci Biotechnol Biochem* (2001) 65(7):1673–5. doi: 10.1271/bbb.65.1673
17. Tian H, Qu S, Wang Y, Lu Z, Zhang M, Gan Y, et al. Calcium and Oxidative Stress Mediate Perillaldehyde-Induced Apoptosis in Candida Albicans. *Appl Microbiol Biotechnol* (2017) 101(8):3335–45. doi: 10.1007/s00253-017-8146-3
18. Duelund L, Amiot A, Fillon A, Mouritsen OG. Influence of the Active Compounds of Perilla Frutescens Leaves on Lipid Membranes. *J Nat Prod* (2012) 75(2):160–6. doi: 10.1021/np200713q
19. Fuyuno Y, Uchi H, Yasumatsu M, Morino-Koga S, Tanaka Y, Mitoma C, et al. Perillaldehyde Inhibits AH Signaling and Activates NRF2 Antioxidant Pathway in Human Keratinocytes. *Oxid Med Cell Longev* (2018) 2018:9524657. doi: 10.1155/2018/9524657
20. Zhang Y, Liu S, Feng Q, Huang X, Wang X, Peng Y, et al. Perilaldehyde Activates AMP-Activated Protein Kinase to Suppress the Growth of Gastric Cancer Via Induction of Autophagy. *J Cell Biochem* (2018) 120(2):1716–25. doi: 10.1002/jcb.27491
21. Elegbede JA, Flores R, Wang RC. Perillyl Alcohol and Perillaldehyde Induced Cell Cycle Arrest and Cell Death in Broto and A549 Cells Cultured in Vitro. *Life Sci* (2003) 73(22):2831–40. doi: 10.1016/s0024-3205(03)00701-x
22. Lou X, Sun S, Chen W, Zhou Y, Huang Y, Liu X, et al. Negative Feedback Regulation of NF-Kappab Action by CITED2 in the Nucleus. *J Immunol* (2011) 186(1):539–48. doi: 10.4049/jimmunol.1001650
23. Li S, Hong Z, Wang Z, Li F, Mei J, Huang L, et al. The Cyclopeptide Astin C Specifically Inhibits the Innate Immune CDN Sensor STING. *Cell Rep* (2018) 25(12):3405–21.e7. doi: 10.1016/j.celrep.2018.11.097
24. Wang C, Guan Y, Lv M, Zhang R, Guo Z, Wei X, et al. Manganese Increases the Sensitivity of the Cgas-STING Pathway for Double-Stranded DNA and is Required for the Host Defense Against DNA Viruses. *Immunity* (2018) 48 (4):675–87.e7. doi: 10.1016/j.immuni.2018.03.017
25. Aguirre S, Luthra P, Sanchez-Aparicio MT, Maestre AM, Patel J, Lamothe F, et al. Dengue Virus NS2B Protein Targets Cgas for Degradation and Prevents Mitochondrial DNA Sensing During Infection. *Nat Microbiol* (2017) 2:17037. doi: 10.1038/nmicrobiol.2017.37
26. Schoggins JW, MacDuff DA, Imanaka N, Gainey MD, Shrestha B, Eitson JL, et al. Pan-Viral Specificity of IFN-Induced Genes Reveals New Roles for Cgas in Innate Immunity. *Nature* (2014) 505(7485):691–5. doi: 10.1038/nature12862
27. Watson RO, Bell SL, MacDuff DA, Kimmey JM, Diner EJ, Olivas J, et al. The Cytosolic Sensor Cgas Detects Mycobacterium Tuberculosis DNA to Induce Type I Interferons and Activate Autophagy. *Cell Host Microbe* (2015) 17 (6):811–9. doi: 10.1016/j.chom.2015.05.004
28. Garcia-Belmonte R, Perez-Nunez D, Pittau M, Richt JA, Revilla Y. African Swine Fever Virus Armenia/07 Virulent Strain Controls Interferon Beta Production Though the Cgas-STING Pathway. *J Virol* (2019) 93(12). doi: 10.1128/JVI.02298-18
29. Li XD, Wu J, Gao D, Wang H, Sun L, Chen ZJ. Pivotal Roles of Cgas-Cgamp Signaling in Antiviral Defense and Immune Adjuvant Effects. *Science* (2013) 341(6152):1390–4. doi: 10.1126/science.1244040
30. West AP, Khoury-Hanold W, Staron M, Tal MC, Pineda CM, Lang SM, et al. Mitochondrial DNA Stress Primes the Antiviral Innate Immune Response. *Nature* (2015) 520(7548):553–7. doi: 10.1038/nature14156
31. Vincent J, Adura C, Gao P, Luz A, Lama L, Asano Y, et al. Small Molecule Inhibition of Cgas Reduces Interferon Expression in Primary Macrophages From Autoimmune Mice. *Nat Commun* (2017) 8(1):750. doi: 10.1038/s41467-017-00833-9
32. Lama L, Adura C, Xie W, Tomita D, Kamei T, Kuryavyi V, et al. Development of Human Cgas-Specific Small-Molecule Inhibitors for Repression of Dsdna-Triggered Interferon Expression. *Nat Commun* (2019) 10(1):2261. doi: 10.1038/s41467-019-08620-4
33. Hall J, Brault A, Vincent F, Weng S, Wang H, Dumlao D, et al. Discovery of PF-06928215 as a High Affinity Inhibitor of Cgas Enabled by a Novel Fluorescence Polarization Assay. *PLoS One* (2017) 12(9):e0184843. doi: 10.1371/journal.pone.0184843
34. An J, Woodward JJ, Sasaki T, Minie M, Elkon KB. Cutting Edge: Antimalarial Drugs Inhibit IFN-Beta Production Though Blockade of Cyclic GMP-AMP Synthase-DNA Interaction. *J Immunol* (2015) 194(9):4089–93. doi: 10.4049/jimmunol.1402793
35. An J, Woodward JJ, Lai W, Minie M, Sun X, Tanaka L, et al. Inhibition of Cyclic GMP-AMP Synthase Using a Novel Antimalarial Drug Derivative in Trex1-Deficient Mice. *Arthitis Rheumatol* (2018) 70(11):1807–19. doi: 10.1002/art.40559
36. Ji WW, Wang SY, Ma ZQ, Li RP, Li SS, Xue JS, et al. Effects of Perillaldehyde on Alternations in Serum Cytokines and Depressive-Like Behavior in Mice After Lipopolysaccharide Administration. *Pharmacol Biochem Behav* (2014) 116:1–8. doi: 10.1016/j.pbb.2013.10.026
37. Yu L, Liu H. Perillaldehyde Prevents the Formations of Atherosclerotic Plaques Though Recoupling Endothelial Nitric Oxide Synthase. *J Cell Biochem* (2018) 119(12):10204–15. doi: 10.1002/jcb.27362
38. Omari-Siaw E, Wang Q, Sun C, Gu Z, Zhu Y, Cao X, et al. Tissue Distribution and Enhanced in Vivo Anti-Hyperlipidemic-Antioxidant Effects of Perillaldehyde-Loaded Liposomal Nanoformulation Against Poloxamer 407-Induced Hyperlipidemia. *Int J Pharm* (2016) 513(1-2):68–77. doi: 10.1016/j.ijpharm.2016.08.042
39. Ahn J, Xia T, Konno H, Konno K, Ruiz P, Barber GN. Inflammation-Driven Carcinogenesis is Mediated Though STING. *Nat Commun* (2014) 5:5166. doi: 10.1038/ncomms6166
40. Chen Q, Boire A, Jin X, Valiente M, Er EE, Lopez-Soto A, et al. Carcinoma-Astrocyte Gap Junctions Promote Brain Metastasis by Cgamp Transfer. *Nature* (2016) 533(7604):493–8. doi: 10.1038/nature18268
41. Bakhoum SF, Ngo B, Laughney AM, Cavallo JA, Murphy CJ, LY P, et al. Chomosomal Instability Drives Metastasis Though a Cytosolic DNA Response. *Nature* (2018) 553(7689):467–72. doi: 10.1038/nature25432

Conflict of Interest: The authors declare that the research was conducted in the absence of any commercial or financial relationships that could be construed as a potential conflict of interest.

frontiers in Immunology

ORIGINAL RESEARCH
published: 14 May 2021
doi: 10.3389/fimmu.2021.654463

A Small Molecule Antagonist of PD-1/PD-L1 Interactions Acts as an Immune Checkpoint Inhibitor for NSCLC and Melanoma Immunotherapy

Yuanyuan Wang[1,2†], Tingxuan Gu[1,2†], Xueli Tian[1,2], Wenwen Li[2], Ran Zhao[1,2], Wenqian Yang[1,2], Quanli Gao[3], Tiepeng Li[3], Jung-Hyun Shim[4], Chengjuan Zhang[5], Kangdong Liu[1,2] and Mee-Hyun Lee[1,2,6]*

[1] Department of Pathophysiology, School of Basic Medical Sciences, Zhengzhou University, Zhengzhou, China, [2] China-US (Henan) Hormel Cancer Institute, Zhengzhou, China, [3] Department of Immunology, The Affiliated Cancer Hospital of Zhengzhou University and Henan Cancer Hospital, Zhengzhou, China, [4] Department of Pharmacy, College of Pharmacy, Mokpo National University, Mokpo, South Korea, [5] Department of Pathology, The Affiliated Cancer Hospital of Zhengzhou University, Zhengzhou, China, [6] College of Korean Medicine, DongShin University, Naju, South Korea

OPEN ACCESS

Edited by:
Xuanming Yang,
Shanghai Jiao Tong University, China

Reviewed by:
Haidong Tang,
Tsinghua University, China
Alessandro Poggi,
San Martino Hospital (IRCCS), Italy

***Correspondence:**
Mee-Hyun Lee
mhyun_lee@hanmail.net

[†]*These authors have contributed equally to this work*

Specialty section:
This article was submitted to Cancer Immunity and Immunotherapy, a section of the journal Frontiers in Immunology

Received: *16 January 2021*
Accepted: *06 April 2021*
Published: *14 May 2021*

Citation:
Wang Y, Gu T, Tian X, Li W, Zhao R, Yang W, Gao Q, Li T, Shim J-H, Zhang C, Liu K and Lee M-H (2021) A Small Molecule Antagonist of PD-1/PD-L1 Interactions Acts as an Immune Checkpoint Inhibitor for NSCLC and Melanoma Immunotherapy. Front. Immunol. 12:654463. doi: 10.3389/fimmu.2021.654463

Immune checkpoint inhibitors, such as monoclonal antibodies targeting programmed death 1 (PD-1) and programmed death ligand-1 (PD-L1), have achieved enormous success in the treatment of several cancers. However, monoclonal antibodies are expensive to produce, have poor tumor penetration, and may induce autoimmune side effects, all of which limit their application. Here, we demonstrate that PDI-1 (also name PD1/PD-L1 inhibitor 1), a small molecule antagonist of PD-1/PD-L1 interactions, shows potent anti-tumor activity *in vitro* and *in vivo* and acts by relieving PD-1/PD-L1-induced T cell exhaustion. We show that PDI-1 binds with high affinity to purified human and mouse PD-1 and PD-L1 proteins and is a competitive inhibitor of human PD-1/PD-L1 binding *in vitro*. Incubation of *ex vivo* activated human T cells with PDI-1 enhanced their cytotoxicity towards human lung cancer and melanoma cells, and concomitantly increased the production of granzyme B, perforin, and inflammatory cytokines. Luciferase reporter assays showed that PDI-1 directly increases TCR-mediated activation of NFAT in a PD-1/PD-L1-dependent manner. In two syngeneic mouse tumor models, the intraperitoneal administration of PDI-1 reduced the growth of tumors derived from human PD-L1-transfected mouse lung cancer and melanoma cells; increased and decreased the abundance of tumor-infiltrating CD8+ and FoxP3+ CD4+ T cells, respectively; decreased the abundance of PD-L1-expressing tumor cells, and increased the production of inflammatory cytokines. The anti-tumor effect of PDI-1 *in vivo* was comparable to that of the anti-PD-L1 antibody atezolizumab. These results suggest that the small molecule inhibitors of PD-1/PD-L1 may be effective as an alternative or complementary immune checkpoint inhibitor to monoclonal antibodies.

Keywords: PD-1/PD-L1 inhibitor 1, PDI-1, PD-1/PD-L1, small molecule compound, immunotherapy, T cell activation

INTRODUCTION

In recent years, interest has been rekindled in immunotherapy for the treatment of cancer and other immune disorders (1). In particular, the introduction of immune checkpoint inhibitors (ICIs), which act by blocking negative regulatory pathways triggered by receptor–ligand interactions between tumor cells and T cells, has revolutionized the treatment of many cancers (2, 3). One example is the PD-1/PD-L1 immune checkpoint. PD-1 is an inhibitor of T cell proliferation and function (4) and plays a vital role in the physiological maintenance of immune tolerance as well as in tumor surveillance (5). PD-1 by its ligand PD-L1, expressed on antigen-presenting cells and tumor cells (6), induces negative signaling that counters signaling through the antigen-specific T cell receptor (TCR) and the costimulatory protein CD28 (7), leading to inhibition of T cell activation, proliferation, and cytokine production, and ultimately to apoptosis (8). Inhibition of PD-1/PD-L1 interactions therefore effectively rescues the activity of "exhausted" T cells and promotes their activation by antigen-expressing cells (9, 10). Accordingly, monoclonal antibodies (mAbs) that block the PD-1 or PD-L1 axis have shown remarkable benefits in clinical trials (11). Several mAbs have been approved by the US Food and Drug Administration for the treatment of various cancers, including nivolumab (anti-PD-1, Bristol Myers Squibb) for the treatment of melanoma (12) and non-small cell lung cancer [NSCLC (13)]; and atezolizumab (anti-PD-L1, Roche) for the treatment of triple-negative breast cancer (14), NSCLC (15). Anti-PD-1/PD-L1 mAbs have not only shown long-lasting beneficial responses in patients with a broad range of human cancers, but also displayed reduced toxicity compared with other ICIs, such as anti-CTLA-4 mAbs (16).

Small molecule compounds offer several advantages over mAbs as therapeutic agents, such as lower manufacturing costs, and less stringent storage conditions (17). Most importantly, the pharmacokinetics of small molecules are generally associated with good oral bioavailability, high tissue and tumor penetration, and long half-lives (18). Small molecule compounds can relatively easily traverse cellular membranes and other biological barriers, thus facilitating their access to intracellular targets. Finally, small molecules can be modified to ensure high efficacy and selectivity, and benign toxicity profiles. Therefore, small molecule drugs that target the PD-1/PD-L1 checkpoint could offer an attractive alternative and complementary therapies to existing mAbs (19).

In the present study, we performed computer modeling of the crystal structures of PD-1 and PD-L1 together with *in silico* screening to identify PDI-1 as a potential small molecule inhibitor of the PD-1/PD-L1 axis. To investigate the mechanism of action of PDI-1, we analyzed its binding to PD-1 and PD-L1 proteins *in vitro* and its ability to rescue TCR/CD28-dependent activation of T cells *ex vivo* and *in vivo* using melanoma and non-small-cell lung cancer (NSCLC) cell lines and mouse tumor models. We show that PDI-1 is a potent competitive inhibitor of PD-1/PD-L1 binding and suppresses tumor growth *in vivo* through a mechanism involving inhibition of TCR/CD28-dependent signaling, enhancement of anti-tumor cytotoxicity, and increased inflammatory cytokine production. Our results suggest that PDI-1 holds promise as a novel small molecule anti-cancer therapeutic agent.

MATERIALS AND METHODS

Cell Culture

Lenti-X-293T (Human embryonic kidney cell line) were purchased from TaKaRa Bio, Inc. (Shiga, Japan). NCI-H1975, A549 (human non-small cell lung cancer), A375, SK-MEL-2 (human malignant melanoma)), and Jurkat (Human T-lymphocytes) cells were purchased from Cell Bank Australia (Shanghai, China), respectively. KLN205 (Murine lung cancer) and B16-F10 (Murine melanoma) cells were purchased from Cobioer bio (Nanjing, China). NCI-H1975, A549 and Jurkat cells were maintained in RPMI-1640 (Cat#01-100-1ACS, Biological Industries, Kibbutz Beit-Haemek, Israel) supplemented with 10% fetal bovine serum (FBS) (Cat#04-001-1ACS, Biological Industries) and 100U/ml penicillin-streptomycin (Cat#P1400, Solarbio, Beijing, China). A375, SK-MEL-2 and Lenti-X-293T cells were maintained in DMEM (Cat#01-052-1ACS, Biological Industries) supplemented with 10% FBS and 100 U/ml penicillin/streptomycin. B16-F10 was maintained in DMEM supplemented with 10% FBS and 100 U/ml penicillin/streptomycin. KLN205 was maintained in MEM (Biological Industries, Kibbutz Beit-Haemek, Israel) supplemented with 10% FBS, 100 U/ml penicillin/streptomycin, 0.1 mM non-essential amino acids (Cat#11140050, Gibco, Grand Island, NY, USA), 1 mM Sodium Pyruvate (Cat#11360070, Gibco, Grand Island, NY, USA).

Isolation of Human PBMCs

PBMCs (Human peripheral blood mononuclear cells) were purchased from TPCS (Milestone Biotechnologies, Shanghai, China). CD3+ T cells were negatively selected from PBMCs by CD3 magnetic negative selection using EasySep Human T Cell Isolation Kit (Cat#17951, STEMCELL Technologies, Cologne, Germany) per manufacturer's instructions. Human primary T cells were cultured in X-VIVO^{TM}15 medium (Cat#: BE02-060F, Lonza Group, Basel, Switzerland) with 5% FBS and 200 U/ml IL-2 (Cat#PHC0026, Thermo, Pudong, Shanghai, China). To activate T cells, a total of 3 million CD3+ T cells were treated by anti-CD3/CD28 magnetic Dynabeads (Cat#11161D, Thermo, Pudong, Shanghai, China) at the ratio of 1:1 together with 200 U/ml of IL-2, 50 ng/ml of IL-7 (Cat#PHC0075, Thermo, Pudong, Shanghai, China) and 50 ng/ml of IL-15 (Cat#PHC9151, Thermo, Pudong, Shanghai, China). After 48 h, activated CD3+ T cells were maintained by culture medium previously described at a density of 1 million cells per ml of culture medium and change the fresh medium every 2-3 days.

Surface Plasmon Resonance (SPR) Assay

A BIACORE T200 (GE Healthcare, UK) was used to perform the SPR assay. Before starting the experiment, the machine was primed twice with ddH_2O. Then a research-grade CM5 sensor chip was docked to the device and continued to prime twice with

filtered phosphate-buffered saline (PBS). The PD-1 protein (Cat#10377-H08H, Sino Biological, Beijing, China) was immobilized using amine-coupling chemistry according to the wizard template. Briefly, the surface was first activated with a 1:1 mixture solution of 0.1 M NHS (N-hydroxy succinimide) and 0.1 M EDC (1-Ethyl-3-(3-dimethylaminopropyl)-carbodiimide hydrochloride) at 5 µl/min. Then a 20 ug/ml PD-1 protein, which was diluted in 10 mM sodium acetate (pH 4.5), was immobilized to channel 2 and then reached an expected density of 5000 RU. Channel 1 was left blank as a reference surface. Then channel 2 was blocked with an ethanolamine solution. To evaluate the binding ability, the PDI-1 (CAS#1675201-83-8, DC chemicals, Pudong, Shanghai, China) in PBS was injected over the two channels at a range that varies from 0.2 to 125 nM of PDI-1 concentration at a flow rate of 30 µl/min. The compound was designed for 90 and 300 s to associate and dissociated, respectively. The surfaces were renewed with a 5 s injection of 10 mM glycine (pH 2.5). PD-L1 protein (Cat#10084-H08H, Sino Biological, Beijing, China) was immobilized to channel 4 with the same method. The interaction of PD-L1 and PDI-1 was measured the same as above. The data were adjusted to a simple 1:1 interaction model within BiaEvaluation 3.1 software (Biacore, Uppsala, Sweden).

Competitive ELISA Assay

To measure the inhibitory effects of PDI-1on interaction between PD-1 and PD-L1, we used the Acro Biosystems ELISA assay kit (Cat#EP-101, Acro Biosystems, Beijing, China) following the manufacturer's instructions. Briefly, human PD-L1 were coated in a 96-well plate and incubated overnight at 4°C. Then, biotin-labeled human PD-1 protein was added, and incubation was performed for 20 min at room temperature. Next, the concentrations gradient of PDI-1 was added by dilution buffer, followed by incubation for 1 h at 37°C. After two washes followed by incubation with Streptavidin-HRP for 1h and TMB for 20 minutes at 37°C. Lastly, the absorbance at 450 nm was measured with Thermo Scientific Multiskan GO spectrophotometer (ThermoFisher Scientific, Vartaa, Finland).

T Cell Cytotoxicity *In Vitro*

To validate the effect of primary T cells on cancer cells, we co-cultured primary T cell with cancer cells. H1975, A549, A375 or SK-MEL-2 cells were labeled by CFSE (carboxyfluorescein diacetate succinimidyl ester) (Cat# 65-0850-84, Invitrogene™ Bioscience, Shanghai, China) per manufacturer's instructions, respectively. CFSE labeled H1975, A549, A375 or SK-MEL-2 cells (5×10^4) were seeded into 12 well-plate overnight, then the next day incubated with primary T cells by the ratio of H1975, A549, A375 or SK-MEL-2 cells to T cells 1:5 for 18 h at the treatment of PDI-1. Next, co-culture cells were harvested, and then propidium iodide (PI) was stained 15 min on ice, last analyzed the sample using a BD FACSCalibur Flow Cytometer (BD Biosciences, San Jose, CA, USA).

To validate the effect of primary T cell on the cancer cells, we co-cultured primary T cell with hPD-L1-TCR-HEK-293T or TCR-HEK-293T cells labeled by CFSE per manufacturer's instructions, respectively. CFSE labeled hPD-L1-TCR-HEK-293T or TCR-HEK-293T cells (5×10^4) were seeded into 12 well-plate overnight, then the next day incubated with primary T cells by the ratio of hPD-L1-TCR-HEK-293T or TCR-HEK-293T cells to T cells 1:5 for 18 h at the treatment of PDI-1. Next, co-culture cells were harvested, and then propidium iodide (PI) was stained 15 min on ice, last analyzed the sample using a BD FACSCalibur Flow Cytometer (BD Biosciences, San Jose, CA, USA).

hPD-L1 Expression of hPD-L1-TCR-HEK293T and TCR-HEK293T Cells

To validate the expression of hPD-L1 on hPD-L1-TCR-HEK293T and TCR-HEK293T cells, we incubated hPD-L1-TCR-HEK293T and TCR-HEK293T cells with PerCP/Cyanine5.5 anti-human PD-L1 antibody (Cat #329737, Biolegend) for 20 min on ice. Finally, we analyzed the sample using a BD FACSCalibur Flow Cytometer (BD Biosciences, San Jose, CA, USA).

Construction of hPD-L1-TCR-HEK293T, TCR-HEK293T and hPD-1-NFAT-Jurkat Cells

hPD-L1-TCR-HEK293T and TCR-HEK293T: One day before transfection, seed HEK293T cells at a density of $2x10^6$ cells per ml, when cells reached 80% confluent at the time of transfection. The next day, transfect 1 µl TCR activator and hPD-L1 (Cat#79455, BPS Bioscience) or the only TCR activator (Cat#79455, Cat#79455) into cells following the manufacturer's protocol. To sort the hPD-L1-TCR -HEK293T cells, we stain the cells with anti-human PD-L1 antibody (Cat #329706, Biolegend) by the FACSAria (BD) after 3 days transfection.

hPD-1-NFAT-Jurkat cells: Lentiviral packaging of the plasmid pLenti-NFAT-IRES-EGFP-PD-1 were performed by Gene Pharma. Lentivirus were infected into Jurkat cells at MOI 20 with 2µg/ml Polybrene, 7 days post infection, hPD-1-NFAT-Jurkat cells were sorted by FACSAria (BD), with staining of anti-human PD1 antibody (Cat #329906, Biolegend). Single clones were performed and selected by expression of PD-1.

Fluorescent Multiplex Immunohistochemistry (mIHC)

The expression of murine CD8a, FoxP3 and PD-L1 were analyzed using Fluorescent multiplex immunohistochemistry. Tumor tissue sections were cut onto slides and heated at 60°C for 2h. Tumor tissue slides were then subjected to deparaffinization, rehydration and antigen retrieval, prior to endogenous peroxidase blocking. The slides were incubated with PD-L1(1:500, Cat#13684S, Cell Signaling Technology, Danvers, MA, USA), CD8a (1:100, Cat# 14-0081-86, eBioscience, Vienna, Austria) or FoxP3 (1:500, Cat# 14-5773-82, eBioscience, Vienna, Austria) primary antibody followed by the application of polymeric Horseradish peroxidase (HRP)-conjugated secondary antibodies ((Invitrogen™ eBioscience, Shanghai, China)). An appropriate fluorophore conjugated TSA (Invitrogen™ eBioscience, Shanghai, China) was then added at 1:100 dilution. The slides were rinsed with PBS after each step. Following TSA deposition, the slides

were again subjected to antigen retrieval to strip the tissue-bound primary/secondary antibody complexes and ready for labeling of the next marker. These steps were repeated until all three markers were labeled and finally added with DAPI (Cat#P36935, Invitrogen™ eBioscience, Shanghai, China) at 1:20000 dilution. Then images were analyzed by Confocal microscopy at 60x magnification using the Nikon A1 laser confocal microscope (Nikon Instruments, Melville, NY, USA). For statistical analysis of grey intensities of fluorescent IHC signals, Image-Pro Plus 6.0 software (Media Cybernetics Inc, Maryland, USA) was used.

Multiplex Cytokines Assay

The production in mice serum was measured by LEGEND plex™ Mouse Inflammation Panel. Blood was collected from the abdominal aorta of the mice after sacrifice and the serums were separated by centrifuge at 350g, 4°C for 15 min. Next, concentrations of IL-1α, IL-1β, IL-6, IL-10, IL-12p70, IL-17A, IL-23, IL-27, MCP-1, IFN-β, IFN-γ, TNF-α, and GM-CSF were measured using LEGEND plex™ Mouse Inflammation Panel (13-plex) (Cat#740446, Biolegend, Shenzhen, China). The samples were analyzed by FACS using FACSCalibur (BD). The data were analyzed *via* LEGENDplexv8.0.

Single-Cell Dissociation From Tumor Tissues

The expression of CD3, CD4, CD8a in the TEM were measured by flow cytometry. Tumor tissues were harvested after injection and digested with Collagenase II (1 mg/ml, Sigma-Aldrich, C685, Pudong, Shanghai, China) in DMEM, which contained DNase (0.3mg/ml, Sigma-Aldrich, DN25) at 37°C with 800 rpm for 1 h. Afterward, the cell suspensions were filtered through a 70 μm strainer. Single-cell suspensions were stained with PerCP/Cyanine5.5 conjugated anti-mouse CD3 (Cat # 100217, clone 17A2, Biolegend), PE-conjugated anti-mouse CD8a (Cat #100707, clone 53-6.7, Biolegend), and APC conjugated anti-mouse CD4 (Cat #100411, clone GK15, Biolegend) for 30 min on ice, following the manufacturer's instructions. Samples were analyzed by flow cytometry system and the data were analyzed by FlowJo software (Ashland, OR, USA).

MRM

The PDI-1 was solved by ethanol to obtain the 2.6mg/ml working solution. Working standard solutions were diluted at 10ng/ml, 50ng/ml, 200ng/ml, 400ng/ml, 600ng/ml, 800ng/ml, 1000ng/ml, 1200ng/ml, 1400ng/ml concentration by ethanol. The serum calibration standards were obtained by adding working standard solutions into blank mice serum. A dose of 8mg/kg PD-I1 was administrated by i.p. to study the pharmacokinetic of PD-I1 in Balb/c male mice (5-week). Blood samples were collected at 1min, 5min, 10min, 20min, 0.5h, 1h, 2h, 4h, 8h, 16h, 24h time-point, and harvest the serum by centrifuging at 500g, 5 min. To extract PDI-1, serum was treated with ten volumes of ethanol and vortex. After centrifuging for 10 min at 10000 x g (4°C), the supernatant was dried in a SpeedVac, suspended in 50 μL of ethanol, and injected into the LC-MS/MS system. An Eclipse Plus C18 (100 × 2.1 mm; 3.5 μm) from Agilent (ZORBAX, USA) was used for chromatographic separation and isocratic elution consisted of water (A) and methanol (B), the ratio of A and B is 20:80. The injection volume was 5 μL and a flow rate of 0.3 ml/min was used. Concentration curves were used for quantitation of the peptides in the serum samples. The mass spectrometry analysis was processed using an Agilent Technologies 6460 Triple Quadrupole LC/MS (ZORBAX, USA).

Mice

For this research, C57BL/6 and DBA/2 mice free of pathogens were purchased from Beijing Vital River Laboratory Animal Technology Co., Ltd (Beijing, China). Male and female mice between 4-5 weeks old were used for the syngeneic model. Mice were housed in a pathogen-free environment under conditions of 20°C ± 2°C, 50% ± 10% relative humidity, 12-h light/dark cycles. They were provided with food and water ad libitum. All animal experiments were generated with the institutional guidelines and approved by the Ethics Review Commission of Zhengzhou University (CUHCI2019001).

Syngeneic Animal Experiments

PD-L1 humanized B16F10 and KLN205 (5 x 10^6) cells were inoculated subcutaneously (s.c.) on the flank of mice with 100 μl of sterile PBS. Seven days following injection when the tumor volume reached 100 mm^3, mice were randomized into three groups, and treatment was initiated. The vehicle or PDI-1 (2/4/8 mg/kg per mice) was administered intraperitoneally (i.p) every day. The tumor's volume was measured twice a week using the formula (L * W * H * 0.52). When the average tumor volume of the vehicle group reached 1000 mm^3, mice were sacrificed and the amount of liver, spleen and tumor were measured.

Statistical Analysis

Data analysis was performed using GraphPad Prism7 (GraphPad Software Inc. La Jolla, CA, USA). Unpaired two-tailed Student's t test was used to compare two groups; One way ANOVA followed by Bonferroni's posttest was applied to assess the statistical significance of differences between multiple treatment groups. P values ≤ 0.05 were considered statistically significant.

Graphical Illustrations

Schematic illustrations were established with Bio Render (BioRender.com).

RESULTS

PDI-1 as a Small Molecule Inhibitor of PD-1/PD-L1 Binding

PDI-1 was first reported by BMS (CN105705489A) and has been identified as a potent and selective small-molecule inhibitor that blocks the interaction between PD-1 and PD-L1. However, the *in-vivo* antagonist effect of PDI-1 to the PD-1/PD-L1 checkpoint still under investigation, so we selected PDI-1, an hPD-L1 inhibitor, as a candidate antagonist. Modeling of PDI-1 docking to hPD-1 and hPD-L1 (**Figures 1A, B**), demonstrates that PDI-1 may interact with the side-chain of serine 57 in hPD-1 and phenylalanine 19 in hPD-L1.

To determine the effectivity of PDI-1 on PD-1/PD-L1 binding, we performed a competitive ELISA assay with solid-phase hPD-1 and solution-phase hPD-L1. We found that PDI-1 dose-dependently inhibited hPD-1 binding to solid-phase PD-L1 with a 50% inhibitory concentration of 4.655 μM (**Figure 1C**). We next investigated whether PDI-1 could bind to human and/or mouse (m) PD-1 and/or PD-L1 using chip-immobilized purified proteins and surface plasmon resonance assays. Interestingly, we found that PDI-1 could bind directly to all four molecules, but had the highest affinity for hPD-L1 and mPD-1 (**Figures 1D, E**). The equilibrium dissociation constants of PDI-1 were 3.021×10^{-6} M for hPD-1, 4.163×10^{-8} M for mPD-1, 4.266×10^{-8} M for hPD-L1, and 1.250×10^{-7} M for mPD-L1. Thus, PDI-1 binds to PD-1 and PD-L1 from both species and inhibits the hPD-1/hPD-L1 interaction *in vitro*.

PDI-1 Increases Anti-Tumor Cytotoxicity and Cytokine Production of T Cells *Ex Vivo*

We then investigated the effects of PDI-1 on the anti-tumor activity of purified human CD3+ T cells *ex vivo*. To confirm that PDI-1 was not directly cytotoxic to human T cells or tumor cells, we examined the effects of incubation with up to 10 μM PDI-1 for 24 hours on the viability of activated human CD3+ T cells (incubated with anti-CD3/CD28-coupled beads for 2 days), two human NSCLC cell lines, NCI-H1975 and A549, and two human melanoma cell lines, A375 and SK-MEL-2. Importantly, we detected no significant effects of PDI-1 on the viability of these cells over the 24- hours incubation (**Supplementary Figures 1A–C**). To measure the effects of PDI-1 on T cell cytotoxicity, activated CD3+ T cells were incubated for 18 h with CFSE-labeled NCI-H1975, A549, A375, and SK-MEL-2 cells at a ratio of 5:1 (E:T) in the presence or absence of PDI-1 or the

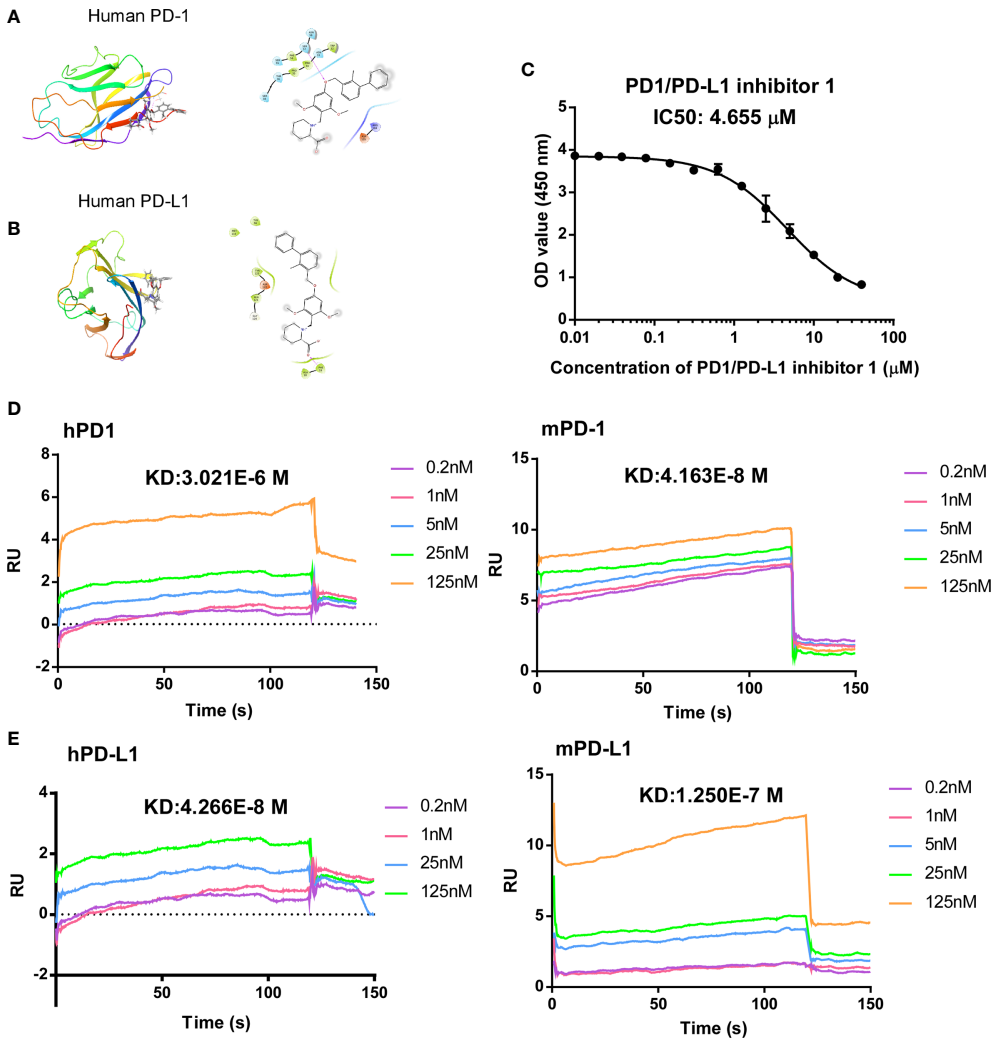

FIGURE 1 | Computer modeling of predicted antagonism of PD-1/PD-L1 binding by PDI-1. **(A, B)** Ribbon representations of a predicted binding pocket for PDI-1 in human PD-1 **(A)** and human PD-L1 **(B)**. Magnified views of the side-chain of Ser567 **(A)** and Phe19 **(B)** with PDI-1 are shown on the right. **(C)** PD-1/PD-L1 binding by PDI-1 *in vitro*, measured using a competitive binding ELISA assay. Data represent the mean ± SEM of three replicates. **(D, E)** Surface plasmon resonance assay of binding of PDI-1 to chip-bound purified human and mouse PD-1 **(D)** or PD-L1 **(E)**.

anti-PD-1 mAb nivolumab. After 18 h co-culture, the cells were labeled with PI and subjected to flow cytometry quantify live (CFSE +) and dead or dying (CFSE+ PI+) cancer cells. We found that T cell cytotoxicity against all four cancer cell lines was significantly higher in the presence of 4 μM PDI-1 compared with vehicle (**Figures 2A, B**). To determine whether PDI-1 also inhibits tumor-cell-induced cytokine production by activated CD3+ T cells, we collected the culture supernatants after 18 h incubation and performed ELISAs to

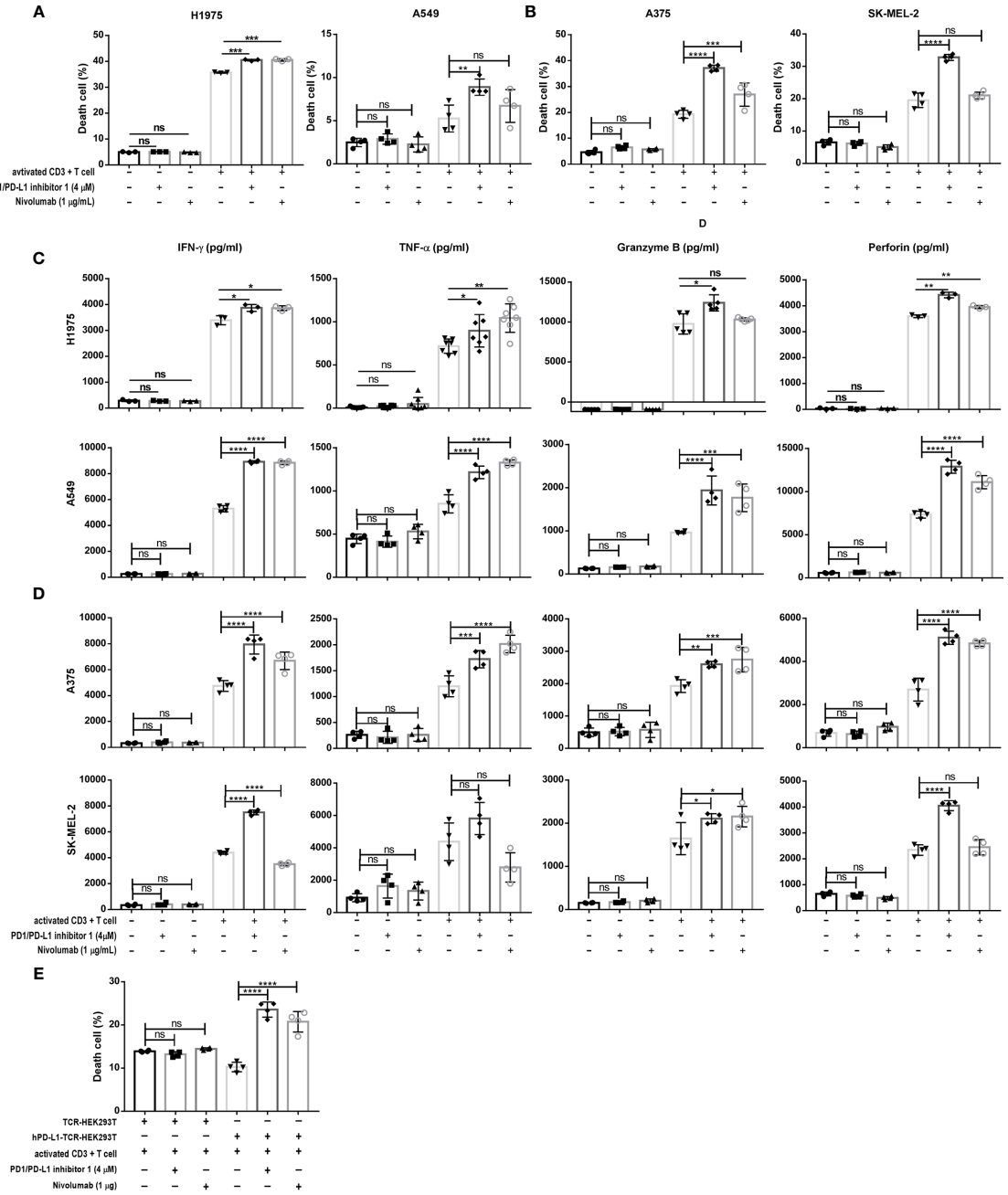

FIGURE 2 | PDI-1 restores T cell cytotoxicity and cytokine production. **(A, B)** Cytotoxicity assay of activated CD3+ T cells cultured for 18 h at an effector to target ratio of 5 to 1 with CFSE-labeled H1975, A549 **(A)** A375, or SK-MEL-2 **(B)** cells alone or in the presence of either PDI-1 (4 μM), nivolumab (1 μg/ml), or an isotype control Ab. At the end of the incubation, cells were labeled with PI and dead or dying tumor cells (CFSE+ PI+) were quantified by flow cytometry. **(C, D)** Cytokine production by activated CD3+ T cells incubated for 18 h, as described for **(A, B)**. Culture supernatants were collected and levels of IFN-γ, TNF-α, perforin, and granzyme B were measured by ELISA assay. **(E)** Activated CD3+ T cells were cultured for 18 h with hPD-L1-TCR-HEK293T cells or TCR-HEK293 T cells in the presence or absence of PDI-1 (4 μM) or nivolumab (1 μg/ml). Dead/dying HEK293 cells were quantified by flow cytometry as described for **(A, B)**. Data represent the mean ± SEM of three replicates. *$p < 0.05$; **$p < 0.01$; ***$p < 0.001$; ****$p < 0.0001$; ns, not significant.

measure secretion of the cytolytic proteins granzyme B and perforin and the inflammatory cytokines IFN-γ and TNF-α. As expected, secretion of all four mediators was induced by incubation of T cells with the cancer cells alone, but a striking increase in mediator secretion was detected after treatment with PDI-1 compared with vehicle (**Figures 2C, D**).

To confirm that PDI-1-mediated enhancement of TCR-triggered apoptosis was dependent on disruption of PD-1/PD-L1 interactions, we incubated activated CD3+ T cells with HEK293T cells co-expressing a TCR activator with or without hPD-L1 (hPD-L1-TCR-HEK293T and TCR-HEK293T cells, respectively; **Supplementary Figure 1D**). Co-expression of PD-L1 reduced the ability of activated T cells to induce TCR-HEK293T cell apoptosis, as expected. However, incubation with PDI-1 reversed the PD-L1-mediated suppression of apoptosis, and the level of hPD-L1-TCR-HEK293T cell death exceeded that of TCR-HEK293T cells (**Figure 2E**).

PDI-1 Promotes T Cell Activation *via* the CD28-TCR Axis

As shown in **Figure 3A**, engagement of the antigen-specific TCR and CD28 costimulatory molecule by tumor cells or antigen-presenting cells triggers a T cell signaling cascade involving ZAP70, PI3K, and RAS pathways (7). Ultimately, this pathway activates the transcription factors NF-κB, AP-1, and NFAT and increases the production of inflammatory cytokines (20). However, activation of this pathway is blocked when the PD-1/PD-L1 axis is engaged (21). Therefore, we next investigated whether PDI-1 enhances T cell activation by blockingPD-1/PD-L1 inhibitory signals. To this end, we employed an assay in which Jurkat T cells were transfected with hPD-1 and an NFAT luciferase reporter (hPD-1-NFAT-Jurkat cells) and incubated with HEK293T cells expressing a TCR activator alone (TCR-HEK293T) or co-expressing hPD-L1 and a TCR activator (hPD-L1-TCR-HEK293T). This system thus serves as a reporter of the effects of PD-1/PD-L1 modulators on TCR signaling. As shown in **Figure 3B**, co-culture of hPD-1-NFAT-Jurkat cells with hPD-L1-TCR-HEK293T cells for 6 h significantly reduced the baseline activity of NFAT. However, addition of either PDI-1 or nivolumab to the culture significantly reversed the inhibition of NFAT activity induced by hPD-L1-TCR-HEK293T cells. This rescue effect of PDI-1 was dependent on PD-1/PD-L1 engagement, because PDI-1 had no effect on NFAT activity in hPD-1-NFAT-Jurkat cells cultured with TCR-HEK293T cells, which lack hPD-L1 expression (**Figure 3C**). Finally, we verified that these results could not simply be explained by a toxic effect by demonstrating that PDI-1 had no effect on the viability of hPD-1-NFAT-Jurkat cells alone (**Figure 3D**). These results indicate that PDI-1 augments T cell activation by preventing PD-1/PD-L1-triggered inhibition of the TCR/CD28-mediated signaling cascade.

PDI-1 Inhibits the Growth of Melanoma and NSCLC Tumors *In Vivo*

Having demonstrated that PDI-1 effectively blocks PD-1/PD-L1-mediated suppression of anti-tumor cytotoxicity and cytokine production by human T cells *ex vivo*, we next determined whether PDI-1 would have beneficial effects on tumor growth *in vivo*. We transfected the mouse NSCLC cell line KLN205 and the mouse melanoma cell line B16F10 with hPD-L1 and verified that the transfectants expressed much higher levels of hPD-L1 relative to the levels of endogenous mPD-L1 (**Supplementary Figure 2**). To determine whether PDI-1 was directly toxic to mice, groups of wild-type C57BL/6 mice were injected intraperitoneally with vehicle or 2, 4, or 8 mg/kg PDI-1 once daily for 13-days. As shown in **Supplementary Figure 3**, there were no detectable effects of PDI-1 treatment on the liver, spleen, or body weights of the treated mice. To examine the effects of PDI-1 treatment on tumor growth, groups of C57BL/6 mice (B16-F10 syngeneic) were subcutaneously injected with hPD-L1-B16-F10 melanoma cells (**Figure 4**) or groups of DBA/2 mice (KLN205 syngeneic) were injected subcutaneously with hPD-L1-KLN205 cells (**Figure 5**), and the mice were injected intraperitoneally with the vehicle, 4 mg/kg PDI-1, or 8 mg/kg PDI-1 once daily for either 29 days (C57BL/6) or 33 days (DBA/2). Compared with vehicle-treated mice, PDI-1 treatment dramatically attenuated the growth of hPD-L1-B16F10 tumors (**Figures 4A, B**, **Supplementary Figure 4A**), and a similar trend, albeit not statistically significant, was observed for the effect of PDI-1 on the growth of hPD-L1-KLN205 tumors (**Figures 5A–C**). Importantly, the spleen, liver, and body weights of the tumor-bearing mice were not affected by PDI-1 treatment compared with vehicle treatment (**Supplementary Figures 4B, C**). At the end of the experiment (days 29 or 33), the tumors were excised for further analysis. H&E staining of hPD-L1-B16-F10 tumors (**Figure 4C**) and hPD-L1-KLN205 tumors (**Figure 5D**), showed that PDI-1 treatment caused a marked increase in tumor infiltration by inflammatory cells and necrosis of tumor cells compared with tumors from vehicle-treated mice. The abundance of CD8+ T cells and FoxP3+ T regulatory cells (Tregs), as well as PD-L1 expression by tumor and stromal cells in the tumor microenvironment (TME), are predictors of prognosis and response to immunotherapy in human NSCLC and melanoma (22). Fluorescent multiplex immunohistochemical (mIHC-F) staining of CD8a, FoxP3, and PD-L1 proteins in sections of hPD-L1-B16-F10 tumors (**Figures 4C, D**) demonstrated that PDI-1 treatment resulted in an increase in CD8+ T cells, decrease in FoxP3+ Tregs, and reduction in PD-L1 expression compared with vehicle treatment, although only the effects of PDI-1 on CD8+ T cells abundance reached the level of statistical significance (**Figure 4D**). In contrast, mIHC-F of hPD-L1-KLN205 tumor sections showed highly significant increases in CD8+ T cells and reductions in FoxP3+ Tregs and PD-L1 expression in PDI-1-treated mice compared with vehicle-treated mice (**Figures 5D, E**). These results demonstrate that PDI-1 treatment inhibits the growth of NSCLC and melanoma tumor cells, likely through a mechanism involving increased recruitment/activation of cytotoxic T cells and reduced recruitment/activation of inhibitory Tregs.

PDI-1 Rapidly Promotes Activation of the Anti-Tumor T Cell Response *In Vivo*

To investigate the immune mechanism of action of PDI-1 in more detail, we compared the serum cytokine content of tumor-bearing mice on day 29 (hPD-L1-B16-F10) or day 33 (hPD-L1-KLN205)

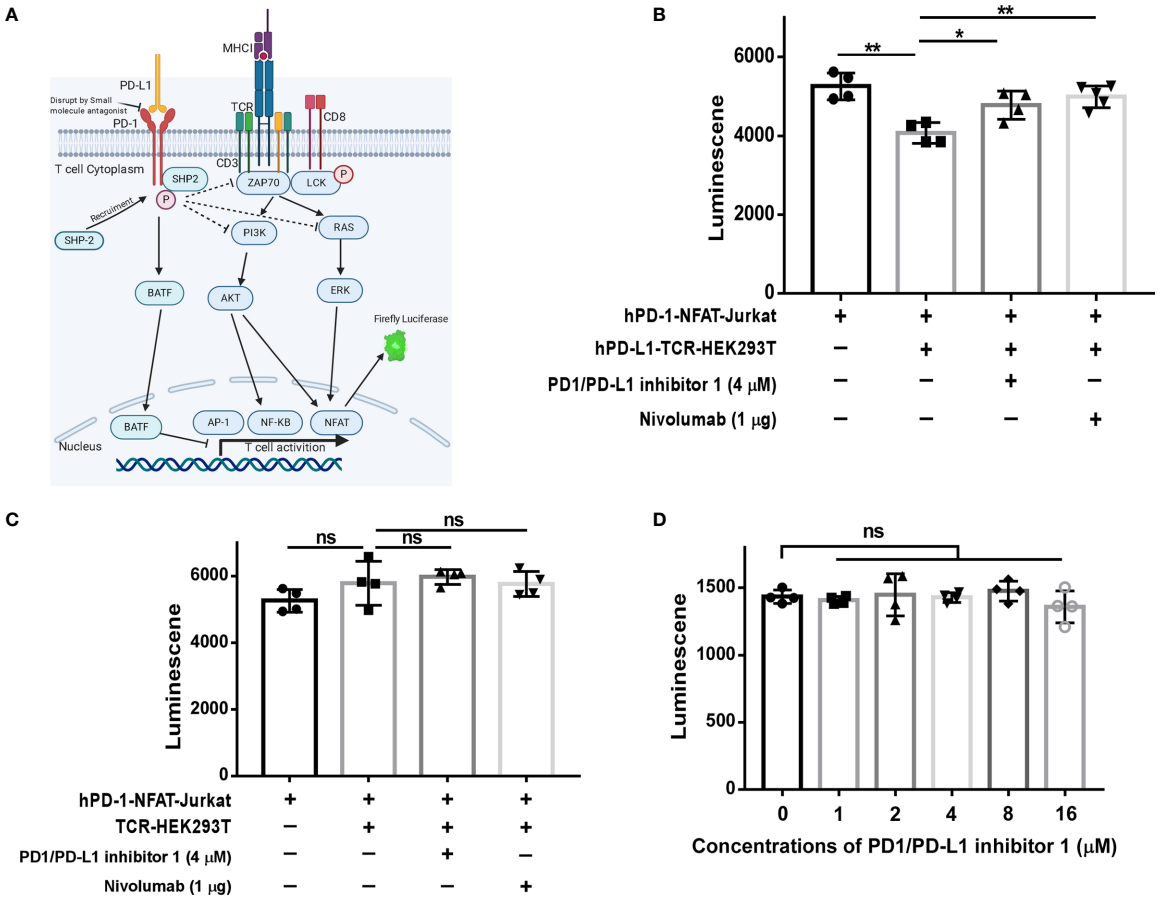

FIGURE 3 | PDI-1 reverses inhibition of NFAT activity by PD-1/PD-L1. **(A)** Schematic of the principle underlying the luciferase reporter assay, in which luciferase expression in Jurkat cells was driven by the NFAT promoter. **(B, C)** hPD-1-NFAT-Jurkat cells were cultured alone or with hPD-L1-TCR-HEK293T cells **(B)** or TCR-HEK293T cells **(C)** overnight. PDI-1 or nivolumab was then added to the cells and luciferase activity was measured after 6 h. **(D)** hPD-1-NFAT-Jurkat cells were cultured with PDI-1 alone for 6 h and luciferase activity was measured. Data represent the mean ± SEM of three replicates. *$p < 0.05$; **$p < 0.01$; ns, not significant.

after treatment with vehicle or PDI-1. Using a multiplex flow cytometry assay, we measured serum concentrations of IL-1α, IL-1β, IL-6, IL-10, IL-12p70, IL-17A, IL-23, IL-27, monocyte chemotactic protein-1 (MCP-1), interferon (IFN)-β, IFN-γ, tumor necrosis factor-α (TNF-α), and granulocyte macrophage-colony stimulating factor (GM-CSF). We found that PDI-1 significantly increased serum levels of several cytokines, most notably IFN-γ, IFN-β, IL-1α, and IL-1β, compared with vehicle (**Figures 6A, B**). We also analyzed the abundance of total CD3+ T cells and/or CD4+ and CD8+ T cell subsets in the peripheral blood and dissociated tumor tissues by flow cytometry. In hPD-L1-B16-F10 tumor-bearing mice, treatment with 4 mg/kg PDI-1 significantly increased the percentage of CD3+ T cells in the peripheral blood compared with vehicle-treated mice, and there was a similar, albeit not significant, trend in the effects of PDI-1 on the abundance of intratumoral CD3+ T cells (**Figure 6C**). Interestingly, treatment with PDI-1 at 8 mg/kg had a smaller effect than 4 mg/kg PDI-1 on CD3+ T cell percentages in both the peripheral blood and tumor tissue (**Figure 6C**). In the PD-L1-KLN205 tumor-bearing mice, the effects of PDI-1 on peripheral blood T cells were more variable than in hPD-L1-B16-F10-bearing mice, although the percentage of CD8 + cells was significantly higher in PDI-1-treated mice than in vehicle-treated mice (**Figure 6C**). Notably, the percentage of intratumoral CD3+ T cells was significantly and dose-dependently increased in hPD-L1-KLN205 tumors from PDI-1-treated compared with vehicle-treated mice (**Figure 6D**).

PDI-1 Rapidly Boosts the Host Anti-Tumor Immune Response

Because the analyses of tumor-infiltrating T cells in the preceding section were performed on days 29 and 33, we next asked whether the effects of PD-L1 blockade might be apparent much earlier in the response. The experiments were therefore repeated with hPD-L1-KLN205 tumors, and the mice were sacrificed on day 7 (**Figure 7A**). Indeed, tumors excised from PDI-1-treated mice displayed enhanced necrosis of cancer cells and infiltration by inflammatory cells compared with tumors from vehicle-treated mice (**Figure 7B**). Furthermore, mIHC-F staining showed that PDI-1 caused a marked increase in CD8a expression and a decrease in PD-L1 and FoxP3 expression in hPD-L1-KLN205 tumors (**Figure 7C**). Evaluation of

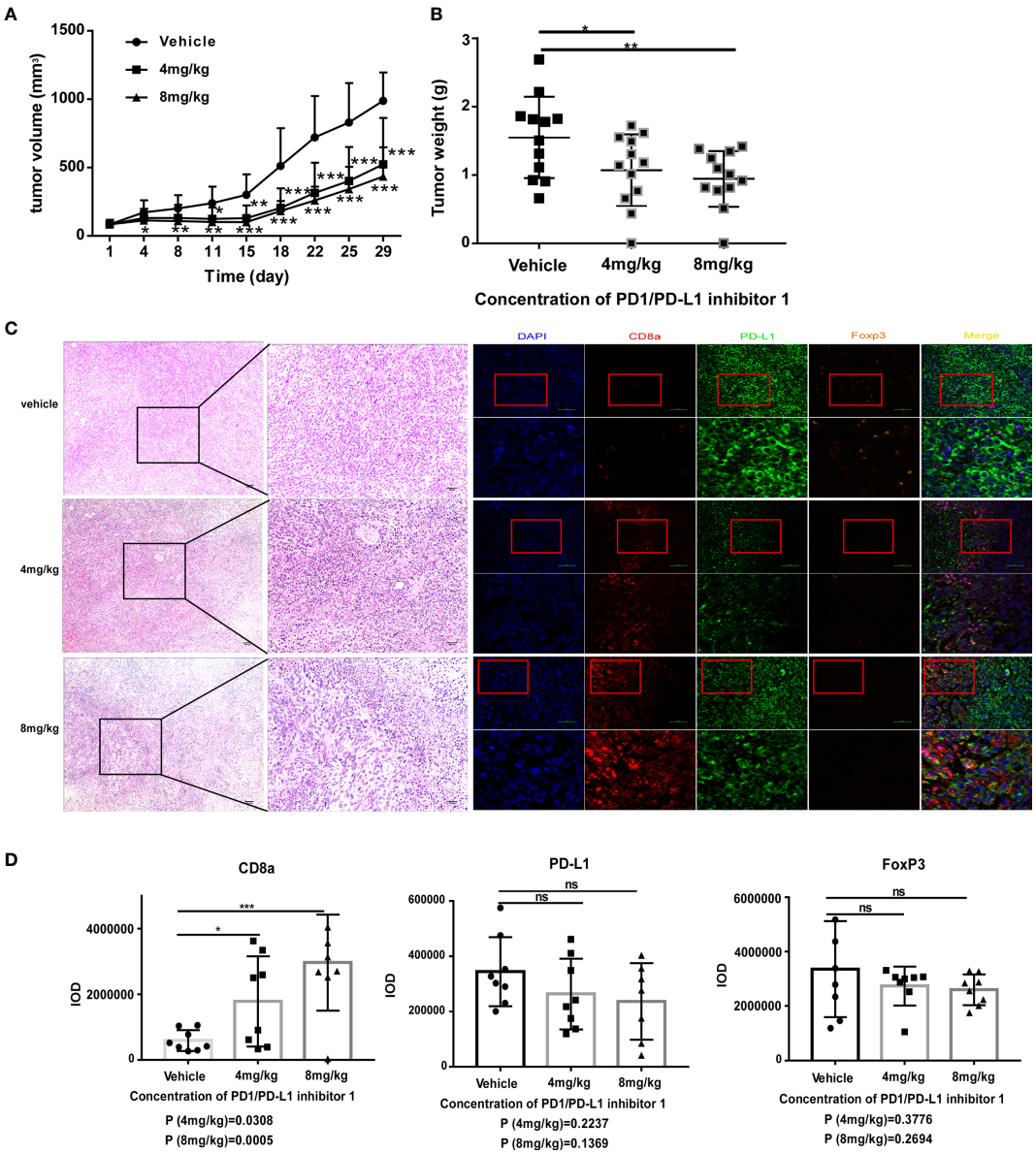

FIGURE 4 | PDI-1 inhibits the growth of human PD-L1-transfected B16-F10 melanoma cells in a mouse model. **(A–D)** B16F10 murine melanoma cells were transfected with hPD-L1 and injected subcutaneously into the flanks of three groups of syngeneic C57BL/6J mice (n=11/group). The mice were then injected intraperitoneally once daily with vehicle, 4 mg/kg PDI-1, or 8 mg/kg PDI-1. **(A, B)** Tumor volumes were measured for up to 29 days. **(B)** Tumors were excised on day 29 and weighed. **(C)** Left: Representative images of H&E-stained tumor sections on day 29. Right: Fluorescent multiplex immunohistochemical staining of PD-L1, CD8a, and FoxP3 proteins in tumors excised on day 29. Nuclei were stained with DAPI. **(D)** Quantification of CD8a, PD-L1, and FoxP3 staining intensity in the images shown in **(C)**. Data represent the mean ± SEM of three replicates. $^{*}p < 0.05$; $^{**}p < 0.01$; $^{***}p < 0.001$; ns, not significant.

serum cytokine levels revealed elevated levels of inflammatory cytokines, including IL-1α, IL-1β, IFN-γ, and TNF-α, in PDI-1-treated compared with vehicle-treated mice (**Figure 7D**). Finally, we analyzed the percentage of CD3+, CD4+, and/or CD8+ T cells in the peripheral blood and dissociated tumor tissues of the treatment mice (**Figures 7E, F**). Although PDI-1 treatment did not affect the percentage of total CD3+ T cells in peripheral blood, the relative abundance of CD8+ and CD4+ T cells was increased and decreased, respectively, in PDI-1-treated mice compared with vehicle-treated mice (**Figure 7E**). In addition, treatment with 4 mg/kg PDI-1 caused a significant increase in the abundance of tumor-associated CD3+ T cells (**Figure 7F**). Importantly, the beneficial anti-cancer effects of PDI-1 on T cell abundance, cytokine production, and PD-L1 expression were as good as or superior to the effects of the anti-PD-L1 mAb atezolizumab (**Supplementary Figures 7A–C**).

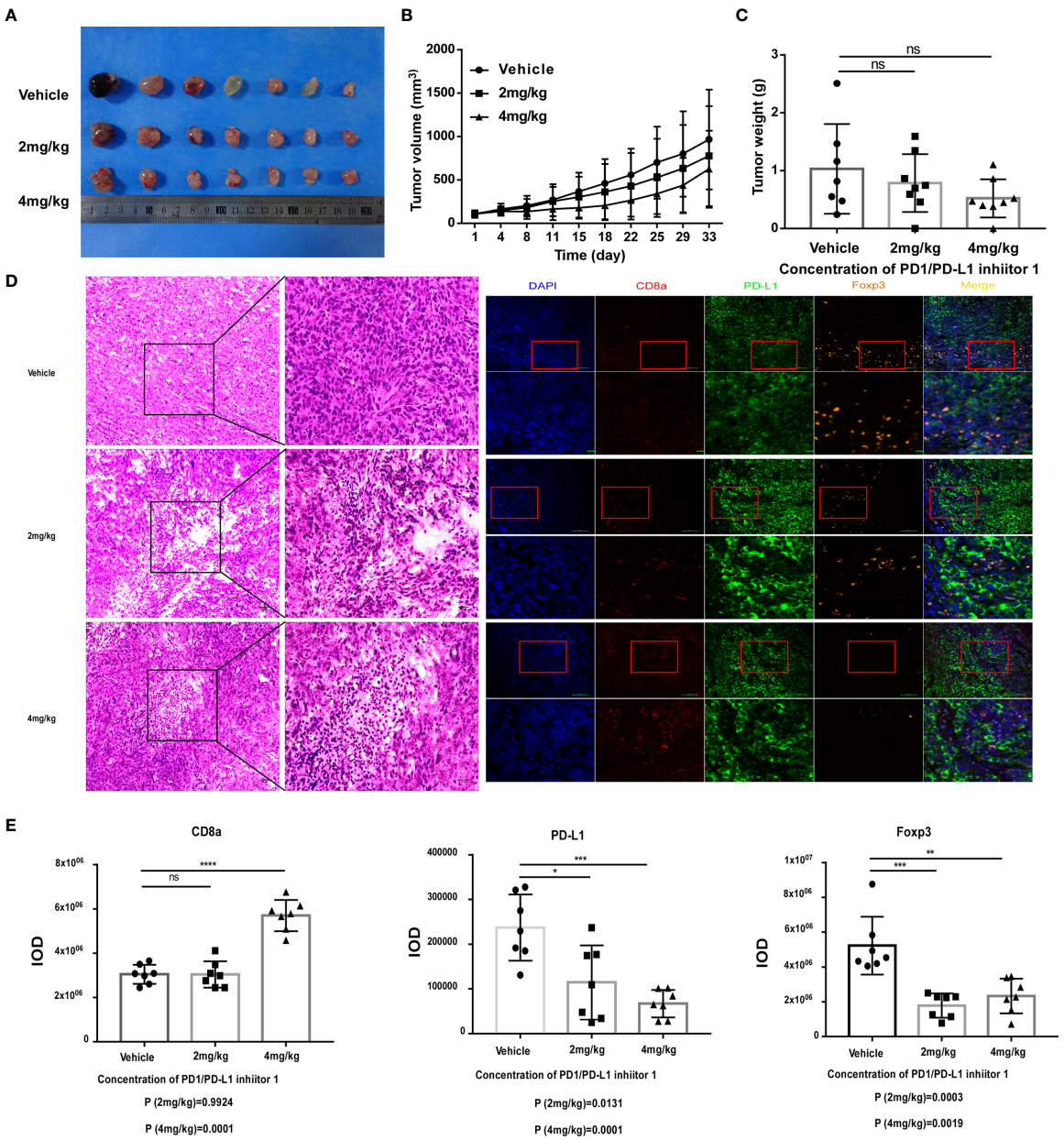

FIGURE 5 | PDI-1 inhibits the growth of human PD-L1-transfected KLN205 NSCLC cells in a mouse model. **(A–E)** KLN205 cells were transfected with hPD-L1 and injected subcutaneously into the flanks of three groups of syngeneic DBA/2 mice (n=8/group). The mice were then injected intraperitoneally once daily with vehicle, 2 mg/kg PDI-1, or 4 mg/kg PDI-1. **(A)** Representative photographs of tumors excised on day 33. **(B)** Tumor volumes measured for up to 33 days. **(C)** Tumor weights on day 33. **(D)** Left: Representative images of H&E-stained tumor sections on day 33. Right: Fluorescent multiplex immunohistochemical staining of PD-L1, CD8a, and FoxP3 proteins in tumors excised on day 33. Nuclei were stained with DAPI. **(E)** Quantification of CD8a, PD-L1, and FoxP3 staining intensity in the images shown in **(D)**. Data represent the mean ± SEM of three replicates. $^{*}p < 0.05$; $^{**}p < 0.01$; $^{***}p < 0.001$; ns, not significant.

DISCUSSION

Accumulating preclinical and clinical data support the crucial role of immune checkpoint pathways as therapeutic targets for cancer. Elucidation of the molecular mechanisms of PD-1 activity and the identification of its ligands (23, 24) has enabled detailed investigation of the involvement of this receptor–ligand pair in the anti-tumor immune response. As noted earlier, PD-1/PD-L1 interactions play a physiological role in maintaining tolerance through suppression of T cell activation, and expression of PD-L1 by cancer cells enables them to evade host immune surveillance (25). Several anti-PD-1 mAbs have been

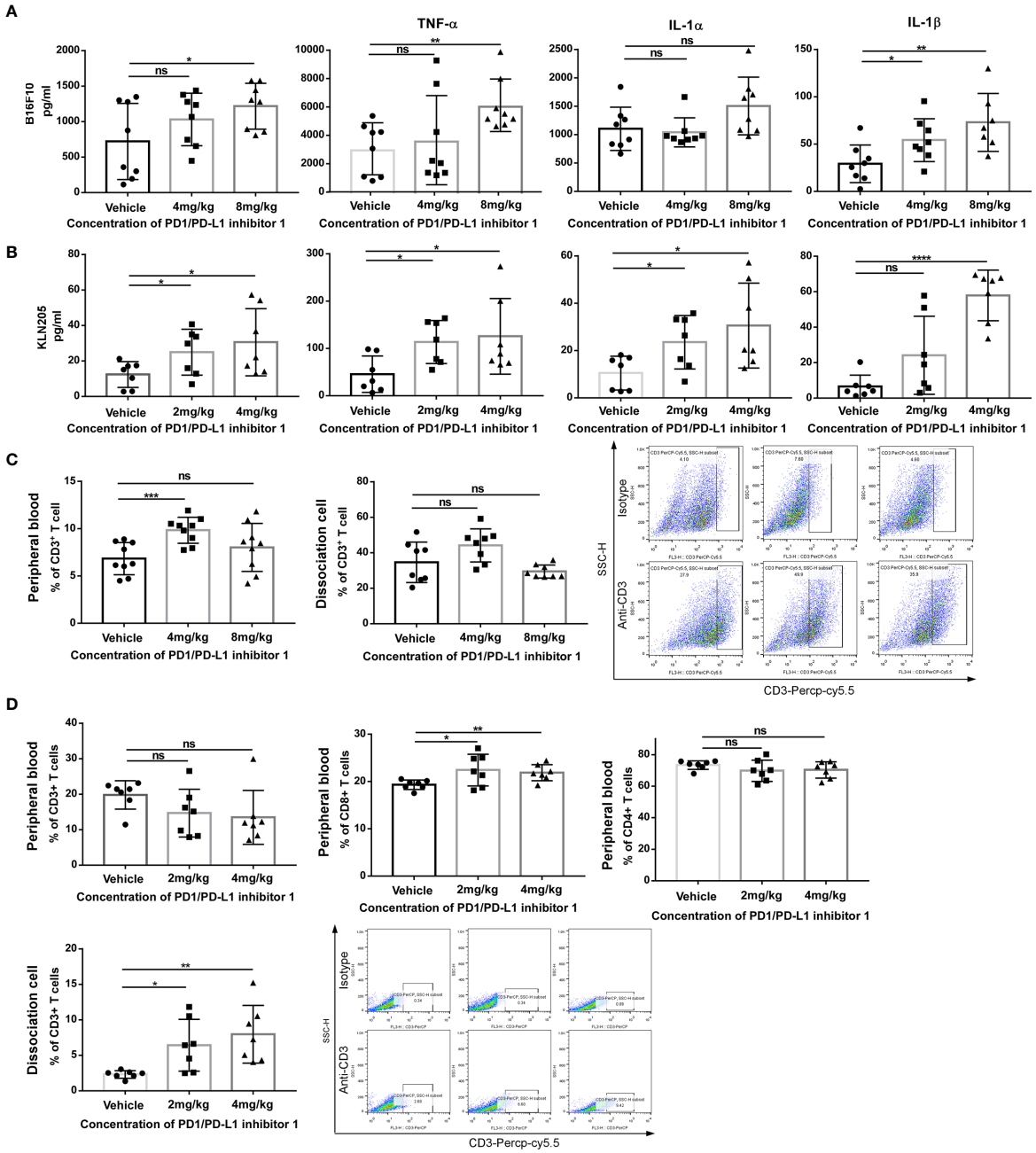

FIGURE 6 | PDI-1 increases T cell-mediated anti-tumor responses *in vivo*. **(A, B)** Blood samples were collected on day 29 from hPD-L1-B16F10 tumor-bearing mice **(A)** or on day 33 from hPD-L1-KLN205 tumor-bearing mice, as described in **Figures 4** and **5**. Serum levels of IFN-γ, TNF-α, IL-1α, and IL-1β were analyzed using a multiplex flow cytometry assay. **(C)** Flow cytometric analysis of CD3+ T cells in peripheral blood mononuclear cells (left) or dissociated tumor tissue (middle) on day 29 after injection of hPD-L1-B16F10 cells. Dot plots (right) show representative FACS analysis of CD3 + T cells derived from tumor specimens. **(D)** Flow cytometric analysis of CD3+, CD4+, and CD8 + T cells in peripheral blood or of intratumorally CD3+ T cells on day 33 after injection of hPD-L1-KLN205 cells. Dot plots show representative FACS analysis of CD3 + T cells derived from tumor specimens. Data represent the mean ± SEM of three replicates. *$p < 0.05$; **$p < 0.01$; ***$p < 0.001$; ****$p < 0.0001$; ns, not significant.

developed and approved for cancer therapy, including nivolumab, pembrolizumab, and atezolizumab (26); nevertheless, about 70% of patients with small cell lung cancer do not respond well to anti-PD-1 mAbs (27). The reason for such unresponsiveness is unclear and is under intense investigation.

Although small molecule blockers of the PD-1/PD-L1 interaction would have intrinsic advantages over mAbs, their development has progressed more slowly. In addition to the benefits already described, small molecules have the potential to enter cells and thus target the molecular mechanisms of

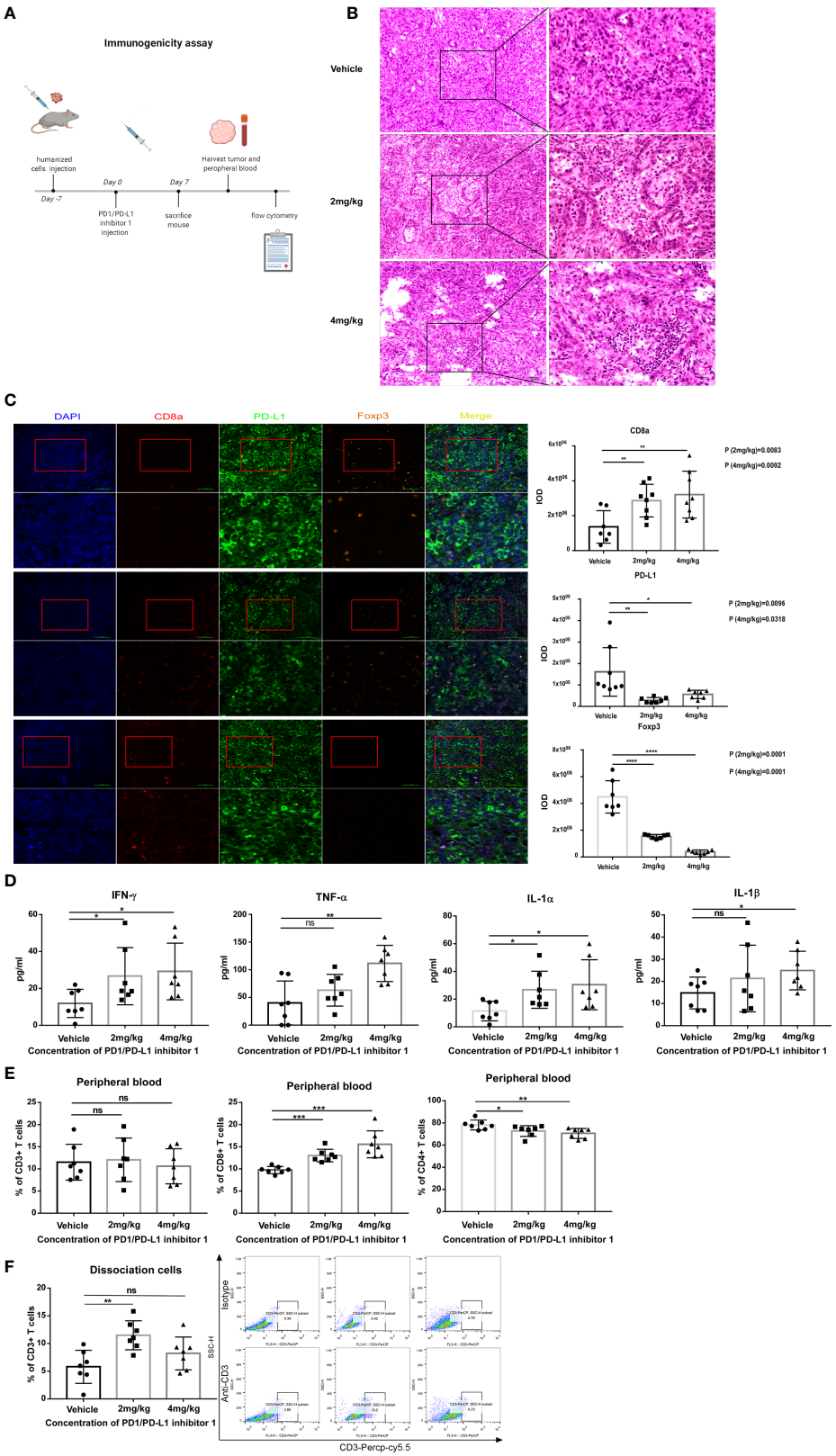

FIGURE 7 | Continued

FIGURE 7 | PDI-1 treatment rapidly boosts the host immune response to hPD-L1-KLN205 NSCLC tumors. **(A)** Schematic of the experimental design. DBA/2 mice were injected subcutaneously with hPD-L1-KLN205 cells and administered vehicle, 2 mg/kg PDI-1, or 4 mg/kg PDI-1 by intraperitoneal injection. Mice were sacrificed on day 7 and peripheral blood and tumors were collected for analysis. **(B)** Representative images of H&E-stained tumor sections. **(C)** Fluorescent multiplex immunohistochemical staining of CD8a, PD-L1, and FoxP3 protein in excised tumors. Nuclei were stained with DAPI. **(D)** Serum levels of IFN-γ, TNF-α, IL-1α, and IL-1β were analyzed using a multiplex flow cytometry assay. **(E, F)** Flow cytometric analysis of CD3+, CD4+, and CD8+ T cells in peripheral blood **(E)** or of intratumoral CD3+ T cells **(F)** on day 7. Dot plots indicate representative FACS analysis of CD3 + T cells derived from tumor specimens. Data represent the mean ± SEM of three replicates. $^{*}p < 0.05$; $^{**}p < 0.01$; $^{***}p < 0.001$; ns, not significant.

immunosuppression not accessible to mAb therapies (28). Thus, novel small molecule compounds that could be used alone or in combination with mAbs provide an alternative therapeutic approach for patients with poor clinical responses and/or resistance to existing drugs.

In this study, we identified PDI-1 as a small molecule that binds to hPD-1 and hPD-L1 and disrupts their interactions *in vitro* and *in vivo*. Nivolumab binds to hPD-1 at amino acids 25–34 (29), whereas our docking simulations suggest that PDI-1 binds in the region of serine 57 of hPD-1. Thus, the binding sites of nivolumab and PDI-1 are non-overlapping and the combination of both agents could potentially provide superior efficacy compared with either agent alone.

We demonstrated that PDI-1 blocks PD-1/PD-L1-mediated negative regulation of TCR-activated T cells (30), thereby promoting T cell cytotoxicity and cytokine production, cancer cell apoptosis, and recruitment of inflammatory cells to the TME (31, 32). In syngeneic mouse tumor models, PDI-1 inhibited the growth of hPD-L1-expressing melanoma and NSCLC by increasing the abundance of effector CD8+ T cells and decreasing that of inhibitory FoxP3 CD4+ Tregs. We also verified that the PD-1/PD-L1 axis contributes to tumor immune evasion, and our results suggest that PDI-1 may rejuvenate immunosurveillance by relieving T cell anergy induced by potent and chronic stimulation by tumor antigens (33). PD-1 engagement by PD-L1 on cancer cells is known to interfere with TCR/CD28-dependent T cell signaling by blocking exhaustion-associated transcription factors, including the AP-1, NF-κB, and NFAT (34). Martinez et al. showed that different *styles of NFAT* trigger transcriptional profiles associated with exhausted *versus* effector T cell phenotypes (35). PD-L1 binding to PD-1 induces phosphorylation of the immunoreceptor tyrosine switch motif in the cytoplasmic domain of PD-1, which leads to recruitment of SHP2 phosphatase, inhibition of downstream signaling through ZAP70 and PI3K, and inhibition of T cell proliferation, differentiation, and cytokine production (36–38). Consistent with this, we demonstrated that PDI-1 enhances NFAT activity in Jurkat T cells in a TCR- and PD-L1-dependent manner, thus providing a molecular mechanism by which PDI-1 enhances anti-tumor responses to NSCLC and melanoma in mice. Importantly, treatment of mice with PDI-1 alone did not affect organ or body weights, suggesting that PDI-1 has a favorable safety profile. We detected the distribution of PDI-1 in mice (**Supplementary Figure 8**). The MRM chromatograms in **Supplementary Figure 8** show the serum concentrations of PDI-1 increase at 5 minutes.

Our finding, that PDI-1 is efficacious and safe in two *in vivo* models of cancer, suggests that this compound could be clinically developed as a new ICI. Small molecule compounds represent an important potential source of novel anti-cancer drugs; however, few small molecules affecting immune regulation have been developed to date. Further studies on the immunomodulatory activity of compounds such as PDI-1 will be of considerable importance in advancing the development of small molecule anti-cancer drugs.

DATA AVAILABILITY STATEMENT

The original contributions presented in the study are included in the article/**Supplementary Material**, further inquiries can be directed to the corresponding author/s.

ETHICS STATEMENT

The animal study was reviewed and approved by the Ethics Committee of China-US (Henan) Hormel Cancer Institute (CUHCI2019001).

AUTHOR CONTRIBUTIONS

YW, TG and M-HL were involved in study concept and design, acquisition of data, analysis, and interpretation of data, and drafting of the manuscript. YW, TG, XT, WL, RZ and WY performed the experiments. QG, TL, CZ, J-HS, and KL provided material support. YW, TG and M-HL wrote the manuscript. M-HL supervised the study. All authors contributed to the article and approved the submitted version.

FUNDING

This work was supported by grant funding from the National Natural Science Foundation of China NSFC81972839, and the Key Program of Henan Province, China Grant NO.161100510300 and Henan Provincial Government, China.

ACKNOWLEDGMENTS

We thank Anne M. O'Rourke, PhD, from Liwen Bianji, Edanz Group China (www.liwenbianji.cn/ac), for editing the English text of a draft of this manuscript.

SUPPLEMENTARY MATERIAL

The Supplementary Material for this article can be found online at: https://www.frontiersin.org/articles/10.3389/fimmu.2021.654463/full#supplementary-material

Supplementary Figure 1 | PDI-1 is not toxic to cancer cells or CD3+ T cells. **(A–C)** Proliferation of NCI-H1975, A549 **(A)** A375, SK-MEL-2 **(B)** tumor cells or CD3+ T cells **(C)**. Cells were cultured overnight and then incubated with the indicated concentrations of PDI-1 for an additional 24 hours. Viability was measured using an MTS assay. **(D)** Flow cytometric analysis of hPD-L1 expression on TCR-HEK293T and hPD-L1-TCR-HEK293T cells. Data represent the mean ± SEM of three replicates. $^{*}p < 0.05$; $^{**}p < 0.01$; $^{***}p < 0.001$.

Supplementary Figure 2 | Mouse and human PD-L1 expression in transfected cancer cell lines. (A, B) Flow cytometric analysis of double staining of human (h) and mouse (m) PD-L1 on murine KLN205 NSCLC cells **(A)** and murine B16-F10 melanoma cells **(B)** after transfection with human PD-L1. Cells were stained with hPD-L1 or an isotype control IgG antibody.

Supplementary Figure 3 | PDI-1 exhibits no toxicity in wild-type C57BL/6 mice. **(A–C)** Groups of 5–6-week-old wild-type C57BL/6 mice were administered vehicle or the indicated doses of PDI-1 by intraperitoneal injection once daily for 13 days. Liver **(A)**, spleen **(B)** and body **(C)** weights were determined on day 13. Data represent the mean ± SEM of 6 mice/group. ns, not significant.

Supplementary Figure 4 | PDI-1 exhibits no toxicity in mice bearing hPD-L1-transfected melanoma or NSCLC tumors. **(A, B)** Groups of C57BL/6 mice (n=11) were injected with hPD-L1-B16-F10 melanoma cells and administered vehicle or the indicated doses of PDI-1 by intraperitoneal injection once daily for 29 days. Tumors were excised and photographed **(A)** and the liver, spleen, and body weights **(B)** were then determined. **(C)** Groups of DBA/2 mice (n=8) were injected with hPD-L1-KLN205 NSCLC cells and administered vehicle or the indicated doses of PDI-1 by intraperitoneal injection once daily for 33 days. Liver, spleen, and body weights were then determined. Data represent the mean ± SEM. ns, not significant.

Supplementary Figure 5 | PDI-1 increases inflammatory cytokine production in hPD-L1-transfected tumor-bearing mice. **(A, B)** Blood samples were collected from C57BL/6 mice bearing hPD-L1-B6F10 tumors on day 29 **(A)** or from DBA/2 mice bearing hPD-L1-KLN205 tumors on day 33 **(B)**. Sera were analyzed for the indicated inflammatory mediators using a multiplex flow cytometry assay. Data represent the mean ± SEM of 8 mice/group. $^{*}p < 0.05$; $^{**}p < 0.01$; $^{***}p < 0.001$; $^{****}p < 0.0001$; ns, not significant.

Supplementary Figure 6 | PDI-1 rapidly boosts the host immune response to hPD-L1-bearing tumor cells. DBA/2 mice harboring hPD-L1-KLN205 tumors were bled on day 7 and sera were analyzed for the indicated inflammatory mediators using a multiplex flow cytometry assay. Data represent the mean ± SEM of 7 mice/group. $^{*}p < 0.05$; $^{**}p < 0.01$; ns, not significant.

Supplementary Figure 7 | Comparison of PDI-1 with Atezolizumab in an animal model. **(A–C)** Groups of C57BL/6 (n=6) mice were injected with hPD-L1-B16-F10 murine melanoma cells and administered vehicle, 4 or 8 mg/kg PDI-1, or the anti-PD-L1 mAb atezolizumab (10 mg/kg) by intraperitoneal injection once daily for 7 days. Tumors and blood samples were collected on day 14. **(A)** Representative images of H&E-stained tumor sections. **(B)** Fluorescent multiplex immunohistochemical staining of PD-L1, CD8a, and FoxP3 protein in excised tumors. **(C)** Serum levels of the indicated cytokines were determined using a multiplex flow cytometry assay. $^{*}p < 0.05$; $^{**}p < 0.01$; $^{***}p < 0.001$; $^{****}p < 0.0001$; ns, not significant.

Supplementary Figure 8 | Distribution of PDI-1 in mice. MRM chromatograms for PDI-1 detected in the serum of C57BL/C male mice.

REFERENCES

1. Topalian SL, Weiner GJ, Pardoll DM. Cancer Immunotherapy Comes of Age. *J Clin Oncol: Off J Am Soc Clin Oncol* (2011) 29(36):4828–36. doi: 10.1200/JCO.2011.38.0899
2. Hanahan D, Weinberg RA. Hallmarks of Cancer: The Next Generation. *Cell* (2011) 144(5):646–74. doi: 10.1016/j.cell.2011.02.013
3. Seliger B. Basis of PD1/PD-L1 Therapies. *J Clin Med* (2019) 8(12):2168. doi: 10.3390/jcm8122168
4. Mahoney KM, Rennert PD, Freeman GJ. Combination Cancer Immunotherapy and New Immunomodulatory Targets. *Nat Rev Drug Discovery* (2015) 14(8):561–84. doi: 10.1038/nrd4591
5. Lesokhin AM, Callahan MK, Postow MA, Wolchok JD. On Being Less Tolerant: Enhanced Cancer Immunosurveillance Enabled by Targeting Checkpoints and Agonists of T Cell Activation. *Sci Trans Med* (2015) 7 (280):280sr1. doi: 10.1126/scitranslmed.3010274
6. Wang X, Teng F, Kong L, Yu J. Pd-L1 Expression in Human Cancers and its Association With Clinical Outcomes. *OncoTargets Ther* (2016) 9:5023–39. doi: 10.2147/OTT.S105862
7. Ostrand-Rosenberg S, Horn LA, Haile ST. The Programmed Death-1 Immune-Suppressive Pathway: Barrier to Antitumor Immunity. *J Immunol (Baltimore Md 1950)* (2014) 193(8):3835–41. doi: 10.4049/jimmunol.1401572
8. Ai L, Xu A, Xu J. Roles of PD-1/PD-L1 Pathway: Signaling, Cancer, and Beyond. *Adv Exp Med Biol* (2020) 1248:33–59. doi: 10.1007/978-981-15-3266-5_3
9. Blackburn SD, Shin H, Freeman GJ, Wherry EJ. Selective Expansion of a Subset of Exhausted CD8 T Cells by PD-L1 Blockade. *Proc Natl Acad Sci* (2008) 105(39):15016–21. doi: 10.1073/pnas.0801497105
10. Pauken KE, Wherry EJ. Overcoming T Cell Exhaustion in Infection and Cancer. *Trends Immunol* (2015) 36(4):265–76. doi: 10.1016/j.it.2015.02.008
11. Zhan MM, Hu XQ, Liu XX, Ruan BF, Xu J, Liao C. From Monoclonal Antibodies to Small Molecules: The Development of Inhibitors Targeting the PD-1/PD-L1 Pathway. *Drug Discovery Today* (2016) 21(6):1027–36. doi: 10.1016/j.drudis.2016.04.011
12. Gomes F, Serra-Bellver P, Lorigan P. The Role of Nivolumab in Melanoma. *Future Oncol (London England)* (2018) 14(13):1241–52. doi: 10.2217/fon-2017-0484
13. Gettinger S, Rizvi NA, Chow LQ, Borghaei H, Brahmer J, Ready N, et al. Nivolumab Monotherapy for First-Line Treatment of Advanced non-Small-Cell Lung Cancer. *J Clin Oncol: Off J Am Soc Clin Oncol* (2016) 34(25):2980–7. doi: 10.1200/JCO.2016.66.9929
14. Reddy SM, Carroll E, Nanda R. Atezolizumab for the Treatment of Breast Cancer. *Expert Rev Anticancer Ther* (2020) 20(3):151–8. doi: 10.1080/14737140.2020.1732211
15. Santini FC, Rudin CM. Atezolizumab for the Treatment of non-Small Cell Lung Cancer. *Expert Rev Clin Pharmacol* (2017) 10(9):935–45. doi: 10.1080/17512433.2017.1356717
16. Farkona S, Diamandis EP, Blasutig IM. Cancer Immunotherapy: The Beginning of the End of Cancer? *BMC Med* (2016) 14(1):73. doi: 10.1186/s12916-016-0623-5
17. Adams JL, Smothers J, Srinivasan R, Hoos A. Big Opportunities for Small Molecules in Immuno-Oncology. *Nat Rev Drug Discovery* (2015) 14(9):603–22. doi: 10.1038/nrd4596
18. Zhu HF, Li Y. Small-Molecule Targets in Tumor Immunotherapy. *Natural Products Bioprospect* (2018) 8(4):297–301. doi: 10.1007/s13659-018-0177-7
19. Vladimer GI, Snijder B, Krall N, Bigenzahn JW, Huber KVM, Lardeau CH, et al. Global Survey of the Immunomodulatory Potential of Common Drugs. *Nat Chem Biol* (2017) 13(6):681–90. doi: 10.1038/nchembio.2360
20. Okazaki T, Chikuma S, Iwai Y, Fagarasan S, Honjo T. A Rheostat for Immune Responses: The Unique Properties of PD-1 and Their Advantages for Clinical Application. *Nat Immunol* (2013) 14(12):1212–8. doi: 10.1038/ni.2762
21. Arasanz H, Gato-Cañas M, Zuazo M, Ibañez-Vea M, Breckpot K, Kochan G, et al. PD1 Signal Transduction Pathways in T Cells. *Oncotarget* (2017) 8:10. doi: 10.18632/oncotarget.17232
22. Morihiro T, Kuroda S, Kanaya N, Kakiuchi Y, Kubota T, Aoyama KT, et al. Pd-L1 Expression Combined With Microsatellite Instability/CD8+ Tumor Infiltrating Lymphocytes as a Useful Prognostic Biomarker in Gastric Cancer. *Sci Rep* (2019) 9(1):4633. doi: 10.1038/s41598-019-41177-2

23. Freeman GJ, Long AJ, Iwai Y, Bourque K, Chernova T, Nishimura H, et al. Engagement of the PD-1 Immunoinhibitory Receptor by a Novel B7 Family Member Leads to Negative Regulation of Lymphocyte Activation. *J Exp Med* (2000) 192(7):1027–34. doi: 10.1084/jem.192.7.1027
24. Latchman Y, Wood CR, Chernova T, Chaudhary D, Borde M, Chernova I, et al. Pd-L2 is a Second Ligand for PD-1 and Inhibits T Cell Activation. *Nat Immunol* (2001) 2(3):261–8. doi: 10.1038/85330
25. Sun Z, Fourcade J, Pagliano O, Chauvin JM, Sander C, Kirkwood JM, et al. IL10 and PD-1 Cooperate to Limit the Activity of Tumor-Specific Cd8+ T Cells. *Cancer Res* (2015) 75(8):1635–44. doi: 10.1158/0008-5472.can-14-3016
26. Freeman-Keller M, Kim Y, Cronin H, Richards A, Gibney G, Weber JS. Nivolumab in Resected and Unresectable Metastatic Melanoma: Characteristics of Immune-Related Adverse Events and Association With Outcomes. *Clin Cancer Res an Off J Am Assoc Cancer Res* (2016) 22(4):886–94. doi: 10.1158/1078-0432.ccr-15-1136
27. Topalian SL, Hodi FS, Brahmer JR, Gettinger SN, Smith DC, McDermott DF, et al. Safety, Activity, and Immune Correlates of Anti-PD-1 Antibody in Cancer. *N Engl J Med* (2012) 366(26):2443–54. doi: 10.1056/NEJMoa1200690
28. Chen S, Song Z, Zhang A. Small-Molecule Immuno-Oncology Therapy: Advances, Challenges and New Directions. *Curr Topics Medicinal Chem* (2019) 19(3):180–5. doi: 10.2174/1568026619666190308131805
29. Tan S, Zhang H, Chai Y, Song H, Tong Z, Wang Q, et al. An Unexpected N-terminal Loop in PD-1 Dominates Binding by Nivolumab. *Nat Commun* (2017) 8:14369. doi: 10.1038/ncomms14369
30. Butte MJ, Keir ME, Phamduy TB, Sharpe AH, Freeman GJ. Programmed Death-1 Ligand 1 Interacts Specifically With the B7-1 Costimulatory Molecule to Inhibit T Cell Responses. *Immunity* (2007) 27(1):111–22. doi: 10.1016/j.immuni.2007.05.016
31. Scheurich P, Thoma B, Ucer U, Pfizenmaier K. Immunoregulatory Activity of Recombinant Human Tumor Necrosis Factor (TNF)-Alpha: Induction of TNF Receptors on Human T Cells and TNF-alpha-mediated Enhancement of T Cell Responses. *J Immunol (Baltimore Md 1950)* (1987) 138(6):1786–90.
32. Perez C, Albert I, DeFay K, Zachariades N, Gooding L, Kriegler M. A Nonsecretable Cell Surface Mutant of Tumor Necrosis Factor (TNF) Kills by Cell-to-Cell Contact. *Cell* (1990) 63(2):251–8. doi: 10.1016/0092-8674(90)90158-b
33. Sotomayor EM, Borello I, Levitsky HI. Tolerance and Cancer: A Critical Issue in Tumor Immunology. *Crit Rev Oncogene* (1996) 7:433–56. doi: 10.1615/critrevoncog.v7.i5-6.30
34. Kahan SM, Wherry EJ, Zajac AJ. T Cell Exhaustion During Persistent Viral Infections. *Virology* (2015) 479-480:180–93. doi: 10.1016/j.virol.2014.12.033
35. Martinez GJ, Pereira RM, Äijö T, Kim EY, Marangoni F, Pipkin ME, et al. The Transcription Factor NFAT Promotes Exhaustion of Activated Cd8+ T Cells. *Immunity* (2015) 42(2):265–78. doi: 10.1016/j.immuni.2015.01.006
36. Chemnitz JM, Parry RV, Nichols KE, June CH, Riley JL. SHP-1 and SHP-2 Associate With Immunoreceptor Tyrosine-Based Switch Motif of Programmed Death 1 Upon Primary Human T Cell Stimulation, But Only Receptor Ligation Prevents T Cell Activation. *J Immunol (Baltimore Md: 1950)* (2004) 173(2):945–54. doi: 10.4049/jimmunol.173.2.945
37. Riley JL. PD-1 Signaling in Primary T Cells. *Immunol Rev* (2009) 229(1):114–25. doi: 10.1111/j.1600-065X.2009.00767.x
38. Sheppard KA, Fits LJ, Lee JM, Benander C, George JA, Wooters J, et al. PD-1 Inhibits T-cell Receptor Induced Phosphorylation of the ZAP70/CD3zeta Signalosome and Downstream Signaling to Pkctheta. *FEBS Lett* (2004) 574:37–41. doi: 10.1016/j.febslet.2004.07.083

Conflict of Interest: The authors declare that the research was conducted in the absence of any commercial or financial relationships that could be construed as a potential conflict of interest.

frontiers in Oncology

ORIGINAL RESEARCH
published: 14 June 2021
doi: 10.3389/fonc.2021.644197

The Novel Curcumin Derivative 1g Induces Mitochondrial and ER-Stress-Dependent Apoptosis in Colon Cancer Cells by Induction of ROS Production

Hao Wang[1,2], *Yingxing Xu*[1,2], *Jialin Sun*[1,2] *and Zhongguo Sui*[1]*

[1] Department of Medicine, Affiliated Hospital of Qingdao University, Qingdao, China, [2] Department of Medicine, Qingdao University, Qingdao, China

OPEN ACCESS

Edited by:
Bin Zhang,
Northwestern University,
United States

Reviewed by:
Do-Hee Kim,
Kyonggi University, South Korea
Fang Cheng,
Sun Yat-sen University, China

***Correspondence:**
Zhongguo Sui
zhongguosui6120@126.com

Specialty section:
This article was submitted to Pharmacology of Anti-Cancer Drugs, a section of the journal Frontiers in Oncology

Received: *20 December 2020*
Accepted: *25 May 2021*
Published: *14 June 2021*

Citation:
Wang H, Xu Y, Sun J and Sui Z (2021) The Novel Curcumin Derivative 1g Induces Mitochondrial and ER-Stress-Dependent Apoptosis in Colon Cancer Cells by Induction of ROS Production. Front. Oncol. 11:644197. doi: 10.3389/fonc.2021.644197

Reactive oxygen species (ROS) play an important role in cellular metabolism. Many chemotherapeutic drugs are known to promote apoptosis through the production of ROS. In the present study, the novel curcumin derivative, 1g, was found to inhibit tumor growth in colon cancer cells both *in vitro* and *in vivo*. Bioinformatics was used to analyze the differentially expressed mRNAs. The mechanism of this effect was a change in mitochondrial membrane potential caused by 1g that increased its pro-apoptotic activity. In addition, 1g produced ROS, induced G1 checkpoint blockade, and enhanced endoplasmic reticulum (ER)-stress in colon cancer cells. Conversely, pretreatment with the ROS scavenging agent N-acetyl-l-cysteine (NAC) inhibited the mitochondrial dysfunction caused by 1g and reversed ER-stress, cell cycle stagnation, and apoptosis. Additionally, pretreatment with the p-PERK inhibitor GSK2606414 significantly reduced ER-stress and reversed the apoptosis induced by colon cancer cells. In summary, the production of ROS plays an important role in the destruction of colon cancer cells by 1g and demonstrates that targeted strategies based on ROS represent a promising approach to inhibit colon cancer proliferation. These findings reveal that the novel curcumin derivative 1g represents a potential candidate therapeutics for the treatment of colon cancer cells, *via* apoptosis caused by mitochondrial dysfunction and endoplasmic reticulum stress.

Keywords: 1g, colon cancer, ROS—reactive oxygen species, apoptosis, ER-stress

Abbreviations: ATCC, American Type Culture Collection; CRC, colorectal cancer; Cur, Curcumin; DMSO, dimethyl sulfoxide; ER, endoplasmic reticulum; GO, gene ontology; HE, hematoxylin-eosin; KEGG, Kyoto Encyclopedia of Genes and Genomes; NAC, N-acetyl-l-cysteine; qRT-PCR, Quantitative real-time PCR; ROS, reactive oxygen species.

INTRODUCTION

According to cancer statistics recently published by the American Cancer Society, the incidence of human colorectal cancer (CRC) is 10.2%, with a mortality rate of 9.2%, a rise from 4th to 2nd place in the ranking of cancer (1, 2). Currently available treatments for CRC include surgical intervention, radiotherapy, and chemotherapeutic drugs. However, the mechanisms by which the treatments operate remain largely unknown (3). Therefore, new treatment strategies are required to improve survival in CRC patients.

Cur (**Figure 1A**), a bioactive ingredient of *Curcuma longa* (turmeric), is a well-known cancer-preventative agent with no significant side effects at a therapeutic dose. Over the past decade, curcuma's anti-cancer properties have been well documented in a variety of cancer types, including lung, breast, pancreatic, and prostate cancer (4–6). In addition, multiple studies have demonstrated that Cur has anti-proliferative and anti-carcinogenic properties in a variety of cell lines and animal models, partly because it blocks the cell cycle, induces apoptosis, and inhibits the proliferation and metastasis of tumor cells (7–9). Various studies have demonstrated the chemoprophylactic and antitumor effects of Cur in CRC *in vivo* (10–14). Despite its safety and extensively documented pharmacological effects, the utilization of Cur is challenging due to its extremely low water solubility, instability, and poor oral bioavailability (15, 16).

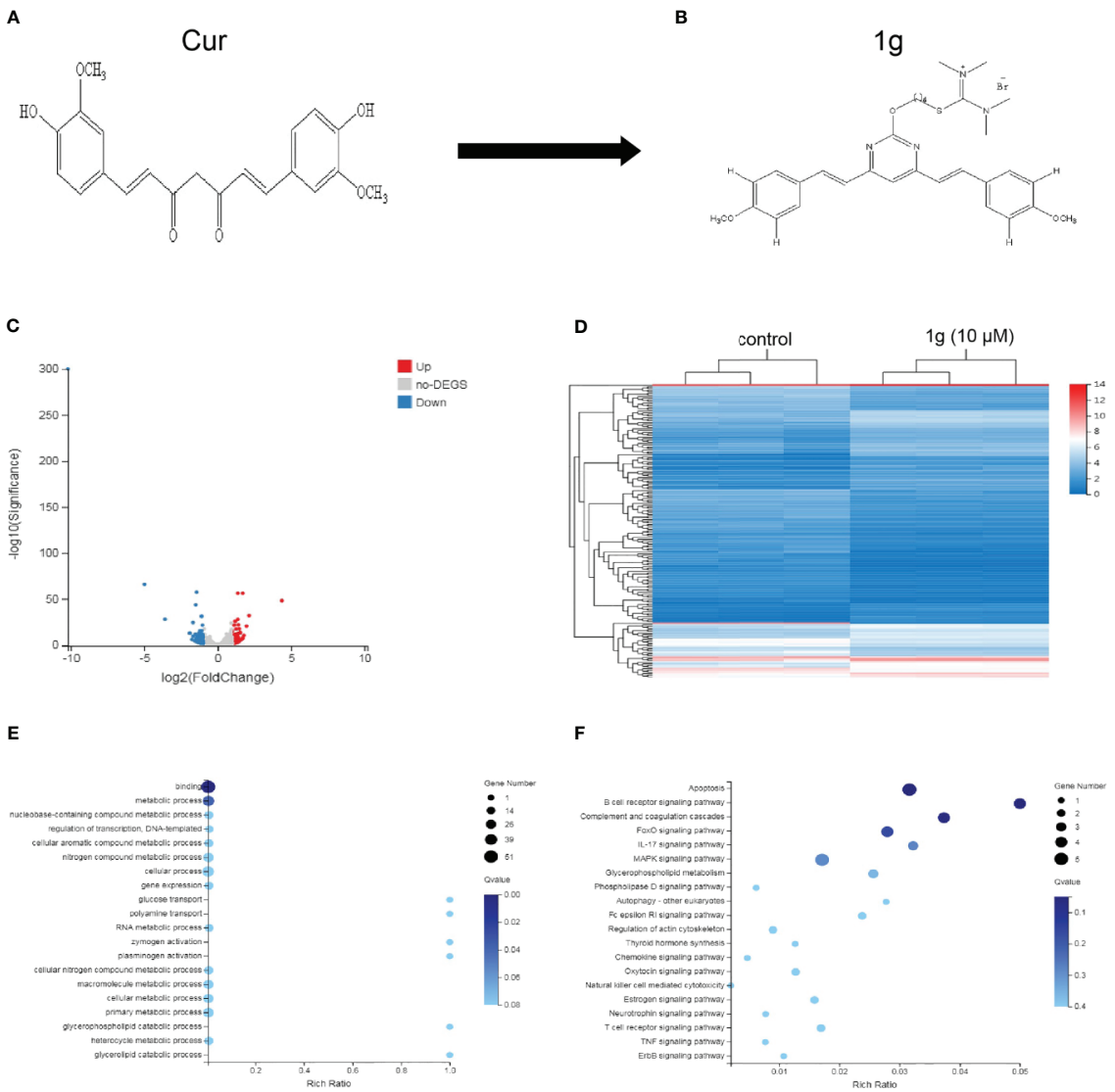

FIGURE 1 | Differentially expressed gene profiles and bioinformatics analysis. HCT116 cells were exposed to 1g (10 μM) for 24 h, after which the transcriptome was sequenced. **(A, B)** The structures of Cur and 1g. **(C)** Volcano plot of differentially expressed mRNAs. **(D)** Heat map of differentially expressed mRNAs. **(E)** GO enrichment bubble map for differentially expressed mRNAs. **(F)** KEGG Pathway enrichment bubble map for differentially expressed mRNAs.

A variety of strategies have been studied to overcome the limitations of Cur, including chemical modification.

ROS are highly active oxygen radicals that are mainly derived from NADPH oxidase in the mitochondria (17). It has been reported that ROS and tumor biology are inherently intertwined (18). Over recent years, this laboratory has investigated the chemical modification of Cur to create novel molecules that are more chemically stable and more pharmacologically powerful than Cur. Previously, a range of pyrimidine-substituted curcumins was synthesized and evaluated as a treatment against a variety of cancer cells (19). One compound: (E,E)-2-(4-(4,6-bis(4-methoxystyryl)pyrimidin-2-yloxy)butyl)-1,1,3,3-tetramethylisothiouronium hydrobromide (**Figure 1B**) exhibited excellent chemical stability combined with anti-cancer properties. Here, RNA-sequencing was conducted to identify differentially expressed mRNAs in a colon cancer cell line (HCT116) treated with the Cur analog 1g and found that those mRNAs identified were closely related to cell apoptosis. Subsequently, the anticancer mechanism and the effectiveness of 1g against colon cancer cells were explored. The results indicate that the anticancer mechanism of action of 1g was possibly *via* the induction of intracellular ROS generation, leading to a change in mitochondrial membrane potential, cell cycle arrest, activation of ER-stress, ultimately leading to cell apoptosis. The present study not only found that 1g inhibited the activity of colon cancer cells to a greater extent than Cur, but also revealed that overproduction of ROS is an important factor in the treatment of CRC.

METHODS

Antibodies and Reagents

The following antibodies were used: GADPH (#2118), anti-CHOP (#2895), anti-GRP78 (#3177), anti-cleaved caspase 9 (#7237), anti-cleaved caspase 3 (#9661), anti-cleaved PARP (#5625), anti-Bax (#5023), anti-Bcl-2 (#3498), anti-Cytochrome c (#4272), anti-PERK (#5683), anti-p44/42 MAPK (Erk1/2) (#9102), anti-phospho-p44/42 MAPK (Erk1/2) (#9101), anti-Cyclin D1 (#2978), anti-phospho-Rb (#8516), anti-IRE1α (#3294), and anti-p21 (#2947), anti-mouse IgG-HRP (#7076), and anti-rabbit IgG-HRP (#7074) were purchased from Cell Signaling (Beverly, MA, USA); anti-Phospho-EIF2 alpha (AF3087) and anti-Phospho-PERK (Thr982) (DF7576) were sourced from Affinity Biosciences Ltd.; anti-ATF4 (0835-1-AP) was obtained from Proteintech (Wuhan Sanying) and anti-p53 (ab26) was acquired from Abcam (Cambridge, UK).

Other reagents used in the present study were: 1g (>98% purity, HPLC) prepared in our laboratory. Cur and DMSO were obtained from Sigma-Aldrich (St. Louis, MO, USA). Cell Counting Kit-8 (CCK-8), N-acetylcysteine (NAC; ROS scavenger), and GSK2606414 were purchased from MedChemExpress (Monmouth Junction, NJ, USA). Antibody diluent and Restore™ PLUS Western Blot Stripping Buffer were purchased from ThermoFisher Scientific (Shanghai, China).

Cell Culture

The human colon cancer cell lines HCT116 and HT29 were obtained from the American Type Culture Collection (ATCC). SW480 and LOVO were obtained from the Cell Resource Center, Shanghai Institute of Life Sciences, Chinese Academy of Sciences. HCT116 and HT29 cells were maintained in Dulbecco's modified Eagle's medium (DMEM; BI, New York, NY, USA), and SW480 in Roswell Park Memorial Institute (RPMI)-1640 medium (BI). LOVO cells were maintained in DMEM/F-12 (Dulbecco's Modified Eagle Medium/Nutrient Mixture F-12). The passage number of all the above cell lines was between 20 and 30. The medium was supplemented with 10% fetal bovine serum (FBS; Biological Industries, Israel) and 1% penicillin G/streptomycin sulfate. Cells were maintained at 37°C in a humidified incubator within 5% CO_2.

Transcriptome Gene Sequencing

Untreated HCT116 cells and those treated with 1g for 24 h (n = 3) underwent transcriptomic analysis by Gooal Gene Technologies Ltd. (Wuhan, China). Briefly, total RNA was processed by mRNA enrichment and rRNA removal. The RNA was fragmented with interrupt buffer, and random N6 primers were reverse transcribed, from which double-stranded cDNA was synthesized. The resultant double-stranded DNA ends were flattened and phosphorylated at the 5'-ends. A "sticky" end was formed at the 3' end from which an 'A' protruded to which a bubblelike junction with a 'T' was connected. The ligands were amplified by PCR using specific primers. The PCR product was thermally denatured into a single strand, which was cycled with a bridge primer to obtain a single-stranded circular DNA library which was finally machine sequenced. The process is detailed in a flowchart in **Additional File 1**.

Cell Proliferation Assay

Cell proliferation was measured using a CCK-8 assay. Briefly, 1g-treated cells were plated at 5×10^3 cells per well in 96-well culture plates and cultured for 12, 24, and 48 h. A 10 μl aliquot of CCK-8 reagent was added to each well then incubated at 37°C for 3 h. The absorbance at 450 nm of each well was recorded using a microplate reader (Tecan Austria GmbH 5082, Austria) (n = 5).

Flow Cytometry Analysis

Cell apoptosis analysis. Cells were seeded in six-well plates (5×10^5 cells/well). After incubation with specified drug treatments, the cells were suspended in Annexin V binding buffer then incubated with Annexin V–FITC and PI in accordance with the manufacturer's instructions (BD Biosciences, Bedford, MA, USA), prior to flow cytometry analysis (n = 3).

Cell cycle analysis. Cells were treated with 1g or Cur for 18 h, collected, fixed, and permeabilized overnight in 75% ethanol overnight at −20°C. All samples were washed twice with PBS and then incubated with PI and RNase at room temperature for 30 min. The results were analyzed using Modifit software (n = 3).

ROS measurement. ROS levels were determined using a dichloro-dihydrofluorescein diacetate (DCF-DA) probe. After treatment, the cells were collected and incubated with 20 μM

DCF-DA for 30 min. After washing twice in PBS, the fluorescence intensity of DCF was measured by flow cytometry. The results were analyzed using Flowjo v10 software (n = 3).

Mitochondrial membrane potential (ΔΨm) evaluation. Following treatment with 1g or Cur for 24 h, the cells were incubated with a JC-1 fluorescent probe (Elabscience, Wuhan, China) in a 5% CO_2 humidified incubator at 37°C for 20 min. The cells were then washed twice with a staining buffer and analyzed using a TMFC500 flow cytometer (Beckman Coulter, CA, USA) (n = 3).

Western Blotting

Cells and tissues were collected in RIPA buffer (50 mM Tris, 10 mM EDTA, 1% v/v Triton-X100), and supplemented with PMSF protease inhibitor and phosphatase inhibitor. The cells and tissues were then sonicated (8 bursts of 12 s, 4°C, 100 W, using a Labsonic sonicator, Hielscher, Teltow, Germany), and the protein concentration of the samples determined using a BCA protein assay. For each sample, the same quantity of protein (35 μg) was added to an appropriate volume of 5× sample buffer (Beyotime Biotechnology, Shanghai, China), and then heated until boiling. Each sample was then separated on a 10–12.5% SDS-polyacrylamide gel (PAGE) after which they were transferred to PVDF membranes using a Bio-Rad electro-transfer system (Bio-Rad Laboratories, Munich, Germany). Each membrane was then hybridized with a primary antibody overnight on a shaking table at 4°C, washed three times with TBST buffer (3 × 10 min), then incubated with the corresponding secondary antibody at room temperature for 1 h. Finally, Immobilon Western chemiluminescent HRP matrix (Millipore, Burlington, MA, USA) was added to develop the membrane. The positive bands were vizualized using an Infrared Imaging System (LI-COR Biosciences, Lincoln, NE, USA), and the density of the digital images measured using ImageJ software (NIH, Bethesda, MD, USA, ver.1.52a) and expressed as a proportion of the GAPDH loading control (n = 3).

Quantitative Real-Time PCR Analysis

qRT-PCR was used to measure the expression of GRP78 and CHOP. Total RNA was extracted using Trizol reagent (Invitrogen; Life Technologies Corporation, Grand Island, NY, USA) in accordance with the manufacturer's instructions. A 1μg quantity of RNA was reverse transcribed using a PrimeScript RT reagent kit (Takara, Tokyo, Japan). The cDNA was diluted (2 μl) and selectively amplified using a real-time PCR with SYBR Green I (Takara) and specific primers. The sequences of human CHOP, GRP78, and GAPDH were obtained from previously published articles (20). The samples were amplified using a Roche LightCycler 480II (Switzerland). The relative quantity of each mRNA was calculated using a comparative method ($2^{-\triangle\triangle Ct}$) against a GAPDH endogenous control (n = 3).

Colon Cancer Xenografts in Nude Mice

All animal husbandry and experimental procedures were approved by the Animal Research Ethics Committee of the Affiliated Hospital of Qingdao University in Shandong Province. Four 6-week-old female Balb/c-nu/nu mice were obtained from the Beijing Viton Lihua Experimental Animal Technology Co. Ltd. The mice were maintained at an ambient temperature of 20–25°C, in specific pathogen-free ventilation chambers at 45–50% relative humidity, in a 12 h light-dark cycle. The mice were adapted to the environment for 7 days prior to experimentation and received sterilized food and water *ad libitum*. Suspensions of HCT116 cells were injected subcutaneously into each mouse (at a cell density of 5×10^6 in 150 μl PBS). When the tumor volume had reached approximately 150 mm^3, the mice were randomly divided into control and treatment groups (n = 6). The groups were: control group with vehicle; 1g group (40 mg/kg); 1g group (20 mg/kg), and Cur group (40 mg/kg). Each treatment group received an intraperitoneal injection once per day. The mice were monitored for 14 days during treatment. Bodyweight and tumor volume were measured every 2 days. The tumor volume was calculated using the formula: ($[width]^2 \times [length]/2$). Moreover, weight was recorded throughout the experiment.

HE Staining

Transplanted tumor tissue biopsies were embedded in paraffin, sectioned, then processed in xylene I for 20 min, xylene II for 20 min, ethanol I for 5 min, anhydrous ethanol II for 5 min, and 75% alcohol for 5 min prior to washing in water. Sections were stained with hematoxylin for 3–5 min, rinsed with tap water, differentiated, again rinsed with tap water, immersed in basic bluing reagent prior to rinsing in running water. Sections were then dehydrated through an 85–95% gradient of alcohol for 5 min respectively, then stained in eosin solution for 5 min. The sections were placed in anhydrous ethanol I for 5 min, anhydrous ethanol II for 5 min, anhydrous ethanol III for 5 min, dimethyl I for 5 min, xylene II for 5 min for clearing, then sealed in neutral rubber. Finally, the sections were examined by light microscopy and images were acquired then analyzed (n = 3).

Statistical Analysis

GraphPad InStat 8.0 software (GraphPad Software, Inc., La Jolla, CA, USA) was used for statistical analysis. The results were expressed as the means of arbitrary units ± SD. Differences were analyzed using a one-way analysis of variance followed by a Bonferroni's post-hoc test. *P*-values <0.05 were considered significant.

RESULTS

Bioinformatics Analysis of Differentially Expressed mRNAs and Microarray Data of 1g-Treated Colon Cancer Cells

A total of 181 differentially expressed mRNAs were identified in the HCT116 cells after exposure to 1g (10 μM) for 24 h. Of these, 80 were up-regulated and 101 were down-regulated compared with the control group. From the results, a volcano plot was created (**Figure 1C**) and a heat map of the mRNA expression

levels (**Figure 1D**). To determine the key factors that inhibit colon cancer cells by 1g, gene ontology (GO) and pathway analyses were performed. From the GO enrichment bubble map (**Figure 1E**), it is apparent that 1g inhibits HCT116 cells principally *via* regulation of the metabolic processes related to adhesion, biological regulation, cellular processes, and catalytic activity. Enrichment was conducted from information in the KEGG database to identify pathways that mediate significant change to the function of the differentially expressed genes, identifying 20 significant pathways associated with those genes that may play a key role in the processing of HCT116 cells by 1g (**Figure 1F**). Interestingly, of these, the apoptotic pathway was the most significant. Therefore, we further explored the effects and mechanisms of 1g on apoptosis in HCT116 cells.

The Cur Derivative, 1g, Inhibits Colon Cancer Cell Proliferation

Using a CCK-8 assay, the effect of 1g on the proliferation of HCT116, HT29, SW480, and LOVO colon cancer cell lines at increasing concentrations for 12, 24, or 48 h, was investigated. The results indicated that 1g significantly inhibited the proliferation of the four different colon cancer cell lines in a time and dose-dependent manner (**Figures 2A–D**). However, the activity of normal CHO fibroblasts was not affected by 1g (10 μM), as reported previously (19). This suggests that 1g displays the similar safety and stability as Cur but is more selective against colon cancer cells.

1g Induces Apoptosis and Cell Cycle Arrest in Colon Cancer Cells

To confirm that the apoptosis caused by 1g was consistent with transcriptomic sequencing, HCT116 cells were further treated with 1g and Cur for 24 h then analyzed after Annexin V-FITC/PI double staining by flow cytometry. The number of apoptotic colon cancer cells was positively correlated with the concentration of 1g, and the number of apoptotic HCT116 cells was significantly greater when treated with 10 μM 1g than with 10 μM Cur (**Figures 3A, B**). 1g was also able to induce apoptosis in HT29 cells (**Figures 3C, D**). In addition, the apoptosis-related proteins cleaved-PARP, p-ERK, cleaved-caspase 9, and cleaved-caspase 3 were measured by Western blotting. HCT116 cells were treated with 1g (10 μM) during cell culture (0–24 h), followed by DMSO, 1g or Cur for 24 h. The results demonstrate that the protein expression levels increased after treatment with 1g in a time and dose-dependent manner (**Figures 3E–H**). Cyclin is closely involved in the checkpoint control mechanism and represents the signal to undergo apoptosis (21). Flow cytometric analysis of PI stained cells was also conducted to ascertain whether 1g induced HCT116 cell cycle arrest. HCT116 cells undergoing exponential growth were treated with 1g or Cur for 24 h then analyzed by flow cytometry. Interestingly, after treatment with 1g (10 μM), the number of cells in the G1 phase increased significantly, the number in the S phase decreased significantly while no significant change in number was observed in the G2/M phase (**Figures 3I–L**). These observations are different from those previously reported for Cur treatment of colon cancer cells, which were observed to undergo cycle arrest in the G2/M phase (8). Subsequently, the colon cancer cells were treated with 1g (10 μM) for up to 24 h. The expression levels of p-Rb and Cyclin D1 were greatest at 4 h and then decreased, while the expression levels of p21 were highest at 8 h (**Figures 3M, N**). In addition, the expression levels of P-Rb and Cyclin D1 were measured in HCT116 cells treated with increasing concentrations of 1g or Cur at 24 h. The expression levels of p21 and p53 were measured at 8 h. P-Rb and Cyclin D1 expression decreased with increasing 1g

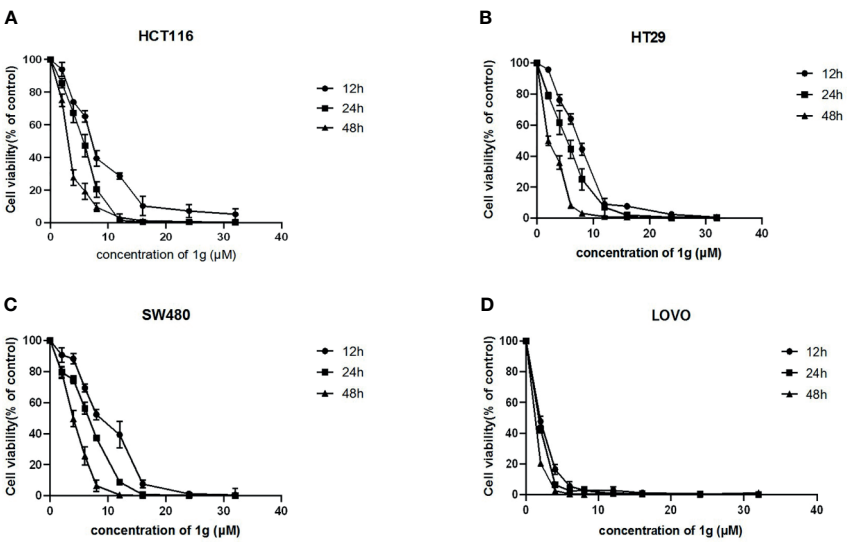

FIGURE 2 | 1g inhibited the proliferation of colon cancer cells. **(A)** HCT116, **(B)** HT29, **(C)** SW480, and **(D)** LOVO cells were treated with 1g (2–32 μM) for 12, 24, and 48 h. The inhibition effect of 1g on cell proliferation was dose-dependent and time-dependent (n = 5).

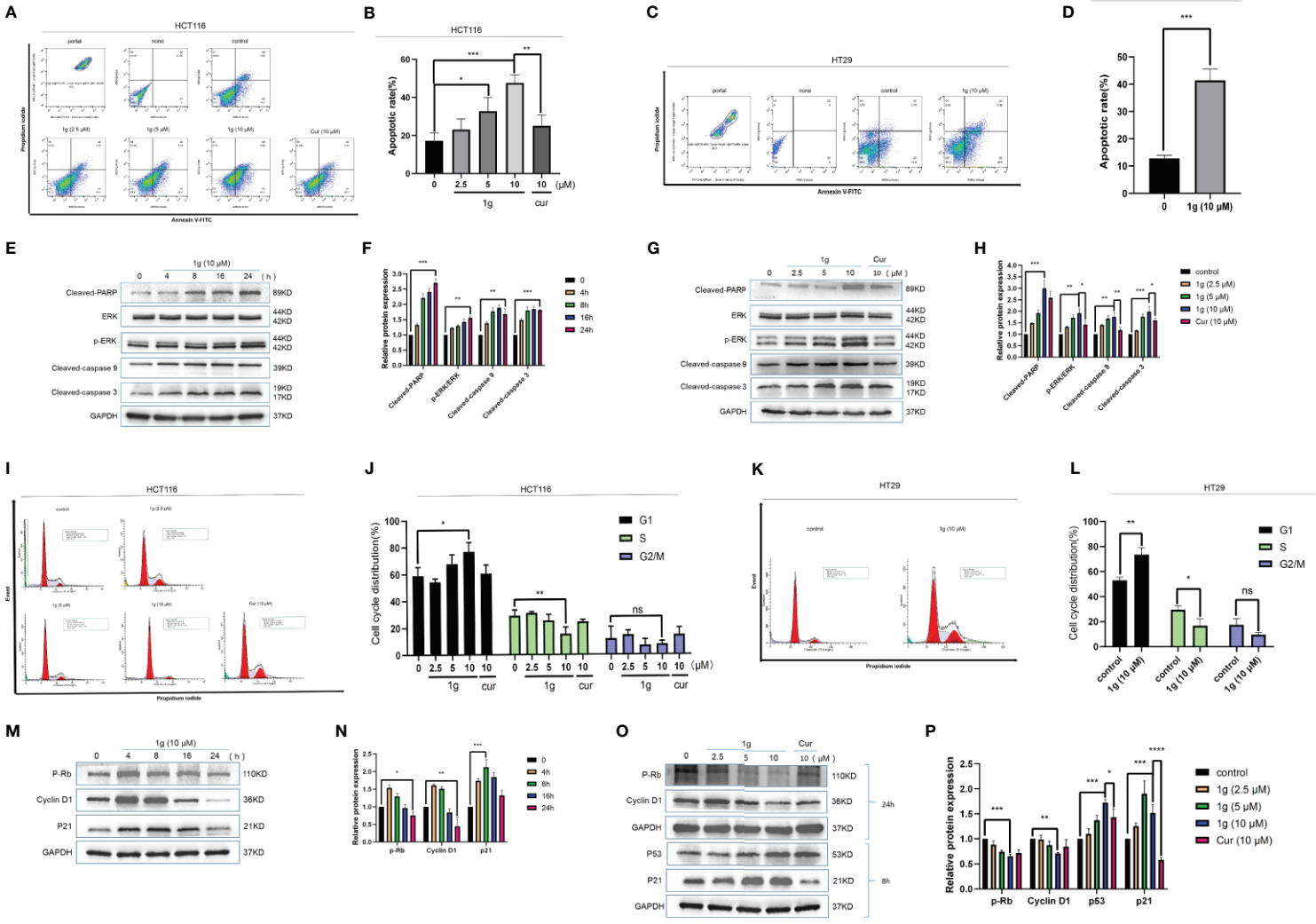

FIGURE 3 | 1g induced colon cancer apoptosis and inhibited cell cycle arrest in the G1 phase. **(A, B)** Flow cytometry was used to detect the induction of apoptosis of HCT116 cells after treatment with 1g or Cur for 24 h. **(C, D)** Flow cytometry was used to detect the induction of apoptosis of HT29 cells after treatment with 1g for 24 h. **(E, F)** The number of apoptotic cells was determined using GraphPad Prism software. **(C)** Levels of apoptotic proteins were evaluated in HCT116 cells treated with 1g (10 μM) over varying durations. **(G, H)** Protein levels evaluated by Western blot analysis of 1g or Cur-treated HCT116 cells for 24 h. **(I, J)** Flow cytometry was used to determine the induction of cell cycle arrest in HCT116 cells after treatment with 1g or Cur for 24 h. **(K, L)** Flow cytometry was used to determine the induction of cell cycle arrest in colon HT29 cells after treatment with 1g for 24 h. **(M, N)** Expression of relative protein levels of the cell cycle determined by Western blot analysis after treatment with 1g (10 μM) over varying durations. **(O, P)** Protein levels evaluated by Western blot analysis of 1g or Cur-treated HCT116 cells for the time indicated. Data represent means ± SD. Statistical significance was determined by one-way analysis of variance (ANOVA) followed by a Bonferroni's *post-hoc* test. Statistical significance indicated as $^{*}P < 0.05$, $^{**}P < 0.01$, $^{***}P < 0.001$, $^{****}P < 0.0001$. ns indicates that the comparison was not statistically significant.

concentration, while the expression levels of p21 and p53 increased. This is consistent with the regulation of the cell cycle by these proteins (**Figures 3O, P**).

1g Induces Changes in Mitochondrial Membrane Potential in Colon Cancer Cells

It is well-known that many cytotoxic stimuli, including chemotherapeutic drugs, induce apoptosis *via* endogenous pathways with which mitochondria are involved (22, 23). Apoptosis-related gene expression was assessed to test the hypothesis that 1g operates similarly, finding that Bax and Cyto C expression levels increased and anti-apoptotic Bcl-2 expression levels decreased after the treatment of HCT116 cells with 1g, in a time and dose-dependent manner (**Figures 4A–D**). As the ratio of Bax/Bcl-2 expression increased, mitochondrial membrane dysfunction and permeability increased (24). The mitochondrial membrane potential of HCT116 and HT29 cells treated with 1g or Cur for 24 h was found to have undergone a clear change (**Figures 4E, F**).

1g Induces Colon Cancer Apoptotic Death by Evoking ROS Generation and Transduction of the ER Stress-Related Cell Death Pathway

As is well known, mitochondria are the principal source of ROS in eukaryotic cells. The destruction of mitochondrial function is generally related to an enhancement of the production of mitochondrial ROS (25). Excessive production of ROS can

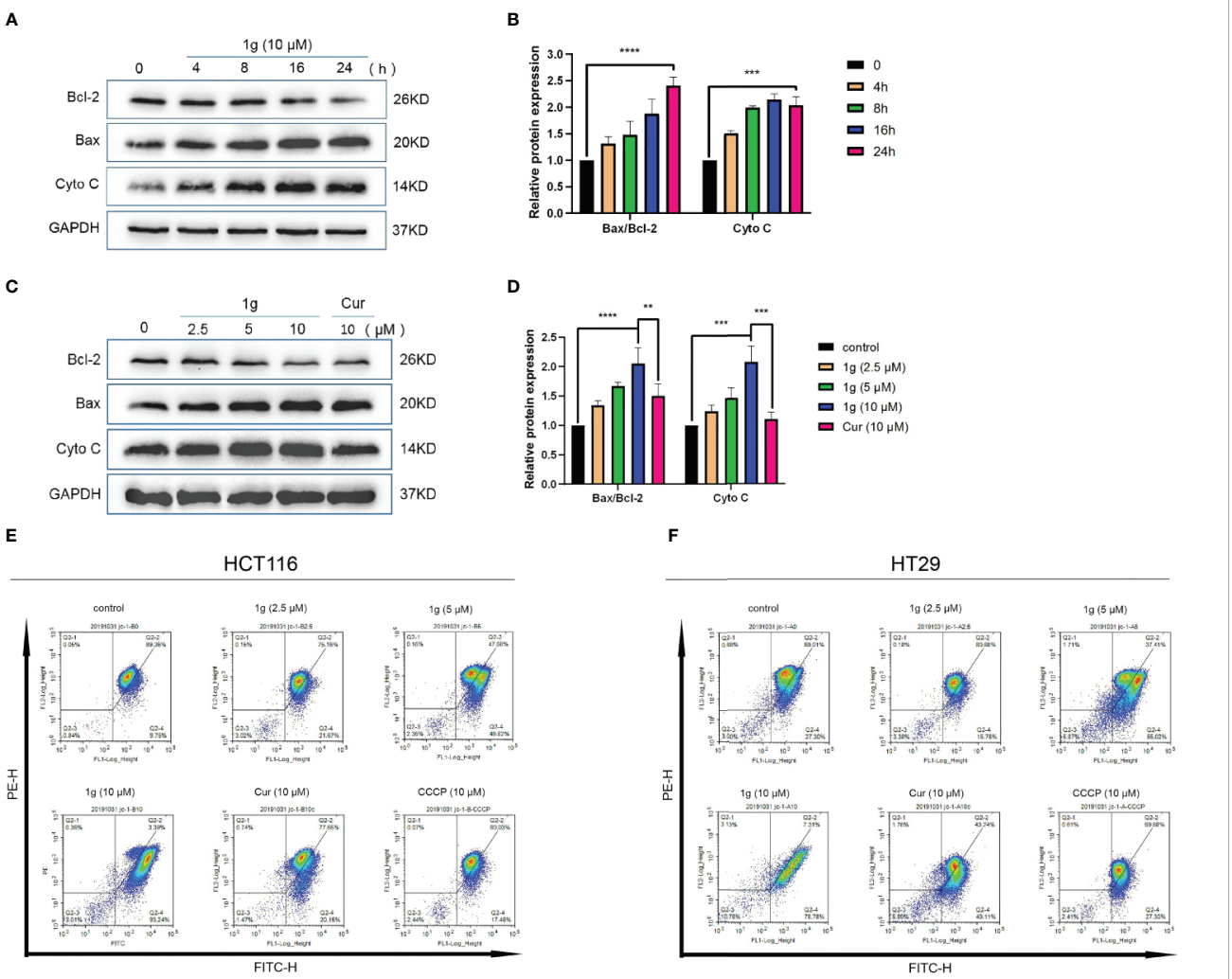

FIGURE 4 | 1g changes the mitochondrial membrane potential in colon cancer cells. **(A, B)** HCT116 cells were treated with 1g (10 μM) over varying durations. **(C, D)** Protein levels evaluated by Western blot analysis of 1g or Cur-treated HCT116 cells for 24 h. **(E)** Mitochondrial membrane potential was analyzed by flow cytometry in HCT116 cells treated with 1g or Cur for 24 h (n = 3). **(F)** Mitochondrial membrane potential was analyzed by flow cytometry in HT29 cells treated with 1g for 24 h (n = 3). Data represents means ± SD. Statistical significance was determined by one-way analysis of variance (ANOVA) followed by a Bonferroni's *post-hoc* test. Statistical significance indicated as $^{**}P < 0.01$, $^{***}P < 0.001$, $^{****}P < 0.0001$.

lead to DNA damage (26), endoplasmic reticulum stress (27), and apoptosis (28). To test the hypothesis that 1g was able to stimulate colon cancer cells to produce ROS, production was measured in 1g-treated cells, which demonstrated increased ROS production in a time-dependent manner (0–120 min) (**Figure 5A**). N-acetyl-l-cysteine (NAC) is an antioxidant that can eliminate all ROS subclasses (29). The ROS produced by HCT116 cells was measured after treatment with different concentrations of 1g and pretreatment with 10 mM NAC for 1 h. ROS increased with increasing concentrations of 1g, while ROS production was significantly reduced in the NAC pretreatment group (**Figure 5B**). To verify that the ROS produced in colon cancer cells led to cell apoptosis and cell cycle stagnation, ultimately leading to decreased cell activity, the cells were pretreated with NAC for 1 h, followed by treatment with 1g (10 μM) for 24 h. The expression of mitochondrial proteins and cycle proteins was detected by Western blotting (**Figures 5C–F**). As demonstrated by flow cytometry, NAC significantly reversed 1g-induced apoptosis of colon cancer (**Figures 5G–J**). The activity of HCT116 and HT29 cells was measured using a CCK-8 assay (**Figures 5K, L**). To further explore whether 1g (10 μM)-stimulated ROS production of colon cancer cells can cause their endogenous apoptosis by ER-stress, the gene expression of CHOP and GRP78 was quantified by RT-PCR in HCT116 cells at various times (0 to 8 h) (**Figures 6A, B**), and CHOP and GRP78 gene expression in 1g and Cur-treated HCT116 cells for 8 h (**Figures 6C, D**). The results demonstrated that the mRNA transcription of GRP78 and CHOP was time-dependent and increased with the increasing 1g concentration. The time dependency of ER-stress related protein expression was then measured by the Western blotting of PERK, p-PERK, and p-EIF2α (0–120 min); ATF4 and CHOP (0–12 h); and IRE1α and BIP (0–24 h). Maximum protein expression of p-PERK occurred at 1 h, p-EIF2α at 2 h, ATF4 and CHOP after 6 h, and IRE1α and BIP at 24 h (**Figures 6E, F**). The effect on ER-stress related protein expression of different concentrations of 1g and Cur was investigated at the specific exposure times above. The protein expression of p-EIF2α, p-PERK, CHOP, and ATF4 were increased with increasing 1g concentration, while the expression of IRE1α and BIP was greatest at 1g (10 μM) (**Figures 6G, H**). After 1 h of pretreatment with NAC, HCT116 cells were treated with 1g (10 μM) after which they were analyzed for protein expression. It demonstrated that the expression of CHOP, ATF4, and p-PERK was almost entirely blocked by pretreatment with NAC and the expression of BIP significantly reduced (**Figures 6I, J**). Similarly, in HT29 cells, NAC reversed the expression of CHOP and BIP proteins (**Figures 6K, L**). To determine whether ER-stress was the cause of 1g-induced apoptosis and death of the colon cancer cells, they were treated with the p-PERK inhibitor GSK2606414 (30). Compared with the untreated group, p-PERK was significantly reduced after 1 h pretreatment with GSK2606414 (2 μM). Similarly, the expression of proteins downstream of CHOP decreased significantly (**Figures 6M, N**). These results indicate that ER stress signal activation at least partially mediated 1g-induced apoptosis of HCT116 cells.

1g Significantly Inhibits HCT116 Cell Growth in a Mouse Model

To verify the anti-tumor effect of 1g *in vivo*, HCT116 cells were injected into mice to establish an *in vivo* tumor xenograft model. The results demonstrated that the volume of the resultant tumors in mice treated with saline increased in a time-dependent manner, while both 1g and Cur displayed antitumor effects (**Figure 7A**). The size of the tumors in mice of the 1g group was distinctly smaller than those in the mice of the Cur and control groups (**Figure 7B**). Furthermore, all mice survived 14 days of treatment and were approximately the same weight. The results indicate that 1g was shown to be safe at the specified dose (**Figure 7C**). Western blotting and immunohistochemical analysis indicated that 1g significantly enhanced the expression of cleaved-caspase 3 and CHOP (**Figures 7D, E**). From the results of hematoxylin-eosin (HE) staining, a large number of pathological mitotic figures were observed in the tumor tissue treated with 1g (**Figure 7F**). These data are consistent with the results of 1g in anti-colon cancer cell proliferation experiments *in vitro*. In addition, 1g exhibited stronger anti-tumor effects *in vivo* than Cur at the same dose.

DISCUSSION

Cur is the biologically active ingredient in turmeric, known since ancient times for its medicinal properties (31). Cur is thought to induce apoptosis in all types of cancer cell (32–34). Over the past decade, cur has demonstrated remarkable biological properties, but its clinical use has been limited by its instability at physiological pH and low bioavailability (35, 36). Multiple studies have shown that the reason for Cur's poor bioavailability is its early biological transformation and metabolism (37, 38). In order to overcome this limitation, Cur has been chemically modified to improve its stability and bioavailability. Interestingly, a series of isothiourea-modified compounds with important pharmacological activity, including anti-tumor properties, were produced (39–41). Based on these compounds, we introduced the positively charged isothiourea group into the pyrimidine-substituted curcumin analog. Our data indicated that 1g significantly enhanced anticancer activity compared to the unmodified compounds, in addition to its unique Golgi body localization. However, the mechanism by which 1g inhibits colon cancer growth remains unclear (19).

Here, we identified 181 differentially expressed mRNAs in HCT116 cells following exposure to 1g (10 μM) for 24 h, and additional bioinformatics analysis indicated that these differentially expressed mRNAs were closely related to cell apoptosis. As a result, we explored the effects and mechanisms of 1g on apoptosis in HCT116 cells. The data indicate that 1g reduced the activity of colon cancer cells in a time and dose-dependent manner. Furthermore, transcriptional genome sequencing revealed that it mainly induced apoptosis and death of colon cancer cells. As described above, it has been confirmed the molecular mechanism by which Cur induces apoptosis is

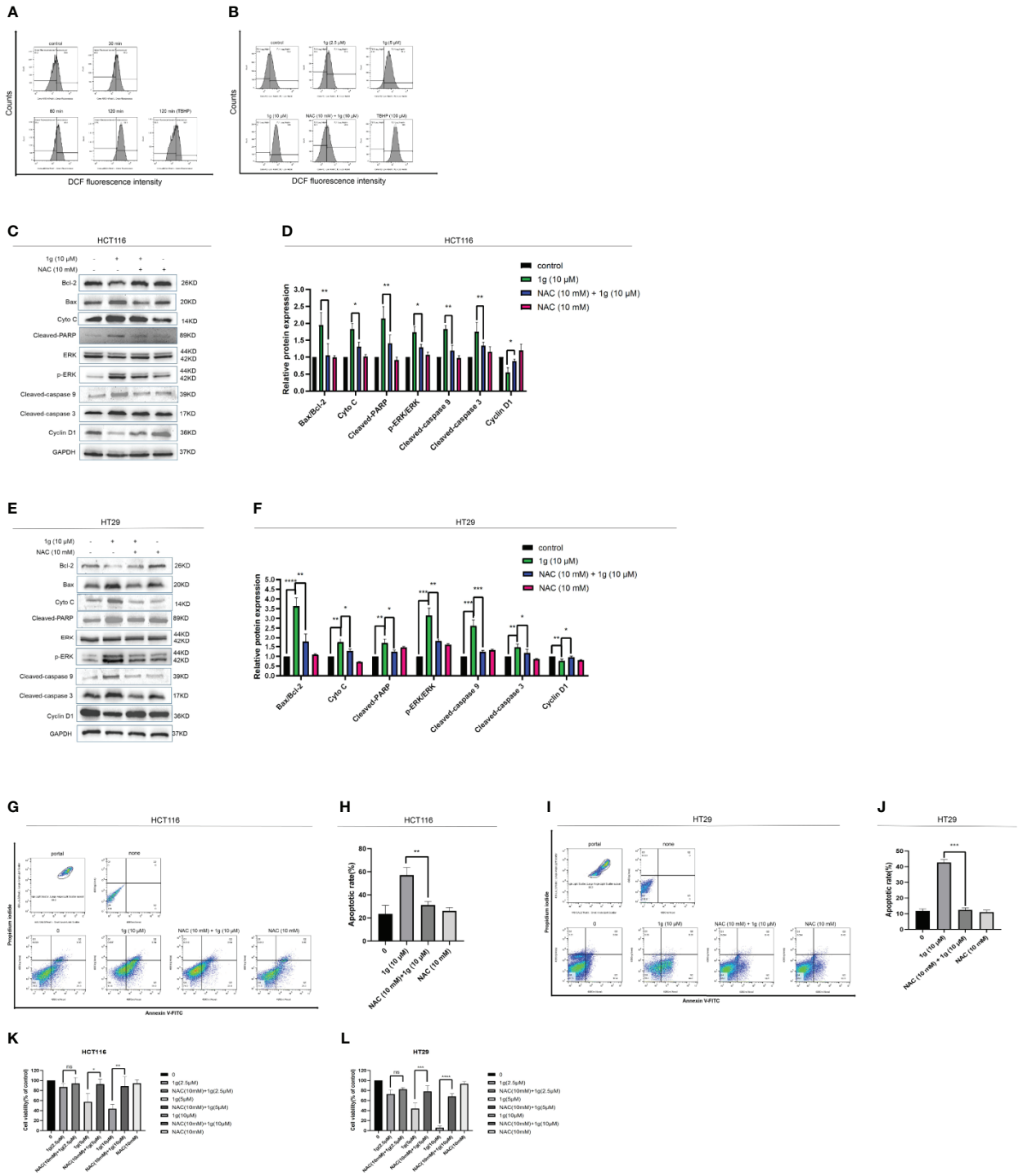

FIGURE 5 | Cytotoxicity of 1g toward colon cancer cells depends on the production of intracellular ROS. **(A)** Flow cytometric analysis of intracellular ROS generation induced by 1g over increasing durations measured in HCT116 cells after staining with DCFH-DA (10 μM). **(B)** HCT116 cells pre-incubated with NAC (10 mM) for 1 h prior to exposure to 1g (10 μM) for 8 h. **(C, D)** HCT116 cells pretreated with NAC (10 mM) for 1 h, then treated with 1g (10 μM) for 24 h. Apoptotic proteins and cyclins measured by Western blotting. **(E, F)** HCT116 cells pretreated with NAC (10 mM) for 1 h, then treated with 1g (10 μM) for 24 h. **(G, H)** Flow cytometry was used to detect the induction of apoptosis of HCT116 cells. **(I, J)** Flow cytometry was used to detect the induction of apoptosis of HCT116 cells. **(K, L)** HCT116 and HT29 cell activity measured using a CCK-8 assay. Data represent means ± SD. Statistical significance was determined by one-way analysis of variance (ANOVA) followed by a Bonferroni's *post-hoc* test. Statistical significance is indicated as $^{*}P < 0.05$, $^{**}P < 0.01$, $^{***}P < 0.001$, $^{****}P < 0.0001$. ns indicates that the comparison was not statistically significant.

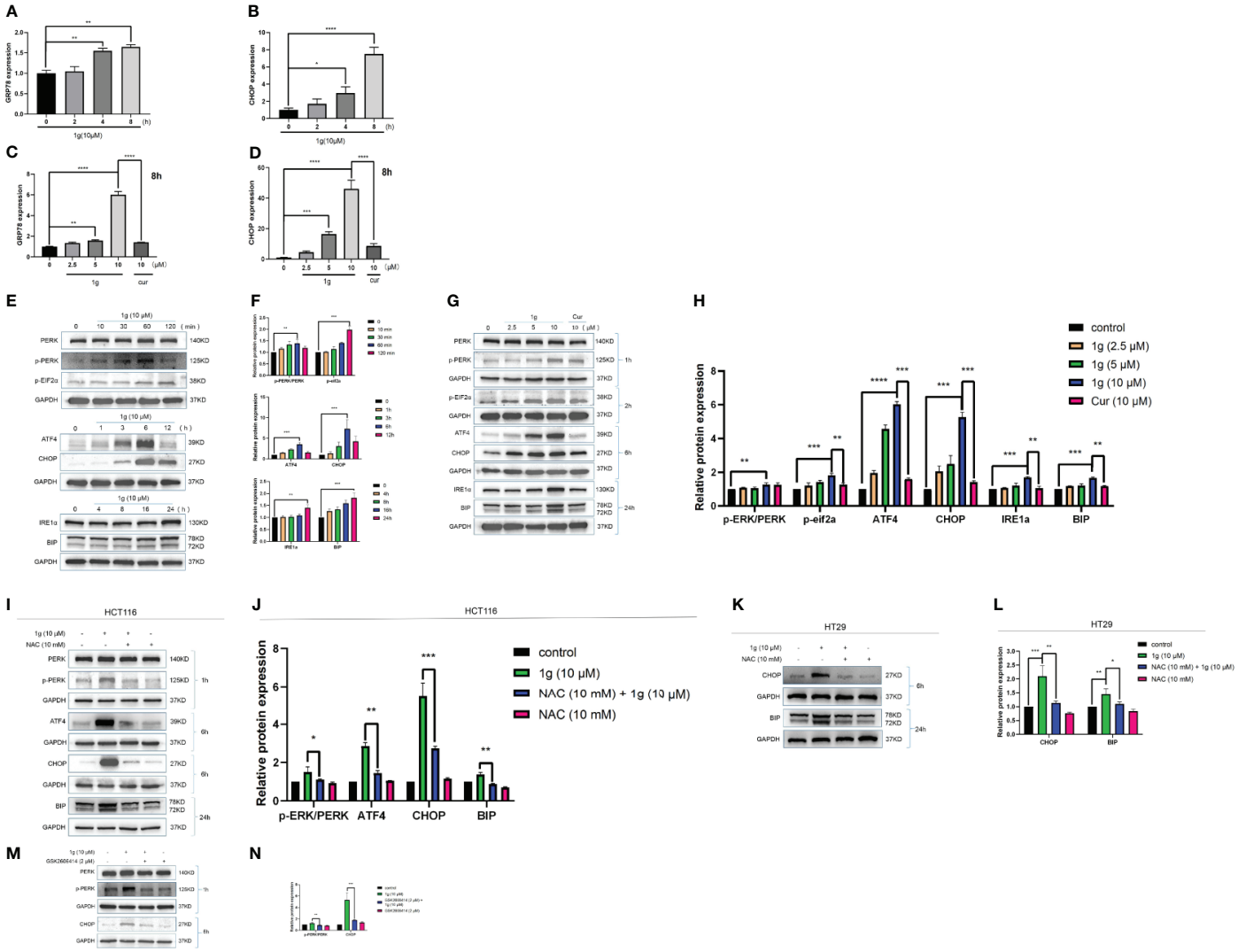

FIGURE 6 | ER-stress is involved in 1g-induced apoptosis of colon cancer cells. **(A, B)** GRP78 and CHOP mRNA levels of HCT116 cells were measured after treatment 1g (10 μM) from 0 to 8 h. **(C, D)** GRP78 and CHOP mRNA levels of HCT116 cells were measured after treatment with various concentrations of 1g ranged from 0 to 10 μM for 8 h. **(E, F)** ER-stress protein levels were measured by Western blot analysis of HCT116 cells treated with 1g (10 μM) for various durations. **(G, H)** Protein levels were measured by Western blot analysis of HCT116 cells treated with 1g or Cur for the duration indicated. **(I, J)** Expression of proteins measured by Western blot analysis of HCT116 cells pre-incubated with 10 mM NAC for 1 h prior to treatment with 1g (10 μM) for the duration indicated. **(K, L)** Expression of proteins measured by Western blot analysis of HT29 cells pre-incubated with 10mM NAC for 1 h prior to treatment with 1g (10 μM) for the duration indicated. **(M, N)** Expression of PERK, p-PERK, or CHOP determined by Western blot analysis of HCT116 cells incubated with p-PERK inhibitor (GSK2606414), after stimulation with 1g (10 μM) for 2 or 6 h. Data represent means ± SD. Statistical significance was determined by one-way analysis of variance (ANOVA) followed by a Bonferroni's *post-hoc* test. Statistical significance is indicated as $^{*}P < 0.05$, $^{**}P < 0.01$, $^{***}P < 0.001$, $^{****}P < 0.0001$. ns indicates that the comparison was not statistically significant.

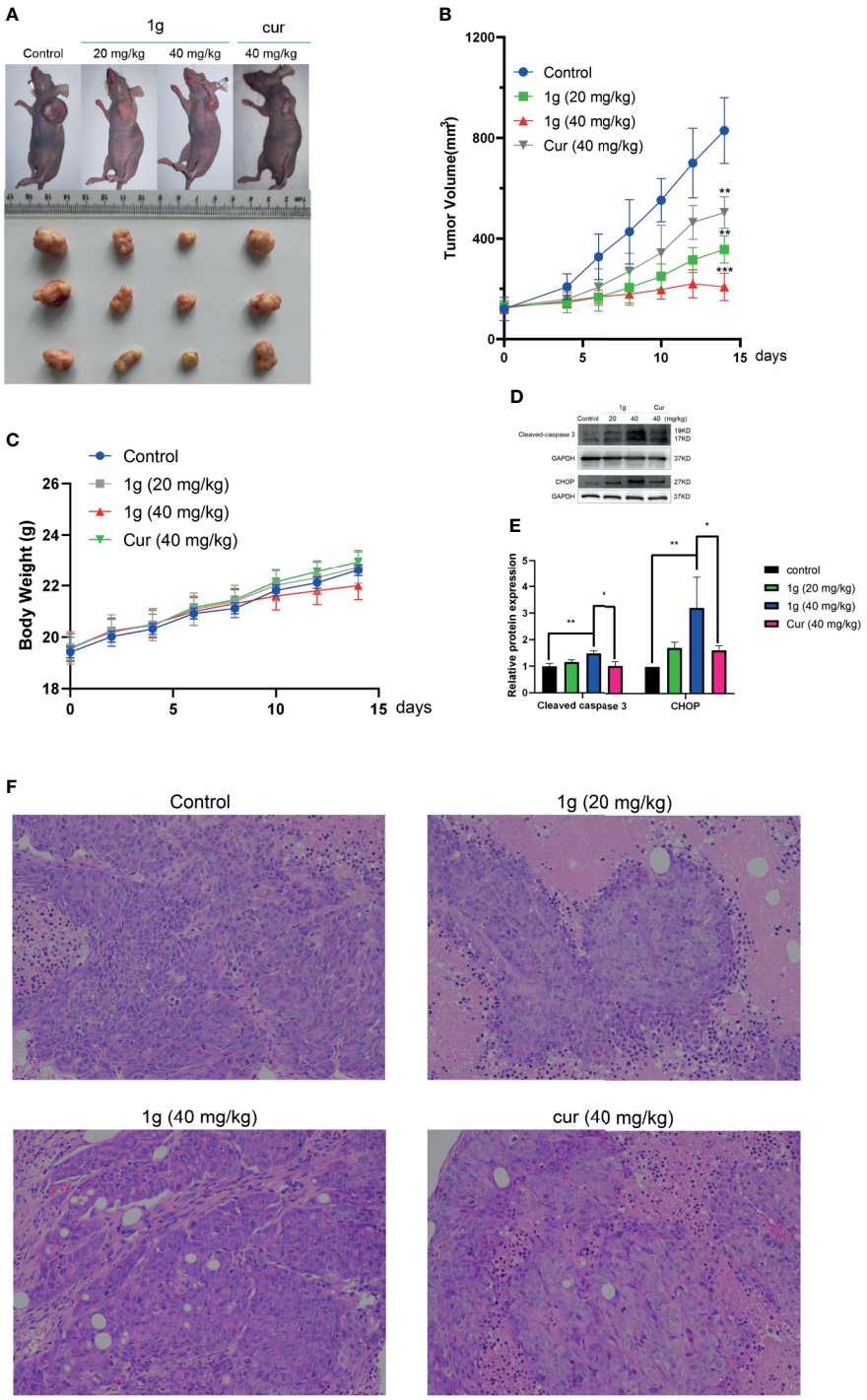

FIGURE 7 | 1g inhibits tumor growth in a xenograft mouse model of human colon cancer. **(A)** 7 days after HCT116 cell implantation, the mice were treated with either vehicle (control), 1g (20 mg/kg), 1g (40 mg/kg), or Cur (40 mg/kg) for an additional 14 days. The size of the tumor in each group is shown (n = 6 each group). **(B)** Representative images of tumors in each treatment group. **(C)** Weight of Balb/c mice (n = 6). **(D, E)** Cleaved caspase 3 and CHOP levels evaluated in 1g-treated and Cur-treated xenografts. Relative density measurements correspond to Western blot band intensities normalized to an internal control (n = 3). **(F)** HE staining of tumor tissue treated with 1g and curcumin. Data represent means ± SD. Statistical significance was determined by one-way analysis of variance (ANOVA) followed by a Bonferroni's *post-hoc* test. Statistical significance is indicated as $^{*}P < 0.05$, $^{**}P < 0.01$, $^{***}P < 0.001$.

principally through the mitochondria-dependent pathway (32, 38). Flow cytometry analysis and Western blotting revealed that 1g modified the mitochondrial membrane potential of HCT116 cells and induced apoptosis. Interestingly, the change in mitochondrial membrane potential induced by 1g activated apoptotic signals, unlike the mechanism of Cur. In addition, Western blot analysis of apoptotic proteins demonstrated that 1g effectively induced apoptosis by releasing cytochrome c and activating downstream caspase-9 and caspase-3 cascade reactions.

In recent years, increasing attention has focused on therapeutic drugs that can regulate different stages of the cell cycle in cancer cells, including G0/G1, S, and G2/M (42). Regulation by inhibition of the cell cycle may be considered a beneficial event that leads to the induction of apoptotic cell death when treating colon cancer (43). In the present study, in comparison with Cur (8), 1g induced cell blockade of the G1 phase in HCT116 cells. Thus, the results indicate that 1g caused apoptosis in colon cancer cells by blocking the cell cycle.

Cur also produced ROS, leading to apoptosis in cancer cells (44, 45). As important multifaceted signaling molecules, ROS regulate multiple cellular pathways and play an important role in deciding cell fate (46). There is growing evidence that excessive oxidative stress may be an effective method of eliminating cancer cells (47). After excessive production of ROS, a number of pro-apoptotic signaling pathways, including ER-stress, are activated (48). ER-stress is a conservative cellular defense mechanism that responds to the environment within the ER (49). A number of anticancer drugs have previously been reported to induce apoptosis in cancer cells by ER-stress, such as sphenol (50), farnicol (51), or polyfiline D (52). Similarly, 1g also promoted

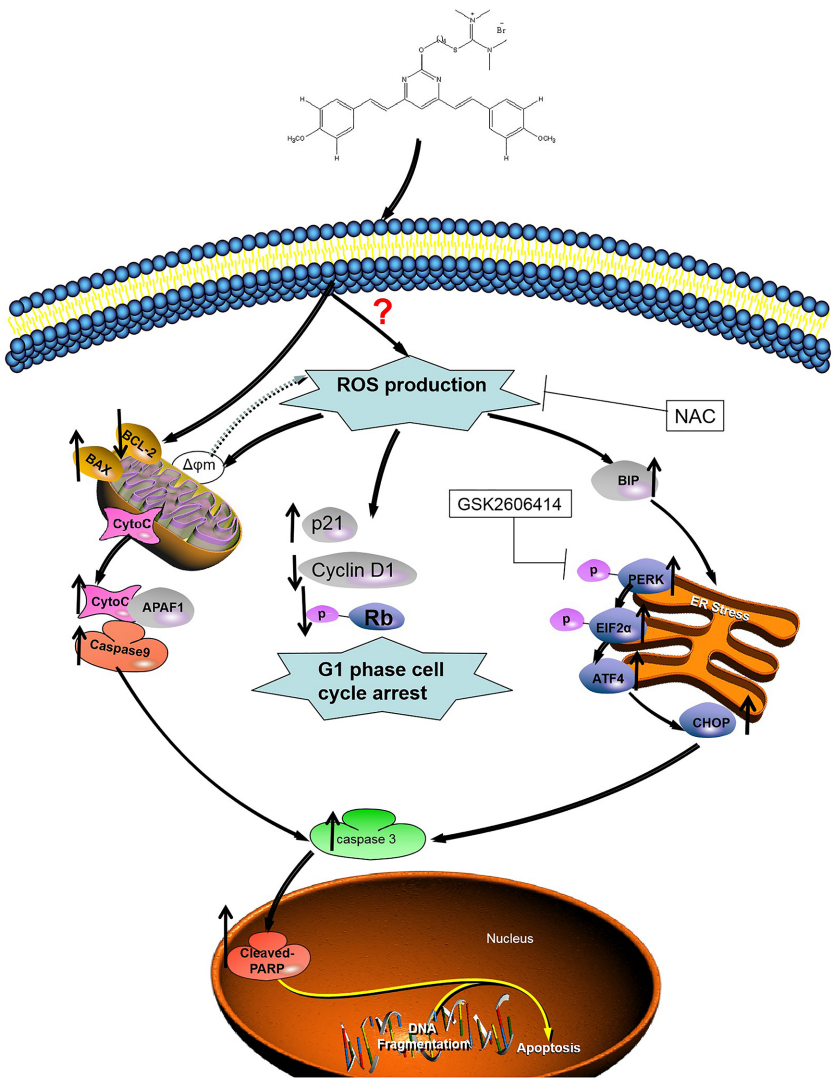

FIGURE 8 | Illustration of the mechanism of inhibition of colon cancer growth by 1g. 1g causes the production of mitochondrial ROS, which then leads to cell cycle stagnation and ER-stress, resulting in apoptotic cell death.

ROS-mediated ER-stress. The unfolded protein response causes ER stress over a long period and activates the mammalian apoptosis pathway (53). During the commitment stage of ER-stress-induced apoptosis, activation of the downstream transcription factor CHOP caused by ATF-4 signaling can trigger pro-apoptotic signals, thereby triggering the specific cascade of ER-stress that results in apoptosis (54). We used Western blotting to identify the association between apoptosis and ER-stress in colon cancer cells induced by 1g. We further investigated whether apoptosis induced by 1g was related to ER stress. HCT116 cells were pretreated with PERK inhibitor. Inhibition of P-PERK by GSK2606414 significantly inhibited the expression of CHOP and p-PERK in 1g-induced HCT116 cells. Importantly, however, the inhibition of ROS production by combined NAC treatment almost completely reversed HCT116-induced apoptosis, including cell cycle blockade, mitochondrial apoptosis, and ER-stress. These results further demonstrate that ROS production plays a critical role in cell survival. The results suggest, as illustrated in **Figure 8**, that 1g can induce the production of ROS in colon cancer cells, resulting in cell cycle stagnation, a change in mitochondrial membrane potential and ER-stress, thus leading to apoptosis in colon cancer cells. Indeed, in addition to cellular effects, we demonstrated that 1g has a strong inhibitory effect on tumor growth in an HCT116 transplant tumor mouse model. Moreover, 1g displayed an excellent safety profile.

In summary, The Cur derivative 1g significantly reduced the activity of colon cancer cells and induced apoptosis of colon cancer cells *in vitro* and *in vivo* through the production of ROS. The properties of 1g should be further studied in order to develop an effective anticancer drug to treat human colon cancer. The results also suggest that activation of ROS production may be a key factor in the treatment of CRC. Nevertheless, the direct target of the 1g molecule remains unknown and the specific origin of ROS is still unclear. Current data indicate a high probability that it is generated in mitochondria, but other aspects require additional study. Therefore, we believe that the over-production of ROS following the modification of natural anticancer drugs may provide a novel strategy for anticancer treatment.

DATA AVAILABILITY STATEMENT

The datasets presented in this study can be found in online repositories. The names of the repository/repositories and accession number(s) can be found below: https://www.ncbi.nlm.nih.gov/bioproject/?term=PRJNA716135.

ETHICS STATEMENT

The animal study was reviewed and approved by the Ethics Committee of Experimental Animal Welfare of the Affiliated Hospital of Qingdao University (AHQU20200605).

AUTHOR CONTRIBUTIONS

HW and JS designed the experiments and helped write the manuscript. YX designed the experiments and checked the text of the article. ZS designed the and raised the funding for the experiments. All authors contributed to the article and approved the submitted version.

FUNDING

This study was supported by grants from the National Youth Foundation of China (81903872) and the Natural Science Foundation of Shandong Province (ZR2019MH077).

ACKNOWLEDGMENTS

Thanks to all the authors listed for their contributions to this study.

SUPPLEMENTARY MATERIAL

The Supplementary Material for this article can be found online at:https://www.frontiersin.org/articles/10.3389/fonc.2021.644197/full#supplementary-material

REFERENCES

1. Bray F, Ferlay J, Soerjomataram I, Siegel RL, Torre LA, Jemal A. Global Cancer Statistics 2018: GLOBOCAN Estimates of Incidence and Mortality Worldwide for 36 Cancers in 185 Countries. *CA Cancer J Clin* (2018) 68 (6):394–424. doi: 10.3322/caac.21492
2. Siegel RL, Miller KD, Jemal A. Cancer Statistics, 2017. *CA Cancer J Clin* (2017) 67(1):7–30. doi: 10.3322/caac.21387
3. Mishra J, Drummond J, Quazi SH, Karanki SS, Shaw JJ, Chen B, et al. Prospective of Colon Cancer Treatments and Scope for Combinatorial Approach to Enhanced Cancer Cell Apoptosis. *Crit Rev Oncol Hematol* (2013) 86(3):232–50. doi: 10.1016/j.critrevonc.2012.09.014
4. Radhakrishna Pillai G, Srivastava AS, Hassanein TI, Chauhan DP, Carrier E. Induction of Apoptosis in Human Lung Cancer Cells by Curcumin. *Cancer Lett* (2004) 208(2):163–70. doi: 10.1016/j.canlet.2004.01.008
5. Terlikowska K, Witkowska A, Terlikowski S. [Curcumin in Chemoprevention of Breast Cancer]. *Postepy Hig Med Dosw (Online)* (2014) 68:571–8. doi: 10.5604/17322693.1102294
6. Xue X, Yu JL, Sun DQ, Kong F, Qu XJ, Zou W, et al. Curcumin Induces Apoptosis in SGC-7901 Gastric Adenocarcinoma Cells *Via* Regulation of Mitochondrial Signaling Pathways. *Asian Pac J Cancer Prev* (2014) 15 (9):3987–92. doi: 10.7314/APJCP.2014.15.9.3987
7. Subramaniam D, May R, Sureban SM, Lee KB, George R, Kuppusamy P, et al. Diphenyl Difluoroketone: A Curcumin Derivative With Potent *In Vivo* Anticancer Activity. *Cancer Res* (2008) 68(6):1962–9. doi: 10.1158/0008-5472.CAN-07-6011
8. Agarwal A, Kasinathan A, Ganesan R, Balasubramanian A, Bhaskaran J, Suresh S, et al. Curcumin Induces Apoptosis and Cell Cycle Arrest *Via* the Activation of Reactive Oxygen Species-Independent Mitochondrial Apoptotic Pathway in Smad4 and P53 Mutated Colon Adenocarcinoma HT29 Cells. *Nutr Res* (2018) 51:67–81. doi: 10.1016/j.nutres.2017.12.011
9. Freudlsperger C, Greten J, Schumacher U. Curcumin Induces Apoptosis in Human Neuroblastoma Cells *Via* Inhibition of Nfkappab. *Anticancer Res* (2008) 28(1a):209–14.
10. Kawamori T, Lubet R, Steele VE, Kelloff GJ, Kaskey RB, Rao CV, et al. Chemopreventive Effect of Curcumin, a Naturally Occurring

Anti-Inflammatory Agent, During the Promotion/Progression Stages of Colon Cancer. *Cancer Res* (1999) 59(3):597–601.
11. Roy M, Chakraborty S, Siddiqi M, Bhattacharya RK. Induction of Apoptosis in Tumor Cells by Natural Phenolic Compounds. *Asian Pac J Cancer Prev* (2002) 3(1):61–7.
12. Chearwae W, Anuchapreeda S, Nandigama K, Ambudkar SV, Limtrakul P. Biochemical Mechanism of Modulation of Human P-Glycoprotein (ABCB1) by Curcumin I, II, and III Purified From Turmeric Powder. *Biochem Pharmacol* (2004) 68(10):2043–52. doi: 10.1016/j.bcp.2004.07.009
13. Anand P, Sundaram C, Jhurani S, Kunnumakkara AB, Aggarwal BB. Curcumin and Cancer: An "Old-Age" Disease With an "Age-Old" Solution. *Cancer Lett* (2008) 267(1):133–64. doi: 10.1016/j.canlet.2008.03.025
14. Bar-Sela G, Epelbaum R, Schaffer M. Curcumin as an Anti-Cancer Agent: Review of the Gap Between Basic and Clinical Applications. *Curr Med Chem* (2010) 17(3):190–7. doi: 10.2174/092986710790149738
15. Safavy A, Raisch KP, Mantena S, Sanford LL, Sham SW, Krishna NR, et al. Design and Development of Water-Soluble Curcumin Conjugates as Potential Anticancer Agents. *J Med Chem* (2007) 50(24):6284–8. doi: 10.1021/jm700988f
16. Sun M, Su X, Ding B, He X, Liu X, Yu A, et al. Advances in Nanotechnology-Based Delivery Systems for Curcumin. *Nanomedicine (Lond)* (2012) 7 (7):1085–100. doi: 10.2217/nnm.12.80
17. Radak Z, Zhao Z, Koltai E, Ohno H, Atalay M. Oxygen Consumption and Usage During Physical Exercise: The Balance Between Oxidative Stress and ROS-Dependent Adaptive Signaling. *Antioxid Redox Signal* (2013) 18 (10):1208–46. doi: 10.1089/ars.2011.4498
18. Bazhin AV, Philippov PP, Karakhanova S. Reactive Oxygen Species in Cancer Biology and Anticancer Therapy. *Oxid Med Cell Longev* (2016) 2016:4197815. doi: 10.1155/2016/4197815
19. Tong S, Zhang M, Wang S, Yin R, Yu R, Wan S, et al. Isothiouronium Modification Empowers Pyrimidine-Substituted Curcumin Analogs Potent Cytotoxicity and Golgi Localization. *Eur J Med Chem* (2016) 123:849–57. doi: 10.1016/j.ejmech.2016.07.071
20. Jin HR, Zhao J, Zhang Z, Liao Y, Wang CZ, Huang WH, et al. The Antitumor Natural Compound Falcarindiol Promotes Cancer Cell Death by Inducing Endoplasmic Reticulum Stress. *Cell Death Dis* (2012) 3(8):e376. doi: 10.1038/cddis.2012.122
21. Evan GI, Brown L, Whyte M, Harrington E. Apoptosis and the Cell Cycle. *Curr Opin Cell Biol* (1995) 7(6):825–34. doi: 10.1016/0955-0674(95)80066-2
22. Green DR, Kroemer G. The Pathophysiology of Mitochondrial Cell Death. *Science* (2004) 305(5684):626–9. doi: 10.1126/science.1099320
23. Fulda S, Debatin KM. Extrinsic Versus Intrinsic Apoptosis Pathways in Anticancer Chemotherapy. *Oncogene* (2006) 25(34):4798–811. doi: 10.1038/sj.onc.1209608
24. Saelens X, Festjens N, Vande Walle L, van Gurp M, van Loo G, Vandenabeele P. Toxic Proteins Released From Mitochondria in Cell Death. *Oncogene* (2004) 23(16):2861–74. doi: 10.1038/sj.onc.1207523
25. Murphy MP. How Mitochondria Produce Reactive Oxygen Species. *Biochem J* (2009) 417(1):1–13. doi: 10.1042/BJ20081386
26. Jena NR. DNA Damage by Reactive Species: Mechanisms, Mutation and Repair. *J Biosci* (2012) 37(3):503–17. doi: 10.1007/s12038-012-9218-2
27. Zhang J, Feng Z, Wang C, Zhou H, Liu W, Kanchana K, et al. Curcumin Derivative WZ35 Efficiently Suppresses Colon Cancer Progression Through Inducing ROS Production and ER Stress-Dependent Apoptosis. *Am J Cancer Res* (2017) 7(2):275–88.
28. Circu ML, Aw TY. Reactive Oxygen Species, Cellular Redox Systems, and Apoptosis. *Free Radic Biol Med* (2010) 48(6):749–62. doi: 10.1016/j.freeradbiomed.2009.12.022
29. Rushworth GF, Megson IL. Existing and Potential Therapeutic Uses for N-Acetylcysteine: The Need for Conversion to Intracellular Glutathione for Antioxidant Benefits. *Pharmacol Ther* (2014) 141(2):150–9. doi: 10.1016/j.pharmthera.2013.09.006
30. Rojas-Rivera D, Delvaeye T, Roelandt R, Nerinckx W, Augustyns K, Vandenabeele P, et al. When PERK Inhibitors Turn Out to be New Potent RIPK1 Inhibitors: Critical Issues on the Specificity and Use of GSK2606414 and GSK2656157. *Cell Death Differ* (2017) 24(6):1100–10. doi: 10.1038/cdd.2017.58
31. Aggarwal BB, Sundaram C, Malani N, Ichikawa H. Curcumin: The Indian Solid Gold. *Adv Exp Med Biol* (2007) 595:1–75. doi: 10.1007/978-0-387-46401-5_1
32. Anto RJ, Mukhopadhyay A, Denning K, Aggarwal BB. Curcumin (Diferuloylmethane) Induces Apoptosis Through Activation of Caspase-8, BID Cleavage and Cytochrome C Release: Its Suppression by Ectopic Expression of Bcl-2 and Bcl-Xl. *Carcinogenesis* (2002) 23(1):143–50. doi: 10.1093/carcin/23.1.143
33. Mackenzie GG, Queisser N, Wolfson ML, Fraga CG, Adamo AM, Oteiza PI. Curcumin Induces Cell-Arrest and Apoptosis in Association With the Inhibition of Constitutively Active NF-Kappab and STAT3 Pathways in Hodgkin's Lymphoma Cells. *Int J Cancer* (2008) 123(1):56–65. doi: 10.1002/ijc.23477
34. Park S, Cho DH, Andera L, Suh N, Kim I. Curcumin Enhances TRAIL-Induced Apoptosis of Breast Cancer Cells by Regulating Apoptosis-Related Proteins. *Mol Cell Biochem* (2013) 383(1-2):39–48. doi: 10.1007/s11010-013-1752-1
35. Anand P, Thomas SG, Kunnumakkara AB, Sundaram C, Harikumar KB, Sung B, et al. Biological Activities of Curcumin and its Analogues (Congeners) Made by Man and Mother Nature. *Biochem Pharmacol* (2008) 76(11):1590–611. doi: 10.1016/j.bcp.2008.08.008
36. Tang H, Murphy CJ, Zhang B, Shen Y, Van Kirk EA, Murdoch WJ, et al. Curcumin Polymers as Anticancer Conjugates. *Biomaterials* (2010) 31 (27):7139–49. doi: 10.1016/j.biomaterials.2010.06.007
37. Sharma RA, McLelland HR, Hill KA, Ireson CR, Euden SA, Manson MM, et al. Pharmacodynamic and Pharmacokinetic Study of Oral Curcuma Extract in Patients With Colorectal Cancer. *Clin Cancer Res* (2001) 7 (7):1894–900.
38. Garcea G, Jones DJ, Singh R, Dennison AR, Farmer PB, Sharma RA, et al. Detection of Curcumin and its Metabolites in Hepatic Tissue and Portal Blood of Patients Following Oral Administration. *Br J Cancer* (2004) 90(5):1011–5. doi: 10.1038/sj.bjc.6601623
39. Davis PD, Elliott LH, Harris W, Hill CH, Hurst SA, Keech E, et al. Inhibitors of Protein Kinase C. 2. Substituted Bisindolylmaleimides With Improved Potency and Selectivity. *J Med Chem* (1992) 35(6):994–1001. doi: 10.1021/jm00084a004
40. Danilenko VN, Simonov AY, Lakatosh SA, Kubbutat MH, Totzke F, Schächtele C, et al. Search for Inhibitors of Bacterial and Human Protein Kinases Among Derivatives of Diazepines[1,4] Annelated With Maleimide and Indole Cycles. *J Med Chem* (2008) 51(24):7731–6. doi: 10.1021/jm800758s
41. Heger M, van Golen RF, Broekgaarden M, Michel MC. The Molecular Basis for the Pharmacokinetics and Pharmacodynamics of Curcumin and its Metabolites in Relation to Cancer. *Pharmacol Rev* (2014) 66(1):222–307. doi: 10.1124/pr.110.004044
42. Garrett MD, Collins I. Anticancer Therapy With Checkpoint Inhibitors: What, Where and When? *Trends Pharmacol Sci* (2011) 32(5):308–16. doi: 10.1016/j.tips.2011.02.014
43. Hwang SK, Piao L, Lim HT, Minai-Tehrani A, Yu KN, Ha YC, et al. Suppression of Lung Tumorigenesis by Leucine Zipper/EF Hand-Containing Transmembrane-1. *PLoS One* (2010) 5(9). doi: 10.1371/journal.pone.0012535
44. Shen HM, Liu ZG. JNK Signaling Pathway is a Key Modulator in Cell Death Mediated by Reactive Oxygen and Nitrogen Species. *Free Radic Biol Med* (2006) 40(6):928–39. doi: 10.1016/j.freeradbiomed.2005.10.056
45. Chen Q, Wang Y, Xu K, Lu G, Ying Z, Wu L, et al. Curcumin Induces Apoptosis in Human Lung Adenocarcinoma A549 Cells Through a Reactive Oxygen Species-Dependent Mitochondrial Signaling Pathway. *Oncol Rep* (2010) 23(2):397–403. doi: 10.3892/or_00000648
46. Zhou Y, Shu F, Liang X, Chang H, Shi L, Peng X, et al. Ampelopsin Induces Cell Growth Inhibition and Apoptosis in Breast Cancer Cells Through ROS Generation and Endoplasmic Reticulum Stress Pathway. *PLoS One* (2014) 9 (2):e89021. doi: 10.1371/journal.pone.0089021
47. Samoylenko A, Hossain JA, Mennerich D, Kellokumpu S, Hiltunen JK, Kietzmann T. Nutritional Countermeasures Targeting Reactive Oxygen Species in Cancer: From Mechanisms to Biomarkers and Clinical Evidence. *Antioxid Redox Signal* (2013) 19(17):2157–96. doi: 10.1089/ars.2012.4662
48. Wang CL, Liu C, Niu LL, Wang LR, Hou LH, Cao XH. Surfactin-Induced Apoptosis Through ROS-ERS-Ca2+-ERK Pathways in Hepg2 Cells. *Cell Biochem Biophys* (2013) 67(3):1433–9. doi: 10.1007/s12013-013-9676-7
49. Jheng JR, Ho JY, Horng JT. ER Stress, Autophagy, and RNA Viruses. *Front Microbiol* (2014) 5:388. doi: 10.3389/fmicb.2014.00388

50. Kawashima M, Kondo H. Comparison of Therapeutic G-CSF Cycles and Prophylactic G-CSF Cycles in Patients Receiving Paclitaxel and Carboplatin Combination Chemotherapy for Ovarian Cancer: A Retrospective Study Report. *J Rural Med* (2014) 9(2):86–9. doi: 10.2185/jrm.2889
51. Park JS, Kwon JK, Kim HR, Kim HJ, Kim BS, Jung JY. Farnesol Induces Apoptosis of DU145 Prostate Cancer Cells Through the PI3K/Akt and MAPK Pathways. *Int J Mol Med* (2014) 33(5):1169–76. doi: 10.3892/ijmm.2014.1679
52. Chan JY, Koon JC, Liu X, Detmar M, Yu B, Kong SK, et al. a Steroidal Saponin From Paris Polyphylla, Inhibits Endothelial Cell Functions *In Vitro* and Angiogenesis in Zebrafish Embryos In Vivo. *J Ethnopharmacol* (2011) 137 (1):64–9. doi: 10.1016/j.jep.2011.04.021
53. Fabrizio G, Di Paola S, Stilla A, Giannotta M, Ruggiero C, Menzel S, et al. ARTC1-Mediated ADP-Ribosylation of GRP78/Bip: A New Player in Endoplasmic-Reticulum Stress Responses. *Cell Mol Life Sci* (2015) 72 (6):1209–25. doi: 10.1007/s00018-014-1745-6
54. Zhang X, Zhang HQ, Zhu GH, Wang YH, Yu XC, Zhu XB, et al. A Novel Mono-Carbonyl Analogue of Curcumin Induces Apoptosis in Ovarian Carcinoma Cells *Via* Endoplasmic Reticulum Stress and Reactive Oxygen Species Production. *Mol Med Rep* (2012) 5(3):739–44. doi: 10.3892/mmr.2011.700

Conflict of Interest: The authors declare that the research was conducted in the absence of any commercial or financial relationships that could be construed as a potential conflict of interest.

frontiers in Pharmacology

REVIEW
published: 06 July 2021
doi: 10.3389/fphar.2021.665387

A Promising Anticancer Agent Dimethoxycurcumin: Aspects of Pharmacokinetics, Efficacy, Mechanism, and Nanoformulation for Drug Delivery

Muhammad Sohail[1†], Wenna Guo[1†], Xin Yang[2], Zhiyong Li[1], Yanli Li[1,3], Hui Xu[1] and Feng Zhao[1]*

[1]School of Pharmacy, Collaborative Innovation Center of Advanced Drug Delivery System and Biotech Drugs in Universities of Shandong, Key Laboratory of Molecular Pharmacology and Drug Evaluation (Yantai University) Ministry of Education, Yantai University, Yantai, China, [2]School of Chemistry and Chemical Engineering, Yantai University, Yantai, China, [3]Department of Pharmaceutics, Binzhou Hospital of TCM, Binzhou, China

Curcumin is a well-known anticancer natural product with various significant bioactivities that has been well documented, but its widespread use is mainly hindered by insufficient ADME properties such as poor solubility and low metabolic stability. Dimethoxycurcumin (DiMC) is a kind of lipophilic compound derived from curcumin that maintains its anticancer potency and has greatly improved systematic bioavailability. Therefore, DiMC is regarded as a promising plant-derived anticancer agent that deserves to be well developed. Herein, we concentrate on the published work by those from original research groups concerned with the pharmacokinetics, efficacy, and mechanism of DiMC involved in the treatment of various tumors, as well as the nanoformulations for effective drug delivery.

Keywords: anticancer agent, dimethoxycurcumin, pharmacokinetics, mechanism of action, nanoformulation

OPEN ACCESS

Edited by:
Xuanming Yang,
Shanghai Jiao Tong University, China

Reviewed by:
Nina Hermans,
University of Antwerp, Belgium
Xueqing Zhang,
Shanghai Jiao Tong University, China

****Correspondence:***
Hui Xu
xuhui@ytu.edu.cn

†These authors have contributed equally to this work

Specialty section:
This article was submitted to Pharmacology of Anti-Cancer Drugs, a section of the journal Frontiers in Pharmacology

Received: *08 February 2021*
Accepted: *04 June 2021*
Published: *06 July 2021*

Citation:
Sohail M, Guo W, Yang X, Li Z, Li Y, Xu H and Zhao F (2021) A Promising Anticancer Agent Dimethoxycurcumin: Aspects of Pharmacokinetics, Efficacy, Mechanism, and Nanoformulation for Drug Delivery. Front. Pharmacol. 12:665387. doi: 10.3389/fphar.2021.665387

INTRODUCTION

Curcumin is the principal curcuminoid of turmeric (*Curcuma longa* L.), a member of the ginger family. As a kind of natural product, curcumin has been extensively noticed in herb medicine due to various striking bioactivities beneficial to human health such as antioxidant, antiviral, anti-inflammatory, and antiangiogenic effects, especially the great potential of the anticancer effect by disturbing multiple molecular targets (Yang et al., 2017). However, the pharmaceutical function and clinical application of curcumin are severely limited by low water solubility, instability, poor absorption, and rapid systemic elimination *in vivo* (Sun et al., 2018). Therefore, a great deal of research has long been performed to find appropriate solutions to the problems mentioned above, for which chemical structure modification provides an effective way and attracts much interest (Yallapu et al., 2013; Heger et al., 2014).

Dimethoxycurcumin (DiMC), also called dimethylcurcumin or ASC-J9, is a lipophilic compound structurally derived from curcumin with a minor modification of both hydroxyls into methoxyls (Lin et al., 2013; Liu et al., 2015). As illustrated in **Figure 1**, DiMC is chemically similar to curcumin, and they both have tautomerism between the bis-keto and enolate forms depending on the pH value of the medium, while the methylene group among the β-diketone structure provides them with similarly remarkable antioxidant properties (Hadjidemetriou et al., 2013). Meanwhile, the methylation of both hydroxyl groups makes DiMC

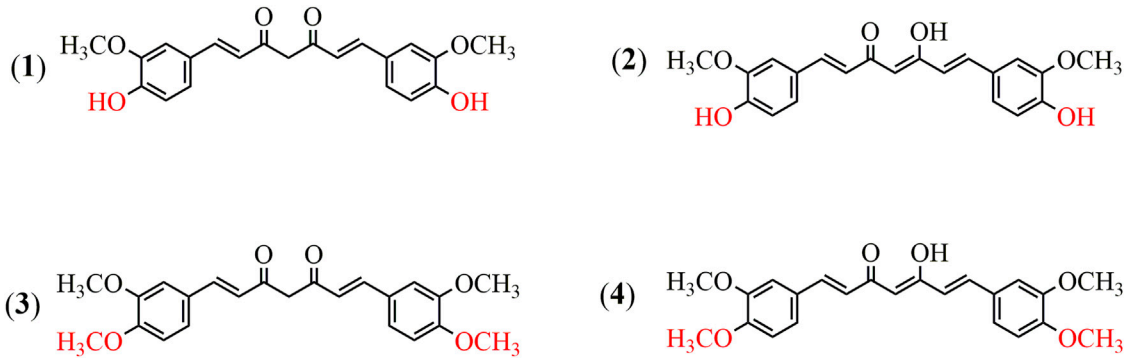

FIGURE 1 | Chemical structures of curcumin and dimethoxycurcumin. **(1)** Curcumin (the bis-keto form). **(2)** Curcumin (the enolate form). **(3)** Dimethoxycurcumin (the bis-keto form). **(4)** Dimethoxycurcumin (the enolate form).

more stable and lipophilic than curcumin, further providing it with a significantly reduced degradation rate and a much improved drug delivery system (Hassan et al., 2015; Dützmann et al., 2016; Jayakumar et al., 2016). It was also found that DiMC could respond to normal healthy cells in a way that is similar to curcumin but exerted more potent antioxidant properties (Kunwar et al., 2011a; Kim et al., 2016; Arrue et al., 2017). Resultantly, DiMC usually displays various pharmacological activities that are mostly maintained and even more improved in contrast to curcumin, which mainly includes anti-inflammatory, antihypertensive, neuroprotective, nephroprotective, and anticancer effects that are primarily attributed to its stability and potent anti-oxidant and free radical scavenger properties (Karimian et al., 2017). Much attention has lately been given to DiMC due to its potency against various cancer cell lines in many cases, such as the ability to serve as an androgen receptor antagonist in human prostate cancer cells *in vivo* (Ramkumar et al., 2017; Hatamipour et al., 2018; Hatamipour et al., 2019). Recent research has further revealed the miraculous power of DiMC as an anticancer agent *via* special actions on various molecular targets, including inactivation of enzymes, regulation of P-glycoprotein activity, inducing apoptosis and promoting autophagy of cancer cells, inhibiting migration, and DNA transcription (Munigunti et al., 2014; Yoon et al., 2014).

In order to provide relatively comprehensive basic data for further development, the present review systematically summarized the literature about the promising anticancer agent DiMC for the first time, which mainly included its pharmacokinetic characteristics, anticancer effects against various cancer cells, and the molecular mechanism of action. The research on drug delivery systems was also involved, especially the nanoformulations of DiMC that focused on improving stability and ADME profiles *in vivo*.

PHARMACOKINETICS OF DIMC

As previously described, DiMC is more effective in inhibiting proliferation and inducing apoptosis of different types of human cancer cells than curcumin and its analogs. In addition, in terms of pharmacokinetics, DiMC also has multiple advantages compared with curcumin. It has been reported that the reason behind the low bioavailability of curcumin was its rapid metabolization into tetrahydrocurcumin and some other less active product *in vivo* (Wang et al., 2019). DiMC is a methylated analog of curcumin, where the phenolic -OH groups in curcumin are replaced with methoxyl groups and the symmetric structure offers better chemical and biological stability.

Hassan et al. found that DiMC could effectively induce cell apoptosis and cell cycle arrest even at low concentrations, which might be due to metabolic stability. For further verification, the authors compared the metabolism of curcumin and DiMC *in vivo* by using human liver microsomal enzymes at different time intervals. The results showed that the retention time of curcumin and DiMC was 2.3 and 4.8 min, respectively, and the inherent clearance rate conformed to the first-order kinetics. In the meantime, it was found that in the presence of UDPGA (reflecting phase II metabolism), DiMC was more stable than curcumin, while in the absence of UDPGA, DiMC was less stable than curcumin (Hassan et al., 2015). It is speculated that because hydroxyl group compounds are easily exposed to phase II metabolism (glucuronidation), DiMC is more resistant to phase II metabolism than curcumin under physiological conditions and at the same molar concentration.

In addition, consistent research studies of the modern era have demonstrated that even at higher doses, the bioavailability and metabolic stability of DiMC were higher than those of curcumin. At high doses (10–20 μM), the clearance rate of DiMC was significantly lower than that of curcumin ($p < 0.05$), and the plasma stability of DiMC was 3 times that of curcumin at a dose of 5 mg/kg (Tamvakopoulos et al., 2007; Mach et al., 2010; Hassan et al., 2015). The higher oral bioavailability and metabolic stability of DiMC could to some extent make up for the clinical limitations of curcumin and at the same time significantly improve its ability to induce apoptosis of cancer cells (Chainoglou and Hadjipavlou, 2019). Therefore, DiMC may be the better choice for effective treatment of cancer with lower side effects (Zhang et al., 2017).

TABLE 1 | Anti-cancer activities of DiMC on different cancer cell line models.

Model	Dose	Duration of treatment	Outcomes	Reference
MCF-7 and T47D	0–30 μM *in vitro* and 25 mg/kg *in vivo*	20 days *in vivo* and 0–24 h *in vitro*	Cellular vacuolation, ROS ↑, ubiquitinated proteins ↑, ER 37 stress-related ATF438 and CHOP 39 ↑, and Bim 40 and Noxa proteins ↑	Yoon et al. (2014)
MCF-7	5–50 μM	2–6 h	ATP/ADP ↓, DNA damage, ATP synthase subunits ↓, p53 and p21 ↑, CDK4 and cyclin-D1 ↓, S-phase cell cycle arrest, Bax/BCl2 ↑, ROS ↑, GSH/GSSG ↓, and mitochondrial membrane potential ↓	Kunwar et al. (2012)
A549	1.5–10 μM	15 min–48 h	Apoptosis ↑, clonogenicy ↓, ROS ↑, GSH/GSSG ↓, DNA damage ↑, and TrxR ↓	Jayakumar et al. (2016)
SW480 and SW620	25–30 μM	48 h *in vitro*	Apoptosis ↑, colon cancer growth ↓, protein expression of Bax and Cyt c ↑, ROS ↑, G0/G1 phase arrest, and endoplasmic reticulum expansion	Zhao et al. (2017)
HT-29 and SW480	12.5–100 μM	24–72 h	Apoptosis ↑, survivin ↓, and caspase-3 and PARP ↓	Chen et al. (2016)
Caki cell	40–80 μM	6–24 h	Apoptosis ↑, ROS ↑, Cyt C ↑, and caspase 3 activity ↑	Lee et al. (2010)
786-O	10–40 μM	24 h	CDKN1A ↑, p21 ↑, MYC, BBC3, and CASP7 ↑, caspase 9 and 3/7 ↑, and TNF ↓	Zanetti et al. (2021)
LNCaP	5 μM	24 h	Activation of the proteasome-dependent pathway and phosphorylation of Akt and Mdm2 ↑	Lai et al. (2013)
C4-2 and LNCaP	10 μM	0–24 h	FASN ↓ and PI3K/AKT ↑	Wen et al. (2016)
PC3	5 μM	24 h	Phosphorylation of STAT3 ↓, PIAS3 ↓, and CCL2↓	Lin et al. (2013)
CEM and Jurkat	2 μM	24 h	p15 and cdh-1 ↑, DNMT enzyme ↓, nuclear protein ↓, and H3K27Ac mark ↑	Hassan et al. (2016)
PBMC	5 μM	24 h	Catalase ↑, PBMC ↓, GR ↓, glutathione ↓, and lipid peroxidation↓	Simon et al. (2018)

ANTITUMOR EFFECTS AND MECHANISMS

DiMC has good metabolic stability and a wide range of pharmacological activities. It is provided with significantly anti-inflammatory, antihypertensive, neuroprotective, anti-infection, nephroprotective, and antifungal effects. More importantly, DiMC has a significant therapeutic effect on a variety of life-threatening diseases including cancer. DiMC can produce different cytotoxicities due to the difference in the uptake of tumor cells and normal cells, thereby producing significant anticancer effects while protecting normal cells, and the anticancer effect is better than that of curcumin. The difference in chemical structure is the fundamental reason for the different pharmacokinetics, epigenetic performance, transcription process, and cellular uptake of DiMC. In this section, we will briefly highlight DiMC's anticancer activity and the mechanism of action (**Table 1** and **Figure 2**).

Breast Cancer

Breast cancer is a common malignant tumor and a serious threat to the lives of women. The morbidity and mortality data of breast cancer are gradually increasing. Approximately 249,260 breast cancer cases with 40,890 deaths were revealed in the U.S. statistical report in 2016 (Siegel et al., 2016). Therefore, it is necessary to find new, alternative anticancer drugs.

DiMC has demonstrated that it has an inhibitory effect on breast cancer cells. Kunwar et al. evaluated the anticancer activity of DiMC against human breast cancer MCF-7 cells with curcumin as a positive control (Kunwar et al., 2011a). The results showed that both DiMC and curcumin could induce cytotoxicity, which increased with increasing treatment concentration from 5 to 50 μM. Concurrently, they both also showed similar concentration-dependent cytotoxicity to spleen lymphocytes, but the level of cytotoxicity was much lower than that of MCF-7 cells. The results suggested that DiMC has selective toxicity to breast cancer cells. Another study by Kunwar et al. found that the basal ROS level of MCF-7 cells stained with dihydroethidium increased significantly after 2 h of DiMC treatment, that is, DiMC had a pro-oxidative effect on MCF-7 cells, which was equivalent to that of curcumin (Kunwar et al., 2012). Yoon et al. further compared the anticancer activity of DiMC and curcumin on various breast cancer cells (Yoon et al., 2014). The results showed that DiMC had a more potent *in vitro* anticancer effect than curcumin on breast cancer cells T-47D, MCF-7, MDAMB435S, and MDA-MB 231. Further *in vivo* pharmacodynamics research in human breast cancer–bearing nude mice found that both DiMC and curcumin reduced tumor volume in a dose-dependent manner, but the tumor-reducing effect of DiMC at 25 mg/kg was greater than that of curcumin at 50 mg/kg. It suggested that the anticancer effect of DiMC *in vivo* was greater than that of curcumin, and a lower concentration of DiMC could produce a stronger anticancer effect.

The elucidation of the mechanism is of great significance for disease treatment and drug discovery. Studies have found that there were complex mechanisms of DiMC against breast cancer, mainly related to oxidative stress, proteasome inhibition, mitochondrial dysfunction, and regulation of the expression of related signaling pathway factor genes and proteins (**Figure 3**).

Excessive reactive oxygen species (ROS) can oxidize specific chemical clusters in cells, further lead to DNA mutations, or activate the release pathway of inflammatory factors, which can eventually lead to the activation of oncogenes or the initiation of normal cell apoptosis (Moloney and Cotter, 2018). Therefore, controlling the content of ROS in tumor cells can effectively promote cell apoptosis and inhibit cell differentiation. Kunwar

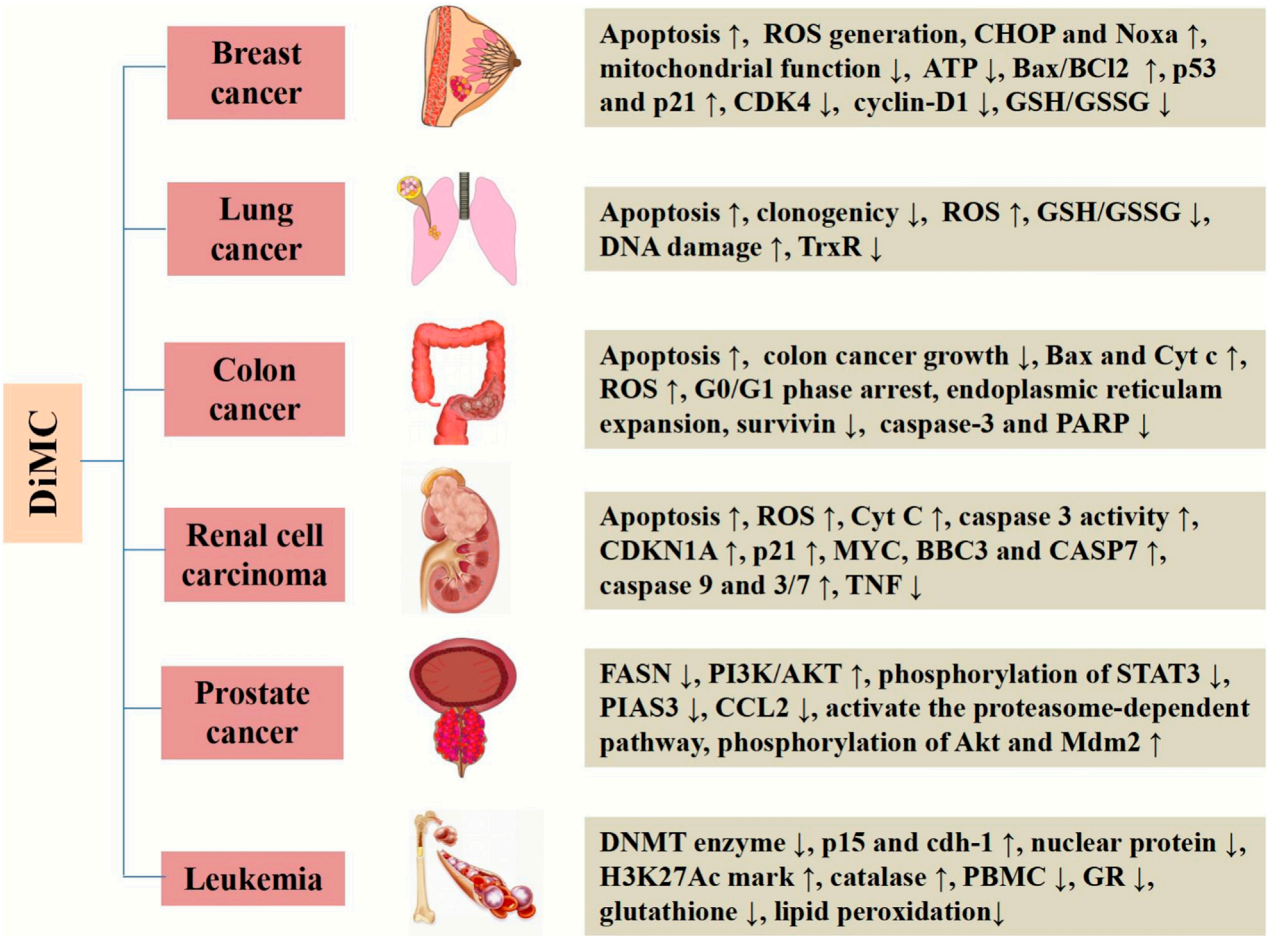

FIGURE 2 | Systemic activities and mechanisms of DiMC against various cancers.

et al. showed that the production of intracellular ROS was decreased when the concentration of DiMC was 5 μM, while at 25 and 50 μM, the production of intracellular ROS was significantly increased (Kunwar et al., 2011b). It was speculated that the increase in the ROS level observed after DiMC treatment might be due to intracellular production or the diffusion of exogenous ROS. Furthermore, with the known cell-permeable free radical scavenger N-acetylcysteine as the positive control, the viability of DiMC (50 μM)-treated cells was evaluated. It was found that N-acetylcysteine inhibited DiMC-induced cytotoxicity with a concentration dependency, confirming the involvement of ROS in DiMC-induced toxicity (Kunwar et al., 2012). Yoon et al. also found that DiMC increased the level of ROS in MDA-MB 435S cells to a greater extent than curcumin (Yoon et al., 2014).

Paraptosis is an alternative, non-apoptotic form of programmed cell death (Fontana et al., 2020), and various stimuli, including paclitaxel, curcumin, and ophiobolin A, reportedly induce paraptosis or paraptosis-like cell death in resistant malignant cancer cells (Lee et al., 2016; Kessel, 2019). Yoon et al. found that DiMC inhibited proteasome activity more strongly than curcumin, which might lead to severe endoplasmic reticulum stress and promote the observed expansion (Yoon et al., 2014). Concurrently, DiMC treatment could upregulate the protein levels of CCAAT–enhancer-binding protein homologous protein (CHOP) and Noxa, which is a candidate mediator of p53-induced apoptosis. It was suggested that DiMC could selectively induce paraptosis of breast cancer cells while retaining normal cells. Furthermore, DiMC could also induce oxidative stress, leading to further weakening of proteasome activity (Yoon et al., 2014).

Moreover, the mechanisms of DiMC against breast cancer were also related to DNA damage, mitochondrial function, expression of cell cycle regulatory proteins, and induction of apoptosis (Kunwar et al., 2012). DiMC could induce the production of ROS, which leads to mitochondrial dysfunction and cell death. In the meantime, DiMC could also reduce the level of ATP in cells by downregulating ATP synthase subunits, resulting in a state of energy depletion. At higher concentrations (25 and 50 μM), DiMC could also induce secondary apoptosis or necrotic cell death in MCF-7 cells by regulating the expression of proapoptotic proteins Bax and Cytochrome c (Cyt c) and antiapoptotic protein Bcl-2. In addition, it has been found that DiMC could inhibit the

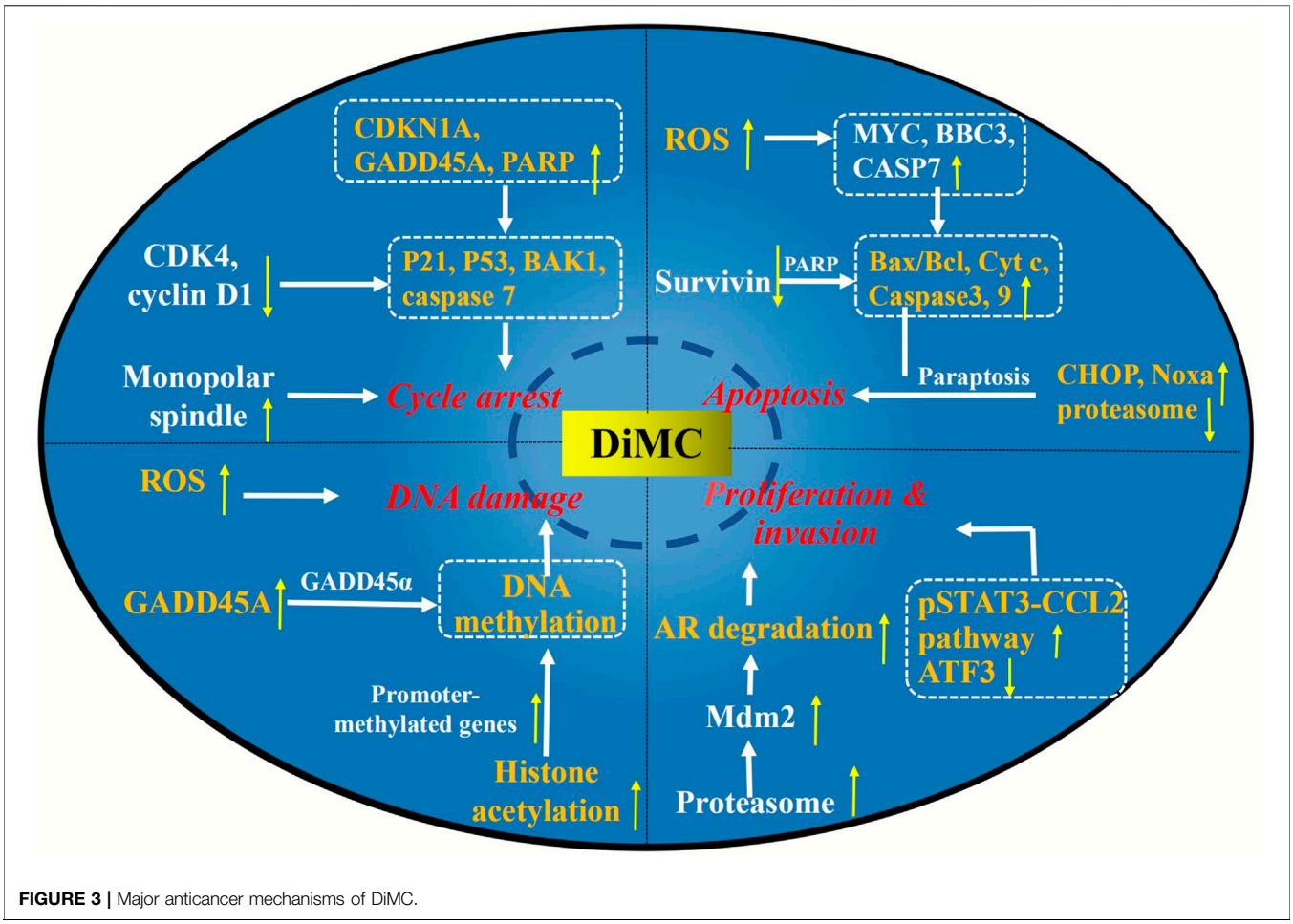

FIGURE 3 | Major anticancer mechanisms of DiMC.

expression of cyclin-dependent kinase four (CDK4) and cyclin-D1 while inducing the expression of p53 and p21, which may play a key role in cell cycle arrest (Kunwar et al., 2012).

Lung Cancer

In general, the untreated nodules in the lungs are identified as a pulmonary cancer. Approximately 224,390 lung cancer cases with 158,080 deaths were revealed in the U.S. statistical report in 2016, of which the disease/death ratio was 117,920/85,920 for males and 106,470/72,160 for females, respectively (Siegel et al., 2016).

Lung adenocarcinoma is a common type of non–small-cell lung cancer. Wada et al. studied the drug resistance of 37 novel curcumin analogs including DiMC and curcumin *in vitro* using gefitinib-resistant lung adenocarcinoma cell lines CL1-5 and H1975 (Wada et al., 2015). The results showed that compared with other curcumin analogs, DiMC significantly decreased the total epidermal growth factor receptor (EGFR) and pEGFR levels of CL1-5 cells carrying wild-type EGFR and also decreased the expression level of total EGFR in EGFR double mutated gefitinib-resistant H1975 cells. The expression level of total EGFR effectively induced gefitinib-insensitive EGFR degradation. It is speculated that the existence of methoxyl groups of C3′ and C4′ in the DiMC chemical structure is beneficial to the EGFR inhibitory activity of gefitinib resistance. Jayakumar et al. investigated the radiosensitizing effect of DiMC in A549 lung cancer cells with curcumin as a positive control. At 2.5 mM, DiMC combined with radiation could significantly increase the apoptosis and mitotic death of A549 cells. In contrast, curcumin at this concentration of 2.5 mM neither showed toxicity toward tumor cells nor exhibited radiosensitizing activity (Jayakumar et al., 2016).

Further study on the possible mechanism of DiMC against lung cancer found that DiMC enhanced the radiosensitivity of lung cancer cells mainly by participating in the regulation of ROS and thioredoxin reductase (TrxR) (**Figure 3**). After DiMC was combined with radiation, the intracellular ROS level increased significantly, the GSH/GSSG ratio decreased significantly, and DNA repair was significantly slowed down, indicating that the treatment with DiMC could make cells sensitive to radiation-induced cytotoxicity by promoting oxidation and inhibiting DNA repair. The thioredoxin system is one of the main antioxidant systems, which can maintain redox balance and participate in DNA synthesis and apoptosis, and is related to radiation resistance of tumor cells. Jayakumar et al. found through computer docking analysis that the binding energies of DiMC and curcumin with TrxR were 7.4 and 7.6 kcal/mol, respectively, which showed high affinity binding and indicated that they could be potential inhibitors of TrxR. The cell experiment further found that DiMC inhibited TrxR in a dose-dependent manner with a half

maximal inhibitory concentration (IC_{50}) value of 5.4 mM. It was inferred that DiMC could increase oxidative stress by inhibiting TrxR, thus slowing down DNA repair and inhibiting DNA synthesis, and resulting in mitotic death (Jayakumar et al., 2016).

Colon Cancer

Colon cancer is the third most prevalent malignant tumor in the world, with an incidence of 10.2% and a mortality rate of 9.2% of all cancer types. It has a trend of increasing year by year, seriously threatening human health. DiMC is a potential candidate for the treatment of colon cancer. It has increased potential to induce apoptosis in colon cancer cells with less toxicity to normal cells and has a higher bioactivity than curcumin.

Chen et al. found that the IC_{50} for DiMC was 43.4 and 28.2 μM on colon cancer cells HT-29 and SW480 (Chen et al., 2016). Simultaneously, the tumors of SW480 and HT29 cells treated with DiMC were significantly smaller than those in mice treated with normal saline. It was suggested that DiMC significantly inhibited the growth of colon cancer cells in a dose-dependent manner. In contrast, the IC_{50} for DiMC was 454.8 μM on normal colonic mucosal epithelial cell NCM460, which was much higher than that of colon cancer cell lines, indicating that DiMC was less toxic to normal colonic epithelium. Flow cytometry further showed that compared with curcumin, the inhibition rate of proliferation of DiMC was higher, the rate of apoptosis increased, and the cell density decreased at a concentration of 5–15 μM (Tamvakopoulos et al., 2007). It is speculated that the phenolic -OH groups in curcumin are replaced with methoxyl groups, and the symmetric structure in DiMC offered better chemical and biological stability.

5-fluorouracil (5-Fu) is the standard chemotherapy treatment for colon cancer. However, the response rates are only 10–15% as a result of the severe side effects and resistance. Zhao et al. investigated the anticancer efficacy of DiMC and 5-fluorouracil (5-FU) in colon cancer cell lines SW480 and SW620 (Zhao et al., 2017). The results showed that both DiMC and 5-Fu significantly inhibited the growth of SW480 and SW620 cells in a dose-dependent manner, and the maximum effect was observed at 128 μmol/L and 128 mg/L, respectively. Moreover, they both had an additive anticancer effect on colon cancer cells. From the information above, DiMC can significantly inhibit the proliferation of colon cancer cells in a dose-dependent manner *in vitro* and *in vivo*.

As a potential therapeutic agent for colon cancer, the mechanism of DiMC has also been deeply studied (**Figure 3**). Caspase-3 is the most important effect or protease in apoptosis, which can be activated by enzymatic cleavage to regulate the apoptotic cascade (Zhou et al., 2018). Survivin (BIRC5) belongs to the apoptotic (IAP) gene family and is thought to be able to directly inhibit the activity of caspase-3 to prevent apoptosis in various cancer tissues and cancer cell lines (Jaiswal et al., 2015; Li et al., 2019). Chen et al. found that DiMC treatment could downregulate survivin, while caspase-3 and PARP (the specific substrate of caspase-3) were cleaved to its active fragments (Chen et al., 2016). The results suggested that DiMC might activate caspase-3 by downregulating survivin to induce apoptosis. In addition, the mobility of DiMC-treated cells decreased significantly, which might be related to the upregulation of E-cadherin expression (Chen et al., 2016).

Many biological processes such as oxidative stress, cell apoptosis, cell cycle phase arrest, and mitochondrial membrane potential play key roles in tumor regulation. Zhao et al. found that DiMC could also increase the level of ROS to upregulate CHOP and Noxa to prevent and treat colon cancer (Zhao et al., 2017). At the same time, DiMC could also induce apoptosis of colon cancer cells by increasing the expression of Bax and Cyt c and reducing the expression of Bcl2. In addition, the anti–colon cancer activity was also closely related to the induction of G0/G1 phase arrest, endoplasmic reticulum expansion, and decreased mitochondrial membrane potential (Zhao et al., 2017).

Renal Cell Carcinoma

Renal cell carcinoma (RCC) is one of the common clinical malignant tumors of the genitourinary system, accounting for 90% of the primary malignant tumors of the kidney in adults. At present, curcumin has been widely proven to have a clear therapeutic effect on RCC. Curcumin can exert its anti-RCC activity by inhibiting the NF-κB signal pathway, regulating autophagy, regulating the RK5/AP-1 pathway, and so on (Li et al., 2017a; Deng et al., 2018; Zhang et al., 2020). DiMC, as a curcumin analog, has higher biological stability and lower metabolism *in vivo*, so it has been paid attention to with regard to the treatment of RCC. Several studies have also demonstrated that DiMC also has an effect of anti-RCC which is higher than that of curcumin.

Lee et al. compared the effect of DiMC and bis-demethoxycurcumin to induce apoptosis in human RCC Caki with curcumin as a positive control (Lee et al., 2010). The results demonstrated that at 80 μM, the three compounds significantly reduced the cell viability, and DiMC was the most potent compound, followed by curcumin and bis-demethoxycurcumin. The typical ladder pattern of DNA fragmentation, which is considered a hallmark of apoptotic cell death, was observed when Caki cells were treated for 24 h. It was suggested that curcumin, DiMC, and bis-demethoxycurcumin could reduce cell viability by inducing apoptosis, and DiMC has the strongest anti–renal cell carcinoma activity. It was speculated that the methoxyl groups contribute to the enhancement of cell apoptosis. The latest study showed that DiMC also has better anti-RCC activity than curcumin and demethoxycurcumin in human RCC line 786-O (Zanetti et al., 2021). In this study, curcumin, demethoxycurcumin, and DiMC exerted their cytotoxic effects in a dose-dependent manner, and DiMC had the most significant antitumor activity. In addition, demethoxycurcumin and DiMC also showed genotoxicity (Zanetti et al., 2021).

The mechanism of DiMC inhibiting the activity of RCC is mainly related to oxidative stress, DNA damage, cell cycle arrest, and induction of cell apoptosis (**Figure 3**). Excess ROS can easily lead to the depolarization of the mitochondrial membrane and releases proapoptotic molecules from mitochondria into the cytosol, which may act to induce apoptosis. Moreover, the

release of Cyt c from the mitochondrial membrane leads to an increased level of Cyt c in the cytoplasm and nucleus, which may activate caspase-9 and trigger the effector caspase-3, to eventually lead to apoptosis. DiMC could induce apoptosis by increasing the level of ROS in Caki cells, promoting the release of Cyt c and the activation of caspase-3 (Lee et al., 2010). DNA damage is one of the main ways to inhibit the proliferation of tumor cells. RCC treated with DiMC could increase the expression of the GADD45A gene, which encodes the GADD45 α protein, and participated in DNA repair and induced DNA damage. The cell cycle is the basic process of cell life activities, and cyclin-dependent kinase (CDK) is one of the main related molecules in cell cycle regulation. CDKN1A encodes for the p21 protein involved in cell cycle regulation and is an important inhibitor of CDK. In the 786-O RCC line, DiMC could activate the p21 protein by upregulating the expression of CDKN1A and then induce cell cycle arrest (Zanetti et al., 2021). In addition, DiMC could also induce apoptosis by increasing the expression of apoptosis genes MYC, BBC3, and CASP7, as well as decreasing the expression of the pro-inflammatory gene TNF (Zanetti et al., 2021).

Prostate Cancer

The androgen receptor (AR) signaling pathway plays an important role in the development of prostate cancer. The change and reactivation of the AR signal transduction pathway are the core factors that promote the development of castration-resistant prostate cancer (CRPC) and the generation of drug resistance. ASC9, the enol isomer of DiMC, is a recently developed anti-AR agent which effectively suppresses castration-resistant prostate cancer cell proliferation and invasion.

Cheng et al. found that when dissolved in FDA-approved solvents such as DMSO, PEG-400, and Tween-80, ASC-J9 had AR degradation effects. Compared with those in AR-negative prostate cancer cells (IC_{50} 16.0 μM) or those in normal prostate cells (IC_{50} 27.0 μM), ASC-J9 was found to exhibit a decreased IC_{50} value in AR-positive prostate cancer cells (IC_{50} 6.5 μM) (Cheng et al., 2018). In another study, ASC-J9 also suppressed the tumor growth of prostate cancer cell lines C81, C4-2, and CWR22Rv1 xenografted into castrated nude mice (Lai et al., 2013). It could selectively degrade the AR protein *via* interruption of the AR–AR selective coregulator interaction. In addition, it was reported that androgens were able to induce fatty acid synthase (FASN) expression in prostate cancer, and addition of the anti-androgen might suppress the androgen-induced FASN expression. Wen et al. found that anti-androgen bicalutamide (Casodex) or enzalutamide MDV3100 had little inhibitory effect on FASN expression and FASN-mediated cell growth and invasion in prostate cancer cell lines C4-2 and LNCaP when the androgen concentration was 1 nM (Wen et al., 2016). In contrast, ASC-J9 inhibited the expression of FASN and the growth and invasion of various prostate cancer cell lines mediated by FASN.

Another study showed that ASC-J9 could not only degrade wild-type AR but also has the ability to target the AR mutant AR-F876L. The production of AR mutants will lead to the occurrence of multidrug resistance, so the consequence of suppressing AR-F876L may then abrogate AR-F876L which mediated the proliferation and metastasis of CRPC, thereby better suppressing CRPC that has already developed resistance (Wang et al., 2016). The above results suggest that ASC-J9 successfully induces the regress of the prostate cancer, which provides a new and more effective treatment against prostate cancer in the future.

The mechanisms of ASC-J9 against prostate cancer have been deeply studied, which can be divided into the AR-dependent pathway and the AR-independent pathway (**Figure 3**). First of all, ASC-J9 could activate the proteasome-dependent pathway to promote AR degradation through the enhanced association of the AR-murine double minute protein 2 (Mdm2) complex (Lai et al., 2013). ASC-J9 could also inhibit the proliferation and metastasis of prostate cancer by regulating pSTAT3-C-C motif chemokine-2 (CCL2) signal transduction through an AR-dependent pathway *via* inhibiting the expression of the protein inhibitor of STAT3 (PIAS3) (Lin et al., 2013). STATs are transcription factors that play an important role in the process of inflammation, and STAT3 is highly expressed and may be related to the progression of many types of cancer, including prostate cancer (Pencik et al., 2016). CCL2 is highly expressed in malignant tumor cells and may play an important role in the recruitment of tumor-associated macrophages. The regulation of the pSTAT3-CCL2 signaling pathway can better battle the growth and metastasis of prostate cancer at the castration-resistant stage (Wu et al., 2017; Lee et al., 2018). Additionally, Wen et al. also found that in AR-positive C4-2 and LNCaP cells, ASC-J9 could suppress significant FASN expression and FASN-mediated prostate cancer progression through the AR-dependent pathway (Wen et al., 2016).

In addition to the AR-dependent pathway above, the AR-independent pathway is also an important mechanism for ASC-J9 to inhibit the proliferation of prostate cancer. It was found that ASC-J9 treatment resulted in significant suppression of the STAT3 phosphorylation/activation and CCL2 expression, with little influence on the PIAS3 expression in the AR-negative PC3 cells, confirming that ASC-J9 could also go through an AR-independent pathway to modulate STAT3 phosphorylation/activation and CCL2 expression (Lin et al., 2013). Lin et al. further found that ASC-J9 could suppress prostate cancer cell invasion by inducing the sumoylation of STAT3, thereby inhibiting the STAT3 phosphorylation that led to the suppression of the EMT-SNAIL2 signals in both prostate cancer DU145 and PC3 AR-negative cells (Lin et al., 2018). Transcription factor ATF3 plays an important role in tumor formation, invasion, and metastasis by finely regulating the delicate balance between proliferation and apoptosis. ASC-J9 could increase the expression of ATF3 by reducing the expression of the glutamate–cysteine ligase catalytic subunit, thus suppressing the proliferation and invasion of prostate cancer (Tian et al., 2021).

Leukemia

Leukemia is a malignant proliferative disease originating from hematopoietic stem cells, and its morbidity and mortality rank

first among cancers in children and adolescents. At present, chemotherapy is still the main treatment method for leukemia, but the emergence of multidrug resistance often leads to an effect of chemotherapy that does not meet expectations. Finding new antitumor drugs is of great significance for the treatment of leukemia.

Epigenetic regulation is a modification mechanism that affects gene expression without DNA sequence changes, which is closely related to the occurrence and development of leukemia. DNA methyltransferase (DNMT) is an important protease related to epigenetic modification, which undertakes the *de novo* methylation of DNA. Inhibition of DNMT can induce DNA hypomethylation and restore the high expression/activation of tumor suppressor genes. Using the DNMT inhibitor 5-azacytidine (5 AC) as a positive control, it was found that at clinically relevant concentrations (2 μM), DiMC could induce the gene expression of promoter methylated genes such as p15 and CDH-1 in leukemia cells, suggesting a possible DNA hypomethylating effect by DiMC, similar to 5 AC (Hassan et al., 2015). However, DiMC did not induce the expression of any of the DNMT isotypes in leukemia cells, that is, no DNA hypomethylation activity. The above results suggested that DiMC induced the expression of promoter methylation genes through a mechanism that did not involve the reversal of DNA methylation, thereby playing a key role in the treatment of leukemia (Hassan et al., 2015).

On the basis of the studies above, Hassan et al. further investigated the cytotoxic effects and epigenetic changes associated with the combination of DiMC and the DNMT inhibitor decitabine (DAC) in primary leukemia samples and cell lines CEM and Jurkat (Hassan et al., 2016). The results clearly showed that compared with a single agent, the combination of DiMC and DAC demonstrated antagonistic cytotoxic effects and induced minimal apoptosis in primary leukemia cells. At the same time, the combination of drugs inhibited the gene expression of the DNMT enzyme and downregulated the level of nuclear protein. However, compared to the use of DAC as a single agent, the DNA hypomethylating activity of the combination did not significantly increase. In addition, the analysis of the histone marks associated with actively transcribed genes such as acetylated H3K27 (H3K27Ac) and trimethylated H3K36 (H3K36me3) near the promoter region of both genes demonstrated a significant increase in the H3K27Ac mark (Hassan et al., 2016). The above results suggest that the combination of DiMC and DAC can enhance the induction of promoter-methylated genes through the mechanism involved in increasing histone acetylation, so as to play a role in the treatment of leukemia.

Oxidative stress is closely related to the occurrence and development of leukemia. Under physiological conditions, the synergistic effect of antioxidant enzymes and antioxidants keeps free radicals at a very low level. When its production exceeds the scavenging and repairing capacity of the body, high concentrations of ROS in plasma can directly oxidize, attack, and destroy antioxidant enzymes, resulting in the decrease or loss of enzyme activity. At the same time, ROS attack the polyunsaturated fatty acids in the biofilm, triggering lipid peroxidation. Studies have shown that both curcumin and DiMC could inhibit the lipid peroxidation state of human peripheral blood mononuclear cells (PBMCs) by increasing the activity of catalase and significantly reduce the activity of glutathione reductase (GR) and the content of glutathione (Simon et al., 2018). It was speculated that DiMC may enhance the activity of catalase by increasing the level of mRNA and protein.

Others

In addition to the cancers mentioned above, the therapeutic effects of DiMC on hepatocellular carcinoma and bladder cancer are also being studied.

Zanetti et al. evaluated the inhibitory effect of DiMC on the HepG2/C3A human hepatocellular carcinoma cell line (Zanetti et al., 2019). The results showed that DiMC had cytotoxic effect. Treatment with 10–50 μM of DiMC for 24 h decreased the cell viability from 71 to 39% in a dose–response manner, and the IC_{50} value was 37 μM. It was further found that the cytotoxicity of DiMC was mainly related to mitotic disorder and DNA damage. DiMC could cause mitotic arrest by inducing the formation of monopolar spindles. In the meantime, it could also activate the key effector factors BCL2-homologous antagonist/killer one (BAK1) and caspase-7 in cell cycle arrest and the DNA repair pathway by increasing the expression of the CDKN1A, GADD45A, and PARP1 genes, thus resulting in genotoxicity (Zanetti et al., 2019). Another study showed that sorafenib, a standard treatment to suppress the progression of hepatocellular carcinoma, combined with ASC-J9 could synergistically suppress the progression of HCC by altering cell cycle regulation, apoptosis, and invasion. Its mechanism was related to the inhibition of the expression of pSTAT3 and its downstream genes including CCL2 and Bcl2 (Xu et al., 2017).

Bladder cancer is a common malignant tumor in the urinary system. Emerging preclinical findings have indicated that androgen-mediated androgen receptor signals have been shown to correlate with the promotion of tumor development and progression (Li et al., 2017b). Studies have shown that DiMC could prevent and treat bladder cancer by inducing AR degradation (Shang et al., 2015). In a study, the daily i. p. co-injection of a carcinogen [N-butyl-N-(4-hydroxybutyl)-nitrosamine or BBN] and DiMC (75 mg/kg for 24 weeks) reduced the incidence of bladder cancer by 4-fold as compared to the DiMC-deprived group (Shang et al., 2015). DiMC treatment had little effect on serum testosterone concentration, suggesting that AR was deprived after DiMC treatment. In addition, DiMC could also be used in combination with Bacillus Calmette–Guerin, a very successful adjuvant for the treatment of bladder cancer, to better suppress bladder cancer progress (Shang et al., 2015).

NANOFORMULATIONS OF DIMC

The poor water solubility is one of the main challenges in cancer chemotherapy since it usually results in low bioavailability at the tumor sites and reduces therapeutic efficacy (Sun et al., 2014). It is

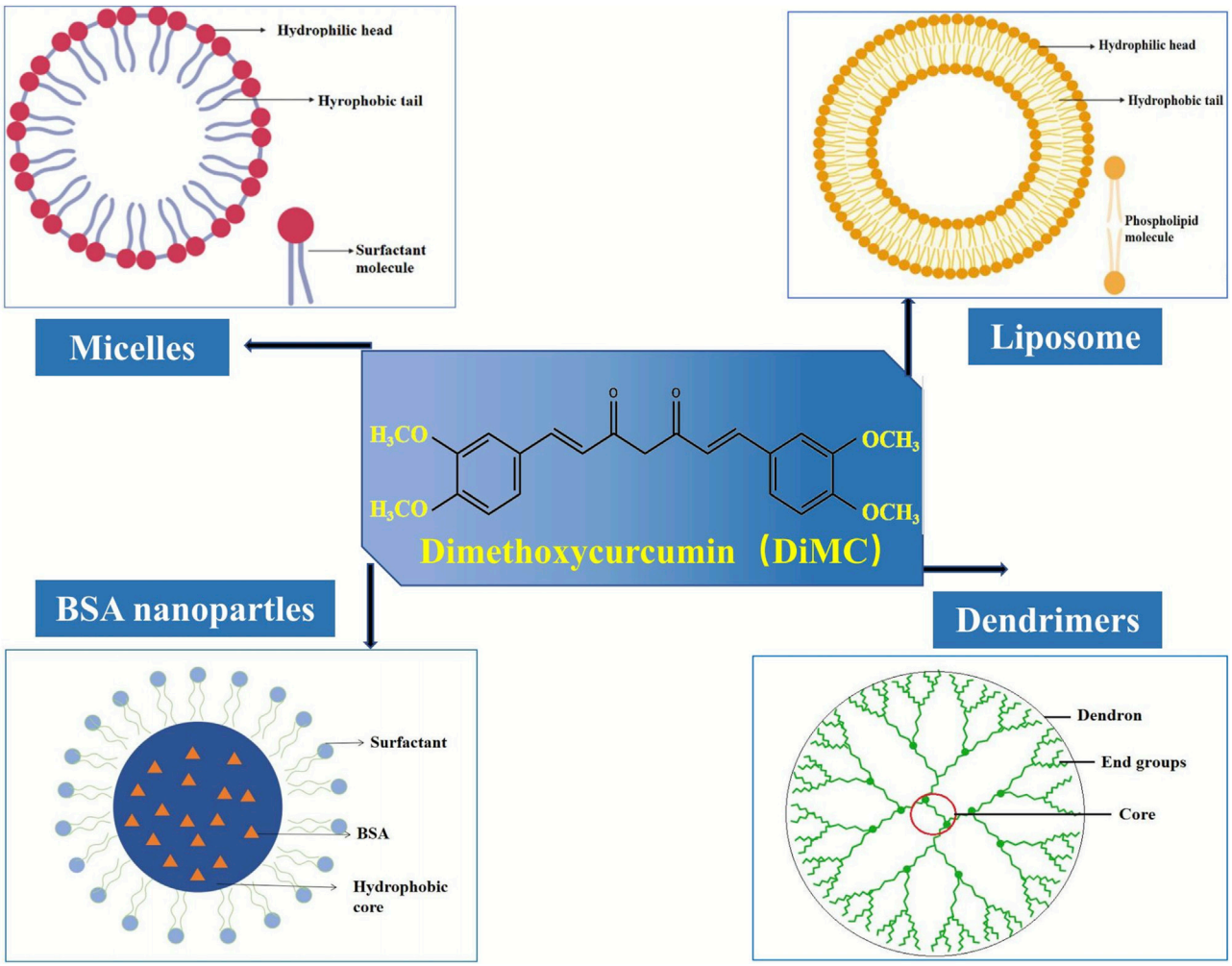

FIGURE 4 | Main nanoformulations of DiMC.

indeed the case for DiMC, a hydrophobic analog of curcumin with superior activity against various cancer cell lines such as breast cancer, lung cancer, colon cancer, and prostate cancer. Therefore, it is a matter of the utmost importance to develop a suitable drug delivery system for further clinical application of this anticancer agent. In recent years, a certain amount of research has been carried out to deliver DiMC, mainly including some polymer-based nanoformulations (**Figure 4**) that provide an efficient alternative to overcome the therapeutic limitation from its poor water solubility (**Table 2**).

Nanoparticles

The first work reported on nanoformulation of DiMC was demonstrated by using an alternative technology of dendrimers due to the attractive properties such as well-defined structures and low polydispersity (Markatou et al., 2007). Appropriate quantities of DiMC and the water-soluble poly (amidoamine) (PAMAM) (G3.5 or G4) were dissolved in methanol and then stirred for 24 h. After evaporating under vacuum to remove the methanol completely, buffer solution was added, stirred for another 24 h in the dark, and then centrifuged to obtain the DiMC-PAPMAM complex dispersed in the aqueous medium. The results indicated that hydrophobic DiMC could be incorporated to PAMAM dendrimers in an enolic form *via* electrostatic or covalent complexation on the surface or entrapment within the dendrimer architecture, while its interaction with the integer generation dendrimer involved the major conformational change of the terminal ethylene amine groups. Although the drug–dendrimer interactions determine the bioavailability enhancement, this formulation of DiMC suffered from glaring shortcomings such as a time-consuming and complicated preparation process, as well as rather low drug-loading capacity (<5%) and poor incorporation efficiency (about 50%).

Bovine serum albumin (BSA), which has ligand-binding properties and is widely available, cheap, and easily purified, is extensively used for drug delivery and well accepted in the pharmaceutical industry. In recent years, BSA nanoparticles have been used as an effective delivery system for hydrophobic drugs like DiMC (Das et al., 2017; Das et al., 2019). Using the

TABLE 2 | Drug delivery systems for DiMC with improved and effective responses.

Drug delivery system	Method of preparation	Outcomes	Model	Reference
Dendrimer	Thin film	*Via* electrostatic or covalent complexation on the surface or entrapment within the dendrimer architecture; enhanced bioavailability	Spleen lymphocytes and bone marrow hematopoietic cells	Markatou et al. (2007)
BSA nanoparticles	Thermal denaturation	Mean hydrodynamic diameters ranging from 28 to 62 nm and corresponding zeta-potential values of −7.0 to −6.0 mV; increased cellular uptake and toxicity of DiMC	A549 human lung cells	Das et al. (2017); Das et al. (2019)
Liposomes	Thin-film hydration	Cholesterol played a key role in the interaction between DiMC and lipid bilayers; the DPPC:DODAP:chol:DiMC liposomal formulation (9:1:1:1 molar ratio) was the most effective with the incorporation efficiency up to 3.84%	—	Hadjideme-triou et al. (2013)
Solid dispersions	Solvent evaporation	Significantly improved drug dissolution rate; the cumulative dissolution was more than 83% in 5 min	—	Xu et al. (2019)
Polymeric micelles	Thin-film hydration	A low initial burst release followed by a sustained release *in vitro*; significantly increased drug exposure and prolonged it *in vivo*; improved the biodistribution profile of DiMC and increased drug accumulation in tumors	A549 human lung cells	Liu et al. (2015)
Stiffness-tunable nanocarriers	Thin-film hydration	Improved the cellular uptake and anticancer activity of ASC-J9; enhanced the tumor penetration in HCT 116 3D colorectal cancer spheroids	HCT 116 human colorectal adenocarcinoma cells	Tomeh et al. (2021)

thermal denaturation method, BSA nanoparticles were prepared with mean hydrodynamic diameters ranging from 28 to 62 nm and corresponding zeta-potential values of −7.0 to −6.0 mV, which could easily bind DiMC to obtain drug-loaded nanoparticles. Using the A549 cell model, Das's group further revealed such a kind of particle size effect that the cellular uptake and toxicity of DiMC increased with the increase in the particle size of these BSA-based nanoparticles (Das et al., 2017). Their latest research demonstrated significant changes in the secondary structure of BSA upon particle formation and also a decrease in helicity (Das et al., 2019). DiMC could be bound within the sub-domain IIA of BSA with a distance of about 24 Å between the hydrophobic core and the ligand, where it experienced a more rigid environment than in the native form of BSA. Also, it displayed a much higher binding constant with BSA nanoparticles than with the native BSA ($1.5 \pm 0.5 \times 105\ M^{-1}$ vs. $2.7 \pm 0.4 \times 104\ M^{-1}$).

Liposomes

Liposomes represent one of the most thoroughly studied categories of colloidal nanocarriers and are proven candidates for delivery of a wide range of therapeutics (Yan et al., 2020). So far, most of the research has been concentrated on developing suitable liposomal formulations of DiMC to improve the thermal stability and water solubility. Charged liposomes incorporating DiMC were investigated for the first time by using the phospholipids composed of 1,2-dipalmitoyl-sn-glycero-3-phosphocholine (DPPC), 1,2-dipalmitoyl-sn-glycero-3-phospho-(1′-rac-glycerol) (DPPG), 1,2-dioleoyl-3-dimethylammonium-propane (DODAP), and cholesterol (chol) (Hadjidemetriou et al., 2013). Three different liposomal formulations have been prepared using the thin-film hydration method, and the charged liposomes composed of DPPC:DPPG:chol or DPPC:DODAP:chol were found to be more efficient in contrast to those uncharged liposomes using DPPC only. The results showed that cholesterol played a key role in the interaction between DiMC and lipid bilayers by affecting their organization and consequently their stability, and incorporating DiMC into cationic liposomes was favored due to their thermodynamically stable liposomal dispersion. Moreover, the DPPC:DODAP:chol:DiMC liposomal formulation (9:1:1:1 molar ratio) was the most effective with an incorporation efficiency up to 3.84%, which reacted as an electrophile *via* the positive charge of the DODAP lipid molecule with ASC-J9 at phosphate buffer saline (pH 7.4).

Particle size effect on the anticancer ability of liposomes encapsulating DiMC also attracted research interest. The liposomes with different sizes were prepared by using the film dispersion technique, and then through the liposome extruder and dialysis. The results showed that the anticancer ability could be enhanced with the decrease in particle size, and the liposomes with a size of 184 nm could more efficiently induce the prostate cancer cell death than those with a size of 250.5 nm (Zhou et al., 2016).

Thereafter, various studies were performed on the preparation and properties of DiMC (namely, ASC-J9) liposomes (Li et al., 2018a; Li et al., 2018b; Sun et al., 2020). By using the thin-film dispersion method and using ethanol as a solvent, the optimal preparation conditions were obtained as the mass ratio of phospholipid to cholesterol of 10:1 and the mass ratio of phospholipid to DiMC of 1,000:10, with the hydration temperature set at 60 °C and the concentration of phospholipid at 6.67 mg/ml (Li et al., 2018a). This manufacturing technique had various advantages such as environmental friendliness, simple operation, and good product performance. In more detail, the liposomes can protect the entrapped DiMC well and be well dispersed in water and remain stable at 4 °C with the entrapment efficiency up to 97% and a mean particle size of 145 nm, with a very narrow particle size distribution (a polymer dispersity index of 0.36). The liposomes could be used as a water-soluble molecular fluorescence probe for the recognition of Fe^{3+}, Fe^{2+}, and Cu^{2+} through fluorescence quenching (Li et al., 2018b), as well as an

inhibitor against cell proliferation *in vivo* and *in vitro* (Sun et al., 2020).

Others

Inclusion complexes and solid dispersions are also involved in formulations of DiMC, mainly to improve its solubility and stability. By complexation with hydroxypropyl-γ-cyclodextrin, the commercial curcumin that contains DiMC could acquire increased solubility and stability (Benediktsdottir et al., 2015). Recently, the solid dispersions (SDs) of DiMC were prepared with polyethylene glycol (PEG) 4,000, PEG 6,000, and poloxamer 188 as carriers using the fusion method and with polyvinylpyrrolidone (PVP K30) as a carrier using the solvent evaporation method, respectively (Xu et al., 2019). The results showed that the drug dissolution rate could be significantly improved by all SDs, and the formulation using PVP K30 at a ratio to DiMC of 10:1 was the best one, where DiMC dispersed in an amorphous form with a cumulative dissolution of more than 83% in 5 min.

A kind of polymeric micellar formulation of DiMC for injection use in cancer therapy was first developed on the basis of the amphiphilic block copolymer with fairly low critical micelle concentration and passive targeting potential to tumor tissue (Liu et al., 2015). By using the copolymer mPEG-PCL-Phe (Boc), N-t-butoxycarbonyl-phenylalanine terminated monomethoxyl poly (ethylene glycol)-b-poly (ε-caprolactone) and the DiMC-loaded micelles could be easily prepared *via* the thin-film hydration method. Through high-affinity interaction between DiMC and the copolymer, the micelles had a typical shell-core structure with an average particle size of 17.9 ± 0.4 nm and a polydispersity index of 0.045 ± 0.011. The drug-loading capacity and entrapment efficiency were 9.94 ± 0.15% and 97.22 ± 0.18%, respectively. At a concentration of 2 mg/ml, the reconstituted micelle solution could be maintained for at least 10 days at room temperature and displayed a low initial burst release, followed by a sustained release *in vitro*. Pharmacokinetic study in rats revealed that *in vivo* drug exposure was significantly increased and prolonged by intravenously administering DMC-loaded micelles. This micellar formulation also greatly improved the biodistribution profile of DiMC and increased drug accumulation in tumors.

DiMC niosomes were recently prepared using the thin-film dispersion ultrasonic method, and the prescription composition and preparation process were optimized using the single-factor investigation method (Li et al., 2017c). The highest encapsulation rate was 88.1 ± 1.7%, and the drug-loading amount was 4.03 ± 1.05%. Moreover, the average particle size was 310.3 ± 0.9 nm, and the leakage rate was below 2% within 45 days, indicating that the niosomes as a vector could significantly improve the solubility and stability of DiMC.

Lately, novel stiffness-tunable nanocarriers were developed for the controlled delivery of the hydrophobic anticancer agent ASC-J9 into colorectal cancer cells (Tomeh et al., 2021). The core-shell nanocarriers composed of naturally derived polymers silk fibroin (SF) and sodium alginate (SA) inside a liposomal shell were prepared using the thin-film hydration method, followed by extrusion and cross-linking of SA to induce structural transformation of SF to obtain a uniform size and shape, avoiding harsh processing conditions. The nanocarriers had high encapsulation efficiency (62–78%) and were physically stable for up to 5 months at 4°C. The stiffness of the nanocarriers has a significant effect on drug release, cellular uptake, and anticancer efficacy. The release profile was directed by their stiffness and was easily tunable by changing the ratio of SF to SA in the core. Also, the designed nanocarriers improved the cellular uptake and anticancer activity of ASC-J9 and enhanced its tumor penetration in HCT 116 3D colorectal cancer spheroids, which thus can be used as a highly efficient drug delivery system for cancer therapy.

DISCUSSION AND CONCLUSION

Natural products have been the most productive source for modern drug discovery and development. Curcumin is a kind of herb-derived natural polyphenol with various bioactivities such as anticancer activity. However, chemical modification of curcumin is usually needed since its systemic bioavailability and therapeutic potency are seriously constricted by poor solubility, low absorption, and hasty metabolism and elimination. DiMC is a striking curcuminoid derivative with significantly improved drug likeness and enhanced power. In the present review, we just systematically summarized the published research about DiMC as a promising anticancer agent, for which pharmacokinetics, pharmacological effects, molecular mechanisms, and nanoformulations for drug delivery were involved.

It has been demonstrated that the methylation of both free hydroxyl groups in curcumin provides the derivate DiMC with greatly improved biochemical stability and pharmacokinetic characteristics when compared with the parent molecule curcumin and other curcuminoids. Meanwhile, research has proven DiMC as a multi-target anticancer agent, which plays an exceptional role in the treatment of various malignant cancers through its superior effectiveness against cancer by triggering cell cycle arrest and apoptosis. More to the point, its efficacies toward cancer cell survival, attachment, movement, and invasion are closely related with the regulation of signal factors such as ROS, Cyt c, caspase-3/7/9, Bax/BCl2, GSH/GSSG, p53, and p21. It also has special chemosensitizing activity and photosensitizing property and thus could be developed as an anticancer adjuvant for cancer chemotherapy.

A reliable delivery system is usually one of the major challenges for drug development, and it is indeed the case for the anticancer agent DiMC. Despite the research on the subject, the drug delivery system of DiMC is still in its infancy; so far, a few nanoformulations have been investigated. Due to the great improvement in hydrophobicity, DiMC could be well incorporated by lipophilic substances to form liposomes, nanoparticles, and micelles, among which the polymeric micellar system is very promising as it can be easily produced with high drug-loading capacity, sustainable drug-releasing features, and satisfactory biodistribution. Recently, the development of complex nanoformulations dually-loaded adjuvant agent and classic first-line chemotherapeutic drugs

such as doxorubicin and paclitaxel have attracted more and more research attention. Thus, we have no reason to doubt that such a novel drug delivery system of DiMC would provide an effective alternative to improving traditional cancer chemotherapies by acquiring synergic efficacy and overcoming adverse effects, especially some dose-limiting and cumulative toxicities, including doxorubicin-induced severe cardiac dysfunction.

In short, it is the first time that the basic information about research on DiMC has been comprehensively reviewed, and it will benefit in-depth development of this promising anticancer agent for clinical application in the near future.

AUTHOR CONTRIBUTIONS

MS prepared and commented on the published work. WG revised the manuscript and participated in preparing the figures. ZL and YL commented during the pre- and postpublication stages. HX and XY were responsible for supervision, project administration, and funding acquisition. FZ was responsible for critical revision during the pre- and postpublication stages.

FUNDING

This work was supported by grants from the Natural Science Foundation of Shandong Province (ZR2019MB054), the Science and Technology Projects of TCM in Shandong Province, China (nos. 2020Y25, 2020M190), and the Innovation Fund of Science and Technology for Graduate Students of Yantai University, China (no. YDZD 2031). The funding agencies had no role in the study design, the collection, analysis, or interpretation of data, the writing of the report, or the decision to submit the article for publication.

REFERENCES

Arrue, L., Barra, T., Camarada, M. B., Zarate, X., and Schott, E. (2017). Electrochemical and Theoretical Characterization of the Electro-Oxidation of Dimethoxycurcumin. *Chem. Phys. Lett.* 677, 35–40. doi:10.1016/j.cplett.2017.03.067

Benediktsdottir, B. E., Baldursson, O., Gudjonsson, T., Tønnesen, H. H., and Masson, M. (2015). Curcumin, Bisdemethoxycurcumin and Dimethoxycurcumin Complexed with Cyclodextrins Have Structure Specific Effect on the Paracellular Integrity of Lung Epithelia *In Vitro*. *Biochem. Biophys. Rep.* 4, 405–410. doi:10.1016/j.bbrep.2015.11.004

Chainoglou, E., and Hadjipavlou-Litina, D. (2019). Curcumin Analogues and Derivatives with Anti-proliferative and Anti-inflammatory Activity: Structural Characteristics and Molecular Targets. *Expert Opin. Drug Discov.* 14, 821–842. doi:10.1080/17460441.2019.1614560

Chen, D., Dai, F., Chen, Z., Wang, S., Cheng, X., Sheng, Q., et al. (2016). Dimethoxy Curcumin Induces Apoptosis by Suppressing Survivin and Inhibits Invasion by Enhancing E-Cadherin in colon Cancer Cells. *Med. Sci. Monit.* 22, 3215–3222. doi:10.12659/msm.900802

Cheng, M. A., Chou, F.-J., Wang, K., Yang, R., Ding, J., Zhang, Q., et al. (2018). Androgen Receptor (AR) Degradation Enhancer ASC-J9 in an FDA-Approved Formulated Solution Suppresses Castration Resistant Prostate Cancer Cell Growth. *Cancer Lett.* 417, 182–191. doi:10.1016/j.canlet.2017.11.038

Das, R. P., Singh, B. G., Kunwar, A., and Priyadarsini, K. I. (2019). Interaction of a Model Hydrophobic Drug Dimethylcurcumin with Albumin Nanoparticles. *Protein J.* 38 (6), 649–657. doi:10.1007/s10930-019-09866-z

Das, R. P., Singh, B. G., Kunwar, A., Ramani, M. V., Subbaraju, G. V., Hassan, P. A., et al. (2017). Tuning the Binding, Release and Cytotoxicity of Hydrophobic Drug by Bovine Serum Albumin Nanoparticles: Influence of Particle Size. *Colloids Surf. B: Biointerfaces* 158, 682–688. doi:10.1016/j.colsurfb.2017.07.048

Deng, Q., Liang, L., Liu, Q., Duan, W., Jiang, Y., and Zhang, L. (2018). Autophagy Is a Major Mechanism for the Dual Effects of Curcumin on Renal Cell Carcinoma Cells. *Eur. J. Pharmacol.* 826, 24–30. doi:10.1016/j.ejphar.2018.02.038

Dützmann, S., Schiborr, C., Kocher, A., Pilatus, U., Hattingen, E., Weissenberger, J., et al. (2016). Intratumoral Concentrations and Effects of Orally Administered Micellar Curcuminoids in Glioblastoma Patients. *Nutr. Cancer* 68, 943–948. doi:10.1080/01635581.2016.1187281

Fontana, F., Raimondi, M., Marzagalli, M., Di Domizio, A., and Limonta, P. (2020). The Emerging Role of Paraptosis in Tumor Cell Biology: Perspectives for Cancer Prevention and Therapy with Natural Compounds. *Biochim. Biophys. Acta (Bba) - Rev. Cancer* 1873 (2), 188338. doi:10.1016/j.bbcan.2020.188338

Hadjidemetriou, M., Pippa, N., Pispas, S., and Demetzos, C. (2013). Incorporation of Dimethoxycurcumin into Charged Liposomes and the Formation Kinetics of Fractal Aggregates of Uncharged Vectors. *J. Liposome Res.* 23, 94–100. doi:10.3109/08982104.2012.747534

Hassan, H. E., Carlson, S., Abdallah, I., Buttolph, T., Glass, K. C., and Fandy, T. E. (2015). Curcumin and Dimethoxycurcumin Induced Epigenetic Changes in Leukemia Cells. *Pharm. Res.* 32, 863–875. doi:10.1007/s11095-014-1502-4

Hassan, H. E., Keita, J. A., Narayan, L., Brady, S. M., Frederick, R., Carlson, S., et al. (2016). The combination of dimethoxycurcumin with DNA methylation inhibitor enhances gene re-expression of promoter-methylated genes and antagonizes their cytotoxic effect. *Epigenetics* 11, 740–749. doi:10.1080/15592294.2016.1226452

Hatamipour, M., Ramezani, M., Tabassi, S. A. S., Johnston, T. P., Ramezani, M., and Sahebkar, A. (2018). Demethoxycurcumin: A Naturally Occurring Curcumin Analogue with Antitumor Properties. *J. Cel Physiol.* 233, 9247–9260. doi:10.1002/jcp.27029

Hatamipour, M., Ramezani, M., Tabassi, S. A. S., Johnston, T. P., and Sahebkar, A. (2019). Demethoxycurcumin: A Naturally Occurring Curcumin Analogue for Treating Non-cancerous Diseases. *J. Cel Physiol.* 234, 19320–19330. doi:10.1002/jcp.28626

Heger, M., van Golen, R. F., Broekgaarden, M., and Michel, M. C. (2014). The Molecular Basis for the Pharmacokinetics and Pharmacodynamics of Curcumin and its Metabolites in Relation to Cancer. *Pharmacol. Rev.* 66, 222–307. doi:10.1124/pr.110.00404410.1124/pr.110.004044

Jaiswal, P. K., Goel, A., and Mittal, R. D. (2015). Survivin: A Molecular Biomarker in Cancer. *Indian J. Med. Res.* 141 (4), 389–397. doi:10.4103/0971-5916.159250

Jayakumar, S., Patwardhan, R. S., Pal, D., Sharma, D., and Sandur, S. K. (2016). Dimethoxycurcumin, a Metabolically Stable Analogue of Curcumin Enhances the Radiosensitivity of Cancer Cells: Possible Involvement of ROS and Thioredoxin Reductase. *Biochem. Biophysical Res. Commun.* 478, 446–454. doi:10.1016/j.bbrc.2016.06.144

Karimian, M. S., Pirro, M., Majeed, M., and Sahebkar, A. (2017). Curcumin as a Natural Regulator of Monocyte Chemoattractant Protein-1. *Cytokine Growth Factor. Rev.* 33, 55–63. doi:10.1016/j.cytogfr.2016.10.001

Kessel, D. (2019). Pathways to Paraptosis after ER Photodamage in OVCAR -5 Cells. *Photochem. Photobiol.* 95 (5), 1239–1242. doi:10.1111/php.13103

Kim, B., Kim, H. S., Jung, E.-J., LeeTsang, J. Y. B., K. Tsang, B., Lim, J. M., et al. (2016). Curcumin Induces ER Stress-Mediated Apoptosis through Selective Generation of Reactive Oxygen Species in Cervical Cancer Cells. *Mol. Carcinog.* 55, 918–928. doi:10.1002/mc.22332

Kunwar, A., Barik, A., Sandur, S. K., and Indira Priyadarsini, K. (2011a). Differential Antioxidant/pro-Oxidant Activity of Dimethoxycurcumin, a Synthetic Analogue of Curcumin. *Free Radic. Res.* 45, 959–965. doi:10.3109/10715762.2011.571681

Kunwar, A., Jayakumar, S., Srivastava, A. K., and Priyadarsini, K. I. (2012). Dimethoxycurcumin-induced Cell Death in Human Breast Carcinoma MCF7 Cells: Evidence for Pro-oxidant Activity, Mitochondrial Dysfunction, and Apoptosis. *Arch. Toxicol.* 86, 603–614. doi:10.1007/s00204-011-0786-y

Kunwar, A., Simon, E., Singh, U., Chittela, R. K., Sharma, D., Sandur, S. K., et al. (2011b). Interaction of a Curcumin Analogue Dimethoxycurcumin with DNA. *Chem. Biol. Drug Des.* 77, 281–287. doi:10.1111/j.1747-0285.2011.01083.x

Lai, K.-P., Huang, C.-K., Chang, Y.-J., Chung, C.-Y., Yamashita, S., Li, L., et al. (2013). New Therapeutic Approach to Suppress Castration-Resistant Prostate Cancer Using ASC-J9 *via* Targeting Androgen Receptor in Selective Prostate Cells. *Am. J. Pathol.* 182 (2), 460–473. doi:10.1016/j.ajpath.2012.10.029

Lee, D., Kim, I. Y., Saha, S., and Choi, K. S. (2016). Paraptosis in the Anti-cancer Arsenal of Natural Products. *Pharmacol. Ther.* 162, 120–133. doi:10.1016/j.pharmthera.2016.01.003

Lee, G. T., Kwon, S. J., Kim, J., Kwon, Y. S., Lee, N., Hong, J. H., et al. (2018). WNT5A Induces Castration-Resistant Prostate Cancer *via* CCL2 and Tumour-Infiltrating Macrophages. *Br. J. Cancer* 118 (5), 670–678. doi:10.1038/bjc.2017.451

Lee, J. W., Hong, H. M., Kwon, D. D., Pae, H.-O., and Jeong, H. J. (2010). Dimethoxycurcumin, a Structural Analogue of Curcumin, Induces Apoptosis in Human Renal Carcinoma Caki Cells through the Production of Reactive Oxygen Species, the Release of Cytochrome C, and the Activation of Caspase-3. *Korean J. Urol.* 51, 870–878. doi:10.4111/kju.2010.51.12.870

Li, F., Aljahdali, I., and Ling, X. (2019). Cancer Therapeutics Using Survivin BIRC5 as a Target: what Can We Do after over Two Decades of Study?. *J. Exp. Clin. Cancer Res.* 38 (1), 368. doi:10.1186/s13046-019-1362-1

Li, G., Wang, Z., Chong, T., Yang, J., Li, H., and Chen, H. (2017a). Curcumin Enhances the Radiosensitivity of Renal Cancer Cells by Suppressing NF-Kb Signaling Pathway. *Biomed. Pharmacother.* 94, 974–981. doi:10.1016/j.biopha.2017.07.148

Li, P., Chen, J., and Miyamoto, H. (2017b). Androgen Receptor Signaling in Bladder Cancer. *Cancers* 9 (2), 20. doi:10.3390/cancers9020020

Li, R., Xu, D. F., Yang, X. Q., Ma, S. X., Ge, X. A., and Zhou, S. W. (2017c). Preparation and Stability Studies of Dimethyl Curcumin Niosomes. *J. Chin. Pharm. Sci.* 26 (4), 265–270.

Li, Z. Y., Shao, D. D., Xu, D. F., He, H. M., and Sun, X. Q. (2018a). Studies on Preparation and Properties of Dimethyl Curcumin Liposome. *Xiandai Huagong* 38 (11), 132–135.

Li, Z. Y., Shao, D. D., Yin, Y., Xiao, T. X., and Sun, X. Q. (2018b). Fluorescent Recognition of Metal Ions in Water Using Dimethyl Curcumin Liposome. *Fenxi Ceshi Xuebao* 37 (9), 1046–1050.

Lin, T.-H., Izumi, K., Lee, S. O., Lin, W.-J., Yeh, S., and Chang, C. (2013). Anti-androgen Receptor ASC-J9 versus Anti-androgens MDV3100 (Enzalutamide) or Casodex (Bicalutamide) Leads to Opposite Effects on Prostate Cancer Metastasis *via* Differential Modulation of Macrophage Infiltration and STAT3-CCL2 Signaling. *Cell Death Dis.* 4 (8), e764. doi:10.1038/cddis.2013.270

Lin, W., Luo, J., Sun, Y., Lin, C., Li, G., Niu, Y., et al. (2018). ASC-J9 Suppresses Prostate Cancer Cell Invasion *via* Altering the Sumoylation-Phosphorylation of STAT3. *Cancer Lett.* 425, 21–30. doi:10.1016/j.canlet.2018.02.007

Liu, H., Xu, H., Jiang, Y., Hao, S., Gong, F., Mu, H., et al. (2015). Preparation, Characterization, *In Vivo* Pharmacokinetics, and Biodistribution of Polymeric Micellar Dimethoxycurcumin for Tumor Targeting. *Int. J. Nanomedicine* 10, 6395–6410. doi:10.2147/IJN.S91961

Mach, C. M., Chen, J. H., Mosley, S. A., Kurzrock, R., and Smith, J. A. (2010). Evaluation of Liposomal Curcumin Cytochrome P450 Metabolism. *Anticancer Res.* 30, 811–814. doi:10.1097/CAD.0b013e32833418c0

Markatou, E., Gionis, V., Chryssikos, G. D., Hatziantoniou, S., Georgopoulos, A., and Demetzos, C. (2007). Molecular Interactions between Dimethoxycurcumin and Pamam Dendrimer Carriers. *Int. J. Pharmaceutics* 339, 231–236. doi:10.1016/j.ijpharm.2007.02.037

Moloney, J. N., and Cotter, T. G. (2018). ROS Signalling in the Biology of Cancer. *Semin. Cel Dev. Biol.* 80, 50–64. doi:10.1016/j.semcdb.2017.05.023

Munigunti, R., Gathiaka, S., Acevedo, O., Sahu, R., Tekwani, B., and Calderón, A. I. (2014). Determination of Antiplasmodial Activity and Binding Affinity of Curcumin and Demethoxycurcumin towardsPfTrxR. *Nat. Product. Res.* 28, 359–364. doi:10.1080/14786419.2013.866112

Pencik, J., Pham, H. T. T., Schmoellerl, J., Javaheri, T., Schlederer, M., Culig, Z., et al. (2016). JAK-STAT Signaling in Cancer: From Cytokines to Non-coding Genome. *Cytokine* 87, 26–36. doi:10.1016/j.cyto.2016.06.017

Ramkumar, M., Rajasankar, S., Gobi, V. V., Dhanalakshmi, C., Manivasagam, T., Justin Thenmozhi, A., et al. (2017). Neuroprotective Effect of Demethoxycurcumin, a Natural Derivative of Curcumin on Rotenone Induced Neurotoxicity in SH-SY 5Y Neuroblastoma Cells. *BMC Complement. Altern. Med.* 17, 217. doi:10.1186/s12906-017-1720-5

Shang, Z., Li, Y., Zhang, M., Tian, J., Han, R., Shyr, C.-R., et al. (2015). Antiandrogen Therapy with Hydroxyflutamide or Androgen Receptor Degradation Enhancer ASC-J9 Enhances BCG Efficacy to Better Suppress Bladder Cancer Progression. *Mol. Cancer Ther.* 14 (11), 2586–2594. doi:10.1158/1535-7163.MCT-14-1055-T

Siegel, R. L., Miller, K. D., and Jemal, A. (2016). Cancer Statistics, 2016. *CA: A Cancer J. Clinicians* 66, 7–30. doi:10.3322/caac.21332

Simon, E., Aswini, P., Sameer Kumar, V. B., and Mankadath, G. (2018). Curcumin and its Synthetic Analogue Dimethoxycurcumin Differentially Modulates Antioxidant Status of normal Human Peripheral Blood Mononuclear Cells. *Free Radic. Res.* 52, 583–591. doi:10.1080/10715762.2018.1455002

Sun, T., Zhang, Y. S., Pang, B., Hyun, D. C., Yang, M., and Xia, Y. (2014). Engineered Nanoparticles for Drug Delivery in Cancer Therapy. *Angew. Chem. Int. Ed.* 53 (46), a–n. doi:10.1002/anie.201403036

Sun, Z., Wei, T., and Zhou, X. (2018). Liposomes Encapsulated Dimethyl Curcumin Regulates Dipeptidyl Peptidase I Activity, Gelatinase Release and Cell Cycle of Spleen Lymphocytes *In-Vivo* to Attenuate Collagen Induced Arthritis in Rats. *Int. Immunopharmacology* 65, 511–521. doi:10.1016/j.intimp.2018.10.039

Sun, Z. Y., Guo, Y. M., Ge, X., Lu, C. X., Shao, D. D., and Zhou, X. Y. (2020). Liposomal Dimethyl Curcumin Inhibits Cell Proliferation and Regulates Cell Cycle of Rat Spleen Lymphocytes *In Vivo* and *In Vitro*. *J. Changzhou Univ. (Natural Sci. Edition)* 32 (4), 63–70.

Tamvakopoulos, C., Dimas, K., Sofianos, Z. D., Hatziantoniou, S., Han, Z., Liu, Z.-L., et al. (2007). Metabolism and Anticancer Activity of the Curcumin Analogue, Dimethoxycurcumin. *Clin. Cancer Res.* 13, 1269–1277. doi:10.1158/1078-0432.CCR-06-1839

Tian, H., Chou, F.-j., Tian, J., Zhang, Y., You, B., Huang, C.-P., et al. (2021). ASC-J9 Suppresses Prostate Cancer Cell Proliferation and Invasion *via* Altering the ATF3-PTK2 Signaling. *J. Exp. Clin. Cancer Res.* 40 (1), 3. doi:10.1186/s13046-020-01760-2

Tomeh, M. A., Hadianamrei, R., Sun, W., Xu, D., Brown, S., and Zhao, X. (2021). Stiffness-tuneable Nanocarriers for Controlled Delivery of ASC-J9 into Colorectal Cancer Cells. *J. Colloid Interf. Sci.* 594, 513–521. doi:10.1016/j.jcis.2021.03.086

Wada, K., Lee, J.-Y., Hung, H.-Y., Shi, Q., Lin, L., Zhao, Y., et al. (2015). Novel Curcumin Analogs to Overcome EGFR-TKI Lung Adenocarcinoma Drug Resistance and Reduce EGFR-TKI-Induced GI Adverse Effects. *Bioorg. Med. Chem.* 23 (7), 1507–1514. doi:10.1016/j.bmc.2015.02.003

Wang, R., Han, J., Jiang, A., Huang, R., Fu, T., Wang, L., et al. (2019). Involvement of Metabolism-Permeability in Enhancing the Oral Bioavailability of Curcumin in Excipient-free Solid Dispersions Co-formed with Piperine. *Int. J. Pharmaceutics* 561, 9–18. doi:10.1016/j.ijpharm.2019.02.027

Wang, R., Lin, W., Lin, C., Li, L., Sun, Y., and Chang, C. (2016). ASC-J9 Suppresses Castration Resistant Prostate Cancer Progression *via* Degrading the Enzalutamide-Induced Androgen Receptor Mutant AR-F876L. *Cancer Lett.* 379 (1), 154–160. doi:10.1016/j.canlet.2016.05.018

Wen, S., Niu, Y., Lee, S. O., Yeh, S., Shang, Z., Gao, H., et al. (2016). Targeting Fatty Acid Synthase with ASC-J9 Suppresses Proliferation and Invasion of Prostate Cancer Cells. *Mol. Carcinog.* 55 (12), 2278–2290. doi:10.1002/mc.22468

Wu, C.-Y., Yang, Y.-H., Lin, Y.-Y., Kuan, F.-C., Lin, Y.-S., Lin, W.-Y., et al. (2017). Anti-cancer Effect of Danshen and Dihydroisotanshinone I on Prostate Cancer: Targeting the Crosstalk between Macrophages and Cancer Cells *via* Inhibition of the STAT3/CCL2 Signaling Pathway. *Oncotarget* 8 (25), 40246–40263. doi:10.18632/oncotarget.14958

Xu, D. F., Liu, Y. L., Wang, W. J., and Zhou, H. (2019). Preparation and Characterization of Dimethylcurcumin Solid Dispersions. *J. Chin. Pharm. Sci.* 50 (2), 210–215.

Xu, J., Lin, H., Li, G., Sun, Y., Shi, L., Ma, W.-L., et al. (2017). Sorafenib with ASC-J9synergistically Suppresses the HCC Progressionviaaltering the pSTAT3-CCL2/Bcl2 Signals. *Int. J. Cancer* 140 (3), 705–717. doi:10.1002/ijc.30446

Yallapu, M. M., Jaggi, M., and Chauhan, S. C. (2013). Curcumin Nanomedicine: A Road to Cancer Therapeutics. *Curr. Pharm. Des.* 19, 1994–2010. doi:10.2174/138161213805289219

Yan, W., Leung, S. S., and To, K. K. (2020). Updates on the Use of Liposomes for Active Tumor Targeting in Cancer Therapy. *Nanomedicine* 15 (3), 303–318. doi:10.2217/nnm-2019-0308

Yang, X., Zhang, D., Song, L. M., Xu, Q., Xu, H., and Liu, K. (2017). Spectroscopic Studies on Alkaline Autoxidation of Curcumin and Antioxidative Activities of the Product. *Chem. J. Chin. U.* 38, 1549–1555. doi:10.7503/cjcu20170147

Yoon, M. J., Kang, Y. J., Lee, J. A., Kim, I. Y., Kim, M. A., Lee, Y. S., et al. (2014). Stronger Proteasomal Inhibition and Higher CHOP Induction Are Responsible for More Effective Induction of Paraptosis by Dimethoxycurcumin Than Curcumin. *Cell Death Dis.* 5, e1112. doi:10.1038/cddis.2014.85

Zanetti, T. A., Biazi, B. I., Coatti, G. C., Baranoski, A., Marques, L. A., Corveloni, A. C., et al. (2021). Dimethoxycurcumin Reduces Proliferation and Induces Apoptosis in Renal Tumor Cells More Efficiently Than Demethoxycurcumin and Curcumin. *Chemico-Biological Interactions* 338, 109410. doi:10.1016/j.cbi.2021.109410

Zanetti, T. A., Biazi, B. I., Coatti, G. C., Baranoski, A., Marques, L. A., Corveloni, A. C., et al. (2019). Mitotic Spindle Defects and DNA Damage Induced by Dimethoxycurcumin lead to an Intrinsic Apoptosis Pathway in HepG2/C3A Cells. *Toxicol. Vitro* 61, 104643. doi:10.1016/j.tiv.2019.104643

Zhang, D., Xu, Q., Wang, N., Yang, Y., Liu, J., Yu, G., et al. (2017). A Complex Micellar System Co-delivering Curcumin with Doxorubicin against Cardiotoxicity and Tumor Growth. *Ijn* Vol. 13, 4549–4561. doi:10.2147/IJN.S170067

Zhang, T., Zhao, L., Zhang, T., Wu, W., Liu, J., Wang, X., et al. (2020). Curcumin Negatively Regulates Cigarette Smoke-Induced Renal Cell Carcinoma Epithelial-Mesenchymal Transition through the ERK5/AP-1 Pathway. *Ott* Vol. 13, 9689–9700. doi:10.2147/OTT.S265847

Zhao, H., Liu, Q., Wang, S., Dai, F., Cheng, X., Cheng, X., et al. (2017). *In Vitro* additive Antitumor Effects of Dimethoxycurcumin and 5-fluorouracil in colon Cancer Cells. *Cancer Med.* 6, 1698–1706. doi:10.1002/cam4.1114

Zhou, M., Liu, X., Li, Z., Huang, Q., Li, F., and Li, C.-Y. (2018). Caspase-3 Regulates the Migration, Invasion and Metastasis of colon Cancer Cells. *Int. J. Cancer* 143 (4), 921–930. doi:10.1002/ijc.31374

Zhou, S. W., Xu, D. F., Yang, X. Q., Ma, S. X., Ge, X. A., and Feng, Z. G. (2016). Anti-tumor Effect *via* Different Sizes of Liposomes Encapsulating Dimethyl Curcumin *In Vitro*. *J. Changzhou Univ. (Natural Sci. Edition)* 28 (6), 63–70.

Conflict of Interest: The authors declare that the research was conducted in the absence of any commercial or financial relationships that could be construed as a potential conflict of interest.

frontiers in Immunology

ORIGINAL RESEARCH
published: 19 August 2021
doi: 10.3389/fimmu.2021.712936

Tumor Temporal Proteome Profiling Reveals the Immunological Triple Offensive Induced by Synthetic Anti-Cancer *Salmonella*

Shuxin Yang[1†], Wenjuan Zhao[1†], Muchun Zhu[2†], Huijuan Hu[1], Weijie Wang[1], Zhongsheng Zang[1], Meiling Jin[1], Jiacheng Bi[1], Jiandong Huang[1], Chenli Liu[1], Xuefei Li[1], Peng Yin[2] and Nan Li[1]*

[1] Chinese Academy of Sciences (CAS) Key Laboratory for Quantitative Engineering Biology, Shenzhen Institute of Synthetic Biology, Shenzhen Institute of Advanced Technology, Chinese Academy of Sciences, Shenzhen, China, [2] Guangdong-Hong Kong-Macao Joint Laboratory of Human-Machine Intelligence-Synergy Systems, Shenzhen Institute of Advanced Technology, Chinese Academy of Sciences, Shenzhen, China

OPEN ACCESS

Edited by:
Yan-feng Gao,
Sun Yat-sen University, China

Reviewed by:
Roslyn Kemp,
University of Otago, New Zealand
Yichuan Xiao,
Chinese Academy of Sciences (CAS), China

***Correspondence:**
Nan Li
nan.li@siat.ac.cn

†These authors have contributed equally to this work and share first authorship

Specialty section:
This article was submitted to Cancer Immunity and Immunotherapy, a section of the journal Frontiers in Immunology

Received: 21 May 2021
Accepted: 03 August 2021
Published: 19 August 2021

Citation:
Yang S, Zhao W, Zhu M, Hu H, Wang W, Zang Z, Jin M, Bi J, Huang J, Liu C, Li X, Yin P and Li N (2021) Tumor Temporal Proteome Profiling Reveals the Immunological Triple Offensive Induced by Synthetic Anti-Cancer Salmonella. Front. Immunol. 12:712936. doi: 10.3389/fimmu.2021.712936

The engineered "obligate" anaerobic *Salmonella typhimurium* strain YB1 shows a prominent ability to repress tumor growth and metastasis, which has great potential as a novel cancer immunotherapy. However, the antitumor mechanism of YB1 remains unelucidated. To resolve the proteome dynamics induced by the engineered bacteria, we applied tumor temporal proteome profiling on murine bladder tumors after intravenous injection of either YB1 or PBS as a negative control. Our data suggests that during the two weeks treatment of YB1 injections, the cured tumors experienced three distinct phases of the immune response. Two days after injection, the innate immune response was activated, particularly the complement and blood coagulation pathways. In the meantime, the phagocytosis was initiated. The professional phagocytes such as macrophages and neutrophils were recruited, especially the infiltration of $iNOS^+$ and $CD68^+$ cells was enhanced. Seven days after injection, substantial amount of T cells was observed at the invasion margin of the tumor. As a result, the tumor shrunk significantly. Overall, the temporal proteome profiling can systematically reveal the YB1 induced immune responses in tumor, showing great promise for elucidating the mechanism of bacteria-mediated cancer immunotherapy.

Keywords: quantitative proteomics, cancer immunotherapy, engineered *Salmonella*, blood coagulation, phagocytosis, antitumor T cell response

INTRODUCTION

Globally cancer is an important leading cause of death, accounting for nearly 10 million deaths in 2020 alone (WHO). The vast majority of cancers are solid tumors, which develop in a variety of organs, such as breast, lung, colorectum, liver, prostate and bladder etc. To date, the conventional methods of cancer treatment such as surgery, radiation therapy and chemotherapy are still the preferred choice. However, surgery is not an effective therapy for metastatic cancer and needs to be

used in combination with other traditional therapies such as radiation or chemotherapy. The procedure and therapeutic effects of radiotherapy and chemotherapy are impeded by the necrotic and hypoxic regions in tumors (1). Cancer immunotherapy had emerged as a standard treatment with great potential in cancer therapy. It includes adoptive T cell therapy, immune checkpoint inhibitors and cancer vaccines etc. The earliest cancer immunotherapy could be traced back to the bacteria-mediated cancer therapy 200 years ago (2). So far, various kinds of bacterial infection or injection have been reported to relieve cancer symptoms or were specifically used for cancer treatment, such as *Streptococcus pyogenes* (*S. pyogenes*), Coley's toxins, *Clostridium histolyticum* and the Bacillus Calmette-Guerin (BCG) vaccine (3–7).

Recent progress in the fields of immunology and biotechnology has generated new interest in the modification of tumor-targeting bacteria, returning them to the forefront of cancer research (8). Many non-pathogenic obligate anaerobes and facultative anaerobes have been shown selectively proliferate in tumor cells possessing hypoxia and abnormal angiogenesis. Attenuated *Salmonella* is an outstanding example of one such obligate anaerobe (9–12). In our previous studies, synthetic biology techniques were applied to construct an engineered "obligate" anaerobic *Salmonella typhimurium* strain YB1 (*Salmonella* YB1). The engineered *Salmonella* YB1 acted as an obligate anaerobe, targeting the hypoxic and necrotic regions in tumors and significantly suppressing the growth and metastasis of a broad range of cancers, including bladder tumor (13), neuroblastoma, liver cancer and breast cancer (14–17). Systemic administration of *Salmonella* YB1 can effectively stimulate the immune system, resulting in the increased production of tumor necrosis factor-α (TNF-α), and interferon-γ (IFN-γ), as well as activation of both innate and adaptive immune cells (14–17). These stimulated immune responses might create a hostile environment for tumor progression (18). However, the underlying systemic therapeutic mechanism of *Salmonella* YB1 remains to be elucidated.

The proteomic approach is a promising technique that can facilitate the systematic characterization of the proteome dynamics in pharmacology and interspecies interactions (19–21). Systematically revealing the dynamics of the tumor proteome after YB1 treatment will contribute to understanding its mechanism. The quantitative proteomics of tumors undergoing bacterial treatment can especially contribute to understanding of the interaction process between bacteria and tumors. We profiled the temporal proteome of the bladder tumor xenografts on mice after *Salmonella* YB1 injection. We then applied a label-free quantitative proteomic approach with in-solution digestion to identify the differentially expressed proteins by mass spectrometry analysis. The tumors with YB1 injection experienced three distinct phases of immune responses, including the activation of complement and blood coagulation pathways, $iNOS^+$ and $CD68^+$ cells mediated phagocytosis, and the accumulation of T cells at the invasion margin of tumors. In summary, we performed the systematic temporal analysis to the proteome of the tumor with YB1 treatment. It will be beneficial to reveal the therapeutic mechanism of YB1 and its application in cancer immunotherapy in the future.

MATERIALS AND METHODS

Salmonella YB1 and Tumor Cells Culture

S. typhimurium strain YB1 was cultivated in Luria-Bertani (LB) broth containing 25μg/mL chloramphenicol at 37°C, with shaking at 220 rpm overnight. The YB1 cultures were then transferred twice and grown until the logarithmic phase. OD600 was measured to determine the bacterial count. The MB49 mouse bladder cancer cell line was maintained in Dulbecco's modified Eagle's medium-high glucose (DMEM-HG) supplemented with 10% FBS (fetal bovine serum), 1% streptomycin and 1% penicillin. The medium was renewed every other day. Cells were cultivated at 37°C in a humidified atmosphere of 5% CO_2.

Animals and Tumor Tissues Collection

All animal experiments were approved by the animal care regulations of the Institutional Animal Care and Use Committee of the Shenzhen Institutes of Advanced Technology, Chinese Academy of Sciences. Four-to six-week-old female C57BL/6 mice (Vital River Laboratory Animal Technology Co. Ltd, CHN) were subcutaneously injected with MB49 cells (1×10^{6}) in the flank region. Tumor volume was calculated according to the following formula: tumor volume = length × (width) 2/2. When the average volumes of the MB49 tumors reached approximately 200 mm^3, the C57BL/6 mice were randomly divided into two groups. One group was inoculated *via* the tail vein of the mice with YB1 (1×10^{7}) dissolved in 125μL PBS, whereas the control group was treated with 125μL PBS only. The mice were killed at different time points after injection. The whole tumor tissues were washed twice with ice-cold phosphate-buffered saline (PBS) to remove blood and other contaminants, quick-frozen in liquid N_2 and stored at –80°C for protein extractions.

Protein Preparation and Peptide Extraction

At least 1 mg samples of tumor tissues were cut off and lysed in a buffer that consisted of 5mM EDTA, 150mM NaCl, 20mM HEPES (pH8.5), 1% SDS, and a Roche complete protease inhibitor cocktail tablet for 10 min on ice. Following lysis, tissues debris was further lysed using sonication under suitable conditions. The lysates were centrifuged at 20,000 g for 15 min at 4°C, and the supernatants were harvested. The protein concentration was measured by BCA Assay Kit (Thermo Fisher Scientific, P/N 23225). Approximately 100μg protein solution was reduced and alkylated for 30 min at 37°C using 1μl 0.5 M TCEP, and 2μl 1 M CAA. After alkylation, quantitative precipitation of soluble and hydrophobic proteins from dilute solutions was based on a defined methanol-chloroform-water mixture method as described in Wessel D et al. (22). In brief, an aliquot (0.200μl) of methanol was added to 50μl of protein

sample (approximately 100μg proteins) and the samples were vortexed. Then, chloroform (50μl) was added and the samples were vortexed again. For phase separation, 150μl of water (HPLC grade) was added, and the samples were vortexed vigorously and centrifuged at 9000 g for 2 min at room temperature. The upper phase was carefully removed and discarded. A further 150μl methanol was added slowly to the rest of the lower chloroform phase and the interphase with the precipitated protein. The samples were mixed gently and centrifuged again at 9000 g for 2 min at room temperature to pellet the protein. The supernatant was removed and the protein pellet was dried under a stream of air for 5 min. The protein pellets were re-disolved by the addition of 20μl of Urea buffer (8 M Urea, 100mM HEPES) and vortexed fully. The protein pellets were reconstituted by the addition of 180μl of 20mM HEPES and vortexed fully. For digestion, 2μg mass spectrometry grade trypsin (Promega, P/N V5280) were added for digestion overnight at 37°C. The peptide digestions were quenched by 10μl of 10% formic acid (FA).

Peptides Desalting

The acidifying peptide samples were desalted using a 100 mg desalting column (Thermo Fisher Scientific, P/N 60108-302). In short, the desalting column was activated with 1 ml acetonitrile (ACN)) twice, and 1 ml buffer B (80% ACN, 0.5% FA in water) twice. The buffer A was loaded twice to equilibrate the desalting column. Subsequently, the peptide solution was loaded onto the column, washed with 1 ml buffer A three times and eluted with buffer B to a clean tube. The eluent was dried completely in a SpeedVac centrifuge at 45°C and store at -80°C.

LC-MS/MS Analysis

All peptides were reconstituted in 0.1% FA (vol/vol) and separated on on reversed-phase columns (trapping column: particle size = 3 μm, C18, length = 20 mm (Thermo Fisher Scientific, P/N 164535); analytical column: particle size = 2 μm, C18, length =150 mm(Thermo Fisher Scientific, P/N 164534)) on an Ultimate™ 3000 RSLCnano system (Thermo Fisher Scientific, San Jose, CA, USA) coupled to Orbitrap Q-Exactive™ HF (Thermo Fisher Scientific). Peptide separation was achieved using a 120 min gradient (buffer A: 0.1% FA in water, buffer B: 0.1% FA in 80% ACN) at a flow rate of 300 nl/min, then analyzed by Orbitrap Q-Exactive™ HF in a data-dependent mode. The Orbitrap Q-Exactive™ HF mass spectrometer was operated in positive ion mode with the ion transfer tube temperature set at 320°C. The positive ion spray voltage was 2.1 kV. Full-scan MS spectra (m/z 350–2000) was acquired in the Orbitrap with a resolution of 60,000. HCD fragmentation was performed at normalized collision energy of 28%. The MS2 automatic gain control (AGC) target was set to 5e4 with a maximum injection time (MIT) of 50 ms and dynamic exclusion was set to 45 s.

Proteomics Data Processing and Bioinformatic Analysis

The MS/MS data were searched against a Swiss-Prot database (Musculus release-20190412 and Salmonella release-20190426 downloaded from UniProt) with MaxQuant 1.5.3.30. Data were searched with a precursor mass tolerance of 20 ppm and a fragment mass tolerance of 0.5 Da. Searches were performed with enzyme specificity and only tryptic peptides were allowed to remain in the final data sets, and up to two mis-cleavages allowed. Cysteine carboxamidomethylation was specified as a static modification; oxidation of methionine residue and acetylation, (protein-N) were allowed as variable modifications. Reverse decoy databases were included for all searches to estimate false discovery rates. Peptide and protein identifications were also quantified and filtered for less than 1% false-discovery rate (FDR).

The intensity values from MaxQuant were normalized and further processed using the VSN method. We removed proteins with fewer than two samples in each group of samples at each time point. Then, the missing values were imputed by using the QRILC method. The Limma package was used for determining differentially expressed proteins between tumor mice and tumor mice injected with Salmonella. Proteins with an average fold change >1 and p-value <0.05 were considered different. For proteins of significant difference, their molecular functions and associated biological processes were analyzed using the DAVID (https://david.ncifcrf.gov/home.jsp) analysis tool, the FDR threshold was set at 5%. In order to observe the protein change panels at seven time points, we used the CLUSTER package (23) to create a k-means cluster analysis.

Immunohistochemical Analysis

Tumor tissues were collected from MB49-bearing mice intravenously injected with bacteria ($1x10^7$ CFU per mice) or PBS for hematoxylin and eosin (H&E) staining. Macrophages were labeled with F-4/80 antibody (Servicebio, GB11027). M1 subset macrophages were marked with iNOS and CD68 antibody (Servicebio, GB11119, GB11067). Neutrophils were labeled with Ly-6G antibody (Servicebio, GB11229). The complement activity was recognized by C3 antibody (Abcam, ab200999). T and B cells were labeled respectively with CD3 antibody (Servicebio, GB13014) and CD19 antibody (Servicebio, GB11061). The collagen was stained with Sirius red staining. The mouse primary antibodies was detected using a goat anti-mouse secondary antibody (Servicebio, gb111739).

Quantification of the Immunohistochemical Staining

Expression levels of effector proteins as well as the abundance of various type of immune cells were quantified using images of tumor sections with immunohistochemical staining. Nine regions of interest (ROI) were manually selected from the whole scan image of the each tumor under 40x magnification (about 250um x 480 um), and there are three tumor-bearing mice for each experimental condition. First, we adopted a color deconvolution model (24) to separate the unstained and stained regions into separate channels with the deconvolution matrix set as [0.650 0.704 0.286; 0.268 0.570 0.776; 0.711 0.423 0.561]. Then, image binarization with an appropriate threshold setting (C3 w/70, CD3 w/10, CD11c w/30, CD68 w/20, F4/80 w/70, iNOS w/70, Ly6G w/25 and CD19 w/10) were applied to extract

the area of different markers. Next, nuclei boundaries were detected by using a level set segmentation and detection technique as previously described (25). Note that we used the area of cell nucleus instead of cytoplasm to represent the area of cell regions, for it is more difficult to define the regions of cytoplasm, and we hypothesized that the nucleus/cytoplasm area-ratio is consistent across different regions. Finally, the area of stained signals (S) and all cell nucleus (N) can be obtained, and a ratio of S to N (S/N) was defined to evaluate the expression levels of effector proteins or the abundance of various type of immune cells in the tumor-section images.

T Cell Separation and ELISpot Assay

The mouse spleen was separated and grinded in RPMI1640 medium, then the T cells were isolated by magnetic negative selection using the $CD8^+$ T cell isolation kit (Miltenyi Biotec.). The activity of $CD8^+$ T cells was tested using the Mouse IFN-γ precoated ELISPOT Kit (DAKEWE, 2210005) as the described in the product manual.

1×10^5 freshly spleen $CD8^+$ T cells were plated in triplicates into 96-well Elispot plates precoated with anti-mouse-IFN-γ antibody and stimulated for 18 h at 37°C under 5% CO_2 with either 1×10^4 MB49 cells or 1×10^5 YB1 resuspended in PBS (positive control). As unstimulated control, cells were incubated for 18 h in cell culture medium (background value). The PMA stimulation was used as a positive control as well. After cell removal, plates were incubated with biotinylated antibody and streptavidin-HRP respectively for 1 h. Spot detection was performed by FluoroSpot and ELISpot Reader (Mabtech IRIS™).

Statistical Analysis

All values are expressed as means ± SD. Statistically significant differences among individual treatments and the corresponding control groups were determined by the Kolmogorov–Smirnov test (K–S test or KS test) or analysis of variance (ANOVA). Experiments were independently repeated at least three times. All analyses were carried out using GraphPad Prism 9. A p-value <0.05 was considered to be statistically significant.

RESULTS

Temporal Proteome Profiling Unraveling Diverse Tumor Responses During YB1 Treatment

To build the tumor model, C57BL/6 mice were subcutaneously injected with MB49 cells in the flank region (detail in method). In brief, when the average size of the MB49 tumors reached approximately $200mm^3$, the C57BL/6 mice were randomly divided into two groups and injected intravenously with *Salmonella* strain YB1 (treatment group) or PBS (control group). The tumor growth was inhibited by YB1 treatment (**Supplementary Figure 1**), same as our previous study (13). To map the proteomic atlas of the *Salmonella* YB1 treatment bladder tumors, we collected the whole tumors in four replicates from each group at each time point. There were seven time points in total, including 6 hours, 12 hours, 24 hours, 2days, 3 days, 7 days and 14 days post *Salmonella* YB1 or PBS injection. We applied a label-free quantitative proteomic approach with in-solution digestion to 56 identified samples by mass spectrometry analysis (**Figure 1A**). To better understand the molecular functions of tumor proteins during *Salmonella* YB1 treatment, GO term enrichment analysis for YB1 proteins displaying ≥1 ± log2(fold-change) revealed a total of 454 enriched GO terms ($p \leq 0.05$, right-sided hypergeometric test, Bonferroni corrected), with 397 being upregulated and 57 downregulated (**Figure 1B**, **Supplementary Table 1**).

We observed a number of infection-related GO terms were significantly enriched, as well as the integrin-mediated signaling pathway related to bacterial invasion at 6 hours (20), an apoptotic pathway at 24 hours and response to virus at 2 days. These findings demonstrate that YB1 could invade the tumor and cause cell apoptosis, consistent with our previous study (14). Moreover, a strong innate immune response occurred at 24 hours last to 7 days, including acute-phase response, blood cogulation and complement activation etc. (**Figure 1B**, **Supplementary Table 1**). Overall, our results are in line with previous observation in Salmonella based tumor therapy, where Salmonella demonstrates an intrinsic anti-tumor effect, largely attributed to its immune stimulatory activity, as well as activation of both innate and adaptive immune cells (18, 26).

A Dynamic Proteomic Atlas of the YB1 Treated Tumors

Summing up all the 56 samples, 4,812 proteins were quantified at a 1% peptide FDR (false discovery rate) (**Figure 2A**, **Dataset1** in **Supplementary Table 2**). A total of 4,516 proteins were identified as high-quality IDs by selecting those that have been measured with at least one unique peptide (**Figure 2A**, **Dataset2** in **Supplementary Table 3**). Further filtering for proteins identified in at least 2 of the 4 replicates at one time point resulted in a final list of 2,739 proteins for bioinformatic analyses (**Figure 2A**, **Dataset3** in **Supplementary Table 4**). Replicate correlation of samples showed good consistency and a high degree of correlation (R = 0.85–0.93) between the YB1 and PBS experiments (**Figure 2B**, **Supplementary Figure 2**). Principal component analysis (PCA) showed that replicates clustered closely and the YB1 separation from control clusters PBS (**Figure 2C**, **Supplementary Figure 3**). Overall, our tumor proteomic dataset is of high quality and reproducibility.

After these filtering steps, we performed relative protein quantification based on the log2 fold change of protein intensity of YB1 versus PBS samples and p-value from the Limma test (**Figure 2D**, **Supplementary Figure 4**). This analysis showed that, 1097 out of the 2739 quantified proteins were significantly up or down regulated leastwise at one timepoint (p-value ≤0.05, |log2 fold change| ≥1) (**Supplementary Table 5**). These results revealed that the majority of differential expression of proteins occurred from 24 hours to 7 days (947 of 1097). Most notably, at 24 hours and 2 days, there were 453 and 412 differentially expressed proteins respectively (**Figure 2E**).

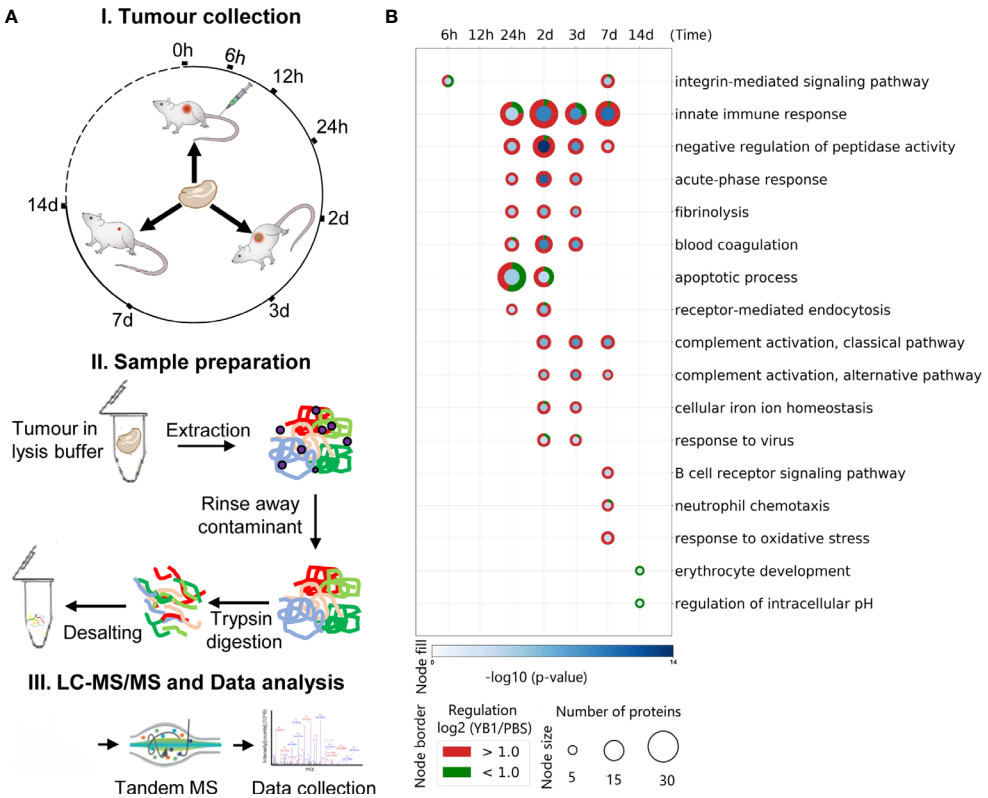

FIGURE 1 | Temporal proteome profiling for exploring the anti-cancer mechanism of *Salmonella* YB1. **(A)** Experimental design and data analysis workflow of the tumor proteome. (I) Illustration of the tumor collection after *Salmonella* YB1 strain treatment at different time points. (II). General workflow of proteomic sample preparation process. (III) The workflow of MS-based quantitative proteomics and bioinformatics analysis. **(B)** GO term enrichment of differentially expressed tumor proteins. Selected enriched GO terms are depicted; all enriched GO terms can be found in **Supplementary Table 1**. Node size and colors depict significance, [–log10 (*p*-value)] right-sided hypergeometric test, Bonferroni corrected) (blue shading) and number of proteins (Node size), respectively. n = 4 biologically independent samples.

Key Immune Responses Revealed by K-Means Clustering Analysis

To better exhibit biological processes induced by YB1 treatment, we applied the *k*-means algorithm to classify the 1097 differentially expressed tumor proteins, according to their dynamic co-expression patterns. We obtained six protein modules with the unsupervised k-mean clustering analysis (**Supplementary Table 6**). Then we analyze GO Biological Process terms in each of the modules (**Figure 3**, **Supplementary Table 7**).

Proteins in Module 1 and 2 were gradually downregulated, dropped to a trough at 24 hours and 2 days respectively, including proteins of RAD50, CCAR2, CDK5 etc. These proteins are mainly involved in cell-cycle, including DNA repair and regulation of cell grows. It has recently been shown that cell-cycle are correlated with *Salmonella* intracellular proliferation (20). The suppression of cell-cycle may indicate a host-driven response to *Salmonella*. Module 2 proteins also participate in the post-translational modification of proteins, such as dephosphorylation and ubiquitination. It appears that cell proliferation and protein degradation are the predominant downregulated pathways during *Salmonella* YB1 treatment.

Proteins in Module 3, 4, 5 and 6 were progressive upregulated and respectively peaked at 24 hours, 2 days, 7 days and 14 days. Module 3 proteins were mainly involved in response to oxidative stress, endothelial cell migration and regulation of intracellular pH. The latter behavior is consistent with the previous study that protein synthesis and cell proliferation and mitosis could make a change in cytosolic pH (27). Although proteins in Module 4-6 peaked at different time point, they were significantly enriched in similar biological processes including innate and adaptive immune response. In particular, we detected a strong response to blood coagulation and complement activation (C3, C9, C4, C5, etc.) in Module 4. This finding indicated that YB1 treatment would trigger blood coagulation within the tumor, consistent with the previous report (23).

We also observed strong induction of endocytosis such as phagocytosis signaling response in both Module 4 and 5, including proteins iNOS, CD14, CD177, NGP, CD68, etc. CD14, which is well known mediate the innate immune response to bacterial lipopolysaccharide (28), was gradually

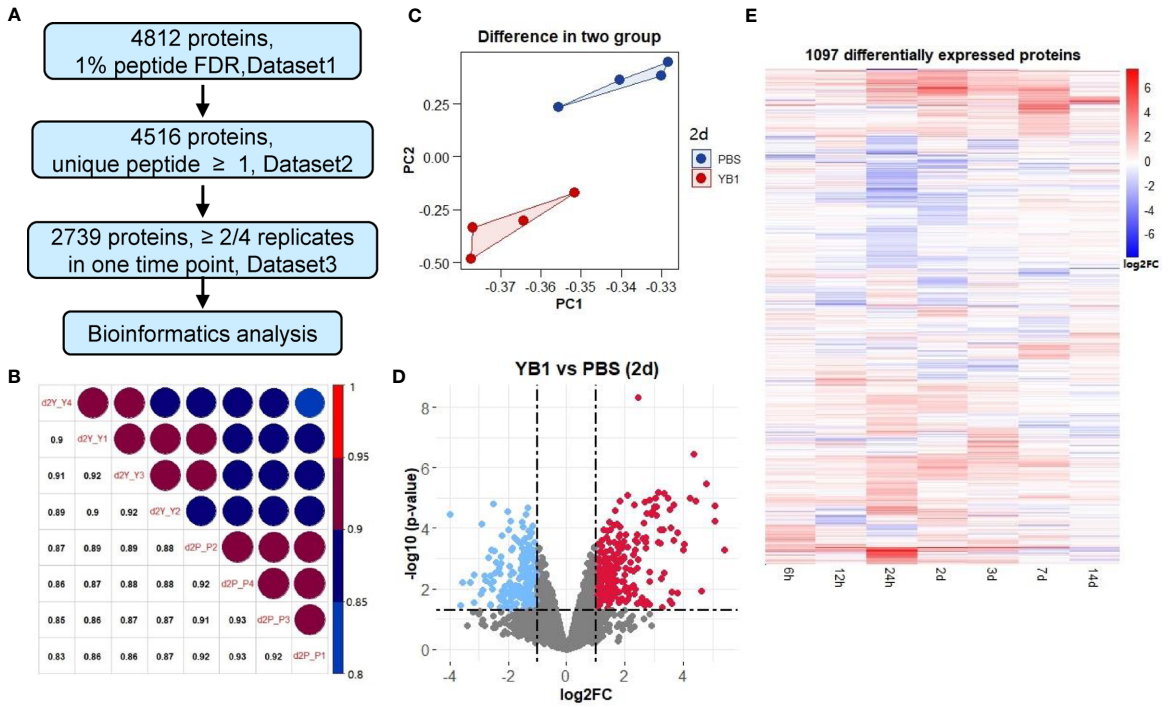

FIGURE 2 | Quantitative proteomics revealed differential protein expressions in tumor induced by YB1 treatment. **(A)** Multiple data sets with different filtering criteria. **(B)** Replicate correlation of YB1 *versus* PBS samples for the indicated time points (2 day). **(C)** Principal component analysis of the proteomics data at 2 day. Each dot represents an independent biological replicate. **(D)** Analysis of significantly dysregulated proteins in YB1 (determined by *t*-test). Volcano plots of YB1 *versus* control comparisons. *p*-values (-log base 10) are plotted as a function of the proteins ratio (log base 2) for YB1 *versus* PBS group. **(E)** Hierarchical clustering of differentially expressed proteins by semi-supervised, Ward's hierarchical clustering.

upregulated from 12 hours, peaked at 2 days (+2.91 Log2 Fold change, adjusted p=3.38E-05). The expression of iNOS reached a peak at 2 days (+2.84 Log2 Fold change, adjusted p=2.75E-03). As a marker of M1 type macrophages, iNOS produces nitric oxide (NO) which mediates tumoricidal and bactericidal activity (29). Likewise, CD177 and NGP was upregulated from 24 hours and peaked at 2 days. CD177 plays an important role in neutrophils recruitment caused by bacterial infection *in vivo* (30). NGP plays a role as a negative regulator of tumor vascular development and metastasis (31) (**Figure 1B**). Proteins in Module 5 were also enriched in positive regulation of T cell proliferation (32). Proteins in Module 6 were involved in B cell receptor signaling pathway and immunoglobulin mediated immune response. Together, these findings highlighted the roles of *Salmonella*-induced immune responses in bacteria mediated anti-tumor effects. However, the functional significance of many of these proteins will require further study.

Thrombosis and Complement Were Initiated After YB1 Treatment

To confirm the complement and blood coagulation in the proteomics analysis results, we performed the immunohistochemical analysis to the mice tumor tissues from the YB1 and PBS injection groups. We collected the tumors of the mice injected with YB1 and PBS at 2 days post injection for hematoxylin and eosin (H&E) staining (**Figure 4A**). In a large view, we could find severe hemorrhagic inflammation in the tumor on mice injected with YB1. Compared to the control group, the mice with YB1 injection showed significant erythrocyte diapedesis in tumors, along with inflammatory cell infiltration. Erythrocyte could be abundantly found inside the tumor after bacterial infection (**Figure 4A**). The results above are representative features in bacterial infection. We observed that the colonization of bacteria in tumor could trigger thrombosis by disrupting tumor blood vessels, which was consistent with the previous study (33). On the other hand, we performed the immunohistochemical analysis to C3, a canonical marker of complement, in the tumor slices. It showed that the expression of C3 in tumor with YB1 injection is significantly higher than the control group (**Figure 4B**). As the description above, not limited to C3, a series of complement related proteins, such as Serpind1, Cfd, C5, C1qbp, etc., were upregulated in tumor with YB1 treatment. The immunohistochemical results confirmed the proteomics analysis and showed that YB1 injection could initiate the activation of complement and blood coagulation in tumor. The activation of the complement system could also induce the recruitment of macrophages and neutrophils into tumor tissues (34, 35), which may indicate a tumoricidal activity.

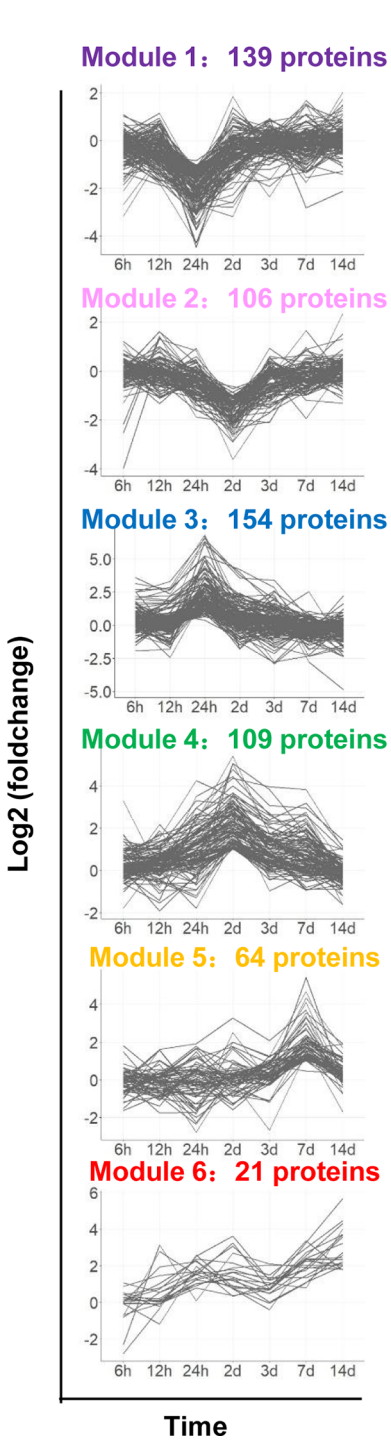

Biological Processes	p-value
mRNA processing	1.20E-04
cell cycle	5.21E-04
intracellular protein transport	1.52E-03
apoptosis	2.91E-03
positive regulation of cell growth	4.16E-03
DNA repair	8.51E-03
phosphorylation	3.41E-02
mRNA processing	6.84E-05
protein amino acid dephosphorylation	9.70E-04
cell cycle	6.50E-03
positive regulation of I-kappaB kinase/NF-kappaB cascade	9.11E-03
protein K48-linked ubiquitination	2.84E-02
positive regulation of apoptosis	3.70E-02
positive regulation of protein ubiquitination	4.28E-02
proteasomal ubiquitin-dependent protein catabolic process	4.85E-02
regulation of intracellular pH	1.62E-04
response to oxidative stress	6.63E-04
proteolysis involved in cellular protein catabolic process	1.07E-03
positive regulation of endothelial cell migration	4.14E-03
translational initiation	8.95E-03
cell adhesion	1.51E-02
oxidation reduction	4.23E-02
blood coagulation	5.26E-15
innate immune response	6.77E-14
acute-phase response	7.03E-13
complement activation, alternative pathway	3.06E-07
complement activation, classical pathway	1.24E-06
receptor-mediated endocytosis	2.09E-06
transport	3.67E-04
oxidation reduction	1.15E-03
response to oxidative stress	8.94E-03
phagocytosis	1.21E-02
positive regulation of T cell proliferation	1.79E-02
cell migration	2.34E-02
response to hypoxia	2.37E-02
response to organic cyclic substance	2.72E-02
phosphorylation	4.61E-02
complement activation, classical pathway	2.49E-08
immunoglobulin mediated immune response	2.56E-07
positive regulation of B cell activation	9.05E-07
B cell receptor signaling pathway	4.32E-06

FIGURE 3 | Dynamic protein co-expression modules classified by *k*-means analysis with GO annotation. The left panel shows the six modules classified by the *k*-means clustering analysis, according to their dynamic co-expression patterns. x-axis represents sampling time, y-axis represents log2 fold-change of protein intensity. The right panel shows the corresponding GO Biological Process terms to each module.

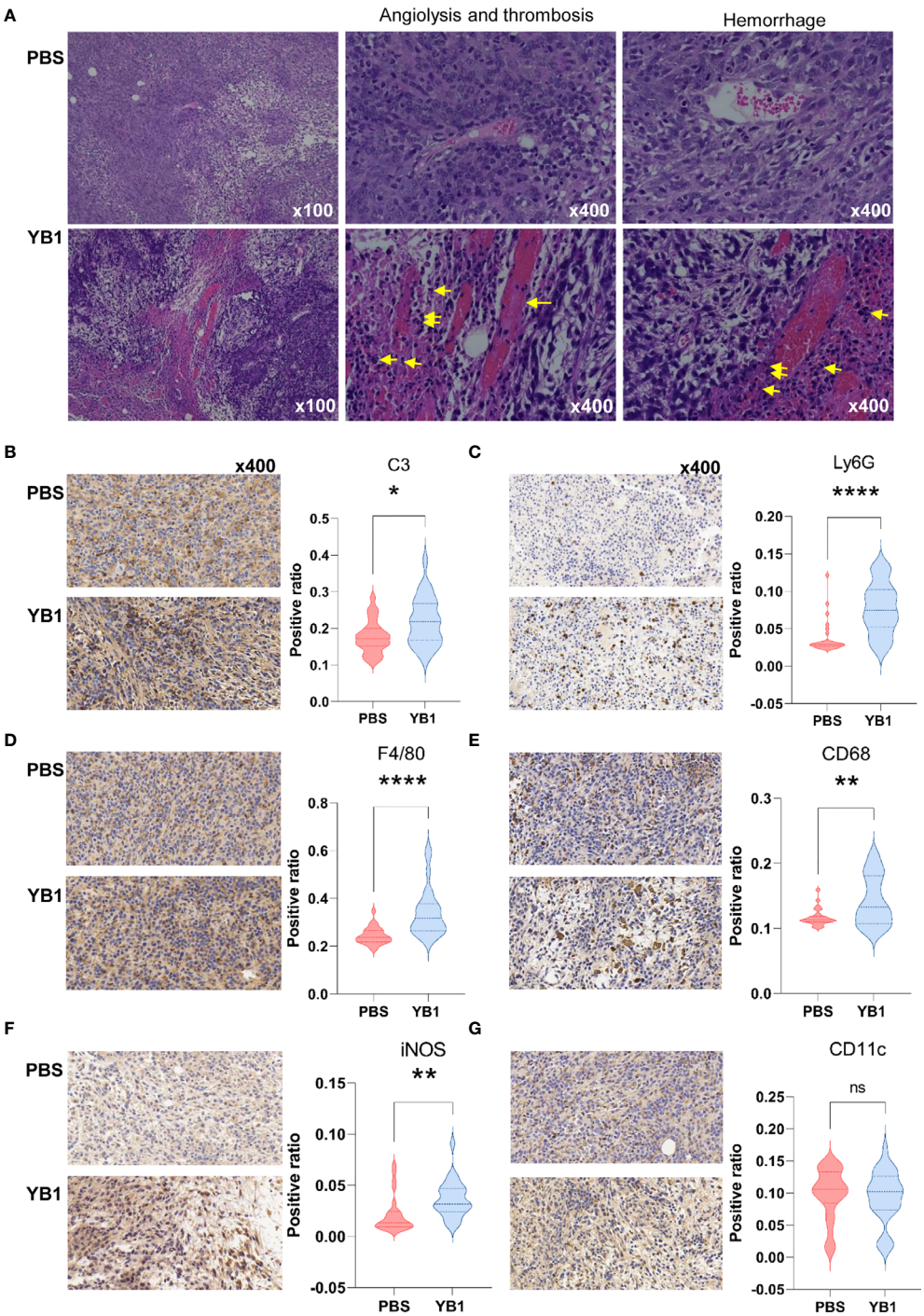

FIGURE 4 | *Salmonella* YB1 induced the innate immune responses in tumors. **(A)** Representative images of hematoxylin and eosin (H&E)–stained tumor slices collected from mice injected with phosphate-buffered saline (PBS) or YB1 at 2 days post injection. The yellow arrow indicates angiolysis, thrombosis and neutrophils infiltration. Area ratio (see methods) of **(B)** $C3^+$ cells, **(C)** $Ly6G^+$ cells, **(D)** F4/80+ cells, **(E)** $CD68^+$ cells, **(F)** $iNOS^+$ cells, **(G)** $CD11c^+$ cells based on immunohistochemical-stained images. Three biological replicates of images with nine random views under 40x magnification per image were collected for statistical analysis which was performed using the K–S test.*$p < 0.05$, **$p < 0.01$, ****$p < 0.0001$, ns, no significant difference.

Phagocytosis Were Activated After YB1 Treatment

We performed immunohistochemical analysis to the professional phagocytes in the tumors at 2 days post injection. F4/80 and CD68 markers were used to identify macrophages. F4/80 is well-known as a highly restricted macrophage molecule in mice. CD68 is exploited as a valuable cytochemical marker to immunostain monocyte/macrophages in the histochemical analysis of tumor tissues. The results showed that there were significantly higher numbers of $F4/80^+$ cells and $CD68^+$ cells in tumors with YB1 injection than the control group (**Figures 4D, E**). In addition, the results showed there was an increased number of the $iNOS^+$ cells in the immunohistochemical slices of YB1 injected tumors (**Figure 4F**). This result consisted with the observation in the above proteomics data, where the iNOS was upregulated at 2 days post YB1 injection (**Figure 4F**, **Supplementary Table 5**). These results further confirmed our proteomic analysis results.

Then we detected another two typical phagocytes, neutrophils and dendritic cells (DCs). We detected the expression of Ly6G and CD11c in the tumor slices. Ly6G is a marker for monocytes, granulocytes and neutrophils. CD11c is the most widely used defining marker for dendritic cells (DCs). The results showed that there was more $Ly6G^+$ cells in tumors with YB1 injection than the control group. But there was no significant difference of the $CD11c^+$ cell number in these two groups (**Figures 4C, G**). These results indicate that the YB1 could induce neutrophils and macrophages gathering, which mediated phagocytosis in tumors. In addition, iNOS is often used as a marker of M1-like macrophages (36), its upregulation may indicate the possible enrichment of M1 macrophages.

T Cells Accumulated at the Invasion Margin of the Tumor After YB1 Treatment

In our proteomics data, the positive regulation of T cell proliferation was significantly upregulated at 7days post YB1 injection. To further confirm this result, we performed the immunohistochemical staining to the CD3 of the T cells in the mice tumor sections. The CD3 protein complex is a defining feature of T cell lineage. Compared to the tumors in the control group, we found that the T cells in the tumors with YB1 injection accumulated at the invasion margin of the tumors, and the $CD3^+$ T cells in the tumors with PBS injection tend to congregate at the tumor center. And the number of T cells at the margin area in YB1 injection group was significantly higher than that in the control group (**Figure 5A**). As previously reported, the location of T cells, such as at the invasive margin, rather than the center of the tumor, is an important positive predictor of outcome (37, 38). These results may indicate a good prognosis of the tumors with YB1 injection. Moreover, we compared the antitumor effects of $CD8^+$ T cells in the spleens of the YB1 treated and control mice. The $CD8^+$ T cells were isolated from mice spleen and stimulated with MB49 mouse bladder tumor cells for 18 hours. IFN-γ secreted by spleen $CD8^+$ T cells was measured through IFN-γ ELISpot assay. We found that the IFN-γ secretion by the spleen $CD8^+$ T cells in the YB1 treated mice was significantly higher than that in the control group (**Figure 5B**). These results indicate YB1 could promote the antitumor T cell effects in the tumor-bearing mice.

B Cells Accumulated in the Tumor After YB1 Treatment

At two weeks after YB1 treatment, the B cells related signaling pathways were activated in the proteomics profiling. We detected the expression of CD19, a biomarker for normal and neoplastic B cells, in YB1 injected mice tumors at 14 days. The results showed that there were more $CD19^+$ B cells in the YB1 injected mice tumor than the control group (**Figure 5C**). These results demonstrate that *Salmonella* YB1 strain could induce the recruitment of B cells in tumors.

DISCUSSION

The development of a "perfect" bacteria strain for cancer therapy relies greatly on the understanding of host–bacteria interactions (32). Our tumor proteome profiling systematically revealed the dynamics of the tumor proteome after YB1 treatment, which can be beneficial for uncovering the underlying immunological mechanism of YB1-mediated tumor shrink. Nevertheless, this global proteomics approach cannot distinguish proteins from different cell types, therefore, the IHC staining were applied on tumor section images to validate the enrichment of several key marker proteins in the YB1-treated group. Furthermore, the IHC staining can also provide the information on the spatial distribution of various types of cells within tumors. Overall, our present study demonstrated three distinct stages of immune responses induced by YB1 in tumors: the complement and coagulation activation, phagocytosis mediated by macrophage and neutrophils, and T-cell infiltration at the invasion margin of the tumor (**Figure 6**), revealing the complexity of YB1-mediated tumor response at the proteome level.

Our analyses indicate that the complement and blood coagulation pathways were activated soon after YB1 injection. The complement serves as a functional bridge between innate and adaptive immune response that allows an integrated host defense to pathogenic challenges (39). More importantly, angiolysis and thrombosis were observed in the tumors with YB1 treatment. In response to bacteria injection, the innate immune cells and platelets cooperate to induce blood coagulation, which block the nutrition supplement in tumors (33). In addition, YB1 in the tumor anaerobic region could still proliferate robustly and compete with the tumor cells for nutrition (40). It appears that these processes could play important roles in the anti-tumor effects induced by YB1. An independent experiment would be required to validate the phenomena we observed.

Probably due to the presence of the complement component (41) and YB1 aggregation in the anaerobic region, the macrophages and neutrophils are recruited into the tumor to mediate the immune response like phagocytosis. Particularly it is noteworthy that the $iNOS^+$ and $CD68^+$ cells in the tumors with YB1 treatment was higher than the control group, which may suggest that YB1 could

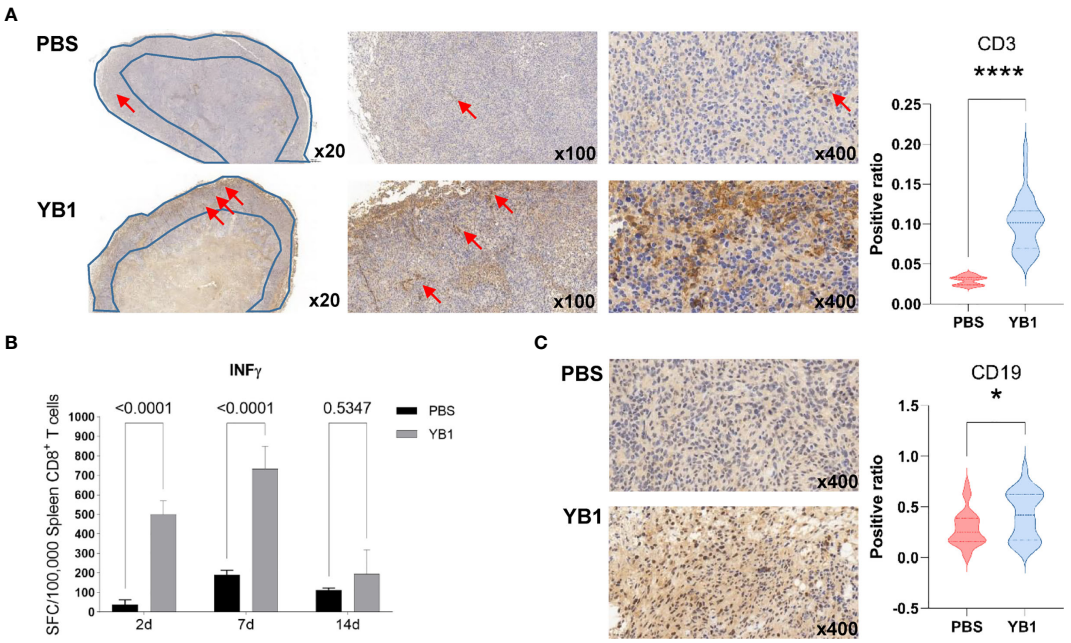

FIGURE 5 | *Salmonella* YB1 induced the adaptive immune responses in tumors. **(A)** Representative images of immunohistochemical stained tumor slices collected from mice injected with phosphate-buffered saline (PBS) or YB1 at 7 days post injection. The area of the blue polygon indicates the invasive margin of the tumor, the red arrow represents $CD3^+$ T cells. An S/N ratio of $CD3^+$ cells in the invasion margin of tumors. **(B)** $CD8^+$ T cells from YB1 (gray) and PBS (black) treated mice spleen were stimulated by MB49 cells. The background value of IFN-γ expression of $CD8^+$ T cells has been removed. IFN-γ ELISpot results of three replicates are expressed as mean SFC (IFN-γ-specific spot-forming cells)/100,000 $CD8^+$ T cells. Error bars represent standard deviations. Statistical analysis was performed using the two-way ANOVA with Šidák's multiple comparisons test. **(C)** A ratio of $CD19^+$ cells versus total cell numbers in the tumors. Statistical analysis in **(A, C)** was performed using the K–S test. $^*p < 0.05$, $^{****}p < 0.0001$.

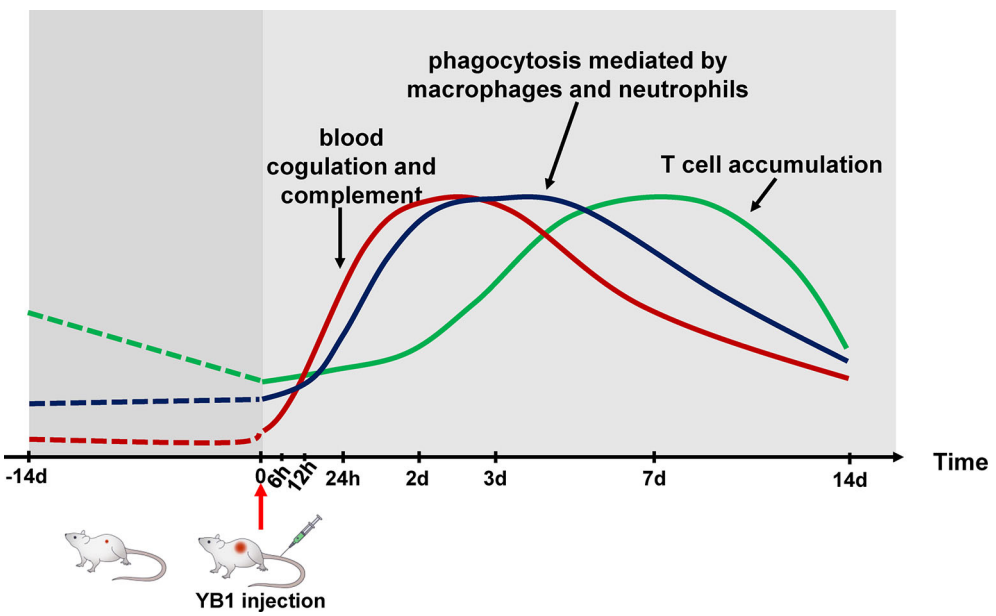

FIGURE 6 | Schematic temporal dynamics of the immunological offensive triggered by YB1 treatment. The red line represents the blood coagulation and complement. The blue line represents phagocytosis mediated by macrophages and neutrophils. The green line represents T cell accumulation in the invasion margin.

induce anti-tumor effects through improving the infiltration of M1-like macrophages in tumors, though the definition and biological functions of macrophage subpopulations are still under debate (42, 43). It is well known that M1 macrophages play critical roles in innate host defense and killing tumor cells by producing reactive oxygen/nitrogen species (ROS/RNS) and pro-inflammatory cytokines, and hence they are considered as antitumor or "good" macrophages (44, 45). On the other hand, it is worth to note that several inflammatory stimuli can induce the expression of iNOS in various cell types including macrophages, dendritic cells and neutrophils (46–48), the overexpression of iNOS alone does not necessarily indicate the enrichment of M1-like macrophages. Therefore, the reshaping of macrophage subpopulation induced by YB1 remains to be explored further. For the dendritic cells, we did not find the significant difference of the number of $CD11c^+$ cells between the YB1 and PBS injection tumors. However, in view of the different subtypes of DCs exhibit differential pro-tumorigenic or anti-tumorigenic functions (49), the contribution of DCs in the bacteria mediated immunotherapy is still to be explored.

As antigen presenting cells, macrophages can present the tumor specific antigens to T cells. In a previous study, the authors demonstrated that the induction of antigen presentation by tumor associated macrophages enhances the accumulation of specific $CD8^+$ T cells at the tumor site (50). Furthermore, we found that INF-γ production of spleen $CD8^+$ T cells were enhanced after tumor cell challenge, in YB1 treated mice. In addition, the $CD3^+$ T cells in the tumors with YB1 treatment accumulated significantly at the invasion margin. As previously described, the presence of T cells at the invasive margin, rather than the center of the tumor, is an important positive predictor of outcome (37, 38). But the mechanism involved in this interplay remains to be investigated.

For collagen in tumors, in our proteomic data, the type I, VI and VII collagens were down regulated. And it was reported that the upregulation of these types of collagen are correlated with the tumor metastasis (51–53). So we hypothesized that the downregulation of the collagen might be involved in the YB1 mediated tumor metastasis inhibition, which could help to explain the reduction of tumor metastasis in YB1 treated tumors (17, 20).

Although bacteria-mediated tumor therapy could be recognized as the oldest type of cancer immunotherapy, its proper clinical application still needs to fulfill very strict requirements of safety and efficacy in both mechanistic and large scale (pre-)clinical studies (8, 54). Early bacteria-based antitumor drug like Coley's toxin was made of natural pathogen, which showed clear efficacy against multiple types of tumor but suffered from toxicity (4, 8). Nearly Two decades ago, the attenuated salmonella VNP20009 was approved to enter a phase I clinical trial, in which its safety was clearly proved but efficacy was insignificant (55). These days, the emerging synthetic biology technology provided more possibilities for engineering both safe and efficient antitumor bacteria, and combining the synthetic bacteria with other tumor killing agents (13, 15, 54, 56, 57). These advances together shed a light on the future of understanding and applying the bacteria-mediated tumor therapy clinically.

According to our previous studies, YB1 significantly improved the survival rate of tumor-bearing mice in various solid tumor models. On the other hand, in term of safety, YB1 can induce moderate inflammation in the liver and spleen. Nevertheless, within 7 days, the bacteria can be effectively cleared from normal organs (13–17). Furthermore, in a recent study, Lin Q et al. extended the YB1-treatment to several other experimental metastasis models, and found that YB1 has potent suppressive effects on cancer metastasis *via* the host innate immunity (32). Taking all these together, engineered *Salmonella* mediated cancer therapy could be an promising and safe strategy in the future, due to its characteristics including proliferation only in tumors, self-targeting and ease of genetic manipulation (58). Systemic understanding of the curing mechanisms will accelerate its development and application in clinical settings.

In summary, we used a proteomics approach to quantify the temporal changes of the bladder tumor proteome during *Salmonella* YB1 treatment. And the reliability of the proteomics results was verified by the immunohistochemical analysis. We profiled the immunological triple offensive, blood coagulation and complement, phagocytosis, and T-cell infiltration at the tumor invasion margin induced by *Salmonella* YB1, and demonstrate the temporal dynamics of these processes. Our study demonstrated the proteomics technique shows great promises in elucidating mechanisms underlying bacteria mediated immunotherapy.

DATA AVAILABILITY STATEMENT

The original contributions presented in the study are publicly available. This data can be found here: https://www.ebi.ac.uk/pride/, PXD026288.

ETHICS STATEMENT

The animal study was reviewed and approved by Shenzhen Institutes of Advanced Technology Chinese Academy of Sciences Committee on Animal Care.

AUTHOR CONTRIBUTIONS

Conceptualization was carried out by CL, JH, XL, PY, and NL. Investigation was done by SY, WZ, WW, and NL (proteomics), and by SY, MJ, ZZ, JH, and CL (immunohistochemistry, biochemistry and animal experiments), MZ, HH, XL, JB, and PY (data analysis and statistics). The article was written by SY, WZ, MZ, and NL with input from all authors. The figures were made by SY, WZ, MZ, and HH, with input from XL, PY, and NL. The study was supervised by CL, JH, XL, PY and NL. Funding acquisition was carried out by NL and PY. All authors contributed to the article and approved the submitted version.

FUNDING

The research was supported by the National Key Research and Development Program of China (2018YFA0902703), the National Natural Science Foundation of China (11801542 31800694 and 31971354), the Natural Science Foundation of Guangdong Province (2020B1515120034), and the Shenzhen Science and Technology Innovation Committee (JCYJ20170818164014753, JCYJ20180507182250795, and JCYJ20180302145723601).

ACKNOWLEDGMENTS

We would like to thank Diana V. Czuchry for English language editing.

SUPPLEMENTARY MATERIAL

The Supplementary Material for this article can be found online at: https://www.frontiersin.org/articles/10.3389/fimmu.2021.712936/full#supplementary-material

REFERENCES

1. Nguyen VH, Min J-J. Salmonella-Mediated Cancer Therapy: Roles and Potential. *Nucl Med Mol Imaging* (2017) 51(2):118–26. doi: 10.1007/s13139-016-0415-z
2. Minton NP. Clostridia in Cancer Therapy. *Nat Rev Microbiol* (2003) 1 (3):237–42. doi: 10.1038/nrmicro777
3. Coley WB. The Treatment of Inoperable Sarcoma by Bacterial Toxins (the Mixed Toxins of the Streptococcus Erysipelas and the Bacillus Prodigiosus). *Proc R Soc Med* (1910) 3(Surg Sect):1–48. doi: 10.1177/003591571000301601
4. McCarthy EF. The Toxins of William B. Coley and the Treatment of Bone and Soft-Tissue Sarcomas. *Iowa Orthop J* (2006) 26:154–8.
5. Morales A, Eidinger D, Bruce AW. Intracavitary Bacillus Calmette-Guerin in the Treatment of Superficial Bladder Tumors (Reprinted From J Urol, Vol 116, Pg 180-183, 1976). *J Urol* (2002) 167(2):891–3. doi: 10.1016/S0022-5347(17)58737-6
6. Shintani Y, Sawada Y, Inagaki T, Kohjimoto Y, Uekado Y, Shinka T. Intravesical Instillation Therapy With Bacillus Calmette-Guerin for Superficial Bladder Cancer: Study of the Mechanism of Bacillus Calmette-Guerin Immunotherapy. *Int J Urol* (2007) 14(2):140–6. doi: 10.1111/j.1442-2042.2007.01696.x
7. Connell HC. The Study and Treatment of Cancer by Proteolytic Enzymes: Preliminary Report. *Can Med Assoc J* (1935) 33(4):364–70. doi: 10.1186/1746-1596-2-8
8. Duong MT-Q, Qin Y, You S-H, Min J-J. Bacteria-Cancer Interactions: Bacteria-Based Cancer Therapy. *Exp Mol Med* (2019) 51(12):1–15. doi: 10.1038/s12276-019-0297-0
9. Zhou S, Gravekamp C, Bermudes D, Liu K. Tumour-Targeting Bacteria Engineered to Fight Cancer. *Nat Rev Cancer* (2018) 18(12):727–43. doi: 10.1038/s41568-018-0070-z
10. Avogadri F, Martinoli C, Petrovska L, Chiodoni C, Transidico P, Bronte V, et al. Cancer Immunotherapy Based on Killing of Salmonella-Infected Tumor Cells. *Cancer Res* (2005) 65(9):3920–7. doi: 10.1158/0008-5472.CAN-04-3002
11. Low KB, Ittensohn M, Le T, Platt J, Sodi S, Amoss M, et al. Lipid A Mutant Salmonella With Suppressed Virulence and Tnfα Induction Retain Tumor-Targeting *In Vivo*. *Nat Biotechnol* (1999) 17(1):37–41. doi: 10.1038/5205
12. Zheng JH, Nguyen VH, Jiang S-N, Park S-H, Tan W, Hong SH, et al. Two-Step Enhanced Cancer Immunotherapy With Engineered Salmonella Typhimurium Secreting Heterologous Flagellin. *Sci Trans Med* (2017) 9 (376):eaak9537. doi: 10.1126/scitranslmed.aak9537
13. Chen F, Zang Z, Chen Z, Cui L, Chang Z, Ma A, et al. Nanophotosensitizer-Engineered Salmonella Bacteria With Hypoxia Targeting and Photothermal-Assisted Mutual Bioaccumulation for Solid Tumor Therapy. *Biomaterials* (2019) 214:119226. doi: 10.1016/j.biomaterials.2019.119226
14. Yu B, Yang M, Shi L, Yao Y, Jiang Q, Li X, et al. Explicit Hypoxia Targeting With Tumor Suppression by Creating an "Obligate" Anaerobic Salmonella Typhimurium Strain. *Sci Rep* (2012) 2:436–6. doi: 10.1038/srep00436
15. Guo Z-L, Yu B, Ning B-T, Chan S, Lin Q-B, Li JC-B, et al. Genetically Modified "Obligate" Anaerobic Salmonella Typhimurium as a Therapeutic Strategy for Neuroblastoma. *J Hematol Oncol* (2015) 8:99–9. doi: 10.1186/s13045-015-0196-3
16. Ning BT, Yu B, Chan S, Chan JL, Huang JD, Chan GC. Treatment of Neuroblastoma With an Engineered "Obligate" Anaerobic Salmonella Typhimurium Strain Yb1. *J Cancer* (2017) 8(9):1609–18. doi: 10.7150/jca.18776
17. Li CX, Yu B, Shi L, Geng W, Lin QB, Ling CC, et al. 'Obligate' Anaerobic Salmonella Strain YB1 Suppresses Liver Tumor Growth and Metastasis in Nude Mice. *Oncol Lett* (2017) 13(1):177–83. doi: 10.3892/ol.2016.5453
18. Lin Q, Rong L, Jia X, Li R, Yu B, Hu J, et al. IFN-γ-Dependent NK Cell Activation is Essential to Metastasis Suppression by Engineered Salmonella. *Nat Commun* (2021) 12(1):2537. doi: 10.1038/s41467-021-22755-3
19. Mo Y, Wang Y, Xiong F, Ge X, Li Z, Li X, et al. Proteomic Analysis of the Molecular Mechanism of Lovastatin Inhibiting the Growth of Nasopharyngeal Carcinoma Cells. *J Cancer* (2019) 10(10):2342–9. doi: 10.7150/jca.30454
20. Selkrig J, Li N, Hausmann A, Mangan MSJ, Zietek M, Mateus A, et al. Spatiotemporal Proteomics Uncovers Cathepsin-Dependent Macrophage Cell Death During Salmonella Infection. *Nat Microbiol* (2020) 5(9):1119–33. doi: 10.1038/s41564-020-0736-7
21. Wang Y, Chiu J-F. Proteomic Approaches in Understanding Action Mechanisms of Metal-Based Anticancer Drugs. *Metal-Based Drugs 2008* (2008) p:716329–9. doi: 10.1155/2008/716329
22. Wessel D, Flugge UI. A Method for the Quantitative Recovery of Protein in Dilute Solution in the Presence of Detergents and Lipids. *Anal Biochem* (1984) 138(1):141–3. doi: 10.1016/0003-2697(84)90782-6
23. Maechler MCluster analysis extended Rousseeuw, et al. (2013). R CRAN.
24. Pham N-A, Morrison A, Schwock J, Aviel-Ronen S, Iakovlev NV, Tsao M-S, et al. Quantitative Image Analysis of Immunohistochemical Stains Using a CMYK Color Model. *Diagn Pathol* (2007) 2:8–8. doi: 10.1186/1746-1596-2-8
25. Zhang K, Zhang L, Song H, Zhou W. Active Contours With Selective Local or Global Segmentation: A New Formulation and Level Set Method. *Image Vision Computing* (2010) 28(4):668–76. doi: 10.1016/j.imavis.2009.10.009
26. Brown JM, Wilson WR. Exploiting Tumour Hypoxia in Cancer Treatment. *Nat Rev Cancer* (2004) 4(6):437–47. doi: 10.1038/nrc1367
27. Lardner A. The Effects of Extracellular pH on Immune Function. *J Leukoc Biol* (2001) 69(4):522–30. doi: 10.1189/jlb.69.4.522
28. Gangloff SC, Zahringer U, Blondin C, Guenounou M, Silver J, Goyert SM. Influence of CD14 on Ligand Interactions Between Lipopolysaccharide and Its Receptor Complex. *J Immunol* (2005) 175(6):3940–5. doi: 10.4049/jimmunol.175.6.3940
29. Connelly L, Palacios-Callender M, Ameixa C, Moncada S, Hobbs AJ. Biphasic Regulation of NF-Kappa B Activity Underlies the Pro- and Anti-Inflammatory Actions of Nitric Oxide. *J Immunol* (2001) 166(6):3873–81. doi: 10.4049/jimmunol.166.6.3873
30. Xie Q, Klesney-Tait J, Keck K, Parlet C, Borcherding N, Kolb R, et al. Characterization of a Novel Mouse Model With Genetic Deletion of CD177. *Protein Cell* (2015) 6(2):117–26. doi: 10.1007/s13238-014-0109-1
31. Boutte AM, Friedman DB, Bogyo M, Min Y, Yang L, Lin PC. Identification of a Myeloid-Derived Suppressor Cell Cystatin-Like Protein That Inhibits Metastasis. *FASEB J* (2011) 25(8):2626–37. doi: 10.1096/fj.10-180604
32. Lin Q, Rong L, Jia X, Li R, Yu B, Hu J, et al. IFN-Gamma-Dependent NK Cell Activation is Essential to Metastasis Suppression by Engineered Salmonella. *Nat Commun* (2021) 12(1):2537. doi: 10.1038/s41467-021-22755-3
33. Yi X, Zhou H, Chao Y, Xiong S, Zhong J, Chai Z, et al. Bacteria-Triggered Tumor-Specific Thrombosis to Enable Potent Photothermal Immunotherapy of Cancer. *Sci Adv* (2020) 6(33):eaba3546. doi: 10.1126/sciadv.aba3546
34. Allendorf DJ, Yan J, Ross GD, Hansen RD, Baran JT, Subbarao K, et al. C5a-Mediated Leukotriene B4-Amplified Neutrophil Chemotaxis is Essential in

Tumor Immunotherapy Facilitated by Anti-Tumor Monoclonal Antibody and β-Glucan. *J Immunol* (2005) 174(11):7050–6. doi: 10.4049/jimmunol.174.11.7050
35. Benoit ME, Clarke EV, Morgado P, Fraser DA, Tenner AJ. Complement Protein C1q Directs Macrophage Polarization and Limits Inflammasome Activity During the Uptake of Apoptotic Cells. *J Immunol* (2012) 188 (11):5682–93. doi: 10.4049/jimmunol.1103760
36. Orecchioni M, Ghosheh Y, Pramod AB, Ley K. Corrigendum: Macrophage Polarization: Different Gene Signatures in M1(LPS+) vs. Classically and M2 (LPS-) vs. Alternatively Activated Macrophages. *Front Immunol* (2020) 11:234. doi: 10.3389/fimmu.2020.00234
37. Munoz-Erazo L, Rhodes JL, Marion VC, Kemp RA. Tertiary Lymphoid Structures in Cancer - Considerations for Patient Prognosis. *Cell Mol Immunol* (2020) 17(6):570–5. doi: 10.1038/s41423-020-0457-0
38. Pagès F, Mlecnik B, Marliot F, Bindea G, Ou F-S, Bifulco C, et al. International Validation of the Consensus Immunoscore for the Classification of Colon Cancer: A Prognostic and Accuracy Study. *Lancet* (2018) 391(10135):2128–39. doi: 10.1016/S0140-6736(18)30789-X
39. Dunkelberger JR, Song W-C. Complement and its Role in Innate and Adaptive Immune Responses. *Cell Res* (2010) 20(1):34–50. doi: 10.1038/cr.2009.139
40. Wall DM, Srikanth CV, McCormick BA. Targeting Tumors With Salmonella Typhimurium- Potential for Therapy. *Oncotarget* (2010) 1(8):721–8. doi: 10.18632/oncotarget.206
41. Zhang R, Liu Q, Li T, Liao Q, Zhao Y. Role of the Complement System in the Tumor Microenvironment. *Cancer Cell Int* (2019) 19(1):300. doi: 10.1186/s12935-019-1027-3
42. Murray PJ, Allen JE, Biswas SK, Fisher EA, Gilroy DW, Goerdt S, et al. Macrophage Activation and Polarization: Nomenclature and Experimental Guidelines. *Immunity* (2014) 41(1):14–20. doi: 10.1016/j.immuni.2014.06.008
43. Noy R, Pollard JW. Tumor-Associated Macrophages: From Mechanisms to Therapy. *Immunity* (2014) 41(1):49–61. doi: 10.1016/j.immuni.2014.06.010
44. Jeannin P, Paolini L, Adam C, Delneste Y. The Roles of CSF s on the Functional Polarization of Tumor-Associated Macrophages. *FEBS J* (2018) 285(4):680–99. doi: 10.1111/febs.14343
45. Chen Y, Song Y, Du W, Gong L, Chang H, Zou Z. Tumor-Associated Macrophages: An Accomplice in Solid Tumor Progression. *J Biomed Sci* (2019) 26(1):78. doi: 10.1186/s12929-019-0568-z
46. Sonar SA, Lal G. The iNOS Activity During an Immune Response Controls the CNS Pathology in Experimental Autoimmune Encephalomyelitis. *Front Immunol* (2019) 10:710. doi: 10.3389/fimmu.2019.00710
47. Saini R, Patel S, Saluja R, Sahasrabuddhe A, Singh M, Habib S, et al. Nitric Oxide Synthase Localization in the Rat Neutrophils: Immunocytochemical, Molecular, and Biochemical Studies. *J Leukocyte Biol* (2006) 79(3):519–28. doi: 10.1189/jlb.0605320
48. Jaramillo M, Gowda DC, Radzioch D, Olivier M. Hemozoin Increases IFN-γ-Inducible Macrophage Nitric Oxide Generation Through Extracellular Signal-Regulated Kinase-and NF-κb-Dependent Pathways. *J Immunol* (2003) 171 (8):4243–53. doi: 10.4049/jimmunol.171.8.4243
49. Ma Y, Shurin GV, Peiyuan Z, Shurin MR. Dendritic Cells in the Cancer Microenvironment. *J Cancer* (2013) 4(1):36–44. doi: 10.7150/jca.5046
50. Muraoka D, Seo N, Hayashi T, Tahara Y, Fujii K, Tawara I, et al. Antigen Delivery Targeted to Tumor-Associated Macrophages Overcomes Tumor Immune Resistance. *J Clin Invest* (2019) 129(3):1278–94. doi: 10.1172/JCI97642
51. Nissen NI, Karsdal M, Willumsen N. Collagens and Cancer Associated Fibroblasts in the Reactive Stroma and its Relation to Cancer Biology. *J Exp Clin Cancer Res: CR* (2019) 38(1):115–5. doi: 10.1186/s13046-019-1110-6
52. Karagiannis GS, Petraki C, Prassas I, Saraon P, Musrap N, Dimitromanolakis A, et al. Proteomic Signatures of the Desmoplastic Invasion Front Reveal Collagen Type XII as a Marker of Myofibroblastic Differentiation During Colorectal Cancer Metastasis. *Oncotarget* (2012) 3(3):267–85. doi: 10.18632/oncotarget.451
53. Liu J, Shen JX, Wu HT, Li XL, Wen XF, Du CW, et al. Collagen 1a1 (COL1A1) Promotes Metastasis of Breast Cancer and Is a Potential Therapeutic Target. *Discov Med* (2018) 25(139):211–23.
54. Lou XY, Chen ZC, He ZG, Sun MC, Sun J. Bacteria-Mediated Synergistic Cancer Therapy: Small Microbiome Has a Big Hope. *Nano-Micro Lett* (2021) 13(1):37. doi: 10.1007/s40820-020-00560-9
55. Toso JF, Gill VJ, Hwu P, Marincola FM, Restifo NP, Schwartzentruber DJ, et al. Phase I Study of the Intravenous Administration of Attenuated Salmonella Typhimurium to Patients With Metastatic Melanoma. *J Clin Oncol* (2002) 20(1):142–52. doi: 10.1200/JCO.20.1.142
56. Din MO, Danino T, Prindle A, Skalak M, Selimkhanov J, Allen K, et al. Synchronized Cycles of Bacterial Lysis for *In Vivo* Delivery. *Nature* (2016) 536 (7614):81–5. doi: 10.1038/nature18930
57. Ho CL, Tan HQ, Chua KJ, Kang A, Lim KH, Ling KL, et al. Engineered Commensal Microbes for Diet-Mediated Colorectal-Cancer Chemoprevention. *Nat Biomed Eng* (2018) 2(1):27–37. doi: 10.1038/s41551-017-0181-y
58. Mi Z, Feng Z-C, Li C, Yang X, Ma M-T, Rong P-F, et al. Salmonella-Mediated Cancer Therapy: An Innovative Therapeutic Strategy. *J Cancer* (2019) 10 (20):4765–76. doi: 10.7150/jca.32650

Conflict of Interest: The authors declare that the research was conducted in the absence of any commercial or financial relationships that could be construed as a potential conflict of interest.

Publisher's Note: All claims expressed in this article are solely those of the authors and do not necessarily represent those of their affiliated organizations, or those of the publisher, the editors and the reviewers. Any product that may be evaluated in this article, or claim that may be made by its manufacturer, is not guaranteed or endorsed by the publisher.

frontiers in Immunology

CASE REPORT
published: 26 October 2021
doi: 10.3389/fimmu.2021.728750

Axitinib Reverses Resistance to Anti-Programmed Cell Death-1 Therapy in a Patient With Renal Cell Carcinoma

Yonghao Yang, Hao Huang, Tiepeng Li, Quanli Gao, Yongping Song and Zibing Wang**

Department of Immunotherapy, Affiliated Cancer Hospital of Zhengzhou University & Henan Cancer Hospital, Zhengzhou, China

OPEN ACCESS

Edited by:
Xuanming Yang, Shanghai Jiao Tong University, China

Reviewed by:
Lu Si, Peking University Cancer Hospital, China
Deng Liufu, Shanghai Jiao Tong University, China
Graham Robert Leggatt, The University of Queensland, Australia

***Correspondence:**
Zibing Wang
zlyywzb2118@zzu.edu.cn
Yongping Song
songyongping001@126.com

Specialty section:
This article was submitted to Cancer Immunity and Immunotherapy, a section of the journal Frontiers in Immunology

Received: *22 June 2021*
Accepted: *11 October 2021*
Published: *26 October 2021*

Citation:
Yang Y, Huang H, Li T, Gao Q, Song Y and Wang Z (2021) Axitinib Reverses Resistance to Anti-Programmed Cell Death-1 Therapy in a Patient With Renal Cell Carcinoma. Front. Immunol. 12:728750. doi: 10.3389/fimmu.2021.728750

Owing to broad and notable clinical anti-tumor activity, anti-programmed cell death-1 (PD-1)/anti-programmed cell death-ligand 1 (PD-L1) antibodies have been indicated for almost all types of cancer, and form a part of the current standard of care. However, a large proportion of patients do not respond to anti-PD-1/PD-L1 therapy (primary resistance), and responders often develop progressive disease (acquired resistance). The mechanisms of resistance are complex and largely unknown; therefore, overcoming resistance remains clinically challenging, and data on reversing anti-PD-1 resistance are scarce. Herein, we report the case of a 58-year-old woman with renal cell carcinoma associated with Xp11.2 translocation/transcription factor E3 gene fusion, who had already showed resistance to both anti-PD-1 monotherapy and standard-dose axitinib. However, she finally achieved a partial response with a continuous combination therapy comprising low-dose axitinib and anti-PD-1. We speculate that axitinib played a key role in reversing the primary resistance to anti-PD-1 therapy. Interestingly, we observed that the number of peripheral regulatory T cells increased after the standard-dose axitinib therapy, with accompanied tumor enlargement; however, after the dose was reduced, the number of regulatory T cells decreased gradually, and the tumor regressed. We also reviewed relevant literature, which supported the fact that low-dose axitinib might be more beneficial than standard-dose axitinib in assisting immunotherapy. Given that this is a single-case report, the immunomodulatory effect of axitinib requires further investigation.

Keywords: anti-angiogenic, PD-1, immunotherapy, low-dose, resistance, axitinib

Abbreviations: AE, Adverse event; CT, Computed tomography; MDSCs, Myeloid-derived suppressor cells; ORR, Objective response rates; PD, Progressive disease; PD-1, Programmed cell death-1; PD-L1, Programmed cell death-ligand 1; PR, Partial response; RCC, Renal cell carcinoma; RECIST, Response evaluation criteria in solid tumors; STAT3, Signal transducer and activator of transcription 3; TKIs, Tyrosine kinase inhibitors; TME, Tumor microenvironment; Tregs, Regulatory T cells; VEGF, Vascular endothelial growth factor.

INTRODUCTION

There have been considerable advances in cancer immunotherapy in recent years, these are mainly due to in-depth studies on the programmed cell death protein 1 (PD-1)/programmed cell death-ligand 1 (PD-L1) pathway. Binding of PD-1 to its ligands on tumor cells suppresses T cells through a negative feedback loop, thereby leading to immune response evasion (1, 2). Antibodies targeting PD-1 or PD-L1 can block this inhibitory signaling pathway and reactivate the anti-tumor immune response. Presently, based on clinical data from many phase III clinical trials, an anti-PD-1 or anti-PD-L1 agent is part of the standard of care for most types of advanced malignancies (3).

Despite the broad and notable anti-tumor activity of anti-PD-1/PD-L1 antibodies, a large proportion of patients still do not respond to anti-PD-1/PD-L1 therapy (primary resistance), and the patients who respond to them would often develop tumor progression again (acquired resistance). With the rapid expansion of the population treated with anti-PD-1/PD-L1 antibodies, the issue of resistance to anti-PD-1 therapy is of increasing concern. The mechanisms of resistance are complex and largely unknown; therefore, overcoming resistance remains clinically challenging (4, 5), and data on reversing anti-PD-1 resistance are scarce. Herein, we present a case in which axitinib successfully reversed primary resistance to anti-PD-1 therapy in a patient with renal cell carcinoma (RCC) associated with Xp11.2 translocation/transcription factor E3 gene fusion (Xp11.2/TFE3). We also reviewed relevant literature on the subject.

CASE DESCRIPTION

The patient's treatment process is shown in **Figure 1**. A 58-year-old woman presented to our hospital in early July 2020 with pain in the left flank region, gross hematuria, and minor vaginal bleeding. Before this time, she was in good health and had no history of chronic diseases, such as hypertension, diabetes, and coronary heart disease. She was allergic to cephalosporin antibiotics, characterized by rashes. Enhanced whole-body computed tomography (CT) revealed an 8.6 × 7.2 × 6.5 cm left renal mass with obvious enhancement, which we highly suspected was a left renal carcinoma. Simultaneously, pelvic magnetic resonance imaging revealed a 7 × 7 mm nodule at the vaginal end. She underwent laparoscopic radical nephrectomy and vaginal mass resection on July 14, 2020. Results of the pathological investigations of specimens from the two sites were consistent for RCC associated with Xp11.2/TFE3, which is a rare type of RCC in adults and a pathology with a poor prognosis (6). There is currently no standard treatment for this rare type of RCC; therefore, an intra-departmental consultation was convened. This patient already had vaginal metastasis, which reflected the aggressive nature of the RCC. In the end, we agreed to start postoperative adjuvant treatment with sintilimab, which is an anti-PD-1 antibody that has been developed and approved in China. From July 26, 2020, our patient received sintilimab (200 mg) every 3 weeks.

Three months later, she presented with a moderate gradual-onset left abdominal pain, poor appetite, and fatigue. On October 22, 2020, a whole-body enhanced CT was performed and disease relapse was apparent with evidence of newly emerged multiple metastases in the abdominal cavity and liver (**Figures 2A–D**). Following further consultation, we switched her treatment to a combination treatment regimen comprising standard-dose axitinib (5 mg, twice daily) and sintilimab (200 mg, every 3 weeks) and discharged her from hospital. After about 6 weeks, she developed binocular pain that gradually worsened and affected her eyesight more severely on the left side. On December 19, 2020, she visited a local hospital and was

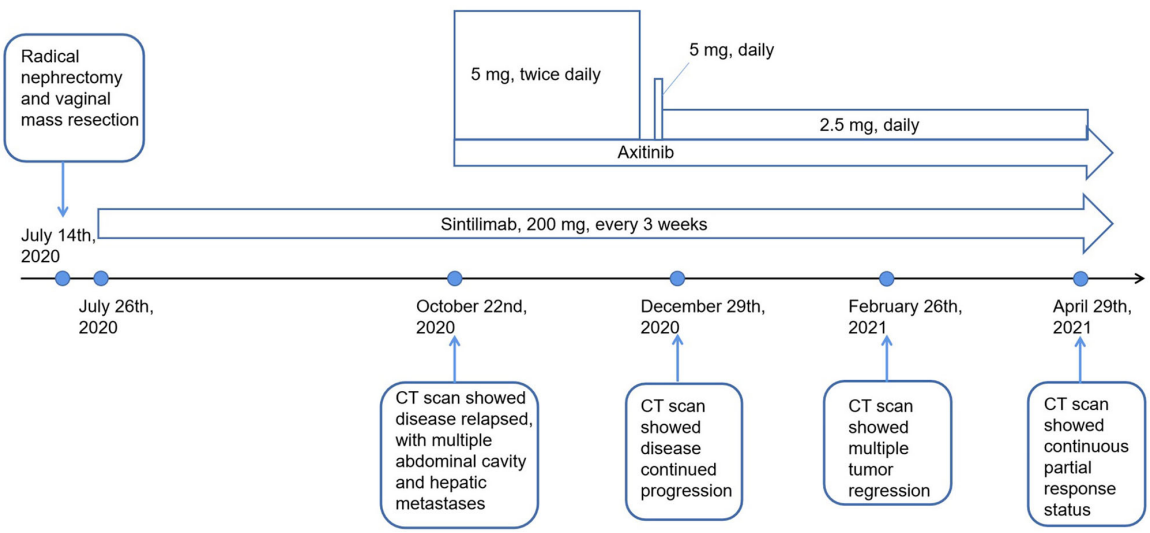

FIGURE 1 | Flow chart of patient's main management process.

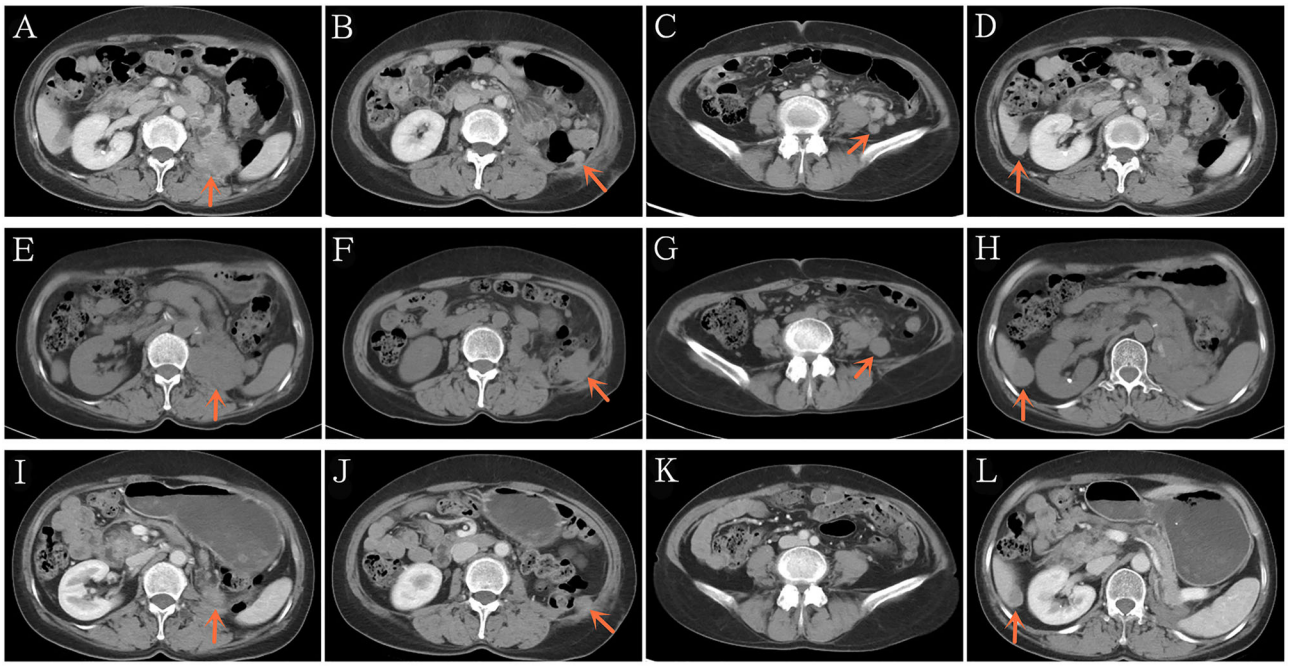

FIGURE 2 | Representative computed tomography showing recurrence after 3 months of post-operative adjuvant anti-PD-1 therapy **(A–D)**. Disease continued to progress after 2 additional months of standard-dose axitinib plus anti-PD-1 therapy **(E–H)**. Significant reduction in the tumor burden after 2 additional months of low-dose axitinib plus anti-PD-1 therapy **(I–L)**. PD-1/PD-L1, Programmed death-1/programmed death ligand-1.

diagnosed with iridocyclitis. She was prescribed three eye drops: pranoprofen, tobramycin plus dexamethasone, and atropine. Simultaneously, axitinib therapy was discontinued, following the doctor's advice. Five days later, her eye symptoms improved significantly. Due to concerns of tumor progression, she decided to restart axitinib therapy at a reduced dose of 5 mg daily. Three days later, the pain in her eyes returned; therefore, the axitinib dosage was reduced to 2.5 mg daily, after which the eye symptoms did not recur.

On December 29, 2020 (two months after treatment with axitinib plus sintilimab), she returned to our hospital for re-examination. Whole-body CT revealed progressive disease (PD), per the Response Evaluation Criteria in Solid Tumors (RECIST) 1.1 and when compared to the CT findings of October 22, 2020 (**Figures 2E–H**). These findings were supportive of the persistent abdominal pain and worsened asthenia she presented with. Since there was no particularly effective treatment regimen, and the patient had limited finances, she insisted that her previous regimen (sintilimab plus oral axitinib at a dose of 2.5 mg daily) should be continued. She was then discharged from the hospital.

We presumed that her condition would continue to gradually deteriorate, even to a life-threatening stage. However, 2 months post-discharge, on February 26, 2021, she re-visited our hospital. In the past two months, she felt that the abdominal pain has gradually relieved, her appetite and performance status have also improved. Subsequent CT revealed that the multiple metastases, including the hepatic metastases, had shrank significantly (**Figures 2I–L**), and a partial response (PR) had been achieved. To date, our patient is receiving treatment with sintilimab and axitinib at a dose of 2.5 mg daily. The most recent CT results confirmed her PR status.

DISCUSSION

Our patient received adjuvant treatment with anti-PD-1 therapy immediately after radical surgery. However, three months later, surveillance CT revealed multiple enhanced nodules in the abdominal cavity and liver, accompanied by clinical deterioration; this was consistent with disease relapse and resistance to anti-PD-1 therapy. Subsequently, she was administered rescue treatment with standard-dose axitinib and sintilimab for two months. However, the lesions increased significantly, and her clinical state worsened; this was assessed as PD per RECIST 1.1. This result confirmed the primary resistance to anti-PD-1 therapy and simultaneous resistance to standard-dose axitinib. After two additional months of continuous anti-PD-1 therapy and low-dose axitinib, she achieved PR, which has been observed till now. Therefore, we speculated that axitinib successfully reversed the primary resistance to anti-PD-1 therapy.

There are many studies that are consistent with our speculation: Despite the fact that the mechanisms of resistance to anti-PD-1/PD-L1 therapy are complex, and largely unknown, it is reported that the immunosuppressive tumor microenvironment (TME) plays an important role in

conveying resistance, and the mechanisms include hypoxia, increased inhibitory immune cells and immune molecules, and inhibition of immune-cell trafficking and infiltration (4, 7, 8). Interestingly, evidence from numerous preclinical studies suggests that anti-angiogenic agents such as bevacizumab and vascular endothelial growth factor receptor (VEGFR) tyrosine kinase inhibitors (TKIs) including axitinib, can improve the immunosuppressive TME significantly (9–13). Directly, anti-angiogenic therapies can inhibit immunosuppressive cells and molecules, and activate anti-tumor effector immune cells. For example, axitinib can hamper myeloid-derived suppressor cells (MDSCs) by downregulating signal transducer and activator of transcription 3 (STAT3) expression in murine RCC xenografts (9), and promote immune-mediated anti-tumor activity by promoting natural killer cell recognition and degranulation in human RCC cells (10). Indirectly, anti-angiogenic therapies can promote normalization of tumor vasculature, which includes reduction in the tortuosity of tumor vessels and interstitial fluid pressure, enhancement of vessel maturation, higher pericyte coverage, and normalization of the basement membrane. Eventually, these result in an alleviation of hypoxia and an increase in tumor-infiltrating lymphocytes. Therefore, even though axitinib did not exhibit any anti-tumor effect of itself after the initial two months' treatment, it may have assisted sintilimab in eliciting a powerful anti-tumor immune response, which resulted in subsequent tumor regression.

Given that anti-angiogenic agents are advantageous for immunotherapy, it raises an important issue: Is the dose in the drug notice optimal for them to act as immunopotentiators? Many clinical trials involving a combination of anti-angiogenic agents and anti-PD-1/PD-L1 antibodies in various types of cancers have been conducted. Now we summarized the relevant data in RCC (**Table 1**), in which anti-angiogenic agents were all administered at the dose in the drug notice. Based on clinical trial data, the objective response rates (ORRs) for the combination regimens were all significantly higher than those for single-agent treatment with multi-targeted VEGFR TKIs, such as sunitinib, sorafenib, axitinib, pazopanib, and lenvatinib. However, from a clinical perspective, it remains unclear whether anti-angiogenic agents enhance the immunotherapeutic effect of anti-PD-1/PD-L1 antibodies. Additionally, if this synergistic effect exists, it is unclear whether it has been fully exploited. As we know, except bevacizumab, both VEGFR TKIs and anti-PD-1/PD-L1 antibodies have shown a considerable single-agent efficacy for metastatic RCC, and more interestingly, the bevacizumab-based regimen was associated with the lowest ORR. Furthermore, no association has been observed between the expression of PD-L1 and outcomes in patients treated with axitinib plus pembrolizumab (16) or axitinib plus avelumab (17). Therefore, it is possible that the marked efficacy of the combination regimen was almost directly additive from that of the individual agents, or that the synergistic effect of anti-angiogenic agents on the anti-PD-1/PD-L1 antibodies in this combination regimen was limited. Furthermore, the combination regimens were often associated with severe toxicities, especially in the first three trials of pazopanil or sunitinib plus anti-PD-1 therapy (14, 15) (**Table 1**). With the severe toxicities, further phase III trials have been prohibited.

Our patient also experienced the treatment related adverse event (AE), iridocyclitis, and the dosage of axitinib was decreased to 2.5mg daily. Interestingly, the tumor remission occurred after the dose reduction, so we guess whether the dose reduction was related to the extraordinary efficacy. We retrospectively reviewed findings of the analysis of the patient's peripheral immune cells (**Supplementary Table S1**) during her treatment course and focused on the changes in regulatory T cells (Tregs), which are reportedly detrimental to anti-tumor immunity (20, 21). As shown in **Figure 3**, before the addition of axitinib, the level of Tregs was relatively low. Two months after the addition of standard-dose axitinib, the level of Tregs increased markedly, and after the dose reduction, the level of Tregs decreased gradually, accompanied by tumor regression. The increase in levels of peripheral Tregs was likely related to standard-dose axitinib, and it was likely that there was a better synergy between low-dose axitinib and sintilimab, which induced tumor regression without affecting the Tregs. Furthermore, two studies (22, 23) of murine models (Lewis lung carcinoma and syngeneic breast cancer) demonstrated that, only low-dose anti-VEGFR2 antibody or apatinib (a novel multi-targeted VEGFR2-TKI) could maximumly alleviate hypoxia, increase the infiltration and activation of immune cells, and eventually assist anti-PD-1 therapy to maximize the anti-tumor effect in mouse models, when compared to intermediate and high doses. One explanation for this phenomenon is that the high-dose anti-angiogenic agents can lead to shorter time-windows of normalization due to rapid and excessive pruning of tumor vessels, further restricting access into the tumor

TABLE 1 | Summary of clinical trials evaluating the combination of PD-1/PD-L1 inhibitors plus different anti-angiogenesis agents in treatment-naïve mRCC.

Phase	Number of patients	Regimen	ORR	PFS (months)	OS (months)	Grade 3-5 AEs
I/II	20	Pazopanib+pembrolizumab (14)	20-60%	NR	NR	90%
I	33	Sunitinib+nivolumab (15)	55.0%	12.7	NR	82.0%
I	20	Pazopanib+nivolumab (15)	45.0%	7.2	27.9	70.0%
III	432	Axitinib+pembrolizumab (16)	59.3%	15.1	NR	75.8%
III	442	Axitinib+avelumab (17)	56.0%	13.8	NR	71.2%
III	454	Bevacizumab+atezolizumab (18)	37.0%	11.2	33.6	40.0%
III	355	Lenvatinib+pembrolizumab (19)	71.0%	23.9	NR	82.4%

PD-1/PD-L1, Programmed death-1/programmed death ligand-1; mRCC, metastatic renal cell carcinomas; ORR, overall response rate; PFS, progression-free survival; OS, overall survival; AEs, adverse events; NR, not reported.

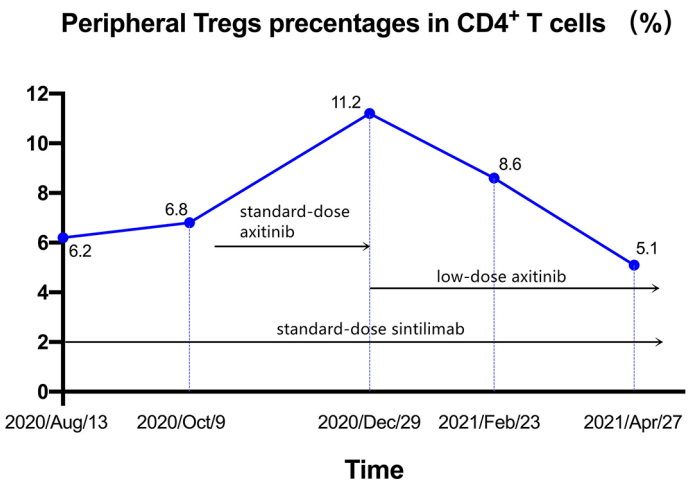

FIGURE 3 | Changes of peripheral Tregs percentages in $CD4^+$ T cells.

parenchyma to effector T cells. Moreover, this would result in more severe hypoxia, which will further worsen the immunosuppressive TME, and thus compromise the efficacy of immunotherapy (24). Contrarily, it is possible that vascular-normalizing lower doses of anti-angiogenic agents can better alleviate hypoxia, increase the infiltration of lymphocytes, and further enhance the efficacy of immunotherapy, with fewer side-effects.

Another issue worth discussing is the iridocyclitis, which is a rare AE of anti-PD-1 therapy (25), however, iridocyclitis is not a known AE of axitinib monotherapy. Interestingly, in our patient, the aggravation and mitigation of iridocyclitis was closely related to the re-initiation and dose reduction of axitinib, and the continuous treatment with sintilimab did not cause relapse of iridocyclitis. As an immune-suppressive pathway, PD-1/PD-L1 signaling is very important to the immunity homeostasis of the body (26). Therefore, we highly suspect that axitinib induced iridocyclitis in the context of anti-PD-1 therapy and was correlated with the axitinib dosage.

There are many anti-angiogenic agents currently in clinical use. Despite inhibition of the VEGF pathway being a common characteristic of them, they also possess considerable heterogeneity. Some of these agents are monoclonal antibodies, and some are TKIs with different targets that generate different biological effects and even have unknown properties. Nevertheless, based on clinical trial data, axitinib should be a preferred option in combination with immunotherapy. The combination regimen consisting of axitinib plus pembrolizumab/avelumab has been approved as a first-line treatment option for patients with metastatic RCC. Furthermore, promising outcomes (ORR, 67.5%; progression free survival, 7.5 months) were reported in a phase I trial (27) of axitinib plus toripalimab (an anti-PD-1 antibody) in patients with advanced mucosal melanoma, who reacted poorly to anti-PD-1 monotherapy.

In conclusion, this is the first report of axitinib successfully reversing primary resistance to anti-PD-1 therapy in a patient with RCC. It's worth noting that low-dose axitinib might be more beneficial than standard-dose axitinib in assisting immunotherapy. Given that this is a single-case report, the immunomodulatory effect of axitinib requires further investigation.

PATIENT PERSPECTIVE

A written informed consent for the publication has been obtained from the patient. From patient perspective, although she felt pain and weakness as the disease recurred and progressed, fortunately, she did not have too much fear and anxiety. She just insisted on treatment without paying too much attention to the effect of treatment.

DATA AVAILABILITY STATEMENT

The original contributions presented in the study are included in the article/**Supplementary Material**. Further inquiries can be directed to the corresponding authors.

ETHICS STATEMENT

The studies involving human participants were reviewed and approved by Henan Cancer Hospital Medical Ethics Committee. The patients/participants provided their written informed consent to participate in this study.

AUTHOR CONTRIBUTIONS

YY collected data and wrote the manuscript. ZW and YS conceived and corrected the manuscript. QG appraised and

edited the manuscript. TL and HH reviewed and edited the manuscript. All authors contributed to the article and approved the submitted version.

FUNDING

This work was supported by the Henan Medical Science and Technology Research Plan (Grant No. LHGJ20190646), the Medical Science and Technology Research Project of Health Commission of Henan Province (2018010033), and the Henan Provincial Scientific and Technological Project (212102310750). The funding bodies played no role in the design of the study; the collection, analysis, and interpretation of data; or manuscript preparation.

ACKNOWLEDGMENTS

We would like to thank the patient and her family for their cooperation. We would also like to thank Editage (www.editage.cn) for English language editing.

SUPPLEMENTARY MATERIAL

The Supplementary Material for this article can be found online at: https://www.frontiersin.org/articles/10.3389/fimmu.2021.728750/full#supplementary-material

REFERENCES

1. Iwai Y, Ishida M, Tanaka Y, Okazaki T, Honjo T, Minato N. Involvement of PD-L1 on Tumor Cells in the Escape From Host Immune System and Tumor Immunotherapy by PD-L1 Blockade. *Proc Natl Acad Sci USA* (2002) 99:12293–7. doi: 10.1073/pnas.192461099
2. Dong H, Strome SE, Salomao DR, Tamura H, Hirano F, Flies DB, et al. Tumor-Associated B7-H1 Promotes T-Cell Apoptosis: A Potential Mechanism of Immune Evasion. *Nat Med* (2002) 8:793–800. doi: 10.1038/nm730
3. Munari E, Mariotti FR, Quatrini L, Bertoglio P, Tumino N, Vacca P, et al. PD-1/PD-L1 in Cancer: Pathophysiological, Diagnostic and Therapeutic Aspects. *Int J Mol Sci* (2021) 22:5123. doi: 10.3390/ijms22105123
4. Weiss SA, Sznol M. Resistance Mechanisms to Checkpoint Inhibitors. *Curr Opin Immunol* (2021) 69:47–55. doi: 10.1016/j.coi.2021.02.001
5. Shergold AL, Millar R, Nibbs RJB. Understanding and Overcoming the Resistance of Cancer to PD-1/PD-L1 Blockade. *Pharmacol Res* (2019) 145:104258. doi: 10.1016/j.phrs.2019.104258
6. Armah HB, Parwani AV. Xp11.2 Translocation Renal Cell Carcinoma. *Arch Pathol Lab Med* (2010) 134:124–9. doi: 10.5858/2008-0391-RSR.1
7. Liu D, Jenkins RW, Sullivan RJ. Mechanisms of Resistance to Immune Checkpoint Blockade. *Am J Clin Dermatol* (2019) 20:41–54. doi: 10.1007/s40257-018-0389-y
8. Gide TN, Wilmott JS, Scolyer RA, Long GV. Primary and Acquired Resistance to Immune Checkpoint Inhibitors in Metastatic Melanoma. *Clin Cancer Res* (2018) 24:1260–70. doi: 10.1158/1078-0432.CCR-17-2267
9. Yuan H, Cai P, Li Q, Wang W, Sun Y, Xu Q, et al. Axitinib Augments Antitumor Activity in Renal Cell Carcinoma *via* STAT3-Dependent Reversal of Myeloid-Derived Suppressor Cell Accumulation. *BioMed Pharmacother* (2014) 68:751–6. doi: 10.1016/j.biopha.2014.07.002
10. Morelli MB, Amantini C, Santoni M, Soriani A, Nabissi M, Cardinali C, et al. Axitinib Induces DNA Damage Response Leading to Senescence, Mitotic Catastrophe, and Increased NK Cell Recognition in Human Renal Carcinoma Cells. *Oncotarget* (2015) 6:36245–59. doi: 10.18632/oncotarget.5768
11. Shigeta K, Datta M, Hato T, Kitahara S, Chen IX, Matsui A, et al. Dual Programmed Death Receptor-1 and Vascular Endothelial Growth Factor Receptor-2 Blockade Promotes Vascular Normalization and Enhances Antitumor Immune Responses in Hepatocellular Carcinoma. *Hepatology* (2020) 71:1247–61. doi: 10.1002/hep.30889
12. Hirsch L, Flippot R, Escudier B, Albiges L. Immunomodulatory Roles of VEGF Pathway Inhibitors in Renal Cell Carcinoma. *Drugs* (2020) 80:1169–81. doi: 10.1007/s40265-020-01327-7
13. Viallard C, Larrivee B. Tumor Angiogenesis and Vascular Normalization: Alternative Therapeutic Targets. *Angiogenesis* (2017) 20:409–26. doi: 10.1007/s10456-017-9562-9
14. Chowdhury S, Infante JR, Hawkins R, Voss MH, Perini R, Arkenau T, et al. Phase I/II Study to Assess the Safety and Efficacy of Pazopanib and Pembrolizumab Combination Therapy in Patients With Advanced Renal Cell Carcinoma. *Clin Genitourin Cancer* (2021) 19:434–46. doi: 10.1016/j.clgc.2021.04.007
15. Amin A, Plimack ER, Ernstoff MS, Lewis LD, Bauer TM, McDermott DF, et al. Safety and Efficacy of Nivolumab in Combination With Sunitinib or Pazopanib in Advanced or Metastatic Renal Cell Carcinoma: The Checkmate 016 Study. *J Immunother Cancer* (2018) 6:109. doi: 10.1186/s40425-018-0420-0
16. Rini BI, Plimack ER, Stus V, Gafanov R, Hawkins R, Nosov D, et al. Pembrolizumab Plus Axitinib *Versus* Sunitinib for Advanced Renal-Cell Carcinoma. *N Engl J Med* (2019) 380:1116–27. doi: 10.1056/NEJMoa1816714
17. Motzer RJ, Penkov K, Haanen J, Rini B, Albiges L, Campbell MT, et al. Avelumab Plus Axitinib *Versus* Sunitinib for Advanced Renal-Cell Carcinoma. *New Engl J Med* (2019) 380:1103–15. doi: 10.1056/NEJMoa1816047
18. Rini BI, Powles T, Atkins MB, Escudier B, McDermott DF, Suarez C, et al. Atezolizumab Plus Bevacizumab *Versus* Sunitinib in Patients With Previously Untreated Metastatic Renal Cell Carcinoma (Immotion151): A Multicentre, Open-Label, Phase 3, Randomised Controlled Trial. *Lancet* (2019) 393:2404–15. doi: 10.1016/S0140-6736(19)30723-8
19. Motzer R, Alekseev B, Rha SY, Porta C, Eto M, Powles T, et al. Lenvatinib Plus Pembrolizumab or Everolimus for Advanced Renal Cell Carcinoma. *N Engl J Med* (2021) 384:1289–300. doi: 10.1056/NEJMoa2035716
20. Linehan DC, Goedegebuure PS. CD25+ CD4+ Regulatory T-Cells in Cancer. *Immunol Res* (2005) 32:155–68. doi: 10.1385/IR:32:1-3:155
21. Sharma P, Hu-Lieskovan S, Wargo JA, Ribas A. Primary, Adaptive, and Acquired Resistance to Cancer Immunotherapy. *Cell* (2017) 168:707–23. doi: 10.1016/j.cell.2017.01.017
22. Li Q, Wang Y, Jia W, Deng H, Li G, Deng W, et al. Low-Dose Anti-Angiogenic Therapy Sensitizes Breast Cancer to PD-1 Blockade. *Clin Cancer Res* (2020) 26:1712–24. doi: 10.1158/1078-0432.CCR-19-2179
23. Zhao S, Ren S, Jiang T, Zhu B, Li X, Zhao C, et al. Low-Dose Apatinib Optimizes Tumor Microenvironment and Potentiates Antitumor Effect Of PD-1/PD-L1 Blockade in Lung Cancer. *Cancer Immunol Res* (2019) 7:630–43. doi: 10.1158/2326-6066.CIR-17-0640
24. Huang Y, Goel S, Duda DG, Fukumura D, Jain RK. Vascular Normalization as an Emerging Strategy to Enhance Cancer Immunotherapy. *Cancer Res* (2013) 73:2943–8. doi: 10.1158/0008-5472.CAN-12-4354
25. Haanen J, Carbonnel F, Robert C, Kerr KM, Peters S, Larkin J, et al. Management of Toxicities From Immunotherapy: ESMO Clinical Practice Guidelines for Diagnosis, Treatment and Follow-Up. *Ann Oncol* (2018) 29:v264–6. doi: 10.1093/annonc/mdy162
26. Buchbinder EI, Desai A. CTLA-4 and PD-1 Pathways: Similarities, Differences, and Implications of Their Inhibition. *Am J Clin Oncol* (2016) 39:98–106. doi: 10.1097/COC.0000000000000239
27. Sheng X, Yan X, Chi Z, Si L, Cui C, Tang B, et al. Axitinib in Combination With Toripalimab, a Humanized Immunoglobulin G4 Monoclonal Antibody Against Programmed Cell Death-1, in Patients With Metastatic Mucosal

Melanoma: An Open-Label Phase IB Trial. *J Clin Oncol* (2019) 37:2987–99. doi: 10.1200/JCO.19.00210

Conflict of Interest: The authors declare that the research was conducted in the absence of any commercial or financial relationships that could be construed as a potential conflict of interest.

Publisher's Note: All claims expressed in this article are solely those of the authors and do not necessarily represent those of their affiliated organizations, or those of the publisher, the editors and the reviewers. Any product that may be evaluated in this article, or claim that may be made by its manufacturer, Is not guaranteed or endorsed by the publisher.

frontiers in Immunology

REVIEW
published: 12 November 2021
doi: 10.3389/fimmu.2021.765906

Vitamin C, From Supplement to Treatment: A Re-Emerging Adjunct for Cancer Immunotherapy?

*Léonce Kouakanou[1], Christian Peters[2], Christine E. Brown[3], Dieter Kabelitz[2] and Leo D. Wang[1,4]**

[1] Department of Immuno-Oncology, Beckman Research Institute, City of Hope National Medical Center, Duarte, CA, United States, [2] Institute of Immunology, Christian-Albrechts University of Kiel and University Hospital Schleswig-Holstein, Kiel, Germany, [3] Department of Hematology and Hematopoietic Cell Transplantation, Beckman Research Institute, City of Hope National Medical Center, Duarte, CA, United States, [4] Department of Pediatrics, Beckman Research Institute, City of Hope National Medical Center, Duarte, CA, United States

Vitamin C (VitC), in addition to its role as a general antioxidant, has long been considered to possess direct anti-cancer activity at high doses. VitC acts through oxidant and epigenetic mechanisms, which at high doses can exert direct killing of tumor cells *in vitro* and delay tumor growth *in vivo*. Recently, it has also been shown that pharmacologic-dose VitC can contribute to control of tumors by modulating the immune system, and studies have been done interrogating the role of physiologic-dose VitC on novel adoptive cellular therapies (ACTs). In this review, we discuss the effects of VitC on anti-tumor immune cells, as well as the mechanisms underlying those effects. We address important unanswered questions concerning both VitC and ACTs, and outline challenges and opportunities facing the use of VitC in the clinical setting as an adjunct to immune-based anti-cancer therapies.

Keywords: immune checkpoint therapy (ICT), CAR (chimeric antigen receptor) T cells, vitamin C (ascorbic acid), cancer immunotherapies, cancer biology

OPEN ACCESS

Edited by:
Xuanming Yang,
Shanghai Jiao Tong University, China

Reviewed by:
Enrique J. Arenas,
Vall d'Hebron Institute of Oncology (VHIO), Spain
Jiao Wang,
Purdue University, United States
Gang Zhou,
Augusta University, United States

***Correspondence:**
Leo D. Wang
leo.wang@coh.org

Specialty section:
This article was submitted to Cancer Immunity and Immunotherapy, a section of the journal Frontiers in Immunology

Received: *27 August 2021*
Accepted: *08 October 2021*
Published: *12 November 2021*

Citation:
Kouakanou L, Peters C, Brown CE, Kabelitz D and Wang LD (2021) Vitamin C, From Supplement to Treatment: A Re-Emerging Adjunct for Cancer Immunotherapy? Front. Immunol. 12:765906. doi: 10.3389/fimmu.2021.765906

INTRODUCTION

Vitamin C (or L-ascorbic acid, hereafter referred to as VitC) is a nutrient with a six-carbon structure, synthesized from glucose and abundant in fruits, vegetables and in the kidney and liver of most animals (1). Species such as guinea pigs, fruit bats, and humans are unable to synthesize VitC, due to a mutation in the gene encoding L-gulonolactone oxidase, which catalyzes the last step of VitC synthesis (2, 3). In nature, VitC exists in two different redox forms. The ascorbic acid (reduced) form enters cells using sodium-dependent VitC transporters (SVCTs), whereas the dehydroascorbic acid (oxidized) form enters cells *via* glucose transporters (GLUTs) (4). Inside the cells, the

Abbreviations: ACT, adoptive cellular therapy; BET, bromodomain and extra-terminal motif proteins; CAR, chimeric antigen receptor; CTLA-4, Cytotoxic T-lymphocyte-associated protein 4; DC, dendritic cells; Erk, extracellular signal-regulated kinases; GLUTs, glucose transporters; H_2O_2, hydrogen peroxide; ICT, Immune checkpoint therapy; IKK, IκB Kinase; i.v., intravenous; mTOR/C1, mammalian target of rapamycin/complex 1; NAC, N-Acetyl-cysteine; NFAT, Nuclear factor of activated T cells; PD-1, Programmed cell death protein 1; pVC, phospho-modified Vitamin C; ROS, reactive oxygen species; SVCTs, sodium-dependent VitC transporters; TCR, T-cell receptor; TET, ten-eleven-translocation; VitC, Vitamin C.

dehydroascorbic acid is reduced back to ascorbic acid which then interacts with different enzymatic systems such as monooxygenases, dioxygenases and hydroxylases, involved in the regulation of numerous biological processes (5). When VitC is not transported inside the cells, it is converted into 2,3-L-diketoglutonate, which is further degraded into oxalate, CO_2 and L-erythrulose (1). VitC was initially described to play a crucial role in extracellular matrix composition by acting as cofactor for prolyl hydroxylase, the enzyme responsible for collagen biosynthesis (6). Defective collagen synthesis due to VitC deficiency causes scurvy, a bleeding diathesis secondary to poor wound healing.

VitC has also long been investigated as anti-cancer agent, either in monotherapy or in combination therapy (7), although its effectiveness in cancer has been a subject of controversy. Cameron and colleagues first reported the clinical efficacy of high doses of intravenous (i.v.) VitC in advanced cancer patients (8, 9). In these studies, patients with different types of cancer, who received 10 g of VitC intravenously daily for 10 days and orally thereafter, showed superior overall survival rate compared to the untreated group. These encouraging results could not be reproduced in other early-phase clinical trials, which used the same total dose, delivered entirely orally (10, 11). However, later work revealed that differences in the route of delivery probably explained the discrepant results (12), and it is now proposed that the anti-cancer benefits of VitC require high systemic concentrations that can only be achieved by intravenous delivery. Recent studies have also reported that VitC supplementation at physiologic doses also improves the function of anti-cancer immunotherapies – notably, ACTs-suggesting beneficial roles for VitC at both high (pharmacologic) and low (physiologic) doses. **Figure 1** depicts the timeline in the development of the VitC usage for anti-cancer therapy.

VitC has mostly been understood to exert its anticancer activity through reactive oxygen species-induced oxidative stress (13–18), as well as through modulation of epigenetic programs (19, 20). These mechanisms preferentially affect cancer cells, and VitC is not toxic to normal cells at these doses. Indeed, previous studies have shown a critical and beneficial function of VitC in immune cells, as VitC is present at high intracellular concentrations in lymphocytes (25, 26), and VitC deficiency has been associated with impaired immunity (27). Such immune-modulatory functions of VitC were shown to be regulated at the epigenetic level (28). As it is now quite clear that immune cells have a profound impact on tumors, it is not surprising that recent *in vivo* murine studies have demonstrated that VitC can also contribute to tumor control by modulating the immune system and, interestingly, by enhancing the efficacy of immune checkpoint inhibitor therapy (21–24).

In this review, we focus on what is known about how VitC modulates anti-tumor immune cell function and shed some light on the mechanistic basis of its activity. We also discuss its relevance for current translational immunotherapeutic approaches, highlighting outstanding challenges and unanswered questions as well as current evidence to support the contention that VitC therapy may be a safe and powerful adjunct for cancer immunotherapy, improving efficacy while limiting toxicity.

PHARMACOKINETICS OF VITAMIN C

Following the original observations reporting the controversy on the use of VitC as anticancer agent, pharmacokinetic studies have been performed both in humans and mice to investigate the effects of high-dose VitC, considering different routes of administration and elucidating underlying mechanisms (12, 29). These studies delivered increasing doses of VitC *via* oral and/or i.v. routes and subsequently measured VitC concentrations in the plasma and tissue. Oral administration of high dose VitC resulted in physiologic plasma concentrations, resulting from tight control by factors such as intestinal absorption, tissue transport, and renal reabsorption and excretion (12). In contrast, repeated i.v. administration, which bypasses intestinal regulation, resulted in high plasma and tissue concentrations (12, 29).

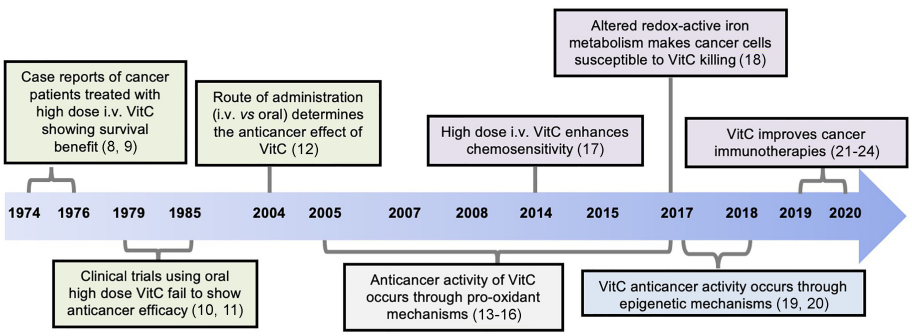

FIGURE 1 | Timeline of discoveries related to the anti-cancer function of Vitamin C (VitC). Advances made over past decades identified VitC as potential anti-cancer agent at high dose yielding remarkable clinical efficacy when given intravenously, and not through oral administration. Mechanistically, VitC at high dose preferentially kills tumor cells *in vitro* or delays tumor growth *in vivo* by exerting pro-oxidant effects and by disrupting iron metabolism, as well as through modulation of epigenetic mechanisms mediated by TET enzymes. Numbers in brackets refer to corresponding references.

VITAMIN C AND TUMOR CELLS

VitC at pharmacologic (high, 1 mM) doses was reported to kill tumor cells *in vitro* and delay tumor growth *in vivo*, essentially through pro-oxidant mechanisms (13, 14). Pharmacologic-dose VitC induces the generation of hydrogen peroxide, which reacts with labile ferrous iron to generate hydroxyl radical known to its action in compromising membrane and DNA integrity as well as glucose metabolism, ultimately leading to cell death (30, 31). Several other mechanisms underlying increased tumor susceptibility to death after high-dose VitC treatment were recently reviewed (32) and include the increased expression of VitC transporters [SVCTs (33) and GLUTs (34)], as well as the decreased concentrations of antioxidant defenses (catalase and superoxide dismutase) and the enhanced cellular levels of prooxidant metal ions (18). These mechanisms likely contribute to VitC-mediated killing of tumor cells; Shenoy et al., testing the effect of VitC on clear cell renal cell carcinoma (ccRCC), showed that short-term exposure (6h) to 1 mM VitC was toxic to ccRCC. However, although the tumor killing effect was forestalled by the addition of catalase, this protective effect disappeared with longer exposures (96h), suggesting an additional, oxidant-independent mechanism of VitC. In subsequent analyses, the authors demonstrated that this effect of VitC was epigenetically mediated (35). Similar observations were also made using lymphoma models (19, 22), and it was shown that pharmacologic-dose VitC exerts antitumor activity through Ten-eleven-translocation (TET)-mediated DNA demethylation (19, 22, 35). In these settings, epigenomic and transcriptomic interrogations from tumor cell samples treated with high-dose VitC revealed enhanced TET-mediated global genome-wide demethylation (increased 5-hydroxymethylcytosine levels) and increased expression of genes encoding human endogenous retroviruses (HERVs) associated with elevated locus-specific demethylation (22). Increased TET expression promotes the effectiveness of cancer immunotherapy (21), and HERVs are known to increase tumor immunogenicity both by increasing tumor mutational burden (36). Furthermore, data from Luchtel et al. showed that VitC-pretreatment of lymphoma cells enhanced their killing by CD8 T cells *in vitro* (22). Together, these data indicate that VitC-facilitated epigenetic modifications enhance tumor immunogenicity, accounting for improved antitumor effect. Based on these and other findings, investigation into high-dose VitC therapy is ongoing in cancer clinical trials.

MECHANISM OF ACTION OF VITAMIN C ON IMMUNE CELLS

As stated above, VitC acts on tumor cells through oxidant and epigenetic mechanisms. Emerging data indicate that VitC also acts on immune cells in these ways. Free radicals and other reactive oxygen species (ROS), at low dose, are crucial regulators of cell signaling and activation. Indeed, ROS produced in small amounts can positively regulate T-cell receptor (TCR) signaling pathways, thus promoting T-cell activation and proliferation. In support of this, ROS have been shown to be essential for TCR signaling-associated events (37, 38). For example, the moderate generation of ROS following TCR-signaling modulates the phosphorylation of the extracellular signal-regulated kinases (Erk)1/2 (39, 40). In addition, ROS such as H_2O_2 can lead to activation of the IκB kinase complex (IKK) (38). However, an overproduction of ROS in the microenvironment causes oxidative stress, leading to damage including cellular dysfunction, cell death, cellular aging, and cancer (41, 42). VitC is a critical non-enzymatic antioxidant that exerts antioxidant activity at micromolar concentrations. This ROS-buffering activity influences cell signal transduction, and the influence of physiologic doses of VitC on TCR signal transduction in general has been recently reviewed. Possible targets include molecules in the proximal TCR signaling complex, as well as downstream signaling molecules such as p38, Erk1/2, NF-κB, NFAT, and PI3K-Akt-mTOR pathway members (43, 44).

Several other studies have described the role of VitC in modulating gene expression in different settings. Duarte et al. reported a genome-wide effect of physiologic-dose VitC in human dermal fibroblasts (45), and Chung et al. identified a number of important genes selectively regulated in human embryonic stem cells cultured in the presence of physiologic dose of VitC (46). Several genes controlling immune function are known to be epigenetically regulated by physiologic dose of VitC, independently of its antioxidant activities. Indeed, compelling evidence suggests that VitC regulates many epigenetic processes, including DNA demethylation and histone modification (28, 46) by interacting with TET (47, 48) and Jumonji C-domain-containing (JmjC) enzymes (49, 50), respectively. TET enzymes convert 5-methylcytosine into 5-hydroxymethylcytosine and further into 5-formylcytosine and 5-carboxylcytosine (47, 48), whereas JmjC demethylases largely regulate chromatin through lysine demethylation of histones (49). VitC-facilitated DNA and histone demethylation is independent of its antioxidant activity. The current model proposes that VitC acts by converting ferric iron (Fe^{3+}) into ferrous iron (Fe^{2+}), which is essential to maintain the enzymes in their fully catalytic form (51). Interestingly, VitC appears to be highly effective in reducing Fe^{3+} over other reducing agents (52). Several other epigenetic modifying enzymes were also reported to rely on VitC as a cofactor (53), which maintain them in their fully catalytic form, thereby facilitating active gene demethylation crucial for T cell differentiation and function.

Oxidant effects and epigenetic modification are the two best understood mechanisms by which VitC regulates various biological processes. However, the interdependence between these two mechanisms has not yet been investigated. Considering that the availability of VitC inside cells is largely controlled by redox status, Young et al. speculated that redox status in the nucleus could impact the availability of VitC to DNA and histones (28). This view becomes much more complicated by a consideration of the complex and redox-independent influences of other factors, such as cytokines, on

epigenetic processes. Indeed, previous murine studies examining the role of IL-2 and IL-6 in the DNA methylation process in regulatory T cells (Treg) have demonstrated the crucial role of IL-2 in the recruitment and binding of TET to the Treg-specific demethylated region (TSDR), whereas IL-6 was reported to hinder that binding (54, 55). Further study is clearly required to fill the gaps in our knowledge of how redox status and epigenetic processes are linked to each other.

VITAMIN C AND ANTITUMOR IMMUNE EFFECTS

In addition to the direct antitumor effect of VitC at high doses, recent studies show that the effect of VitC on immune cells can mediate indirect antitumor effects (22, 23). Interestingly, many of these effects also occur at physiologic doses of VitC. Here, we summarize what is known about the effects of VitC on immune cells with anti-tumor activity (namely NK cells, CD4 and CD8 T cells, and γδ T cells) in the context of cancer immunotherapy. We also discuss the mechanistic basis of its effect with a brief focus on potential targets in TCR signaling. A schematic overview of the influence of VitC on different immune cells is presented in **Figure 2**.

Natural Killer Cells

NK cells, part of the innate immune system, are capable of rapid and potent killing of virally infected or malignant cells without any prior priming (56, 57). A previous study by Huijskens et al. demonstrated that addition of physiologic-dose VitC to peripheral blood mononuclear cells (PBMC) *in vitro* cultures resulted in a moderately increased proportion of NK cells (58) expressing both inhibitory and activating NK receptors. However, the expression of these receptors was not significantly affected by VitC. Subsequent studies fractionated NK cells further according to their CD56 surface expression to differentiate less mature ($CD56^{bright}$) from more mature ($CD56^{dim}$) NK cells (59–61). Immature $CD56^{bright}$ NK cells exhibit high levels of activating CD94/NKG2C but low frequencies of inhibitory receptors 2DL1 and 2DL3; conversely, mature $CD56^{dim}$ NK cells are 2DL1 and 2DL3 high (59, 60, 62, 63). In this setting, addition of VitC *in vitro* resulted in increased expression of inhibitory receptors on immature $CD56^{bright}$ (both at the gene and protein levels), but not on mature $CD56^{dim}$ NK cells (63). These results suggest that VitC preferentially affects immature NK cells, influencing peripheral NK cell development by inducing a more inhibitory phenotype. It is not known whether VitC influences the developmental expression of other NK cell receptors, or how VitC-mediated changes affect NK cell anti-tumor function. It is possible that VitC-induced upregulation of inhibitory receptors inhibits NK cell cytotoxicity against tumor cells, as upregulation of inhibitory receptors by another epigenetic-modifying drug, decitabine, impaired NK cell anti-tumor activity (64). Furthermore, impaired NK cytotoxic function in the presence of VitC has been reported in *in vitro* studies (58, 65). In contrast, some murine and human (66, 67) studies have reported that VitC augmented the cytotoxic function of NK cells; these studies typically compared VitC depletion with supplementation at physiologic doses, suggesting that there may be an optimal dose range. Clearly, more extensive investigation is needed to fully understand the effect of VitC on NK cell function.

αβ T Cells

T cells expressing the αβ T-cell receptor (TCR), comprising CD4 and CD8 T cells, release cytolytic granules (68, 69) and produce cytokines, including IFN-γ; after tumor antigen challenge [reviewed in (70)]. Physiologic-dose VitC enhances human T-cell proliferation (44, 71), and exerts both direct and indirect effects on CD4 and CD8 T-cell subsets. A murine study reported that VitC treatment of dendritic cells (DCs) increased phosphorylation of p38, Erk1/2 and NF-κB relevant for DC activation, resulting in elevated production of IL-12, which in turn drove naïve T cells towards the Th1 phenotype, increasing IFN-γ and decreasing IL-5 secretion (72). This was confirmed in a follow-up study demonstrating that murine CD4 and CD8 T cells showed increased IFN-γ production when cocultured with VitC-pretreated DC (73). Furthermore, *in vivo* injection of VitC-pretreated DCs increased IL-12 and IL-15 levels and augmented the generation of memory CD8 T cells; these cells exhibited strong cytotoxic activity against melanoma cells both *in vitro* and *in vivo* (73). Less has been reported on the direct effects of VitC on αβ T cells, and to our knowledge no studies have been reported describing the effects of physiologic-dose VitC on αβ T cells against cancer. Luchtel et al. reported that VitC-pretreatment of isolated human CD8 T cells led to an increase in global 5-hmC levels and enhanced their *in vitro* cytotoxic activity against lymphoma cells (22). Notably, this increase in CD8 T cell cytotoxicity also occurred *in vivo*; however, physiologic-dose VitC has not been tested in this context.

γδ T Cells

γδ T cells are prototypical unconventional T lymphocytes and express a TCR composed of variable Vδ genes paired with different Vγ elements. Studies have shown that infiltration of γδ T cells into tumors correlates with favorable prognosis in several cancer types (74); however, γδ T cells have not yet been widely adopted as anti-cancer cellular therapies. Approaches to improve γδ T-cell expansion and effector function were recently reviewed (75), and we have previously shown that VitC and its derivative, L-ascorbic acid 2-phosphate (pVC), can increase the *in vitro* proliferation of γδ T cells. We have also shown that pVC and VitC (at low dose) treatment led to reduced intracellular ROS levels, increased proportion of cells in G2/M phase, and increased Ki-67 expression, as well as increased glycolysis and mitochondrial respiration (76). These findings are consistent with the induction of effector and memory programs within γδ T cells (77–79). Indeed, treatment of γδ T cells with physiologic-dose VitC improved *ex vivo* expansion and yielded cell products that expressed higher levels of costimulatory molecules, increased cytokine production, and superior cytotoxic activity against tumor cells (24). These data suggest that VitC may be a useful adjunct for γδ T cell immunotherapies. Along these lines, this study showed that the adoptive transfer of VitC-expanded γδ

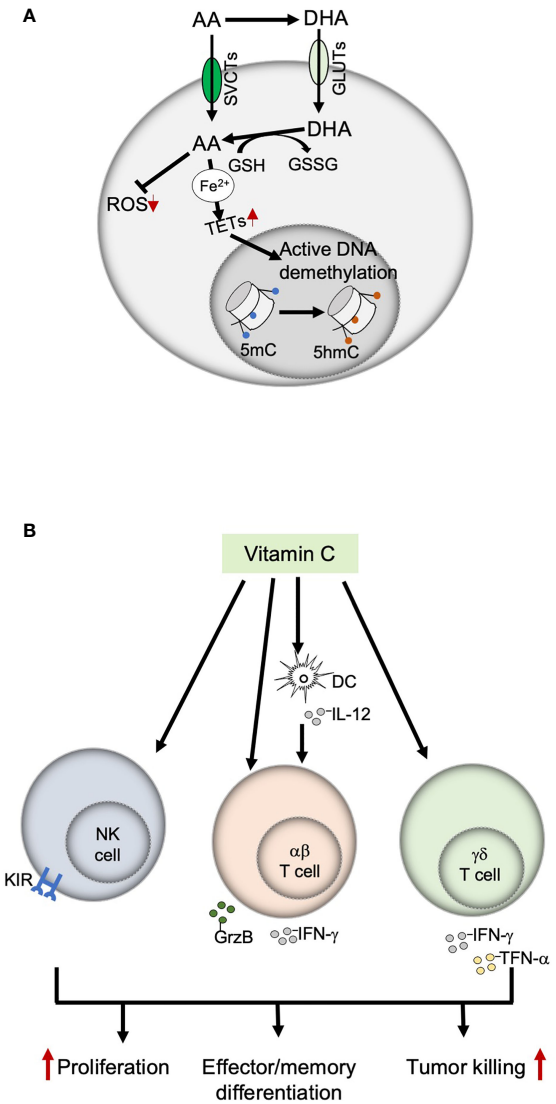

FIGURE 2 | Immunomodulatory functions of Vitamin C. **(A)** Mechanisms of action of Vitamin C; VitC exerts an immune-modulatory effect on immune cells through two main mechanisms, antioxidant activity and epigenetic modulation (by providing ferrous iron to the TET enzymes, which maintains them in their fully catalytic form, thereby ensuring an active DNA demethylation). **(B)** Effects of Vitamin C on immune cells with anti-tumor functions. VitC exerts both direct and indirect effects on NK, αβ and γδ T cells by modulating their proliferation, differentiation, and effector functions. AA, ascorbic acid; DHA, dehydroascorbic acid; GSH, glutathione; GSSG, glutathione disulfide: SVCTs, sodium-dependent vitamin C transporters: GLUTs, glucose transporters: TETs, ten-eleven translocation enzymes; ROS, reactive oxygen species; 5mC, 5-methylcytosine; 5hmC, 5-hydroxymethylcytosine.

T cells, but not control γδ T cells, significantly prolonged the survival of humanized mice transplanted with human lung tumor cells (24). Remarkably, a subsequent phase I clinical trial found that repeated infusion of VitC-treated allogeneic γδ T cells increased overall survival rates in lung and liver cancer patients (24).

In summary, VitC appears to exert its effects on immune cells in a dose- and context-dependent manner. At *in vitro* doses above 57 μM, VitC is toxic to human γδ T cells (76); 1mM VitC treatment of human αβ T cells enhanced cytotoxic activity against lymphoma cells (22), but required pretreatment with catalase to protect against VitC-mediated αβ T cell toxicity. Thus, an alternative to the use of pharmacologic-dose VitC may be pVC, which resists oxidation in culture medium and releases the reduced VitC form once inside the cells *via* alkaline phosphatase-mediated hydrolysis (80). pVC therefore has no extracellular prooxidant effect, but still facilitates intracellular biological effects. Indeed, we have seen no toxicity with pVC at doses approaching 1mM, while continuing to see marked metabolic (76) and epigenetic effects (81).

VITAMIN C AND CANCER IMMUNOTHERAPY

Chimeric Antigen Receptor T Cells

CAR design, biology, and clinical efficacy have been extensively reviewed elsewhere (82, 83). Very briefly, CARs are TCR surrogates with a modular design comprising an antigen-binding domain, an extracellular hinge region, a transmembrane domain, and an intracellular tail incorporating the TCR signaling domain CD3ζ. Despite their overall structural similarity, there are significant differences in proximal signaling after antigen recognition between CARs and TCRs (83, 84). However, given that VitC can modulate activation-induced TCR signaling (43), it is probable that VitC affects proximal CAR signaling. Additionally, γδ T cells treated with pVC have reduced ROS levels, and ROS are known to interact with molecules involved in proximal TCR signaling (85). Moreover, VitC may increase c-Jun levels (43) and Nuclear Factor of Activated T cell (NFAT) activity (86), and both c-Jun and NFAT have been shown to influence CAR T cell function (87). Specific studies on the effects of VitC on CAR signaling have not yet been reported.

Immunomodulatory effects of antioxidants and epigenetic activators on CAR T cell function and development have been described (88–90). Manufacturing anti-CD19-CAR T cells in the presence of the antioxidant N-acetyl-cysteine (NAC) resulted in enforcement of a stem cell memory-like phenotype (T_{scm}), including displayed T_{scm}-specific metabolic features, improved self-renewal, and superior anti-tumor function *in vivo* (88). Similar observations were also made when manufacturing anti-CD19-CAR T cells in the presence of JQ1, an inhibitor of bromodomain and extra-terminal motif (BET) proteins (90). Interestingly, VitC was also reported to play a crucial role in the generation and maintenance of induced pluripotent stem cells (91), and the combination of NAC and VitC promotes the acquisition of long-term T cell memory in aged mice (92). Additionally, we recently demonstrated that VitC increased the proliferation of IL-2/IL-15-expanded human γδ T cells, which was accompanied by a switch to memory T cell-like metabolism and improved anti-tumor function (24, 76). IL-15-expanded CAR T cells also exhibit an enhanced proliferative capacity and anti-tumor function *in vivo* in part through reduced mammalian target of rapamycin complex 1 (mTORC1) signaling, which enforces a T_{scm} phenotype (93). Taken together, these findings suggest that VitC may be a beneficial addition to the CAR T cell manufacturing process, and we are currently investigating this possibility.

Immune Checkpoint Therapy

The antagonistic potential of monoclonal antibodies to suppress the function of immune inhibitory receptors such as CTLA-4 and PD-1, known as ICT, has led to remarkable clinical responses against many tumors (94). Unfortunately, ICT is not universally effective (95, 96), and expanding the therapeutic scope of this revolutionary modality would be of great value.

Interestingly, evidence is mounting that VitC can augment the effects of ICT. Recent studies showed that pharmacologic-dose VitC potentiates PD-1 blockade, resulting in increased macrophage and CD8 T-cell tumor infiltration, increased granzyme B production, and significant tumor regression (21, 22). Similarly, addition of high doses of VitC to CTLA-4 and/or PD-1/PD-L1 blockade delayed tumor growth and led to pronounced tumor regression in different tumor mouse models (23). Although mechanistic data are not completely elucidated in these studies, it is interesting that VitC treatment enhances T cell trafficking in solid tumors (97). VitC may also amplify the effects of checkpoint inhibitor therapy through its role as an epigenetic facilitator possibly increasing the expression of retroviral elements and neoantigens (22). Taken together, these studies point the way to therapeutic combination of VitC and ICT in early-phase clinical trials.

CONCLUDING REMARKS

Recent advances in immunotherapy have ushered in a new era in cancer treatment, but many challenges remain to be solved for successful implementation of cancer immunotherapy, including adverse side effects of treatment, off-target toxicity, tumor resistance, tumor evolution, and an immunosuppressive tumor microenvironment, all of which limit translational efficacy across a wide variety of tumors. VitC has recently reemerged as a potent immunomodulatory small molecule, acting on immune cells through well-known antioxidant and epigenetic mechanisms as well as emerging direct signaling effects. Mounting evidence suggests that VitC may be of great therapeutic benefit in combination with immunotherapies, in particular CAR T-cell therapy and immune checkpoint inhibition. Pharmacologic i.v. concentrations of VitC possess anticancer properties, but combinatorial immunotherapeutic approaches may be required for tumor clearance. The addition of physiologic doses of VitC (or pVC) during manufacturing of adoptive cellular therapies may also be beneficial for enhancing T cell proliferation and maintenance of T stem cell phenotype. Although it has been demonstrated that VitC may have some synergistic effects when combined with ACTs, further investigation is needed to better define the optimal dosing, route, and schedule strategies as well as predictive biomarkers of susceptibility of immune/tumor cells to VitC treatment as it pertains to ACT. It is of great interest to study these interactions in more detail, and potentially to incorporate VitC into future immunotherapeutic clinical protocols.

AUTHOR CONTRIBUTIONS

LK, LDW, and DK conceived of the manuscript. LK wrote the manuscript and created the figures. LDW, CEB, CP, and DK edited the manuscript and figures.

FUNDING

CEB is supported by grants from the California Institute of Regenerative Medicine (CIRM; CLIN2-10248), the National

Cancer Institute (NCI, R01CA236500), and the Ivy Foundation. LDW is supported by NCI K08CA201591, CIRM CLIN2-12153, and the Pediatric Cancer Research Foundation. DK was supported by a grant from the Deutsche Forschungsgemeinschaft (Ka 502/19-3).

ACKNOWLEDGMENTS

The authors thank Joseph Aldahl for critical review and editing of the manuscript.

REFERENCES

1. Linster CL, Van Schaftingen E. Vitamin C. Biosynthesis, Recycling and Degradation in Mammals. *FEBS J* (2007) 274:1–22. doi: 10.1111/j.1742-4658.2006.05607.x
2. Nishikimi M, Kawai T, Yagi K. Guinea Pigs Possess a Highly Mutated Gene for L-Gulono-Gamma-Lactone Oxidase, the Key Enzyme for L-Ascorbic Acid Biosynthesis Missing in This Species. *J Biol Chem* (1992) 267:21967–72. doi: 10.1016/S0021-9258(19)36707-9
3. Nishikimi M, Fukuyama R, Minoshima S, Shimizu N, Yagi K. Cloning and Chromosomal Mapping of the Human Nonfunctional Gene for L-Gulono-Gamma-Lactone Oxidase, the Enzyme for L-Ascorbic Acid Biosynthesis Missing in Man. *J Biol Chem* (1994) 269:13685–8. doi: 10.1016/S0021-9258(17)36884-9
4. Corti A, Casini AF, Pompella A. Cellular Pathways for Transport and Efflux of Ascorbate and Dehydroascorbate. *Arch Biochem Biophys* (2010) 500:107–15. doi: 10.1016/j.abb.2010.05.014
5. Padayatty SJ, Levine M. Vitamin C: The Known and the Unknown and Goldilocks. *Oral Dis* (2016) 22:463–93. doi: 10.1111/odi.12446
6. Myllyla R, Kuutti-Savolainen ER, Kivirikko KI. The Role of Ascorbate in the Prolyl Hydroxylase Reaction. *Biochem Biophys Res Commun* (1978) 83:441–8. doi: 10.1016/0006-291x(78)91010-0
7. Nauman G, Gray JC, Parkinson R, Levine M, Paller CJ. Systematic Review of Intravenous Ascorbate in Cancer Clinical Trials. *Antioxid (Basel)* (2018) 7:89. doi: 10.3390/antiox7070089
8. Cameron E, Campbell A. The Orthomolecular Treatment of Cancer. II. Clinical Trial of High-Dose Ascorbic Acid Supplements in Advanced Human Cancer. *Chem Biol Interact* (1974) 9:285–315. doi: 10.1016/0009-2797(74)90019-2
9. Cameron E, Pauling L. Supplemental Ascorbate in the Supportive Treatment of Cancer: Prolongation of Survival Times in Terminal Human Cancer. *Proc Natl Acad Sci U.S.A.* (1976) 73:3685–9. doi: 10.1073/pnas.73.10.3685
10. Creagan ET, Moertel CG, O'Fallon JR, Schutt AJ, O'Connell MJ, Rubin J, et al. Failure of High-Dose(Ascorbic Acid) Therapy to Benefit Patients With Advanced Cancer. A Controlled Trial. *N Engl J Med* (1979) 301:687–90. doi: 10.1056/NEJM197909273011303
11. Moertel CG, Fleming TR, Creagan ET, Rubin J, O'Connell MJ, Ames MM. High-Dose Vitamin C Versus Placebo in the Treatment of Patients With Advanced Cancer Who Have had No Prior Chemotherapy. A Randomized Double-Blind Comparison. *N Engl J Med* (1985) 312:137–41. doi: 10.1056/NEJM198501173120301
12. Padayatty SJ, Sun H, Wang Y, Riordan HD, Hewitt SM, Katz A, et al. Vitamin C Pharmacokinetics: Implications for Oral and Intravenous Use. *Ann Intern Med* (2004) 140:533–7. doi: 10.7326/0003-4819-140-7-200404060-00010
13. Chen Q, Espey MG, Krishna MC, Mitchell JB, Corpe CP, Buettner GR, et al. Pharmacologic Ascorbic Acid Concentrations Selectively Kill Cancer Cells: Action as a Pro-Drug to Deliver Hydrogen Peroxide to Tissues. *Proc Natl Acad Sci USA* (2005) 102:13604–9. doi: 10.1073/pnas.0506390102
14. Chen Q, Espey MG, Sun AY, Pooput C, Kirk KL, Krishna MC, et al. Pharmacologic Doses of Ascorbate Act as a Prooxidant and Decrease Growth of Aggressive Tumor Xenografts in Mice. *Proc Natl Acad Sci USA* (2008) 105:11105–9. doi: 10.1073/pnas.0804226105
15. Serrano OK, Parrow NL, Violet PC, Yang J, Zornjak J, Basseville A, et al. Antitumor Effect of Pharmacologic Ascorbate in the B16 Murine Melanoma Model. *Free Radic Biol Med* (2015) 87:193–203. doi: 10.1016/j.freeradbiomed.2015.06.032
16. Xia J, Xu H, Zhang X, Allamargot C, Coleman KL, Nessler R, et al. Multiple Myeloma Tumor Cells Are Selectively Killed by Pharmacologically-Dosed Ascorbic Acid. *EBioMedicine* (2017) 18:41–9. doi: 10.1016/j.ebiom.2017.02.011
17. Ma Y, Chapman J, Levine M, Polireddy K, Drisko J, Chen Q. High-Dose Parenteral Ascorbate Enhanced Chemosensitivity of Ovarian Cancer and Reduced Toxicity of Chemotherapy. *Sci Transl Med* (2014) 6:222ra18. doi: 10.1126/scitranslmed.3007154
18. Schoenfeld JD, Sibenaller ZA, Mapuskar KA, Wagner BA, Cramer-Morales KL, Furqan M, et al. O2(-) and H2O2-Mediated Disruption of Fe Metabolism Causes the Differential Susceptibility of NSCLC and GBM Cancer Cells to Pharmacological Ascorbate. *Cancer Cell* (2017) 32:268. doi: 10.1016/j.ccell.2017.07.008
19. Shenoy N, Bhagat T, Nieves E, Stenson M, Lawson J, Choudhary GS, et al. Upregulation of TET Activity With Ascorbic Acid Induces Epigenetic Modulation of Lymphoma Cells. *Blood Cancer J* (2017) 7:e587. doi: 10.1038/bcj.2017.65
20. Gerecke C, Schumacher F, Edlich A, Wetzel A, Yealland G, Neubert LK, et al. Vitamin C Promotes Decitabine or Azacytidine Induced DNA Hydroxymethylation and Subsequent Reactivation of the Epigenetically Silenced Tumour Suppressor CDKN1A in Colon Cancer Cells. *Oncotarget* (2018) 9:32822–40. doi: 10.18632/oncotarget.25999
21. Xu YP, Lv L, Liu Y, Smith MD, Li WC, Tan XM, et al. Tumor Suppressor TET2 Promotes Cancer Immunity and Immunotherapy Efficacy. *J Clin Invest* (2019) 129:4316–31. doi: 10.1172/JCI129317
22. Luchtel RA, Bhagat T, Pradhan K, Jacobs WR Jr, Levine M, Verma A, et al. High-Dose Ascorbic Acid Synergizes With Anti-PD1 in a Lymphoma Mouse Model. *Proc Natl Acad Sci USA* (2020) 117:1666–77. doi: 10.1073/pnas.1908158117
23. Magri A, Germano G, Lorenzato A, Lamba S, Chila R, Montone M, et al. High-Dose Vitamin C Enhances Cancer Immunotherapy. *Sci Transl Med* (2020) 12:eaay8707. doi: 10.1126/scitranslmed.aay8707
24. Xu Y, Xiang Z, Alnaggar M, Kouakanou L, Li J, He J, et al. Allogeneic Vgamma9Vdelta2 T-Cell Immunotherapy Exhibits Promising Clinical Safety and Prolongs the Survival of Patients With Late-Stage Lung or Liver Cancer. *Cell Mol Immunol* (2020) 18:427–39. doi: 10.1038/s41423-020-0515-7
25. Evans RM, Currie L, Campbell A. The Distribution of Ascorbic Acid Between Various Cellular Components of Blood, in Normal Individuals, and Its Relation to the Plasma Concentration. *Br J Nutr* (1982) 47:473–82. doi: 10.1079/bjn19820059
26. Omaye ST, Schaus EE, Kutnink MA, Hawkes WC. Measurement of Vitamin C in Blood Components by High-Performance Liquid Chromatography. Implication in Assessing Vitamin C Status. *Ann N Y Acad Sci* (1987) 498:389–401. doi: 10.1111/j.1749-6632.1987.tb23776.x
27. Kennes B, Dumont I, Brohee D, Hubert C, Neve P. Effect of Vitamin C Supplements on Cell-Mediated Immunity in Old People. *Gerontology* (1983) 29:305–10. doi: 10.1159/000213131
28. Young JI, Zuchner S, Wang G. Regulation of the Epigenome by Vitamin C. *Annu Rev Nutr* (2015) 35:545–64. doi: 10.1146/annurev-nutr-071714-034228
29. Campbell EJ, Vissers MCM, Wohlrab C, Hicks KO, Strother RM, Bozonet SM, et al. Pharmacokinetic and Anti-Cancer Properties of High Dose Ascorbate in Solid Tumours of Ascorbate-Dependent Mice. *Free Radic Biol Med* (2016) 99:451–62. doi: 10.1016/j.freeradbiomed.2016.08.027
30. Du J, Cullen JJ, Buettner GR. Ascorbic Acid: Chemistry, Biology and the Treatment of Cancer. *Biochim Biophys Acta* (2012) 1826:443–57. doi: 10.1016/j.bbcan.2012.06.003
31. Ma E, Chen P, Wilkins HM, Wang T, Swerdlow RH, Chen Q. Pharmacologic Ascorbate Induces Neuroblastoma Cell Death by Hydrogen Peroxide Mediated DNA Damage and Reduction in Cancer Cell Glycolysis. *Free Radic Biol Med* (2017) 113:36–47. doi: 10.1016/j.freeradbiomed.2017.09.008
32. Ngo B, Van Riper JM, Cantley LC, Yun J. Targeting Cancer Vulnerabilities With High-Dose Vitamin C. *Nat Rev Cancer* (2019) 19:271–82. doi: 10.1038/s41568-019-0135-7

33. Lv H, Wang C, Fang T, Li T, Lv G, Han Q, et al. Vitamin C Preferentially Kills Cancer Stem Cells in Hepatocellular Carcinoma *via* SVCT-2. *NPJ Precis Oncol* (2018) 2:1. doi: 10.1038/s41698-017-0044-8
34. Yun J, Mullarky E, Lu C, Bosch KN, Kavalier A, Rivera K, et al. Vitamin C Selectively Kills KRAS and BRAF Mutant Colorectal Cancer Cells by Targeting GAPDH. *Science* (2015) 350:1391–6. doi: 10.1126/science.aaa5004
35. Shenoy N, Bhagat TD, Cheville J, Lohse C, Bhattacharyya S, Tischer A, et al. Ascorbic Acid-Induced TET Activation Mitigates Adverse Hydroxymethylcytosine Loss in Renal Cell Carcinoma. *J Clin Invest* (2019) 129:1612–25. doi: 10.1172/JCI98747
36. Attermann AS, Bjerregaard AM, Saini SK, Gronbaek K, Hadrup SR. Human Endogenous Retroviruses and Their Implication for Immunotherapeutics of Cancer. *Ann Oncol* (2018) 29:2183–91. doi: 10.1093/annonc/mdy413
37. Bienert GP, Schjoerring JK, Jahn TP. Membrane Transport of Hydrogen Peroxide. *Biochim Biophys Acta* (2006) 1758:994–1003. doi: 10.1016/j.bbamem.2006.02.015
38. Oliveira-Marques V, Marinho HS, Cyrne L, Antunes F. Role of Hydrogen Peroxide in NF-kappaB Activation: From Inducer to Modulator. *Antioxid Redox Signal* (2009) 11:2223–43. doi: 10.1089/ARS.2009.2601
39. Devadas S, Zaritskaya L, Rhee SG, Oberley L, Williams MS. Discrete Generation of Superoxide and Hydrogen Peroxide by T Cell Receptor Stimulation: Selective Regulation of Mitogen-Activated Protein Kinase Activation and Fas Ligand Expression. *J Exp Med* (2002) 195:59–70. doi: 10.1084/jem.20010659
40. Jackson SH, Devadas S, Kwon J, Pinto LA, Williams MS. T Cells Express a Phagocyte-Type NADPH Oxidase That is Activated After T Cell Receptor Stimulation. *Nat Immunol* (2004) 5:818–27. doi: 10.1038/ni1096
41. Finkel T, Holbrook NJ. Oxidants, Oxidative Stress and the Biology of Ageing. *Nature* (2000) 408:239–47. doi: 10.1038/35041687
42. Reuter S, Gupta SC, Chaturvedi MM, Aggarwal BB. Oxidative Stress, Inflammation, and Cancer: How Are They Linked? *Free Radic Biol Med* (2010) 49:1603–16. doi: 10.1016/j.freeradbiomed.2010.09.006
43. Peters C, Kouakanou L, Kabelitz D. A Comparative View on Vitamin C Effects on Alphabeta- Versus Gammadelta T-Cell Activation and Differentiation. *J Leukoc Biol* (2020) 107:1009–22. doi: 10.1002/JLB.1MR1219-245R
44. Manning J, Mitchell B, Appadurai DA, Shakya A, Pierce LJ, Wang H, et al. Vitamin C Promotes Maturation of T-Cells. *Antioxid Redox Signal* (2013) 19:2054–67. doi: 10.1089/ars.2012.4988
45. Duarte TL, Cooke MS, Jones GD. Gene Expression Profiling Reveals New Protective Roles for Vitamin C in Human Skin Cells. *Free Radic Biol Med* (2009) 46:78–87. doi: 10.1016/j.freeradbiomed.2008.09.028
46. Chung TL, Brena RM, Kolle G, Grimmond SM, Berman BP, Laird PW, et al. Vitamin C Promotes Widespread Yet Specific DNA Demethylation of the Epigenome in Human Embryonic Stem Cells. *Stem Cells* (2010) 28:1848–55. doi: 10.1002/stem.493
47. Tahiliani M, Koh KP, Shen Y, Pastor WA, Bandukwala H, Brudno Y, et al. Conversion of 5-Methylcytosine to 5-Hydroxymethylcytosine in Mammalian DNA by MLL Partner TET1. *Science* (2009) 324:930–5. doi: 10.1126/science.1170116
48. Ito S, Shen L, Dai Q, Wu SC, Collins LB, Swenberg JA, et al. Tet Proteins can Convert 5-Methylcytosine to 5-Formylcytosine and 5-Carboxylcytosine. *Science* (2011) 333:1300–3. doi: 10.1126/science.1210597
49. Klose RJ, Kallin EM, Zhang Y. JmjC-Domain-Containing Proteins and Histone Demethylation. *Nat Rev Genet* (2006) 7:715–27. doi: 10.1038/nrg1945
50. Tsukada Y, Fang J, Erdjument-Bromage H, Warren ME, Borchers CH, Tempst P, et al. Histone Demethylation by a Family of JmjC Domain-Containing Proteins. *Nature* (2006) 439:811–6. doi: 10.1038/nature04433
51. Hore TA, von Meyenn F, Ravichandran M, Bachman M, Ficz G, Oxley D, et al. Retinol and Ascorbate Drive Erasure of Epigenetic Memory and Enhance Reprogramming to Naive Pluripotency by Complementary Mechanisms. *Proc Natl Acad Sci USA* (2016) 113:12202–7. doi: 10.1073/pnas.1608679113
52. Hore TA. Modulating Epigenetic Memory Through Vitamins and TET: Implications for Regenerative Medicine and Cancer Treatment. *Epigenomics* (2017) 9:863–71. doi: 10.2217/epi-2017-0021
53. Kuiper C, Vissers MC. Ascorbate as a Co-Factor for Fe- and 2-Oxoglutarate Dependent Dioxygenases: Physiological Activity in Tumor Growth and Progression. *Front Oncol* (2014) 4:359. doi: 10.3389/fonc.2014.00359
54. Yang R, Qu C, Zhou Y, Konkel JE, Shi S, Liu Y, et al. Hydrogen Sulfide Promotes Tet1- and Tet2-Mediated Foxp3 Demethylation to Drive Regulatory T Cell Differentiation and Maintain Immune Homeostasis. *Immunity* (2015) 43:251–63. doi: 10.1016/j.immuni.2015.07.017
55. Nair VS, Song MH, Ko M, Oh KI. DNA Demethylation of the Foxp3 Enhancer Is Maintained Through Modulation of Ten-Eleven-Translocation and DNA Methyltransferases. Mol. *Cells* (2016) 39:888–97. doi: 10.14348/molcells.2016.0276
56. Trinchieri G. Biology of Natural Killer Cells. *Adv Immunol* (1989) 47:187–376. doi: 10.1016/s0065-2776(08)60664-1
57. Biron CA, Nguyen KB, Pien GC, Cousens LP, Salazar-Mather TP. Natural Killer Cells in Antiviral Defense: Function and Regulation by Innate Cytokines. *Annu Rev Immunol* (1999) 17:189–220. doi: 10.1146/annurev.immunol.17.1.189
58. Huijskens MJ, Walczak M, Sarkar S, Atrafi F, Senden-Gijsbers BL, Tilanus MG, et al. Ascorbic Acid Promotes Proliferation of Natural Killer Cell Populations in Culture Systems Applicable for Natural Killer Cell Therapy. *Cytotherapy* (2015) 17:613–20. doi: 10.1016/j.jcyt.2015.01.004
59. Cooper MA, Fehniger TA, Turner SC, Chen KS, Ghaheri BA, Ghayur T, et al. Human Natural Killer Cells: A Unique Innate Immunoregulatory Role for the CD56(bright) Subset. *Blood* (2001) 97:3146–51. doi: 10.1182/blood.v97.10.3146
60. Bjorkstrom NK, Riese P, Heuts F, Andersson S, Fauriat C, Ivarsson MA, et al. Expression Patterns of NKG2A, KIR, and CD57 Define a Process of CD56dim NK-Cell Differentiation Uncoupled From NK-Cell Education. *Blood* (2010) 116:3853–64. doi: 10.1182/blood-2010-04-281675
61. Chan A, Hong DL, Atzberger A, Kollnberger S, Filer AD, Buckley CD, et al. CD56bright Human NK Cells Differentiate Into CD56dim Cells: Role of Contact With Peripheral Fibroblasts. *J Immunol* (2007) 179:89–94. doi: 10.4049/jimmunol.179.1.89
62. Yu J, Mao HC, Wei M, Hughes T, Zhang J, Park IK, et al. CD94 Surface Density Identifies a Functional Intermediary Between the CD56bright and CD56dim Human NK-Cell Subsets. *Blood* (2010) 115:274–81. doi: 10.1182/blood-2009-04-215491
63. Wu CY, Zhang B, Kim H, Anderson SK, Miller JS, Cichocki F. Ascorbic Acid Promotes KIR Demethylation During Early NK Cell Differentiation. *J Immunol* (2020) 205:1513–23. doi: 10.4049/jimmunol.2000212
64. Niu C, Li M, Zhu S, Chen Y, Zhou L, Xu D, et al. Decitabine Inhibits Gamma Delta T Cell Cytotoxicity by Promoting KIR2DL2/3 Expression. *Front Immunol* (2018) 9:617. doi: 10.3389/fimmu.2018.00617
65. Huwyler T, Hirt A, Morell A. Effect of Ascorbic Acid on Human Natural Killer Cells. *Immunol Lett* (1985) 10:173–6. doi: 10.1016/0165-2478(85)90073-2
66. Kim JE, Cho HS, Yang HS, Jung DJ, Hong SW, Hung CF, et al. Depletion of Ascorbic Acid Impairs NK Cell Activity Against Ovarian Cancer in a Mouse Model. *Immunobiology* (2012) 217:873–81. doi: 10.1016/j.imbio.2011.12.010
67. Atasever B, Ertan NZ, Erdem-Kuruca S, Karakas Z. *In Vitro* Effects of Vitamin C and Selenium on NK Activity of Patients With Beta-Thalassemia Major. *Pediatr Hematol Oncol* (2006) 23:187–97. doi: 10.1080/08880010500506420
68. Pasternack MS, Verret CR, Liu MA, Eisen HN. Serine Esterase in Cytolytic T Lymphocytes. *Nature* (1986) 322:740–3. doi: 10.1038/322740a0
69. Beal AM, Anikeeva N, Varma R, Cameron TO, Vasiliver-Shamis G, Norris PJ, et al. Kinetics of Early T Cell Receptor Signaling Regulate the Pathway of Lytic Granule Delivery to the Secretory Domain. *Immunity* (2009) 31:632–42. doi: 10.1016/j.immuni.2009.09.004
70. Smyth MJ, Dunn GP, Schreiber RD. Cancer Immunosurveillance and Immunoediting: The Roles of Immunity in Suppressing Tumor Development and Shaping Tumor Immunogenicity. *Adv Immunol* (2006) 90:1–50. doi: 10.1016/S0065-2776(06)90001-7
71. Huijskens MJ, Walczak M, Koller N, Briede JJ, Senden-Gijsbers BL, Schnijderberg MC, et al. Technical Advance: Ascorbic Acid Induces Development of Double-Positive T Cells From Human Hematopoietic Stem Cells in the Absence of Stromal Cells. *J Leukoc Biol* (2014) 96:1165–75. doi: 10.1189/jlb.1TA0214-121RR
72. Jeong YJ, Hong SW, Kim JH, Jin DH, Kang JS, Lee WJ, et al. Vitamin C-Treated Murine Bone Marrow-Derived Dendritic Cells Preferentially Drive Naive T Cells Into Th1 Cells by Increased IL-12 Secretions. *Cell Immunol* (2011) 266:192–9. doi: 10.1016/j.cellimm.2010.10.005

73. Jeong YJ, Kim JH, Hong JM, Kang JS, Kim HR, Lee WJ, et al. Vitamin C Treatment of Mouse Bone Marrow-Derived Dendritic Cells Enhanced CD8 (+) Memory T Cell Production Capacity of These Cells *In Vivo*. *Immunobiol* (2014) 219:554–64. doi: 10.1016/j.imbio.2014.03.006
74. Tosolini M, Pont F, Poupot M, Vergez F, Nicolau-Travers ML, Vermijlen D, et al. Assessment of Tumor-Infiltrating TCRVgamma9Vdelta2 Gammadelta Lymphocyte Abundance by Deconvolution of Human Cancers Microarrays. *Oncoimmunology* (2017) 6:e1284723. doi: 10.1080/2162402X.2017.1284723
75. Kabelitz D, Serrano R, Kouakanou L, Peters C, Kalyan S. Cancer Immunotherapy With Gammadelta T Cells: Many Paths Ahead of Us. *Cell Mol Immunol* (2020) 17:925–39. doi: 10.1038/s41423-020-0504-x
76. Kouakanou L, Xu Y, Peters C, He J, Wu Y, Yin Z, et al. Vitamin C Promotes the Proliferation and Effector Functions of Human Gammadelta T Cells. *Cell Mol Immunol* (2020) 17:462–73. doi: 10.1038/s41423-019-0247-8
77. van der Windt GJ, Everts B, Chang CH, Curtis JD, Freitas TC, Amiel E, et al. Mitochondrial Respiratory Capacity is a Critical Regulator of CD8+ T Cell Memory Development. *Immunity* (2012) 36:68–78. doi: 10.1016/j.immuni.2011.12.007
78. Pearce EL, Poffenberger MC, Chang CH, Jones RG. Fueling Immunity: Insights Into Metabolism and Lymphocyte Function. *Science* (2013) 342:1242454. doi: 10.1126/science.1242454
79. Sukumar M, Liu J, Ji Y, Subramanian M, Crompton JG, Yu Z, et al. Inhibiting Glycolytic Metabolism Enhances CD8+ T Cell Memory and Antitumor Function. *J Clin Invest* (2013) 123:4479–88. doi: 10.1172/JCI69589
80. Hata R. Senoo H. L-Ascorbic Acid 2-Phosphate Stimulates Collagen Accumulation, Cell Proliferation, and Formation of a Three-Dimensional Tissuelike Substance by Skin Fibroblasts. *J Cell Physiol* (1989) 138:8–16. doi: 10.1002/jcp.1041380103
81. Kouakanou L, Peters C, Sun Q, Floess S, Bhat J, Huehn J, et al. Vitamin C Supports Conversion of Human Gammadelta T Cells Into FOXP3-Expressing Regulatory Cells by Epigenetic Regulation. *Sci Rep* (2020) 10:6550. doi: 10.1038/s41598-020-63572-w
82. Weber EW, Maus MV, Mackall CL. The Emerging Landscape of Immune Cell Therapies. *Cell* (2020) 181:46–62. doi: 10.1016/j.cell.2020.03.001
83. Wu L, Wei Q, Brzostek J, Gascoigne NRJ. Signaling From T Cell Receptors (TCRs) and Chimeric Antigen Receptors (CARs) on T Cells. *Cell Mol Immunol* (2020) 17:600–12. doi: 10.1038/s41423-020-0470-3
84. Lindner SE, Johnson SM, Brown CE, Wang LD. Chimeric Antigen Receptor Signaling: Functional Consequences and Design Implications. *Sci Adv* (2020) 6:eaaz3223. doi: 10.1126/sciadv.aaz3223
85. Griffith CE, Zhang W, Wange RL. ZAP-70-Dependent and -Independent Activation of Erk in Jurkat T Cells. Differences in Signaling Induced by H2o2 and Cd3 Cross-Linking. *J Biol Chem* (1998) 273:10771–6. doi: 10.1074/jbc.273.17.10771
86. Sommer D, Fakata KL, Swanson SA, Stemmer PM. Modulation of the Phosphatase Activity of Calcineurin by Oxidants and Antioxidants *In Vitro*. *Eur J Biochem* (2000) 267:2312–22. doi: 10.1046/j.1432-1327.2000.01240.x
87. Lynn RC, Weber EW, Sotillo E, Gennert D, Xu P, Good Z, et al. C-Jun Overexpression in CAR T Cells Induces Exhaustion Resistance. *Nature* (2019) 576:293–300. doi: 10.1038/s41586-019-1805-z
88. Pilipow K, Scamardella E, Puccio S, Gautam S, De Paoli F, Mazza EM, et al. Antioxidant Metabolism Regulates CD8+ T Memory Stem Cell Formation and Antitumor Immunity. *JCI Insight* (2018) 3:e122299. doi: 10.1172/jci.insight.122299
89. Das RK, O'Connor RS, Grupp SA, Barrett DM. Lingering Effects of Chemotherapy on Mature T Cells Impair Proliferation. *Blood Adv* (2020) 4:4653–64. doi: 10.1182/bloodadvances.2020001797
90. Kagoya Y, Nakatsugawa M, Yamashita Y, Ochi T, Guo T, Anczurowski M, et al. BET Bromodomain Inhibition Enhances T Cell Persistence and Function in Adoptive Immunotherapy Models. *J Clin Invest* (2016) 126:3479–94. doi: 10.1172/JCI86437
91. Esteban MA, Wang T, Qin B, Yang J, Qin D, Cai J, et al. Vitamin C Enhances the Generation of Mouse and Human Induced Pluripotent Stem Cells. *Cell Stem Cell* (2010) 6:71–9. doi: 10.1016/j.stem.2009.12.001
92. Meryk A, Grasse M, Balasco L, Kapferer W, Grubeck-Loebenstein B, Pangrazzi L. Antioxidants N-Acetylcysteine and Vitamin C Improve T Cell Commitment to Memory and Long-Term Maintenance of Immunological Memory in Old Mice. *Antioxid (Basel)* (2020) 9:1152. doi: 10.3390/antiox9111152
93. Alizadeh D, Wong RA, Yang X, Wang D, Pecoraro JR, Kuo CF, et al. IL15 Enhances CAR-T Cell Antitumor Activity by Reducing Mtorc1 Activity and Preserving Their Stem Cell Memory Phenotype. *Cancer Immunol Res* (2019) 7:759–72. doi: 10.1158/2326-6066.CIR-18-0466
94. Sharma P, Allison JP. Immune Checkpoint Targeting in Cancer Therapy: Toward Combination Strategies With Curative Potential. *Cell* (2015) 161:205–14. doi: 10.1016/j.cell.2015.03.030
95. Adams S, Schmid P, Rugo HS, Winer EP, Loirat D, Awada A, et al. Pembrolizumab Monotherapy for Previously Treated Metastatic Triple-Negative Breast Cancer: Cohort A of the Phase II KEYNOTE-086 Study. *Ann Oncol* (2019) 30:397–404. doi: 10.1093/annonc/mdy517
96. Gong J, Hendifar A, Tuli R, Chuang J, Cho M, Chung V, et al. Combination Systemic Therapies With Immune Checkpoint Inhibitors in Pancreatic Cancer: Overcoming Resistance to Single-Agent Checkpoint Blockade. *Clin Transl Med* (2018) 7:32. doi: 10.1186/s40169-018-0210-9
97. Lim WA, June CH. The Principles of Engineering Immune Cells to Treat Cancer. *Cell* (2017) 168:724–40. doi: 10.1016/j.cell.2017.01.016

Conflict of Interest: CEB receives royalty payments from and is an advisory board member for Mustang Bio.

The remaining authors declare that the research was conducted in the absence of any commercial or financial relationships that could be construed as a potential conflict of interest.

Publisher's Note: All claims expressed in this article are solely those of the authors and do not necessarily represent those of their affiliated organizations, or those of the publisher, the editors and the reviewers. Any product that may be evaluated in this article, or claim that may be made by its manufacturer, is not guaranteed or endorsed by the publisher.

frontiers in Oncology

ORIGINAL RESEARCH
published: 25 November 2021
doi: 10.3389/fonc.2021.736882

Pseudomonas aeruginosa PcrV Enhances the Nitric Oxide-Mediated Tumoricidal Activity of Tumor-Associated Macrophages *via* a TLR4/PI3K/AKT/mTOR-Glycolysis-Nitric Oxide Circuit

Hua Yu[1†], Ying Bai[2†], Jing Qiu[1], Xiaomei He[1], Junzhi Xiong[1], Qian Dai[1], Xingmin Wang[1], Yuanyuan Li[1], Halei Sheng[1], Rong Xin[1], Lu Jiang[1], Qiaoqiao Li[1], Defeng Li[1], Hong Zhang[3], Le Zhang[1], Qian Chen[1], Jin Peng[1], Xiaomei Hu[4] and Kebin Zhang[1*]*

[1] Clinical Medical Research Center, Xinqiao Hospital, Army Medical University, Chongqing, China, [2] Health Management Center, First Affiliated Hospital, Army Medical University, Chongqing, China, [3] Administration Department of Nosocomial Infection, Xinqiao Hospital, Army Medical University, Chongqing, China, [4] Department of Microbiology, College of Basic Medical Sciences, Army Medical University, Chongqing, China

Tumor-associated macrophages (TAMs), which display a tumor-supportive M2 phenotype, are closely related to tumor growth and metastasis. The reprogramming of TAMs toward a tumoricidal M1 profile has emerged as an attractive strategy for cancer immunotherapy. In this study, we found that the intratumoral injection of PcrV protein, a component of the *Pseudomonas aeruginosa* type 3 secretion system, suppressed tumor growth and increased apoptosis, inducible nitric oxide synthase (iNOS) expression, and the percentage of M1-polarized TAMs in tumor tissues. Furthermore, the intratumoral injection of PcrV-primed macrophages exerted a similar tumoricidal effect. *In vitro* analyses revealed that PcrV reeducated TAMs toward an antitumoral M1 phenotype and augmented their nitric oxide (NO)-mediated cytotoxicity against cancer cells. Mechanistically, we found that these effects were dependent on the activation of Toll-like receptor 4 (TLR4)/myeloid differentiation factor 88 (MyD88)-mediated regulation of a PI3K/AKT/mTOR-glycolysis-NO feedback loop *via* direct interaction with TLR4. Collectively, these results revealed a potential role for PcrV in cancer immunotherapy through the targeting of TAM plasticity.

Keywords: *Pseudomonas aeruginosa* PcrV protein, TAM reeducation, tumoricidal efficacy, TLR4/PI3K/AKT/mTOR-glycolysis-NO feedback loop, PcrV–TLR4 interaction

OPEN ACCESS

Edited by:
Xuanming Yang,
Shanghai Jiao Tong University, China

Reviewed by:
Yuli Lin,
Fudan University, China
Fang Wei,
Shanghai Jiao Tong University, China

***Correspondence:**
Kebin Zhang
zhangkebin12@163.com
Xiaomei Hu
huxiaomei@tmmu.edu.cn

†These authors share first authorship

Specialty section:
This article was submitted to Cancer Immunity and Immunotherapy, a section of the journal Frontiers in Oncology

Received: *06 July 2021*
Accepted: *04 November 2021*
Published: *25 November 2021*

Citation:
Yu H, Bai Y, Qiu J, He X, Xiong J, Dai Q, Wang X, Li Y, Sheng H, Xin R, Jiang L, Li Q, Li D, Zhang H, Zhang L, Chen Q, Peng J, Hu X and Zhang K (2021) Pseudomonas aeruginosa PcrV Enhances the Nitric Oxide-Mediated Tumoricidal Activity of Tumor-Associated Macrophages via a TLR4/PI3K/AKT/mTOR-Glycolysis-Nitric Oxide Circuit. Front. Oncol. 11:736882. doi: 10.3389/fonc.2021.736882

INTRODUCTION

Tumor-associated macrophages (TAMs) form the major component of the immune cell infiltrate in the tumor microenvironment (TME) and are correlated with tumor development and progression. Macrophages infiltrated in the immunosuppressive TME are generally induced into the tumor-supportive M2 phenotype. These M2-like TAMs play roles in supporting tumor growth and metastasis and maintaining an immunosuppressive TME by generating a series of anti-inflammatory and protumoral cytokines and mediators (1). As macrophages are highly heterogeneous and plastic, TAMs exposed to M1-associated stimuli can undergo a reversal from the protumoral M2 to the tumoricidal M1 phenotype. M1-like TAMs exert tumoricidal activity through the production of proinflammatory cytokines (e.g., TNFA and IL12), cytotoxic nitric oxide (NO), and reactive oxygen species (ROS) and the activation of Th1 immune responses *via* increasing the expression of associated major histocompatibility complex class I and class II (MHCI/II) and costimulatory molecules (CD86 and CD80) (2). Accordingly, the reeducation of TAMs from an M2 to an M1 phenotype has emerged as an attractive strategy for cancer immunotherapy.

Recent studies have shown that drugs such as paclitaxel (3) and astragaloside IV (4) can suppress tumor growth by reprogramming TAMs into an M1 phenotype. In addition, several reports have highlighted the potential efficacy of bacteria or their products in antitumoral therapy. For instance, *Mycobacterium bovis*-derived bacillus Calmette–Guérin (BCG) has already been utilized as a preferred first-line treatment for non-muscle invasive bladder carcinoma (5, 6). Additionally, modified lipopolysaccharide (LPS), a Toll-like receptor 4 (TLR4) agonist, has been tested for its antitumoral efficacy in a clinical trial (7). Given that a large number of bacterial components, such as *Brucella abortus* cell-surface protein 31 (BCSP31) protein (8) and *Vibrio cholerae* porin OmpU (9), can induce functional macrophage M1 polarization by activating the TLR-mediated signaling axis (8, 9), these results imply that bacterial products have great potential for exploitation as therapeutic reagents for cancer treatment.

PcrV, a secretory needle tip protein component of the *Pseudomonas aeruginosa* type 3 secretion system (T3SS), helps the translocator proteins PopB and PopD form a functional pore on the target cell membrane (10). PcrV, a V-antigen, elicits protective immune responses against *P. aeruginosa* infection (11, 12). However, the mechanism underlying the PcrV-mediated regulation of the host immune response remains unknown. We have previously reported that PcrV reverses host immune suppression elicited following bacterial biofilm infection *via* the activation of macrophage-mediated immune responses (13). Considering that TAMs exhibit diverse phenotypes and given their function as tumor-resident macrophages, using PcrV to reeducate TAMs and thereby enhance M1 TAM-mediated antitumoral properties is an attractive possibility that requires further investigation.

In the current study, we found that PcrV inhibited tumor growth by reprogramming TAMs to a tumoricidal M1 phenotype. We further found that PcrV-mediated TAM reprogramming potentiated their NO-mediated cytotoxicity against cancer cells, effects that were exerted through the activation of a PI3K/AKT/mTOR-glycolysis-NO feedback loop *via* direct interaction with TLR4. Our findings demonstrated that PcrV exerts an immunomodulatory effect on TAMs, providing the basis for further investigation into the potential of PcrV as a therapeutic agent for cancer immunotherapy.

MATERIALS AND METHODS

Cell Culture

Macrophages, mouse Lewis lung cancer (LLC) cells, and HEK293T cells were cultured in Dulbecco's modified Eagle's medium (DMEM) (Thermo Fisher, USA) supplemented with 10% fetal bovine serum (FBS) (HyClone, USA) at 37°C with 5% CO_2.

Animals and Ethics Statement

Male C57BL/6 mice were purchased from Biocytogen Co., Ltd (Beijing, China). The $TLR4^{-/-}$ and myeloid differentiation factor 88 $(MyD88)^{-/-}$ C57BL/6 mice were provided by Professor Qingwu Yang. Animal experiments were conducted according to the experimental animal guidelines of the Army Medical University of China.

Expression and Purification of PcrV Protein

Recombinant PcrV protein was expressed from the expression strain *Escherichia coli* JM109/pQE31-PcrV as described previously (13). Protein purification was performed using His-Trap HP affinity columns (GE Healthcare, Sweden), and endotoxin was removed using Detoxi-Gel endotoxin removing gel (Thermo Fisher, USA), according to the manufacturer's instructions.

Induction of Bone Marrow-Derived Macrophages and Tumor-Associated Macrophages *In Vitro*

Mouse bone marrow cells were isolated from the tibia and femur of C57BL/6 mice. Bone marrow-derived macrophages (BMDMs) were induced by the administration of mouse macrophage colony-stimulating factor (M-CSF; 30 ng/ml) in DMEM supplemented with 10% FBS and 100 U/ml of penicillin for 7 days at 37°C with 5% CO_2. For *in vitro* TAM induction, BMDMs were cultured in DMEM/FBS (10%) containing 20% (*v*/*v*) LLC cell culture supernatant for 24 h (14).

Mouse Tumor Models and Treatment

For PcrV administration, C57BL/6 mice were subcutaneously inoculated with 1×10^6 LLC cells. On day 9, the animals were randomly divided into two groups and were intratumorally injected with either phosphate-buffered saline (PBS; control group) or PcrV (0.5 mg/kg, every 4 days). For the BMDM inoculation experiment, mice were subcutaneously inoculated with 1×10^6 LLC cells (day 0). On days 0 and 7, the animals were peritoneally injected with 200 μl of clodronate liposomes (Liposoma BV, Netherlands) to deplete endogenous macrophages. PBS or PcrV (0.5 mg/kg) was intratumorally injected at days 12, 14, 16, and 18, while the wild type (WT),

TLR4$^{-/-}$, or MyD88$^{-/-}$ BMDMs (2×10^6 cells) primed or not with PcrV were intratumorally inoculated at days 16 and 18. At the end of the experiment, the mice were euthanized with pentobarbital, and tumor tissues were harvested for subsequent analyses.

Fluorescence-Activated Cell Sorting

Tumor tissues were minced and incubated with collagenase type II (1 mg/ml, Thermo Fisher) at 37°C for 40 min to obtain a single-cell suspension. For the staining of extracellular target proteins, 1×10^6 cells were first incubated in a mixture of PBS, 1% FBS, and anti-CD16/32 antibody (BioLegend, #101301) to block non-specific binding and then labeled with the indicated antibodies at room temperature for 30 min. Fluorescence-activated cell sorting (FACS) was performed using a Beckman Coulter Gallios flow cytometer (USA), and the results were analyzed using FlowJo software version 10.0.7 (TreeStar). The following fluorochrome-coupled antibodies were used in the experiment: anti-CD45 (#103115), anti-CD206 (#141711), anti-CD3 (#100235), anti-CD4 (#100203), anti-CD8 (#100733), anti-NK1.1 (#108709), and anti-Gr1 (#108425) (all from BioLegend); and anti-CD11b (#12-0112), anti-F4/80 (#11-4801), anti-CD11c (25–0114), anti-MHCII (#17-5321), and anti-CD86 (#17-0862) (all from eBioscience) antibodies; the fixable viability dye eFluor 506 was from eBioscience (#65-0866).

TUNEL Assay

Tissue apoptosis was detected using the TdT-mediated dUTP nick end labeling (TUNEL) assay by staining the tissue sections using an *In Situ* Cell Death Detection Kit, POD (Roche, USA), at 37°C for 30 min. Nuclei were counterstained with Hoechst 33342, and images were obtained by laser scanning confocal microscopy (Leica TCS SP5, Germany).

Immunofluorescence Staining

Murine macrophages (Raw264.7 cells) cultured on coverslips were treated with PcrV (10 μg/ml) for 24 h, fixed in 4% paraformaldehyde at room temperature for 15 min, and stained with antibodies targeting TLR4 (ProteinTech, #19811-1-AP) and PcrV (generated in our laboratory). For tissue staining, paraffin-embedded tumor tissues were sectioned and stained first with antibodies against inducible NO synthase (iNOS) (ProteinTech, # 18985-1-AP), ARG1 (ProteinTech, # 16001-1-AP), and/or F4/80 (Abcam, #ab6640) and then with the corresponding secondary antibodies (labeled with fluorescein isothiocyanate (FITC) or Alexa Fluor 647). Nuclei were counterstained with 4′,6-diamidino-2-phenylindole (DAPI) (Beyotime, China). Images were acquired by laser scanning confocal microscopy (Leica).

Co-culture and Detection of Apoptosis

BMDMs were seeded at 5×10^5 cells/well in a six-well plate and treated or not with PcrV (10 μg/ml) for 24 h. After the supernatants were discarded, the macrophages (lower chamber of a Transwell plate [0.4-μm pore; Corning, USA]) were co-cultured with LLC cells (upper chamber) in DMEM/FBS (10%) at a ratio of 1:1 for another 24 h. LLC cells were harvested and stained using an Annexin V/7-AAD apoptosis detection kit (BD Biosciences, USA) according to the manufacturer's instructions. Apoptosis was determined by FACS.

Western Blotting

Protein extraction and concentration determination were performed following the manufacturer's instructions (Beyotime). Primary antibodies targeting iNOS (BioLegend, #696802), p-AKT (Ser473) (CST, #4060), AKT (Epitomics, #1081), p-mTOR (Ser2448) (CST, #5536), mTOR (CST, #2983), COX2 (ProteinTech, #12375-1-AP), vimentin (CST, #5741), HA tag (CST, #3724), His tag (ProteinTech, #10001-0-AP), and GAPDH (ProteinTech, #60004-1-Ig) were used in this study. The relative optical densities of the protein bands were quantified using ImageJ software.

RNA Extraction and Real-Time Quantitative PCR

Total RNA extraction, reverse transcription, and RT-qPCR were performed according to the manufacturer's protocols. Primers were provided in the Supplementary Material (Table S1).

Cytokine Level

The levels of TNFA and IL12 p40/70 in the cell culture supernatants were quantified by ELISA kits (BD Biosciences, USA) according to the manufacturer's instructions.

Detection of Nitric Oxide Level

NO level in the culture supernatants was measured by Griess reagent (Beyotime, China) according to the manufacturer's instruction.

Measurement of Intracellular Reactive Oxygen Species

Cells were incubated with 2′7′-dichlorodihydrofluorescein diacetate (H2DCFDA) (Santa Cruz, USA) dye in DMEM at a final concentration of 5 μM at room temperature for 30 min. Intracellular ROS was measured by FACS.

Analysis of Lactic Acid Level

Lactic acid level in cell supernatant was measured according to the manufacturer's instruction (Dojindo Laboratories, Japan).

Extracellular Acidification Rate Determination

Cells were cultured in a Seahorse XFp cell culture microplate (Agilent, USA) at 5×10^4 cells/well. After pretreatment with the corresponding inhibitors or PcrV, the cells were washed with Seahorse XF Base Medium (103193-100, Agilent) supplemented with 2 mM of glutamine (103579, Agilent). The extracellular acidification rate (ECAR) was measured using a Seahorse XFp Glycolysis Stress Test Kit (103020-100, Agilent) with a Seahorse XFp Analyzer (Agilent) according to the manufacturer's instructions.

Migration Assay

LLC cells (3×10^4 cells in serum-free DMEM) that had been serum-starved overnight were seeded in the upper chamber of a Transwell insert (8-μm pore, 24-well, Corning). DMEM supplemented with 20% FBS and with or without PcrV (20 μg/ml) was added to the lower chamber as a chemoattractant. After incubation for 24 or 48 h, the non-migrated LLC cells in the upper chambers were removed. Migrated cells in the bottom

chamber were fixed and then stained with 0.5% crystal violet solution for 5 min. The number of migrated cells was counted under an optical microscope (Olympus, Tokyo, Japan).

Cytotoxicity Assay

Tumor cells and TAMs were treated with various concentrations of PcrV for 48 h. Cytotoxicity was assessed using a Cell Counting Kit-8 (CCK-8; Dojindo Laboratories, Japan) according to the manufacturer's protocol.

ATP Assay

Cells were lysed in lysis buffer, and the ATP concentration was tested using an enhanced ATP assay kit (Beyotime) according to the manufacturer's protocol. The luminescence data as determined using a microplate reader (Varioskan Flash, Thermo Fisher) were normalized against protein concentration.

Co-Immunoprecipitation

HEK293T cells were transfected with the pCDNA3.1-TLR4 vector using Lipofectamine 2000 (Invitrogen, USA) and cultured in an incubator at 37°C with 5% CO_2 for 48 h. The obtained cell lysates were incubated with purified PcrV (5 μg) at 4°C for 4 h before the addition of 20 μl of His Mag Sepharose™ Ni (GE Healthcare) and incubation at 4°C for 1 h. PcrV and TLR4 were detected by Western blotting using anti-His and anti-HA-tag antibodies, respectively.

Surface Plasmon Resonance

For surface plasmon resonance (SPR) analysis, 30 μg/ml of human recombinant TLR4 protein containing a 6×His tag (Abcam, #ab233665) was fixed on the NH2 sensor chip (Nicoya, Canada) using Amine Coupling Kit (Nicoya). Then, PcrV at the indicated concentrations was sequentially injected into the chamber in PBS running buffer. TLR4-PcrV interaction was detected using OpenSPR (Nicoya). The parameters of the binding reactions were calculated and analyzed using Trace Drawer software (Nicoya).

Statistical Analysis

Data were analyzed using unpaired Student's *t*-tests or one-/two-way ANOVA in GraphPad Prism version 7.0. Tumor volume data were reported as means ± SEM. Other data were expressed as means ± SD.

RESULTS

PcrV Inhibits Tumor Growth by Reprogramming Tumor-Associated Macrophages to a Tumoricidal M1 Phenotype

As PcrV has been reported to activate the host immune response (11, 12), we investigated whether PcrV exerts similar effects in the immunosuppressive TME. First, we assessed the efficacy of PcrV *in vivo* by subcutaneously inoculating LLC cells into the right flanks of C57BL/6 mice followed by intratumoral injection of PcrV (**Figure 1A**). Compared with the control group, PcrV treatment decreased tumor growth (**Figure 1B**) and weight (**Figure 1C**). We previously demonstrated that PcrV significantly increased NO production in normal BMDMs (13). Considering that NO-mediated cytotoxicity is associated with tissue apoptosis and the inhibition of tumor growth, we then evaluated the levels of tumor cell apoptosis and the expression of the NO-generating enzyme—iNOS—in PcrV-treated tumor tissues. The results showed that PcrV treatment increased the levels of apoptosis (**Figure 1D**) and iNOS expression (**Figure 1E**) in the tumor tissues, indicating that PcrV-induced NO generation is associated with the suppression of tumor growth. In addition, we also treated LLC cells and TAMs with PcrV to assess whether PcrV administration might directly cause cytotoxicity or affect tumor cell growth and metastasis. We found that at the concentrations tested, PcrV did not cause significant cytotoxicity against either tumor cells or TAMs (**Supplementary Figure 1A**). Moreover, PcrV treatment did not affect the expression levels of genes (e.g., *Cox2*, *Mmp9*, *Vegfa*, and *Hif1a*; **Supplementary Figure 1B**) or proteins (e.g., COX2 and vimentin; **Supplementary Figure 1C**) related to tumor growth and metastasis, or the metastatic ability of LLC cells (**Supplementary Figure 1D, E**).

Given that immune cells infiltrated in the TME, such as TAMs, $CD4^+$ and $CD8^+$ T cells, NK cells, and myeloid-derived suppressor cells (MDSCs), play a critical role in modulating antitumoral immune responses (15), we further analyzed the ratios of these cells in the TME following PcrV treatment. The results showed that exposure to PcrV did not significantly affect the percentages of $CD4^+$ and $CD8^+$ T cells, NK cells, or MDSCs in tumor tissues (**Supplementary Figure 2A–F**). However, even though PcrV treatment did not alter the percentage of TAMs infiltrated in the TME (**Supplementary Figure 2G, H**), the ratios of M1-polarized TAMs ($F4/80^+CD11c^+CD206^-$, $F4/80^+MHCII^+$, and $F4/80^+CD86^+$ macrophages) were increased in PcrV-treated tumor tissues (**Figures 2A–D**), whereas those of M2-polarized TAMs ($F4/80^+CD11c^-CD206^+$ macrophages) were decreased (**Figures 2A, B**). Subsequent analysis of $iNOS^+$ TAMs by immunofluorescence (IF) staining indicated that PcrV treatment increased the percentage of $F4/80^+iNOS^+$ M1 TAMs (**Figure 2E**), whereas that of $F4/80^+ARG1^+$ M2 TAMs was decreased (**Figure 2F**). Collectively, these results suggested that PcrV reeducates TAMs to a tumoricidal M1 phenotype *in vivo*.

To determine whether PcrV directly affects TAM polarization *in vitro*, we generated *in vitro*-trained TAMs by incubating BMDMs with LLC cell culture supernatant. These cells showed increased expression of genes related to tumor growth (*Cox2* and *Vegfa*), metastasis (*Cox2*, *Mmp2*, and *Mmp9*), and immune suppression (*Ido2*) (**Supplementary Figure 3A**), indicating that TAM generation *in vitro* had been successful. The levels of tumoricidal M1 polarization markers, including *iNos*, *Cd11c*, *MhcI*, *MhcII*, *Cd86* (**Supplementary Figure 3B**), iNOS (**Supplementary Figure 3C**), NO (**Supplementary Figure 3D**), IL12 p40/70, TNFA (**Supplementary Figure 3E**), MHCII, and CD86 (**Supplementary Figure 3F, G**), were found to be higher in PcrV-primed than mock-treated TAMs, whereas the levels of the protumoral M2 polarization markers *c-Myc*, *Egr2*, *Fn1*, *Arg1* (13), and *Cd206* were lower (**Supplementary Figure 3B**), demonstrating that PcrV directly reprograms TAMs to an antitumoral M1 profile *in vitro*.

To further determine whether the PcrV-mediated M1 polarization of TAMs is responsible for tumor growth inhibition, LLC tumor-bearing mice were peritoneally injected with clodronate

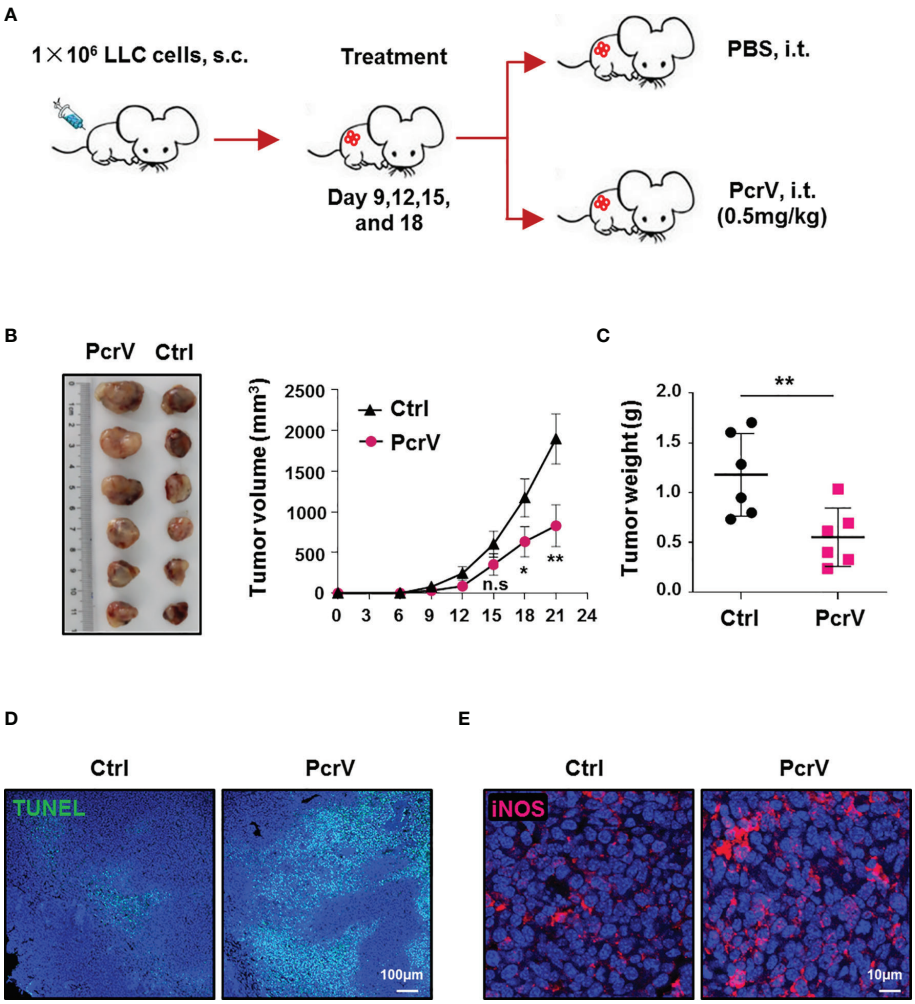

FIGURE 1 | PcrV-mediated suppression of tumor growth is associated with the increased levels of apoptosis and iNOS expression in tumor tissues. Mice bearing LLC cell-derived tumors were treated with PBS or PcrV. **(A)** Schematic of mouse models used. Tumor growth **(B)** and weight **(C)** were measured in LLC tumor-bearing mice treated with PBS or PcrV. Apoptosis **(D)** and iNOS protein level **(E)** in tumor tissues were detected by TUNEL assay and immunofluorescence staining, respectively. Data were expressed as means ± SEM (**B**, $n = 6$) or means ± SD (C, $n = 6$) and were analyzed by two-way ANOVA **(B)** or unpaired Student's t-test **(C)**. $^{*}p < 0.05$; $^{**}p < 0.01$. n.s, no significance; s.c, subcutaneous injection; i.t., intratumoral injection; iNOS, inducible nitric oxide synthase; LLC, Lewis lung cancer; PBS, phosphate-buffered saline.

liposomes to deplete endogenous macrophages, after which the mice were intratumorally injected with PBS, PcrV, or BMDMs primed or not with PcrV (**Figure 3A**). The results showed that clodronate liposome treatment reduced macrophage infiltration in tumor tissues (**Figure 3B**). The treatment with PcrV-primed BMDMs decreased tumor growth (**Figure 3C**) and weight (**Figure 3D**) and increased the levels of apoptosis (**Figure 3E**) and iNOS expression (**Figure 3F**), and the percentage of $iNOS^{+}F4/80^{+}$ TAMs (**Figure 3F**) in tumor tissues; however, PcrV treatment did not affect either tumor growth (**Figure 3C**) or weight (**Figure 3D**) in mice depleted of endogenous macrophages due to clodronate liposome administration. Collectively, these results demonstrated that the PcrV-mediated tumoricidal effect is associated with the reprogramming of TAMs to an M1 phenotype.

PcrV-Primed Tumor-Associated Macrophages Induce the Apoptosis of Cancer Cells by Enhancing Nitric Oxide-Associated Cytotoxicity *In Vitro*

Based on the above *in vivo* and *in vitro* results, we next investigated the direct cytotoxic effect of PcrV-primed BMDMs on tumor cells by co-culturing these cells with LLC cells. The co-culture of BMDMs with tumor cells polarized normal BMDMs into TAMs. Hence, BMDMs are referred to as TAMs after their co-culture with tumor cells. We found that co-culture increased the rate of apoptosis among the tumor cells (**Figures 4A, B**). Considering that ROS and NO are critical mediators of cancer cell cytotoxicity, we also examined the levels of these factors in the co-culture system. Unexpectedly, PcrV treatment did not

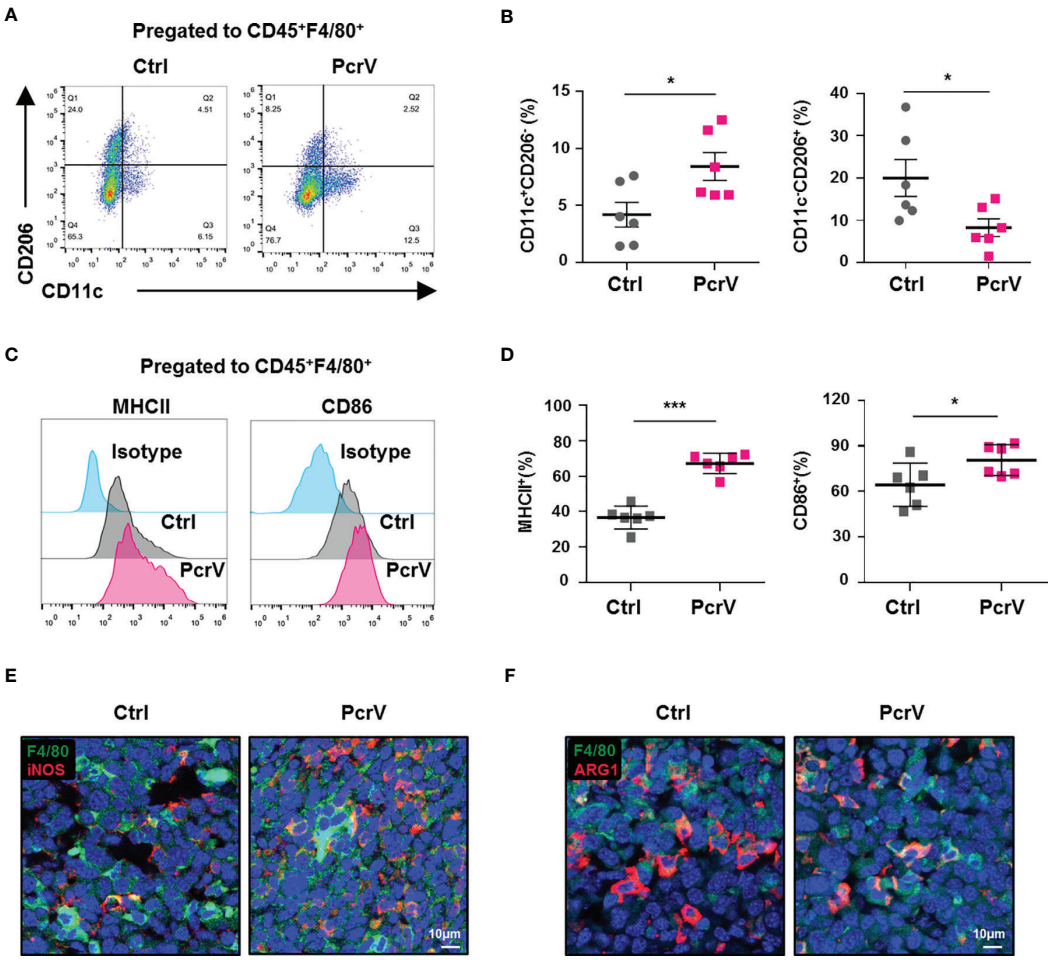

FIGURE 2 | PcrV reeducates tumor-associated macrophages (TAMs) into a tumoricidal M1 phenotype *in vivo*. Mice bearing LLC cell-derived tumors were treated with PBS or PcrV. **(A–D)** FACS analysis of the percentages of M1 ($CD45^+F4/80^+CD11c^+CD206^-$, $CD45^+F4/80^+MHCII^+$, and $CD45^+F4/80^+CD86^+$) and M2 ($CD45^+F4/80^+CD11c^-CD206^+$) TAMs in tumor tissues. **(E, F)** Immunofluorescence staining for visualizing $F4/80^+iNOS^+$ M1 and $F4/80^+Arg1^+$ M2 TAMs in tumor tissues. Data were expressed as means ± SD [**(B, D)**, $n = 6$] and analyzed by unpaired Student's *t*-test. $^*p < 0.05$ and $^{***}p < 0.001$. Ctrl indicates control. LLC, Lewis lung cancer; PBS, phosphate-buffered saline; FACS, fluorescence-activated cell sorting.

affect the levels of ROS either in TAMs or LLC cells (**Supplementary Figure 4**). In contrast, NO production was found to be higher in the PcrV/TAM-LLC cell co-culture medium than in that of the TAM-LLC cell group (**Figure 4C**). The levels of *iNos* (**Figure 4D**) and iNOS (**Figures 4E, F**) were also higher in both TAMs and LLC cells. The inhibition of NO production in PcrV/TAMs through *S*-methyl thiourea (SMT) treatment decreased apoptosis (**Figures 4A, B**) in LLC cells. The addition of the NO donor DETA-NONOate (DETA-NO) into a co-culture system in which TAMs had been pretreated with SMT led to an increase in NO levels in the culture medium (**Figure 4C**) while also promoting the apoptosis of LLC cells (**Figures 4G, H**) in the PcrV/TAM-LLC cell co-culture group, thus providing further evidence that PcrV-primed TAMs display enhanced NO-associated cytotoxicity against tumor cells.

Even though the levels of NO were similar among the three groups [LLC cells (**Supplementary Figure 5A**), TAM-LLC cell co-culture group (**Figure 4C**), and PcrV/TAM-LLC cell co-culture group (**Figure 4C**)] following the addition of DETA-NO to the culture medium, the increased concentrations of NO did not enhance the apoptosis rate of LLC cells cultured individually (**Supplementary Figure 5B**) or with BMDMs (**Figures 4G, H**) compared with that of the PcrV/TAM-LLC cell co-culture system, suggesting that the PcrV-mediated augmentation of TAM-associated cytotoxicity against cancer cells relies on a synergistic effect of NO and other factors generated by PcrV-primed TAMs.

In addition, to observe whether PcrV-primed TAMs can affect tumor growth and metastasis, BMDMs treated or not with PcrV were co-cultured with LLC cells, and the levels of related genes were analyzed. No differences in the expression levels of genes related to tumor growth and metastasis, such as *Cox2*, *Mmp9*, *Vegfa*, and *Hif1a*, were found in LLC cells that were co-cultured with PcrV-primed TAMs (**Figure 4D**).

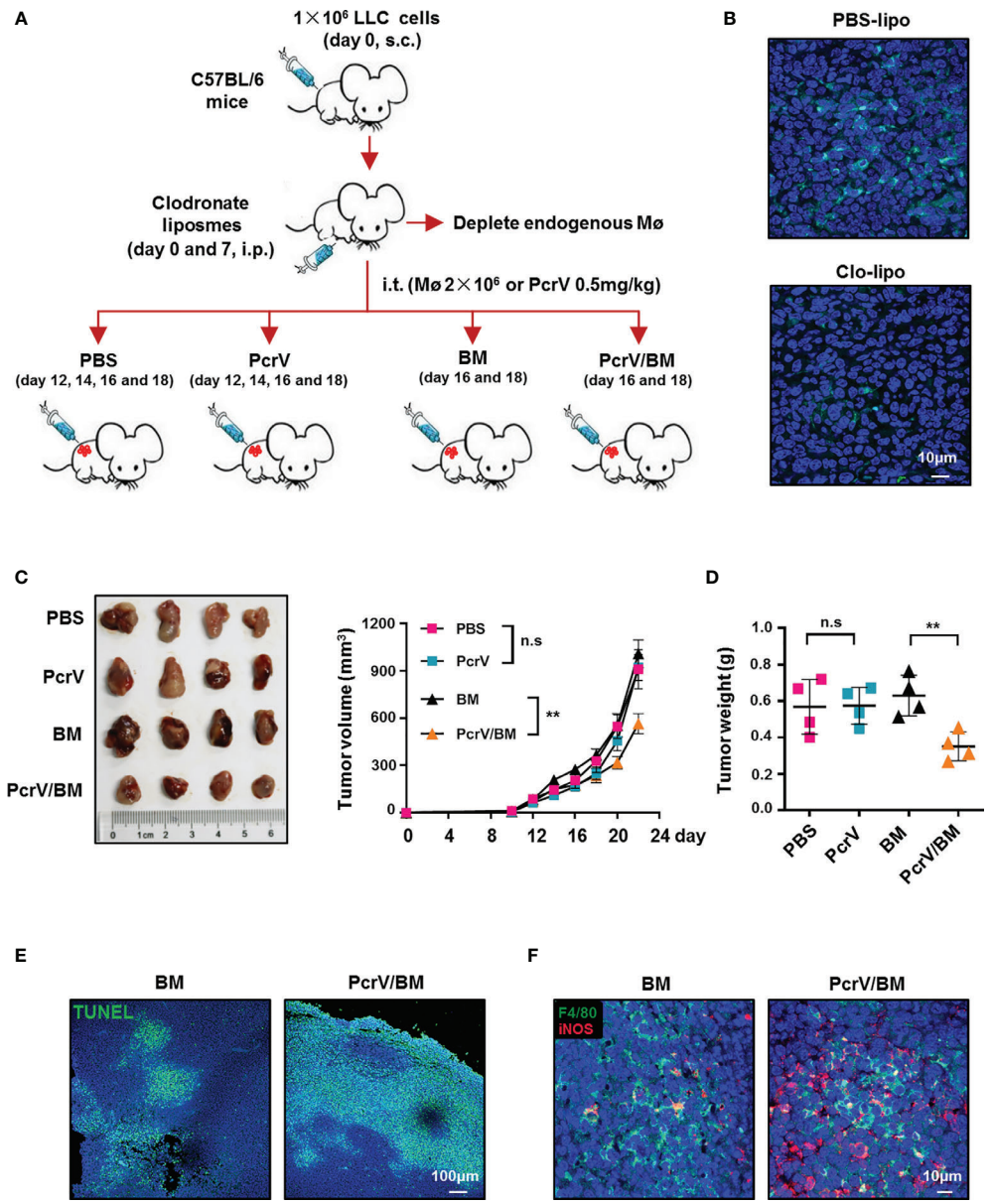

FIGURE 3 | PcrV-primed macrophages suppress tumor growth by increasing the levels of apoptosis and iNOS expression in tumor tissues. **(A)** Schematic of the mouse models used. **(B)** Immunofluorescence staining of F4/80$^+$ macrophages in the tumor tissues (harvested on day 16) of mice treated with PBS liposomes or clodronate liposomes (day 0 and 7). Tumor growth **(C)** and weight **(D)** were measured in LLC cell-derived tumor-bearing mice treated with PBS, PcrV, or bone marrow-derived macrophages (BMDMs) primed or not with PcrV. **(E)** Apoptosis was detected by TUNEL assay. **(F)** iNOS protein level and F4/80$^+$iNOS$^+$ M1 TAMs in tumor tissues were detected by immunofluorescence staining. Data were expressed as means ± SEM (**C**, $n = 4$) or means ± SD (**D**, $n = 4$), and were analyzed by two-way ANOVA **(C)** or unpaired Student's *t*-test **(D)**. $^{**}p < 0.01$. s.c, subcutaneous injection; i.p., intraperitoneal injection; i.t., intratumoral injection; BM, BMDMs; PBS-lipo, PBS liposomes; Clo-lipo, clodronate liposomes; iNOS, inducible nitric oxide synthase; PBS, phosphate-buffered saline; LLC, Lewis lung cancer. n.s, no significance.

The Rewiring of Glycolysis in Tumor-Associated Macrophages by PcrV Enhances Their Nitric Oxide-Mediated Tumoricidal Activity

M1 macrophages are reported to rely on aerobic glycolysis for their energy supply (16), suggesting that the PcrV-mediated increase in TAM cytotoxic activity against cancer cells might involve the regulation of glycolysis. Similar to that seen with LPS/IFNG-primed M1-like TAMs, PcrV treatment increased the glycolysis-related ECAR (**Figure 5A**), lactic acid production (**Figure 5B**), and ATP generation (**Figure 5C**) in TAMs. The inhibition of glycolysis in TAMs by the application of 2-deoxy-D-glucose (2-DG) suppressed the PcrV-induced production of lactic acid (**Figure 5B**) and ATP (**Figure 5C**), as well as the

levels of NO (**Figure 5D**), IL12 p40/70, and TNFA (**Figure 5E**), indicating that PcrV reprograms TAMs toward an M1 profile through increasing glycolysis. In addition, to examine the role of glycolysis in PcrV-induced, TAM-mediated cytotoxicity against cancer cells, BMDMs pretreated with 2-DG and PcrV were co-cultured with LLC cells. We found that 2-DG treatment decreased the PcrV-induced production of NO (**Figure 5F**) and the rate of apoptosis in LLC cells (**Figures 5G, H**), demonstrating that the enhancement of glycolysis by PcrV promotes the NO-associated tumoricidal activity of TAMs.

PcrV-Mediated Activation of a PI3K/AKT/mTOR-Glycolysis-Nitric Oxide Feedback Loop Promotes Tumor-Associated Macrophage Repolarization and Cytotoxicity Against Cancer Cells

Studies have shown that the PI3K/AKT/mTOR pathway is closely related to macrophage activation (17) as well as glycolysis in pulmonary fibrosis (18). To observe whether the PcrV-mediated regulation of TAM repolarization might involve this signaling pathway, we examined AKT and mTOR phosphorylation levels in TAMs treated or not with PcrV. The results revealed that PcrV treatment increased the phosphorylation levels of both proteins (**Figure 6A**) in TAMs. The treatment of PI3K, AKT, or mTOR with the corresponding inhibitor suppressed the levels of M1 markers in PcrV-treated TAMs, including that of *iNos* (**Supplementary Figure 6A**), iNOS (**Figure 6B**), NO (**Figure 6C**), IL12 p40/70, and TNFA (**Supplementary Figure 6B**) while increasing the levels of the M2 markers *Fn1*, *c-Myc*, and *Egr2* (**Supplementary Figure 6A**), suggesting that PcrV repolarizes TAMs into an M1 phenotype through the activation of the PI3K/AKT/mTOR signaling pathway. To further investigate whether the PI3K/AKT/mTOR signaling pathway is involved in the enhancement of the tumoricidal effect of TAMs elicited by PcrV, TAMs pretreated with the AKT or mTOR inhibitor plus PcrV were co-cultured with LLC cells. The suppression of AKT or mTOR activation reduced NO production in the co-culture medium (**Figure 6D**) and also decreased the levels of PcrV/TAM-induced apoptosis in LLC cells (**Figures 6E, F**).

We also investigated the cross-talk among PI3K/AKT/mTOR, glycolysis, and NO. The inhibition of PI3K, AKT, or mTOR led

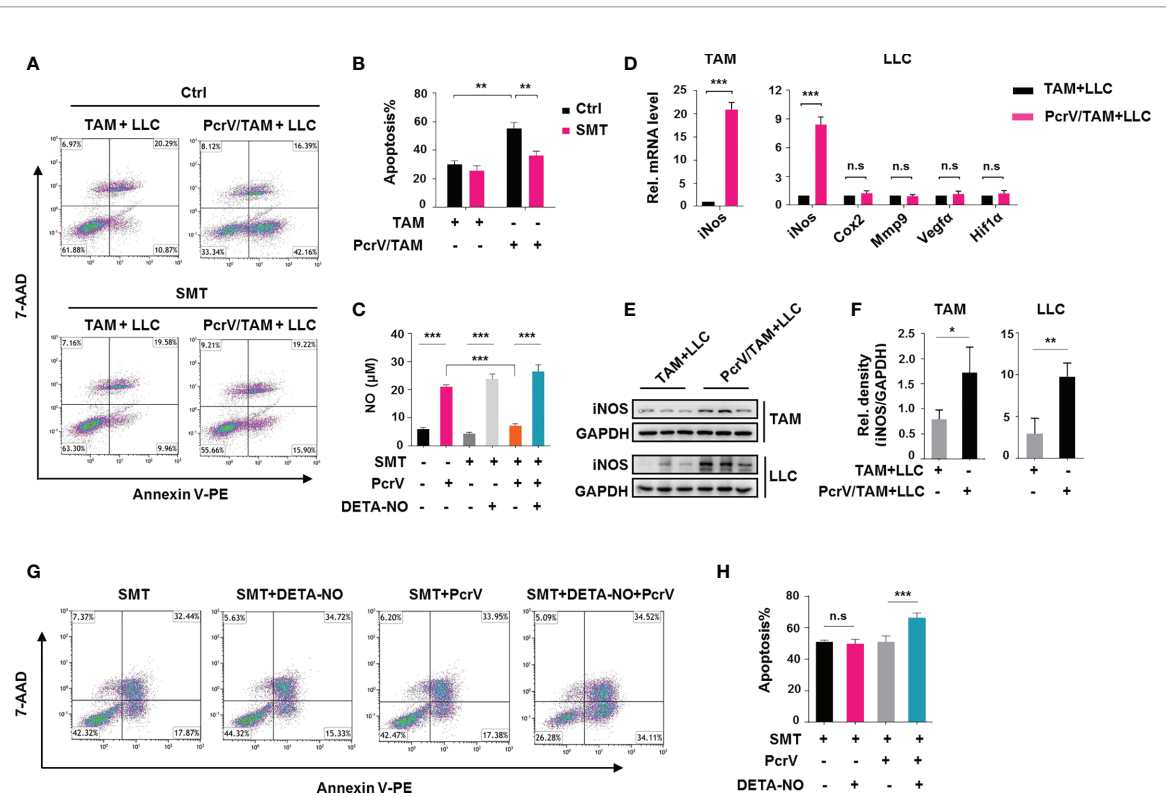

FIGURE 4 | PcrV-primed tumor-associated macrophages (TAMs) induce the apoptosis of tumor cells by enhancing nitric oxide (NO)-associated cytotoxicity *in vitro*. Bone marrow-derived macrophages (BMDMs) were treated or not with PcrV (10 μg/ml) for 24 h and then co-cultured with LLC cells for another 24 h For the inhibition of nitric oxide (NO) production, BMDMs were pretreated with *S*-methyl thiourea (SMT; 0.5 mM) for 2 h followed by exposure to PcrV. To increase the NO level, the culture medium was supplemented with the NO donor DETA-NO (20 μM). **(A, B)** LLC cell apoptosis was detected by FACS using Annexin V/7-AAD staining. **(C)** The NO level in the macrophage-LLC cell co-culture medium was detected using Griess reagent. **(D)** Gene expression levels in TAMs and LLC cells were analyzed by RT-qPCR. **(E, F)** Protein expression was analyzed by Western blotting. **(G, H)** Apoptosis in LLC cells was analyzed by FACS. Data were expressed as means ± SD and analyzed by unpaired Student's *t*-test. $^{*}p < 0.05$, $^{**}p < 0.01$, and $^{***}p < 0.001$. Rel. mRNA level indicates relative mRNA level. LLC, Lewis lung cancer; FACS, fluorescence-activated cell sorting.

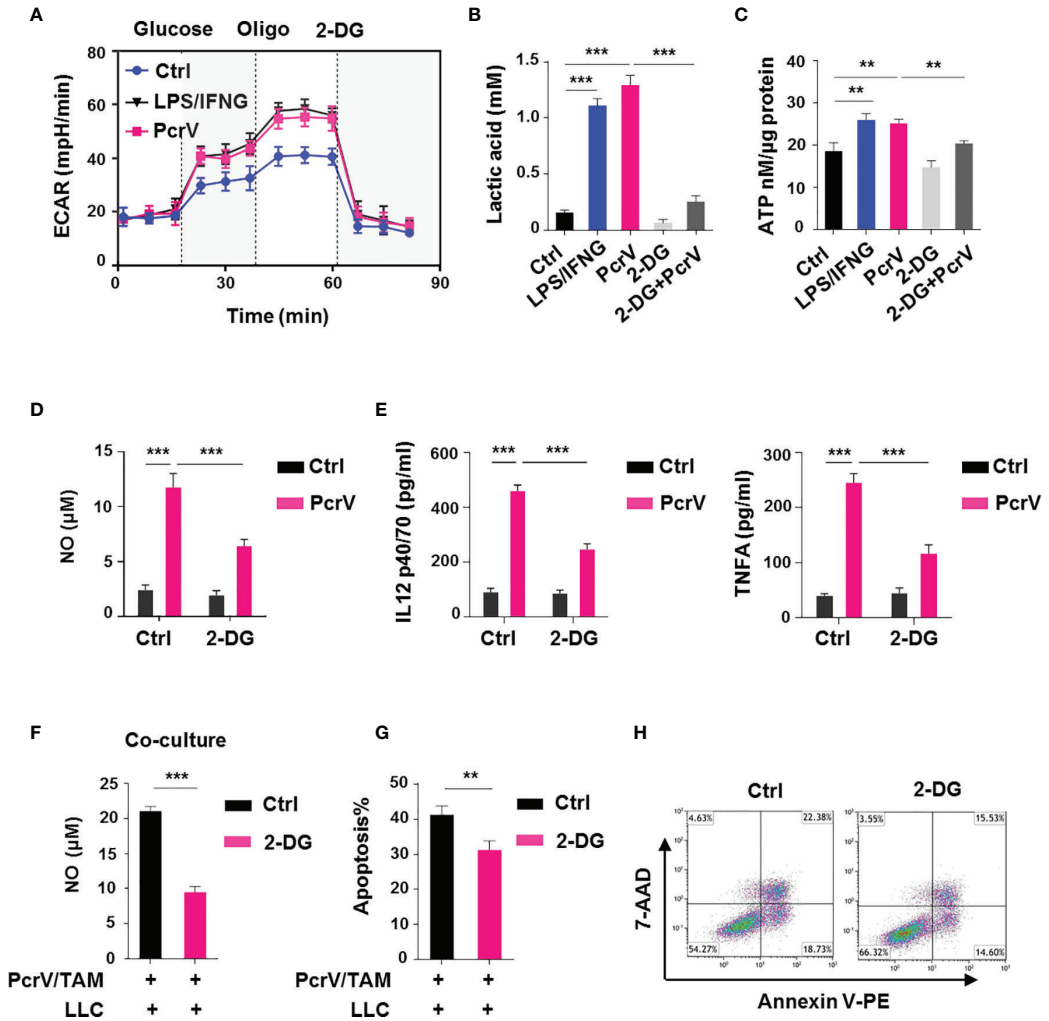

FIGURE 5 | PcrV-induced stimulation of glycolysis augments tumor-associated macrophage (TAM)-mediated tumoricidal activity. To induce TAMs *in vitro*, bone marrow-derived macrophages (BMDMs) were cultured in 10% FBS/DMEM containing 20% (*v/v*) LLC cell culture supernatant for 24 h and then primed or not with PcrV (10 μg/ml) for another 24 h For the induction of an M1-like phenotype, TAMs were pulsed with LPS (10 ng/ml) and IFNG (10 ng/ml) for 24 h For the inhibition of glycolysis, TAMs were pretreated with 2-deoxy-D-glucose (2-DG; 2 mM) for 2 h followed by exposure to PcrV for another 24 h **(A)** Assay for the extracellular acidification rate (ECAR). **(B)** Measurement of the lactic acid level in the culture supernatant. **(C)** Assay for ATP levels in cell lysates. **(D)** The NO level in the culture supernatant was detected using Griess reagent. **(E)** IL12 p40/70 and TNFA levels in the culture supernatant were analyzed by ELISA. BMDMs pretreated with 2-DG (2 mM, 2 h) were primed with PcrV (10 μg/ml) for 24 h and then co-cultured with LLC cells for another 24 h **(F)** Detection of NO level in the culture medium. **(G, H)** The apoptosis of LLC cells was detected by FACS. Data were expressed as means ± SD and analyzed by unpaired Student's *t*-test. $^{**}p < 0.01$ and $^{***}p < 0.001$. Oligo, oligomycin; FBS, fetal bovine serum; DMEM, Dulbecco's modified Eagle's medium; LLC, Lewis lung cancer; FACS, fluorescence-activated cell sorting.

to impaired glycolysis-related ECAR and lactic acid production in PcrV-primed TAMs (**Figures 6G, H**). Inversely, the suppression of glycolysis by 2-DG led to impaired AKT and mTOR phosphorylation and iNOS expression (**Figure 6I**), suggesting that glycolysis positively regulates AKT/mTOR activation and NO generation in PcrV-primed TAMs. Given that NO promotes glycolysis in neurons (19) and also activates the PI3K/AKT axis in cancer cells (20, 21), we next examined the role of NO in triggering AKT/mTOR activation and glycolysis in PcrV-primed TAMs. Inhibiting NO generation in PcrV-primed TAMs with SMT treatment reduced AKT and mTOR phosphorylation (**Figure 6J**) as well as the ECAR (**Figure 6G**) and lactic acid levels (**Figure 6H**). Intriguingly, the exogenous administration of DETA-NO in combination with PcrV, but not DETA-NO alone, promoted AKT/mTOR activation in TAMs (**Figure 6K**) and upregulated lactic acid production (**Figure 6L**), indicating that NO-associated regulation of glycolysis and the AKT/mTOR signaling pathway in TAMs requires the involvement of other factors activated by PcrV. Collectively, these results indicated that the PcrV-mediated increase in the antitumoral effects of TAMs is associated with the activation of a PI3K/AKT/mTOR-glycolysis-NO feedback loop.

TLR4/MyD88-Mediated Activation of the PI3K/AKT/mTOR-Glycolysis-Nitric Oxide Circuit Is Involved in Enhancing the Tumoricidal Activity of PcrV-Primed Tumor-Associated Macrophages

TLR4, a key pattern recognition receptor (PPR), is abundantly expressed on immune cells, where it functions in the recognition of pathogen-associated molecular patterns (PAMPs). Following pathogen recognition, TLR4 activates host immune response through both MyD88-dependent and MyD88-independent mechanisms (22). Given that PcrV is a needle tip protein component of the T3SS of *P. aeruginosa*, it seems likely that it can interact with host PPRs and thus activate immune responses. To address this possibility, we investigated the role of the TLR4/MyD88 signaling pathway in PcrV-mediated regulation of TAM polarization. Compared with WT PcrV-primed TAMs, TLR4$^{-/-}$ or MyD88$^{-/-}$ PcrV-primed TAMs showed reduced levels of NO (**Figure 7A**), *iNos* (**Figure 7B**), iNOS (**Figure 7C**), IL12 p40/70, and TNFA (**Supplementary Figure 7A**) but higher levels of *c-Myc*, *Egr2*, and *Fn1* (**Supplementary Figure 7B**), suggesting that PcrV skews the TAM phenotype toward an M1 profile through the TLR4-MyD88 signaling pathway.

As it has been reported that the PI3K/AKT/mTOR pathway is under the control of the TLR4/MyD88 signaling axis (23), we next examined PI3K/AKT/mTOR pathway activation in TLR4$^{-/-}$ or MyD88$^{-/-}$ PcrV-primed TAMs. The results showed that the PcrV-induced activation of AKT and mTOR was impaired in TLR4$^{-/-}$ or MyD88$^{-/-}$ TAMs, respectively (**Figure 7C**). Analyses of glycolysis-related factors demonstrated that the PcrV-induced increase in the ECAR (**Figure 7D**) and lactic acid production (**Figure 7E**) was reduced in TLR4$^{-/-}$ and MyD88$^{-/-}$ TAMs.

We further analyzed the role of the TLR4/MyD88 axis in the PcrV-mediated regulation of the tumoricidal effect of TAMs. The co-culture of LLC cells with PcrV-primed TLR4$^{-/-}$ or MyD88$^{-/-}$

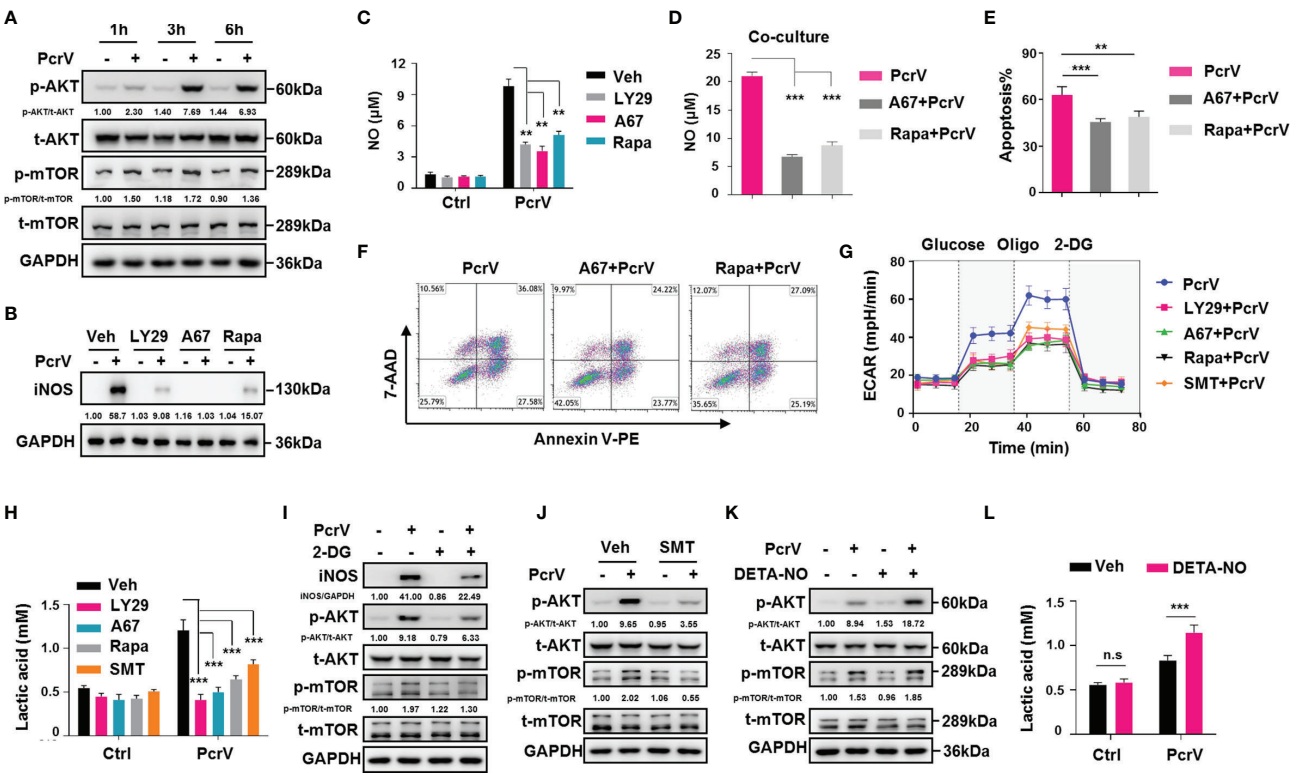

FIGURE 6 | PcrV-mediated activation of the PI3K/AKT/mTOR-glycolysis-NO feedback loop reeducates tumor-associated macrophage (TAMs) and enhances TAM-mediated cytotoxicity against cancer cells. For the inhibition of the PI3K/AKT/mTOR axis, TAMs were pretreated with a PI3K (LY294002, 20 μM), AKT (A674563, 1 μM), or mTOR (rapamycin, 50 μM) inhibitor for 1 h and then primed with PcrV (10 μg/ml) for the indicated times. **(A, B)** Protein levels were analyzed by Western blotting. **(C)** The nitric oxide (NO) level in the culture supernatant (24 h) was detected using Griess reagent. Bone marrow-derived macrophages (BMDMs) pretreated with AKT or mTOR for 1 h were primed with PcrV (10 μg/ml) for 24 h and then co-cultured with LLC cells for another 24 h **(D)** Detection of NO levels in the culture medium. **(E, F)** The apoptosis of LLC cells was detected by FACS. TAMs pretreated with the PI3K/AKT/mTOR inhibitors (1 h), *S*-methyl thiourea (SMT; 0.5 mM, 2 h), or 2-deoxy-D-glucose (2-DG; 2 mM, 2 h) were primed with PcrV (10 μg/ml) for another 24 h **(G)** Extracellular acidification rate (ECAR) measurement. **(H)** Measurement of lactic acid levels in the culture supernatant. **(I, J)** Protein levels were analyzed by Western blotting. For increasing the NO concentration, TAM culture medium was supplemented with DETA-NO (20 μM) in combination or not with PcrV (1 μg/ml) for 24 h **(K)** Protein levels were analyzed by Western blotting. **(L)** Measurement of lactic acid level in the culture supernatant. Data were expressed as means ± SD and analyzed by unpaired Student's *t*-test. $^{**}p < 0.01$ and $^{***}p < 0.001$. Oligo, oligomycin; Veh, vehicle; LY29, LY294002; A67, A674563; Rapa, rapamycin; LLC, Lewis lung cancer; FACS, fluorescence-activated cell sorting.

TAMs, but not WT TAMs, reduced NO production in the culture medium (**Figure 7F**) as well as the levels of apoptosis in LLC cells (**Figures 7G, H**). In addition, the LLC tumor-bearing mice in which endogenous macrophages were depleted by clodronate liposomes were intratumorally injected with WT, TLR4$^{-/-}$, or MyD88$^{-/-}$ BMDMs primed or not with PcrV (**Supplementary Figure 8A**). The result showed that treatment with PcrV-primed WT BMDMs, but not TLR4$^{-/-}$ or MyD88$^{-/-}$ BMDMs, decreased tumor growth (**Supplementary Figure 8B**) and weight (**Supplementary Figure 8C**). Collectively, these results indicated that the TLR4/MyD88 signaling axis participates in the PcrV-mediated modulation of the PI3K/AKT/mTOR-glycolysis-NO circuit and the tumoricidal effect of TAMs.

Direct Interaction Between PcrV and TLR4 Is Required for the PcrV-Mediated Reeducation of Tumor-Associated Macrophages

To further explore whether PcrV alters TAM polarization through interaction with TLR4, we performed immunoprecipitation by incubating purified PcrV protein with the lysate of HEK293T cells overexpressing recombinant human TLR4 protein. The result showed a successful pull-down of TLR4 protein by PcrV (**Figure 7I**). SPR analysis using purified protein further revealed a direct interaction between TLR4 and PcrV (**Figure 7J**). Moreover, IF staining result showed that PcrV colocalized with TLR4 in Raw264.7 macrophages (**Figure 7K**). In addition, to examine the effect of PcrV–TLR4 interaction on PcrV-mediated regulation of TAMs, we blocked TLR4 using an antibody, and we found that the PcrV-induced production of IL12 p40/70, TNFA (**Supplementary Figure 7C**), and NO (**Supplementary Figure 7D**) in TAMs was reduced, indicating that PcrV-mediated regulation of TAM repolarization involves direct interaction between PcrV and TLR4.

DISCUSSION

TAMs can constitute up to 50% of a tumor mass, forming the major component of the tumor immune cell infiltrate. In the TME, M2-like TAMs promote tumor cell growth, invasion, and metastasis, angiogenesis, and infiltration of immune-suppressive cells, while suppressing antitumoral immune surveillance (24). In addition, TAMs are known to increase resistance to standard-of-care therapeutics, including chemotherapy, irradiation, and angiogenic inhibitors (25). In contrast, tumoricidal M1-like macrophages, which express high levels of TNF, iNOS, and MHC molecules and low levels of ARG1, IL-10, CD163, and CD206 (26), play roles in reversing immune suppression in the TME and enhancing macrophage- or T cell-mediated killing of cancer cells. In tumor-initiating conditions, macrophages exhibit antitumoral activity; however, once tumors are established, macrophages are reeducated into a protumoral phenotype (27), likely because macrophages are highly plastic in terms of functional reprogramming in response to stimuli in the TME, such as hypoxia, cytokines, and chemokines, as well as in response to varied interactions with components of the extracellular matrix (24, 28). Hence, approaches that can potentiate TAM reprogramming into a tumoricidal M1 phenotype show great promise in cancer immunotherapy. In this study, we found that intratumoral injection of PcrV reduces tumor growth and increases the rate of apoptosis in tumor tissues by reeducating TAMs into an M1 profile characterized by the elevated expression of M1 markers (e.g., iNOS, MHCII, and CD86) and reduced levels of M2 markers (e.g., ARG1 and CD206). Additionally, we found that PcrV-induced NO production increased M1 TAM-mediated cytotoxicity against cancer cells *in vitro*. These results highlight the feasibility of utilizing *P. aeruginosa*-derived PcrV in immunomodulation and cancer therapy. Similarly, other well-known bacterial molecules, such as MPT63 (*M. bovis*), arginine deiminase (*Mycoplasma arginine*), lapidated-azurin (*Neisseria meningitidis*), and azurin (*P. aeruginosa*), have been reported as potential anticancer drugs (29). However, factors such as bacterial endotoxin, manufacturing technique, protein stability, administration mode, and biosafety still need to be addressed when utilizing bacteria-derived proteins as antitumoral drugs (29, 30).

TLR4, which is expressed on immune cells such as macrophages, dendritic cells (DCs), T cells, neutrophils, and epithelial cells, is one of the major sensors of PAMPs/damage-associated molecular patterns (DAMPs) that activate adaptive immune responses. The activation of TLR4 on multiple immune cells, such as T cells and DCs, represents a powerful means of suppressing tumor growth (31–33). In addition, several studies have reported that TLR4-dependent TAM reprogramming into an M1 profile reduces tumor growth (3, 34). In this study, we found that PcrV directly interacts with TLR4 expressed on macrophages, which induces TAM M1 polarization and enhances TAM-mediated killing of tumor cells *via* the TLR4/MyD88 signaling pathway. Surprisingly, the activation of TLR4 expressed on tumor cells has been proposed to also promote tumor development by increasing the production of oncogenic mediators (e.g., COX2, IL6, VEGF, and TGFβ) *via* the activation of proinflammatory and protumoral signaling pathways, such as the NF-κB, MAPK, and COX2/PGE2 pathways (35, 36). However, in this study, LLC cells treated with PcrV or PcrV-primed macrophages did not show significantly increased production of oncogenic mediators or metastatic ability, indicating that PcrV exerts its antitumoral effects mainly through the targeting of TAMs. The differences observed between macrophages and cancer cells might be partially attributable to differences in the expression levels of TLR4 or other accessory molecules expressed on these cells.

The PI3K/AKT/mTOR axis, which is regulated by TLR4, functions as a critical signaling pathway in modulating macrophage polarization. The inhibition of the PI3K/AKT/mTOR or the PI3K/AKT signaling pathway in macrophages suppresses M1 macrophage polarization (17) and polarizes M1 macrophages into an M2-like phenotype (37). In addition, both the PI3K/AKT/mTOR and AKT/mTOR axes are reported to be involved in enhancing glycolysis in tumor cells (38) and TAMs (39), which, in turn, promotes tumor cell survival and proliferation. In line with these findings, our results showed

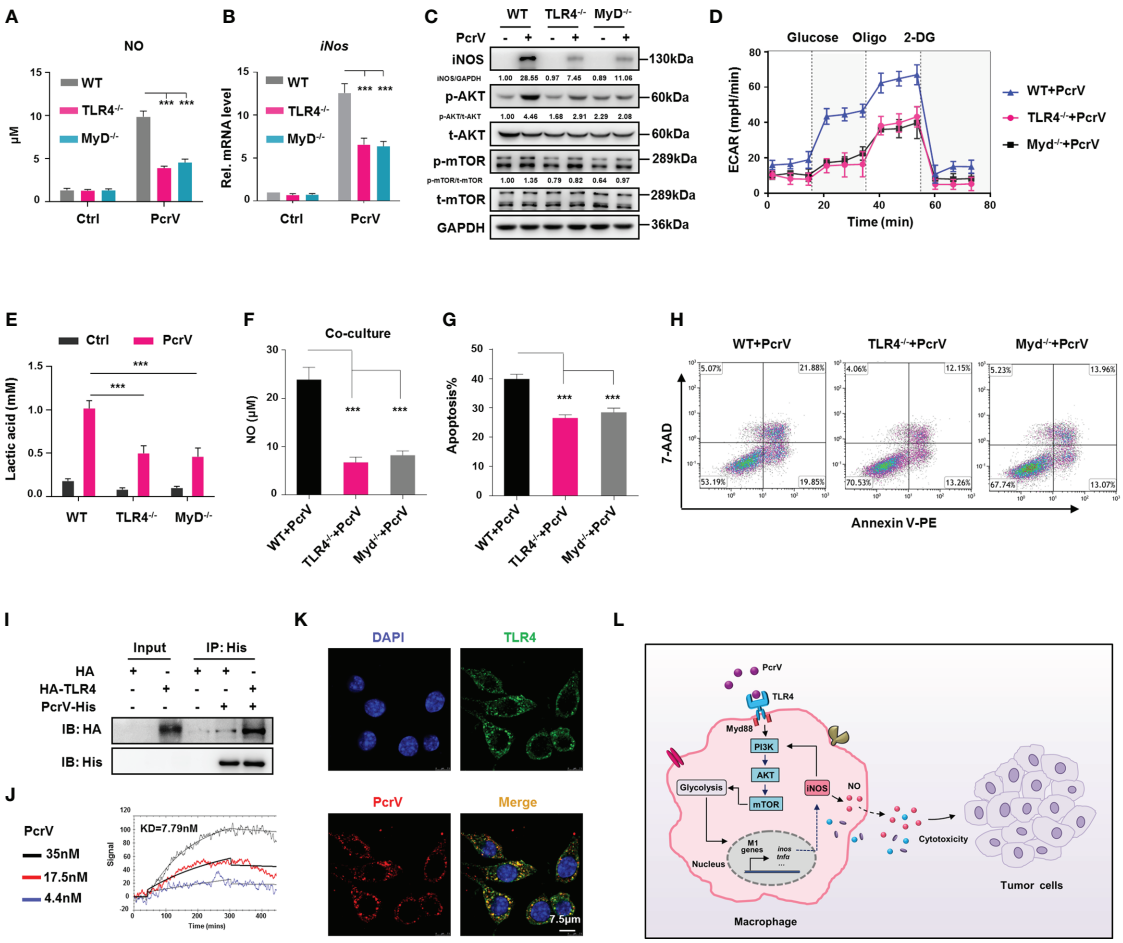

FIGURE 7 | TLR4/MyD88-mediated activation of the PI3K/AKT/mTOR-glycolysis-NO circuit promotes PcrV-induced M1 polarization and tumor-associated macrophage (TAM)-mediated cytotoxicity. Wild type (WT), TLR4$^{-/-}$, and MyD88$^{-/-}$ TAMs were treated with PcrV (10 μg/ml) for 24 h **(A)** The nitric oxide (NO) level in the culture supernatant was measured using Griess reagent. **(B)** *iNos* expression levels were analyzed by RT-qPCR. **(C)** Protein levels were analyzed by Western blotting. **(D)** Assay for the extracellular acidification rate (ECAR). **(E)** Measurement of the lactic acid level in the culture supernatant. WT, TLR4$^{-/-}$, and MyD88$^{-/-}$ bone marrow-derived macrophages (BMDMs) were pretreated with PcrV (10 μg/ml) for 24 h and then co-cultured with LLC cells for another 24 h **(F)** Detection of NO level in the culture medium. **(G, H)** The apoptosis of LLC cells was detected by FACS. **(I)** The lysates of HEK293T cells overexpressing recombinant human TLR4 were incubated with purified PcrV protein. A co-immunoprecipitation (Co-IP) assay and Western blotting were performed to detect the interaction between PcrV and TLR4. **(J)** Direct interaction between TLR4 and PcrV was analyzed using surface plasmon resonance (SPR). **(K)** PcrV/TLR4 co-colonization on Raw264.7 cells was visualized using immunofluorescence (IF) staining. **(L)** Schematic diagram of the molecular mechanism by which PcrV reeducates TAMs and enhances TAM-mediated antitumoral activity. Data were expressed as means ± SD and analyzed by unpaired Student's *t*-test. ***$p < 0.001$. MyD indicates MyD88. TLR4, Toll-like receptor 4; MyD88, myeloid differentiation factor 88; LLC, Lewis lung cancer; FACS, fluorescence-activated cell sorting.

that PcrV-induced activation of the PI3K/AKT/mTOR pathway promotes both M1 polarization and glycolysis in TAMs. However, in contrast to previously reported results, we found that PcrV-primed TAMs exert cytotoxic effects against cancer cells rather than protumoral activity. These discrepant results might be partially explained by the contrasting (cytoprotective/cytotoxic) effects elicited by NO.

NO, a gas with diverse biological activities produced from arginine by NO synthases, has long been known as a cytotoxic agent that can directly induce the apoptosis of cancer cells (40), as well as enhance radiation-/chemotherapeutic agent-induced apoptosis of cancer cells (41, 42). In our study, we found that the co-culture of LLC cells with PcrV-primed TAMs leads to a marked increase in NO levels in the co-culture medium as well as iNOS expression in LLC cells, which, in turn, induces LLC cell apoptosis in a NO-dependent manner. Intriguingly, the supplementation of exogenous NO to LLC cells or TAM-LLC cell co-culture medium did not enhance LLC cell apoptosis, whereas increased levels of LLC cell apoptosis were seen when exogenous NO was applied to co-cultures of LLC cells and PcrV-primed TAMs. These results indicate that NO-associated cytotoxicity relies on the involvement of other mediators supplied by macrophages following PcrV priming. In contrast to the NO-associated cytotoxic effects, NO has been suggested to enhance tumor cell growth and metastasis (43) and help tumor cells resist chemotherapeutic agent-induced apoptosis (44).

These contradictory effects might be due to the concentration and duration of exposure to NO encountered by cancer cells (45). NO is cytoprotective at low/physiological levels or with short exposure time but is cytotoxic when produced at high concentrations or under long periods of exposure (46). We and others have reported that PI3K/AKT/mTOR activation and glycolysis rewire TAMs into an M1-polarized phenotype that, in turn, promotes NO production (47, 48). Here, we further found that NO, in combination with PcrV, activates the PI3K/AKT/mTOR-glycolysis signaling pathway in TAMs, resulting in the formation of a PI3K/AKT/mTOR-glycolysis-NO feedback loop that increases NO generation and, consequently, NO-associated cytotoxicity against cancer cells (**Figure 7L**).

Combined, our findings revealed a tumoricidal role for PcrV mediated by the reeducation of TAMs into a tumoricidal M1 phenotype through the modulation of a PI3K/AKT/mTOR-glycolysis-NO feedback loop *via* a direct interaction with TLR4. Our findings provide an alternative therapeutic approach for inhibiting tumor development.

DATA AVAILABILITY STATEMENT

The raw data supporting the conclusions of this article will be made available by the authors, without undue reservation.

ETHICS STATEMENT

The animal study was reviewed and approved by Army Medical University of China.

AUTHOR CONTRIBUTIONS

KZ, XHe, and HY designed the experiment. KZ, HY, YB, and XHu analyzed the data and wrote the manuscript. YB, HY, JQ, JX, QD, XW, YL, HS, RX, LJ, QL, DL, HZ, LZ, QC, and JP performed the experiments. All authors contributed to the article and approved the submitted version.

FUNDING

This project was supported by grants from the National Natural Science Foundation of China (No. 31872634 and No. 31700129), Basic Foundation of Army Medical University (2021-2018-067) and Special Financial Aid to Postdoctoral Research Fellow in Chongqing.

ACKNOWLEDGMENTS

We thank Professor Qingwu Yang for providing the $TLR4^{-/-}$ and $MyD88^{-/-}$ C57BL/6 mice.

SUPPLEMENTARY MATERIAL

The Supplementary Material for this article can be found online at: https://www.frontiersin.org/articles/10.3389/fonc.2021.736882/full#supplementary-material

Supplementary Figure 1 | PcrV does not exert apparent cytotoxicity and protumoral effect. LLC cells and TAMs were treated with PcrV at the indicated concentrations for 48 h. **(A)** Cell viability was analyzed by CCK8 assay. **(B)** Gene expression levels of LLC cells were analyzed by RT-qPCR. **(C)** Protein levels of LLC cells were detected by Western blotting. **(D, E)** Metastatic ability of LLC cells treated with or without PcrV (10 μg/mL) for 24 or 48 h was analyzed. Data were expressed as means ± SD and analyzed by one-way ANOVA **(A, B)** or unpaired Student's t-test **(E)**. n.s (No significance); Rel. mRNA level (Relative mRNA level).

Supplementary Figure 2 | PcrV treatment does not affect the percentages of CD4+ and CD8+ T cells, NK cells and MDSCs in tumor tissues of LLC tumor-bearing mice. FACS analysis of the percentages of CD4+ T (CD45+CD4+), CD8+ T (CD45+CD8+) **(A, B)**, NK cells (CD45+NK1.1+) **(C, D)**, MDSCs (CD45+CD11b +Gr1+) **(E, F)** and TAMs (CD45+F4/80+) **(G, H)** in tumor tissues of LLC tumor-bearing mice treated with PBS or PcrV. Data were expressed as means ± SD (n = 6) and analyzed by unpaired Student's t-test.

Supplementary Figure 3 | PcrV skews TAMs towards an M1 phenotype in vitro. TAMs were induced by treating BMDMs with 10% FBS/DMEM containing 20% (v/v) LLC cell culture supernatant for 24 h. TAMs were then primed with or without PcrV (10 μg/mL) for another 24 h. **(A, B)** Gene expression levels were analyzed by RT-qPCR. **(C)** iNOS protein level was analyzed by Western blotting. **(D)** NO production in culture supernatant was measured by Griess reagent. **(E)** IL12 p40/70 and TNFA levels in culture supernatants were analyzed by ELISA. **(F, G)** Cell surface markers, MHCII and CD86, were analyzed by FACS. Data were expressed as means ± SD and analyzed by unpaired Student's t-test. $^{**}P < 0.01$ and $^{***}P < 0.001$.

Supplementary Figure 4 | PcrV does not affect ROS production in TAMs or LLC cells. BMDMs were pretreated with or without PcrV (10 μg/mL) for 24 h. Then, the supernatants were discarded, and cells were cocultured with LLC cells for 24 h by using Transwell plate (0.4-μm pore). TAMs and LLC cells were separately harvested and stained with H2DCFDA at RT for 30 min. Intracellular ROS in TAMs **(A, B)** and LLC cells **(C, D)** were measured by FACS. Data were expressed as means ± SD and analyzed by unpaired Student's t-test.

Supplementary Figure 5 | NO does not enhance the apoptosis rate of LLC cells cultured individually. The NO donor, DETA-NO, was supplemented into the culture medium of LLC cells, and then cells were incubated at 37°C with 5% CO2 for 24 h. **(A)** NO production in culture supernatant was measured by Griess reagent. **(B)** Apoptosis was analyzed by FACS. Data were expressed as means ± SD, and analyzed by one-way ANOVA. $^{**}P < 0.01$ and $^{***}P < 0.001$.

Supplementary Figure 6 | PI3K/AKT/mTOR signaling pathway is involved in PcrV-mediated regulation of TAM polarization. TAMs were pretreated with the inhibitor of PI3K (LY294002, 20 μM), AKT (A674563, 1 μM) or mTOR (Rapamycin, 50 μM) for 1 h. Then, the cells were primed with PcrV (10 μg/mL) for another 24 h. **(A)** Gene expression levels were analyzed by RT-qPCR. **(B)** IL12 p40/70 and TNFA levels in culture supernatants were detected by ELISA. Data were expressed as means ± SD and analyzed by unpaired Student's t-test. $^{**}P < 0.01$ and $^{***}P < 0.001$. Veh (Vehicle), LY29 (LY294002), A67 (A674563) and Rapa (Rapamycin).

Supplementary Figure 7 | PcrV regulates TAM polarization via the TLR4-MyD88 signaling pathway. WT, TLR4-/- and MyD88-/- TAMs were treated with PcrV (10 μg/mL) for 24 h. **(A)** IL12 p40/70 and TNFA levels in culture supernatants were analyzed by ELISA. **(B)** Gene expression levels were analyzed by RT-qPCR. TAMs were pretreated with TLR4 antibody (5 μg/mL)at 37°C for 1 h to block TLR4 expressed on TAMs. Then, the cells were primed with PcrV (10 μg/mL) for 24 h. **(C)** Detection of IL12 p40/70 and TNFA levels in culture supernatants. **(D)** NO level in culture supernatant was measured by Griess reagent. Data were expressed as means ± SD and compared by unpaired Student's t-test. $^{*}P < 0.05$, $^{**}P < 0.01$ and $^{***}P < 0.001$. Ab indicates antibody.

Supplementary Figure 8 | PcrV-primed BMDMs, but not TLR4$^{-/-}$ or MyD88$^{-/-}$ BMDMs, suppress tumor growth. **(A)** Schematic of the mouse models used. Tumor growth **(B)** and weight **(C)** were measured in LLC cell-derived tumor-bearing mice treated with WT, TLR4$^{-/-}$ or MyD88$^{-/-}$ BMDMs primed or not with PcrV. Data were expressed as means ± SEM [**(B)**, n = 4] or means ± SD [**(C)**, n = 4], and were analyzed by two-way ANOVA **(B)** or unpaired Student's t-test **(C)**. **P < 0.01.

REFERENCES

1. Gambardella V, Castillo J, Tarazona N, Gimeno-Valiente F, Martínez-Ciarpaglini C, Cabeza-Segura M, et al. The Role of Tumor-Associated Macrophages in Gastric Cancer Development and Their Potential as a Therapeutic Target. *Cancer Treat Rev* (2020) 86:102015. doi: 10.1016/j.ctrv.2020.102015
2. Pathria P, Louis TL, Varner JA. Targeting Tumor-Associated Macrophages in Cancer. *Trends Immunol* (2019) 40(4):310–27. doi: 10.1016/j.it.2019.02.003
3. Wanderley CW, Colón DF, Luiz JPM, Oliveira FF, Viacava PR, Leite CA, et al. Paclitaxel Reduces Tumor Growth by Reprogramming Tumor-Associated Macrophages to an M1 Profile in a TLR4-Dependent Manner. *Cancer Res* (2018) 78(20):5891–900. doi: 10.1158/0008-5472.CAN-17-3480
4. Xu F, Cui WQ, Wei Y, Cui J, Qiu J, Hu LL, et al. Astragaloside IV Inhibits Lung Cancer Progression and Metastasis by Modulating Macrophage Polarization Through AMPK Signaling. *J Exp Clin Cancer Res* (2018) 37 (1):207. doi: 10.1186/s13046-018-0878-0
5. Kiselyov A, Bunimovich-Mendrazitsky S, Startsev V. Treatment of non-Muscle Invasive Bladder Cancer With Bacillus Calmette-Guerin (BCG): Biological Markers and Simulation Studies. *BBA Clin* (2015) 4:27–34. doi: 10.1016/j.bbacli.2015.06.002
6. Svatek RS, Zhao XR, Morales EE, Jha MK, Tseng TY, Hugen CM, et al. Sequential Intravesical Mitomycin Plus Bacillus Calmette-Guérin for non-Muscle-Invasive Urothelial Bladder Carcinoma: Translational and Phase I Clinical Trial. *Clin Cancer Res* (2015) 21(2):303–11. doi: 10.1158/1078-0432.CCR-14-1781
7. Shetab Boushehri MA, Lamprecht A. TLR4-Based Immunotherapeutics in Cancer: A Review of the Achievements and Shortcomings. *Mol Pharm* (2018) 15(11):4777–800. doi: 10.1021/acs.molpharmaceut.8b00691
8. Li JY, Liu Y, Gao XX, Gao X, Cai H. TLR2 and TLR4 Signaling Pathways are Required for Recombinant Brucella Abortus BCSP31-Induced Cytokine Production, Functional Upregulation of Mouse Macrophages, and the Th1 Immune Response *In Vivo* and In Vitro. *Cell Mol Immunol* (2014) 11(5):477–94. doi: 10.1038/cmi.2014.28
9. Khan J, Sharma PK, Mukhopadhaya A. Vibrio Cholerae Porin OmpU Mediates M1-Polarization of Macrophages/Monocytes *via* TLR1/TLR2 Activation. *Immunobiology* (2015) 220(11):1199–209. doi: 10.1016/j.imbio.2015.06.009
10. Mueller CA, Broz P, Cornelis GR. The Type III Secretion System Tip Complex and Translocon. *Mol Microbiol* (2008) 68(5):1085–95. doi: 10.1111/j.1365-2958.2008.06237.x
11. Wan C, Zhang J, Zhao L, Cheng X, Gao C, Wang Y, et al. Rational Design of a Chimeric Derivative of PcrV as a Subunit Vaccine Against Pseudomonas Aeruginosa. *Front Immunol* (2019) 10:781. doi: 10.3389/fimmu.2019.00781
12. Hamaoka S, Naito Y, Katoh H, Shimizu M, Kinoshita M, Akiyama K, et al. Efficacy Comparison of Adjuvants in PcrV Vaccine Against Pseudomonas Aeruginosa Pneumonia. *Microbiol Immunol* (2017) 61(2):64–74. doi: 10.1111/1348-0421.12467
13. Yu H, Xiong J, Qiu J, He X, Sheng H, Dai Q, et al. Type III Secretion Protein, PcrV, Impairs Pseudomonas Aeruginosa Biofilm Formation by Increasing M1 Macrophage-Mediated Anti-Bacterial Activities. *Front Microbiol* (2020) 11:1971. doi: 10.3389/fmicb.2020.01971
14. Liu L, Yi H, He H, Pan H, Cai L, Ma Y. Tumor Associated Macrophage-Targeted microRNA Delivery With Dual-Responsive Polypeptide Nanovectors for Anti-Cancer Therapy. *Biomaterials* (2017) 134:166–79. doi: 10.1016/j.biomaterials.2017.04.043
15. Chiossone L, Dumas PY. Natural Killer Cells and Other Innate Lymphoid Cells in Cancer. *Nat Rev Immunol* (2018) 18(11):671–88. doi: 10.1038/s41577-018-0061-z
16. Zhihua Y, Yulin T, Yibo W, Wei D, Yin C, Jiahao X, et al. Hypoxia Decreases Macrophage Glycolysis and M1 Percentage by Targeting microRNA-30c and mTOR in Human Gastric Cancer. *Cancer Sci* (2019) 110(8):2368–77. doi: 10.1111/cas.14110
17. Bai D, Zhao Y, Zhu Q, Zhou Y, Zhao Y, Zhang T, et al. LZ205, a Newly Synthesized Flavonoid Compound, Exerts Anti-Inflammatory Effect by Inhibiting M1 Macrophage Polarization Through Regulating PI3K/AKT/mTOR Signaling Pathway. *Exp Cell Res* (2018) 364(1):84–94. doi: 10.1016/j.yexcr.2018.01.033
18. Hu X, Xu Q, Wan H, Hu Y, Xing S, Yang H, et al. PI3K-Akt-mTOR/PFKFB3 Pathway Mediated Lung Fibroblast Aerobic Glycolysis and Collagen Synthesis in Lipopolysaccharide-Induced Pulmonary Fibrosis. *Lab Invest* (2020) 100 (6):801–11. doi: 10.1038/s41374-020-0404-9
19. Bolaños JP, Delgado-Esteban M, Herrero-Mendez A, Fernandez-Fernandez S, Almeida A. Regulation of Glycolysis and Pentose-Phosphate Pathway by Nitric Oxide: Impact on Neuronal Survival. *Biochim Biophys Acta* (2008) 1777 (7-8):789–93. doi: 10.1016/j.bbabio.2008.04.011
20. Ridnour LA, Barasch KM, Windhausen AN, Dorsey TH, Lizardo MM, Yfantis HG, et al. Nitric Oxide Synthase and Breast Cancer: Role of TIMP-1 in NO-Mediated Akt Activation. *PloS One* (2012) 7(9):e44081. doi: 10.1371/journal.pone.0044081
21. Fujita M, Imadome K, Endo S, Shoji Y, Yamada S, Imai T. Nitric Oxide Increases the Invasion of Pancreatic Cancer Cells *via* Activation of the PI3K-AKT and RhoA Pathways After Carbon Ion Irradiation. *FEBS Lett* (2014) 588 (17):3240–50. doi: 10.1016/j.febslet.2014.07.006
22. Firmal P, Shah VK, Chattopadhyay S. Insight Into TLR4-Mediated Immunomodulation in Normal Pregnancy and Related Disorders. *Front Immunol* (2020) 11:807. doi: 10.3389/fimmu.2020.00807
23. Wei CY, Wang L, Zhu MX, Deng XY, Wang DH, Zhang SM, et al. TRIM44 Activates the AKT/mTOR Signal Pathway to Induce Melanoma Progression by Stabilizing TLR4. *J Exp Clin Cancer Res* (2019) 38(1):137. doi: 10.1186/s13046-019-1138-7
24. Kim J, Bae JS. Tumor-Associated Macrophages and Neutrophils in Tumor Microenvironment. *Mediators Inflamm* (2016) 2016:6058147. doi: 10.1155/2016/6058147
25. DeNardo DG, Ruffell B. Macrophages as Regulators of Tumour Immunity and Immunotherapy. *Nat Rev Immunol* (2019) 19(6):369–82. doi: 10.1038/s41577-019-0127-6
26. Mantovani A, Sozzani S, Locati M, Allavena P, Sica A. Macrophage Polarization: Tumor-Associated Macrophages as a Paradigm for Polarized M2 Mononuclear Phagocytes. *Trends Immunol* (2002) 23(11):549–55. doi: 10.1016/S1471-4906(02)02302-5
27. Qian BZ, Pollard JW. Macrophage Diversity Enhances Tumor Progression and Metastasis. *Cell* (2010) 141(1):39–51. doi: 10.1016/j.cell.2010.03.014
28. Ruffell B, Affara NI, Coussens LM. Differential Macrophage Programming in the Tumor Microenvironment. *Trends Immunol* (2012) 33(3):119–26. doi: 10.1016/j.it.2011.12.001
29. Chakrabarty AM, Bernardes N, Fialho AM. Bacterial Proteins and Peptides in Cancer Therapy: Today and Tomorrow. *Bioengineered* (2014) 5(4):234–42. doi: 10.4161/bioe.29266
30. Fialho AM, Chakrabarty AM. Recent Patents on Bacterial Proteins as Potential Anticancer Agents. *Recent Pat Anticancer Drug Discov* (2007) 2 (3):224–34. doi: 10.2174/157489207782497163
31. Wang RF, Miyahara Y, Wang HY. Toll-Like Receptors and Immune Regulation: Implications for Cancer Therapy. *Oncogene* (2008) 27(2):181–9. doi: 10.1038/sj.onc.1210906
32. Iribarren K, Bloy N, Buqué A, Cremer I, Eggermont A, Fridman WH, et al. Trial Watch: Immunostimulation With Toll-Like Receptor Agonists in Cancer Therapy. *Oncoimmunology* (2016) 5(3):e1088631. doi: 10.1080/2162402X.2015.1088631
33. Long T, Liu Z, Shang J, Zhou X, Yu S, Tian H, et al. Polygonatum Sibiricum Polysaccharides Play Anti-Cancer Effect Through TLR4-MAPK/NF-κb Signaling Pathways. *Int J Biol Macromol* (2018) 111:813–21. doi: 10.1016/j.ijbiomac.2018.01.070
34. Zhuang H, Dai X, Zhang X, Mao Z, Huang H. Sophoridine Suppresses Macrophage-Mediated Immunosuppression Through TLR4/IRF3 Pathway and Subsequently Upregulates CD8(+) T Cytotoxic Function Against

Gastric Cancer. *BioMed Pharmacother* (2020) 121:109636. doi: 10.1016/j.biopha.2019.109636
35. Pandey N, Chauhan A, Jain N. TLR4 Polymorphisms and Expression in Solid Cancers. *Mol Diagn Ther* (2018) 22(6):683–702. doi: 10.1007/s40291-018-0361-9
36. Chen CY, Kao CL, Liu CM. The Cancer Prevention, Anti-Inflammatory and Anti-Oxidation of Bioactive Phytochemicals Targeting the TLR4 Signaling Pathway. *Int J Mol Sci* (2018) 19(9):2729. doi: 10.3390/ijms19092729
37. Hyam SR, Lee IA, Gu W, Kim KA, Jeong JJ, Jang SE, et al. Arctigenin Ameliorates Inflammation In Vitro and *In Vivo* by Inhibiting the PI3K/AKT Pathway and Polarizing M1 Macrophages to M2-Like Macrophages. *Eur J Pharmacol* (2013) 708(1-3):21–9. doi: 10.1016/j.ejphar.2013.01.014
38. Takashima Y, Hayano A, Yamanaka R. Metabolome Analysis Reveals Excessive Glycolysis *via* PI3K/AKT/mTOR and RAS/MAPK Signaling in Methotrexate-Resistant Primary CNS Lymphoma-Derived Cells. *Clin Cancer Res* (2020) 26(11):2754–66. doi: 10.1158/1078-0432.CCR-18-3851
39. Arts RJ, Plantinga TS. Transcriptional and Metabolic Reprogramming Induce an Inflammatory Phenotype in non-Medullary Thyroid Carcinoma-Induced Macrophages. *Oncoimmunology* (2016) 5(12):e1229725. doi: 10.1080/2162402X.2016.1229725
40. Zhang X, Jin L. Nitric Oxide Inhibits Autophagy and Promotes Apoptosis in Hepatocellular Carcinoma. *Cancer Sci* (2019) 110(3):1054–63. doi: 10.1111/cas.13945
41. Chung P, Cook T, Liu K, Vodovotz Y, Zamora R, Finkelstein S, et al. Overexpression of the Human Inducible Nitric Oxide Synthase Gene Enhances Radiation-Induced Apoptosis in Colorectal Cancer Cells *via* a Caspase-Dependent Mechanism. *Nitric Oxide* (2003) 8(2):119–26. doi: 10.1016/S1089-8603(02)00147-7
42. Ye S, Yang W, Wang Y, Ou W, Ma Q, Yu C, et al. Cationic Liposome-Mediated Nitric Oxide Synthase Gene Therapy Enhances the Antitumor Effects of Cisplatin in Lung Cancer. *Int J Mol Med* (2013) 31(1):33–42. doi: 10.3892/ijmm.2012.1171
43. Girotti AW, Fahey JM. Upregulation of Pro-Tumor Nitric Oxide by Anti-Tumor Photodynamic Therapy. *Biochem Pharmacol* (2020) 176:113750. doi: 10.1016/j.bcp.2019.113750
44. Perrotta C, Cervia D, Di Renzo I, Moscheni C, Bassi MT, Campana L, et al. Nitric Oxide Generated by Tumor-Associated Macrophages Is Responsible for Cancer Resistance to Cisplatin and Correlated With Syntaxin 4 and Acid Sphingomyelinase Inhibition. *Front Immunol* (2018) 9:1186. doi: 10.3389/fimmu.2018.01186
45. Huerta S, Chilka S, Bonavida B. Nitric Oxide Donors: Novel Cancer Therapeutics (Review). *Int J Oncol* (2008) 33(5):909–27. doi: 10.3892/ijo_00000079
46. Star RA. Nitric Oxide. *Am J Med Sci* (1993) 306(5):348–58. doi: 10.1097/00000441-199311000-00015
47. Karar J, Maity A. PI3K/AKT/mTOR Pathway in Angiogenesis. *Front Mol Neurosci* (2011) 4:51. doi: 10.3389/fnmol.2011.00051
48. Viola A, Munari F, Sánchez-Rodríguez R, Scolaro T, Castegna A. The Metabolic Signature of Macrophage Responses. *Front Immunol* (2019) 10:1462. doi: 10.3389/fimmu.2019.01462

Conflict of Interest: The authors declare that the research was conducted in the absence of any commercial or financial relationships that could be construed as a potential conflict of interest.

Publisher's Note: All claims expressed in this article are solely those of the authors and do not necessarily represent those of their affiliated organizations, or those of the publisher, the editors and the reviewers. Any product that may be evaluated in this article, or claim that may be made by its manufacturer, is not guaranteed or endorsed by the publisher.

frontiers in Immunology

REVIEW
published: 12 January 2022
doi: 10.3389/fimmu.2021.730666

Toripalimab: the First Domestic Anti-Tumor PD-1 Antibody in China

Lin Zhang[1†], *Bo Hao*[1†], *Zhihua Geng*[2*] *and Qing Geng*[1*]

[1] *Department of Thoracic Surgery, Renmin Hospital of Wuhan University, Wuhan, China,* [2] *Department of Orthopedics of Union Hospital, Tongji Medical College, Huazhong University of Science and Technology, Wuhan, China*

Toripalimab (Tuoyi™) is a selective, recombinant, humanized monoclonal antibody against programmed death protein 1 (PD-1) developed by Shanghai Junshi Bioscience Co., Ltd. Toripalimab is able to bind to PD-1 and block the interaction with its ligands. The binding of toripalimab to PD-1 is mainly attributed to the heavy chain of the former and the FG loop of the latter. Toripalimab received a conditional approval in China for the treatment of melanoma (second-line) in December, 2018. It has also received approvals to treat nasopharyngeal carcinoma (first-line and third-line) and urothelial carcinoma (second-line) in 2021. Additionally, several orphan drug designations were granted to toripalimab by the US Food and Drug Administration. Toripalimab has exhibited primary anti-tumor effects in tumors such as melanoma, lung cancer, digestive tract tumors, hepatobiliary and pancreatic tumors, neuroendocrine neoplasms, nasopharyngeal carcinoma and urothelial carcinoma. It showed a satisfactory anti-tumor effect and long-term survival benefits in Chinese melanoma patients, while the combination of axitinib with toripalimab exhibited an impressive result in metastatic mucosal melanoma. As a checkpoint inhibitor, toripalimab was generally well-tolerated in the enrolled patients. Due to different study populations, comparisons could not be made directly between toripalimab and other drugs in most cases. Nevertheless, the introduction of toripalimab may offer a valuable choice for decision-making in the treatment of tumors in the future.

Keywords: toripalimab, programmed death protein 1, programmed death ligand 1, immunotherapy, tumor, adverse effect

OPEN ACCESS

Edited by:
Xuanming Yang,
Shanghai Jiao Tong University, China

Reviewed by:
Fang Wei,
Shanghai Jiao Tong University, China
Zhida Liu,
Shanxi Academy of Advanced Research and Innovation, China

***Correspondence:**
Qing Geng
gengqingwhu@whu.edu.cn
Zhihua Geng
drgzh91@gmail.com

[†]*These authors have contributed equally to this work*

Specialty section:
This article was submitted to Cancer Immunity and Immunotherapy, a section of the journal Frontiers in Immunology

Received: *25 June 2021*
Accepted: *14 December 2021*
Published: *12 January 2022*

Citation:
Zhang L, Hao B, Geng Z and Geng Q (2022) Toripalimab: the First Domestic Anti-Tumor PD-1 Antibody in China. Front. Immunol. 12:730666. doi: 10.3389/fimmu.2021.730666

INTRODUCTION

T cells are important immune cells in the human body and express co-stimulating immune checkpoint proteins on their surface. Through immune checkpoints, cancer cells can block the activation of T cells and their cytotoxic effects on tumors, leading to immune evasion (1). As surface receptor proteins, immune checkpoints can be effectively inhibited by antibodies known as checkpoint inhibitors. The emergence of checkpoint inhibitors has radically changed the landscape of cancer therapy. Among all clinically applied checkpoint inhibitors, anti-programmed death protein 1 (PD-1)/programmed death ligand 1 (PD-L1) antibodies are the most successful (2). Antibody blockade of PD-1 prevents its interaction with PD-L1 and PD-L2, blocking their downstream pathways and recovering the anti-tumor response of T cells (3). There are already well-studied PD-1 inhibitors on the market such as nivolumab and pembrolizumab, two

drugs that have been approved by the China National Medical Product Administration (NMPA) and US Food and Drug Administration (FDA) for use in various tumors (4).

Toripalimab (Tuoyi™) is the first domestic anti-PD-1 monoclonal antibody in China with completely independent intellectual property rights (5). Toripalimab has received a conditional approval for the treatment of unresectable or metastatic melanoma that has not responded to previous systemic therapy in December, 2018 (6). Recently, toripalimab was approved by the NMPA for the treatment of recurrent/metastatic nasopharyngeal carcinoma (NPC) and locally advanced or metastatic urothelial carcinoma (UC) (7–9). Showing an acceptable safety profile in clinical studies, it has exhibited promising anti-tumor effects in tumors like melanoma, neuroendocrine neoplasms and urothelial carcinoma, with obvious economic advantages. Here, we summarize the preclinical studies, pharmacological characteristics, anti-tumor effects, and adverse effects (AEs) of this drug in order to provide valuable information for decision-making in the treatment of tumors in the future.

PRECLINICAL DATA AND PHARMACOLOGICAL CHARACTERISTICS OF TORIPALIMAB

Toripalimab is the first monoclonal anti-PD-1 antibody approved by the China NMPA onto the market (10). It consists of two heavy chains of 452 amino acids, two light chains of 219 amino acids, and includes an N-linked glycosylation site at N302 in each heavy chain. The average molecular weight of toripalimab is 149,670 Daltons (11–14) (**Figure 1**). Toripalimab is able to bind to PD-1, efficiently blocking the interaction with its ligands; the blockade is mainly attributed to the stereospecific hindrance of the heavy chain (12). The interaction of toripalimab with PD-1 is mainly attributed to the complementarity determining regions of the heavy chain of the former and the FG loop of the latter; the light chain complementarity determining regions of toripalimab participate mainly in recognizing the epitopes on PD-1 (12, 17, 18). Comparatively, nivolumab mainly binds to the N-terminal loop of PD-1, while the binding of pembrolizumab primarily involves the C' D loop (12, 15, 16) (**Figure 1**).

Preclinical Safety and Effectiveness

Toripalimab has low effective and inhibitory concentrations. *In vitro*, the effective concentration of toripalimab was determined to be 21 nmol/L and 0.89 ± 0.15 ng/mL by two studies (17, 18). *In vivo*, the effective concentration dose for toripalimab in the MC38 tumor model is between 0.3 and 1 mg/kg (12). In *in vitro* flow cytometry assays, the inhibitory concentrations of toripalimab were 3.0 nmol/L and 3.1 nmol/L for PD-1/PD-L1 and PD-1/PD-L2, respectively (18). In *in vivo* mouse models, by blocking the binding of PD-1 to PD-L1 or PD-L2 using a protein-based enzyme-linked immunosorbent assay, the inhibitory concentrations of toripalimab were determined to be 0.8 nmol/L for PD-L1 and 1.3 nmol/L for PD-L2. Using a cell-based flow cytometry assay, the concentrations were 1.3 nmol/L and 3.7 nmol/L for PD-L1 and PD-L2, respectively (12).

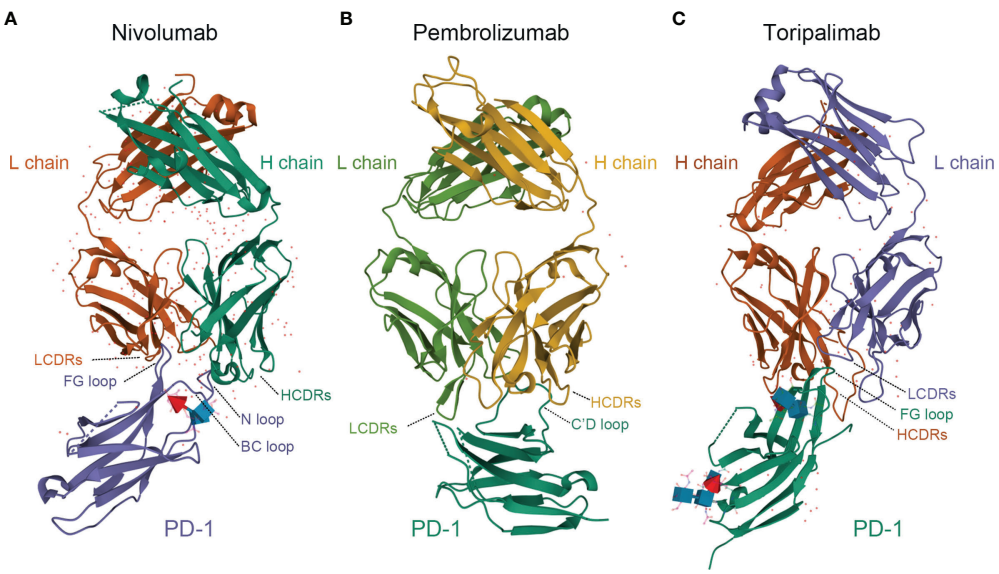

FIGURE 1 | Comparison of structures of PD-1 in complex with nivolumab-Fab **(A)** (PDB code: 5WT9), pembrolizumab-Fab **(B)** (PDB code: 5JXE) and toripalimab-Fab **(C)** (PDB code: 6JBT). L chain, light chain; H chain, heavy chain; LCDRs, complementary determining regions of the light chain; HCDRs, complementary determining regions of the heavy chain; PD-1, programmed death protein 1. Images were acquired from Protein Data Bank and relevant research was conducted by Tan S et al., Na Z et al., and Liu H et al., respectively (12–16).

The blockage by toripalimab is effective. *In vivo*, toripalimab can dramatically inhibit the elevated expression of PD-1 on $CD4^+$ and $CD8^+$ T cells in a dose-dependent manner, while PD-1 receptor occupancy can reach up to 90% at 1 mg/kg and 100% at 10 mg/kg in cynomolgus monkeys (18). In three phase I studies, toripalimab can also bind to the PD-1 receptor on activated T lymphocytes and maintain complete PD-1 receptor occupancy (> 80%) on $CD4^+$ and $CD8^+$ T cells; this was observed in the majority of the patients in all dose cohorts throughout the observation period (19–21). In mice inoculated with tumor cells, toripalimab can significantly decrease tumor sizes after a 23-day treatment compared with IgG-treated controls (12). Treatment with toripalimab (0.01–10 μg/mL) can also dose-dependently stimulate human T cell proliferation, as well as IFN-γ and TNF-α secretion (18).

Immunogenicity

Toripalimab provoked only a weak immune response in animal experiments and clinical trials. In an animal experiment, 18 cynomolgus monkeys were treated with toripalimab at low (1 mg/kg), medium (10 mg/kg) and high (75 mg/kg) doses; 10% of monkeys from each group were positive for anti-drug antibodies 28 d after the first administration, indicating a low immunogenicity of this drug (18). In NCT03013101, detection of anti-drug antibodies was performed in 128 melanoma patients treated with toripalimab at 3 mg/kg intravenously once every 2 weeks; samples from 10.2% (13/128) patients were positive after toripalimab treatment and only one positive patient had a decreased toripalimab plasma concentration (22). In NCT02857166, patients were assigned to receive 0.3 mg/kg, 1 mg/kg, 3 mg/kg, 10 mg/kg or 240 mg toripalimab *via* intravenous infusion every 2 weeks; anti-drug antibodies were detected in one (33.3%) patient in the 0.3 mg/kg group, three (42.9%) patients in the 1 mg/kg group, and one (16.7%) patient in the 3 mg/kg group, but were not detected in the 10 mg/kg group or the 240 mg group (19). These results indicate a low immunogenicity of toripalimab in the body.

Pharmacological Characteristics

In the phase II study POLARIS-01, when toripalimab was given at 3 mg/kg per 2 weeks (Q2W), its steady-state median trough plasma concentration was 39.8 μg/mL (22). In phase I studies, the serum concentrations of toripalimab reached a maximum at about 1 h, within 2 h and within 6 h after infusion, respectively (19–21). In NCT02836795 and NCT02836834, the steady state trough concentration of toripalimab was 8.9 ± 4.4, 37.8 ± 17.5, 174.3 ± 95.6 μg/mL and 8.5 ± 2.6, 34.5 ± 10.0, and 195.8 ± 104.6 μg/mL for the 1 mg/kg, 3 mg/kg, and 10 mg/kg cohorts, respectively (20, 21). In NCT02857166, the analyses of blood samples of patients receiving toripalimab showed a serum half-life of 150–222 h after a single infusion and 188–525 h after multi-dose infusions (19). In another two studies, the average serum half-lives for the 1, 3 and 10 mg/kg cohorts were 6.2, 7.7, 9.8 days and 7.7, 8.0 and 14.2 days respectively after a single infusion; after multi-dose infusions, the half-lives were 9.5, 16.5, 13.9 days and 10.7, 12.1 20.1 days, respectively (20, 21). Based on the preclinical and pharmacological data, toripalimab was tested in therapeutic clinical trials.

EFFICACY OF TORIPALIMAB IN TUMORS

Based on the above preclinical studies, toripalimab was tested in phase I clinical studies. The recommended phase II dose was determined to be 3 mg/kg Q2W in a first-in-human phase I trial (NCT02836795) (23). In NCT02836795, patients in the dose escalation cohorts received intravenous infusion of toripalimab at 1 mg/kg, 3 mg/kg, and 10 mg/kg Q2W; 28 days after the first dose, subjects continued to receive toripalimab at the intended dose level Q2W. The confirmed dosage of toripalimab laid the foundation for further clinical trials. The primary endpoints are usually safety and tolerability in phase I studies; overall response rate (ORR), defined as the percentage of patients achieving complete response (CR) or partial response (PR), in phase II studies; and overall survival (OS) and progression-free survival (PFS) in phase III studies (24). The basic information of toripalimab studies in these cancers was visualized in **Figures 2**, **3**.

Efficacy of Toripalimab in Melanoma

Melanoma of the skin accounts for 1.7% of newly-diagnosed cancers and 0.6% of cancer-related deaths worldwide (25).Clinical trials in melanoma have largely been unsuccessful, and there are few treatment options when the disease becomes advanced (26). The first approval of toripalimab was for unresectable or metastatic melanoma that has failed to respond to previous systemic therapy, which was based on a phase II study (NCT03013101/POLARIS-01) (22). Additionally, the anti-tumor effects of nivolumab and pembrolizumab were investigated in NCT00730639 and KEYNOTE-151, respectively. The information of toripalimab studies in melanoma was visualized in **Figure 2** and the comparisons between toripalimab, nivolumab and pembrolizumab in melanoma are listed in **Table 1**.

Overall, the toripalimab was effective in melanoma. In POLARIS-01, toripalimab was given at 3 mg/kg Q2W until disease progression or unacceptable toxicity in 128 Chinese patients who had previously received systemic therapy. The achieved ORR was 17.3% (22/127), and the disease control rate (DCR), defined as the percentage of patients achieving CR, PR, or stable disease (SD), was 57.5% (73/127); the median PFS and OS were 3.6 months and 22.2 months, respectively (22). Toripalimab has led to long-term survival benefit, and PD-L1 positive patients show markedly longer OS than PD-L1 negative patients; the data for different subtypes are shown in **Table 1** (22, 27). In 22 melanoma patients from another phase I study (NCT02836795), ORR, DCR, PFS and OS were 18.2% (4/22), 45.5% (10/22), 84 days and 448 days, respectively (20). Comparatively, in KEYNOTE-151, pembrolizumab was administered in previously-treated Chinese melanoma patients; the achieved ORR was 16.7% (17/102) and the DCR was 38.2% (39/102). The ORRs were 15.8% (6/38) for acral, 19.5%(8/41) for non-acral and 13.3% (2/15) for mucosal melanoma patients, the DCRs were 42.1% (16/38) for acral melanoma and 20.0% (3/15) for mucosal melanoma, respectively (29). In NCT00730639, overall response and disease control were achieved by

FIGURE 2 | A summary of prospective clinical studies of toripalimab on solid tumors, melanoma and lung cancer. Dates indicate the time when the results of the studies were available online. Dashed lines perpendicular to the y-axis in the bar graph indicate absence of corresponding available data. Dotted gray line at the edge of column means not less than the indicated number. Approval 1, approval in mucosal melanoma, an orphan designation by the FDA (plus axitinib); approval 2, approval in melanoma, by the NMPA (second-line); HDI, high-dose IFN-α2b; ORR, overall response rate; DCR, disease control rate; RFS, recurrence-free survival; PFS, progression-free survival; OS, overall survival; TRAEs, treatment-related adverse events; FDA, Food and Drug Administration; NMPA, National Medical Products Administration.

nivolumab in 30.8% (33/107) and 37.4% (40/107) patients, respectively; the median PFS and median OS were 3.7 months and 16.8 months (28). The ORR achieved by nivolumab appears to be the highest among all three drugs; however, the efficacies of nivolumab for each subtype are unknown, and the study population in NCT00730639 was not mentioned. In addition, adjuvant toripalimab was able to improve the recurrence-free survival of mucosal melanoma patients, but its comparison with conventional chemotherapy remained to be conducted (31).

The combination of toripalimab and axitinib, a vascular endothelial growth factor inhibitor, has shown a potent effect in treating mucosal melanoma. Vascular endothelial growth factor is an important growth factor for the growth of cancer and is upregulated in melanoma patients (32). Simultaneous blockade of PD-1 and vascular endothelial growth factor receptor 2 can induce a synergistic anti-tumor effect in mice inoculated with colon cancer cells (33). In a phase Ib study (NCT03086174), 33 Chinese patients were given axitinib 5 mg twice a day plus toripalimab 1 or 3 mg/kg every 2 weeks until confirmed disease progression, unacceptable toxicity, or voluntary withdrawal, in a dose-escalation and a cohort-expansion phase. The achieved ORR was 48.3% (14/29) and DCR was 86.2% (25/29), while the median PFS was 7.5 months (23). The combinatorial plan produced a high response rate. Thus, an orphan designation for treatment of mucosal melanoma was granted to the combinational therapy by the US FDA in March 25, 2020 (34). An updated analysis of NCT03086174 revealed a median OS of 20.7 months among these patients (30). Later, toripalimab plus axitinib combination treatment was tested in an adjuvant setting, and led to pathological complete response (pCR), defined as no viable tumor on all slides, in 14.3% (2/14) of patients (35). In addition, the effectiveness of the combination in advanced mucosal melanoma is currently being investigated in a phase II trial (registration number: NCT03941795) (36).

Toripalimab has also been tested for the treatment of melanoma in other settings. For example, the pCR achieved by toripalimab plus OrienX010, a granulocyte-macrophage colony-stimulating factor, is 14.3% (3/21) in resectable stage IIIb–IVM1a acral melanoma patients; and intravenous administration of toripalimab plus intralesional injection of OrienX010 achieved an ORR of 13.3% (2/15) in liver metastasis (37, 38). Toripalimab plus vorolanib achieved a 13.2% (5/38) ORR in advanced mucosal melanoma as a first-line therapy (39). Additionally, a randomized, multi-center, phase II study (NCT03430297) comparing toripalimab as a first-line treatment of metastatic melanoma to dacarbazine (a first-line chemotherapy for melanoma) is currently ongoing (36). The results of these studies may provide more indications for toripalimab in the future.

Efficacy of Toripalimab in Non-Small Cell Lung Cancer

Toripalimab exhibited anti-tumor effects in non-small cell lung cancer (NSCLC) as a single agent (**Figure 2**). In a phase I study

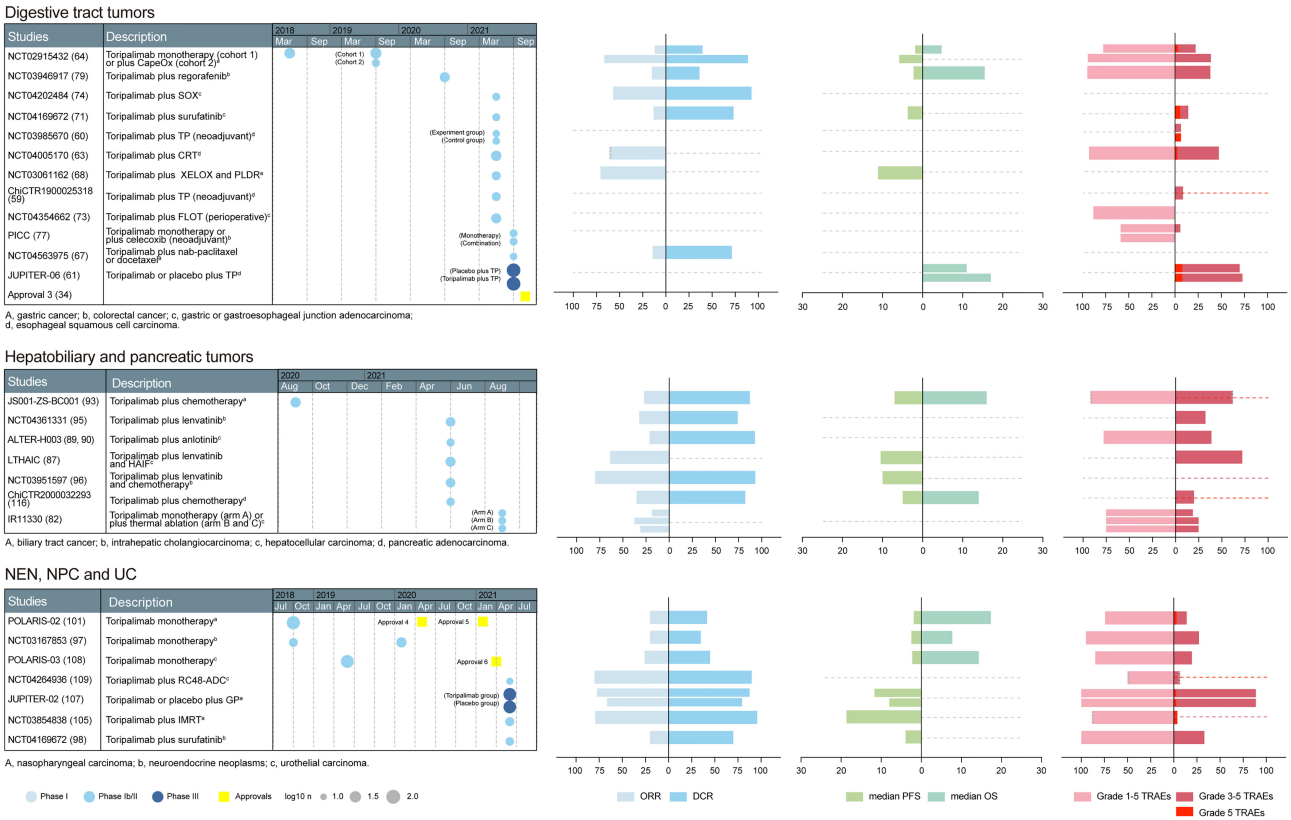

FIGURE 3 | A summary of prospective clinical studies of toripalimab on digestive tract tumors, hepatobiliary and pancreatic tumors, and other tumors. Dates indicate the time when the results of the studies were available online. Dashed lines perpendicular to the y-axis in the bar graph indicate absence of corresponding available data. Dotted gray line at the edge of column means not less than the indicated number. CapeOX, capecitabine and oxaliplatin; SOX, S-1 plus oxaliplatin; TP, paclitaxel plus platinum; CRT, chemoradiotherapy; XELOX, capecitabine and oxaliplatin; PLDR, pulsed low dose rate radiotherapy; FLOT, 5-fluorouracil, leucovorin, oxaliplatin, docetaxel; HAIF,hepatic arterial infusion of oxaliplatin, 5-fluorouracil, and leucovorin; GP, gemcitabine and platinum; IMRT, intensity-modulated radiotherapy; approval 3, approval in esophageal cancer, an orphan designation by the FDA; approval 4, approval in NPC, an orphan designation by the FDA; approval 5, approval in NPC, by the NMPA (third-line); approval 6, approval in UC, by the NMPA (second-line); ORR, overall response rate; DCR, disease control rate; RFS, recurrence-free survival; PFS, progression-free survival; OS, overall survival; TRAEs, treatment-related adverse events; FDA, Food and Drug Administration; NMPA, National Medical Products Administration.

(NCT02836834), the ORR and DCR achieved by toripalimab in seven Chinese NSCLC patients were 14.3% (1/7) and 71.4% (5/7), respectively (21). In another phase I study (NCT03301688), 41 heavily-treated patients were included and treated with a single dose of toripalimab; the ORR and DCR achieved were 7.1% (2/28) and 39.3% (11/28), respectively (40). The effect of toripalimab in NSCLC was also observed in retrospective studies (41). In comparison, nivolumab and pembrolizumab monotherapy achieved ORRs of 17.1% (22/129) and 19.4% (96/495) and DCRs of 27.1% (35/129) and 41.2% (204/495) in NSCLC, as revealed by the phase I studies CHECKMATE-003 and KEYNOTE-001, respectively (42, 43). Due to the small sample size and different patient baseline characteristics such as race of NCT02836834, it is not valid to compare the effect of toripalimab with the other two drugs directly.

Toripalimab plus other therapies has also exerted anti-tumor effects in NSCLC. Multiple target cytotoxic T-lymphocyte cells can restore antitumor immunity to improve patient outcome. In NCT04193098, a combination of multiple target cytotoxic T-lymphocyte cells and toripalimab as a second-line therapy led to an ORR of 38.4% (5/13) and a DCR 76.9% (10/13) in patients with advanced NSCLC, without causing treatment-related death (44). Platinum-based chemotherapy is one of the standard systemic therapies for NSCLC (45). In NCT03513666, 40 Chinese NSCLC patients who failed to respond to first-line EGFR-TKIs and did not harbor T790M mutation were enrolled and received toripalimab combined with carboplatin and pemetrexed every 3 weeks, for up to six cycles, followed by toripalimab and pemetrexed maintenance until disease progression or unacceptable toxicity. The ORR achieved by the combination regime was 50.0% (20/40), the median PFS was 7.0 months and the median OS was 23.5 months, better than historical data for traditional chemotherapy (46). The ORR and DCR achieved by toripalimab combined with chemotherapy in a retrospective study were 39.2% and 96.2% among 79 NSCLC patients (47). In addition, a phase III clinical

TABLE 1 | Comparison of different therapeutic regimens for melanoma.

Therapeutic Regimen		Toripalimab[NCT03013101/ POLARIS-01 [(22, 27)]	Nivolumab [NCT00730639 (28)]	Pembrolizumab [KEYNOTE-151 (29)]	Toripalimab plus axitinib [NCT03086174 (23, 30)]
Patient races		Chinese	Not mentioned	Chinese	Chinese
ORR	total	17.3% (22/127)	30.8% (33/107)	16.7% (17/102)	NA
	cutaneous	20.3% (16/79)	NA	17.7% (14/79)	NA
	mucosal	0 (0/22)	NA	13.3% (2/15)	48.3% (14/29)
DCR	total	57.5% (73/127)	37.4% (40/107)	38.2% (39/102)	NA
	cutaneous	57.0% (45/79)	NA	42.1% (16/38) for acral	NA
	mucosal	40.9% (9/22)	NA	20.0% (3/15)	86.2% (25/29)
Median PFS	total	3.6 months	3.7 months	2.8 months	NA
	cutaneous	3.2 months for acral, 5.5 months for NC	NA	NA	NA
	mucosal	1.9 months	NA	NA	7.5 months
Median OS	total	22.0 months	16.8 months	12.1 months	NA
	cutaneous	16.9 months for acral, 46.1 months for NC	NA	NA	NA
	mucosal	10.3 months	NA	NA	20.7 months
Safety profiles	Grade 1-5 TRAEs	90.6% (116/128)	54.2% (58/107)	84.5% (87/103)	97.0% (32/33)
	Grade ≥3 TRAEs	19.5% (25/128)	22.4% (24/107)	10.7% (11/103)	39.4% (13/33)
	Grade 5 TRAEs	0	0	1.9% (2/103)	0

ORR, overall response rate; DCR, disease control rate; PFS, progression-free survival; OS, overall survival; NA, not available/applicable; NC, nonacral cutaneous; TRAE, treatment-related adverse event.

trial comparing the toripalimab versus placebo in combination with chemotherapy in the same setting as NCT03924050 is ongoing (48). Also, toripalimab in combination with vorolanib, a multi-target tyrosine kinase inhibitor, also exhibited anti-tumor effects as a second-line therapy (49).

A toripalimab-containing regimen in a neoadjuvant setting yielded a high major pathological response (MPR) rate and caused no treatment-related surgical delays. In a phase 2 study (NeoTPD01/NCT04304248), surgically resectable stage IIIA or T3–4N2 IIIB NSCLC patients received three cycles of neoadjuvant treatment with intravenous toripalimab plus carboplatin, and pemetrexed or nab-paclitaxel (50). MPR, defined as less than 10% residual tumor remaining at the time of surgery, was achieved in 66.7% (20/30) of patients, and pCR was achieved in 50.0% (15/30) of patients. Treatment discontinuation or dose reduction was not observed and there were no treatment-related deaths (50). In another study, neoadjuvant toripalimab plus chemotherapy led to a lower pCR rate (18.2%) and MPR rate (40.9%), but resulted in an ORR of 75.0% (30/40) and DCR of 95.0% (38/40) (51). Nivolumab and pembrolizumab monotherapy have also been tested in a neoadjuvant setting in US medical centers and an Israeli medical center; the MPRs achieved were 42.9% (9/21) and 40% (4/10), respectively (52–54). In contrast, Sheng et al. tested pembrolizumab in a Chinese setting; they enrolled 37 Chinese adults with untreated, surgically resectable stage IIB–IIIB squamous NSCLC and treated them with two cycles of pembrolizumab with albumin-bound paclitaxel plus carboplatin (55). All tumors were completely resected and MPR occurred in 24 (64.9%) resected tumors; none of the patients discontinued neoadjuvant therapy due to toxic effects and no treatment-related death was observed (55).

In addition, ongoing trials conferred potential possibilities in NSCLC treatment. For example, in NCT04238169, metastatic NSCLC patients who have previously received first-line platinum-based chemotherapy or immune checkpoint inhibitors (except toripalimab) and diagnosed with confirmed disease progression were included and treated with stereotactic body radiation therapy (30–50 Gy/5 F for 2–4 lesions) plus toripalimab (240 mg, Q3W) with or without bevacizumab (7.5 mg/kg, Q3W) until disease progression or intolerable toxicity (56). Toripalimab was also tested in different NSCLC stages in prospective studies, such as in early-stage NSCLC, and treatment-naive advanced NSCLC (57). Release of these results in the future may lay the foundations for more indications.

Efficacy of Toripalimab in Esophageal Cancer

Toripalimab plus chemotherapy is effective when used as a neoadjuvant therapy in esophageal squamous cell carcinoma (ESCC) (**Figure 3**). Combinational fluoropyrimidine plus platinum-based chemotherapy is a recommended first-line treatment for advanced or metastatic ESCC, but confers limited survival benefits (58). In a phase II study (ChiCTR1900025318), 23 subjects with resectable ESCC were included and given toripalimab combined with paclitaxel and cisplatin as neoadjuvant treatment. Among the evaluable patients, 33.3% (6/18) achieved pCR (59). The combination regime also showed a controllable safety profile, and grade 3–4 treatment-related adverse events (TRAEs) were reported in two patients. Interestingly, when toripalimab was administrated two days after chemotherapy rather than being used simultaneously, the combinational neoadjuvant regime showed a trend toward a higher pCR rate (36.4%, 4/11 versus 7.7%, 1/13, P = 0.079) (60).

Toripalimab plus chemotherapy conferred better OS and PFS than chemotherapy alone in the first-line setting (**Figure 3**). In the randomized, double-blind phase III study JUPITER-06, 514 Chinese patients with treatment-naive, advanced or metastatic ESCC were randomized (1:1) to receive 240 mg toripalimab or placebo in combination with paclitaxel plus cisplatin every

3 weeks for up to six cycles, followed by toripalimab or placebo maintenance (61). Incidence of fatal TRAEs was similar between the groups (8.2% vs 8.2%), while significant advantages in OS and PFS for toripalimab over placebo (HR = 0.58, HR = 0.58) were observed, with median OS being 17.0 months and 11.0 months, respectively (61). In a similar setting (KEYNOTE-590), pembrolizumab plus 5-fluorouracil and cisplatin (n = 373) also led to superior OS (12.6 months versus 9.8 months, HR = 0.72) and PFS (6.3 months versus 5.8 months, HR = 0.65) to placebo plus 5-fluorouracil and cisplatin (n = 376) in patients with advanced ESCC from 168 medical centers in 26 countries, with a lower TRAE-related death rate (7.5%, 28/373; 10.1%, 38/376) (62).

Efficacy of toripalimab was also observed in other combinatorial regimes (**Figure 3**). For example, when combined with concurrent chemoradiotherapy, toripalimab achieved a clinical complete response rate of 60.7% (17/28) in previously untreated ESCC patients at 3 months (63). Based on the satisfactory anti-tumor effects of toripalimab shown above, an orphan designation was designated by FDA on November 8, 2021 (34).

Efficacy of Toripalimab in Gastric and Gastroesophageal Junction Cancer

The efficacy of toripalimab in advanced gastric cancer (GC) has been observed and seems promising (**Figure 3**). In the phase Ib part of the clinical trial NCT02915432, 58 Chinese chemo-refractory advanced GC patients received toripalimab (3 mg/kg d1, Q2W) as a monotherapy plan, which resulted in an ORR of 12.1% (7/58) (64). In cohort 1 of KEYNOTE-059, 259 patients from different countries with advanced GC received pembrolizumab monotherapy; the ORR in the east Asia subgroup was 8.8% (3/34) (65). In the gastric cohort of KEYNOTE-012, pembrolizumab monotherapy was associated with an ORR of 22.2% (8/36) in patients from different countries/regions with PD-L1-positive recurrent or metastatic adenocarcinoma of the stomach or gastro-esophageal junction (66). The east Asian data of KEYNOTE-012 are unavailable. In contrast, KEYNOTE-059 is more comparable to NCT02915432.

The combination of toripalimab and chemotherapy was effective in advanced GC patients (**Figure 3**). For example, the toripalimab plus CapeOx (capecitabine and oxaliplatin) regime (NCT02915432) as a first-line treatment in chemotherapy-naive advanced GC patients achieved an ORR and DCR of 66.7% (12/18) and 88.9% (16/18), respectively (64). In patients with advanced gastric adenocarcinoma, toripalimab plus nab-paclitaxel/docetaxel as second-line treatment resulted in confirmed PR in 1/7 patients, and SD in 4/7 patients, corresponding to an ORR of 14.2% and a DCR of 71.4% (67). The toripalimab plus XELOX (capecitabine and oxaliplatin) chemotherapy regimen and pulsed low dose rate radiotherapy also showed therapeutic effects in abdominal metastasis of advanced GC, with an ORR of 70.8% (17/24) (68). In ATTRACTION-4, nivolumab in combination with CapeOx yielded an ORR and DCR of 76.5% (13/17) and 88.2% (15/17), respectively, in treatment-naive advanced GC patients from Japan and South Korea (69). In cohort 2 of KEYNOTE-059, previously untreated advanced GC patients received pembrolizumab, cisplatin, and 5-fluorouracil (or capecitabine in Japan); the combination plan yielded an ORR of 60.0% (15/25) and a DCR of 80.0% (20/25) (70). The data of NCT02915432 and ATTRACTION-4 are more comparable because their study populations are similar.

Toripalimab showed an anti-tumor effect in gastric or gastroesophageal junction adenocarcinoma (G/GEJ) in different settings (**Figure 3**). Surufatinib is a novel small-molecule kinase inhibitor targeting VEGFRs, FGFR and CSF-1R, and its combination with toripalimab resulted in two confirmed PR and six SD in 15 evaluable G/GEJ patients who did not respond to first-line systemic chemotherapy, with median PFS being 3.71 months (71). FLOT (docetaxel, oxaliplatin, leucovorin, 5-FU) is the standard perioperative treatment for resectable G/GEJ (72). The combination of toripalimab and FLOT produced a 25.0% pCR and 42.9% MPR among 28 G/GEJ patients receiving complete resection (73). A toripalimab plus S-1 and oxaliplatin regimen as a first-line treatment showed effectiveness (ORR 57.1%, and DCR 92.8%) among 14 patients with advanced stage G/GEJ (74).

Efficacy of Toripalimab in Colorectal Cancer

Toripalimab alone or plus celecoxib conferred therapeutic effects in colorectal cancer (CRC) patients in a neoadjuvant setting (**Figure 3**). Cancer cell-intrinsic cyclooxygenases-2 expression contributed to resistance to immune checkpoint blockade (75). Therapeutically targeting the cyclooxygenases-2 pathway with widely used non-steroidal and steroidal anti-inflammatory drugs was able to synergize with immune checkpoint blockers and strengthen their anti-tumor effects in mouse CRC models (76). Celecoxib is a non-steroidal anti-inflammatory drug. In the phase 2 PICC study, toripalimab with or without celecoxib was tested in a neoadjuvant setting. In PICC, 34 patients with histologically-confirmed mismatch repair-deficient or microsatellite instability-high CRC, with clinical stage T3–T4 or any T with lymph node positivity were included and randomly assigned (1:1) to receive either toripalimab plus celecoxib (combination group) or toripalimab monotherapy (monotherapy group). While neither treatment caused surgical delays, pCR was achieved in 88.2% (15/17) in the combination group and 64.7% patients in the monotherapy group (77).

Toripalimab plus regorafenib showed anti-tumor efficacy in metastatic CRC (**Figure 3**). Regorafenib is an oral tyrosine kinase inhibitor targeting angiogenesis, the tumor microenvironment and tumor immunity, and has been approved for the treatment of metastatic CRC after failing standard therapies (78). In the phase I/II study NCT03946917, regorafenib plus toripalimab was tested in relapsed or metastatic CRC patients that had failed ≥ 2 previous lines of chemotherapy or were intolerant to prior systemic treatment (79). Twelve patients were enrolled in the dose escalation phase, which identified a dose of 80 mg regorafenib plus 3 mg/kg toripalimab to be the recommended phase II dose. In the 33 evaluable patients treated with recommended phase II doses, the ORR was 15.2% (5/33), the DCR was 36.4% (12/33), the median PFS was 2.1 months and median OS was 15.5% at the data cutoff of July 12, 2020 (79). In a

retrospective analysis, the ORR in these patients is 12.1% (4/33), DCR is 36.4% (12/33), and median PFS is 3.8 months (80). In a similar setting to NCT03946917, nivolumab achieved an ORR of 36.0% (9/25) in the Japanese population (81).

Efficacy of Toripalimab in Hepatobiliary Cancers

Toripalimab alone or in combination with other treatments showed promising anti-tumor effects in advanced hepatocellular carcinoma (HCC) (**Figure 3**). Toripalimab monotherapy led to an ORR of 18.8% in previously-treated advanced HCC patients (82). Additional ablation increased the response rate in these patients, without causing treatment-related death (82, 83). Lenvatinib has been reported to improve the survival of advanced HCC patients, while hepatic arterial infusion of oxaliplatin, 5-fluorouracil, and leucovorin (HAIF) led to further survival benefit (84, 85). In a retrospective analysis, the addition of toripalimab plus HAIF prolonged PFS and OS and increased ORR in HCC patients receiving lenvatinib (86). The effect of the combination regime was also explored in a prospective phase II trial, showing an ORR of 63.9% and median PFS of 10.5 months among 36 treatment-naive advanced HCC patients (87). Anlotinib, a novel multi-targeting tyrosine kinase inhibitor, has shown promising efficacy and safety as a first- or second-line treatment strategy in advanced HCC (88). The combination of toripalimab and anlotinib conferred an ORR of 21.4% (3/14) and a DCR of 92.9% (13/14) among treatment-naive patients with advanced HCC (89, 90).

Toripalimab plus chemotherapy showed a preliminary efficacy in treatment-naive advanced biliary tract cancer (BTC) (**Figure 3**). Combination chemotherapy with gemcitabine plus cisplatin has been regarded as the standard treatment for patients with advanced BTC, but confers only limited clinical benefit (91). In the phase II trial NCT03796429, treatment-naive patients with advanced BTC received toripalimab combined with gemcitabine and S-1 until progressive disease or unacceptable toxicity. By the data cutoff at January 24, 2021, the ORR was 27.1% (13/48) and DCR was 87.5% (42/48), median PFS was 7.0 months and median OS was 16.0 (92, 93). In a similar phase I study JapicCTI-153098, 30 chemotherapy-naive Japanese patients with unresectable or recurrent BTC were given nivolumab and cisplatin plus gemcitabine chemotherapy; in this cohort, median OS was 15.4 months, median PFS was 4.2 months, and 11 of 30 patients (36.7%) had an objective response (94).

Toripalimab plus lenvatinib showed promising efficacies in intrahepatic cholangiocarcinoma (ICC) (**Figure 3**). In NCT04361331, 31 pathologically-confirmed advanced ICC patients were included and treated with toripalimab plus lenvatinib as a first-line therapy. The combination plan resulted in an ORR of 32.3% (10/31) and a DCR of 74.2% (23/31) (95). When the regime was added to oxaliplatin and gemcitabine chemotherapy, a standard chemotherapy regime for ICC, the ORR became 80% (24/30) and DCR 93.3% (28/30) in treatment-naive patients (96). Treatment-related death was identified in neither of the studies, which indicated an acceptable safety profile.

Efficacy of Toripalimab in Neuroendocrine Neoplasms

Toripalimab has a satisfactory efficacy when used alone or in combination with surufatinib in neuroendocrine neoplasms (NEN) (**Figure 3**). The ORR achieved in previously-treated metastatic Chinese NEN patients was 20.0% (8/40), and DCR was 35.0% (14/40) (NCT02939651) (97). Furthermore, four patients achieved confirmed PR and 10 achieved SD among 20 tumor evaluable patients receiving toripalimab plus surufatinib, with a median PFS of 3.94 months and no treatment-related deaths (98). In contrast, pembrolizumab monotherapy resulted in ORR and DCR of 3.4% (1/29) and 24.1% (7/29), respectively, in grade 3 NEN patients refractory to first-line chemotherapy (NCT02939651) (99). It has been widely acknowledged that the prognosis of NEN based on pathological grading is dependent on the measurement of a proliferative index such as Ki-67 (100). In NCT02939651, patients had Ki-67 > 20%, while in NCT03167853, patients had Ki-67 ≥ 10%. Thus, the higher ORR achieved by toripalimab might be correlated with the lower grade of tumors in NCT03167853 to some extent. In addition, the comparison should still be made cautiously because the patient races in the two studies are different.

Efficacy of Toripalimab in Nasopharyngeal Cancer

Toripalimab was shown to be effective when used alone or with radiotherapy in treating NPC patients (**Figure 3**). In POLARIS-02/NCT02915432, 190 treated Chinese patients with recurrent or metastatic NPC were included and received 3 mg/kg toripalimab Q2W *via* intravenous infusion until disease progression, unacceptable toxicity, or voluntary withdrawal (101). Toripalimab monotherapy led to an ORR of 20.5% (39/190) and a DCR of 41.6% (79/190), which led to its approval for treating patients with recurrent/metastatic NPC as a third-line therapy (8). Due to the satisfactory anti-tumor effect of toripalimab shown in NPC, an orphan designation was also given by the FDA in May 18, 2020 (34). In comparison, the ORRs achieved by nivolumab in NCI-9742/NCT02339558 and pembrolizumab in KEYNOTE-028/NCT02054806 were 20.5% (9/44) and 26.3% (5/19), respectively (102, 103). Patients in these studies have similar tumor stages and treatment status. In NCI-9742, 82.2% (37/45) of patients are Asian; in KEYNOTE-028, this number is 63.0% (17/27). Considering the small sample size and lower proportions of Asian patients in KEYNOTE-028, the comparison between NCT02915432 and NCI-9742 is more valid. Intensity-modulated radiotherapy is the most widely used radiotherapy technique for NPC and significantly improves patient survival (104). In a phase II trial in patients with recurrent NPC, toripalimab in combination with intensity-modulated radiotherapy was prescribed, achieving an ORR of 79.2% (19/24) and a DCR of 95.8% (23/24), causing one treatment-related death (4.0%) (105).

Toripalimab plus chemotherapy showed superior clinical benefit compared to chemotherapy alone in NPC patients (**Figure 3**). Gemcitabine-cisplatin (GP) was the standard first-line

chemotherapy regime for advanced or metastatic NPC (106). Recently, the phase III study JUPITOR-02 was published, making a head-to-head comparison between toripalimab plus GP and placebo plus GP (107). The study involved 289 patients with recurrent or metastatic NPC and no previous chemotherapy history. The patients were randomized (1:1) to receive toripalimab plus GP (combination group) or placebo plus GP (placebo group); longer PFS was observed in the combination group compared to the placebo group (11.7 versus 8.0 months); the data for median OS were not available yet, but a trend toward better OS was observed, with the stratified HR for OS being 0.78 (107). Due to the superior clinical benefit conferred by the combination plan, NMPA have approved the indication of toripalimab plus GP as a first-line therapy in NPC recently (7).

Efficacy of Toripalimab in Urothelial Carcinoma

Toripalimab produced a satisfactory anti-tumor effect in locally advanced or metastatic UC patients (**Figure 3**). In a phase I study NCT02836795, toripalimab monotherapy achieved an ORR of 25.0% (2/8) and a DCR of 67.5% (5/8) among eight Chinese patients with metastatic UC (20). In the phase II study POLARIS-03/NCT03113266, 151 Chinese patients with advanced metastatic UC that had failed prior standard therapy were enrolled and treated with toripalimab until disease progression, unacceptable toxicity or voluntary withdrawal (108). By the cut-off date, there were two CR, 37 PR, and 29 SD, corresponding to an ORR of 25.8% (39/151) and a DCR of 45.0% (68/151) (65). When combined with RC48-ADC, a novel humanized anti-HER2 antibody-drug conjugate, the ORR increased to 80% (8/10) and DCR to 90% (9/10) in patients that were mostly treatment-naive (8/14) (109). The satisfactory anti-tumor effect of toripalimab shown in UC facilitated toripalimab's approval in previously-treated locally advanced or metastatic UC (9). In CHECKMATE-275, nivolumab 3 mg/kg Q2W resulted in an ORR of 19.6% (52/265) in locally advanced or metastatic UC patients (110), and in KEYNOTE-052, pembrolizumab in treatment-naive patients yielded an ORR of 24.1% (89/370) (111). Although the patients had received prior systemic therapy, the response rate in POLARIS-03 is still higher than in KEYNOTE-052. However, it should be noted that study populations of CHECKMATE-275 and KEYNOTE-052 are different from that of POLARIS-03.

Efficacy of Toripalimab in Other Cancers

In addition to the above-mentioned tumors, toripalimab monotherapy has also shown anti-tumor effects in phase I studies on alveolar soft part sarcoma, lymphoma and renal cell carcinoma, achieving ORRs of 25.0% (3/12), 90.9% (10/11) and 33.3% (2/6), respectively (20, 21). In lymphoma patients, the ORR achieved by toripalimab (NCT02836834) is apparently higher than those achieved by nivolumab [CHECKMATE-205, 69.1% (168/243)] or pembrolizumab [KEYNOTE-087, 69.0% (145/210)]. Although the sample size in NCT02836834 is small and the patient race is different from the other two studies, the result suggests a promising anti-tumor effect of toripalimab in lymphoma that is worth exploring in future studies (21, 112, 113). As neoadjuvant therapies, toripalimab-containing regimes were claimed to be effective in penile squamous cell carcinoma and anal canal squamous carcinoma (114, 115). Toripalimab was also effective in cancers such as pancreatic adenocarcinoma and small-cell lung cancer (**Figures 2**, **3**) (116, 117). It is interesting that the regime achieved a 100% ORR in extensive-stage small cell lung cancer (117). In addition, toripalimab in combination with YH-001, an anti-CTLA-4 monoclonal antibody, or YH-003, an anti-CD40 monoclonal antibody, were shown to be effective in phase I studies in advanced solid tumors (**Figure 2**) (118, 119). In other retrospective studies, toripalimab was claimed to be effective when combined with other treatments in patients with soft tissue sarcoma cervical cancer, and head and neck squamous cell carcinoma (120–122). These studies have indicated a bright future for this drug in clinical applications. The efficacies of toripalimab in different clinical studies have been visualized in **Figures 2**, **3**.

ADVERSE EFFECTS

Although toripalimab has shown preliminary efficacy in the treatment of various tumors, there are inevitable side effects. The adverse effects have five grades, which were defined according to the Common Terminology Criteria for Adverse Events from the National Cancer Institute, referring to mild, moderate, severe and life-threatening AEs or death, in ascending order, and were coded using the Medical Dictionary for Regulatory Activities (123, 124).

Generally, the safety profile of toripalimab is acceptable; the incidence of AEs is higher than well-studied checkpoint inhibitors, but is manageable. The incidences of all grade TRAEs have been visualized in **Figures 2**, **3**, and most common TRAEs are summarized in **Table 2**. The safety of checkpoint inhibitors has been assessed in previous research, revealing an incidence varying between 54% and 76% for all TRAEs (125). The incidences of fatal AEs for PD-1 inhibitors and PD-L1 inhibitors were shown to be 0.361% (33/9136) and 0.63% (12/3164) in a study that comprehensively evaluated the spectrum of fatal checkpoint inhibitor-related toxic effects (126). For toripalimab, there was no dose-limiting toxicity in three phase I studies, and the pooled incidence rates of AEs and AE-related death (hereafter "the rates") were 96.8% (91/94) and 2.1% (2/94) (19–21), respectively. The death rate appears to be higher than the average; however, the sample sizes are small, meaning that it is difficult to draw a conclusion. In the first reported phase I study of nivolumab, the rates were 69.9% (207/296) and 1.0% (3/296) (127). The rates for pembrolizumab in a phase I study were 70.9% (351/495) and 0.2% (1/495) (43). When toripalimab was used alone, TRAEs occurred in 42.9–100% patients across the studies, and the death rate ranged from 0–6.7%. In combination regimes, the highest incidence of grade 5 TRAEs was 8.2%, when combined with chemotherapy (**Figure 3**). The incidences may not be compared directly because the baseline characteristics of patients are different.

Toripalimab has shown a better safety profile than pembrolizumab in melanoma. In POLARIS-01, toripalimab

TABLE 2 | Summary of most common treatment-related adverse events of all grades across 15 prospective studies with complete results.

Trials	Tumor	Patient number	Included TRAE	Regimen	Leukopenia	Anemia	Neutropenia	Nausea	Fatigue	ALT elevation	AST elevation	Decreased appetite/ Anorexia	Thrombocytopenia	Rash/ Skin reaction	Vomiting	Hypothyroidism	Fever	Constipation	Diarrhea	Creatine kinase elevation	Pruritus	Hyponatremia	Hyperglycemia	Myalgia	Proteinuria	Peripheral neuropathy
NCT03946917 (79)	CRC	39	All	Toripalimab plus regorafenib	0.0%	5.1%	2.6%	0.0%	10.3%	0.0%	0.0%	5.1%	10.3%	30.8%	0.0%	2.6%	20.5%	0.0%	17.9%	0.0%	2.6%	0.0%	0.0%	12.8%	2.6%	0.0%
PICC (77) (Combination)	CRC	17	All	Toripalimab plus celecoxib (neoadjuvant)	0.0%	0.0%	0.0%	6.0%	12.0%	6.0%	18.0%	0.0%	0.0%	6.0%	0.0%	6.0%	0.0%	0.0%	0.0%	0.0%	12.0%	0.0%	0.0%	0.0%	0.0%	0.0%
PICC (77) (Monotherapy)	CRC	17	All	Toripalimab monotherapy (neoadjuvant)	0.0%	0.0%	0.0%	18.0%	24.0%	6.0%	12.0%	6.0%	0.0%	18.0%	0.0%	0.0%	6.0%	0.0%	0.0%	0.0%	18.0%	0.0%	0.0%	0.0%	0.0%	0.0%
NCT02915432 (64) (Cohort 1)	GC	58	All (>5%)	Toripalimab monotherapy	8.6%	12.1%	1.7%	5.2%	10.3%	8.6%	10.3%	5.2%	6.9%	8.6%	5.2%	12.1%	5.2%	0.0%	5.2%	0.0%	10.3%	0.0%	0.0%	0.0%	8.6%	0.0%
NCT02915432 (64) (Cohort 2)	GC	18	All (>10%)	Toripalimab plus CapeOx	38.9%	27.8%	38.9%	50.0%	16.7%	16.7%	33.3%	27.8%	22.2%	22.2%	38.9%	0.0%	11.1%	16.7%	27.8%	0.0%	22.2%	0.0%	0.0%	0.0%	22.2%	0.0%
NCT03013101 (22)	Melanoma	128	All (>5%)	Toripalimab montherapy	20.3%	0.0%	17.2%	0.0%	14.8%	31.3%	22.7%	10.2%	7.0%	23.4%	0.0%	27.3%	6.3%	0.0%	0.0%	25.8%	0.0%	0.0%	30.5%	5.5%	0.0%	0.0%
NCT03086174 (23)	Mucosal melanoma	33	All (>15%)	Toripalimab plus axitinib	27.3%	21.2%	24.2%	21.2%	48.5%	42.4%	33.3%	24.2%	0.0%	36.4%	0.0%	51.5%	0.0%	0.0%	60.6%	36.4%	0.0%	0.0%	33.3%	0.0%	57.6%	0.0%
NCT03167853 (97)	NEN	40	All (≥10%)	Toripalimab monotherapy	15.0%	22.5%	10.0%	15.0%	20.0%	32.5%	37.5%	10.0%	0.0%	17.5%	0.0%	0.0%	12.5%	0.0%	12.5%	25.0%	25.0%	15.0%	35.0%	0.0%	40.0%	0.0%
POLARIS-02 (101)	NPC	190	All (≥5%)	Toripalimab monotherapy	10.0%	15.3%	5.3%	0.0%	13.2%	13.7%	15.3%	0.0%	0.0%	6.3%	0.0%	23.7%	9.5%	0.0%	0.0%	0.0%	8.4%	0.0%	0.0%	0.0%	12.6%	0.0%
NCT03854838 (105)	NPC	25	All	Toripalimab plus IMRT	16.0%	0.0%	8.0%	76.0%	88.0%	20.0%	12.0%	0.0%	4.0%	40.0%	8.0%	32.0%	4.0%	0.0%	4.0%	20.0%	32.0%	0.0%	36.0%	16.0%	0.0%	0.0%
JUPITER-02 (107) (Toripalimab group)	NPC	146	All (≥10%)	Toripalimab plus GP	91.1%	88.4%	85.6%	69.2%	35.6%	36.3%	37.7%	53.4%	63.0%	27.4%	67.1%	30.8%	30.8%	39.0%	30.1%	17.8%	16.4%	25.3%	0.0%	23.3%	0.0%	30.1%
JUPITER-02 (107) (Placebo group)	NPC	143	All (≥10%)	Placebo plus GP	94.4%	94.4%	93.0%	83.2%	35.7%	39.9%	30.8%	58.7%	62.2%	21.7%	65.7%	16.8%	21.7%	44.8%	23.1%	23.8%	7.0%	36.4%	0.0%	26.6%	0.0%	28.7%
NCT03301688 (40)	NSCLC	41	All	Toripalimab monotherapy	2.4%	0.0%	0.0%	4.9%	2.4%	7.3%	12.2%	0.0%	0.0%	14.6%	0.0%	7.3%	0.0%	0.0%	0.0%	0.0%	2.4%	0.0%	0.0%	0.0%	0.0%	0.0%
NeoTPD01 (50)	NSCLC	33	All	Toripalimab plus chemotherapy (neoadjuvant)	0.0%	51.6%	6.1%	30.3%	15.2%	0.0%	0.0%	12.1%	15.2%	18.2%	3.0%	18.2%	0.0%	0.0%	3.0%	0.0%	3.0%	0.0%	0.0%	15.1%	0.0%	15.1%
NCT03513666 (46)	NSCLC	40	All	Toripalimab plus chemotherapy	82.5%	67.5%	70.0%	47.5%	25.0%	50.0%	52.5%	37.5%	47.5%	15.0%	17.5%	0.0%	10.0%	27.5%	0.0%	0.0%	0.0%	0.0%	0.0%	0.0%	0.0%	0.0%
NCT02857166 (19)	ST	25	All	Toripalimab monotherapy	4.0%	0.0%	0.0%	8.0%	64.0%	4.0%	4.0%	16.0%	0.0%	24.0%	0.0%	12.0%	4.0%	0.0%	12.0%	0.0%	12.0%	0.0%	0.0%	0.0%	16.0%	0.0%
NCT02836834 (21)	ST	33	All (≥10%)	Toripalimab monotherapy	30.0%	18.0%	18.0%	0.0%	18.0%	18.0%	21.0%	0.0%	0.0%	21.0%	0.0%	0.0%	30.0%	0.0%	0.0%	3.0%	15.0%	0.0%	0.0%	0.0%	0.0%	0.0%
NCT02836795 (20)	ST	36	All (≥20%)	Toripalimab monotherapy	25.0%	33.3%	0.0%	0.0%	22.2%	22.2%	25.0%	22.2%	0.0%	44.4%	0.0%	0.0%	38.9%	0.0%	0.0%	0.0%	25.0%	0.0%	58.3%	0.0%	50.0%	0.0%

CRC, colorectal cancer; GC, gastric cancer; NEN, neuroendocrine neoplasms; NPC, nasopharyngeal carcinoma; NSCLC, non-small cell lung cancer; ST, solid tumors; TRAE, treatment-related adverse events; CapeOx, capecitabine and oxaliplatin; IMRT, intensity-modulated radiotherapy; GP, gemcitabine and platinum; ALT, alanine aminotransferase; AST, aspartate aminotransferase.

monotherapy resulted in 90.6% (116/128) TRAEs and 19.5% (25/128) grade 3 or 4 TRAEs, with no TRAE-related deaths, in melanoma patients (22). The rates for combination of toripalimab with axitinib were 97.0% (32/33) and 0% (23). For pembrolizumab monotherapy in melanoma, 84.5% (87/103) patients encountered TRAEs, and 8.7% (9/103) patients encountered grade 3 or 4 TRAEs; 1.9% (2/103) of patients died (one patient died of shock and one died of pulmonary embolism), although the researchers claimed that the deaths were unrelated to treatment (29). In a pooled analysis, nivolumab monotherapy caused 66.3% (57/86), 76.4% (508/665) TRAEs and 8.1% (7/86), 12.5% (83/665) grade 3 or 4 TRAEs in mucosal and cutaneous melanoma patients, without deaths. The pooled incidence of TRAEs and grade 3 or 4 TRAEs were 75.2% (565/751) and 12.0% (90/751), respectively (128). However, the analysis included patients of multiple races, compared to only Chinese patients in POLARIS-01 and KEYNOTE-151.

In other tumors, toripalimab also exhibited manageable adverse effects. Chinese patients may react differently from other populations; thus, the rates of toripalimab and the other two drugs may not be compared directly. The TRAE incidence of toripalimab in prospective clinical studies were shown and compared in **Figures 2**, **3**. The safety profile of toripalimab could be analyzed systematically in future research.

DISCUSSION

Toripalimab is the first domestic PD-1 antibody in China and has received approvals for the treatment of advanced melanoma, NPC and UC (128). The binding of toripalimab to PD-1 is mainly attributed to the heavy chain of the former and the FG loop of the latter. Toripalimab has shown preliminary anti-tumor effects comparable to pembrolizumab or nivolumab in tumors like melanoma, GC, NEN and UC, with acceptable safety profiles. Prospective clinical studies on toripalimab were shown in integrated tables and graphs in **Figures 2**, **3**.

There are some disadvantages and limitations of this review. Firstly, all patients included in toripalimab studies are native Chinese, which makes it difficult to compare the anti-tumor effects with other drugs. Future studies involving other races may provide more comparable data. Secondly, although the comparisons made between studies are based on their identical primary endpoints, there is a lack of direct head-to-head comparisons. The comparisons between studies need to be made prudently, considering the different baseline characteristics of patients. Importantly, there are mainly phase 2 studies for toripalimab at present. Comparisons between drugs could be made using the indirect comparison method, which requires phase 3 randomized controlled studies with control groups (129–131). Furthermore, complete data from some studies, such as JUPITER-06 and ChiCTR1900025318, are not available. The release of complete study results will solve this problem.

Despite these limitations, there are some inherent advantages of this study. Firstly, there are more than 200 ongoing clinical trials of toripalimab, with future results expected (36). Furthermore, toripalimab has a lower cost than the other two well-studied PD-1 inhibitors (nivolumab and pembrolizumab) after the patient-assistant program; after the negotiation of Chinese government with pharmaceutical companies and the inclusion of toripalimab into the medical insurance catalogue, the cost of toripalimab further decreased (132–134). The approval of toripalimab has provided tumor patients with an extra option. Despite the decline in cost of the domestic PD-1 antibody in China, the radical change in the drug price may also exert pressure on foreign pharmaceutical companies and lead to a price decline in their PD-1/PD-L1 antibodies. Moreover, several orphan drug designations have been granted to toripalimab by the US FDA (34). Thus, it may also benefit tumor patients in other countries.

CONCLUSION

In conclusion, toripalimab has shown preliminary efficacy in tumors like melanoma, lung cancer, ESCC, GC, G/GEJ, CRC, HCC, BTC, ICC, NEN, NPC, and UC, with acceptable safety profiles. Specifically, it has a potent efficacy in melanoma according to data from relevant studies. Although there are some limitations, it is hopeful that the introduction of toripalimab will provide a valuable option for tumor patients. Meanwhile, our review has also provided oncologists with information on a potential choice for the treatment of cancers in the future.

AUTHOR CONTRIBUTIONS

Conception and design: LZ. Manuscript writing: LZ and BH. Revision and language editing: LZ, ZG. Supervision: QG. All authors contributed to the article and approved the submitted version

REFERENCES

1. Sun C, Mezzadra R, Schumacher TN. Regulation and Function of the PD-L1 Checkpoint. *Immunity* (2018) 48:434–52. doi: 10.1016/j.immuni.2018.03.014
2. He X, Xu C. Immune Checkpoint Signaling and Cancer Immunotherapy. *Cell Res* (2020) 30:660–9. doi: 10.1038/s41422-020-0343-4
3. Patsoukis N, Wang Q, Strauss L, Boussiotis VA. Revisiting the PD-1 Pathway. *Sci Adv* (2020) 6(38):eabd2712. doi: 10.1126/sciadv.abd2712
4. Lin X, Lu X, Luo G, Xiang H. Progress in PD-1/PD-L1 Pathway Inhibitors: From Biomacromolecules to Small Molecules. *Eur J Med Chem* (2020) 186:111876. doi: 10.1016/j.ejmech.2019.111876
5. National Medical Products Administration. *Toripalimab, the First Domestic Anti-PD-1 Monoclonal Antibody, Was Approved Into Market* (2018). Available at: https://www.nmpa.gov.cn/directory/web/nmpa/zhuanti/ypqxgg/gggzjzh/20181217161101989.html (Accessed November 30, 2021).
6. Keam SJ. Toripalimab: First Global Approval. *Drugs* (2019) 79:573–8. doi: 10.1007/s40265-019-01076-2

7. National Medical Products Administration. *Drug Approval Documents Released on November 26, 2021* (2021). Available at: https://www.nmpa.gov.cn/zwfw/sdxx/sdxxyp/yppjfb/20211126160047176.html (Accessed November 30, 2021).
8. National Medical Products Administration. *Drug Approval Documents Released on February 19, 2021* (2021). Available at: https://www.nmpa.gov.cn/zwfw/sdxx/sdxxyp/yppjfb/20210219085955119.html (Accessed November 30, 2021).
9. National Medical Products Administration. *Drug Approval Documents Released on April 12, 2021* (2021). Available at: https://www.nmpa.gov.cn/zwfw/sdxx/sdxxyp/yppjfb/20210412090005190.html (Accessed November 30, 2021).
10. National Medical Products Administration. *The First Domestic PD-1 Antibody Toripalimab Injection was Approved Into the Market* (2018). Available at: https://www.nmpa.gov.cn/directory/web/nmpa/yaowen/ypjgyw/20181217161101989.html (Accessed November 30, 2021).
11. Tang B, Chi Z, Guo J. Toripalimab for the Treatment of Melanoma. *Expert Opin Biol Ther* (2020) 20:863–9. doi: 10.1080/14712598.2020.1762561
12. Liu H, Guo L, Zhang J, Zhou Y, Zhou J, Yao J, et al. Glycosylation-Independent Binding of Monoclonal Antibody Toripalimab to FG Loop of PD-1 for Tumor Immune Checkpoint Therapy. *MAbs* (2019) 11:681–90. doi: 10.1080/19420862.2019.1596513
13. Burley SK, Bhikadiya C, Bi C, Bittrich S, Chen L, Crichlow GV, et al. RCSB Protein Data Bank: Powerful New Tools for Exploring 3D Structures of Biological Macromolecules for Basic and Applied Research and Education in Fundamental Biology, Biomedicine, Biotechnology, Bioengineering and Energy Sciences. *Nucleic Acids Res* (2021) 49:D437–51. doi: 10.1093/nar/gkaa1038
14. Sehnal D, Bittrich S, Deshpande M, Svobodová R, Berka K, Bazgier V, et al. Mol* Viewer: Modern Web App for 3D Visualization and Analysis of Large Biomolecular Structures. *Nucleic Acids Res* (2021) 49:W431–7. doi: 10.1093/nar/gkab314
15. Tan S, Zhang H, Chai Y, Song H, Tong Z, Wang Q, et al. An Unexpected N-Terminal Loop in PD-1 Dominates Binding by Nivolumab. *Nat Commun* (2017) 8:14369. doi: 10.1038/ncomms14369
16. Na Z, Yeo SP, Bharath SR, Bowler MW, Balikci E, Wang CI, et al. Structural Basis for Blocking PD-1-Mediated Immune Suppression by Therapeutic Antibody Pembrolizumab. *Cell Res* (2017) 27:147–50. doi: 10.1038/cr.2016.77
17. Huang H, Zhu H, Xie Q, Tian X, Yang X, Feng F, et al. Evaluation of 124I-JS001 for Hpd1 Immuno-PET Imaging Using Sarcoma Cell Homografts in Humanized Mice. *Acta Pharm Sin B* (2020) 10:1321–30. doi: 10.1016/j.apsb.2020.02.004
18. Fu J, Wang F, Dong LH, Zhang J, Deng CL, Wang XL, et al. Preclinical Evaluation of the Efficacy, Pharmacokinetics and Immunogenicity of JS-001, a Programmed Cell Death Protein-1 (PD-1) Monoclonal Antibody. *Acta Pharmacol Sin* (2017) 38:710–8. doi: 10.1038/aps.2016.161
19. Wei XL, Ren C, Wang FH, Zhang Y, Zhao HY, Zou BY, et al. A Phase I Study of Toripalimab, an Anti-PD-1 Antibody, in Patients With Refractory Malignant Solid Tumors. *Cancer Commun* (2020) 40:345–54. doi: 10.1002/cac2.12068
20. Tang B, Yan X, Sheng X, Si L, Cui C, Kong Y, et al. Safety and Clinical Activity With an Anti-PD-1 Antibody JS001 in Advanced Melanoma or Urologic Cancer Patients. *J Hematol Oncol* (2019) 12(1):7. doi: 10.1186/s13045-018-0693-2
21. Yang J, Dong L, Yang S, Han X, Han Y, Jiang S, et al. Safety and Clinical Efficacy of Toripalimab, a PD-1 mAb, in Patients With Advanced or Recurrent Malignancies in a Phase I Study. *Eur J Cancer* (2020) 130:182–92. doi: 10.1016/j.ejca.2020.01.028
22. Tang B, Chi Z, Chen Y, Liu X, Wu D, Chen J, et al. Safety, Efficacy, and Biomarker Analysis of Toripalimab in Previously Treated Advanced Melanoma: Results of the POLARIS-01 Multicenter Phase II Trial. *Clin Cancer Res* (2020) 26:4250–9. doi: 10.1158/1078-0432.CCR-19-3922
23. Sheng X, Yan X, Chi Z, Si L, Cui C, Tang B, et al. Axitinib in Combination With Toripalimab, a Humanized Immunoglobulin G4 Monoclonal Antibody Against Programmed Cell Death-1, in Patients With Metastatic Mucosal Melanoma: An Open-Label Phase IB Trial. *J Clin Oncol* (2019) 37:2987–99. doi: 10.1200/JCO.19.00210
24. U.S. Food & Drug Administration. *Clinical Trial Endpoints for the Approval of Cancer Drugs and Biologics Guidance for Industry* (2018). Available at: https://www.fda.gov/media/71195/download (Accessed December 30, 2021).
25. Sung H, Ferlay J, Siegel RL, Laversanne M, Soerjomataram I, Jemal A, et al. Global Cancer Statistics 2020: GLOBOCAN Estimates of Incidence and Mortality Worldwide for 36 Cancers in 185 Countries. *CA Cancer J Clin* (2021) 71:209–49. doi: 10.3322/caac.21660
26. Schadendorf D, van Akkooi A, Berking C, Griewank KG, Gutzmer R, Hauschild A, et al. Melanoma. *Lancet* (2018) 392:971–84. doi: 10.1016/S0140-6736(18)31559-9
27. Tang B, Chi Z, Chen Y, Liu X, Wu D, Chen J, et al. Four-Year Survival Follow-Up of Toripalimab (JS001) as Salvage Therapy in Chinese Melanoma Patients. *J Clin Oncol* (2021) 39:e21522. doi: 10.1200/JCO.2021.39.15_suppl.e21522
28. Topalian SL, Sznol M, McDermott DF, Kluger HM, Carvajal RD, Sharfman WH, et al. Survival, Durable Tumor Remission, and Long-Term Safety in Patients With Advanced Melanoma Receiving Nivolumab. *J Clin Oncol* (2014) 32:1020–30. doi: 10.1200/JCO.2013.53.0105
29. Si L, Zhang X, Shu Y, Pan H, Wu D, Liu J, et al. A Phase Ib Study of Pembrolizumab as Second-Line Therapy for Chinese Patients With Advanced or Metastatic Melanoma (KEYNOTE-151). *Transl Oncol* (2019) 12:828–35. doi: 10.1016/j.tranon.2019.02.007
30. Sheng X, Yan X, Chi Z, Si L, Cui C, Tang B, et al. Overall Survival and Biomarker Analysis of a Phase Ib Combination Study of Toripalimab, a Humanized IgG4 mAb Against Programmed Death-1 (PD-1) With Axitinib in Patients With Metastatic Mucosal Melanoma. *J Clin Oncol* (2020) 38:10007. doi: 10.1200/JCO.2020.38.15_suppl.10007
31. Cui C, Lian B, Si L, Chi Z, Sheng X, Kong Y, et al. Adjuvant Anti-PD-1 Ab (Toripalimab) Versus High-Dose IFN-A2b in Resected Mucosal Melanoma: A Phase Randomized Trial. *J Clin Oncol* (2021) 39:9573. doi: 10.1200/JCO.2021.39.15_suppl.9573
32. Lacal PM, Graziani G. Therapeutic Implication of Vascular Endothelial Growth Factor Receptor-1 (VEGFR-1) Targeting in Cancer Cells and Tumor Microenvironment by Competitive and Non-Competitive Inhibitors. *Pharmacol Res* (2018) 136:97–107. doi: 10.1016/j.phrs.2018.08.023
33. Yasuda S, Sho M, Yamato I, Yoshiji H, Wakatsuki K, Nishiwada S, et al. Simultaneous Blockade of Programmed Death 1 and Vascular Endothelial Growth Factor Receptor 2 (VEGFR2) Induces Synergistic Anti-Tumour Effect *In Vivo*. *Clin Exp Immunol* (2013) 172:500–6. doi: 10.1111/cei.12069
34. U.S. Food and Drug Administration. *Search Orphan Drug Designations and Approvals* (2021). Available at: https://www.accessdata.fda.gov/scripts/opdlisting/oopd/listResult.cfm (Accessed November 18, 2021).
35. Cui C, Wang X, Lian B, Si L, Chi Z, Sheng X, et al. A Phase 2 Clinical Trial of Neoadjuvant Anti-PD-1 Ab (Toripalimab) Plus Axitinib in Resectable Mucosal Melanoma. *J Clin Oncol* (2021) 39:9512. doi: 10.1200/JCO.2021.39.15_suppl.9512
36. U.S. National Library of Medicine. *Clinical Trials on Toripalimab* (2021). Available at: https://clinicaltrials.gov/ct2/results?cond=&term=toripalimab&cntry=&state=&city=&dist (Accessed November 30, 2021).
37. Wang X, Cui C, Si L, Li C, Dai J, Mao L, et al. A Phase Ib Clinical Trial of Neoadjuvant OrienX010, an Oncolytic Virus, in Combination With Toripalimab in Patients With Resectable Stage IIIb to Stage IVM1a Acral Melanoma. *J Clin Oncol* (2021) 39:9570. doi: 10.1200/JCO.2021.39.15_suppl.9570
38. Guo J, Cui C, Wang X, Lian B, Yin S, Cong Y, et al. A Phase 1b Clinical Trial of Anti-PD-1 Ab (Toripalimab) Plus Intralesional Injection of OrienX010 in Stage Melanoma With Liver Metastases. *J Clin Oncol* (2021) 39:9559. doi: 10.1200/JCO.2021.39.15_suppl.9559
39. Si L, Sheng X, Mao L, Li C, Wang X, Bai X, et al. A Phase II Study of Vorolanib (CM082) in Combination With Toripalimab (JS001) in Patients With Advanced Mucosal Melanoma. *J Clin Oncol* (2020) 38:10040. doi: 10.1200/JCO.2020.38.15_suppl.10040
40. Wang Z, Ying J, Xu J, Yuan P, Duan J, Bai H, et al. Safety, Antitumor Activity, and Pharmacokinetics of Toripalimab, a Programmed Cell Death 1 Inhibitor, in Patients With Advanced Non–Small Cell Lung Cancer. *JAMA Netw Open* (2020) 3:e2013770. doi: 10.1001/jamanetworkopen.2020.13770
41. Ruan Z, Zhu B, Wang YN, Liu B, Li M, Xia G, et al. Real-World Outcomes of Toripalimab (JS001) in Advanced Non-Small Cell Lung Cancer: A Multicenter Retrospective Study. *J Clin Oncol* (2021) 39:e21193. doi: 10.1200/JCO.2021.39.15_suppl.e21193

42. Gettinger SN, Horn L, Gandhi L, Spigel DR, Antonia SJ, Rizvi NA, et al. Overall Survival and Long-Term Safety of Nivolumab (Anti-Programmed Death 1 Antibody, BMS-936558, ONO-4538) in Patients With Previously Treated Advanced Non-Small-Cell Lung Cancer. *J Clin Oncol* (2015) 33:2004–12. doi: 10.1200/JCO.2014.58.3708
43. Garon EB, Rizvi NA, Hui R, Leighl N, Balmanoukian AS, Eder JP, et al. Pembrolizumab for the Treatment of Non-Small-Cell Lung Cancer. *N Engl J Med* (2015) 372:2018–28. doi: 10.1056/NEJMoa1501824
44. Ren X, Zhang W. A Single-Arm Phase Ib Study of Multiple Target Cytotoxic T-Lymphocyte (MCTL) in Combination With Toripalimab as Second-Line Therapy in Advanced Non-Small Cell Lung Cancer (NSCLC). *J Clin Oncol* (2021) 39:2535. doi: 10.1200/JCO.2021.39.15_suppl.2535
45. National Comprehensive Cancer Network. *NCCN Guidelines, Non Small Cell Lung Cancer* (2021). Available at: https://www.nccn.org/guidelines/guidelines-detail?category=1&id=1450 (Accessed November 30, 2021).
46. Jiang T, Wang P, Zhang J, Zhao Y, Zhou J, Fan Y, et al. Toripalimab Plus Chemotherapy as Second-Line Treatment in Previously EGFR-TKI Treated Patients With EGFR-Mutant-Advanced NSCLC: A Multicenter Phase-II Trial. *Signal Transduct Target Ther* (2021) 6:355. doi: 10.1038/s41392-021-00751-9
47. Jiang M, Wang Y, Zhang X. 1310p - Toripalimab Combined With Chemotherapy as Second-Line Treatment of Advanced Non-Small Cell Lung Cancer (NSCLC): A Single Center Retrospective Study. *Ann Oncol* (2021) 32:S949–1039. doi: 10.1016/annonc/annonc729
48. U.S. National Library of Medicine. *Search Results for Nct03924050* (2021). Available at: https://clinicaltrials.gov/ct2/results?cond=&term=NCT03924050&cntry=&state=&city=&dist (Accessed November 30, 2021).
49. Zhao J, Li J, Chen H, Yang X, Zhong J, Zhuo M, et al. A Phase II Study of Vorolanib in Combination With Toripalimab in Patients With Non-Small Cell Lung Cancer. *J Clin Oncol* (2021) 39:e21053. doi: 10.1200/JCO.2021.39.15_suppl.e21053
50. Zhao Z, Yang C, Chen S, Yu H, Lin Y, Lin Y, et al. Phase 2 Trial of Neoadjuvant Toripalimab With Chemotherapy for Resectable Stage III Non-Small-Cell Lung Cancer. *Oncoimmunology* (2021) 10(1):1996000. doi: 10.1080/2162402X.2021.1996000
51. Zhu X, Sun L, Song N, Sun F, Yang Y, Duan L, et al. 1176p - Neoadjuvant PD-1 Inhibitor (Toripalimab) Plus Chemotherapy in Patients With Potentially Resectable NSCLC: An Open-Label, Single-Arm, Phase II Trial. *Ann Oncol* (2021) 32:S939–48. doi: 10.1016/annonc/annonc728
52. Forde PM, Chaft JE, Smith KN, Anagnostou V, Cottrell TR, Hellmann MD, et al. Neoadjuvant PD-1 Blockade in Resectable Lung Cancer. *N Engl J Med* (2018) 378:1976–86. doi: 10.1056/NEJMoa1716078
53. Ben Nun A, Golan N, Ofek E, Urban D, Kamer I, Simansky D, et al. Neoadjuvant Pembrolizumab (Pembro) for Early Stage Non-Small Cell Lung Cancer (NSCLC): Initial Report of a Phase I Study, MK3475-223. *Ann Oncol* (2018) 29:i486. doi: 10.1093/annonc/mdy290.011
54. Bar J, Urban D, Ofek E, Ackerstein A, Redinsky I, Golan N, et al. Neoadjuvant Pembrolizumab (Pembro) for Early Stage Non-Small Cell Lung Cancer (NSCLC): Updated Report of a Phase I Study, MK3475-223. *J Clin Oncol* (2019) 37:8534. doi: 10.1200/JCO.2019.37.15_suppl.8534
55. Shen D, Wang J, Wu J, Chen S, Li J, Liu J, et al. Neoadjuvant Pembrolizumab With Chemotherapy for the Treatment of Stage IIB–IIIB Resectable Lung Squamous Cell Carcinoma. *J Thorac Dis* (2021) 13:1760–8. doi: 10.21037/jtd-21-103
56. Sun J, Xie L, Feng Y, Qin S. 1320tip - The Efficacy and Safety of Stereotactic Body Radiation Therapy (SBRT) Plus Toripalimab With or Without Bevacizumab as Second-Line Treatment for Advanced Non-Small Cell Lung Cancer (NSCLC): A Prospective, Multicenter, Open-Label, Phase II Study. *Ann Oncol* (2021) 32:S949–1039. doi: 10.1016/annonc/annonc729
57. U.S. National Library of Medicine. *Studies Registered for: Toripalimab and Non Small Cell Lung Cancer* (2021). Available at: https://clinicaltrials.gov/ct2/results?cond=non+small+cell+lung+cancer&term=toripalimab&cntry=&state=&city=&dist (Accessed November 30, 2021).
58. National Comprehensive Cancer Network. *NCCN Guidelines, Esophageal and Esophagogastric Junction Cancers* (2021). Available at: https://www.nccn.org/guidelines/guidelines-detail?category=1&id=1433 (Accessed November 30, 2021).
59. Liu D, Zhang Q, Zhu J, Qian T, Yin R, Fan Z, et al. Phase-II Study of Toripalimab Combined With Neoadjuvant Chemotherapy for the Treatment of Resectable Esophageal Squamous Cell Carcinoma. *J Clin Oncol* (2021) 39:e16029. doi: 10.1200/JCO.2021.39.15_suppl.e16029
60. Zhao L, Xing W, Yang Y, Zhang Y, Ma B, Fu X, et al. The Sequence of Chemotherapy and Anti-PD-1 Antibody Influence the Efficacy of Neoadjuvant Immunochemotherapy in Locally Advanced Esophageal Squamous Cell Cancer: A Phase II Study. *J Clin Oncol* (2021) 39:4051. doi: 10.1200/JCO.2021.39.15_suppl.4051
61. Xu R, Wang F, Cui C, Yao J, Zhang Y, Wang G, et al. 1373mo - JUPITER-06: A Randomized, Double-Blind, Phase III Study of Toripalimab Versus Placebo in Combination With First-Line Chemotherapy for Treatment Naive Advanced or Metastatic Esophageal Squamous Cell Carcinoma (ESCC). *Ann Oncol* (2021) 32:S1040–75. doi: 10.1016/annonc/annonc708
62. Sun J, Shen L, Shah MA, Enzinger P, Adenis A, Doi T, et al. Pembrolizumab Plus Chemotherapy Versus Chemotherapy Alone for First-Line Treatment of Advanced Oesophageal Cancer (KEYNOTE-590): A Randomised, Placebo-Controlled, Phase 3 Study. *Lancet* (2021) 398:759–71. doi: 10.1016/S0140-6736(21)01234-4
63. Xi M, Zhu Y, Li Q, Zhao L, Yang Y, Hu Y, et al. The Efficacy and Safety of Toripalimab Combined With Definitive Chemoradiotherapy for Patients With Locally Advanced Esophageal Squamous Cell Carcinoma. *J Clin Oncol* (2021) 39:e16043. doi: 10.1200/JCO.2021.39.15_suppl.e16043
64. Wang F, Wei XL, Wang FH, Xu N, Shen L, Dai GH, et al. Safety, Efficacy and Tumor Mutational Burden as a Biomarker of Overall Survival Benefit in Chemo-Refractory Gastric Cancer Treated With Toripalimab, a PD-1 Antibody in Phase Ib/II Clinical Trial NCT02915432. *Ann Oncol* (2019) 30:1479–86. doi: 10.1093/annonc/mdz197
65. Fuchs CS, Doi T, Jang RW, Muro K, Satoh T, Machado M, et al. Safety and Efficacy of Pembrolizumab Monotherapy in Patients With Previously Treated Advanced Gastric and Gastroesophageal Junction Cancer. *JAMA Oncol* (2018) 4:e180013. doi: 10.1001/jamaoncol.2018.0013
66. Muro K, Chung HC, Shankaran V, Geva R, Catenacci D, Gupta S, et al. Pembrolizumab for Patients With PD-L1-Positive Advanced Gastric Cancer (KEYNOTE-012): A Multicentre, Open-Label, Phase 1b Trial. *Lancet Oncol* (2016) 17:717–26. doi: 10.1016/S1470-2045(16)00175-3
67. Zhang T, Yu D, Wang J, Liu J, Ma H, Lin Z, et al. 1403p - Toripalimab Combined With Nab-Paclitaxel/Docetaxel as Second-Line Treatment in Patients With Advanced Gastric Cancer: Preliminary Results From a Single-Arm, Open-Label Phase II Trial. *Ann Oncol* (2021) 32:S1040–75. doi: 10.1016/annonc/annonc70
68. Yang Y, Yan J, Liu J, Li S, Gao S, Wei J, et al. Phase II Study of Combining Immunotherapy and Pulsed Low Dose Rate Radiotherapy for Abdominal Metastasis of Gastric Cancer. *J Clin Oncol* (2021) 39:e16099. doi: 10.1200/JCO.2021.39.15_suppl.e16099
69. Boku N, Ryu MH, Kato K, Chung HC, Minashi K, Lee KW, et al. Safety and Efficacy of Nivolumab in Combination With S-1/Capecitabine Plus Oxaliplatin in Patients With Previously Untreated, Unresectable, Advanced, or Recurrent Gastric/Gastroesophageal Junction Cancer: Interim Results of a Randomized, Phase II Trial (ATTRACTION-4). *Ann Oncol* (2019) 30:250–8. doi: 10.1093/annonc/mdy540
70. Bang Y, Kang Y, Catenacci DV, Muro K, Fuchs CS, Geva R, et al. Pembrolizumab Alone or in Combination With Chemotherapy as First-Line Therapy for Patients With Advanced Gastric or Gastroesophageal Junction Adenocarcinoma: Results From the Phase II Nonrandomized KEYNOTE-059 Study. *Gastric Cancer* (2019) 22:828–37. doi: 10.1007/s10120-018-00909-5
71. Shen L, Lu M, Chen Z, Ye F, Zhang Y, Li Z, et al. Phase II Trial of Surufatinib Plus Toripalimab for Disease Progression After First-Line Chemotherapy With Platinum and Fluoropyrimidine in Advanced Gastric or Gastroesophageal Junction Adenocarcinoma. *J Clin Oncol* (2021) 39:e16040. doi: 10.1200/JCO.2021.39.15_suppl.e16040
72. National Comprehensive Cancer Network. *NCCN Guidelines, Esophageal and Esophagogastric Junction Cancers* (2021). Available at: https://www.nccn.org/guidelines/guidelines-detail?category=1&id=1433 (Accessed November 30, 2021).
73. Li H, Deng J, Ge S, Zang F, Zhang L, Ren P, et al. Phase II Study of Perioperative Toripalimab in Combination With FLOT in Patients With Locally Advanced Resectable Gastric/Gastroesophageal Junction (GEJ)

Adenocarcinoma. *J Clin Oncol* (2021) 39:4050. doi: 10.1200/JCO.2021.39.15_suppl.4050
74. Lin X, Xia Q, Han T, Zhuo M, Yang H, Qiu X, et al. Efficacy and Safety of Toripalimab Combination With SOX Regimen as a First-Line Treatment in Patients With Unresectable Locally Advanced or Recurrent/Metastatic Gastric/Gastroesophageal Junction Cancer: Preliminary Data From a Single-Armed, Exploratory Study. *J Clin Oncol* (2021) 39:e16015. doi: 10.1200/JCO.2021.39.15_suppl.e16015
75. Zelenay S, van der Veen AG, Böttcher JP, Snelgrove KJ, Rogers N, Acton SE, et al. Cyclooxygenase-Dependent Tumor Growth Through Evasion of Immunity. *Cell* (2015) 162:1257–70. doi: 10.1016/j.cell.2015.08.015
76. Pelly VS, Moeini A, Roelofsen LM, Bonavita E, Bell CR, Hutton C, et al. Anti-Inflammatory Drugs Remodel the Tumor Immune Environment to Enhance Immune Checkpoint Blockade Efficacy. *Cancer Discovery* (2021) 11:2602–19. doi: 10.1158/2159-8290.CD-20-1815
77. Hu H, Kang L, Zhang J, Wu Z, Wang H, Huang M, et al. Neoadjuvant PD-1 Blockade With Toripalimab, With or Without Celecoxib, in Mismatch Repair-Deficient or Microsatellite Instability-High, Locally Advanced, Colorectal Cancer (PICC): A Single-Centre, Parallel-Group, Non-Comparative, Randomised, Phase 2 Trial. *Lancet Gastroenterol Hepatol* (2022) 7:38–48. doi: 10.1016/S2468-1253(21)00348-4
78. Loupakis F, Antonuzzo L, Bachet J, Kuan F, Macarulla T, Pietrantonio F, et al. Practical Considerations in the Use of Regorafenib in Metastatic Colorectal Cancer. *Ther Adv Med Oncol* (2020) 12:386357190. doi: 10.1177/1758835920956862
79. Wang F, He M, Yao Y, Zhao X, Wang Z, Jin Y, et al. Regorafenib Plus Toripalimab in Patients With Metastatic Colorectal Cancer: A Phase Ib/II Clinical Trial and Gut Microbiome Analysis. *Cell Rep Med* (2021) 2:100383. doi: 10.1016/j.xcrm.2021.100383
80. Yu W, Tao Q, Zhang Y, Yi F, Feng L. Efficacy and Safety of Regorafenib Combined With Toripalimab in the Third-Line and Beyond Treatment of Advanced Colorectal Cancer. *J Oncol* (2021) 2021:1–7. doi: 10.1155/2021/9959946
81. Fukuoka S, Hara H, Takahashi N, Kojima T, Kawazoe A, Asayama M, et al. Regorafenib Plus Nivolumab in Patients With Advanced Gastric or Colorectal Cancer: An Open-Label, Dose-Escalation, and Dose-Expansion Phase Ib Trial (REGONIVO, Epoc1603). *J Clin Oncol* (2020) 38:2053–61. doi: 10.1200/JCO.19.03296
82. Shi L, Zhou C, Long X, Li H, Chen C, Peng C, et al. 949p - Thermal Ablation Plus Toripalimab in Patients With Advanced Hepatocellular Carcinoma: Phase I Results From a Multicenter, Open-Label, Controlled Phase I/II Trial (IR11330). *Ann Oncol* (2021) 32:S818–28. doi: 10.1016/j.annonc.2021.08.169
83. Lyu N, Kong Y, Li X, Mu L, Deng H, Chen H, et al. Ablation Reboots the Response in Advanced Hepatocellular Carcinoma With Stable or Atypical Response During PD-1 Therapy: A Proof-Of-Concept Study. *Front Oncol* (2020) 10:580241. doi: 10.3389/fonc.2020.580241
84. Kudo M, Finn RS, Qin S, Han KH, Ikeda K, Piscaglia F, et al. Lenvatinib Versus Sorafenib in First-Line Treatment of Patients With Unresectable Hepatocellular Carcinoma: A Randomised Phase 3 Non-Inferiority Trial. *Lancet* (2018) 391:1163–73. doi: 10.1016/S0140-6736(18)30207-1
85. Lyu N, Kong Y, Mu L, Lin Y, Li J, Liu Y, et al. Hepatic Arterial Infusion of Oxaliplatin Plus Fluorouracil/Leucovorin vs. Sorafenib for Advanced Hepatocellular Carcinoma. *J Hepatol* (2018) 69:60–9. doi: 10.1016/j.jhep.2018.02.008
86. He M, Liang R, Zhao Y, Xu Y, Chen H, Zhou Y, et al. Lenvatinib, Toripalimab, Plus Hepatic Arterial Infusion Chemotherapy Versus Lenvatinib Alone for Advanced Hepatocellular Carcinoma. *Ther Adv Med Oncol* (2021) 13:386371531. doi: 10.1177/17588359211002720
87. He M, Ming S, Lai Z, Li Q. A Phase II Trial of Lenvatinib Plus Toripalimab and Hepatic Arterial Infusion Chemotherapy as a First-Line Treatment for Advanced Hepatocellular Carcinoma (LTHAIC Study). *J Clin Oncol* (2021) 39:4083. doi: 10.1200/JCO.2021.39.15_suppl.4083
88. Sun Y, Zhou A, Zhang W, Jiang Z, Chen B, Zhao J, et al. Anlotinib in the Treatment of Advanced Hepatocellular Carcinoma: An Open-Label Phase II Study (ALTER-0802 Study). *Hepatol Int* (2021) 15:621–9. doi: 10.1007/s12072-021-10171-0
89. Lin H, Ma J, Zhuo M, Zhang C, Luo J, Zhuang X, et al. Preliminary Results of the Phase II ALTER-H003 Trial: Anlotinib Plus Toripalimab as a First-Line Treatment for Patients With Unresectable Hepatocellular Carcinoma. *J Clin Oncol* (2021) 39:314. doi: 10.1200/JCO.2021.39.3_suppl.314
90. Lin H, Ma J, Zhuo M, Zhang C, Luo J, Zhuang X, et al. Updated Results of the Phase II ALTER-H003 Trial: Anlotinib Plus Toripalimab as a First-Line Treatment for Patients With Unresectable Hepatocellular Carcinoma. *J Clin Oncol* (2021) 39:e16130. doi: 10.1200/JCO.2021.39.15_suppl.e16130
91. Park K, Kim K, Park S, Chang H. Comparison of Gemcitabine Plus Cisplatin Versus Capecitabine Plus Cisplatin as First-Line Chemotherapy for Advanced Biliary Tract Cancer. *Asia-Pac J Clin Onco* (2017) 13:13–20. doi: 10.1111/ajco.12592
92. Liu L, Li W, Yu Y, Guo X, Xu X, Wang Y, et al. 53p - Toripalimab With Chemotherapy as First-Line Treatment for Advanced Biliary Tract Tumors: A Preliminary Analysis of Safety and Efficacy of an Open-Label Phase II Clinical Study. *Ann Oncol* (2020) 31:S260–73. doi: 10.1016/annonc/annonc259
93. Li W, Yu Y, Xu X, Guo X, Wang Y, Li Q, et al. Toripalimab With Chemotherapy as First-Line Treatment for Advanced Biliary Tract Tumors: Update Analytic Results of an Open-Label Phase II Clinical Study (JS001-ZS-Bc001). *J Clin Oncol* (2021) 39:e16170. doi: 10.1200/JCO.2021.39.15_suppl.e16170
94. Ueno M, Ikeda M, Morizane C, Kobayashi S, Ohno I, Kondo S, et al. Nivolumab Alone or in Combination With Cisplatin Plus Gemcitabine in Japanese Patients With Unresectable or Recurrent Biliary Tract Cancer: A Non-Randomised, Multicentre, Open-Label, Phase 1 Study. *Lancet Gastroenterol Hepatol* (2019) 4:611. doi: 10.1016/S2468-1253(19)30086-X
95. Jian Z, Fan J, Shi G, Huang X, Wu D, Liang F, et al. Lenvatinib Plus Toripalimab as First-Line Treatment for Advanced Intrahepatic Cholangiocarcinoma: A Single-Arm, Phase 2 Trial. *J Clin Oncol* (2021) 39:4099. doi: 10.1200/JCO.2021.39.15_suppl.4099
96. Jian Z, Fan J, Shi G, Huang X, Wu D, Yang G, et al. Gemox Chemotherapy in Combination With Anti-PD1 Antibody Toripalimab and Lenvatinib as First-Line Treatment for Advanced Intrahepatic Cholangiocarcinoma: A Phase 2 Clinical Trial. *J Clin Oncol* (2021) 39:4094. doi: 10.1200/JCO.2021.39.15_suppl.4094
97. Lu M, Zhang P, Zhang Y, Li Z, Gong J, Li J, et al. Efficacy, Safety and Biomarkers of Toripalimab in Patients With Recurrent or Metastatic Neuroendocrine Neoplasms: A Multiple-Center Phase Ib Trial. *Clin Cancer Res* (2020) 626(10):2337–45. doi: 10.1158/1078-0432.CCR-19-4000
98. Shen L, Yu X, Lu M, Zhang X, Cheng Y, Zhang Y, et al. Surufatinib in Combination With Toripalimab in Patients With Advanced Neuroendocrine Carcinoma: Results From a Multicenter, Open-Label, Single-Arm, Phase II Trial. *J Clin Oncol* (2021) 39:e16199. doi: 10.1200/JCO.2021.39.15_suppl.e16199
99. Vijayvergia N, Dasari A, Deng M, Litwin S, Al-Toubah T, Alpaugh RK, et al. Pembrolizumab Monotherapy in Patients With Previously Treated Metastatic High-Grade Neuroendocrine Neoplasms: Joint Analysis of Two Prospective, non-Randomised Trials. *Br J Cancer* (2020) 122:1309–14. doi: 10.1038/s41416-020-0775-0
100. Oberg K, Modlin IM, De Herder W, Pavel M, Klimstra D, Frilling A, et al. Consensus on Biomarkers for Neuroendocrine Tumour Disease. *Lancet Oncol* (2015) 16:e435–46. doi: 10.1016/S1470-2045(15)00186-2
101. Wang F, Wei X, Feng J, Li Q, Xu N, Hu X, et al. Efficacy, Safety, and Correlative Biomarkers of Toripalimab in Previously Treated Recurrent or Metastatic Nasopharyngeal Carcinoma: A Phase II Clinical Trial (POLARIS-02). *J Clin Oncol* (2021) 38:O2002712. doi: 10.1200/JCO.20.02712
102. Ma B, Lim WT, Goh BC, Hui EP, Lo KW, Pettinger A, et al. Antitumor Activity of Nivolumab in Recurrent and Metastatic Nasopharyngeal Carcinoma: An International, Multicenter Study of the Mayo Clinic Phase 2 Consortium (NCI-9742). *J Clin Oncol* (2018) 36:1412–8. doi: 10.1200/JCO.2017.77.0388
103. Hsu C, Lee SH, Ejadi S, Even C, Cohen RB, Le Tourneau C, et al. Safety and Antitumor Activity of Pembrolizumab in Patients With Programmed Death-Ligand 1-Positive Nasopharyngeal Carcinoma: Results of the KEYNOTE-028 Study. *J Clin Oncol* (2017) 35:4050–6. doi: 10.1200/JCO.2017.73.3675
104. Chen YP, Chan A, Le QT, Blanchard P, Sun Y, Ma J. Nasopharyngeal Carcinoma. *Lancet* (2019) 394:64–80. doi: 10.1016/S0140-6736(19)30956-0
105. Hua Y, You R, Wang Z, Huang P, Lin M, Ouyang Y, et al. Toripalimab Plus Intensity-Modulated Radiotherapy for Recurrent Nasopharyngeal Carcinoma: An Open-Label Single-Arm, Phase II Trial. *J Immunother Cancer* (2021) 9:e3290. doi: 10.1136/jitc-2021-003290
106. Zhang L, Huang Y, Hong S, Yang Y, Yu G, Jia J, et al. Gemcitabine Plus Cisplatin Versus Fluorouracil Plus Cisplatin in Recurrent or Metastatic Nasopharyngeal

Carcinoma: A Multicentre, Randomised, Open-Label, Phase 3 Trial. *Lancet* (2016) 388:1883–92. doi: 10.1016/S0140-6736(16)31388-5
107. Mai HQ, Chen QY, Chen D, Hu C, Yang K, Wen J, et al. Toripalimab or Placebo Plus Chemotherapy as First-Line Treatment in Advanced Nasopharyngeal Carcinoma: A Multicenter Randomized Phase 3 Trial. *Nat Med* (2021) 27:1536–43. doi: 10.1038/s41591-021-01444-0
108. Sheng X, Chen H, Hu B, Yao X, Liu Z, Yao X, et al. Safety, Efficacy and Biomarker Analysis of Toripalimab in Patients With Previously Treated Advanced Urothelial Carcinoma: Results From a Multicenter Phase II Trial POLARIS-03. *Clin Cancer Res* (2021) clincanres.2210.2021. doi: 10.1158/1078-0432.CCR-21-2210
109. Zhou L, Xu H, Yan X, Chi Z, Cui C, Si L, et al. RC48-ADC Combined With Toripalimab, an Anti-PD-1 Monoclonal Antibody (Ab), in Patients With Locally Advanced or Metastatic Urothelial Carcinoma (UC): Preliminary Results of a Phase Ib/II Study. *J Clin Oncol* (2021) 39:4534. doi: 10.1200/JCO.2021.39.15_suppl.4534
110. Sharma P, Callahan MK, Bono P, Kim J, Spiliopoulou P, Calvo E, et al. Nivolumab Monotherapy in Recurrent Metastatic Urothelial Carcinoma (CheckMate 032): A Multicentre, Open-Label, Two-Stage, Multi-Arm, Phase 1/2 Trial. *Lancet Oncol* (2016) 17:1590–8. doi: 10.1016/S1470-2045(16)30496-X
111. Balar AV, Castellano D, O'Donnell PH, Grivas P, Vuky J, Powles T, et al. First-Line Pembrolizumab in Cisplatin-Ineligible Patients With Locally Advanced and Unresectable or Metastatic Urothelial Cancer (KEYNOTE-052): A Multicentre, Single-Arm, Phase 2 Study. *Lancet Oncol* (2017) 18:1483–92. doi: 10.1016/S1470-2045(17)30616-2
112. Armand P, Engert A, Younes A, Fanale M, Santoro A, Zinzani PL, et al. Nivolumab for Relapsed/Refractory Classic Hodgkin Lymphoma After Failure of Autologous Hematopoietic Cell Transplantation: Extended Follow-Up of the Multicohort Single-Arm Phase II CheckMate 205 Trial. *J Clin Oncol* (2018) 36:1428–39. doi: 10.1200/JCO.2017.76.0793
113. Chen R, Zinzani PL, Fanale MA, Armand P, Johnson NA, Brice P, et al. Phase II Study of the Efficacy and Safety of Pembrolizumab for Relapsed/Refractory Classic Hodgkin Lymphoma. *J Clin Oncol* (2017) 35:2125–32. doi: 10.1200/JCO.2016.72.1316
114. Han H, An X, Yan R, Guo S, Xue C, Liu T, et al. Immune Checkpoint Inhibitor Plus Anti-EGFR Target Therapy Plus Chemotherapy in Patients With Locally Advanced Penile Squamous Cell Carcinoma. *J Clin Oncol* (2021) 39:e17016. doi: 10.1200/JCO.2021.39.15_suppl.e17016
115. Xiao W, Yuan Y, Wang S, Cai P, Chen B, Zhang R, et al. Neoadjuvant PD-1 Blockade Combined With Chemotherapy Followed by Concurrent Immunoradiotherapy for Locally Advanced Anal Canal Squamous Carcinoma Patients: Antitumor Efficacy, Safety and Biomarker. *J Clin Oncol* (2021) 39:e15500. doi: 10.1200/JCO.2021.39.15_suppl.e15500
116. Cheng K, Lv W, Li X, Tian B, Cao D. Toripalimab With Nab-Paclitaxel/Gemcitabine as First-Line Treatment for Advanced Pancreatic Adenocarcinoma: Updated Results of a Single-Arm, Open-Label, Phase Ib/II Clinical Study. *J Clin Oncol* (2021) 39:e16213. doi: 10.1200/JCO.2021.39.15_suppl.e16213
117. Luo H, Jian D, Feng Y, Zhong L, Chen Q, Guan W, et al. Efficacy and Safety of Toripalimab With Anlotinib and Chemotherapy as First-Line Therapy in Patients With Extensive-Stage Small-Cell Lung Cancer: Preliminary Results of an Open-Label, Single-Arm, Phase II Study. *J Clin Oncol* (2021) 39:e20570. doi: 10.1200/JCO.2021.39.15_suppl.e20570
118. Coward J, Abed A, Nagrial A, Markman B. Phase I Open-Label, Dose Escalation of YH003, an Anti-CD40 Monoclonal Antibody in Combination With Toripalimab (Anti-PD-1 mAb) in Patients With Advanced Solid Tumors. *J Clin Oncol* (2021) 39:2580. doi: 10.1200/JCO.2021.39.15_suppl.2580
119. Ganju V, Cooper A, Gao B, Wilkinson K. A First-in-Human Phase I Dose Escalation of YH001, an Anti-CTLA-4 Monoclonal Antibody (mAb) in Combination With Toripalimab (Anti-PD-1 mAb) in Patients With Advanced Solid Tumors. *J Clin Oncol* (2021) 39:2577. doi: 10.1200/JCO.2021.39.15_suppl.2577
120. Cheng Y, Song Y, Wang C, Li X, Li Y, Zhang C. 782p - A Retrospective Study of Toripalimab Combined With Concurrent Chemoradiotherapy in Patients With Recurrent/Advanced Cervical Cancer. *Ann Oncol* (2021) 32:S725–72. doi: 10.1016/annonc/annonc703
121. Liu Z, Liu C, Yao W, Gao S, Wang J, Zhang P, et al. Efficacy and Safety of Toripalimab Combined With Doxorubicin as First-Line Treatment for Metastatic Soft Tissue Sarcomas. *Anti-Cancer Drugs* (2021) 32:962–8. doi: 10.1097/CAD.0000000000001088
122. Dou S, Li R, Zhang L, Jiang W, Ye L, Zhu G. Adjuvant Toripalimab or Combined With S-1 in Recurrent, Previously Irradiated Head and Neck Squamous Cell Carcinoma Treated With Salvage Surgery: A Phase II Clinical Trial (The RePASS Study). *J Clin Oncol* (2021) 39:6039. doi: 10.1200/JCO.2021.39.15_suppl.6039
123. National Institute of Health. *Common Terminology Criteria for Adverse Events (CTCAE)* (2020). Available at: https://ctep.cancer.gov/protocolDevelopment/electronic_applications/ctc.htm (Accessed November 30, 2021).
124. Brown EG, Wood L, Wood S. The Medical Dictionary for Regulatory Activities (MedDRA). *Drug Saf* (1999) 20:109–17. doi: 10.2165/00002018-199920020-00002
125. Xu C, Chen YP, Du XJ, Liu JQ, Huang CL, Chen L, et al. Comparative Safety of Immune Checkpoint Inhibitors in Cancer: Systematic Review and Network Meta-Analysis. *BMJ* (2018) 363:k4226. doi: 10.1136/bmj.k4226
126. Wang DY, Salem J, Cohen JV, Chandra S, Menzer C, Ye F, et al. Fatal Toxic Effects Associated With Immune Checkpoint Inhibitors. *JAMA Oncol* (2018) 4:1721. doi: 10.1001/jamaoncol.2018.3923
127. Topalian SL, Hodi FS, Brahmer JR, Gettinger SN, Smith DC, McDermott DF, et al. Safety, Activity, and Immune Correlates of Anti-PD-1 Antibody in Cancer. *N Engl J Med* (2012) 366:2443–54. doi: 10.1056/NEJMoa1200690
128. Angelo SP D, Larkin J, Sosman JA, Lebbé C, Brady B, Neyns B, et al. Efficacy and Safety of Nivolumab Alone or in Combination With Ipilimumab in Patients With Mucosal Melanoma: A Pooled Analysis. *J Clin Oncol* (2017) 35:226–35. doi: 10.1200/JCO.2016.67.9258
129. Song F, Xiong T, Parekh-Bhurke S, Loke YK, Sutton AJ, Eastwood AJ, et al. Inconsistency Between Direct and Indirect Comparisons of Competing Interventions: Meta-Epidemiological Study. *BMJ* (2011) 343:d4909. doi: 10.1136/bmj.d4909
130. Bucher HC, Guyatt GH, Griffith LE, Walter SD. The Results of Direct and Indirect Treatment Comparisons in Meta-Analysis of Randomized Controlled Trials. *J Clin Epidemiol* (1997) 50:683–91. doi: 10.1016/s0895-4356(97)00049-8
131. Song F, Altman DG, Glenny AM, Deeks JJ. Validity of Indirect Comparison for Estimating Efficacy of Competing Interventions: Empirical Evidence From Published Meta-Analyses. *BMJ* (2003) 326:472. doi: 10.1136/bmj.326.7387.472
132. National Healthcare Security Administration. *Public Consultation of Work Plan for the Adjustment of the National Insurance Drug List in 2020 (Draft for Comments)* (2020). Available at: http://www.nhsa.gov.cn/art/2020/8/3/art_48_3394.html?from=timeline (Accessed November 30, 2021).
133. National Heathcare Security Administration. *The Notice of Issuing <National Drug Catalogue for Basic Medical Insurance, Work-Related Injury Insurance and Maternity Insurance (2020)>, by National Health Security Administration and Ministry of Human Resouraces and Social Security of the People's Republic of China* (2020). Available at: http://www.nhsa.gov.cn/art/2020/12/28/art_37_4220.html (Accessed November 30, 2021).
134. Central People's Government of the People's Republic of China. *National Medical Insurance Catalogue* (2020). Available at: http://www.gov.cn/zhengce/zhengceku/2020-12/28/5574062/files/4159212adf854117b62d0e91d445a4e2.pdf (Accessed November 30, 2021).

Conflict of Interest: The authors declare that the research was conducted in the absence of any commercial or financial relationships that could be construed as a potential conflict of interest.

Publisher's Note: All claims expressed in this article are solely those of the authors and do not necessarily represent those of their affiliated organizations, or those of the publisher, the editors and the reviewers. Any product that may be evaluated in this article, or claim that may be made by its manufacturer, is not guaranteed or endorsed by the publisher.

frontiers | Frontiers in Immunology

REVIEW
published: 02 May 2022
doi: 10.3389/fimmu.2022.752065

Small Molecule Agents Targeting PD-1 Checkpoint Pathway for Cancer Immunotherapy: Mechanisms of Action and Other Considerations for Their Advanced Development

Pottayil G. Sasikumar and Murali Ramachandra *

Aurigene Discovery Technologies Limited, Bangalore, India

OPEN ACCESS

Edited by:
Bin Zhang,
Northwestern University,
United States

Reviewed by:
Evelien Smits,
University of Antwerp, Belgium
Sung Yong Lee,
Korea University Guro Hospital,
South Korea

***Correspondence:**
Murali Ramachandra
murali_r@aurigene.com

Specialty section:
This article was submitted to Cancer Immunity and Immunotherapy, a section of the journal Frontiers in Immunology

Received: *02 August 2021*
Accepted: *29 March 2022*
Published: *02 May 2022*

Citation:
Sasikumar PG and Ramachandra M (2022) Small Molecule Agents Targeting PD-1 Checkpoint Pathway for Cancer Immunotherapy: Mechanisms of Action and Other Considerations for Their Advanced Development. Front. Immunol. 13:752065. doi: 10.3389/fimmu.2022.752065

Pioneering success of antibodies targeting immune checkpoints such as programmed cell death protein 1 (PD-1) and cytotoxic T-lymphocyte-associated protein 4 (CTLA-4) has changed the outlook of cancer therapy. Although these antibodies show impressive durable clinical activity, low response rates and immune-related adverse events are becoming increasingly evident in antibody-based approaches. For further strides in cancer immunotherapy, novel treatment strategies including combination therapies and alternate therapeutic modalities are highly warranted. Towards this discovery and development of small molecule, checkpoint inhibitors are actively being pursued, and the efforts have culminated in the ongoing clinical testing of orally bioavailable checkpoint inhibitors. This review focuses on the small molecule agents targeting PD-1 checkpoint pathway for cancer immunotherapy and highlights various chemotypes/scaffolds and their characterization including binding and functionality along with reported mechanism of action. The learnings from the ongoing small molecule clinical trials and crucial points to be considered for their clinical development are also discussed.

Keywords: PD-L1 inhibitors, cancer immunotherapy, mechanism of action (MOA), small molecule immunomodulators, small molecule PD-1/PD-L1 inhibitors

BACKGROUND

Checkpoint inhibitors have transformed cancer therapy by harnessing the power of the immune system to fight cancer, and this breakthrough has now been considered as one of the most exciting discoveries of the twenty-first century (1). Among the various cancer immunotherapies such as checkpoint inhibitors, adoptive T-cell transfer, oncolytic viruses and cancer vaccines, immune checkpoint inhibitors have shown remarkable response in clinical trials and are currently regarded as the most successful class of cancer immunotherapy. Since the Food and Drug Administration (FDA) approval of anti-CTLA-4 antibody ipilimumab in 2011, several antibodies targeting PD-1/programmed death-ligand 1 (PD-L1) immune checkpoint pathway have been approved for cancer

therapy in various indications with many more in the pipeline (2). In this review, we have highlighted the progress in the discovery and development of small molecule agents interfering in the PD-1 pathway, with majority of the reported compounds targeting PD-L1, along with their mechanisms of action and specific considerations that are relevant for their advanced development.

LIMITATIONS OF IMMUNE CHECKPOINT BLOCKADE THERAPY ASSOCIATED WITH ANTIBODIES

While these antibody-based therapies show notable clinical activity, they suffer from serious treatment-related toxicities known as immune-related adverse events (irAEs) mostly due to the dysregulation in the immune system balance (3). The wide range of irAEs are reported to involve almost any tissue or organ with most severe complications manifesting as skin rashes, pneumonitis, hypothyroidism, pancreatitis, encephalopathy, hepatitis, myocarditis, and immune cytopenias (4). Antibodies targeting PD-1 pathways are reported to have lower incidence of adverse events than agents targeting CTLA-4 pathway (5), whereas combination therapy with antibodies targeting both CTLA-4 and PD-1 is reported to have higher rate of irAEs with a greater number of grade 3 and 4 treatment-related adverse events and treatment discontinuations (6, 7). Even though irAEs can be resolved by appropriate management of immunosuppression with corticosteroids or other immunosuppressant agents such as infliximab, it may expose patients to a higher risk of developing infections (8). Sustained target inhibition due to long half-life (>15–20 days) and ~70% target occupancy for months are likely contributing to severe irAEs (9–11). Apart from toxicity, one of the major deficiencies of approved PD-1/PD-L1 targeted antibodies is their response only in a subset of patient population, which could be partly due to the compensatory mechanisms such as upregulation of alternative immune checkpoints such as T-cell immunoglobulin and mucin-domain containing-3 (TIM-3) and V-domain Ig suppressor of T-cell activation (VISTA) (12, 13). Physiological barriers of antibodies (14) limit their tumor exposure, and the large size of these agents warrants their intravenous dosing in a hospital setting. Last but not the least is the low affordability, since the treatment cost for a single agent therapy can reach more than US$100,000 per patient annually. Furthermore, the requirement for the rational combination with other therapeutic agents to achieve greater response is expected to make checkpoint antibody therapy prohibitively expensive (15).

OPPORTUNITIES FOR SMALL MOLECULE AGENTS TO ADDRESS THE LIMITATIONS

Even though deficiencies of antibody-based PD-1/PD-L1 targeted agents underscore the need for alternate approaches, the development of small molecule inhibitors has been significantly behind despite the great potential. The advantages of small molecule agents over antibodies to target PD-1 and other immune checkpoint pathways are summarized in **Table 1**. However, small molecule agents also have a few limitations including their shorter half-life, broad drug distribution resulting in on- and off-target toxicity, potential for reduced specificity and selectivity, and species-specific activity in some instances, making it highly challenging to find appropriate preclinical pharmacology models. These shortcomings might have contributed to the initial lack of enthusiasm in the scientific community compared to monoclonal antibody-based inhibitors as reflected in dramatically less preclinical and clinical efforts focused on the small molecule-based approach. Lessons learned from the highly successful development of small molecule therapeutics against specific targets including protein tyrosine kinases, growth factor receptors, and cell cycle regulatory proteins can be adapted to fully exploit the distinct advantages of small molecule approaches (**Table 1**).

CONSIDERATIONS FOR TARGETING PD-1 SIGNALING PATHWAY USING SMALL MOLECULES

The PD-1–PD-L1 receptor–ligand interaction is a classic example of protein–protein interaction (PPI); hence, designing inhibitors for these interactions are highly challenging. Antibodies and fusion proteins are the preferred approach to modulate such PPI dysregulation primarily due to (a) the large interfacial area of the interaction (1,500–3,000 Å), (b) the presence of flat interface without deep and well-defined pockets that are suitable to bind a ligand with high-affinity, (c) the lack of endogenous low molecular ligands that can be considered as reference standards for small molecule chemistry starting points (25, 26)

General perception is that the druggability of an interaction pocket increases logarithmically with total surface area and non-polar contact area, while it decreases logarithmically with polar contact area (27). Efforts to increase the affinity of small molecules to the binding partner often results in increased lipophilicity, which is believed to negatively impact the druggability due to reduced solubility, bioavailability, and increased off-target toxicity. Natural complexes, either protein–protein interactions or protein–peptide ligand interactions, typically engage in more polar contacts than synthetic greasy molecules, with a lot of unmatched hetero atoms bound to proteins. Druggable binding sites are often oversimplified as closed, hydrophobic cavities, but data set analysis reveals that polar groups in druggable binding sites have properties that enable them to play a decisive role in ligand recognition (28). The influence of hotspots, which are small areas of the protein–protein interface contributing most of the binding energy within one hot region, is cooperative to stabilize protein interfaces, and they are networked to provide stability of PPIs, with contributions between various hot regions can be either additive (29) or cooperative (30). Hotspots are also defined as residues that impede protein–protein interactions if mutated (31). Hotspots tend to occur in clusters and are in contact with each

TABLE 1 | Advantages of small molecule agents over antibodies to target PD-1 and other immune checkpoint pathways.

Parameter	Antibody	Small molecule
Route of administration	• Requirement to dose by intravenous or other parenteral route making it inconvenient to patients (16) • Administration in a clinical setting adds to the cost	• Potential for oral bioavailability offering the convenience to patients • No need to visit the clinic for dose administration (17)
Tumor distribution	• Limited tumor distribution because of the larger size (18)	• Better tumor distribution expected and greater opportunities to fine tune the physico-chemical properties for improvement
Clinical response	• Due to high degree of selectivity, response not expected when intrinsic and adaptive resistance are due to another immune checkpoint pathway(s) (12, 13)	• Simultaneous targeting of more than one immune checkpoint proteins with the same agent because of the significant structural homology to drive greater response possible (19, 20)
Management of immune-related toxicity	• Due to long pharmacokinetic half-life, typically in weeks, aggressive treatment with immunosuppressants needed while increasing the infection risk (8)	• Because of the shorter pharmacokinetic half-life, typically in hours, treatment cessation can be employed for better management of any emergent adverse events (21)
Manufacturing and logistics cost	• Due to recombinant mode of production, high cost associated with production, product heterogeneity, and greater regulatory hurdles (18) • Cold chain transport and storage required because of their thermo labile nature	• Synthetic mode of production leading to lower cost of goods, product homogeneity, and lower regulatory hurdles (22) • Cold chain transport and storage not needed due to their thermo stability
Regulatory hurdles	• High due to recombinant production (23, 24)	• Low and straight forward due to synthetic production

other resulting in hot regions, a network of conserved interactions (32). Antibodies are considered widely acceptable approach to target PPIs, since they could target or bind a vast region covering the discontinuos tertiary epitopes. Hence, while designing small molecule agents, the compounds need to be targeted to interact with either in one hot region (either hydrophobic or hydrophilic), which could be a critical contributor to the signaling pathways or need to engage with critical residues in multiple hot regions (both hydrophobic and hydrophilic) if an additive effect on hotspots is required for the desired pharmacological effects. In agreement with the concepts described above, the identification of small molecule PPI inhibitors have been possible because of the presence of PPI hotspots (33, 34).

Advances in solving the crystal structure of PD-1:PD-L1 and PD-1:PD-L2 complexes and mapping of the molecular networks resulted in the identification of several potential hotspots. Three major hot regions identified on PD-L1 based on PD-1:PD-L1 crystal structure are (1) hydrophobic pocket consisting of the side chains of Tyr56, Glu58, Arg113, Met115, and Tyr123; (2) second pocket nearby hydrophobic cleft composed of Met115, Ala121, and Tyr123; and (3) extended groove made up of the main chain and side chains of Asp122, Tyr123, Lys124, and Arg125 (35). In the PD-1:PD-L1 interface, hot region containing hydrophobic regions are involved in hotspots 1 and 2 and are proposed to be ideal for binding to PD-L1 using conventional small molecules. Hotspots in the PD1:PD-L interaction have also been quantitatively predicted based on the theoretical calculations (36). This analysis has identified six hot spots on PD-L1 (Tyr123, Tyr56, Arg125, Met115, Arg113, and Gln66) and two warm spots on PD-L1 (Ile54 and Lys124) (36). Among various hotspots/hot regions reported, the hydrophilic hot region containing polar residues is reported to be a solvent exposed with extended shallow groove and with multiple hydrogen bond donors and acceptors and is considered to be challenging to target *via* conventional small molecules abiding the famous rule of five (37).

TWO MAJOR CLASSES OF SMALL MOLECULES TARGETING PD1-PD-L1 AXIS

A survey of the literature as highlighted in this section below indicates predominantly two different classes of small molecule inhibitors targeting PD-L1, namely, (a) compounds based on the biphenyl scaffold, originally identified by a conventional approach of screening compounds in a binding assay and (b) amino acids-inspired small molecules mimicking the receptor–ligand interface identified in a functional assay.

Biphenyl Derivatives

Scientists from BMS reported a series of substituted biphenyl derivatives based on their ability in preventing the PD-1:PD-L1 interaction. Extensive characterization and elucidation of the mode of action of these compounds (**Figure 1**) have been reported in several publications (discussed in detail in the following section). However, further advancement of these interesting but highly hydrophobic small molecules into the clinic has not been reported. The contributions of hotspots for stabilizing PPIs can be either additive or cooperative, and if the targeting of one of the hotspots is not good enough to achieve the desirable activity, design strategies need to be included to cover one or more hotspots. Based on this rationale, the binding mode of Compound 2a (BMS-1001 in **Figure 2**), which contains the 2,3-dihydro-1,4-benzodioxinyl group and polar groups, is more effective in dimerization of PD-L1 ligands with a network of hydrophobic and polar interactions compared to the first-generation BMS-type compounds, which can bind to only hydrophobic cleft (38). Since the last 6 years, several companies including Incyte Corporation, Arising International Inc., Chemocentryx Inc., Polaris Pharmaceuticals, and Guangzhou Maxinovel Pharmaceuticals Co. have discovered a series of small molecule PD-L1 inhibitors based on the biphenyl core (39–41).

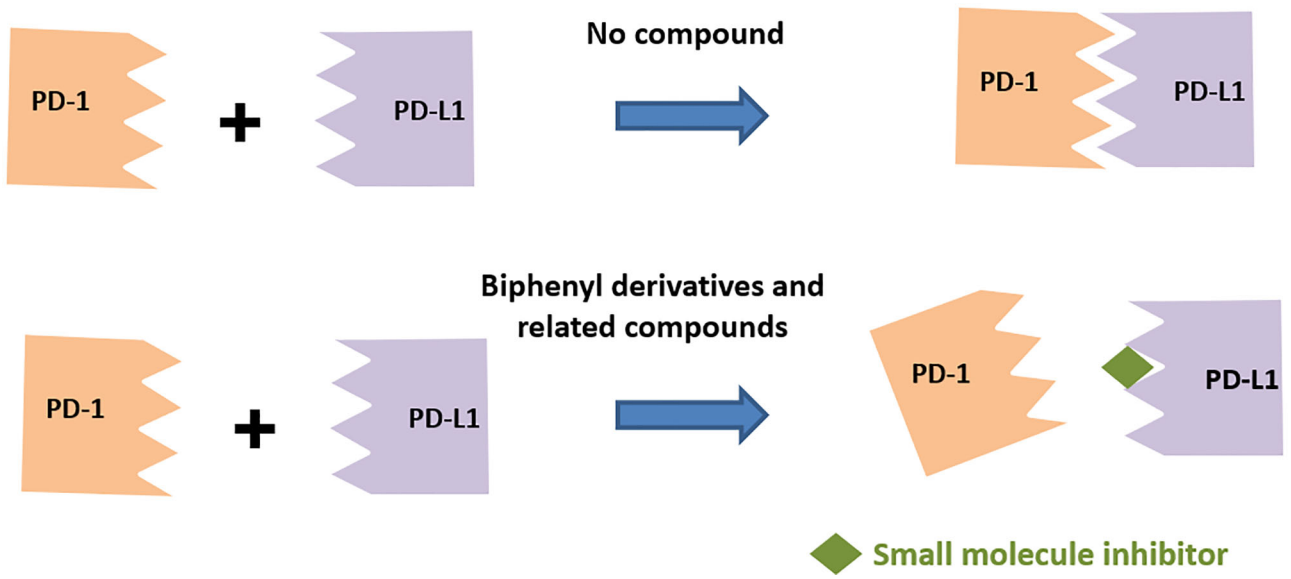

FIGURE 1 | Compounds based on the biphenyl scaffold, originally identified by a conventional approach of screening compounds in an assay for prevention of the PD-1, PD-L1 interaction.

Among the new modified biphenyl scaffolds, compounds with C_2 symmetry or pseudosymmetry containing polar groups are gaining a lot of attention than asymmetric structure (**Figure 2**). The C_2–symmetric small molecule inhibitors of PD-1:PD-L1 interaction containing the lipophilic biphenyl core for binding to PD-L1 at its PD-1 binding site to occupy the hydrophobic cleft have been reported (42). NMR and X-ray co-crystal structural studies indicated that symmetric molecules such as LH1306 and LH1307 induce formation of a more symmetrically arranged PD-L1 dimer than previously reported asymmetric inhibitors. The polar groups 2-(acetamido) ethylamine of BMS-202, incorporated into the C_2 symmetric molecules, LH1306 and LH1307, are reported to extend out the hydrophobic cleft and occupy the solvent-exposed region sandwiched between the AG and C′C β strands of the respective PD-L1 proteins, further enhancing binding to the two PD-L1 monomers *via* hydrogen bonds and electrostatic interactions. It was also hypothesized that a symmetric compound would induce a flip of sidechain of Tyr56 protein residue to form a new cavity, leading to increased binding affinity to PD-L1, and PD-1/PD-L1 inhibitory activity in physiological conditions as reported for Compound 4 (43). The improved cellular activity of the PD-L1 inhibitor ARB-272572 further demonstrated the importance of C_2-biphenyl skeleton and symmetry with polar (2-hydroxyl ethyl) amino group extended from the hydrophobic cleft (44). Representative structures of compounds disclosed by BMS, Incyte, and C_2 symmetric compounds are presented in **Figure 2**.

A number of reports are also emerging recently from the industry and academia using the privileged structure of biphenyl-containing compounds and their various derivatives to improvise the druggability of the molecules. This includes scaffold based on nicotinyl alcohol ether derivative (45–47), resorcinol dibenzyl ether (48), 4-phenylindoline derivatives (49), combining two privileged scaffolds such as biphenyl backbone structure and 2-amino-pyrimidine structure (50), biphenyl-4-carboxamide derivatives (51), incorporating taurine moieties (52), 1-methyl-1H-pyrazolo[4,3-b] pyridine derivatives (53), replacing the linker connecting aryl group and biaryl core with a novel amine linker (54), a series of novel biphenyl pyridines derivatives lacking linker (55), biphenyl methyl nitrophenyl core unit (56), and terphenyl scaffold derived from the rigidified biphenyl inspired structure (57). Representative structures of the compounds disclosed are presented in **Figure 3**.

Amino Acid Inspired Interface Mimics

The presence of distinct interface of PPIs involving the loops/strand sequences can be exploited in identifying peptides that mimic the native interaction interface. Checkpoint proteins are membrane proteins with majority of them from the B7 family (58). Most of the members of the B7 family and their ligands belong to the immunoglobulin superfamily (IgSF). All IgSF proteins have a characteristic Ig-fold structure with an IgG domain consisting of anti-parallel β-strands and loops connecting the β-strands with most strands constituting ~10 amino acids. Receptor–ligand interaction of IgSF proteins is mediated either through loops, strands, or loops and strands. Rational design of peptides based on these interacting interfaces is a proven strategy for design of PPI inhibitors (59). However, due to the inherent limitations of peptides in general, the focus has now shifted to peptide mimics by depeptidizing the short stretch of residues with cyclic linkages, un-natural linkages, retro and retro-inverso amides, urea, and non-amide bonds as peptide bond surrogates.

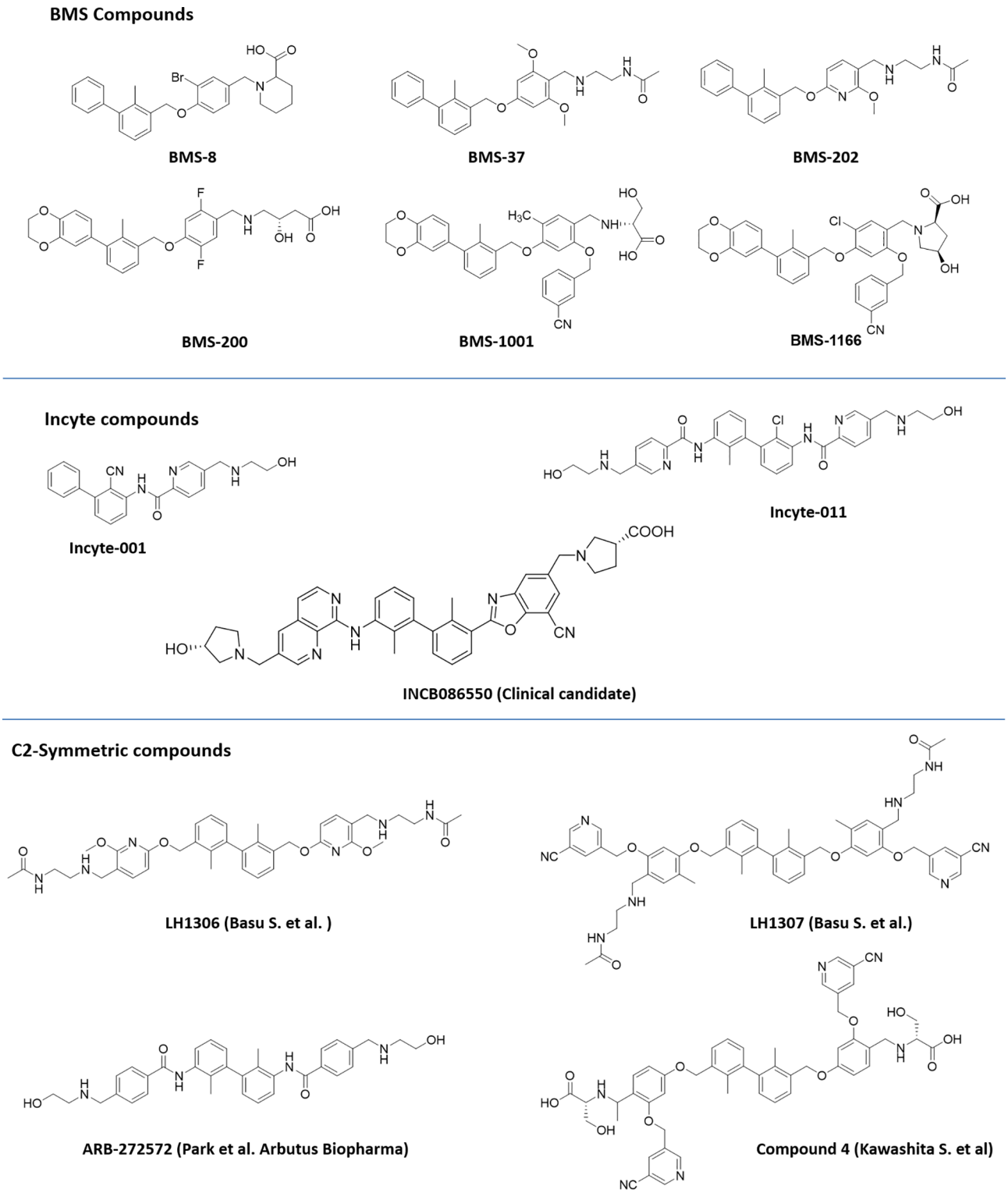

FIGURE 2 | Representative structures of first-generation biphenyl derivatives and C_2 symmetric compounds targeting PD-L1.

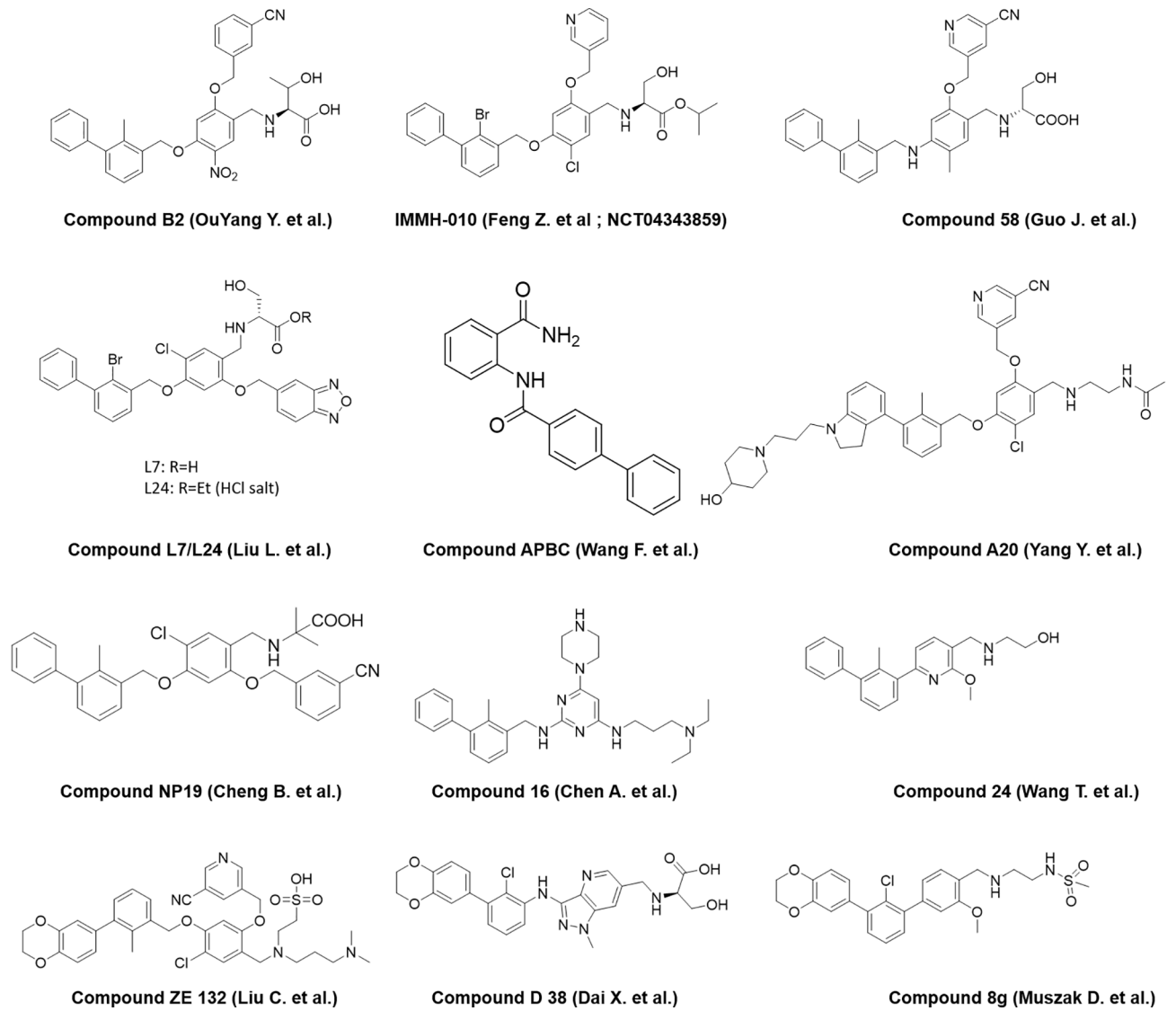

FIGURE 3 | Representative structures of modified biphenyl analogues without C_2 symmetry but with improved druggability.

Proteins are built from a set of only 20 amino acids, and the side chains, which are unique to each amino acid, exhibit different chemistries. The side chains of amino acids involved in hotspots residues are crucial and participate either in polar contacts or hydrophobic interactions in the interface of PPI contributing to stability and specificity of the interaction. In general, a peptidomimetic is referred as bioactive peptide mimicking molecules with the side chain groups of critical amino acids oriented to enable bioactive conformation to yield desirable pharmacological properties (60). The peptidomimetic structure ranges from molecular scaffolds replacing the peptide backbone, to compounds with modified peptide sequences with improved therapeutic properties (61–64).

Utilization of the design principles described above, several peptidomimetics were identified, but none of the peptidomimetics capable of antagonizing the PD-1 signaling exhibit oral bioavailability (65). Therefore, the native interaction pharmacophore first identified by the reductionist approach comprising of three to five amino acids, as in the case of typical peptidomimetic, was radically redesigned (**Figure 4**). In this design strategy, compounds with side chain functionalities of the amino acids from the native interaction pharmacophore protrude from a heterocyclic template with no amide bonds, in which the side chains are the critical interacting motifs of PPI hotspots, while the metabolically stable heterocyclic template anchors the amino acid side chains presumably in a required geometry (**Figure 5**). The novel heterocyclic oxadiazole templates were obtained by fusing two amino acids while presenting the desired amino acid side chains to interact with residues on PD-L1, while bringing in the

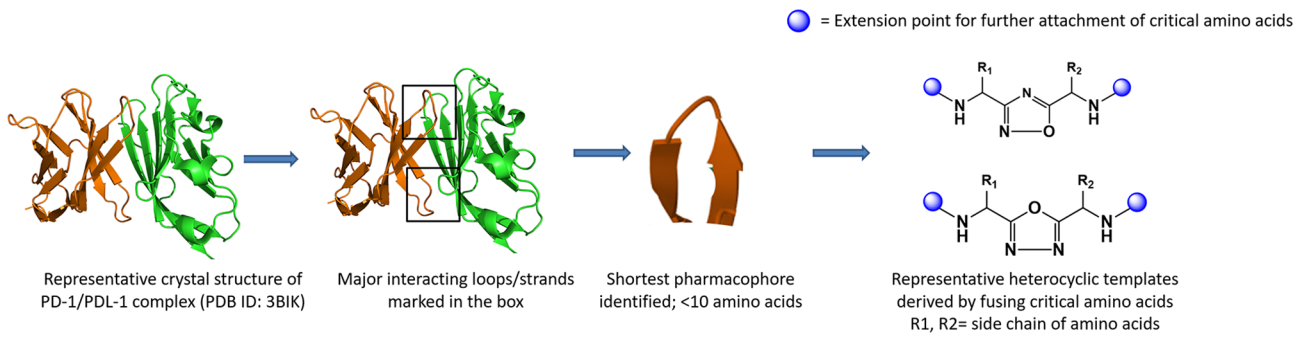

FIGURE 4 | Amino-acid-inspired small molecules mimicking the receptor–ligand interface identified in a functional assay.

remaining amino acid(s) from the pharmacophore through the use of linkers such as urea bonds resulting in the compound such as CA-170 (19, 66–68).

Recently, scientists from Guangzhou Medicine Pharmaceutical Biological Co. Ltd. and Nanjing Sanhome Pharmaceutical disclosed in their patent applications the close analogues of the lead PD-L1 inhibitor compound from Aurigene approach: (a) cyclizing oxadiazole head to tail by a short PEG linker (69) and (b) incorporating unnatural amino acids majorly containing cyclobutyl groups for oxadiazole generation instead of α-amino acid reported by Aurigene (70). The detailed profile of these compounds is yet to be published.

As discussed earlier in this article, to improve the clinical response rate, one of the strategies would be to target

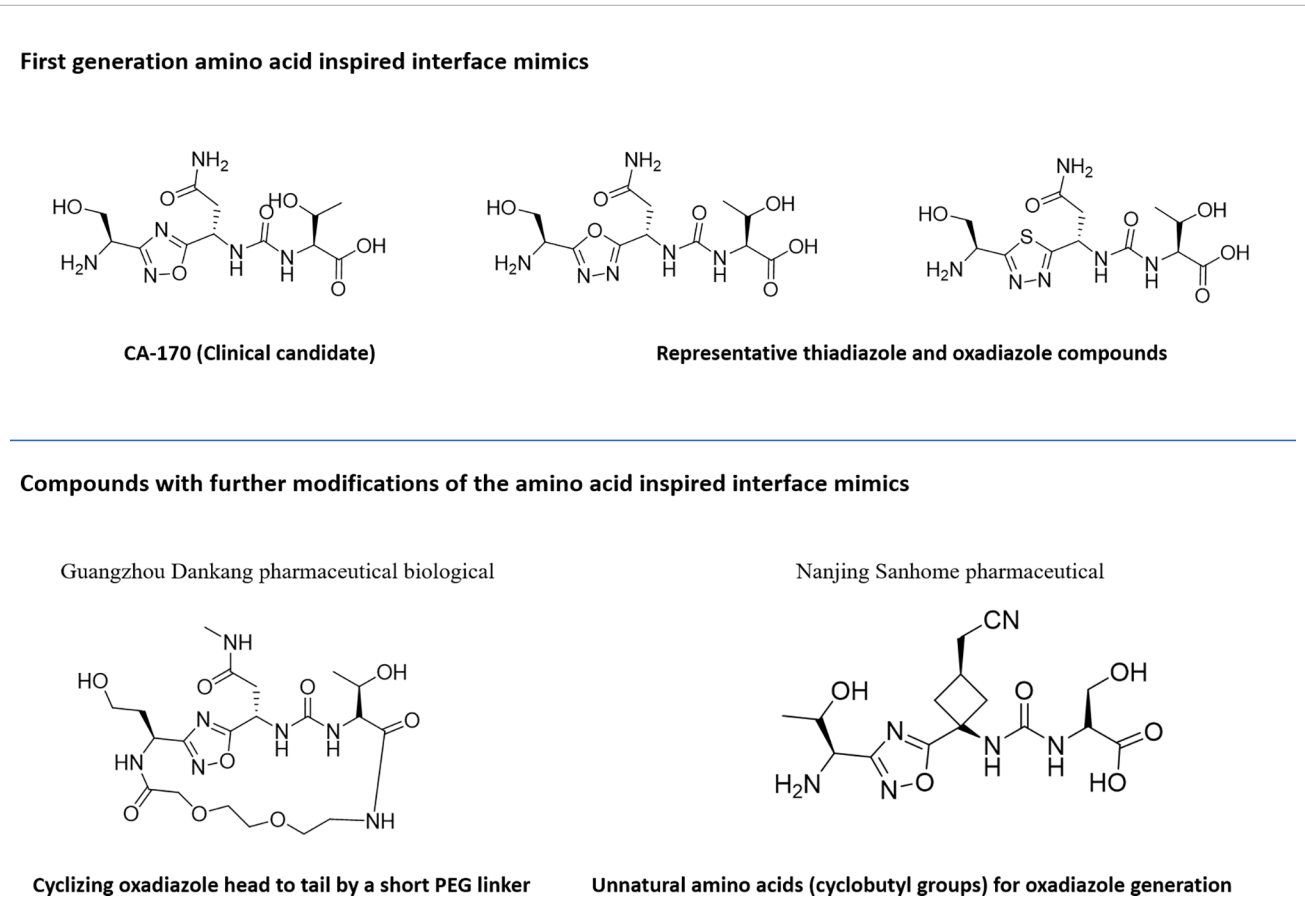

FIGURE 5 | Representative structures of amino-acid-inspired interface mimics targeting PD-L1.

simultaneously more than one non-redundant checkpoint pathways. It was hypothesized that a substantially reduced native pharmacophore derived from protein–protein interacting interfaces of one of the B7 family protein (such as PD-1) also has the potential to interact with other proteins belonging to IgSF (such as VISTA and TIM3) with structurally similar grooves induced by pockets of sequence similarity (71). A focused library was designed and synthesized using amino acids in the hotspot region including conserved residues in the hotspot regions to identify selective or spectrum-selective inhibitors targeting one or more non-redundant checkpoint signaling pathways such as PD-L1 and VISTA (72), PD-L1 and TIM3 (73, 74), VISTA (75), TIM-3 (76), PD-L1 and T-cell immunoreceptor with immunoglobulin and ITIM domain (TIGIT) (77), TIGIT (78), and cluster of differentiation 47 (CD-47) (79) pathways with desirable physicochemical properties and exposure upon oral administration. It is worth noting that small molecules with dual immune checkpoint inhibition have only been reported from the amino-acids-inspired interface mimic approach.

CHARACTERIZATION OF BINDING TO PD-L1 AND PREVENTION OF PD1:PD-L1 COMPLEX FORMATION

Most reported small molecule inhibitors of PD-L1 have been extensively characterized for binding to PD-L1 in various biophysical and biochemical assays using extracellular domain of PD-L1 from heterologous expression system. Scientists from BMS were the first to report biphenyl compounds identified using a homogenous time-resolved fluorescence (HTRF)-based binding assay in order to screen and rank their ability to inhibit PD-1:PD-L1 complex formation (80). Based on BMS scaffold, several molecules up to sub-nanomolar binding potency in HTRF assays have now been reported both from the industry and academia (39, 41, 79, 81). Direct binding of biphenyl compounds such as BMS compound 37 to PD-L1 has been demonstrated *via* SPR and ELISA-based assays (82). Using such biophysical techniques, it was observed that the amino-acids-inspired interface mimic CA-170 did not show observable binding to either PD-L1/PD-1 or inhibition of the PD-1:PD-L1 interaction while acknowledging the key differences in the "expressed" proteins and real-life interacting proteins as expressed on the surface of T cells and APCs (82).

The binding of biaryl scaffold-based compounds from BMS using three independent binding assays was demonstrated using DSF, MST, and SPR techniques and the concentration-dependent inhibitory activity in the PD-1/PD-L1-based biochemical ELISA (83). A higher affinity for BMS macrocycle peptide, which contains hydrophobic amino acids as compared to BMS biaryl scaffold compounds, was reported in DSF. However, the results of high affinity for macrocycles in DSF assay are interpreted with a caution due to the different physicochemical properties of macrocyclic peptide. In a similar assay, the binding affinity of BMS compounds has also been established by MST assays using fluorescent-labeled PD-L1 protein instead of label-free PD-L1 protein as used for DSF for incubation with test compounds.

The recent understanding of C_2 symmetric compounds targeting both hydrophobic cleft and polar groups in PD-L1 revealed that symmetric compounds have a better binding in HTRF assays as compared to asymmetric compounds. The C_2-symmetric inhibitor LH1306 (IC_{50} = 25 nM) was reported to be 3.8-fold more potent than its asymmetric counterpart (42). In this study, authors also illustrated the importance of 1,1′-1,1′-biphenyl core by comparing the core generated with 1,4- or 1,3-phenylene and 1,4- or 2,6-naphthalenylene analogues (micromolar binding activity). The importance of symmetric architecture for PD-L1 inhibitors was demonstrated with the compound, ARB 272542 (44), which inhibited PD-1/PD-L1 in a cell-free HTRF at 400 pM IC_{50} compared to 200 pM (anti-PD-L1 antibody, MIH1) and 200 pM (anti-PD-1 antibody, nivolumab). Incyte compounds with asymmetric and symmetric structure were analyzed by Liu et al., and data further confirmed that C_2 symmetric compound (Incyte 011, 5.3 nM) was almost twice as potent as its asymmetric form (11 nM) (84).

NMR has been extensively used to characterize the binding of reported PD-L1 inhibitors to PD-L1. Prof. Holak and colleagues initially reported SAR-by-NMR approach to demonstrate the direct binding of BMS compounds to PD-L1. In this method, ^{15}N-labeled PD-L1 was titrated with increasing amount of tested compound, and signals were monitored using 2D ^{1}H-^{15}N heteronuclear multiple quantum coherence (HMQC) NMR experiment. Significant shifts in the correlation NMR signals of PD-L1 upon addition of each tested compound documented their direct binding to PD-L1 (85). The ability of BMS-202 to disrupt PD-1/PD-L1 interaction was further demonstrated in a new antagonist-induced dissociation assay NMR screen, called AIDA-NMR (85, 86). In this method, ^{15}N labeled PD-1 was initially titrated with slight excess of non-labeled PD-L1 so that no further changes in the linewidth of the 1^{H}-^{15}N resonance peaks was observed as monitored by HMQC. The addition of test compounds inhibiting interaction or dissociation of this preformed complex results in the narrowing of ^{1}H-^{15}N signals. The NMR competition assay was further improvised, called weak-AIDA, for the fragment screening of weak binders using a low-affinity mutant of PD-1 (87). The weak-AIDA assay was conceptualized by introducing point mutations in the complex's protein that is not targeted by the inhibitor resulting in a low-affinity complex, thus allowing for short fragments to dissociate the complex. The method is illustrated using the compounds that block the Mdm2/X-p53 and PD-1/PD-L1 interactions (87). Among the various mutations attempted, Asn66 to Ala mutation was considered as the ideal mutation to generate mutant PD-1 protein due to its thermal stability as compared to native PD-1, retaining the overall structure and minimum interaction with the binding partner. This methodology was further utilized to determine the minimal fragment of BMS-1166 responsible for the PD-L1 binding (88). Although protein has been mutated at the asparagine position distant from the interacting site, considering the importance of asparagine residues in post-translational modifications, these variations may need to

be checked with its impact in physiological environment (89). PD-1 is heavily glycosylated at Asn49, Asn 58, Asn 74, and Asn 116 in T cells, and Asn 58 is highly critical for PD-1/PD-L1 interaction (89) underscoring the need for structure analysis using the glycosylated protein. Given that glycosylation of PD-L1 (90) is also critical for binding to PD-1, it would be important to determine the structure of PD-1/PD-L1 binding using the glycosylated forms of these proteins in the future to better understand the interaction between PD-1 and PD-L1. The criticality of using protein with all appropriate post-translational modifications for interaction with reported ligands, especially those identified in cell-based assays, has been elegantly shown for the binding of a small molecule to p53 (91, 92).

Published findings utilizing solution NMR (93) and other biophysical techniques (83) have indicated a lack of binding of the amino-acids-inspired interface mimic, CA-170 to PD-L1. The lack of conclusive binding in these studies may be due to the use of protein expressed in *E. coli* deficient in appropriate post-translational modifications and devoid of functional activity. To recapitulate the interaction as in the native environment, a cellular NMR spectroscopy using PD-L1-expressed mammalian cells in the native context along with the parental cell line as a negative control was utilized (19). Cell-based NMR spectroscopy is an ideal tool for studying the binding of macromolecules with a ligand under the physiological environment to obtain biologically relevant structural and functional information (94, 95). This is achieved by monitoring the difference in the nuclear-spin relaxation or transverse relaxation (T_2) rates of a small molecule ligand in the presence and the absence of the macromolecular targets such as cells (96). There is a huge difference in the rotational and translational motion of small molecule ligands and large molecule receptors. Small, rapidly tumbling molecules have much slower relaxation rates than slowly reorienting cells, and therefore, the T_2 of small molecules is generally large compared to the T_2 of large macromolecules or cells. This phenomenon is exploited to detect and characterize binding by measuring the T_2 values of the ligands in the absence and presence of the macromolecular targets like proteins or cells (96, 97). The ligands associated with macromolecules or cells attain the NMR properties of macromolecules or cells. This is analogous to imagining a small molecule agent as an ant and a cell as an elephant and the ant sitting on top of the elephant moving with a speed of the elephant. Based on the different relaxation rates of small molecules and cells, the interaction of CA-170 to PD-L1 was confirmed in the cellular context using PD-L1 overexpressed CHO-K1 cells in comparison to blank CHO-K1 cells (19). The results from these studies demonstrate that the cellular NMR technique is sensitive in determining the complex binding mechanism in a physiologically relevant environment.

CHARACTERIZATION OF BINDING TO PD-L2

Interestingly, despite a flurry of publications in the recent past, limited information is available regarding the interaction of small molecule agents reported to bind to PD-L1 for their binding to PD-L2. In one of the early publications, BMS compounds were evaluated for their interaction with PD-L2 (85). Data indicated their selective binding to PD-L1 and not to PD-L2. In view of the high degree of homology between PD-L1 and PD-L2, it would be of great interest to characterize newer biphenyl compounds including symmetric compounds with greater potency for their interaction with PD-L2.

ANALYSIS OF FUNCTIONALITY

In a simplistic view, because of the presence of domains of PD-L1 interacting with the small molecule agents outside of the cells, a good correlation for potency between binding leading to inhibition of PD-1:PD-L1 complex formation and functional assays is expected. However, it is worth noting that not all molecules with demonstrated binding to PD-L1 and/or capable of preventing PD-1:PD-L1 complex with high affinity have shown good activity in functional assays. Various assays utilized for functional characterization include measurement of impact on signaling components, e.g., the downstream transcription factor such as NFAT, using a luciferase-based reporter assay or signaling intermediate SHP-1 and primary T-cell-based assays in which proliferation or cytokine secretion is monitored in a set-up involving antigen recall or rescue from the inhibitory effect of PD-L1. Details of the most commonly used functional assays are summarized in **Table 2**.

NFAT Reporter Assay

In most of the PD-L1 inhibitor publications, a co-culture assay in which CHO-K1 cells (of Chinese Hamster ovary origin) overexpressing PD-L1 and T-cell receptor activator with the effector Jurkat T cells overexpressing PD-1 and a luciferase gene controlled by the NFAT response element has been used. In such a reporter assay, BMS-1001 and BMS-1166 restored the activation of Jurkat T cells, represented by an increase in luciferase activity (98). However, the potential of the compounds in restoring the activation of effector cells is significantly lower than that observed for the therapeutic antibodies and with lower maximal cell activation levels. Such drastic reduction in the potency of BMS compounds (83) and other derivatives based on the original BMS compounds (49) in the reporter assay has also been confirmed by several other groups (42, 44, 53, 57, 99). In a similar reporter assay system, CA-170, which rescues T cells from the inhibitory activity of PD-L1, did not show activity (93), while a low activity was observed (<1.5 induction of reporter activity at doses ranging from 0.1 to 10 μM) with the most potent small molecule capable (BMS-1166) of potently disrupting the interaction of PD-1:PD-L1 complex (IC_{50} 7 nM in TR-FRET assay). In comparison, a significant activity was observed for macrocyclic peptide or nivolumab in the same study. Another biphenyl compound, L7, has also been reported to show significantly lower potency compared to its activity in HTRF-based biochemical assay for the disruption of PD-1-PD-L1 interaction (99). Interestingly, the more potent two

TABLE 2 | Most commonly used functional assays to monitor the impact of small molecule agents on PD-1 pathway.

Type of assay	Source for PD-1	Source for PD-L1	Consequence of interfering in the PD-1:PD-L1 interaction by small molecules	Detection system	Comments
NFAT reporter	Jurkat (immortalized line of human T cells) overexpressing PD-1 and luciferase gene controlled by the NFAT-response element	CHO-K1 (Chinese hamster ovary cells) cell line overexpressing PD-L1 and T-cell receptor activator	Activation of TCR signaling leading to greater luciferase expression	Chemiluminescence	Engineered cell line as T cells in the assay. Assay commercially available
SHP-1	Jurkat cells expressing PD-1 and SHP-1 each fused with different individually inactive fragments of the β-galactosidase	U-2 OS osteosarcoma cell line expressing PD-L1	Decrease in SHP-1 recruitment leading to lower β-galactosidase activity due to reduced enzyme fragment complementation	Chemiluminescence	Engineered cell line as T cells in the assay. Assay commercially available
PBMC	T cells activated by anti-CD3/anti-CD28	Recombinant protein	Activation of TCR signaling leading to the rescue of proliferation or cytokine release	FACS or ELISA	Primary T cells in the assay—closer to physiological context
PBMC/ whole blood	T cells activated by staphylococcal enterotoxin B (SEB) or CMV antigen	Other cells in PBMCs or blood; not controlled likely leading to greater variability in the assay	Activation of TCR signaling leading to the rescue of proliferation or cytokine release	FACS or ELISA	Primary T cells in the assay—closer to physiological context

C_2-symmetric inhibitors LH1306 and LH1307, with IC_{50} value of 25 and 3 nM, respectively, dose dependently released the PD-1-mediated inhibition of PD-1-expressing Jurkat T cells and induced the activity of luciferase with EC_{50} values of 4.2 and 0.76 μM, respectively, and the asymmetric version of LH1306 was inactive (42). Similarly, ARB-272572, another symmetric molecule with potent activity (400 pM IC_{50}) in PD-1/PD-L1 HTRF showed significantly lower potency (>40-fold less in the reporter assays, whereas anti-PD-L1 and anti-PD-1 antibodies showed comparable potency in binding and reporter assays (44). Taken together, the available data suggest that the reporter assay system, which is far removed from the physiological context, may not be ideally suited for characterizing all classes of small molecule inhibitors.

SHP-1 Signaling Assay

Another heterologous functional assay based on the enzyme fragment complementation technology, the commercial PathHunter cell-based PD-1 (SHP-1) signaling assay, has also been used to investigate the potency of PD-L1 inhibitors. This assay utilizes a stable, engineered cell line with enzyme fragment complementation technology for use in studying drug candidates targeting PD-1/PD-L1 pathway. In this assay format, symmetric compounds LH1306 and LH1307 demonstrated 8.2-fold (EC_{50}, 334 nM) and 2.8-fold (EC_{50}, 79 nM) more activity as compared to their asymmetric analogues in commercial PathHunter cell-based PD-1 (SHP-1) signaling assay underscoring the need for C_2-symmetry for optimal functionality (42). However, it is important to note that as in the NFAT reporter assay, the potency of the compounds in the SHP-1 signaling assay was ~10-fold lower compared their potency in PD-1:PD-L1 disruption.

Primary T-Cell-Based Assay

Only a limited number of publications report the characterization of biphenyl compounds in the primary T-cell-based assays. In a peripheral blood mononuclear cell (PBMC)-based assay, BMS-202, one of the early biphenyl compounds with poor cellular activity in the NFAT reporter assay (53), showed significant rescue of interferon gamma (IFN-γ) secretion inhibited by PD-L1 at a lower concentration (100 nM) similar to another biphenyl compound, Compound 58 (54). The biphenyl compound B2 has been shown to induce IFN-γ secretion from the lymph node T cells co-cultured with LLC cells and rescue the inhibition of IFN-γ secretion from PD-L1 of PBMC treated with anti-CD3/anti-CD28, with a potency similar to that observed in biochemical assay for the disruption of PD-1/PD-L1 interaction (56). During the discovery of amino-acid-inspired interface mimic CA-170, a PBMC-based function assay monitoring the rescue of T cells from the inhibitory activity of PD-L1 in inducing proliferation and cytokine secretion was extensively used. In this assay, CA-170 shows the Emax and potency similar to those observed with an anti-PD1 antibody (19). A functional assay in a similar format was recently employed to establish equipotent functional activity as in biochemical assays of modified biphenyl compound, Compound B2, from researchers of Nanjing University and China Pharmaceutical University (56).

It is important to note that not all studies have reported a good correlation between biochemical and PBMC-based functional assays. For example, Compound 24, a biphenyl asymmetric molecule, showed about 30-fold lower activity in PBMC-based tumor cell line (MDA-MB231) killing assay (Wang 2021). In a co-culture assay using 293T-OS8-hPDL1 cells, and CD3 + T cells, Incyte-011, a symmetric compound, increased IFN-γ production in a dose-dependent manner and reached the peak at the maximum dose of 1 μM, indicating a significant attenuation relative to its biochemical activity (IC_{50} of 5 nM in HTRF assay), whereas the asymmetric compound Incyte-001 and BMS compounds were not active in this assay. In the same assay, the control PD-L1 antibody atezolizumab was highly active, with IFN-γ production reaching up to 350 pg/ml at 5 nM concentration (84).

Based on the observation that PD-1 antibodies have been shown to upregulate T-cell responses in response to superantigens such as staphylococcal enterotoxin B (SEB) or cytomegalovirus (CMV) antigens, these assays have also been

utilized for the characterization of PD-L1 agents. In the SEB-induced PBMC assays, to monitor proliferation and secretion of IL-2 or IFN-γ production, BMS small molecule compounds showed activity only at micromolar concentration, while BMS macrocyclic peptide induced high levels of IL-2 at sub-micromolar concentrations (83). In a separate study, a symmetric compound, ARB-272572, that demonstrated activity in an NAFT reporter assay of 17 nM IC_{50} displayed a potency of 3 nM in CMV antigen recall assay, still a significant drop-off in the potency relative to that observed in biochemical activity (400 pM IC_{50} in a cell-free HTRF assay) (44).

Among all the functional assays employed, the best correlation with biochemical potency was observed for selected biphenyl compounds using primary T cells with PBMCs as the source and in the presence of PD-L1. Interestingly, CA-170, which failed to exhibit activity in HTRF based PD-1:PD-L1 disruption and NFAT-reporter-based functional assay, was highly active in the PBMC-based assays, which has now translated into immune activation observed in the clinic (100). Taken together, these findings raise the possibility of PBMC/primary T-cell-based assays, which are used to monitor rescue from the inhibitory activity of PD-L1, in which the addition of PD-L1 brings in the specificity, as the most relevant assay to analyze the immune activation potential of small molecule PD-L1 agents. While this possibility needs to be validated further, it may not be entirely surprising considering that PD-1:PD-L1 interaction is studied in a setup that is a lot closer to the physiological and therapeutic context. It is also important to note that in the PBMC-based assay format, the substitution of human PBMCs with monkey PBMCs or mouse splenocytes along with PD-L1 of monkey or mouse origin allows to evaluate the cross-species functional activity (19).

In the cellular pharmacology studies using human T cells and the rescue of inhibition by PD-L1, both CA-170 and anti-PD-1 antibodies showed a bell-shaped T-cell activation response (101). In these assays, optimal T-cell activation occurs between concentrations of 125–500 nM beyond which there is a substantial reduction in the activity. Such inverse dose response has also been observed *in vivo* in tumor models with a series of novel benzo[c][1,2,5]oxadiazole derivatives with potent PD-L1 binding and functional activity (99). An inverse dose response was observed with PD-L1-humanized MC38 model, in which compound L24 exhibited significant antitumor efficacy in this model, with 25 mg/kg (TGI 44.2%) exhibiting higher efficacy compared to a higher dose of 50 mg/kg (TGI 30.8%). The likely cause for such a bell-shaped response is the hyperactivation of the immune system leading to activation-induced T-cell death (102), which is detrimental to the effect of the drug.

Functional Antagonism of PD-L2

Among the reported small molecule agents binding and interfering in the function of PD-L1, CA-170 has also been shown to functionally antagonize signalling from PD-L2 (19). In human PBMC or mouse splenocyte-based assays, CA-170 has shown dose-dependent rescue of inhibition of proliferation or cytokine secretion in the presence of either PD-L1 or PD-L2. The potency of CA-170 in these assays for functional antagonisms were similar to that observed with commercially available anti-PD1 antibodies (19), which are known to antagonize signaling originated from either PD-L1 and PD-L2. Unlike PD-L1, the expression of PD-L2 is mainly restricted to professional antigen-presenting cells (APCs) like macrophages and dendritic cells (DCs) and more commonly upregulated in lymphoid malignancies (103). Studies have also indicated that the expression of PD-L2 is independently associated with clinical response in pembrolizumab (anti-PD1)-treated patients, supporting that the presence or absence of PD-L2 expression may also play a role in response to PD-1 axis targeted therapies (104). The consequence of selective inhibition of PD-L1 versus dual inhibition of both PD-L1 and PD-L2 needs to be characterized, specifically in view of greater apparent clinical efficacy of anti-PD1 antibodies capable of blocking signals that originated both from PD-L1 and PD-L relative to the efficacy from anti-PD-L1 antibodies.

MECHANISM OF ACTION OF THE REPORTED SMALL MOLECULE COMPOUNDS TARGETING PD-L1

Even though the functional antagonism of the PD-1 pathway is anticipated from a compound capable of binding to one of the partner in the PD-1:PD-L1 complex and preventing the interaction, emerging data point to additional complexity with which reported compounds antagonize the PD-1 signaling.

Induction of PD-L1 Dimerization and Inhibiting PD-1:PD-L1 Interaction

The detailed characterization of PD-L1 targeting compounds originally described by the BMS group was carried out by Prof. Holak and colleagues, and they have extensively published on the mechanism of action, binding mode based on X-ray structure determination, confirmation of binding, and functionality by various methods (35). One of their major contributions to the field is in identifying the molecular details of the human PD-1/PD-L1 interaction using X-ray structure of hPD-1:PD-L1 complex, which led to the identification of three hotspot pockets in PD-L1, the binding of which can lead to inhibition of PD-1:PD-L1 interaction (35). Among these pockets, two are rich in hydrophobic amino acids with considerable hydrophobicity and one in hydrophilic amino acids. The direct binding of BMS compounds to PD-L1 *via* NMR assays and the structural basis for these compounds (BMS-8 and BMS-202) in targeting PD-L1 were delineated (85). Using crystal structure studies, it was demonstrated that these compounds inhibit the PD-1:PD-L1 interaction by inducing PD-L1 dimerization through PD-1 interacting surface. The BMS compounds reported in these studies were targeted to the reported hydrophobic hotspots 1 and 2. In a subsequent publication, the same group also reported that BMS compounds, specifically BMS-200, based on 2,3-dihydro-1,4-benzdioxinyl group induced an enlarged interaction interface that results in the

open "face-back" tunnel through the PD-L1 dimer (38). This result indicates that BMS-200 induces conformational changes in PD-L1, and the ligand binding site of PD-L1 to be more flexible than it was previously seen. The crystal structure of the less cytotoxic compounds (BMS-1001 and 1166) from the BMS compounds series indicated that the deep hydrophobic pocket harboring BMS-202 is transformed into a tunnel in the PD-L1/BMS-1166 structure by rotation of the Tyr56 sidechain, which may be responsible for increased potency of the compounds compared to their predecessors (98). Using multiple molecular modeling methods, computational insights into the small molecule induced PD-L1 dimerization, suggesting the tendency of BMS small-molecule inhibitors to interact with one PD-L1 monomer first followed by dimer formation for an advantage of stability has been provided (105).

The more active (in both binding and functional assays) C_2-symmetic inhibitor Compound LH1307 was found to extend across the AFGCC' faces of the PD-L1 proteins, forming an extended hydrophobic tunnel through the PD-L1 homodimer (42). In this molecule, the biphenyl moiety helped in anchoring the compound in the hydrophobic core of the homodimer, while the polar groups in the solvent exposed helped in bringing the two PD-L1 monomers through a network of hydrogen bonds and electrostatic interactions with the polar residues on the AB and CC' strands of the PD-L1. Greater potency of such symmetrical compound was due to the binding two equivalent sites in the PD-L1 homodimer by virtue of its C_2-symmetric nature (42). Incyte and Arbutus have also utilized the inherent C2-symmetry in the PD-L1 dimer by symmetrizing their molecules to achieve greater potency (**Figure 6**).

A recent review (106) summarizes the phenomenon of drug-induced protein dimerization, as the mechanism to modulate the target activity is not unique to PD-L1. Other examples of drug-induced protein homodimer stabilization include compounds that stabilize Max and TLR2 homodimers. In these examples, the same dimer sequestration principle occurs with the compounds, which shape an interfacial binding tunnel between two monomeric protein units. Interestingly, compounds used to promote homo-dimerization of matrix metalloproteinases for crystallographic studies also include a biphenyl unit (107).

Blocking of PD-L1 Export From Endoplasmic Reticulum to Golgi

A cellular mechanism for the functional antagonism of the biphenyl compound BMS-1166 based on the role of glycosylation on the critical residues of PD-L1 protein has also been proposed (108). The four N-glycosylation sites (Asn35, Asn192, Asn 200, and Asn 219) present in the extracellular domain of PD-L1 is necessary for the stability of ligand protein, and except Asn 35, all other glycosylation sites are critical for its interaction with receptor (90, 109). BMS-1166 partially and specifically inhibits PD-L1 glycosylation and functionally inactivates PD-L1 by blocking its export from the endoplasmic reticulum to Golgi (108). It is not known if the newer C_2 symmetric compounds also have an impact on PD-L1 by this mechanism.

Induction of PD-L1 Dimerization and Internalization

Induction of a two-step internalization process as the mechanism of action for a C_2-skeleton biphenyl compounds has recently been published by the Arbutus group (44). In this process, Compound ARB-272572 inhibits the PD-1/PD-L1 axis by inducing cell surface PD-L1 dimerization *via* cis-interacting homodimers triggering a rapid loss of cell surface PD-L1 by rapid internalization into the cytosol, thereby preventing any further interaction with PD-1-expressing cell types. The formation of homodimer as illustrated by a crystal structure where ARB 272542 (44) bound within a hydrophobic pocket created between two PD-L1 proteins followed by rapid internalization into the cytosol is reported to be the primary mechanism contributing to cellular potency. Similar to the publication by Arbutus, Incyte had previously described inhibitor-induced internalization, but the structure of the specific compound was not revealed (110). Apart from the clinical candidate, Incyte also reported INCB-090244, which binds and internalizes surface PD-L1 *in vivo* in a dose-dependent manner, and orally dosed INCB-090244 exhibits single agent activity and increases infiltrating T cells in two distinct humanized mouse models (110). Although the induction of PD-L1 internalization has been reported only with C_2-symmetric molecules., it is not clear if the C_2 symmetry and the resulting interaction are prerequisites for inducing internalization.

In the mechanism of action of PD-L1 inhibitor that induces internalization, PD-L1 is no longer available on the cell surface not only to interact with its cognate receptor PD-1 but also for its other reported binding partner Cluster of Differentiation 24 (CD80) (111). This may have unwanted consequences based on the reported finding indicating that PD-L1 also exerts an immunostimulatory effect by repressing the CTLA-4 pathway (112). The reduced cell surface PD-L1 levels could lead to greater availability of CD80 to its cognate receptor CTLA-4 leading to immune suppression. Hence, the disappearance of PD-L1 on the cell surface because of the internalization and its functional consequence may need to be studied further, as the checkpoint biology is still emerging (113).

Binding to PD-L1 Without Interference in the PD1:PD-L1 Complex Formation

Lack of binding of amino-acids-inspired interface mimic CA-170 to either PD-1 or PD-L1 or disruption of PD-1:PD-L1 complex in various biophysical and biochemical assays has been discussed in the literature along with postulating alternative unknown mechanism of action for these compounds (82, 83, 93). In view of the use of proteins expressed in heterologous expression systems lacking appropriate post-translational modifications, recently, the binding of CA-170 to PD-L1 has been established by cellular NMR spectroscopy using full-length PD-L1 expressed in mammalian cells (19). Compared to the biphenyl-based small molecule inhibitors (38, 98), CA-170 is highly polar and thus likely interacts with PD-L1 at a solvent exposed region. Observed functional antagonism in PD-L1 signaling and direct binding to PD-L1 in the cellular context without the disruption of the PD1: PD-L1 complex support the formation of a defective ternary

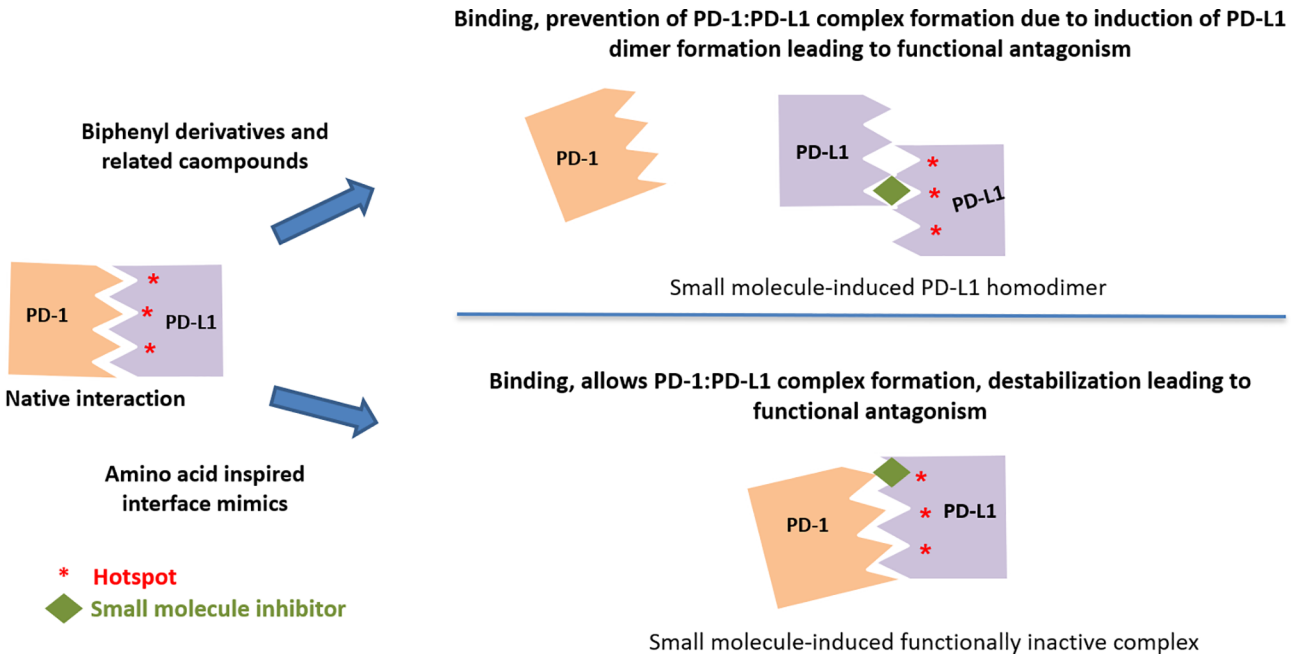

FIGURE 6 | Two distinct mechanisms leading to functional antagonism with reported small molecule PD-L1 inhibitors.

complex as the mechanism of action of CA-170 (19) (**Figure 6**). This mode of action of CA-170 is analogous to that of two reported anti-PD1 antibodies that antagonize PD-1 signaling without interfering in PD-1:PD-L1 complex formation (114, 115).

CLINICAL DEVELOPMENT OF PD-1 SMALL MOLECULE INHIBITORS

CA-170 was the first orally available small molecule PD-L1 inhibitor to enter the clinical trials in 2016, and it is currently in Phase 2b/3 trials (co-development by Curis and Aurigene). The clinical trials of Incyte compound INCB-086550 was initiated in 2018, and Phase 1 is expected to be completed by 2022. The details of all small molecule agents in the clinic with most recent findings are consolidated in **Table 3**.

Considerations in Small Molecule Clinical Development

Several unique features of small molecule agents targeting PD-L1 compared to antibodies against PD-1 and PD-L1 emphasize the potential need to adapt strategies that are different than those that have worked well for approved PD-1 and PD-L1 antibodies. Target engagement analysis in circulation that is widely used for antibody-based therapeutics may not work for small molecule reversible agents because of their distinct binding kinetics including faster off-rate. In the absence of the direct target engagement, dose selection for expansion studies my need to be decided based on the exposure and its correlation with pharmacodynamic effects observed in both preclinical and clinical setting.

Because of the substantially smaller size of small molecule PD-L1 agents, a significantly higher number of molecules (300′ or more) are delivered compared an antibody-based agents at the same dosage level. If the potency of a small molecule PD-L1 agent is similar to anti-PD-1/PD-L1 antibody in primary T-cell-based functional assays, specifically in the rescue of inhibition by PD-L1 (as has been shown for amino-acids-inspired interface mimic CA-170 and several biphenyl derivatives), it is important to think through the consequence of achieving very high molar exposure in the clinic relative to antibodies. As discussed earlier in this article, because of the observed bell-shaped T-cell activation response in preclinical studies, the conventional approach in oncology such as first determining the maximum tolerated dose (MTD), followed by dose expansion at the MTD, may not be ideal and in fact may be highly counterproductive for an immune-activating agent.

Classically, dose–response to drugs is generally considered to be sigmoidal in nature where the biological effect increases linearly with dose until the threshold concentrations whereby inhibition proceeds in a linear fashion until saturation is achieved. However, there are examples in various classes of drugs where the dose–response curve deviates from the sigmoidal curve and exhibits a hormetic (bell-, U-, or J-shaped) dose–response. A classic example of bell-shaped clinical response for an immunomodulating agent was reported for IFN-γ several decades ago with efforts that resulted in identifying optimal immunomodulatory dose (OID) (117).

TABLE 3 | Details of small molecules in clinical trials.

Sl. no.	Drug/ company	Dosing	Indications	Current status	Details of recent status
1	**CA-170** Aurigene/Curis	50 mg QD to 1,200 mg	Lymphoma; advanced solid tumors	Phase 2b/3	In Phase 2 studies, ORR of 30% in classical Hodgkin lymphoma (based on Lugano criteria) and a CBR of >85% at a daily dose of 400 mg and PFS of 19.6 weeks in advanced (stage 4) non-squamous NSCLC (101) CTRI/2017/12/011026 Phase2b/3 studies: Phase 2b/3 randomized study of CA-170 in patients with non-squamous non-small cell lung cancer CTRI/2020/07/026870
2	**INCB-086550** Incyte Corp	QD (100, 200 mg) or BID (200, 400 mg).	NSCLC urothelial cancer Renal cell carcinoma Hepatocellular carcinoma Melanoma	Phase 2	Phase 1 Study Exploring the Safety, Tolerability, PK and PD (NCT03762447). A dose-related 1.2-fold increase in the plasma concentration of soluble target (PD-L1); 3.4-fold increase in IFN- γ; 1.3- and 1.4-fold of CXCL9 and CXCL10, observed post-treatment (116, 086550). Phase 2: Open-label, non-randomized study to evaluate the efficacy and safety (NCT04629339); INCB-086550 will be administered orally twice a day.
3	**MX-10181** Maxinovel Pharma	Dose not disclosed	Advanced solid tumor; cancer	Phase 1	In February 2021, an implied trial approval was granted for advanced solid tumor. Part 1: Dose escalation, MAX-10181 once or twice daily with dose modifications based on tolerability criteria. Part 2: Dose expansion, Recommended doses from Part 1 (NCT04122339).
4	**GS-4224** Gilead Sciences	Starting at 400 mg once a day (QD). Subsequent doses of 700 mg QD, 1,000 mg QD, 1,500 mg QD, and 1,000 mg twice a day (BID)	Advanced solid tumor; Hepatitis B virus infection	Phase 1	In March 2021, Gilead Sciences terminated a phase Ib/II trial to evaluate the safety, tolerability, pharmacokinetics, and efficacy of GS 4224 in patients with advanced solid tumors (NCT04049617).
5	**IMMH-010** Tianjin Chasesun Pharmaceutical Co., LTD	Starting at 60 mg QD. Subsequent doses of 120, 240, and 360 mg QD	Malignant neoplasms	Phase 1	Trial approved in April 2020 and the study is not yet recruited. To determine MTD and RP2D and to evaluate the effects of food on the pharmacokinetic profiles after single dose of IMMH-010 in patients with advanced solid tumors (NCT04343859).

Preclinical and clinical studies have suggested that the OID of may not be the clinical MTD (118–120). Hence, the clinical trials carried out with IFN-γ at MTD resulting in low response rate was attributed to failure in treating the patients at an optimal OID. Such bell-shared clinical response has also been noted with small molecule immunotherapeutic agents such as STING agonists (121) or TLR agonists (122). It is also worth noting that a bell-shaped clinical response has also been reported for anti-PD1 antibody nivolumab (123, 124), a finding that is not widely highlighted.

Clinical exposure-efficacy data of small molecule PD-L1 agents are slowly unfolding, and they indicate an inverse dose relationship in efficacy. Radhakrishnan et al. reported the clinical benefit for CA-170 at a dosage of 400 mg QD compared to 800 mg QD dose (101). Analysis of safety profile of the drug also indicated higher incidence of irAEs at the lower dosage of 400 mg. Additionally, there was a strong overall trend of improved CBR and PFS with 400 mg when compared to the higher dose (800 mg) in both lung cancer and Hodgkin lymphoma. These agree with preclinical findings showing a bell-shaped curve of immune activation likely due to activation-induced cell death with CA-170 (discussed earlier in this article). Observed clinical activity of CA-170 at lower dose is also consistent with the exposure achieved at optimal dose of 10 mg/kg in preclinical models (19). A recent preclinical study also reported potent anticancer efficacy of CA-170 at a dose of 10 mg/kg in carcinogen-induced mouse lung tumorigenesis model (20). Clinical efficacy data are not yet reported for INCB-086550, but peripheral pharmacodynamic activity in Phase 1 studies is reported for a low dose (100, 200 mg QD dosing or 200, 400 mg BID dosing), and Phase 2 dosing is currently ongoing (dosage not disclosed) orally twice a day.

The clinical and preclinical data of CA-170 discussed here highlight the need to adjust the optimal immunomodulatory dose for attaining clinical efficacy. In the absence of any tolerability issues, the recommended Phase 2 dose (RP2D) for a small molecule PD-L1 agent is likely the dose that achieves a reliable immune response/pharmacodynamics (assessed by monitoring T cells or other immune cells in the tumor microenvironment) and hints of clinical efficacy or exposure that shows anti-tumor efficacy in preclinical models. Further studies on the dose–efficacy relationship and the underlying mechanisms need to be understood further to achieve complete benefit of these agents in clinic.

Since most of the reported small molecule inhibitors target PD-L1 as opposed to PD-1, with the exception of limited reports (125), clinical indications in which anti-PD-L1 antibodies have shown good efficacy could be more appropriate for PD-L1 small molecule agents. Unlike PD-1 antibodies that block signaling from both PD-L1 and PD-L2, PD-L1 antibodies do not impact

PD-L2 signaling. On the other hand, PD-L1 antibodies also block the interaction of PD-L1 with CD80. Even though there is a significant overlap in the approved clinical indications for PD-1 antibodies versus PD-L1 antibodies, there are specific indications including Hodgkin lymphoma, head and neck cancer, and colorectal cancers in which only PD-1 antibodies are approved. In the absence of head-to-head comparison and the dependence on cross-study comparisons, it is not clear if these differences are due to differential biology expected from PD-1-targeted agents versus those targeting PD-L1. However, these points may need to be taken into consideration during the development of PD-L1-targeted agents.

CONCLUSIONS AND FUTURE PERSPECTIVES

With the realization that small molecule agents targeting PD-1: PD-L1 immune checkpoint pathway offer distinct advantages, there has been a burst of publications describing several agents targeting PD-L1. Interestingly, while most of these agents interact with PD-L1 and result in the desired phenotype, there has been limited report(s) of small molecule agents binding to PD1 or both PD1 and PD-L1. Because of several elegant studies, the mechanisms of action of PD-L1 agents are unravelling, but we still do not know if targeting PD-1 would be more advantageous. While most of the reported agents derived from the biphenyl scaffold perform very well in the binding and PD-1: PD-L1 disruption assays by inducing dimerization of PD-L1, not all of them show potent functionality in cellular systems. Among the functional assays evaluated, PBMC or primary T-cell-based assays, specifically those in which rescue of inhibition by PD-L1 is monitored, show a better correlation with potency in biochemical assays for disruption of PD-1:PD-L1 interaction. Disconnection in several other functional assays is likely contributed by differences in which these molecules encounter the target on immune cells in a physiological context, which emphasizes the need to use appropriate functional assays in the discovery. Functional assays using primary T cells from human and preclinical species provide their cross-species activity and valuable information for clinical translation with respect to exposure that would likely lead to optimal immune activation. While there is substantial progress in identifying PD-L1 targeted small molecule agents, it is intriguing to note that not many have attempted to characterize the interaction of the reported PD-L1 agents with PD-L2. Similarly, the consequences of the binding to PD-L1 on PD-L1's interaction with CD80 are yet to be characterized for most of the reported PD-L1 agents. Ultimately, the utility of the PD-L1-targeted small molecule agents needs to be delineated by clinical studies, and in this regard, it is encouraging to note that clinical studies are progressing with a few of the molecules. Early clinical data suggest a need for a precise determination of the dose providing optimal immune activation for dose expansion without escalating it to MTD as typically followed for most cytotoxic or targeted oncology drugs. Clinical success with small molecule PD-L1 inhibitors either as a single agent or in combination with current standard of care is eagerly awaited towards fully harnessing this important therapeutic modality.

AUTHOR CONTRIBUTIONS

PS and MR performed the literature review and wrote the manuscript. All authors contributed to the article and approved the submitted version.

REFERENCES

1. Ledford H, Else H, Warren M. Cancer Immunologists Scoop Medicine Nobel Prize. *Nature* (2018) 562(7725):20–1. doi: 10.1038/d41586-018-06751-0
2. Vaddepally RK, Kharel P, Pandey R, Garje R, Chandra AB. Review of Indications of FDA-Approved Immune Checkpoint Inhibitors Per NCCN Guidelines With the Level of Evidence. *Cancers* (2020) 12(3):735. doi: 10.3390/cancers12030738
3. Pardoll DM. The Blockade of Immune Checkpoints in Cancer Immunotherapy. *Nat Rev Cancer* (2012) 12(4):252–64. doi: 10.1038/nrc3239
4. Ghosh A, Barba P, Perales M-A. Checkpoint Inhibitors in AML: Are We There Yet? *Br J Haematol* (2020) 188(1):159–675. doi: 10.1111/bjh.16358
5. Naidoo J, Page DB, Li BT, Connell LC, Schindler K, Lacouture ME, et al. Toxicities of the Anti-PD-1 and Anti-PD-L1 Immune Checkpoint Antibodies. *Ann Oncol* (2015) 26(12):2375–91. doi: 10.1093/annonc/mdv383
6. Larkin J, Chiarion-Sileni V, Gonzalez R, Grob JJ, Cowey CL, Lao CD, et al. Combined Nivolumab and Ipilimumab or Monotherapy in Untreated Melanoma. *New Engl J Med* (2015) 373(1):23–34. doi: 10.1056/NEJMoa1504030
7. Wolchok JD, Chiarion-Sileni V, Gonzalez R, Rutkowski P, Grob J-J, Cowey CL, et al. Overall Survival With Combined Nivolumab and Ipilimumab in Advanced Melanoma. *New Engl J Med* (2017) 377(14):1345–56. doi: 10.1056/NEJMoa1709684
8. Redelman-Sidi G, Michielin O, Cervera C, Ribi C, Aguado JM, Fernández-Ruiz M, et al. ESCMID Study Group for Infections in Compromised Hosts (ESGICH) Consensus Document on the Safety of Targeted and Biological Therapies: An Infectious Diseases Perspective (Immune Checkpoint Inhibitors, Cell Adhesion Inhibitors, Sphingosine-1-Phosphate Receptor Modulators and Proteasome Inhibitors). *Clin Microbiol Infect* (2018) 24: S95–107. doi: 10.1016/j.cmi.2018.01.030
9. Brahmer JR, Drake CG, Wollner I, Powderly JD, Picus J, Sharfman WH, et al. Phase I Study of Single-Agent Anti-Programmed Death-1 (MDX-1106) in Refractory Solid Tumors: Safety, Clinical Activity, Pharmacodynamics, and Immunologic Correlates. *J Clin Oncol* (2010) 28 (19):3167–75. doi: 10.1200/JCO.2009.26.7609
10. Brahmer JR, Tykodi SS, Chow LQM, Hwu W-J, Topalian SL, Hwu P, et al. Safety and Activity of Anti-PD-L1 Antibody in Patients With Advanced Cancer. *New Engl J Med* (2012) 366(26):2455–65. doi: 10.1056/NEJMoa1200694
11. Topalian SL, Hodi FS, Brahmer JR, Gettinger SN, Smith DC, McDermott DF, et al. Safety, Activity, and Immune Correlates of Anti-PD-1 Antibody in Cancer. *New Engl J Med* (2012) 366(26):2443–54. doi: 10.1056/NEJMoa1200690
12. Koyama S, Akbay EA, Li YY, Herter-Sprie GS, Buczkowski KA, Richards WG, et al. Adaptive Resistance to Therapeutic PD-1 Blockade Is Associated With Upregulation of Alternative Immune Checkpoints. *Nat Commun* (2016) 7:10501. doi: 10.1038/ncomms10501
13. Gao J, Ward JF, Pettaway CA, Shi LZ, Subudhi SK, Vence LM, et al. VISTA Is an Inhibitory Immune Checkpoint That Is Increased After Ipilimumab

Therapy in Patients With Prostate Cancer. *Nat Med* (2017) 23(5):551–55. doi: 10.1038/nm.4308
14. Jain RK. Physiological Barriers to Delivery of Monoclonal Antibodies and Other Macromolecules in Tumors. *Cancer Res* (1990) 50(3 Suppl):814s–19.
15. Andrews A. Treating With Checkpoint Inhibitors-Figure $1 Million Per Patient. *Am Health Drug Benefits* (2015) 8(Spec Issue):9–9.
16. Imai K, Takaoka A. Comparing Antibody and Small-Molecule Therapies for Cancer. *Nat Rev Cancer* (2006) 6(9):714–275. doi: 10.1038/nrc1913
17. Yabroff KR, Warren JL, Knopf K, Davis WW, Brown ML. Estimating Patient Time Costs Associated With Colorectal Cancer Care. *Med Care* (2005) 43 (7):640–485. doi: 10.1097/01.mlr.0000167177.45020.4a
18. Chames P, Regenmortel MV, Weiss E, Baty D. Therapeutic Antibodies: Successes, Limitations and Hopes for the Future: Therapeutic Antibodies: An Update. *Br J Pharmacol* (2009) 157(2):220–335. doi: 10.1111/j.1476-5381.2009.00190.x
19. Sasikumar PG, Sudarshan NS, Adurthi S, Ramachandra RK, Samiulla DS, Lakshminarasimhan A, et al. PD-1 Derived CA-170 Is an Oral Immune Checkpoint Inhibitor That Exhibits Preclinical Anti-Tumor Efficacy. *Commun Biol* (2021) 4(1):699. doi: 10.1038/s42003-021-02191-1
20. Pan J, Chen Y, Zhang Q, Khatun A, Palen K, Xin G, et al. Inhibition of Lung Tumorigenesis by a Small Molecule CA170 Targeting the Immune Checkpoint Protein VISTA. *Commun Biol* (2021) 4(1):906. doi: 10.1038/s42003-021-02381-x
21. Findlay M, von Minckwitz G, Wardley A. Effective Oral Chemotherapy for Breast Cancer: Pillars of Strength. *Ann Oncol* (2008) 19(2):212–22. doi: 10.1093/annonc/mdm285
22. Makurvet FD. Biologics vs. Small Molecules: Drug Costs and Patient Access. *Med Drug Discovery* (2021) 9:100075. doi: 10.1016/j.medidd.2020.100075
23. Schneider C. Monoclonal Antibodies - Regulatory Challenges. *Curr Pharm Biotechnol* (2008) 9(6):431–38. doi: 10.2174/138920108786786394
24. Vandivort TC, Horton DB, Johnson SB. Regulatory and Strategic Considerations for Addressing Immunogenicity and Related Responses in Biopharmaceutical Development Programs. *J Clin Trans Sci* (2020) 4 (6):547–55. doi: 10.1017/cts.2020.493
25. Smith MC, Gestwicki JE. Features of Protein–Protein Interactions That Translate Into Potent Inhibitors: Topology, Surface Area and Affinity. *Expert Rev Mol Med* (2012) 14:e16. doi: 10.1017/erm.2012.10
26. Ivanov AA, Khuri FR, Fu H. Targeting Protein–Protein Interactions as an Anticancer Strategy. *Trends Pharmacol Sci* (2013) 34(7):393–4005. doi: 10.1016/j.tips.2013.04.007
27. Guo W, Wisniewski JA, Ji H. Hot Spot-Based Design of Small-Molecule Inhibitors for Protein–Protein Interactions. *Bioorg Med Chem Lett* (2014) 24 (11):2546–545. doi: 10.1016/j.bmcl.2014.03.095
28. Schmidtke P, Barril X. Understanding and Predicting Druggability. A High-Throughput Method for Detection of Drug Binding Sites. *J Med Chem* (2010) 53(15):5858–675. doi: 10.1021/jm100574m
29. Reichmann D, Rahat O, Albeck S, Meged R, Dym O, Schreiber G. The Modular Architecture of Protein-Protein Binding Interfaces. *Proc Natl Acad Sci* (2005) 102(1):57–62. doi: 10.1073/pnas.0407280102
30. Moza B, Buonpane RA, Zhu P, Herfst CA, Rahman AKMN-u, McCormick JK, et al. Long-Range Cooperative Binding Effects in a T Cell Receptor Variable Domain. *Proc Natl Acad Sci* (2006) 103(26):9867–725. doi: 10.1073/pnas.0600220103
31. Ofran Y, Rost B. Protein–Protein Interaction Hotspots Carved Into Sequences. In: A Valencia, editor. *PLoS Computational Biology*, vol. 3 (2007). doi: 10.1371/journal.pcbi.0030119
32. Keskin O, Ma B, Nussinov R. Hot Regions in Protein–Protein Interactions: The Organization and Contribution of Structurally Conserved Hot Spot Residues. *J Mol Biol* (2005) 345(5):1281–945. doi: 10.1016/j.jmb.2004.10.077
33. Bogan AA, Thorn KS. Anatomy of Hot Spots in Protein Interfaces. *J Mol Biol* (1998) 280(1):1–95. doi: 10.1006/jmbi.1998.1843
34. Darnell SJ, LeGault L, Mitchell JC. KFC Server: Interactive Forecasting of Protein Interaction Hot Spots. *Nucleic Acids Res* (2008) 36:W265–69. doi: 10.1093/nar/gkn346
35. Zak KM, Kitel R, Przetocka S, Golik P, Guzik K, Musielak B, et al. Structure of the Complex of Human Programmed Death 1, PD-1, and Its Ligand PD-L1. *Struct (London England: 1993)* (2015) 23(12):2341–485. doi: 10.1016/j.str.2015.09.010
36. Huang D, Wen W, Liu X, Li Y, Zhang JZH. Computational Analysis of Hot Spots and Binding Mechanism in the PD-1/PD-L1 Interaction. *RSC Adv* (2019) 9(26):14944–565. doi: 10.1039/C9RA01369E
37. Lipinski CA, Lombardo F, Dominy BW, Feeney PJ. Experimental and Computational Approaches to Estimate Solubility and Permeability in Drug Discovery and Development Settings 1PII of Original Article: S0169-409x(96)00423-1. *Article Originally Published Adv Drug Deliv Rev* (2001) 23 (1997):3–25. doi: 10.1016/S0169-409X(00)00129-0
38. Guzik K, Zak KM, Grudnik P, Magiera K, Musielak B, Törner R, et al. Small-Molecule Inhibitors of the Programmed Cell Death-1/Programmed Death-Ligand 1 (PD-1/PD-L1) Interaction *via* Transiently Induced Protein States and Dimerization of PD-L1. *J Med Chem* (2017) 60(13):5857–675. doi: 10.1021/acs.jmedchem.7b00293
39. Guzik K, Tomala M, Muszak D, Konieczny M, Hec A, Błaszkiewicz U, et al. Development of the Inhibitors That Target the PD-1/PD-L1 Interaction—A Brief Look at Progress on Small Molecules, Peptides and Macrocycles. *Molecules* (2019) 24(11):20715. doi: 10.3390/molecules24112071
40. Sasikumar PG, Ramachandra M. Small-Molecule Immune Checkpoint Inhibitors Targeting PD-1/PD-L1 and Other Emerging Checkpoint Pathways. *BioDrugs* (2018) 32(5):481–975. doi: 10.1007/s40259-018-0303-4
41. Wu X, Meng Y, Liu L, Gong G, Zhang H, Hou Y, et al. Insights Into Non-Peptide Small-Molecule Inhibitors of the PD-1/PD-L1 Interaction: Development and Perspective. *Bioorg Med Chem* (2021) 33 (March):116038. doi: 10.1016/j.bmc.2021.116038
42. Basu S, Yang J, Xu B, Magiera-Mularz K, Skalniak L, Musielak B, et al. Design, Synthesis, Evaluation, and Structural Studies of C2-Symmetric Small Molecule Inhibitors of Programmed Cell Death-1/Programmed Death-Ligand 1 Protein–Protein Interaction. *J Med Chem* (2019) 62(15):7250–635. doi: 10.1021/acs.jmedchem.9b00795
43. Kawashita S, Aoyagi K, Yamanaka H, Hantani R, Naruoka S, Tanimoto A, et al. Symmetry-Based Ligand Design and Evaluation of Small Molecule Inhibitors of Programmed Cell Death-1/Programmed Death-Ligand 1 Interaction. *Bioorg Med Chem Lett* (2019) 29(17):2464–67. doi: 10.1016/j.bmcl.2019.07.027
44. Park J-J, Thi EP, Carpio VH, Bi Y, Cole AG, Dorsey BD, et al. Checkpoint Inhibition Through Small Molecule-Induced Internalization of Programmed Death-Ligand 1. *Nat Commun* (2021) 12(1):1222. doi: 10.1038/s41467-021-21410-1
45. Feng Z, Chen X, Yang Y, Zheng Y, Lai F, Ji M, et al. *Nicotinyl Alcohol Ether Derivative, Preparation Method Therefor, and Pharmaceutical Composition and Uses Thereof*. United States: Patent and Trademark Office (USPTO) (2021). Available at: https://patents.google.com/patent/US10975049B2/en.US10975049B2.
46. Tianjin Chasesun Pharmaceutical Co., LTD. A Phase I Clinical Trial of IMMH-010 in Patients With Advanced Malignant Solid Tumors. In: *Clinical trial registration NCT04343859*. clinicaltrials.gov (2020). Available at: https://clinicaltrials.gov/ct2/show/NCT04343859.
47. Jiang J, Zou X, Liu Y, Liu X, Dong K, Yao X, et al. Simultaneous Determination of a Novel PD-L1 Inhibitor, IMMH-010, and Its Active Metabolite, YPD-29B, in Rat Biological Matrices by Polarity-Switching Liquid Chromatography-Tandem Mass Spectrometry: Application to ADME Studies. *Front Pharmacol* (2021) 12:677120. doi: 10.3389/fphar.2021.677120
48. Cheng B, Ren Y, Cao H, Chen J. Discovery of Novel Resorcinol Diphenyl Ether-Based PROTAC-Like Molecules as Dual Inhibitors and Degraders of PD-L1. *Eur J Med Chem* (2020) 199:112377. doi: 10.1016/j.ejmech.2020.112377
49. Yang Y, Wang K, Chen H, Feng Z. Design, Synthesis, Evaluation, and SAR of 4-Phenylindoline Derivatives, a Novel Class of Small-Molecule Inhibitors of the Programmed Cell Death-1/Programmed Cell Death-Ligand 1 (PD-1/PD-L1) Interaction. *Eur J Med Chem* (2021) 211(February):113001. doi: 10.1016/j.ejmech.2020.113001
50. Chen A, Wu D-L, Shi J, Narva S, Zhao X-Y, Wu Y-L, et al. Design, Synthesis and Biological Evaluation of 2-Methyl-(1,1′-Biphenyl)-Pyrimidine Conjugates. *Bioorg Med Chem Lett* (2020) 30(16):1273285. doi: 10.1016/j.bmcl.2020.127328
51. Wang F, Ye W, Wang S, He Y, Zhong H, Wang Y, et al. Discovery of a New Inhibitor Targeting PD-L1 for Cancer Immunotherapy. *Neoplasia* (2021) 23 (3):281–93. doi: 10.1016/j.neo.2021.01.001

52. Liu C, Zhou F, Yan Z, Shen L, Zhang X, He F, et al. Discovery of a Novel, Potent and Selective Small-Molecule Inhibitor of PD-1/PD-L1 Interaction With Robust *in Vivo* Anti-Tumour Efficacy. *Br J Pharmacol* (2021) 1778 (13):2651. doi: 10.1111/bph.15457
53. Dai X, Wang K, Chen H, Huang X, Feng Z. Design, Synthesis, and Biological Evaluation of 1-Methyl-1h-Pyrazolo[4,3-B]Pyridine Derivatives as Novel Small-Molecule Inhibitors Targeting the PD-1/PD-L1 Interaction. *Bioorg Chem* (2021) 114:105034. doi: 10.1016/j.bioorg.2021.105034
54. Guo J, Luo L, Wang Z, Hu N, Wang W, Xie F, et al. Design, Synthesis, and Biological Evaluation of Linear Aliphatic Amine-Linked Triaryl Derivatives as Potent Small-Molecule Inhibitors of the Programmed Cell Death-1/Programmed Cell Death-Ligand 1 Interaction With Promising Antitumor Effects *In Vivo*. *J Med Chem* (2020) 63(22):13825–505. doi: 10.1021/acs.jmedchem.0c01329
55. Wang T, Cai S, Wang M, Zhang W, Zhang K, Chen D, et al. Novel Biphenyl Pyridines as Potent Small-Molecule Inhibitors Targeting the Programmed Cell Death-1/Programmed Cell Death-Ligand 1 Interaction. *J Med Chem* (2021) 64(11):7390–403. doi: 10.1021/acs.jmedchem.1c00010
56. OuYang Y, Gao J, Zhao L, Lu J, Zhong H, Tang H, et al. Design, Synthesis, and Evaluation of *O* -(Biphenyl-3-Ylmethoxy)Nitrophenyl Derivatives as PD-1/PD-L1 Inhibitors With Potent Anticancer Efficacy *In Vivo*. *J Med Chem* (2021) 64(11):7646–66. doi: 10.1021/acs.jmedchem.1c00370
57. Muszak D, Surmiak E, Plewka J, Magiera-Mularz K, Kocik-Krol J, Musielak B, et al. Terphenyl-Based Small-Molecule Inhibitors of Programmed Cell Death-1/Programmed Death-Ligand 1 Protein–Protein Interaction. *J Med Chem* (2021) 64(15):11614–36. doi: 10.1021/acs.jmedchem.1c00957
58. Collins M, Ling V, Carreno BM. The B7 Family of Immune-Regulatory Ligands. *Genome Biol* (2005) 6(6):2235. doi: 10.1186/gb-2005-6-6-223
59. Sasikumar PG, Ramachandra M. Peptide and Peptide-Inspired Checkpoint Inhibitors: Protein Fragments to Cancer Immunotherapy. *Med Drug Discovery* (2020) 8:100073. doi: 10.1016/j.medidd.2020.100073
60. Giannis A, Kolter T. Peptidomimetics for Receptor Ligands?Discovery, Development, and Medical Perspectives. *Angew Chem Int Ed English* (1993) 32(9):1244–675. doi: 10.1002/anie.199312441
61. Pelay-Gimeno M, Glas A, Koch O, Grossmann TN. Structure-Based Design of Inhibitors of Protein-Protein Interactions: Mimicking Peptide Binding Epitopes. *Angew Chem Int Ed* (2015) 54(31):8896–89275. doi: 10.1002/anie.201412070
62. Ripka AS, Rich DH. Peptidomimetic Design. *Curr Opin Chem Biol* (1998) 2 (4):441–525. doi: 10.1016/S1367-5931(98)80119-1
63. Azzarito V, Long K, Murphy NS, Wilson AJ. Inhibition of α-Helix-Mediated Protein–Protein Interactions Using Designed Molecules. *Nat Chem* (2013) 5 (3):161–735. doi: 10.1038/nchem.1568
64. Akram ON, DeGraff DJ, Sheehan JH, Tilley WD, Matusik RJ, Ahn J-M, et al. Tailoring Peptidomimetics for Targeting Protein–Protein Interactions. *Mol Cancer Res* (2014) 12(7):967–785. doi: 10.1158/1541-7786.MCR-13-0611
65. Sasikumar PGN, Ramachandra M, Naremaddepalli SS. *Peptidomimetic Compounds as Immunomodulators*. World Intellectual Property Organization (2013). Available at: https://patents.google.com/patent/WO2013132317A1/en.
66. Sasikumar PGN, Ramachandra M, Appukuttan P, Naremaddepalli SSS. *3-Substituted-1,2,4-Oxadiazole and Thiadiazole Compounds as Immunomodulators*. (2016). Available at: https://patents.google.com/patent/WO2016142886A3/en
67. Sasikumar PGN, Ramachandra M, Naremaddepalli SSS. *1,2,4-Oxadiazole Derivatives as Immunomodulators*. World Intellectual Property Organization (2015). Available at: https://patents.google.com/patent/WO2015033299A1/en?oq=WO2015033299.
68. Sasikumar PGN, Ramachandra M, Naremaddepalli SSS. *1,3,4-Oxadiazole and 1,3,4-Thiadiazole Derivatives as Immunomodulators*. World Intellectual Property Organization WO2015033301A1. International Bureau. (2015). Available at: https://patents.google.com/patent/WO2015033301A1/en?oq=WO2015033301.
69. Xu Y, Lu H, Hai H, Lindang. *Cyclic Compounds Inhibiting Programmed Death Receptor Ligand 1 and Uses Thereof*. State Intellectual Property Office of the Peoples Republic of China (2021). Available at: https://patents.google.com/patent/CN108395443B/en?oq=CN108395443B. CN108395443B.
70. Wang Y, Liwen Z, Xin L, Wei Y, Xiao L, Qi Y. Heterocyclic Compound Serving as Pd-L1 Inhibitor. In: *World Intellectual Property Organization WO2018196768A1, filed April 25, 2018, and issued November 1, 2018* (2018). Available at: https://patents.google.com/patent/WO2018196768A1/en?oq=WO2018196768.
71. Yoon KW, Byun S, Kwon E, Hwang S-Y, Chu K, Hiraki M, et al. Control of Signaling-Mediated Clearance of Apoptotic Cells by the Tumor Suppressor P53. *Sci (New York N.Y.)* (2015) 349(6247):1261669. doi: 10.1126/science.1261669
72. Sasikumar PGN, Ramachandra M, Naremaddepalli S. *Dual Inhibitors of Vista and Pd-1 Pathways*. (2018). Available at: https://patents.google.com/patent/WO2018073754A1/en.
73. Sasikumar P, Sudarshan NS, Gowda N, Samiulla DS, Ramachandra R, Chandrasekhar T, et al. Abstract 4861: Oral Immune Checkpoint Antagonists Targeting PD-L1/VISTA or PD-L1/Tim3 for Cancer Therapy. *Immunology* (2016) 76(14_Supplement)4861. doi: 10.1158/1538-7445.AM2016-4861. American Association for Cancer Research.
74. Sasikumar PGN, Ramachandra M, Naremaddepalli SSS, Gowda N. *Dual Inhibitors of Tim-3 and Pd-1 Pathways*. World Intellectual Property Organization. International Bureau WO2019087087A1 (2019). Available at: https://patents.google.com/patent/WO2019087087A1/en?oq=WO2019087087A1.
75. Sasikumar PG, Naremaddepalli SS, Ramachandra RK, Gowda N, Yerramsetti MR, Bandireddy SR, et al. "Abstract B006: Functional Antagonism of VSIG8-Mediated Immune Suppression by Oral VISTA Agents." In: *Immune Modulators*. American Association for Cancer Research. Philadelphia, PA. (2018). p. B006–6. doi: 10.1158/1535-7163.TARG-17-B006
76. Sasikumar PG, Naremaddepalli SS, Ramachandra RK, Gowda N, Devarapalli S, Adurthi S, et al. Abstract 4148: An Orally Bioavailable Small Molecule Antagonist of TIM-3 Signaling Pathway Shows Potent Anti-Tumor Activity. *Clin Res (Excluding Clin Trials)* (2019) 79(13 Suppl):Abstract nr 4148. doi: 10.1158/1538-7445.AM2019-4148. American Association for Cancer Research.
77. Sasikumar PGN, Ramachandra M, Naremaddepalli SS, Gundala C. *Method of Modulating TIGIT and PD-1 Signalling Pathways Using 1,2,4-Oxadiazole Compounds*. (2019). Available at: https://patents.google.com/patent/WO2019175799A2/en?oq=WO2019175799
78. Sasikumar PGN, Ramachandra M, Naremaddepalli SSS, Gundala C. *Compounds as Modulators of TIGIT Signalling Pathway*. (2018). Available at: https://patents.google.com/patent/WO2018047139A1/en?oq=WO2018047139
79. Sasikumar PG, Gundala C, Balasubramanian WR, Naremaddepalli SS, Bhumireddy A, Patil SS, et al. "Abstract B007: Potent Antitumor Activity of a Novel and Orally Available Small-Molecule Antagonist Targeting the CD47/Sirpα Pathway." In: *Immune Modulators*. American Association for Cancer Research. Philadelphia, PA. (2018). p. B007–7. doi: 10.1158/1535-7163.TARG-17-B007
80. Chupak LS, Zheng X. *Compounds Useful as Immunomodulators*. World Intellectual Property Organization (2015). Available at: https://patents.google.com/patent/WO2015034820A1/en. WO2015034820A1.
81. Wu Q, Jiang L, Li S-c, He Q-j, Yang B, Cao J. Small Molecule Inhibitors Targeting the PD-1/PD-L1 Signaling Pathway. *Acta Pharmacol Sin* (2021) 42 (1):1–95. doi: 10.1038/s41401-020-0366-x
82. Blevins DJ, Hanley R, Bolduc T, Powell DA, Gignac M, Walker K, et al. *In Vitro* Assessment of Putative PD-1/PD-L1 Inhibitors: Suggestions of an Alternative Mode of Action. *ACS Med Chem Lett* (2019) 10(8):1187–925. doi: 10.1021/acsmedchemlett.9b00221
83. Ganesan A, Ahmed M, Okoye I, Arutyunova E, Babu D, Turnbull WL, et al. Comprehensive *in Vitro* Characterization of PD-L1 Small Molecule Inhibitors. *Sci Rep* (2019) 9(1):12392. doi: 10.1038/s41598-019-48826-6
84. Liu M, Zhang Y, Guo Y, Gao J, Huang W, Dong X. A Comparative Study of the Recent Most Potent Small-Molecule PD-L1 Inhibitors: What Can We Learn? *Med Chem Res* (2021) 30(6):1230–395. doi: 10.1007/s00044-021-02728-3
85. Zak KM, Grudnik P, Guzik K, Zieba BJ, Musielak B, Dömling A, et al. Structural Basis for Small Molecule Targeting of the Programmed Death Ligand 1 (PD-L1). *Oncotarget* (2016) 7(21):30323–355. doi: 10.18632/

oncotarget.8730
86. Krajewski M, Rothweiler U, D'Silva L, Majumdar S, Klein C, Holak TA. An NMR-Based Antagonist Induced Dissociation Assay for Targeting the Ligand–Protein and Protein–Protein Interactions in Competition Binding Experiments. *J Med Chem* (2007) 50(18):4382–875. doi: 10.1021/jm070365v
87. Musielak B, Janczyk W, Rodriguez I, Plewka J, Sala D, Magiera-Mularz K, et al. Competition NMR for Detection of Hit/Lead Inhibitors of Protein–Protein Interactions. *Molecules* (2020) 25(13):30175. doi: 10.3390/molecules25133017
88. Konieczny M, Musielak B, Kocik J, Skalniak L, Sala D, Czub M, et al. Di-Bromo-Based Small-Molecule Inhibitors of the PD-1/PD-L1 Immune Checkpoint. *J Med Chem* (2020) 63(19):11271–85. doi: 10.1021/acs.jmedchem.0c01260
89. Sun L, Li C-W, Chung EM, Yang R, Kim Y-S, Park AH, et al. Targeting Glycosylated PD-1 Induces Potent Anti-Tumor Immunity. *Cancer Res* (2020) 80(11):2298–10. doi: 10.1158/0008-5472.CAN-19-3133
90. Li C-W, Lim S-O, Xia W, Lee H-H, Chan L-C, Kuo C-W, et al. Glycosylation and Stabilization of Programmed Death Ligand-1 Suppresses T-Cell Activity. *Nat Commun* (2016) 7(1):12632. doi: 10.1038/ncomms12632
91. Krajewski M, Ozdowy P, D'Silva L, Rothweiler U, Holak TA. NMR Indicates That the Small Molecule RITA Does Not Block P53-MDM2 Binding *in Vitro*. *Nat Med* (2005) 11(11):1135–365. doi: 10.1038/nm1105-1135
92. Grinkevich V, Issaeva N, Hossain S, Pramanik A, Selivanova G. Reply to 'NMR Indicates That the Small Molecule RITA Does Not Block P53-MDM2 Binding *in Vitro*. *Nat Med* (2005) 11(11):1136–375. doi: 10.1038/nm1105-1136
93. Musielak B, Kocik J, Skalniak L, Magiera-Mularz K, Sala D, Czub M, et al. CA-170 – A Potent Small-Molecule PD-L1 Inhibitor or Not? *Molecules* (2019) 24(15):28045. doi: 10.3390/molecules24152804
94. Freedberg D, Selenko P. Live Cell NMR. *Annu Rev Biophys* (2014) 43 (1):171–925. doi: 10.1146/annurev-biophys-051013-023136
95. Siegal G, Selenko P. Cells, Drugs and NMR. *J Magn Reson* (2019) 306 (September):202–12. doi: 10.1016/j.jmr.2019.07.018
96. Pellecchia M, Sem DS, Wüthrich K. Nmr in Drug Discovery. *Nat Rev Drug Discovery* (2002) 1(3):211–195. doi: 10.1038/nrd748
97. Shortridge MD, Hage DS, Harbison GS, Powers R. Estimating Protein–Ligand Binding Affinity Using High-Throughput Screening by NMR. *J Comb Chem* (2008) 10(6):948–585. doi: 10.1021/cc800122m
98. Skalniak L, Zak KM, Guzik K, Magiera K, Musielak B, Pachota M, et al. Small-Molecule Inhibitors of PD-1/PD-L1 Immune Checkpoint Alleviate the PD-L1-Induced Exhaustion of T-Cells. *Oncotarget* (2017) 8(42):72167–81. doi: 10.18632/oncotarget.20050
99. Liu L, Yao Z, Wang S, Xie T, Wu G, Zhang H, et al. Syntheses, Biological Evaluations, and Mechanistic Studies of Benzo[c][1,2,5]Oxadiazole Derivatives as Potent PD-L1 Inhibitors With *In Vivo* Antitumor Activity. *J Med Chem* (2021) 64(12):8391–84095. doi: 10.1021/acs.jmedchem.1c00392
100. Powderly J, Patel MR, Lee JJ, Brody J, Meric-Bernstam F, Hamilton E, et al. CA-170, a First in Class Oral Small Molecule Dual Inhibitor of Immune Checkpoints PD-L1 and VISTA, Demonstrates Tumor Growth Inhibition in Pre-Clinical Models and Promotes T Cell Activation in Phase 1 Study. *Ann Oncol* (2017) 28:v405–6. doi: 10.1093/annonc/mdx376.007
101. Radhakrishnan VS, Bakhshi S, Prabhash K, Deshmukh C, Nag S, Lakshmaiah KC, et al. Phase 2 Trial of CA-170, a Novel Oral Small Molecule Dual Inhibitor of Immune Checkpoints VISTA and PD-1, in Patients (Pts) With Advanced Solid Tumor and Hodgkin Lymphoma. *J Immunother Cancer* (2018) 6:P714.
102. Kabelitz D. Antigen-Induced Death of T-Lymphocytes. *Front Biosci* (1997) 2 (4):d61–77. doi: 10.2741/A175
103. Rozali EN, Hato SV, Robinson BW, Lake RA, Lesterhuis WJ. Programmed Death Ligand 2 in Cancer-Induced Immune Suppression. *Clin Dev Immunol* (2012) 2012:1–8. doi: 10.1155/2012/656340
104. Yearley JH, Gibson C, Yu N, Moon C, Murphy E, Juco J, et al. "PD-L2 Expression in Human Tumors: Relevance to Anti-PD-1 Therapy in Cancer." *Clin Cancer Res* (2017) 23(12):3158–67. doi: 10.1158/1078-0432.CCR-16-1761
105. Shi D, An X, Bai Q, Bing Z, Zhou S, Liu H, et al. Computational Insight Into the Small Molecule Intervening PD-L1 Dimerization and the Potential Structure-Activity Relationship. *Front Chem* (2019) 7:764. doi: 10.3389/fchem.2019.00764
106. Bailly C, Vergoten G. Protein Homodimer Sequestration With Small Molecules: Focus on PD-L1. *Biochem Pharmacol* (2020) 174:113821. doi: 10.1016/j.bcp.2020.113821
107. Antoni C, Vera L, Devel L, Catalani MP, Czarny B, Cassar-Lajeunesse E, et al. Crystallization of Bi-Functional Ligand Protein Complexes. *J Struct Biol* (2013) 182(3):246–545. doi: 10.1016/j.jsb.2013.03.015
108. Chen F-F, Li Z, Ma D, Yu Q. Small-Molecule PD-L1 Inhibitor BMS1166 Abrogates the Function of PD-L1 by Blocking Its ER Export. *OncoImmunology* (2020) 9(1):18311535. doi: 10.1080/2162402X.2020.1831153
109. Li C-W, Lim S-O, Chung EM, Kim Y-S, Park AH, Yao J, et al. Eradication of Triple-Negative Breast Cancer Cells by Targeting Glycosylated PD-L1. *Cancer Cell* (2018) 33(2):187–201.e10. doi: 10.1016/j.ccell.2018.01.009
110. Wang L-C, Koblish H, Zhang Y, Kulkarni A, Covington M. *Incyte - Investors - Events & Presentations* (2019). Available at: https://investor.incyte.com/investors/events-and-presentations/default.aspxmodule-scientific-presentations.
111. Butte MJ, Keir ME, Phamduy TB, Sharpe AH, Freeman GJ. Programmed Death-1 Ligand 1 Interacts Specifically With the B7-1 Costimulatory Molecule to Inhibit T Cell Responses. *Immunity* (2007) 27(1):111–225. doi: 10.1016/j.immuni.2007.05.016
112. Zhao Y, Lee CK, Lin C-H, Gassen RB, Xu X, Huang Z, et al. PD-L1:CD80 Cis-Heterodimer Triggers the Co-Stimulatory Receptor CD28 While Repressing the Inhibitory PD-1 and CTLA-4 Pathways. *Immunity* (2019) 51(6):1059–1073.e9. doi: 10.1016/j.immuni.2019.11.003
113. Sugiura D, Maruhashi T, Okazaki I-m, Shimizu K, Maeda TK, Takemoto T, et al. Restriction of PD-1 Function by *Cis* -PD-L1/CD80 Interactions Is Required for Optimal T Cell Responses. *Science* (2019) 364(6440):558–66. doi: 10.1126/science.aav7062
114. Fenwick C, Pellaton C, Farina A, Radja N, Pantaleo G. Identification of Novel Antagonistic Anti-PD-1 Antibodies That Are Non-Blocking of the PD-1/PD-L1 Interaction. *J Clin Oncol* (2016) 34(15_suppl):3072–2. doi: 10.1200/JCO.2016.34.15_suppl.3072
115. Scheuplein F, Ranganath S, McQuade T, Wang L, Spaulding V, Vadde S, et al. Abstract B30: Discovery and Functional Characterization of Novel Anti-PD-1 Antibodies Using *Ex Vivo* Cell-Based Assays, Single-Cell Immunoprofiling, and *in Vivo* Studies in Humanized Mice. *Cancer Res* (2016) 76(15 Supplement):B30–0. doi: 10.1158/1538-7445.TME16-B30
116. Piha-Paul S, Mitchell T, Sahebjam S, Mehnert J, Karasic T, O'Hayer K, et al. 419 Pharmacodynamic Biomarkers Demonstrate T-Cell Activation in Patients Treated With the Oral PD-L1 Inhibitor INCB086550 in a Phase 1 Clinical Trial. *J ImmunoTher Cancer* (2020) 8(Suppl 3):A445–5. doi: 10.1136/jitc-2020-SITC2020.0419
117. Kopp WC, Smith JW, Ewel CH, Alvord WG, Main C, Guyre PM, et al. Immunomodulatory Effects of Interferon-Gamma in Patients With Metastatic Malignant Melanoma. *J Immunother* (1993) 13(3):181–905. doi: 10.1097/00002371-199304000-00005
118. Maluish AE, Urba WJ, Longo DL, Overton WR, Coggin D, Crisp ER, et al. The Determination of an Immunologically Active Dose of Interferon-Gamma in Patients With Melanoma. *J Clin Oncol* (1988) 6(3):434–45. doi: 10.1200/JCO.1988.6.3.434
119. Talmadge JE, Tribble HR, Pennington RW, Phillips H, Wiltrout RH. Immunomodulatory and Immunotherapeutic Properties of Recombinant γ-Interferon and Recombinant Tumor Necrosis Factor in Mice. *Cancer Res* (1987) 47(10):25635.
120. Thompson JA, Cox WW, Lindgren CG, Collins C, Neraas KA, Bonnem EM, et al. Subcutaneous Recombinant Gamma Interferon in Cancer Patients: Toxicity, Pharmacokinetics, and Immunomodulatory Effects. *Cancer Immunol Immunother* (1987) 25(1):47–53. doi: 10.1007/BF00199300
121. Sivick KE, Desbien AL, Glickman LH, Reiner GL, Corrales L, Surh NH, et al. Magnitude of Therapeutic STING Activation Determines CD8+ T Cell-Mediated Anti-Tumor Immunity. *Cell Rep* (2018) 25(11):3074–3085.e5. doi: 10.1016/j.celrep.2018.11.047
122. Lowder JN, Freidberg JW, Kelly J, Freedman AS, Coffman R, Kanzler H, et al. Dose Finding in Human Trials of TLR9 Agonists: Induction of Interferon-α

Inducible Genes in Blood Mononuclear Cells as a Measure of Biologic Activity of 1018 ISS. *Blood* (2007) 110(11):3844–38445. doi: 10.1182/blood.V110.11.3844.3844
123. Agrawal S, Feng Y, Roy A, Kollia G, Lestini B. Nivolumab Dose Selection: Challenges, Opportunities, and Lessons Learned for Cancer Immunotherapy. *J ImmunoTher Cancer* (2016) 4(1):725. doi: 10.1186/s40425-016-0177-2
124. Ratain MJ, Goldstein DA. Time Is Money: Optimizing the Scheduling of Nivolumab. *J Clin Oncol* (2018) 36(31):3074–765. doi: 10.1200/JCO.18.00045
125. Wang Y, Gu T, Tian X, Li W, Zhao R, Yang W, et al. A Small Molecule Antagonist of PD-1/PD-L1 Interactions Acts as an Immune Checkpoint Inhibitor for NSCLC and Melanoma Immunotherapy. *Front Immunol* (2021) 12:654463(May). doi: 10.3389/fimmu.2021.654463

Conflict of Interest: Authors are present or previous employees of Aurigene Discovery Technologies Limited. PS and MR are inventors on several patent applications related to immune checkpoint inhibitors described in this manuscript. MR is the CEO of Aurigene Discovery Technologies Limited, a company that is co-developing CA-170 for cancer therapy.

Publisher's Note: All claims expressed in this article are solely those of the authors and do not necessarily represent those of their affiliated organizations, or those of the publisher, the editors and the reviewers. Any product that may be evaluated in this article, or claim that may be made by its manufacturer, is not guaranteed or endorsed by the publisher.

Advantages of publishing in Frontiers

OPEN ACCESS
Articles are free to read for greatest visibility and readership

FAST PUBLICATION
Around 90 days from submission to decision

HIGH QUALITY PEER-REVIEW
Rigorous, collaborative, and constructive peer-review

TRANSPARENT PEER-REVIEW
Editors and reviewers acknowledged by name on published articles

Frontiers
Avenue du Tribunal-Fédéral 34
1005 Lausanne | Switzerland

Visit us: www.frontiersin.org
Contact us: frontiersin.org/about/contact

REPRODUCIBILITY OF RESEARCH
Support open data and methods to enhance research reproducibility

DIGITAL PUBLISHING
Articles designed for optimal readership across devices

FOLLOW US
@frontiersin

IMPACT METRICS
Advanced article metrics track visibility across digital media

EXTENSIVE PROMOTION
Marketing and promotion of impactful research

LOOP RESEARCH NETWORK
Our network increases your article's readership